Development of Stimuli-Responsive Liposomes for Drug Delivery Applications

A Dissertation Presented for the

Doctor of Philosophy

Degree

The University of Tennessee, Knoxville

Jinchao Lou

May 2022

Acknowledgements

The journey through graduate school is challenging, and I could have never gone this far without the help and support from the people around me. First and foremost, I would like to thank my advisor, Dr. Michael Best, for his help and support over the past six years. He is knowledgeable and is always there if I need any help or suggestions. He taught me so much and helped me to become a real scientist. I know I can be very annoying sometimes, but he is always patient with me and helps me through tough times. Besides being an advisor, he is part of a mentor, part of a friend to me, and I can always feel comfortable going to him with any questions I have, no matter scientific or personal. I feel so lucky to have him as my research advisor, and I am sure things would have been a lot different if I had chosen a different lab. Without him, I could never have accomplished these much as is today.

I would also like to thank Dr. John Brantley, Dr. Chris Baker, and Dr. Andy Sarles for agreeing to serve on my committee. All your insights and questions during defenses helped me understand my projects better. I'd also like to thank Dr. Francisco Barrera and Dr. Josh Baccile for helping with cell studies on multiple of my projects. In addition, I'd like to thank past members from the Best lab, including Dr. Adam Carr, Dr. Sam Mattern-Schain, Dr. Xiaoyu Zhang, Alexa Watson, and Zhengsu Yu, who helped me start research here, and they all helped me with my projects. I also thank current members Christelle Ancajas, Megan Qualls, and Ruhani Sagar for creating a nice and warm working environment, being friends with me, and supporting me during the tough times. We also went through the special COVID time together, which are invaluable memories that I will never forget. Outside the Best lab, I'd like to thank Xinyi Wang and Zhiming Liu for being a friend to me. Thanks to Dr. Carlos Steren for maintaining all the NMR facilities in the department, which definitely makes the challenging research life less stressful.

I believe things happen for a reason and am grateful for everything that happened and all the people I met in the past. I'd like to thank many people I met prior to UT; Without them, I could not have had the opportunity to start my Ph.D. career here at UT, let alone a successful one. First, I'd like to thank my undergraduate advisor Dr. Qi Lin, who willingly allowed me to work in his lab in my freshman year, which gave me invaluable opportunities to learn what research is. I also appreciate that he recommended me to work as a visiting undergraduate research assistant at Nanjing University in Dr. Leyong Wang's lab in my senior year. That six-month intensive training in organic synthesis with one of their graduate students, Dr. Xin Liu, granted me a smooth start to graduate education. I also want to thank my best friend, Jiedan Deng. Even though we haven't seen each other for years, we still have things to talk about, such as research, life, hobbies and all the times we spent together in college. Many times, she stayed up late to talk with me on the phone when I was in crisis. I appreciate the friendship between us.

Finally, I'd like to thank my family for their support throughout the years. Thanks to my parents for raising me well. I know life was not easy after my Dad passed away, but I thank my Mom for being strong and not giving up on me. Although it has been eleven years, the pain is still real, and it is probably something that time will never heal. Part of me feels that Dad has missed so many important moments in my life, and there will be more to miss, but part of me chooses to believe that he is always around me and knows all the things I have accomplished.

This dissertation is dedicated to my father (1955-2011), who did not see this adventure. Hope I make you proud.

Abstract

Liposomes are spherical nano-assemblies that are proven to be effective drug delivery vehicles. Due to their unique bilayer structures, they are able to encapsulate both hydrophilic and hydrophobic drugs in their aqueous inner core and membrane bilayers, respectively. While liposomal delivery platforms exhibit numerous advantages, the therapeutic efficacy of these platforms would be enhanced by developing triggered release strategies such that one can tune the timing and location of the cargo release in a controlled manner. In this dissertation, we mainly present the development of stimuli-responsive liposomes targeting different disease-associated metabolites utilizing rationally designed synthetic lipid switches.

In Chapter 2, we developed stimuli-responsive liposomes based on molecular recognition principles, employing synthetic lipid switches that can undergo programmed conformational changes upon binding to calcium. While simple ions validated that molecular recognition principles can be harnessed for smart liposome design, in Chapters 3-4, we expanded this field by targeting more complicated phosphorylated small molecule metabolites, such as adenosine triphosphate (ATP) and inositol 1,4,5-trisphosphate (IP_3), which are known to be associated with diseases. Utilizing a slightly different strategy, in Chapters 5-6, we present the design of synthetic lipids that can respond to enzymes (esterases, phosphatases, and galactosidases) and reactive oxygen species (ROS). In all of these works, after obtaining the designed synthetic lipid switches, we evaluated release efficacy upon stimulus treatment using fluorescence-based dye release assays. Morphology changes to the lipid nanoparticles were probed with dynamic light scattering (DLS) and electron microscopy (EM) techniques.

Other than triggering release, enhancing the targeting of liposomes to diseased rather than healthy cells can also improve diseased-cell specificity and drug release/potency. In Chapter 7, we introduce a boronate-caged guanidine lipid that can show site-specific targeting properties upon treatment with ROS, which is known to be upregulated in certain diseased cells.

Outside liposome projects, we also attempted to develop high-throughput assays for detection of phospholipase inhibition. In Chapter 8, we designed fluorescent probes containing two pyrene moieties based on the lipids cardiolipin and phosphatidylethanolamine. Taking advantage of the pyrene excimer properties, these lipids are expected to exhibit fluorescent changes upon catalytic hydrolysis by disease-associated phospholipase enzymes.

Table of Contents

Chapter 1. Introduction to lipids, liposomes, and drug delivery 1
1.1. Overview of lipids in biological systems 1
1.2. Structures and properties of lipids 1
1.3. Lipid self-assemblies and liposomes 5
1.3.1. Introduction to packing parameters 5
1.3.2. Introduction to liposomes 7
1.3.3. Introduction to membrane phase behavior 9
1.3.4. Liposome preparation and characterization methods 11
1.4. Liposomes and drug delivery 12
1.4.1. Overview of drug delivery vehicles 12
1.4.2. Liposome as a drug delivery vehicle (overview and considerations) 13
1.4.3. Surface modification of liposomes 16
1.5. Liposomes and triggering release 19
1.6. Summary and outlook 22
Chapter 2. Development of calcium-responsive liposomes 23
2.1. Project overview 23
2.1.1. Calcium in biological systems 24
2.1.2. Lipid switches that undergo conformational changes 25
2.2. Design and synthesis of the calcium responsive synthetic lipid switch 27
2.3. Fluorescence-based dye release assays and DLS studies 30
2.3.1. Nile red release assay and corresponding morphology changes 30
2.3.2. Sulforhodamine B release assay 31
2.3.3. Metal ion selectivity screen with Nile red release assay 33
2.4. Scanning transmission electron microscopy studies 36
2.5. Miscellaneous experiments 36
2.5.1. Quantification of trigger lipid incorporation 36
2.5.2. Release studies with varying conditions 38
2.5.3. Metal ion selectivity screen with SRB release assay 40
2.6. Conclusion 40
2.7. Synthesis and experimental procedure 42
Chapter 3. Development of ATP-responsive liposomes 51
3.1. Project overview 51
3.2. Design and synthesis of the phosphorylated metabolites-responsive synthetic lipid switch 52
3.3. Nile red-based dye release assays for phosphorylated small molecules 54
3.3.1. Phosphorylated metabolite selectivity screen 54
3.3.2. Triphosphate metabolite NR release screens 56
3.3.3. Expanded Nile red titration curves 59
3.4. Dynamic light scattering studies 65
3.5. Transmission electron microscopy (TEM) and cryo-EM studies 65

3.6. Fluorescence microscopy studies on liposome morphology changes 68
3.7. Reversibility of NR release 68
3.8. ATP triggered hydrophilic calcein release assay 74
3.9. Techniques used to prove binding interactions between lipid switches and ATP 79
3.9.1. NMR titration and DOSY experiment 79
3.9.2. UV-Vis titration experiment 83
3.9.3. Zeta potential measurement 83
3.10. Development of alternative lipid structures to elucidate conformational changes 83
3.10.1. Design and synthesis of alternative lipid structures 83
3.10.2. Nile red release studies for all alternative lipids 86
3.10.3. DLS studies for all alternative lipids 92
3.10.4. Calcein release studies for all alternative lipids 92
3.11. Cellular delivery studies 98
3.11.1. Delivery studies with untreated cells 98
3.11.2. Delivery studies with inhibitor-treated cells for intracellular ATP manipulation 100
3.11.3. MTS assay 100
3.11.4. Initial colocalization experiments 104
3.12. Miscellaneous experiments 105
3.12.1. Biphenyl- and naphthyl- linker compound synthesis 105
3.12.2. Initially designed synthetic route 107
3.12.3. Initial release studies with 3.1a 109
3.13. Conclusions 111
3.14. Synthesis and experimental procedure 112
Chapter 4. Development of IP_3-responsive liposomes 150
4.1. Project overview 150
4.2. Design and synthesis of the IP_3-responsive lipid switch 150
4.3. Nile red-based dye release assays 151
4.3.1. Phosphorylated metabolite selectivity screen 151
4.3.2. Expanded Nile red titration experiments 154
4.4. DLS studies on morphology changes 156
4.5. Fluorescence microscopy studies on liposome morphology changes 161
4.6. Zeta potential measurements 161
4.7. Sulforhodamine B release studies 164
4.8. Attempts at NMR and UV-Vis titrations 167
4.9. Miscellaneous experiments 167
4.10. Conclusions 169
4.11. Synthesis and experimental procedure 171
Chapter 5. A general strategy to develop enzyme-responsive liposomes 183
5.1. Project overview 183

5.1.1. Introduction to previous enzyme-responsive liposomes 183
5.1.2. Introduction of enzymes in biology and disease 184
5.1.3. Structure of DOPE and its self-assembly properties 186
5.1.4. Headgroup-modified DOPE based release systems 186
5.1.5. Introduction to self-immolative linkers 188
5.2. Design and synthesis of enzyme-responsive lipids 190
5.3. TLC analysis of enzyme-mediated cleavage of free lipid ERL 193
5.4. Fluorescence-based dye release assays and DLS studies 194
5.4.1. Nile red release assay 194
5.4.2. DLS studies 204
5.4.3. SRB release assay 207
5.5. Miscellaneous experiments 209
5.5.1. ERL related attempts 209
5.5.2. PRL related attempts 214
5.5.3. GRL related attempts 217
5.5.4. Chain extension attempts 221
5.6. Conclusions 228
5.7. Synthesis and experimental procedure 229
Chapter 6. Development of ROS-responsive liposomes 267
6.1. Project overview 267
6.1.1. Introduction of ROS and ROS-responsive nanocarriers 267
6.2. Design and synthesis of the ROS-responsive lipid 6.1 268
6.3. Hydrophobic release assays using Nile red 270
6.3.1. Initial studies 270
6.3.2. NR release with different concentrations of peroxide 272
6.3.3. NR release with diluted liposomes 274
6.4. Dynamic light scattering studies 277
6.5. Transmission electron microscopy studies 277
6.6. Hydrophilic dye release assay with ANTS/DPX 280
6.7. Mechanistic studies 281
6.7.1. Evidence for the formation of DOPE 281
6.7.2. Additional compound to elucidate release mechanism 288
6.7.3. Membrane asymmetry in the release process 290
6.8. Miscellaneous experiments 295
6.8.1. Alternative designs 295
6.8.2. Synthesis and release studies of alternate control lipid 6.22 297
6.8.3. Alternative ROS-responsive lipids based on poly-unsaturated PE scaffold 300
6.9. Conclusion 303
6.10. Synthesis and experimental procedure 305
Chapter 7. Development of ROS-responsive caged guanidine lipids for targeted delivery 325

7.1. Project overview 325
7.1.1. Liposome targeting and cell penetrating peptides 326
7.1.2. Introduction to activable cell penetrating peptide 326
7.2. Design and synthesis of the ROS-responsive caged guanidine lipids 329
7.3. Verification of lipid uncaging 331
7.3.1. Mass spectrometry analysis 331
7.3.2. Zeta potential analysis of lipid uncaging 334
7.4. Microplate-based liposome assay to detect binding/fusion driven by uncaging 336
7.4.1. Assay overview 336
7.4.2. Microplate binding/fusion assay results 336
7.5. Dynamic light scattering studies 341
7.6. Cellular delivery studies 341
7.7. Conclusions 353
7.8. Synthesis and experimental procedure 353
Chapter 8. Fluorescent probes based on cardiolipin and PE for high throughput assays of phospholipase inhibition 363
8.1. Background and project overview 363
8.2. Design and synthesis of cardiolipin probes 8.5 and 8.6 366
8.2.1. Initial synthetic route for 8.5 366
8.2.2. Pyrene-DAG building block synthesis 368
8.2.3. Protected glycerol backbone synthesis 370
8.2.4. CL scaffold build-up 370
8.3. Design and synthesis of the PE probe 373
8.4. Conclusions and future works 375
8.5. Synthesis 377
Chapter 9. Miscellaneous Synthesis 398
9.1. Design and synthesis of disulfide lipids for enhanced cellular delivery 398
9.1.1. Project overview 398
9.1.2. Synthetic procedures 400
9.2. Synthesis of 19-halogen substituted cholesterol analogues 404
9.2.1. Project overview 404
9.2.2. Synthetic procedures 406
9.3. Synthesis of a zinc-responsive lipid based on a DPA scaffold 413
9.3.1. Project overview 413
9.3.2. Synthetic procedures 415
9.4. Synthesis of azide-containing probes for metabolic labeling purposes 418
9.4.1. Project overview 418
9.4.2. Synthetic procedures 424
List of References 438
Appendix 461
Vita 462

List of Tables

Table 1.1. T_m values for selected lipids commonly employed in liposome formation. .10
Table 3.1. Summary of phosphorylated/triphosphate metabolite screen results using NR release assay with all lipid switches studied herein. 93
Table 3.2. Initial NR release studies with different buffer conditions. 110
Table 5.1. Summary of formulations explored for triggered release using ERL containing different percentages of PC, DOPE, DOTAP or PA.....197
Table 5.2. Summary of formulations explored for forming stable PRL liposomes containing different percentages of PC, DOPE, DOTAP or PA. 200
Table 5.3. Summary of formulation explored for triggered release using GRL containing different percentages of PC, DOPE, DOTAP or PA.....202
Table 8.1. Conditions explored to deprotect PMB groups of 8.10. 369
Table 8.2. Conditions explored to deprotect benzyl groups of 8.20. 369
Table 8.3. Conditions explored to deprotect the benzyl protecting group of 8.29. 374
Table 8.4. Conditions explored to deprotect the silyl and cyanoethyl protected CL scaffold 8.32. 374

List of Figures

Figure 1.1. Structure of a typical glycerophospholipid. 3
Figure 1.2. Structures of common fatty acids. 4
Figure 1.3. Packing parameters and self-assembly properties of lipids. 6
Figure 1.4. The common vesicle size and lamellarity classification system..... 8
Figure 1.5. Cartoon illustration for different classes of nanoparticles utilized for drug delivery applications. 14
Figure 1.6. Cartoon illustration for different types of surface-modified liposomes for active targeting purposes. 17
Figure 1.7. Cartoon illustration of commonly explored strategies for triggered release of contents from liposomes by fine-tuning lipid structures and membrane properties. 20
Figure 2.1. Previously reported pH-responsive switchable lipids developed by (A) Leblond and coworkers, and (B) the Menger group. 26
Figure 2.2. Structures of (A) ZnBDPA sensor developed by the Smith group and (B) the first indo-1 calcium sensor reported by Tsien and coworkers. 26
Figure 2.3. NR release and DLS studies of liposomes containing 2.5. 32
Figure 2.4. Sulforhodamine B release study of liposomes containing lipid 2.5. 34
Figure 2.5. Selectivity of triggered release with different common metal cations. 35
Figure 2.6. STEM images of liposomes containing (A) 10% of 2.5 before calcium addition, (B) 0% of 2.5 after 20 mM calcium addition, and (C) 10% of 2.5 after 20 mM calcium addition. 37
Figure 2.7. UV-Vis quantification of lipid 2.5 in the liposomes. 37
Figure 2.8. Nile red release studies performed in HEPES buffer at mM scale. 39
Figure 2.9. Nile red release studies performed in HEPES buffer at μM scale. 39
Figure 2.10. Metal ion selectivity screen with SRB release assay. 41
Figure 3.1. UV-Vis calibration curve for Nile red in chloroform used to measure encapsulation efficiency within liposomes. 57
Figure 3.2. NR release results for liposomes containing lipid switch 3.1a. 58
Figure 3.3. Kinetic curves of NR release from 2 mM 10% (A) and 20% (B) 3.1a/PC liposomes after adding ATP. 60
Figure 3.4. NR release profile using diluted 10% 3.1a/PC liposomes. 62
Figure 3.5. NR release results for liposomes containing 3.1b and PC. 63
Figure 3.6. Kinetic curves of NR release from 2 mM 10% or 20% 3.1b/PC liposomes after adding ATP. 64
Figure 3.7. A. DLS analysis of PC-based liposomes containing different percentages of 3.1a encapsulating NR before and after ATP treatment. 66
Figure 3.8. DLS results for liposomes containing 3.1b (A-C) and ADP selectivity for 3.1a or 3.1b liposomes (D). 67
Figure 3.9. EM images of PC and 3.1a liposomes. 69
Figure 3.10. Fluorescence microscope images for 0% (B) or 10% 3.1a (A) liposomes

labeled with Rd-PE before and after 15 minute incubation with 1 mM ATP.....70
Figure 3.11. Reversibility test for Nile red release assay using 10% 3.1a liposomes....71
Figure 3.12. Reversibility test for Nile red release assay using 20% 3.1a liposomes. ..73
Figure 3.13. Raw distribution curves for calcein-encapsulated PC liposomes containing or lacking all lipid switches/controls studied herein.....75
Figure 3.14. Calcein release results using 10% 3.1a/PC liposomes.....76
Figure 3.15. Calcein release results with 10% 3.1b/PC liposomes.....77
Figure 3.16. Reversibility test for calcein release assay using 10% 3.1a liposomes. ...78
Figure 3.17. Calcein release results with 10X diluted 10% 3.1a/PC liposomes.....80
Figure 3.18. ^{31}P NMR spectra obtained from titration of free 3.1a lipid and ATP.....81
Figure 3.19. DOSY results for lipid 3.1a, ATP and 3.1a-ATP complex in d_6-DMSO containing 8% D_2O.....82
Figure 3.20. UV-Vis titration experiment with free 3.1a and ATP.....84
Figure 3.21. Zeta potential measurements for PC liposomes containing 0, 5%, or 10% 3.1a before and after adding ATP.....84
Figure 3.22. Structures of additional lipid switches designed to probe structural effects on activity. 85
Figure 3.23. NR release results with liposomes composed of different percentages of 3.1c within PC.....89
Figure 3.24. NR release results with liposomes composed of different percentages of 3.1d within PC. 90
Figure 3.25. NR release results with liposomes composed of different percentages of 3.2 within PC.....91
Figure 3.26. DLS results for liposomes containing 3.1c before and after ATP treatment. 94
Figure 3.27. DLS results for liposomes containing 3.2 before and after ATP treatment. 95
Figure 3.28. Calcein release results using 10% 3.1c/PC liposomes.....96
Figure 3.29. Calcein release results using 10% 3.2/PC liposomes.....97
Figure 3.30 Fluorescence images of A375 cells treated with PC/Rd-PE liposomes (A) or 5% 1a/PC/Rd-PE liposomes (B) for 30 minutes.....99
Figure 3.31. ATP assay of intracellular (A) and extracellular (B) ATP levels. 101
Figure 3.32. Fluorescence images of control cells (A), control cells including diluted DMSO (B), cells treated with AA/DG (C), or AICAR (D) followed by addition of PC/3.1a (5%)/Rd-PE liposomes for 30 minutes. 102
Figure 3.33. MTS assay indicating 3.1a does not affect cell viability.....103
Figure 3.34. 3.1a liposomes do not colocalize with mitochondria. 106
Figure 4.1. Results from NR release assay using PC-based liposomes containing lipid switch 4.1.....155
Figure 4.2. NR release titration curve for 5% 4.1-liposomes by titrating with IP_3 to an excess amount (> 5 mM). 157

Figure 4.3. Kinetic curves of NR release from 2 mM 10% and 20% 4.1/PC liposomes after adding IP_3. 157
Figure 4.4. Liposome stability test for NR encapsulated PC-based liposomes containing 0-20% lipid 4.1. 158
Figure 4.5. DLS results for 0-25% 4.1/PC liposomes before (grey) and after (red) IP_3 treatment. 159
Figure 4.6. DLS raw distribution curves for PC and 5-25% 4.1/PC liposomes before and after IP_3 addition. 160
Figure 4.7. Fluorescence microscopy images for Rd-PE labeled 0% (B) and 20% (A) 4.1-liposomes (1 mM) before and after 15 minute 1 mM IP_3 incubation. 162
Figure 4.8. Zeta potential measurements for PC liposomes containing 0, 10%, or 20% 4.1 before and after adding IP_3. 163
Figure 4.9. DLS raw distribution curves for SRB-encapsulated DPPC/DOPE liposomes containing or lacking lipid 4.1. 165
Figure 4.10. SRB release results for DPPC/DOPE liposomes containing or lacking lipid switch 4.1 upon IP_3 treatment. 166
Figure 4.11. Sample raw fluorescence emission spectra for liposomes containing 0 or 10% lipid 4.1, 50% or 40% DPPC and 50% DOPE used in SRB release assay. 166
Figure 4.12. UV-Vis titration results. 168
Figure 5.1. Representative previous reported enzyme-responsive liposomes. 185
Figure 5.2. Lipids designed for triggered release through the production of natural non-bilayer lipid DOPE product. 187
Figure 5.3. Design for general self-immolative systems and examples for self-immolative linkers. 189
Figure 5.4. TLC analysis of free ERL as an esterase substrate. 195
Figure 5.5. Photos of colorimetric assays testing enzyme activity. 195
Figure 5.6. Release of NR over time from different formulations of enzyme-responsive liposomes. 198
Figure 5.7. Liposome stability test for NR-encapsulated PA-containing liposomes with all three enzyme-responsive lipids. 203
Figure 5.8. DLS results from enzyme-responsive liposomes used in NR release experiments. 205
Figure 5.9. Raw DLS size distribution plots for A. ERL-containing liposomes before and after esterase/buffer treatment, and B. control liposomes without ERL before and after esterase addition. 205
Figure 5.10. Raw DLS size distribution plots for A. GRL-containing liposomes before and after β-galactosidase/buffer treatment, and B. control liposomes without GRL before and after β-galactosidase addition. 206
Figure 5.11. Raw DLS size distribution plots for A. PRL-containing liposomes before and after phosphatase/buffer treatment, and B. control liposomes without PRL before and after phosphatase addition. 208

Figure 5.12. SRB release data over time upon esterase addition to liposomes containing 30% ERL, 50% DOPE, 10% PC and 10% PA or control experiments of buffer treatment or liposomes lacking ERL. 208
Figure 5.13. Packing parameters of certain membrane lipids. 211
Figure 5.14. ChemBioDraw 3D prediction of POPE (A) and DOPE (B) conformation. . 211
Figure 5.15. Attempts to acquire STEM images of esterase-responsive lipid ERL. 213
Figure 5.16. Cryo-EM image of liposomes containing 30% ERL, 50% DOPE, 10% PA and 10% PC. 215
Figure 5.17. Cellular delivery studies using liposomes containing ERL. 215
Figure 5.18. Preliminary NR release assays with lipid 5.43 at 40 μM liposome concentrations. 220
Figure 5.19. Raw data for GRL lectin binding and release experiments. 222
Figure 5.20. Substrate accessibility is a common problem in drug delivery research area. 224
Figure 5.21. Initial enzyme mediated depolymerization studies with two polymer intermediates 5.50 and 5.51. 227
Figure 6.1. Nile red release profiles for liposomes containing various percentages (0-100%) of lipid 6.1 mixed with PC as the remaining percentage after adding 98 mM H_2O_2. 271
Figure 6.2. NR fluorescence intensity change over time when treating NR with excess H_2O_2 in MeOH or MeOH/H_2O. 273
Figure 6.3. Triton addition to liposomes post NR release. 273
Figure 6.4. Nile red release profiles for PC liposomes containing 75% of lipid 6.1 after addition of varying concentrations of H_2O_2. 275
Figure 6.5. Nile red release profiles using different concentrations of PC-based liposomes containing 75% of 6.1. 276
Figure 6.6. DLS size distribution plots for 0.1 mM PC-based liposomes containing 75% 6.1 before and after H_2O_2 addition. 278
Figure 6.7. DLS analysis of NR-encapsulated liposomes containing different percentages of lipid 6.1 (0-100%) mixed with the remaining percentage of PC before and after H_2O_2 addition. 278
Figure 6.8. Raw DLS size distribution plots for liposomes containing 6.1 used in NR release assays. 279
Figure 6.9. TEM images of A. liposomes composed of 100% PC after H_2O_2 treatment, and B. and C. liposomes containing 75% of lipid 6.1 and 25% PC after H_2O_2 incubation. 279
Figure 6.10. Hydrophilic dye release results using liposomes containing 30% lipid 6.1, 50% DOPE, 10% PC and 10% PA utilizing an ANTS/DPX leakage assay. 282
Figure 6.11. Sample raw fluorescence emission spectra for liposomes containing 30% lipid 6.1, 10% egg PC, 50% DOPE and 10% PA used in ANTS/DPX release assay after H_2O_2 addition. 282

Figure 6.12. DLS results using liposomes containing 30% lipid 6.1, 50% DOPE, 10% PC and 10% PA before and after release via the ANTS/DPX assay. 283
Figure 6.13. Raw DLS size distribution plots for liposomes used in ANTS/DPX release assays. 283
Figure 6.14. ANTS/DPX release profile for 10X diluted liposomes containing 30% lipid 6.1, 50% DOPE, 10% PC and 10% PA. 284
Figure 6.15. Time-dependent NMR analysis for lipid 6.1 in $CDCl_3/CD_3OD/D_2O$=65/25/4 (v/v) upon treatment with hydrogen peroxide. 286
Figure 6.16. TLC analysis of free lipid 6.1 after adding H_2O_2. 287
Figure 6.17. Mass spectrum including a peak matching DOPE after treating free lipid 6.1 with hydrogen peroxide. 287
Figure 6.18. Release profiles of liposomes containing control lipid 6.6. 291
Figure 6.19. Sample raw fluorescence emission spectra for 6.6 liposomes. 291
Figure 6.20. DLS size distribution plots for 6.6 liposomes. 292
Figure 6.21. NMR analysis for liposomes composed of 100% lipid 6.1 after treatment with H_2O_2 for five minutes. 294
Figure 6.22. A. Alternative designs for ROS-responsive lipids 6.1 and 6.9-6.11. B. Proposed decomposition mechanism for lipid 6.11 upon H_2O_2 addition. 296
Figure 6.23. Release studies for lipid 6.22. 301
Figure 6.24. NMR titration of lipid 6.22 upon treatment of H_2O_2. 301
Figure 6.25. Fluorescence-based assays to evaluate the release properties for poly-unsaturated lipids 6.23-6.25. 304
Figure 7.1. Representative activable CPPs that show cellular uptake only upon treatment of a desired stimulus. 327
Figure 7.2. High-resolution mass spectrometry analysis of lipid 7.1 after H_2O_2 treatment. 333
Figure 7.3. Zeta potential measurements for liposomes containing 0%, 10%, and 20% lipid 7.1 before and after H_2O_2 addition. 335
Figure 7.4. Evidence of successful immobilization of anionic PS liposomes onto streptavidin-coated microplates containing 5% PS, 1% biotin-PE and 1% Rd-PE. 339
Figure 7.5. Results for microplate-based binding/fusion assay. 340
Figure 7.6. Microplate-based binding assay using 10% or 20% DOTAP liposomes. 342
Figure 7.7. DLS raw distribution curves for PC liposomes containing 0%, 10%, or 20% lipid 7.1 before and after H_2O_2 incubation. 343
Figure 7.8. DLS results for 20% 7.1/PC liposomes mixed with 10% PS/PC or PA/PE/PC=10/50/40 liposomes before and after addition of H_2O_2. 344
Figure 7.9. Raw distribution curves for all liposomes analyzed in this experiment. 345
Figure 7.10. Fluorescence images indicating enhanced liposomal delivery to MDA-MB-231 cells with liposomes containing 20% H_2O_2-uncaged 7.1 under buffer dilution conditions. 347

Figure 7.11. Representative 4X fluorescence images indicating enhanced liposomal delivery to MDA-MB-231 cells with liposomes containing 20% H_2O_2-uncaged 7.1 under buffer dilution conditions.....348
Figure 7.12. Fluorescence images indicating enhanced liposomal delivery to MDA-MB-231 cells with liposomes containing 20% H_2O_2-uncaged 7.1 under media dilution conditions.....349
Figure 7.13. Representative 4X fluorescence images indicating enhanced liposomal delivery to MDA-MB-231 cells with liposomes containing 20% H_2O_2-uncaged 7.1 under media dilution conditions. 350
Figure 7.14. Representative 4X fluorescence images for MDA-MB-231 cells treated with liposomes containing 10% H_2O_2-uncaged 7.1 under PBS^{++} or media dilution conditions.....351
Figure 7.15. Representative 20X fluorescence images for MDA-MB-231 cells treated with liposomes containing 10% H_2O_2-uncaged 7.1 under PBS^{++} or media dilution conditions.....352
Figure 8.1. Structures of previous reports of fluorogenic analogues for measurement of phospholipase enzyme activities.....365
Figure 8.2. Structures of the cardiolipin probes we pursued containing two pyrene fluorophores.....367
Figure 8.3. Structure and sensing mechanism of the alternative PE probe 8.33 containing two pyrene fluorophores.....376

List of Schemes

Scheme 2.1. Calcium-triggered liposomal release. 28
Scheme 2.2. Synthesis of calcium-responsive lipid switch 2.5. 29
Scheme 3.1. Design for phosphorylated metabolite-responsive liposomes. 53
Scheme 3.2. Synthetic routes to bis-ZnDPA lipid structures 3.1a (A) and 3.1b (B). 55
Scheme 3.3. Synthetic route for alternative lipid switch 3.1c bearing a hexyl linker. 87
Scheme 3.4. Synthetic route for alternative lipid switch 3.1d bearing only one ZnDPA binding unit. 87
Scheme 3.5. Synthetic route for alternative lipid switch 3.2 bearing altered C12 alkyl tails. 88
Scheme 3.6. Synthetic attempts made to make lipid switches bearing biphenyl linker (3.1e) as well as a naphthyl- linker (3.1f). 106
Scheme 3.7. Initial designed synthetic route to switchable lipid 3.6 through reductive amination reactions. 108
Scheme 3.8. Initially designed synthetic route to switchable lipid through alkylation reactions. 108
Scheme 4.1. Design for IP_3-responsive liposomes. 152
Scheme 4.2. Synthetic route to lipid switch 4.1. 153
Scheme 4.3. Synthetic route to lipid 4.10 bearing a triethylamine linker. 170
Scheme 5.1. Design of enzyme-responsive liposomes. 191
Scheme 5.2. Synthetic routes developed to access ERL (A) PRL (B) and GRL (C). 192
Scheme 5.3. Synthetic route and attempts to make commercially available intermediate 5.7. 210
Scheme 5.4. Synthesis of POPE version esterase-responsive lipid 5.29. 210
Scheme 5.5. Synthetic route and attempts to make the POPE version of phosphatase-responsive lipid 5.33. 216
Scheme 5.6. Initial design and proposed synthetic route for trimethyl lock-based galactosidase-responsive lipid. 218
Scheme 5.7. Synthetic attempts to the make the lipid scaffold of GRL lipid (A-C) and alternative route for direct coupling to make GRL (D). 218
Scheme 5.8. Synthesis of an alternative galactosidase-responsive lipid 5.43, bearing a dodecylamine lipid chain as the scaffold. 220
Scheme 5.9. Self-immolative polymer (SIP) lipid design. 225
Scheme 5.10. Synthetic route for SIP lipid 5.46 with one QM immolating unit. 225
Scheme 5.11. Polymer SIP lipid related synthesis. 227
Scheme 6.1. Design strategy for ROS-responsive liposomes. 269
Scheme 6.2. Synthetic route developed to produce ROS-responsive lipid 6.1. 271
Scheme 6.3. Design and synthetic route for control lipid 6.6. 289
Scheme 6.4. Structure and synthetic route for initially designed ROS-responsive lipid target 6.8. 296
Scheme 6.5. Proposed synthetic route to ester and carbonate version of ROS-

responsive lipid 6.9 and 6.10. 298
Scheme 6.6. Synthetic route for the key building block of di-carbonate immolative lipid 6.11. 299
Scheme 6.7. Synthetic route to control lipid 6.22. 299
Scheme 6.8. Structures and synthetic route to alternative ROS-responsive lipids based on poly-unsaturated PE scaffolds. 302
Scheme 7.1. Design for caged guanidine liposomes containing lipid 7.1 for ROS-mediated targeted delivery. 330
Scheme 7.2. Synthetic route to caged guanidine lipid 7.1. 332
Scheme 7.3. Cartoon illustration for fluorescence-based microplate binding assays. 337
Scheme 8.1. Proposed synthetic route for initially designed CL probe 8.5. 367
Scheme 8.2. Synthetic route to benzyl-protected pyrene-containing DAG building block 8.20. 369
Scheme 8.3. Synthetic route to the extended linker and the resulting alternative DAG scaffold 8.23. 371
Scheme 8.4. Synthetic routes to Bn- (A), silyl- (B) and PMB- (C) protected glycerol backbone. 371
Scheme 8.5. Proposed synthetic route to CL probe through Bn protected glycerol backbone. 372
Scheme 8.6. Proposed synthetic route to CL probe through silyl protected glycerol backbone. 374
Scheme 8.7. Synthetic route to pyrene probe 8.33 based on PE scaffold..... 376
Scheme 9.1. A-C. Synthetic routes to disulfide containing lipids 9.1.1-9.1.3. D. Synthetic route to a TEG-disulfide control compound 9.1.7..... 399
Scheme 9.2. Synthetic routes to 19-iodo or 19-bromo cholesterol..... 405
Scheme 9.3. Synthetic route to zinc-responsive lipid 9.3.1. 414
Scheme 9.4. Synthetic routes to azido-glycerol-based probes for metabolic labeling purposes..... 420
Scheme 9.5. Design and synthetic route to azido-PA probe..... 421
Scheme 9.6. Synthetic route to 3-azido inositol probe 9.4.14..... 423

List of Abbreviations

AA	Antimycin A
AADAC	Arylacetamide deacetylase
AcOH	Acetic acid
ADP	Adenosine diphosphate
AICAR	5-Aminoimidazole-4-carboxamide-1-ß-riboside
AMP	Adenosine monophosphate
AMPK	AMP-activated protein kinase
ANTS	8-Aminonaphthalene-1,3,6-trisulfonic acid
ASGP-R	Asialoglycoprotein receptor
ATP	Adenosine triphosphate
Bn	Benzyl
Boc	*tert*-Butylcarbamate
BSA	Bovine serum albumin
CAN	Ammonium Cerium(IV) Nitrate; $(NH_4)_2Ce(NO_3)_6$
CBz	Benzyloxycarbonyl
$CHCl_3$	Chloroform
CL	Cardiolipin
CO_2	Carbon dioxide
CPP	Cell penetrating peptide
CSA	(±)-10-Camphorsulfonic acid
CTCF	Corrected total cell fluorescence
CTP	Cytidine-5'-triphosphate
CuAAC	Cu(I)-catalyzed azide/alkyne cycloaddition
$Cu(CNCH_3)_4PF_6$	Tetrakis(acetonitrile)copper(I) hexafluorophosphate
CuI	Copper(I) iodide
$CuSO_4$	Copper(II) sulfate
DAG	Diacylglycerol
DAPI	4’,6-Diamidino-2-phenylindole
DART	Direct analysis in real time
DCC	Dicyclohexylcarbodiimide
DCM/CH_2Cl_2	Dichloromethane
DCU	Dicyclohexylurea
DDQ	2,3-Dichloro-5,6-dicyano-1,4- benzoquinone
DG	2-Deoxy-D-glucose
DIB	Iodobenzene diacetate
DIEA	*N,N*-Diisopropylethylamine
DLS	Dynamic light scattering
DMAP	*N,N'*-Dimethylaminopyridine
DMEM	Dulbecco's modified eagle medium

DMF	*N,N*-Dimethylformamide
DMSO	Dimethylsulfoxide
DOPE	1,2-Dioleoyl-*sn*-glycero-3-phosphoethanolamine
DOTAP	1,2-Dioleoyl-3-trimethylammonium propane
Dox	Doxorubicin
DPA	Dipicolylamine
DPPC	1,2-Dipalmitoyl-*sn*-glycero-3-phosphocholine
DPX	*p*-xylene-bis-Pyridinium bromide
DTT	Dithiothreitol
EDCI	1-Ethyl-3-(3-dimethylaminopropyl)carbodiimide hydrochloride
EE	Encapsulation efficiency
EM	Electron microscopy
EPR	Enhanced permeability and retention
ER	Endoplasmic reticulum
ESI	Electrospray ionization
Et_2O	Diethyl ether
EtOAc	Ethyl acetate
EtOH	Ethanol
FA	Fatty acid
FBP	D-Fructose-1,6-bisphosphate
FBS	Fetal bovine serum
FP	D-Fructose-6-phosphate
FRET	Förster resonance energy transfer
Gal	Galactose
GalNAc	*N*-Acetylgalactosamine
GSH	Glutathione
GTP	Guanidine triphosphate
GUV	Giant unilamellar vesicles
H_2O_2	Hydrogen peroxide
HBA	4-Hydroxybenzyl alcohol
HCl	Hydrochloric acid
HEPES	4-(2-Hydroxyethyl)-1-piperazineethanesulfonic acid
$Hg(OTFA)_2$	Mercury(II) trifluoromethanesulfonate
$HO^{\cdot}$	Hydroxyl radicals
HOBt	Hydroxybenzyltriazole
HRMS	High-resolution mass spectrometry
IP_3	D-myo-Inositol-1,4,5-triphosphate
i-PrOH	Isopropanol alcohol
K_2CO_3	Potassium carbonate

KI	Potassium iodide
$KMnO_4$	Potassium permanganate
LPC	*lyso*-Phosphotidylcholine
LUV	Large unilamellar vesicles
m-CPBA	*meta*-Chloroperoxybenzoic acid
MeCN	Acetonitrile
MeOH	Methanol
MLV	Multilamellar vesicles
MQ	Milli-Q purified water
$Na(OAc)_3BH$	Sodium triacetoxyborohydride
Na_2CO_3	Sodium carbonate
Na_2SO_4	Sodium sulfate
$NaBH_4$	Sodium borohydride
NaBr	Sodium bromide
NaCl	Sodium chloride
NaH	Sodium hydride
$NaHCO_3$	Sodium bicarbonate
NaI	Sodium iodide
NaN_3	Sodium azide
NaOH	Sodium hydroxide
NH_4F	Ammonium fluoride
NMR	Nuclear magnetic resonance
NR	Nile red
$^1O_2$	Singlet oxygen
$O_2^{\cdot -}$	Superoxide
PA	Phosphatidic acid
PBS	Phosphate buffered saline
PC	L-α-Phosphatidylcholine
$Pd(OH)_2$	Palladium hydroxide
Pd/C	Palladium on carbon
PDI	Polydispersity index
PE	Phosphatidylethanolamine
PG	Phosphatidylglycerol
PGA	Penicillin G amidase
Pi	Inorganic phosphate
PI	Phosphatidylinositol
PI(4,5)P2	Phosphatidylinositol-4,5-bisphosphate
PIP_n	Phosphoinositides
PLA	Phospholipase A
PLB	Phospholipase B

PLC	Phospholipase C
PLD	Phospholipase D
PMB	*para*-Methoxybenzyl
PMBCl	*para*-Methoxybenzyl chloride
PMTrtCl	*para*-Methoxytrityl chloride
pNPP	*p*-Nitrophenyl phosphate
POPE	1-Palmitoyl-2-oleoyl-*sn*-glycero-3-phosphoethanolamine
PPh_3	Triphenylphosphine
PPi	Inorganic pyrophosphate
PS	Phosphatidylserine
pTLC	Preparative thin layer chromatography
p-TsOH	*p*-Toluenesulfonic acid
QM	1,4-Quinone-methide
R8	*octa*-Arginine
Rd-PE	1,2-Dioleoyl-*sn*-glycero-3-phosphoethanolamine-*N*-(lissamine rhodamine B sulfonyl)(ammonium salt)
RES	Reticuloendothelial system
R_f	Retention factor
ROS	Reactive oxygen species
rt	Room temperature
SATE	*S*-Acetylthioethyl
SEC	Size exclusive chromatography
SIL	Self-immolative linker
SIP	Self-immolative polymer
SRB	Sulforhodamine B
STEM	Scanning Transmission electron microscopy
SUV	Small unilamellar vesicles
TAG	Triacylglycerol
TBAF	Tetrabutylammonium fluoride
TBAI	Tetrabutylammonium iodide
TBDMSCl	*tert*-Butyldimethylsilyl chloride
TBDPSCl	*tert*-Butyldiphenylsilyl chloride
TBS	Tris-buffered saline
TBTA	tris(Benzyltriazolylmethyl)amine
TCEP	tris(2-Carboxyethylphosphine)
TEA/Et_3N	Triethylamine
TEG	Tetra ethylene glycol
TEM	Transmission electron microscopy
TEMPO	2,2,6,6,-Tetramethylpiperidinyloxy radical
Tf_2O	Trifluoromethanesulfonic anhydride

TFA	Trifluoroacetic acid
THF	Tetrahydrofuran
TLC	Thin layer chromatography
T_m	Phase transition temperature
TML	Trimethyl lock
TMS	Trimethylsilyl
TMSBr	Bromotrimethylsilane
TMSI	Iodotrimethylsilane
TPi	Sodium tripolyphosphate
TsCl	Tosyl chloride
UTP	Uridine triphosphate
UV	Ultraviolet
ZP	Zeta potential

Chapter 1. Introduction to lipids, liposomes, and drug delivery

1.1. Overview of lipids in biological systems

Cellular membranes are crucial in maintaining rigid cell structures and regulating cell activities. They are primarily composed of proteins and a variety of chemically diverse lipids embedded within mobile mosaics.[1] Lipids are generally known to be responsible for multiple functions in cell activities. First, lipids were long thought to only be responsible for energy storage and membrane formation. Simple lipids such as triacylglycerol and sterol esters function as an energy reservoir for membrane biogenesis.[2] Second, unlike other major components in biological systems (such as proteins, carbohydrates, and nucleic acids), lipids are distinguished by their solubility in nonpolar organic solvents and are generally defined as amphiphilic molecules that contain both a hydrophilic and a hydrophobic region.[3] Entropically driven by water, lipids spontaneously self-assemble with hydrophobic moieties aggregating and hydrophilic moieties exposed to the aqueous environment. This results in the fundamental structures of cellular membranes that can act as selectively permeable barriers to separate subcellular compartments from one another and from the extracellular environment. In addition, lipids play key roles in cell division,[4] reproduction,[5] intracellular membrane trafficking,[6] and interaction with certain proteins.[7] Other than bulk lipids, which are the major component of cell membranes, there is another category known as signaling lipids, classified based on their functions. These lipids serve as first and second messengers in numerous cell signal transduction and molecular recognition processes.[8-10]

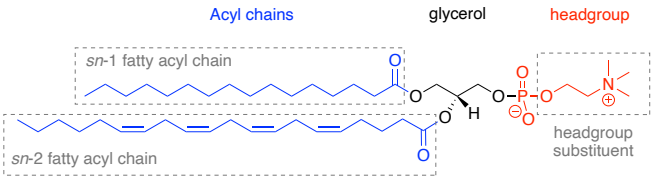
1.2. Structures and properties of lipids

The numerous key functions of lipids in biological systems can be explained by the incredible degree of diversity of these molecules, including variation in both chemical structure and membrane composition.[11] The lipid components of different biological membranes vary between species, organisms, organelles, and even membrane leaflets and microdomains.[11-14] Regarding chemical diversity, this is primarily determined by chemical structures, which can

ultimately affect the physicochemical properties of certain lipids.[11] Membrane lipids can be classified into three major categories based on their chemical structures, including glycerophospholipids, sphingolipids, and sterols.[14] While sphingolipids and sterols are both key components of biomembranes, we mainly focus on phospholipids in this Chapter by introducing their structure and properties.

Common glycerophospholipids are shown in Figure 1.1, which contain three building blocks, including two fatty acyl chains, a glycerol backbone, and a headgroup substituent.[11] The chemical diversity of glycerophospholipids primarily arises from the wide-ranging combinations of these building blocks that exist in nature. The fatty acyl chains (FA) are the simplest natural lipid units, which are connected to the *sn*-1 and *sn*-2 positions of the middle glycerol backbone via an ester bond (or ether bond).[15] The free fatty acids prior to lipid incorporation contain a carboxylic acid headgroup directly attached to a hydrocarbon tail with various numbers of carbons and degrees of saturation (Figure 1.2). In the nomenclature system for FAs, these are described as XX:Y, where XX represents the number of total carbons in the acyl chain and Y indicates the number of double bonds they possess. For glycerophospholipids, their *sn*-1 acyl chains typically have a low degree of unsaturation (saturated or have only one double bond). However, their *sn*-2 acyl chains are normally unsaturated, containing one to up to four double bonds.[16] While unsaturated lipid tails tend to provide membranes with more fluidity, saturated chains result in more rigidity.

On the other hand, the headgroups are attached to the *sn*-3 position of glycerol through a phosphodiester group. The classes of glycerophospholipids are determined by their headgroups (Figure 1.1). When a terminal phosphate group is directly attached to the lipid diacylglycerol (DAG), this produces phosphatidic acid (PA) lipid, which is an important signaling lipid.[9] Due to its unique structure, this lipid can influence membrane curvature and is known to be involved in membrane fission or fusion processes.[17] Phosphatidylcholine (PC) is



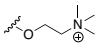
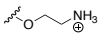
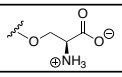
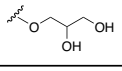
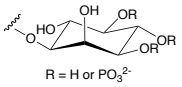
Common glycerophospholipids	Headgroup substituent	Headgroup structures
Phosphatidic acid (PA)	None	--
Phosphatidylcholine (PC)	Choline	
Phosphatidylethanolamine (PE)	Ethanolamine	
Phosphatidylserine (PS)	Serine	
Phosphatidylglycerol (PG)	Glycerol	
Phosphatidylinositol (PI) or Phosphoinositides (PIP_n)	Inositol	

Figure 1.1. Structure of a typical glycerophospholipid. These lipids contain three major parts: a headgroup, a glycerol backbone, and fatty acyl chains. They are classified by the different headgroups. While PA does not have a headgroup substituent, zwitterionic lipids PC and PE have choline and ethanolamine as headgroups, respectively. Anionic lipids PS and PG have serine and glycerol as the headgroups. PI and PIP_ns are important signaling lipids bearing inositol or phosphorylated inositol headgroups.

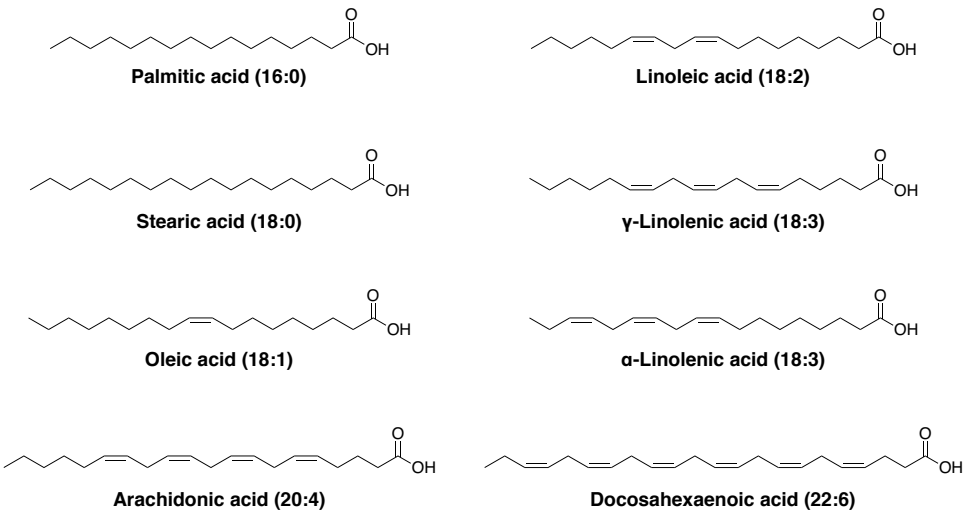


Figure 1.2. Structures of common fatty acids. These differ in chain length, degree of unsaturation, and the position of the double bonds. The numbers in the parentheses indicate the numbers of total carbons in the chain and the number of the double bonds present.

a major constituent of the cell membranes and contains a choline headgroup.[18] It is a zwitterionic lipid under physiological conditions due to the presence of the negatively charged phosphodiester group and the positively charged quaternary ammonium group. Phosphatidylethanolamine (PE) contains ethanolamine as the headgroup. Unlike choline, such headgroup has an unmethylated amine group, resulting in a smaller area in the headgroup region.[19] As a result, PE is also known to promote membrane fusion and regulate membrane curvature.[20] Phosphatidylserine (PS) and phosphatidylglycerol (PG) have serine and glycerol units as the headgroup, respectively. Both of these are anionic lipids and carry one negative charge at physiological pH. PS is crucial in cell cycle signaling, and particularly during apoptosis.[21,22] While PS generally resides in the inner membrane leaflets, the presence of PS on the outer leaflet can be utilized as a disease marker for cancer.[23] Phosphatidylinositol (PI) has a *myo*-inositol headgroup, for which every combination of the hydroxyl groups at the 3, 4, and/or 5 positions of the inositol ring can be phosphorylated, resulting in seven different phosphoinositide lipids (PIP_nS). Although PIs only make up a small portion of membrane phospholipids, they control almost all key aspects of cellular functions since their diverse headgroups can act as built-in “codes” to render the lipids with specific lipid-protein interactions.[10,11,24]

1.3. Lipid self-assemblies and liposomes

1.3.1. Introduction to packing parameters

Due to their unique structures and amphiphilic nature, lipids tend to self-assemble in aqueous media, particularly for glycerophospholipids and sphingolipids. Such processes are driven by multiple factors, including thermodynamics, entropic properties, molecular geometry of a certain lipid, and the condition of the aqueous environment. First proposed by Israelachvili et al.,[25] the structural feature of lipids can be described by the packing parameter P, which is determined by the cross-sectional area of the headgroups and the area occupied by the hydrophobic tails (Figure 1.3A). The lipid assemblages can be classified into three categories,

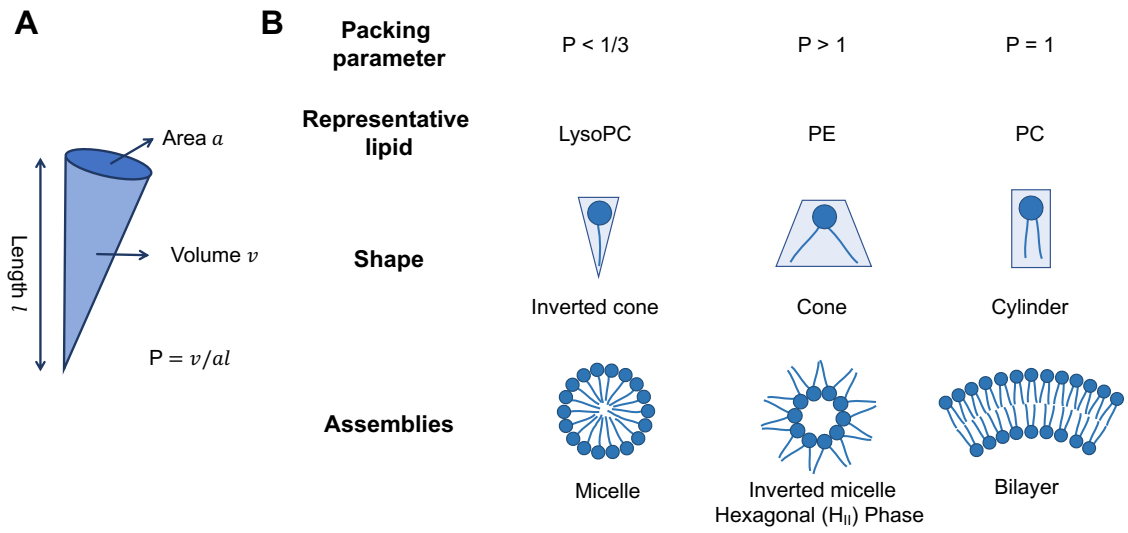


Figure 1.3. Packing parameters and self-assembly properties of lipids. A. Packing parameter is determined by the size of the headgroup and the area occupied by the hydrophobic tail region. The figure is inspired and reproduced based on the work reported by Boyd et al.[26] **B.** The relationship between packing parameters, lipid shapes, and assemblage structures. Lipids with P values of less than 1/3 have an inverted cone shape and favor micelle assemblies in aqueous media. Lipids with P values greater than 1 (such as DOPE) possess a cone shape and favor hexagonal phase assemblies. Lipids with P values around 1 show cylindric geometry and prefer bilayer structures (i.e., PC). The figure is inspired and reproduced based on work reported by Best et al.[27]

depending on their packing parameter (Figure 1.3B) and associated curvature.[28] PC lipids, the most abundant phospholipids in eukaryotic membranes, possess P values around 1. Thus, they show cylindric geometry and favor bilayer assemblies. When the P value is less than 1/3, the resulting lipids present an inverted cone shape and possess positive curvature. The representative lipids for this kind feature lyso-lipids (i.e., *lyso*-phosphatidylcholine (LPC)), which contain only one acyl chain at the *sn*-1 position and favor micelle-like assemblages in the aqueous environment.[29] Oppositely, cone-shaped lipids with a P value greater than 1 possess negative curvatures and thus favor inverted micelle (hexagonal phase) assemblies. A predominant example of this category is the lipid PE. By replacing the choline headgroup from PC into an unmethylated amine, PE lipids exhibit a much smaller headgroup area compared to PC.[19] This feature can be exaggerated particularly in the case of PE bearing unsaturated acyl chains, such as dioleoylphosphatidylethanolamine (DOPE). The introduction of *cis* double bonds into the acyl chains provides kinks in the tails, resulting in a significantly expanded hydrophobic region.

1.3.2. Introduction to liposomes

One of the most ubiquitous assemblages formed by lipids is the liposome, which consist of spherical bilayer structures that possess a hydrophobic bilayer region and aqueous inner core. Bangham first reported liposomes in 1965 and established the structural foundation of biological membranes.[3] The most common classification system for liposomes is based on their sizes and structural parameters, such as lamellarity, as is shown in Figure 1.4. Lamellarity refers to the number of layers of membrane a vesicle possesses. Unilamellar vesicles contain one single bilayer membrane, while multilamellar vesicles have multiple bilayers. Since unilamellar vesicles show similar structural features compared to real biomembranes, they are commonly employed as a model membrane system in biological studies, such as membrane-protein binding.[30] The diameters of liposomes can vary from 20 nm to over 1 μm.[31] Vesicles with diameters smaller than 100 nm are defined as small unilamellar vesicles (SUVs), while

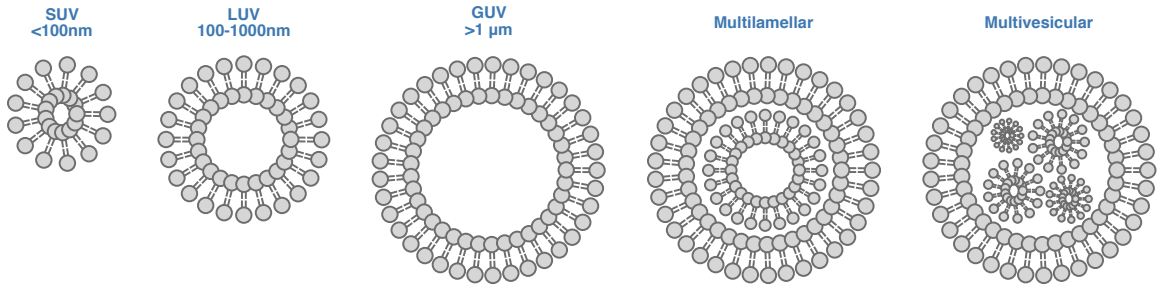


Figure 1.4. The common vesicle size and lamellarity classification system. While small unilamellar vesicles (SUVs) possess diameters less than 100 nm, large unilamellar vesicles (LUVs) have diameters ranging from 100 to 1000 nm. Giant unilamellar vesicles (GUVs), on the other hand, are larger than 1 µm. Multilamellar vesicles (MLVs) have several membrane layers, while multivesicular vesicles encapsulate smaller vesicles. The figure is inspired and reproduced based on the work reported by deMello et al.[32]

those with diameters ranging from 100 to 1000 nm are known as large unilamellar vesicles (LUVs). Giant unilamellar vesicles (GUVs) are typically larger than 1 μm.

1.3.3. Introduction to membrane phase behavior

Since liposomes are widely used as biomimetic model membranes, it is crucial to understand their phase behavior, which can provide substantial information regarding membrane fluidity. The temperature needed for a specific lipid to transition from the ordered gel phase to the disordered crystalline phase is known as phase transition temperature (T_m).[33] The individual lipid tails are fully extended and closely packed in the rigid ordered gel phase below the T_m; however, when the temperature goes above T_m, the hydrocarbon tails become randomly oriented and ultimately reach a disordered fluid crystalline phase. One of the most important physical properties of liposomes is their permeability, which is used to describe how target compounds travel across the membranes. The permeability of certain liposomes is primarily determined by the T_m of its compositional lipids, and this increases when the bilayers transit from an ordered gel phase to a disordered fluid phase.[34,35]

The T_m values for lipids that are commonly used in liposome preparations are listed in Table 1.1. Several factors can affect T_m, including the length of the hydrocarbon tail, charges, unsaturation, and headgroup species.[36] The physicochemical origins that account for these falls on the strength of van der Waals interactions between adjacent lipid molecules.[37] The van der Waals interactions increase when the hydrocarbon tail length increases, which means more energy is required to disrupt membrane packing. Thus, lipids with longer tails generally show greater T_m. Other than tail length, the degree of unsaturation also has a significant effect on T_m. As is described above, the *cis* double bonds can provide kinks in the tail region, resulting in more spaces between adjacent lipids that result in additional freedom. Such disruptions decrease the packing density, which ultimately lowers T_m.

Table 1.1. T_m values for selected lipids commonly employed in liposome formation. For the same type of lipid, lengthening tails yields increases in T_m values of the resulting lipid, while increases in unsaturation can significantly decrease T_m. Data courtesy of Avanti Polar Lipids website[38] and the values reported by Marsh.[39]

Lipid Name (Abbreviation)	**Acyl Chain**	**T_m (°C)**
Dilauroyl phosphatidylcholine (DLPC)	12:0	-1
Dimyristoyl phosphatidylcholine (DMPC)	14:0	23
Dipalmitoyl phosphatidylcholine (DPPC)	16:0	41
Distearoyl phosphatidylcholine (DSPC)	18:0	55
Dioleoyl phosphatidylcholine (DOPC)	18:1	-20
Dimyristoyl phosphatidylethanolamine (DMPE)	14:0	50
Dipalmitoyl phosphatidylethanolamine (DPPE)	16:0	63
Dioleoyl phosphatidylethanolamine (DOPE)	18:1	-16
Dioleoyl phosphatidic acid (DOPA)	18:1	-8
Dioleoyl phosphatidylglycerol (DOPG)	18:1	-18
Dioleoyl phosphatidylserine (DOPS)	18:1	-11
Tetramyristoyl cardiolipin•$(Na)_2$	14:0	59
1,2-Dioleoyl-3-trimethylammonium propane (DOTAP)	18:1	~-0

1.3.4. Liposome preparation and characterization methods

Different methods have been developed to prepare liposomes with various physical properties, such as size and lamellarity. One traditional method is the thin-film hydration technique, which is also recognized as the most convenient liposome preparation method.[31,40] Compositional lipids are first dissolved in organic solvent and transferred into a container. The solvent is next removed to form a lipid film, which is then hydrated in a desired aqueous solution above the T_m, resulting in a liposome suspension. The physical properties of the formed liposomes are largely dependent on the hydration conditions. For example, while gentle hydration may most likely result in GUVs, intensive agitation is more likely to result in MLVs. Since liposomes obtained after hydration are large and heterogeneous in particle sizes, subsequent down-sizing steps are required to obtain liposomes with smaller and uniform sizes. SUVs can be prepared by sonication (probe or bath) techniques. Another effective way to control particle sizes is extrusion, where liposome solutions post-hydration are forced through a polycarbonate membrane of defined pore sizes.[41] The sizes and homogeneity of the resulting liposomes correlate to the number of extrusion cycles. Other liposome preparation methods include reverse phase evaporation,[42] microfluidic hydrodynamic focusing,[43] cross-flow injection, supercritical fluids, etc.[44] All the liposomes we present in this dissertation were prepared using thin-film hydration and extrusion techniques.

Characterization of liposomes after preparation is critical to ensure liposome qualities and avoid batch-batch variations.[45] The most important characteristics of a specific liposome solution include their size and polydispersity, which can be measured and analyzed by dynamic light scattering (DLS), size exclusive chromatography (SEC), nuclear magnetic resonance spectroscopy (NMR), and microscopy techniques, such as electron microscopy (EM) or fluorescence microscopy.[46,47] Among these, DLS is considered the simplest and most efficient method, and it has been widely applied for the size characterization of proteins, polymers, nanoparticles, and colloidal dispersions.[48] The physics foundation of this technique

is the Brownian motion of particles or molecules in solution, which can cause the laser light to be scattered at different intensities. Detection and analysis of these intensity fluctuations can ultimately yield particle sizes and distributions according to the Stokes-Einstein equation. Typical DLS measurements are suitable for particles with submicron sizes, and all the liposomes we prepared in this dissertation were primarily characterized by this technique to verify their size and homogeneity.

Other critical physical properties of prepared liposomes include zeta potential, lamellarity, and encapsulation efficiency. Zeta potential characterizes the surface charge of the liposomes in dispersion, which primarily depends on the lipid compositions and can also be measured with a DLS instrument.[49] Lamellarity can be determined via cryo-EM, small-angle X-ray scattering (SAXS), ^{31}P NMR, and radioactive labeling.[50,51] Encapsulation efficiency (EE%) is a key property to consider for liposomal drug delivery purposes, and it will be discussed in detail in the later sections. EE% is generally determined using spectroscopic methods, such as fluorescence or UV-Vis spectroscopy. Other methods including HPLC, UPLC, LC-MS have also been employed for EE% calculation.[52] Liposomes, being a versatile model system, can be utilized for different purposes in numerous experimental settings. As a result, it is important to choose appropriate preparation methods and characterize the resulting liposomes carefully to ensure they meet the desired requirement.

1.4. Liposomes and drug delivery

1.4.1. Overview of drug delivery vehicles

Free therapeutics commonly suffer from severe drawbacks (i.e., limited solubility, off-site effects, and poor localization) in clinical settings. To overcome these issues, intensive efforts have been made to develop different types of nanomaterials to enhance therapeutic lifetime and potency by improving navigation through biological systems. These nanocarriers can be primarily classified into three categories, including polymeric, inorganic, and lipid-based

nanoparticles.[53] As shown in Figure 1.5, each category contains different subclasses to meet the need for various applications. While the particle characteristics of polymeric and inorganic carriers can be precisely controlled, and studies have shown their potential in theranostic applications, they exhibit major drawbacks, such as high toxicity. On the other hand, lipid-based carriers show excellent biocompatibility and payload flexibility, making them one of the most promising drug delivery candidates. For example, it is worth noting that lipid nanoparticles have been employed in the development of mRNA vaccines to fight against the COVID-19 pandemic.[54]

1.4.2. Liposome as a drug delivery vehicle (overview and considerations)

Liposomes are the earliest version of lipid nanoparticles, and their potential as drug delivery platforms was recognized immediately after realizing their unique structures.[55] Since liposomes are composed of hydrophobic bilayer membranes surrounding hydrophilic cores, they are capable of encapsulating either hydrophobic and/or hydrophilic contents. The initial concept of using liposomes as drug delivery agents was first established by Gregoriadis.[56,57] Since then, numerous liposome-based drug and gene delivery systems have been developed and entered clinical trials.[58] Liposomes are considered as the first nanomedicine delivery platform that was successfully translated from concept to clinical use. So far, there are at least fifteen FDA-approved liposomal drugs that are commercially available, including the Doxil/Caelyx (Johnson & Johnson) formulation for the delivery of the anti-cancer drug doxorubicin and AmBisome (Gilead) encapsulating amphotericin B to treat fungal infections.[59,60] Compared with free drugs, biocompatible liposome platforms can protect against degradation, reduce drug toxicity[61] and side effects[62], as well as optimize the pharmacokinetic properties[63] and therapeutic index of drugs.[64] In addition, since more than 40% of the small molecule drugs designed for cancer treatment exhibit limited hydrophilicity, inclusion within nanocarriers, such as liposomes, can easily solve their solubility issue.[55]

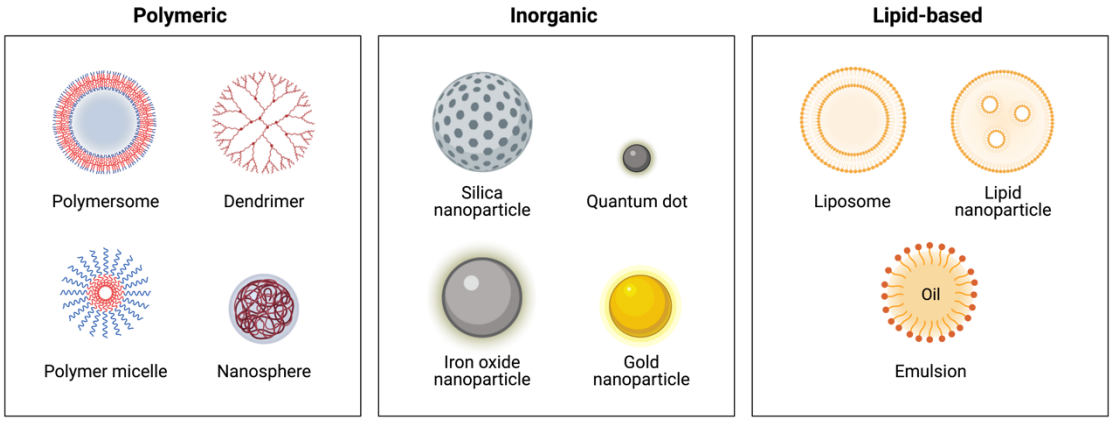


Figure 1.5. Cartoon illustration for different classes of nanoparticles utilized for drug delivery applications. Carriers can be divided into three major categories: polymeric, inorganic, and lipid-based nanoparticles. Each of these exhibit advantages and disadvantages and can be selected wisely based on different potential applications. This figure is inspired by the work reported by Langer et al.[53] and is created with BioRender.com.

Multiple parameters need to be considered and optimized to prepare liposomes specifically for drug delivery applications, and the most critical one is their particle sizes. Commonly utilized liposomal delivery systems feature particles around 100-200 nm,[65] since these show improved extravasation and circulation properties compared to the particles with other sizes. These smaller liposomes are more prone to fuse with cell membranes due to their enhanced curvature.[66,67] They also show prolonged circulation time compared to large particles with diameters (> ~400 nm) by avoiding uptake by the reticulo-endothelial system (RES). In addition, liposomes around these size ranges can also take advantage of the enhanced permeation and retention (EPR) effect. This phenomenon results from the abnormal and heterogeneous vasculature within the tumor sites; the leaky vessels allow nanoparticle extravasation and the ultimate accumulation of particles in tumors.[68,69]

The surface charge of liposomal delivery platforms is another key factor to consider, since this affects interactions between adjacent liposomes or liposomes and counterions, which ultimately contributes to the stability of the resulting liposomes. Uncharged or low-charged liposomes tend to aggregate over time. On the other hand, strongly positively or negatively charged liposomes are less likely to aggregate due to electrostatic repulsion. Zeta potentials are proportional to the charged lipids incorporated within the membrane. Liposomes with zeta potentials less than -30 mV or greater than +30 mV are generally considered to be stable due to the sufficient repulsion to prevent particle clustering.[55]

Encapsulation efficiency (EE%) reflects the ability of liposomes to encapsulate payload and is also of great importance for delivery purposes. Hydrophobic cargo resides in the membrane bilayer and hydrophilic content prefers the aqueous inner core. While conventional liposome preparation methods, such as the thin film hydration technique, are simple and convenient, they result in liposomes with low EE%, considering the cargoes are non-specifically entrapped during the preparation. Enhancing EE% for hydrophilic small molecule drugs has become a

vibrant area in liposomal research.[52] Different active loading strategies have been developed for these purposes, such as transmembrane pH gradient, ammonium sulfate gradient, metal ion gradient, etc. For example, the first FDA-approved liposomal drug Doxil was prepared by the ammonium sulfate gradient method.[70]

1.4.3. Surface modification of liposomes

Despite the advantages liposomal nanocarriers show, conventional liposomes (Figure 1.6A) have major translational obstacles for clinical applications. As the first generation of liposomes developed, they are generally composed of neutral, anionic, or cationic lipids, as well as cholesterol. Although conventional liposomal formulations can reduce toxicity and enhance the pharmacokinetics of therapeutic cargo compared to free drugs, they can be rapidly cleared from the bloodstream.[71] Another major limitation for conventional liposomes is the lack of targeting selectivity. While nanoparticles can take advantage of EPR effects, studies have shown that these only result in approximately two-fold increase in delivery to tumor sites compared to other common accumulation organs.[72] To overcome these obstacles, surface modified liposomes came into play, which show enhanced target selectivity, prolonged circulation, and improved stability.

Sterically stabilized (also known as “stealth”) liposomes (Figure 1.6B) were first invented.[73] By grafting biocompatible hydrophilic polymers onto membrane surfaces, the resulting liposomes exhibit improved stability during circulation. Polyethylene glycol (PEG) polymers were intensively used for such purposes, since they were previously employed in protein drugs to avoid immune response.[74] The length and density of the PEG coating can potentially affect circulation time and *in vivo* biodistribution of the PEGylated liposomes.[75] Prolonged circulation time also allows liposomes to accumulate at the tumor site more effectively by enhancing the EPR effect.

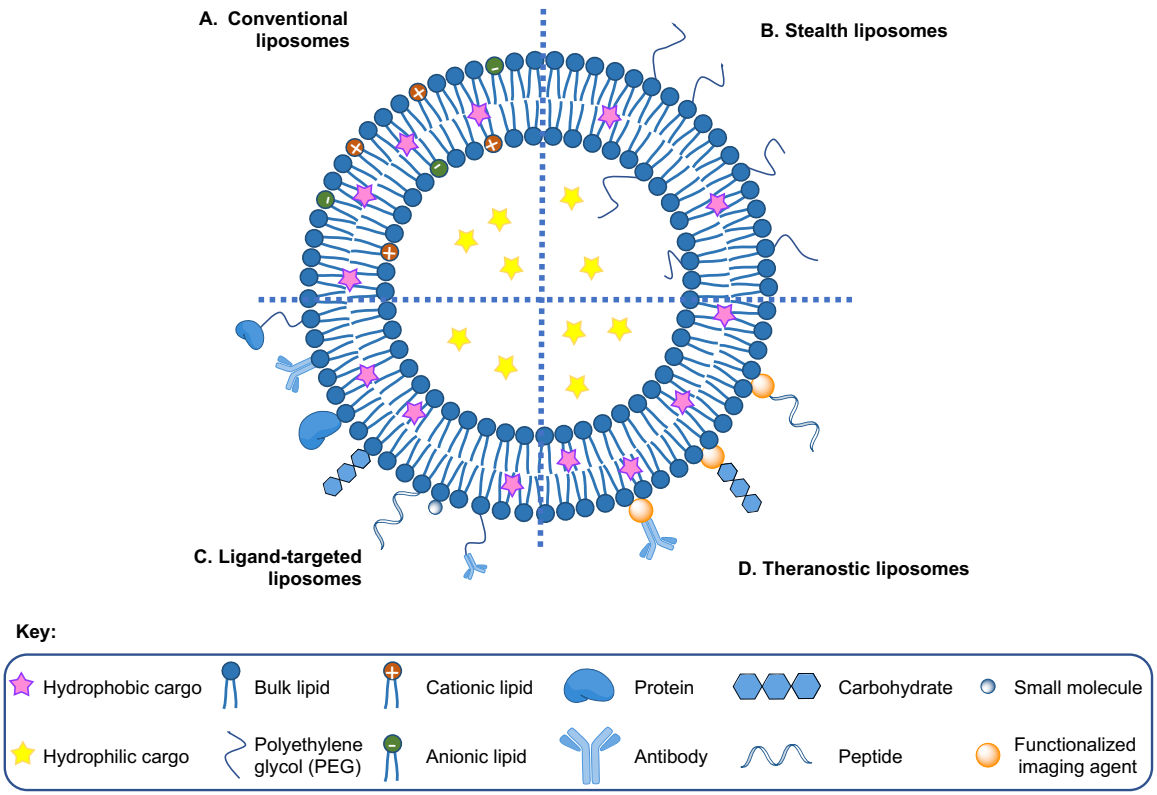


Figure 1.6. Cartoon illustration for different types of surface-modified liposomes for active targeting purposes. A. Conventional liposomes composed of neutral, cationic, or anionic lipids. **B.** Stealth liposomes with polyethylene glycol (PEG) coating. PEGylation provides the resulting liposomes with additional steric stabilization, which show prolonged circulation time *in vivo*. **C.** Surface-functionalized ligand-targeted liposomes bearing active targeting moieties. Commonly explored targeting groups involve protein/peptide, antibody, carbohydrate, and small molecules. PEGylation can also be applied to this type of liposomes. **D.** Theranostic liposomes containing functionalized imaging agents as well as active targeting groups. This figure is inspired by the work reported by Hua et al.[71]

Site-specific delivery can be further enhanced by surface modification of active targeting moieties (Figure 1.6C). Numerous ligands have been employed to deliver liposomes to designated cell types or organs, which primarily include antibody, carbohydrate, small molecule, and peptide/protein. These moieties are normally introduced onto the membrane bilayer through incorporation of headgroup functionalized lipids, or at the end of the PEG polymer coating. Antibodies or antibody fragments are the most intensively studied ligand due to their excellent specificity for target antigens. Antibody modified liposomes are also known as “immunoliposomes” and have shown great potential in specific drug delivery to cancer cells and gene therapy.[76] As an example, studies have shown that IgM-modified liposomes are 100 times more efficient than unmodified liposomes.[77] Cancer cells are known to over-express certain receptors on their surface, providing another opportunity for cell-specific delivery. One of the established ligand-receptor systems involves the asialoglycoprotein receptor (ASGP-R)/N-acetylgalactosamine (GalNAc) pair.[78] Since ASGP-R is exclusively expressed in hepatocytes and plays key roles in eliminating glycoproteins from the blood, and GalNAc is its known natural ligand, numerous galactose-functionalized nanocarriers have been developed to show enhanced delivery to hepatoma cell line (HepG2).[79] Folate receptor is another well-studied example, which is upregulated on many cancer cells.[80] Since it can bind tightly with folic acid ligand, liposomes decorated with folic acid have been studied, allowing specific delivery of drug or imaging reagents to tumor cells over noncancerous cells.[81]

Other than site-specific targeting groups, cell-penetrating peptides (CPPs) have been employed to improve the cellular uptake of liposomes in a non-cell-type specific manner.[82] Representative CPPs include transactivator of transcription (TAT) and octa-arginine (R8) peptides, both of which are highly cationic peptides. While CPPs do not exhibit cell-specificity and show high cytotoxicity, activable CPPs have been developed, allowing spatiotemporal control of CPP-mediated delivery.[83] More background will be introduced in Chapter 7, where we designed a liposomal system bearing a reactive oxygen species (ROS)-responsive caged

guanidine lipid that can potentially mimic CPP functionalities. More recent generations of liposomes tend to combine functionalized imaging agents with the features mentioned above, resulting in liposomes that can be utilized for theranostic purposes (Figure 1.6D).

1.5. Liposomes and triggering release

While liposomes decorated with active targeting ligands allow precise delivery of the therapeutics, additional strategies for quick drug release at therapeutic levels are desired to further increase drug efficacy and reduce adverse effects. Therefore, the development of triggered release systems employing stimuli-responsive liposomes that can release cargo upon specific trigger exposure has emerged as a vibrant research field.[84] Triggering release strategies typically fall into two categories, including passive and active release. Passive release utilizes the pathophysiological differences in conditions between healthy and diseased cells, such as pH,[85] redox environment,[86] enzyme expression,[87] and metabolite concentrations as the source of the stimulus that drives release.[88-90] Active release, on the other hand, exploits external stimuli including light,[91-93] heat[94,95] and ultrasound[96,97] to drive cargo release.

The key aspect in developing stimuli-responsive liposomes is to create liposomes that are stable enough to survive circulation but undergo significant alterations in lipid packing properties when encountering the desired stimuli to destabilize the bilayer and induce encapsulated cargo escape (Figure 1.7).[27] Thus, it is critical to design synthetic lipids whose structures and self-assembly properties can be fine-tuned before and after stimulus treatment.

The strategies developed to alter lipid assembly properties can be primarily classified into four categories (Figure 1.7). Since detailed examples will be discussed in each related Chapter throughout this dissertation, we will simply provide a brief introduction for each category herein. Early examples entail the direct chemical modification of a well-known non-bilayer forming lipid, which results in lipids that favor bilayer formation initially. Once the responsive groups are

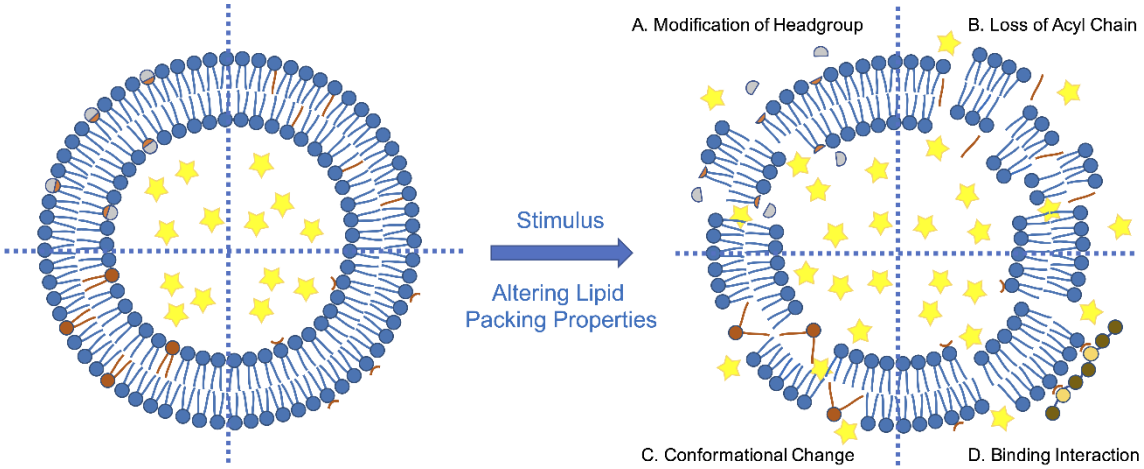


Figure 1.7. Cartoon illustration of commonly explored strategies for triggered release of contents from liposomes by fine-tuning lipid structures and membrane properties. A. Stimuli-driven modification of lipid headgroups; **B.** Loss of acyl chains; **C.** Conformational change, and **D.** Binding interaction. This Figure is adapted from Ref[27], created by Best and co-workers.

removed by the desired stimulus addition, the original non-bilayer lipid will be released to disrupt membrane integrity. The most common modifications are at the lipid headgroups or acyl chains (Figure 1.7A-B). For headgroup medication, DOPE has been intensively studied due to its unique self-assembly properties. DOPE itself is a non-layer lipid that favors hexagonal phase assemblies at physiological conditions; however, *N*-acylation can significantly increase its headgroup to tail ratio and result in lipids that favor lamellar phases.[98] Once the headgroups are removed, the release of DOPE can induce changes in membrane stability and permeability. Lysolipids are typically used for acyl chain modifications, since they possess non-bilayer characteristics that favor micelle assemblies in the aqueous environment. Taking advantage of phospholipase A2 (PLA2) that can selectively remove the *sn*-2 position of glycerophospholipids, a wide variety of *sn*-2 acyl chain modified lipids and prodrugs have been developed.[99-103] Light-responsive liposomes based on lysolipid formation have also been studied, utilizing lipids bearing photo-sensitive moieties at the *sn*-2 acyl chain.[104,105]

Although modifications to these traditional non-bilayer lipids are proven to be effective for triggering release purposes and the chemistry to achieve these targets is simple, they are primarily limited to very few unusual natural lipid scaffolds with unique self-assembly properties. In addition, these responsive liposomes typically require a high percentage of synthetic lipids or additional components such as DOPE or 1,2-dioleoyl-3-trimethylammonium propane (DOTAP) to drive efficient cargo release, which is not ideal for clinical settings. This, in part, results from these lipids not undergoing major structural changes in response to stimuli. To overcome this obstacle, researchers began to develop artificial lipid scaffolds that can undergo dramatic programmed structural changes upon stimuli treatment.[27,90,106] While additional efforts in structural design and synthesis are required, this drastically expands the limited toolbox of natural lipids, offering numerous potential possibilities in modulating membrane properties that can maximize cargo release. Representative strategies involve the development of lipid switches that can undergo conformational changes or binding interactions

on membrane surfaces upon stimuli addition, which can disrupt membrane packing and trigger the encapsulated content release (Figure 1.7C-D). In most of the studies reported by our group or others, incorporating low percentages of these lipid switches in the membrane was enough to induce dramatic membrane disruption, which can significantly improve liposome stability during circulation.

1.6. Summary and outlook

While there is no doubt that liposomes are effective drug delivery nanocarriers, further improvements are needed to optimize their therapeutic potential. Although numerous clever triggering release strategies have been developed that open up possibilities for delivering cargo in a spatiotemporally controlled manner, challenges still exist, and none of these platforms have been approved for clinical use due to significant barriers.

In this dissertation, we mainly focus on advancing this field by developing various stimuli-responsive liposomal platforms targeting different types of disease-associated metabolites via synthetic lipid switches. In Chapters 2-4, we present the design of liposomal platforms that can respond to calcium, adenosine triphosphate (ATP), and inositol 1,4,5-trisphosphate (IP_3) by leveraging the molecular recognition of these metabolites that are upregulated in disease states. Artificial lipids that can undergo dramatic conformational changes upon binding with each metabolite were designed. In Chapter 5-6, utilizing a slightly different strategy, we chemically modified the headgroups of the non-bilayer lipid DOPE to achieve responsive lipids that show alteration in self-assembly properties upon enzyme and ROS addition. Additional efforts were made (Chapter 7) to enhance the targeting properties of liposomes via the development of a ROS-responsive caged guanidine lipid that can mimic CPPs but allow cargo delivery in a controlled manner. Our approaches show strong prospects for enhancing payload delivery and release to diseased cells driven by metabolites, providing an exciting new paradigm for controlled release that is expected to ultimately advance clinical applications.

Chapter 2. Development of calcium-responsive liposomes

(The scientific data used in this Chapter has been published by the authors: Lou, Jinchao; Carr, Adam J.; Watson, Alexa J.; Mattern-Schain, Samuel I.; Best, Michael D., Calcium-Responsive Liposomes via a Synthetic Lipid Switch, *Chem. Eur. J.* **2018**, *24*, 3599-3607.)

2.1. Project overview

Liposomes are effective supramolecular nanocarriers for drug delivery and imaging applications due to their ability to encapsulate and deliver a range of molecular cargo with varying properties. Indeed, liposome formulations have been clinically approved for the delivery of drugs that possess poor pharmacokinetic properties on their own.[70,107,108] Despite this demonstrated efficacy, challenges remain in the optimization of drug delivery characteristics. In particular, the ability to control the release of therapeutic or diagnostic contents to achieve selective delivery within targeted diseased cells is a key aspect to maximize encapsulated drug efficacy while minimizing off-target effects. As a result, a variety of approaches for triggering release from liposomes have been investigated, which have commonly utilized either pathophysiological conditions (passive release) or external stimuli (active release) to drive drug release.[84,109] For passive release, characteristics of diseased cells including acidity, reducing environments, and aberrant enzyme expression have been exploited to stimulate liposomal release. Regarding external stimuli, light-initiated release using photocleavable moieties, ultrasound-mediated leakage, and liposome disruption through heat have been reported.

While these approaches have proven to be successful *in vitro*, many challenges remain for maximizing controlled release in real-world drug delivery applications. Diseased cells possess different properties that can be targeted through passive release mechanisms. However, these conditions often show minimal variation from normal cells. For example, the average extracellular pH of cancer cells has been measured as 6.5-6.9 compared to 7.2-7.4 for normal

tissue, providing a narrow window for differentiation.[110,111] Approaches involving external stimuli on the other hand suffer from the challenges associated with delivering stimuli to a defined target location in a non-destructive manner. For example, while photocleavable liposomes have been extensively studied, release from these systems typically results from irradiation with UV light, which suffers from minimal penetration of tissue and the photodecomposition of many biological molecules that absorb in this range of the electromagnetic spectrum.

In this Chapter, we present a promising new means by which we may distinguish between healthy and diseased cells in triggering drug release. This is to drive release from liposomes based on the chemical compositions of cells, which vary considerably between normal and diseased tissue. Metal ions, and specifically calcium, were chosen to be our target. To achieve this goal, a switchable lipid sensitized to calcium was synthesized and incorporated into liposomes. The lipid trigger contains a calcium binding headgroup that is designed to induce a conformational change that perturbs liposome membrane integrity and thereby causes content release upon calcium binding. A comprehensive evaluation of this delivery platform is presented in this chapter including the design and synthesis of the switchable lipid, assessment of its release behavior with both hydrophobic and hydrophilic dyes, and analysis of morphology changes during the release process.

2.1.1. Calcium in biological systems

Calcium was selected as the target since this is a critical biological cation that regulates cell death,[112] muscle contraction,[113] neuronal transduction,[114,115] immune responses[116] and numerous intra- and extracellular signaling pathways.[117] Human serum concentrations of calcium are in the low millimolar range,[117,118] while cytosolic amounts are lower (~100 nM) since calcium is pumped out of this region.[119] Some cytosolic calcium is pumped into the endoplasmic reticulum (ER), which maintains higher calcium concentrations (~1 mM), as do

mitochondria.[120] Calcium overload, particularly in the ER, has been linked to diseases[121,122] including Alzheimer's disease,[123] amyotrophic lateral sclerosis (ALS),[124,125] Gaucher's disease[126,127] and ischemic stroke.[128] Calcium abundance is a critical aspect associated with malaria,[129] in which *Plasmodium* parasites are reliant upon ~30 calcium-responsive metalloproteins.[120,130] Thus, calcium is required for cell invasion and egress,[131] and calcium concentration increases 10-20 fold in invaded cells above normal concentrations.[132,133] Molecules that diminish free calcium such as chelating ligands inhibit parasite invasion.[131,134,135] Finally, calcium regulates aspects of cancer physiology,[136,137] and is found in greater abundance in certain metastasizing cancer cells.[138] For these reasons, calcium provides an exciting target for triggering release of liposomal therapeutics.

2.1.2. Lipid switches that undergo conformational changes

The work reported here was inspired by previous efforts in switchable lipid design and release, such as acid-responsive lipids. For example, Leblond and co-workers reported bis-(methoxyphenyl)pyridine system **2.1** (Figure 2.1) in which protonation of the central pyridine nitrogen leads to rotation of methoxyphenyl groups to promote hydrogen bonding, thereby disrupting the membrane and triggering release.[139,140] PEGylated liposomes containing this compound and distearoylphosphatidylcholine (DSPC) exhibited high stability at physiological pH, while ~88% encapsulated sulforhodamine B cargo release was observed within 15 min when the pH was dropped to 5. This system also demonstrated cytosolic delivery in HeLa cells with minimal toxicity. Additionally, Menger and co-workers reported a morpholinocyclohexanol-(MOCH)-lipid **2.2** that undergoes a cyclohexanol chair flip upon morpholine protonation to trigger release when the liposomes are tethered to spherical polycationic brushes.[141]

Our design also took advantage of molecular recognition principles, which has received only minimal attention in this field. In a rare example from 2014, the Smith group[142] developed a zinc(II)-dipicolylamine complex (ZnBDPA, **2.3**), as a chemical trigger (Figure 2.2) that can

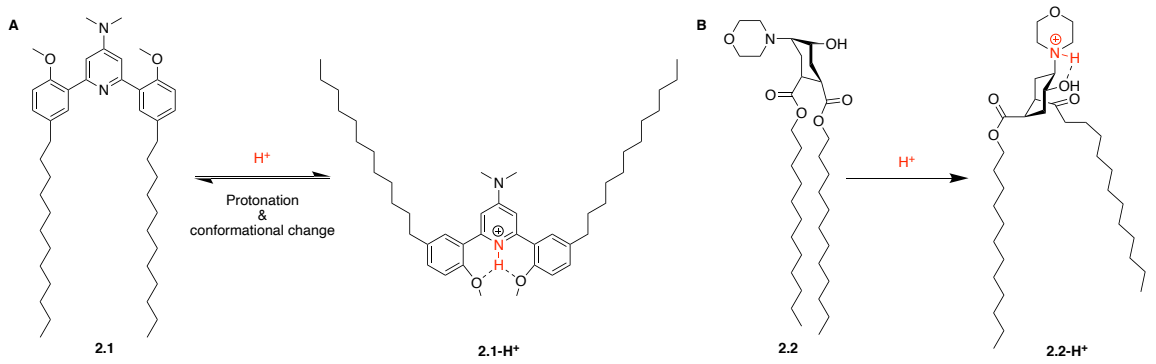


Figure 2.1. Previously reported pH-responsive switchable lipids developed by (A) Leblond and coworkers, and (B) the Menger group. In both cases, enhanced acidic environment induces hydrogen binding interactions in the lipid switches that result in a conformational change.

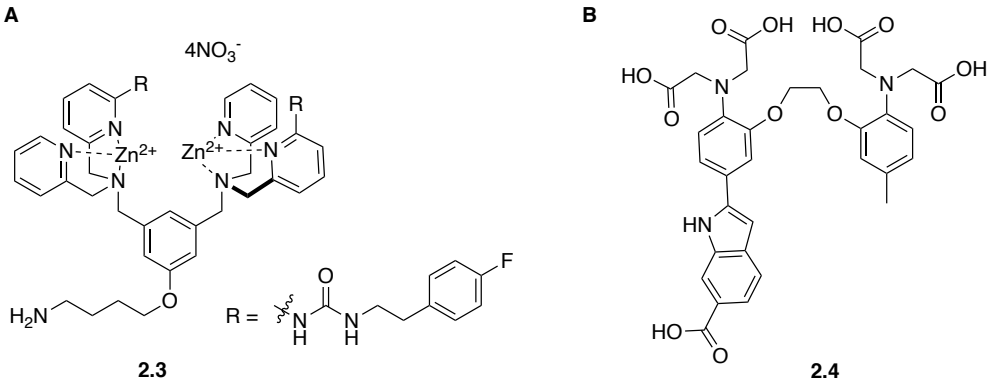


Figure 2.2. Structures of (A) ZnBDPA sensor developed by the Smith group and (B) the first indo-1 calcium sensor reported by Tsien and coworkers.

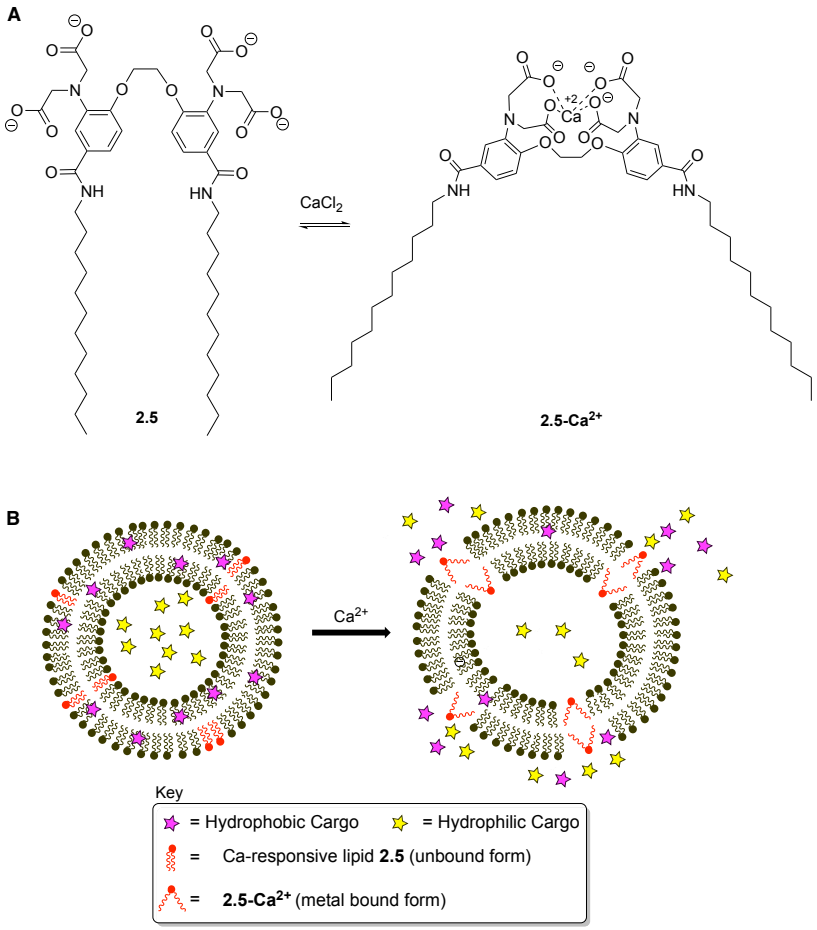
selectively bind liposome membranes containing the lipid phosphatidylserine (PS) and trigger the release of 5-aminolevulinic acid. While this paper demonstrates that membrane disruption and release can be driven by non-covalent binding, our work seeks to build upon this principle by incorporating the sensor motif into the lipid structure so as to engineer liposomes to undergo conformational changes that perturb bilayer packing and trigger release upon recognition.

2.2. Design and synthesis of the calcium responsive synthetic lipid switch

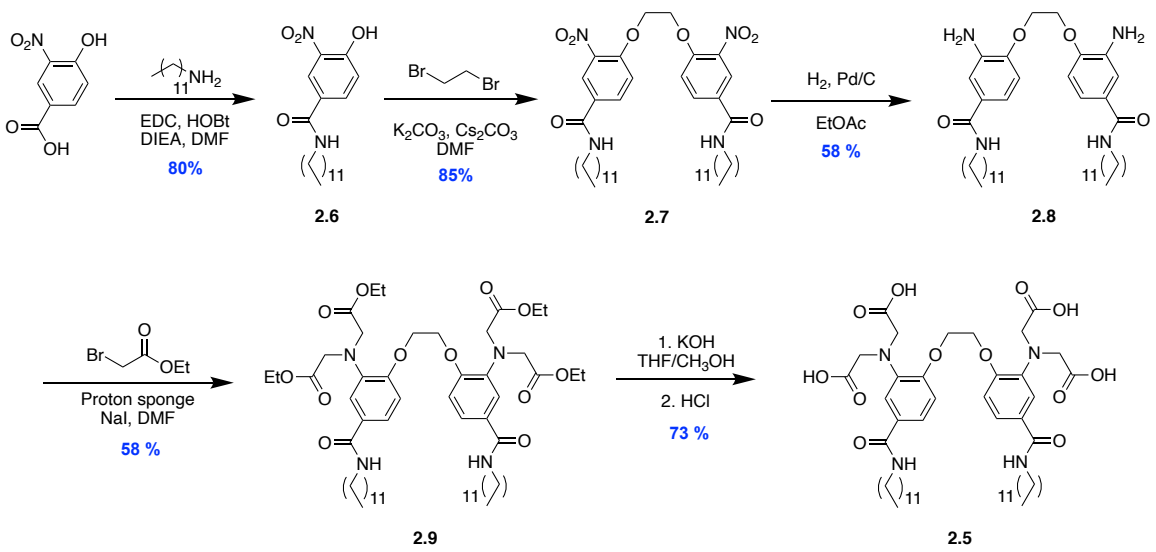
Inspiration for this project also came from well-developed calcium sensors, the most commonly used of which is indo-1. The first calcium fluorescent indicator indo-1 was reported by Tsien in 1985 (**2.4**, Figure 2.2).[143] Over the last 20 years, this sensor has been intensively studied and numerous indo-1 derivatives have been developed for the detection of calcium in complex biological systems.[144-147] The calcium-binding site of indo-1 is a 1,2-bis(2-aminophenoxy)ethane-*N*,*N*,*N*',*N*' -tetraacetic acid moiety. According to Tsien, the apparent K_d of indo-1 for calcium is 250 nM in MOPS buffer, even in the presence of mM scale magnesium.[143]

We hypothesized that we could develop calcium-responsive lipid **2.5** for controlled release from liposomes in the presence of increased calcium abundance (Scheme 2.1). Since we intended to incorporate the trigger into the membrane, lipid tails were installed onto the tetracarboxylate chelating site so that this lipid can rest comfortably within the membrane bilayer in its free form. As is shown in Scheme 2.1, after binding to calcium, this binding region is expected to constrict, causing the hydrophobic lipid chains to move significantly farther away from one another leading to a dramatic increase in lipid cone angle, which can disturb the organization of the membrane bilayer and trigger release of contents.

The synthesis of lipid **2.5** is shown in Scheme 2.2, which is also inspired by Tsien's indo-1 synthesis.[143] We started with 4-hydroxy-3-nitrobenzoic acid, to which the hydrophobic lipid tails



Scheme 2.1. Calcium-triggered liposomal release. A. Structure of calcium-responsive responsive lipid **2.5** and the expected conformational change after adding Ca^{2+}. **B.** Cartoon for liposome release driven by membrane perturbation upon calcium binding.



Scheme 2.2. Synthesis of calcium-responsive lipid switch 2.5. A dodecylamine group was coupled onto precursor 4-hydroxy-3-nitrobenzoic acid to produce the amide of **2.6**, followed by dimerization through reaction of the phenol group with dibromoethane to **2.7**, nitro reduction to the amines of **2.8**, alkylation to introduce four ethylacetate groups to access **2.9**, and finally ester hydrolysis to generate **2.5** in its protonated form.

were coupled using dodecylamine via an amide coupling reaction to give **2.6**. Two equivalents of this compound were then connected together with dibromoethane to yield compound **2.7**. The nitro groups were then reduced into amine groups with Pd/C to **2.8**, followed by alkylation using ethylbromoacetate to add the four ethylacetate moieties of **2.9**. The last step is the deprotection of the ethyl ester functionalities to unveil the tetra-carboxylic acid binding groups and generate our desired lipid **2.5**.

2.3. Fluorescence-based dye release assays and DLS studies

2.3.1. Nile red release assay and corresponding morphology changes

After successfully synthesizing switchable lipid **2.5**, we prepared PC liposomes with different percentages of lipid **2.5** to evaluate release properties. Standard thin film-hydration methods for preparing unilamellar liposomes were used including formation of lipid films, hydration with MilliQ water at 50°C, freeze-thaw cycling and extrusion through a 200 nm membrane for at least 15 passes. The successful preparation of liposomes with desired sizes was determined by dynamic light scattering (DLS) (*vide infra*).

Experimentation began by using a Nile red (NR) release assay to study the release of non-polar contents from liposomes containing **2.5**. NR is a hydrophobic dye widely used in cell biology.[148] It can fluoresce in aqueous media only when it is encapsulated within membranes. After triggering release into aqueous media, NR will no longer fluoresce due to precipitation.[149] The release can then be tracked through reductions in fluorescence intensity. Furthermore, NR is an effective analog for us to investigate the release behavior of commonly used hydrophobic drugs. In this study, we prepared 2 mM phosphatidylcholine (PC) liposomes containing 0%, 3%, 5%, or 10% lipid **2.5**. After an initial fluorescence scan, each sample was titrated with calcium chloride solution until the final calcium concentration reached 10 mM. Since dilution effects will also cause signal decreases, we added a blank sample that was titrated by just adding water into the liposome solution, which was subtracted from study

samples to eliminate dilution effects when processing data. All the experiments were run three times with different batches of liposomes and the error bars shown in Figure 2.3A indicate standard errors.

From the titration curve, we can see that the addition of calcium did cause a fluorescence signal decrease that was dependent on the percentage of **2.5** in liposomes. The 0% sample, which is the negative control liposome, indicated there was an approximately 10% decrease in fluorescence attributed to background dye release. When lipid **2.5** composed 3% and 5% of the total lipid content, the fluorescence signal decreased by ~25% and ~50%, respectively. With 10% lipid **2.5**, the signal decrease was around 65%. Since increased release can be achieved with higher percentages of lipid **2.5**, it is convincing that this compound drives triggered release. DLS was also used to evaluate liposome sizes after release. From Figure 2.3B, we initially prepared liposomes with 0%, 5%, or 10% of **2.5** that exhibit uniform sizes pre-calcium treatment. After introducing calcium, 0% (negative control) liposomes did not show any change while both 5% and 10% showed dramatic changes in size as well as much larger polydispersity indices (PDIs), which is a parameter indicating the distribution of particle size in a given sample. These results provide evidence that the membrane did undergo significant morphological changes driven by calcium when lipid **2.5** was present.

2.3.2. Sulforhodamine B release assay

After the promising results from the NR release assay, we next moved to study the release of hydrophilic contents. Since hydrophilic contents are entrapped in the liposome aqueous interior, as opposed to hydrophobic contents that are contained within the lipid bilayer, more significant membrane disruption must be achieved to release hydrophilic contents. For our studies, sulforhodamine B (SRB) was chosen to run the release assay because it is a highly water soluble fluorescent dye commonly used in release[139] and cytotoxicity assays.[150] The concentration used to encapsulate SRB solution within the aqueous interior was carefully

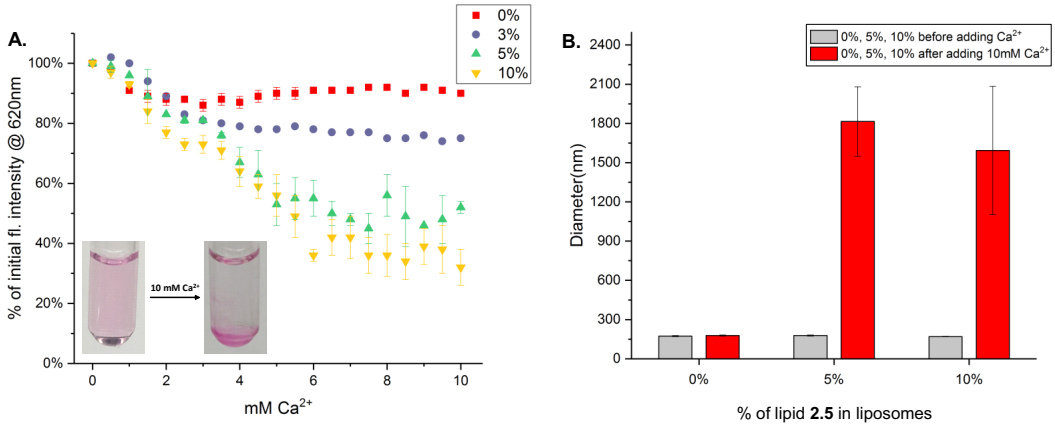


Figure 2.3. NR release and DLS studies of liposomes containing 2.5. A. Dose-dependent release of NR from PC liposomes containing 0%, 3%, 5%, or 10% of lipid **2.5**. Inset shows images before and after release of liposomes containing 10% of **2.5** with 10 mM calcium. **B.** DLS results before and after calcium addition indicate initial stable liposomes that undergo dramatic changes in size only when lipid **2.5** is present. All data represent the averages of at least three replicates with error bars indicating standard errors.

chosen to make sure it is high enough for fluorescence to be self-quenched due to collisional effects. When the dye is released from liposomes, it will be diluted leading to a fluorescence turn-on effect. When preparing the liposomes, similar methods were used with the addition of a size exclusion column (SEC), which is needed after extrusion to remove unencapsulated dye. The successful preparation of liposomes was again determined by DLS. Similar titration experiments were conducted by adding calcium chloride solution into liposomes with 0% or 10% **2.5**. Since a SEC is used during the liposome preparation procedure, the concentration of final liposomes is challenging to control. Therefore, after reaching the titration ending point, Triton X-100 detergent was added to destroy the bilayers and obtain a reference of total release to which each titration point was compared by converting the data into percent release. From Figure 2.4A, we can see that 20 mM calcium causes ~8% background release for PC liposomes, which increased to ~20% release for liposomes including 10% of **2.5**. DLS studies were consistent with this result since dramatic increases in size were again observed for liposomes containing 10% of **2.5** after adding calcium (Figure 2.4B). Addition of Triton X-100 destroyed the bilayers and converted the liposomes into micelles. In the corresponding DLS results, particles with diameters of ~80 nm were detected that are consistent with lipid reorganization into smaller micelle assemblies.

2.3.3. Metal ion selectivity screen with Nile red release assay

The selectivity for calcium of lipid **2.5** over other metal cations commonly found in biological systems was also studied with the NR release assay. Various metal chloride solutions (10 mM) were incubated with liposomes composed of 10% of **2.5**. Cation concentrations of 10 mM were chosen based on the end point from the titration curve of our initial experiments. Figure 2.5 shows the relative fluorescence intensity after adding different cations compared to the blank set incubated with only water. The most abundant metal ions in the human body, potassium and sodium, did not cause any NR release from liposomes. The same phenomenon also can be observed for zinc. Magnesium is commonly thought to be difficult to differentiate from

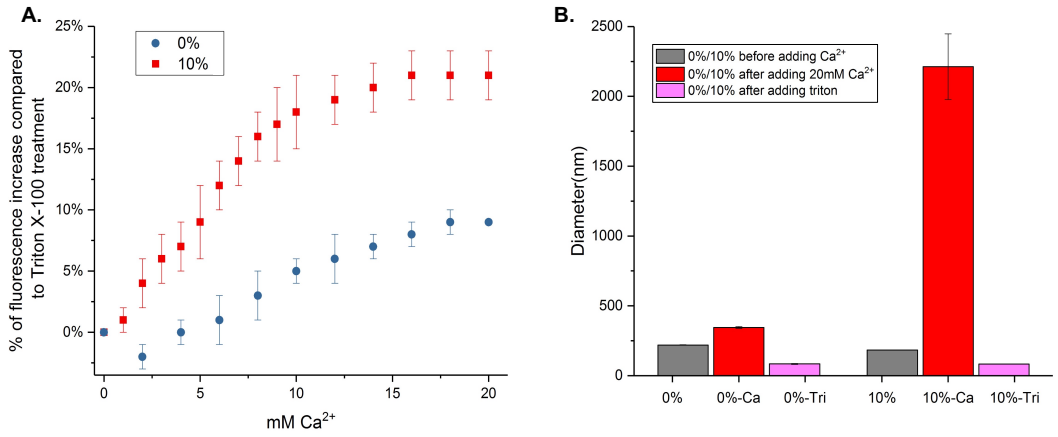


Figure 2.4. Sulforhodamine B release study of liposomes containing lipid 2.5. A. Increase in fluorescence upon calcium titration as a percentage of fluorescence increase following Triton X-100 addition. Liposomes containing 10% of lipid **2.5** yielded a greater fluorescence increase compared to PC liposomes. **B.** DLS studies before and after triggered release driven by Ca^{2+}. Dramatic changes were only observed for liposomes containing **2.5** in the presence of calcium.

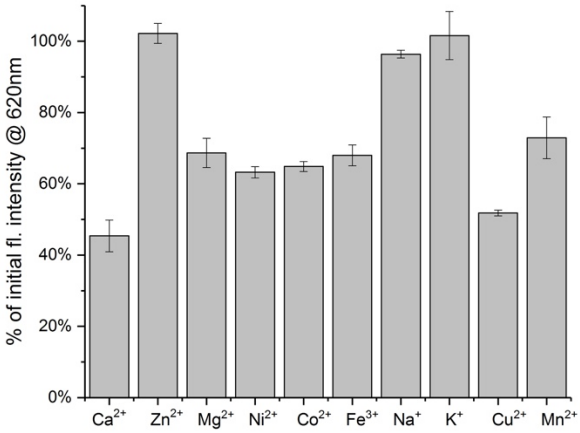


Figure 2.5. Selectivity of triggered release with different common metal cations. NR end point fluorescence values are shown to indicate fluorescence decrease percentages caused by incubation with different cations. K^+, Na^+ and Zn^{2+} did not cause release, while Ca^{2+} resulted in the greatest release.

calcium. In our case, we observed differences, which indicates some calcium selectivity for our trigger. Other common transition metal cations also caused moderate release. However, considering their low abundance in nature and biological systems, release driven by these ions is not expected to be an issue for clinical delivery applications.

2.4. Scanning transmission electron microscopy studies

Scanning transmission electron microscopy (STEM) experiments were also carried out to understand morphological changes in lipid self-assembly driven by calcium binding. Images were taken using liposomes containing 0% or 10% of **2.5** before and after treatment with 20 mM calcium. As can be seen in Figure 2.6, both the liposomes containing 10% of **2.5** before adding calcium (Figure 2.6A) and the liposomes containing entirely PC after adding calcium (Figure 2.6B) show similar images of unilamellar liposomes with defined membranes of the expected sizes. The aggregation of liposomes in these images may be due to the STEM sample preparation procedure, and thus does not reflect their behavior in solution. Based on DLS results shown in Figure 2.6B, the liposomes are not aggregating into larger assemblies in solution. The images obtained from the liposome samples containing 10% of **2.5** after treatment with calcium (Figure 2.6C) show significant changes in liposome morphology. Complicated multilamellar globular assemblies driven by the calcium addition can be observed.

2.5. Miscellaneous experiments

2.5.1. Quantification of trigger lipid incorporation

The percentages of lipid **2.5** and NR incorporation within liposomes were determined by UV-Vis spectroscopy. For this experiment, lipid **2.5** was dissolved in chloroform and a calibration curve was generated, as is shown in Figure 2.7A. After liposome formation, the water was removed, and the components were re-dissolved in chloroform and an additional measurement was taken (Figure 2.7B). The inclusion of lipid trigger **2.5** was evaluated via the characteristic absorbance peak at 235 nm, which confirmed its presence within

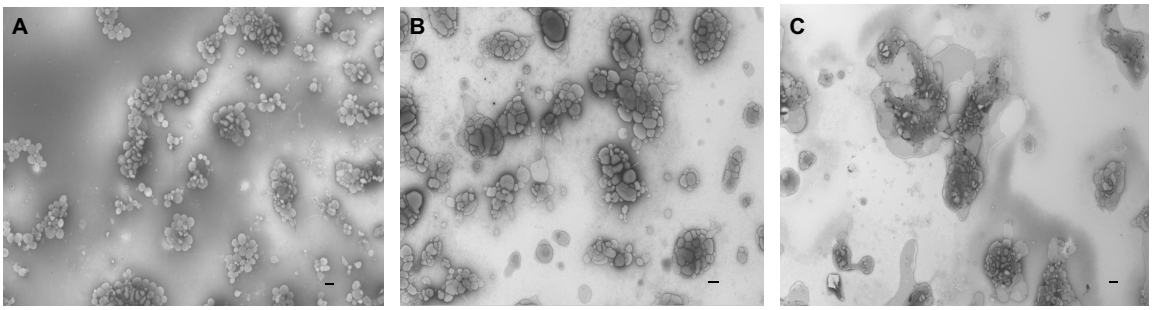


Figure 2.6. STEM images of liposomes containing (A) 10% of 2.5 before calcium addition, (B) 0% of 2.5 after 20 mM calcium addition, and (C) 10% of 2.5 after 20 mM calcium addition. The scale bar in each image denotes 200 nm.

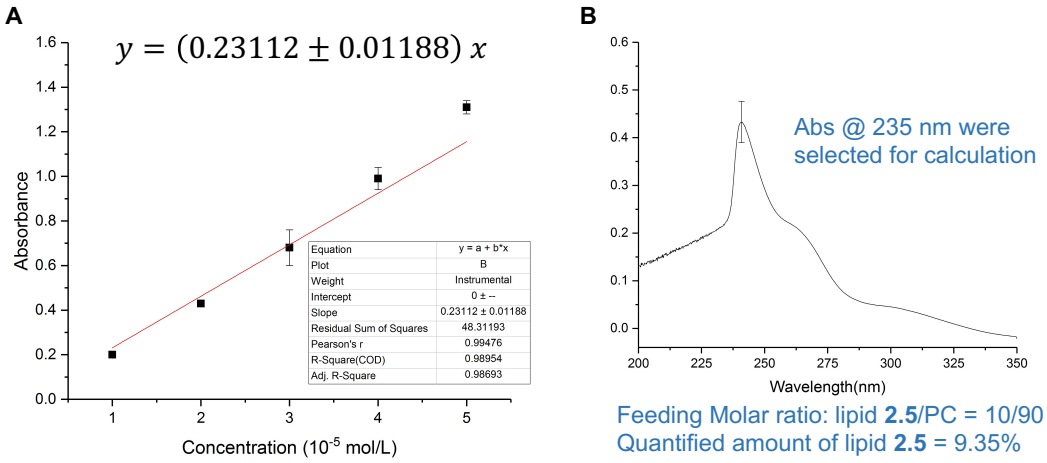


Figure 2.7. UV-Vis quantification of lipid 2.5 in the liposomes. A. Calibration curve of lipid **2.5** in chloroform. **B.** UV-Vis absorbance spectra of the liposomes dissolved in chloroform and the calculation of lipid incorporation.

resulting liposomes. For example, when lipid switch **2.5** was incorporated as 10% of the lipid mix, the final absorbance peak was 94% of the original signal, correlating with 9.4% of lipid **2.5**. This slight decrease in absorbance may result from some loss of materials during the liposome formulation process. The inclusion of NR within liposomes was additionally confirmed using a similar strategy through the characteristic absorbance peak at 540 nm, which was determined to be 0.48% of the total lipid content.

2.5.2. Release studies with varying conditions

Besides the NR release conditions we reported above, we also explored different conditions to investigate how those affected content release. Previous studies were performed in MilliQ purified water; however, we wondered if the release could be affected when using HEPES buffer (pH=7.4). HEPES buffer is ideal since it can maintain pH but also has minimal salt concentrations, considering excess amount of ion could affect our ion-responsive system. As shown in Figure 2.8A, when 2 mM liposomes were prepared in HEPES buffer and treated with calcium, 10% **2.5** liposomes exhibited diminished release from 60% to 40%, with PC liposomes showing ~10% non-specific release. On the corresponding DLS analysis, similar changes in liposomes in morphology was observed. Both PC and 10% liposomes were stable in HEPES buffer pre calcium treatment. After adding calcium, only 10% liposomes showed significant increases in particle sizes, as is shown in Figure 2.8B.

The concentrations of NR-encapsulated liposomes in HEPES were also adjusted and subjected to release studies. When diluting the 2 mM liposomes down to 40 μM, we first observed a much higher (~20%) non-specific release when the PC control liposomes were treated with buffer, as shown in Figure 2.9A, indicating that the encapsulated NR dye is more prone to leak out at such a low liposome concentration. In addition, while PC liposomes and 10% liposomes showed ~40% release, 20% liposomes showed only ~25% release. Since the release extent correlated with the percentages of PC lipid, this is an indication that PC is

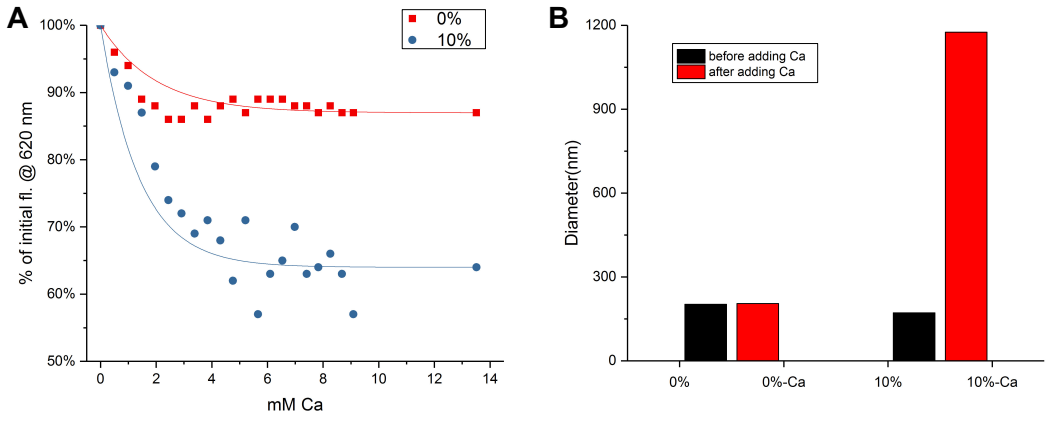


Figure 2.8. Nile red release studies performed in HEPES buffer at mM scale. A. Dose-dependent release curve. While PC liposomes still showed ~10% non-specific NR release, 10% **2.5** liposomes showed reduced release. **B.** DLS analysis of the liposomes before and after adding calcium. Increases in particle sizes were only observed for liposomes containing **2.5** in the presence of calcium.

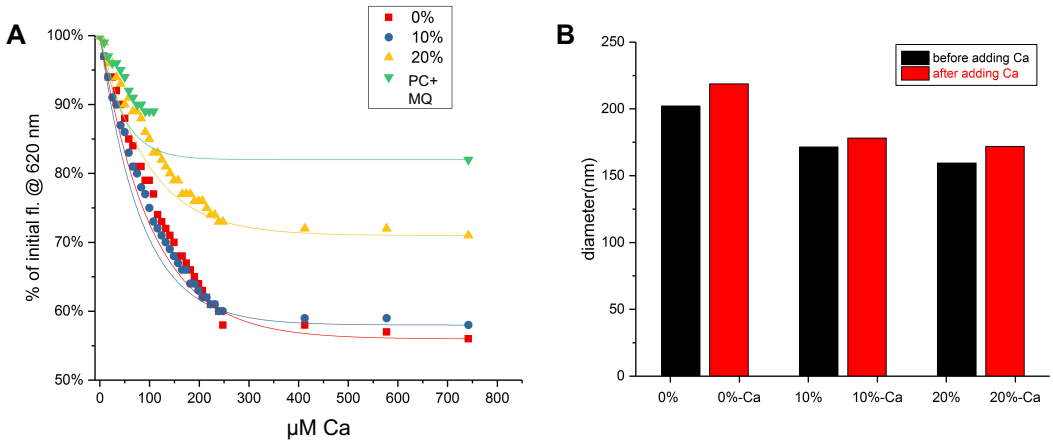


Figure 2.9. Nile red release studies performed in HEPES buffer at μM scale. A. Dose-dependent release curves showing significant background release from buffer dilution and PC lipids. **B.** DLS analysis of the liposomes before and after adding calcium. None of these showed changes in particle sizes in the presence of calcium.

causing background release in HEPES at μM concentrations. When subjecting these liposomes to DLS analysis, none of them showed changes in particle sizes, as is shown in Figure 2.9B. This could because although we noticed NR leakage, the modulation of membrane properties may not have been significant enough to induce membrane fusion to drive particle size increases. Alterations in local membrane packing might be the release mechanism in this case.

2.5.3. Metal ion selectivity screen with SRB release assay

The selectivity towards different metal ions was also screened with SRB release assay. To 50 μL SRB encapsulated liposomes, 10 mM various metal ions were added and the resulting fluorescence intensities were recorded after one hour incubation. From Figure 2.10A, while most of the transition metals (i.e., nickel, copper, and cobalt) as well as magnesium showed medium increase in fluorescence, calcium addition induced more SRB release. However, it is surprising that zinc treatment resulted in ~80% increase in SRB fluorescence, which was slightly higher than calcium treatment. The DLS analysis of liposomes after zinc addition is shown in Figure 2.10B (green bars) and increases in particle sizes were again observed upon metal ion treatment. Considering the fact that zinc addition did not induce release in the NR assay, we postulate that zinc might be interacting with SRB liposomes in a different manner since these did not contain NR in the lipid bilayer. NR, similar to cholesterol, could potentially act as a lipid to tune membrane fluidity or stability, which could ultimately affect cargo release properties and selectivities.

2.6. Conclusion

Our calcium-responsive lipid switch **2.5** opens a new paradigm for controlling the release of therapeutic cargo from liposomes driven by the molecular environment of cells and tissues. We observed lipid **2.5** to play a critical role in triggering release driven by calcium, proven by both NR and SRB release, and correlated release with liposome morphology changes via DLS

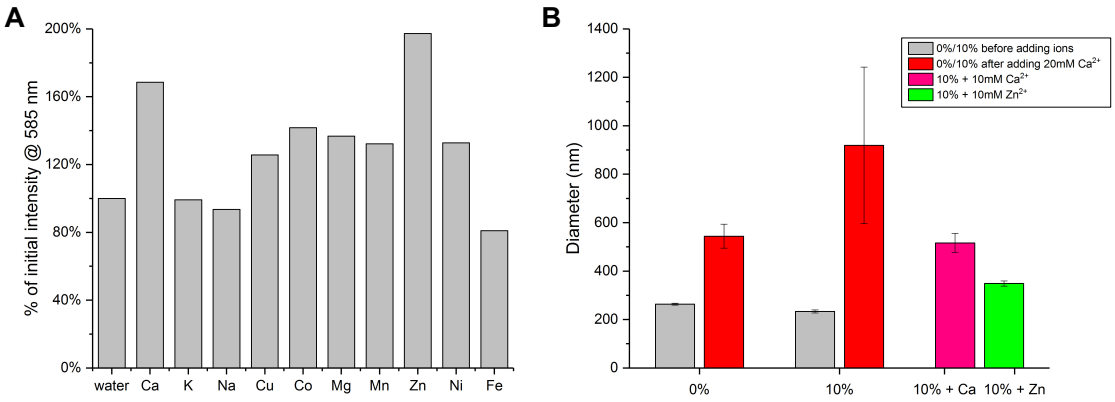


Figure 2.10. Metal ion selectivity screen with SRB release assay. A. Bar graph showing selectivity data that indicate the largest fluorescence increases for Zn and Ca. **B.** DLS analysis of liposomes used in this study. Interestingly, zinc addition resulted in higher increases in SRB fluorescence, and it also induced increases in particle sizes.

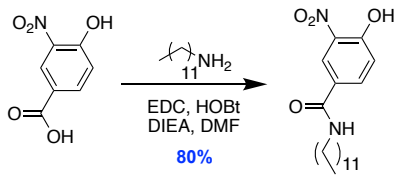
and STEM. This is an exciting new avenue since it is often the abundance of metabolites that exhibits the greatest variation between normal and diseased cells. Thus, calcium-responsive liposomes provide a new avenue for selective delivery and release of therapeutics in and around diseased cells, such as those infected with the *Plasmodium* associated with malaria. In addition, many other biomolecules that are aberrantly expressed in disease could be promising targets for the development of additional membrane release systems driven by lipid switches, as will be discussed in later chapters of this dissertation.

2.7. Synthesis and experimental procedure

General Experimental

Reagents and solvents were generally purchased from Acros, Aldrich, or Fisher Scientific and used without further purification. PC (L-α-phosphatidylcholine, mixed isomers from chicken eggs) was purchased from Avanti Polar Lipids, Inc. Dry solvents were obtained from a Pure solvent delivery system purchased from Innovative Technology, Inc. Column chromatography was performed using 230−400 mesh silica gel purchased from Sorbent Technologies. NMR spectra were obtained using Varian 500 MHz spectrometer. Mass spectra were obtained with JEOL DART-AccuTOF and Q-Star XL quadrupole time-of-flight hybrid mass spectrometer (Applied Biosystems, Foster City, CA). Liposome extruder and polycarbonate membranes were obtained from Avestin (Ottawa, Canada). Ultrapure water was purified via a Millipore water system (≥18 MΩ·cm triple water purification system). Small quantities (<5 mg) were weighed on a OHRUS analytical-grade mass balance. Fluorescence studies were performed using a PerkinElmer LS55 fluorimeter. Plots were generated using Origin Pro 2017. All error bars show the standard errors of at least three experimental replicates.

Synthesis

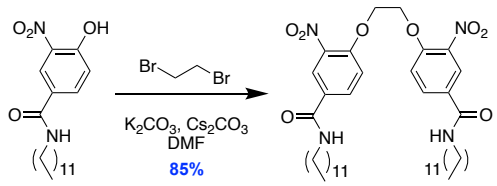


2.6

***N*-Dodecyl-4-hydroxy-3-nitrobenzamide (2.6)**

4-Hydroxy-3-nitrobenzoic acid (1 g, 5.46 mmol), dodecan-1-amine (1.52 g, 8.2 mmol) and hydroxybenzotriazole (HOBt, 1.256 g, 8.2 mmol) were dissolved in 15 mL DMF under argon atmosphere. After being cooled to 0 °C and stirred for 5 minutes, 1-(3-dimethylaminopropyl)-3-ethylcarbodiimide hydrochloride (EDCI•HCl, 1.57 g, 8.2 mmol) and *N*, *N*-diisopropylethylamine (DIEA, 2.4 mL, 13.65 mmol) were added. The reaction mixture was opaque orange. Then, the ice bath was removed and the reaction mixture was further stirred at room temperature for 5 hours. The reaction was quenched by adding 3 mL water and poured into 1M HCl. Ethyl acetate was then added to the mixture and the organic phase was washed five times with water and twice with brine. After the removal of the organic solvent under reduced pressure, the crude product was recrystallized with 95% ethanol to afford compound **2.6** as a pale yellow solid (1.54g, 4.39 mmol, 80% yield).

^{1}H NMR (500 MHz, $CDCl_3$) δ 10.76 (s, 1H), 8.50 (d, *J* = 2.2 Hz, 1H), 8.06 (dd, *J* = 8.8, 2.3 Hz, 1H), 7.23 (d, *J* = 8.7 Hz, 1H), 6.11 (s, 1H), 3.45 (td, *J* = 7.3, 5.7 Hz, 2H), 1.63 (ddd, *J* = 14.8, 8.1, 6.7 Hz, 2H), 1.39 – 1.24 (m, 18H), 0.92 – 0.85 (m, 3H); ^{13}C NMR (126 MHz, $CDCl_3$) δ 164.57, 157.03, 136.09, 127.23, 123.65, 120.48, 40.40, 31.92, 29.65, 29.63, 29.59, 29.54, 29.35, 29.32, 27.00, 22.69, 14.12; HRMS-DART: $[M+H]^+$ calcd for $C_{19}H_{31}N_2O_4$, 351.2283, found 351.2252.

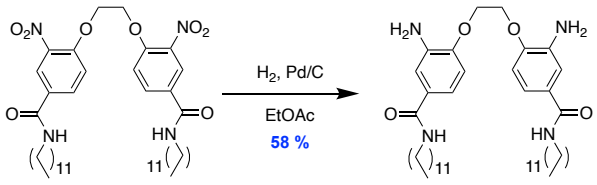


2.6 **2.7**

4,4'-(Ethane-1,2-diylbis(oxy))bis(*N*-dodecyl-3-nitrobenzamide (2.7)

In a round bottom flask, compound **2.6** (1.0381 g, 2.96 mmol) was combined with oven-dried Cs_2CO_3 (1.265 g, 3.88 mmol) and K_2CO_3 (0.691 g, 5 mmol) under nitrogen. Then, 15 mL DMF was added and followed by 1,2-dibromoethane (0.1276 mL, 1.48 mmol). After refluxing for 24 hours, the reaction mixture was cooled down to room temperature. Enough water was added to obtain a yellow suspension and then the suspension was extracted twice by chloroform (determined by TLC). The organic phases were collected and then washed three times with water, once with brine, dried with Na_2SO_4, filtered, and concentrated under reduced pressure. Column chromatography using gradient elution from 50% ethyl acetate-hexanes to 10% methanol-dichloromethane afforded pale yellow compound **2.7** (0.9189 g, 1.264 mmol, 85% yield). R_f = 0.5 (5% methanol-ethyl acetate).

^{1}H NMR (500 MHz, $CDCl_3$) δ 8.20 (d, *J* = 2.3 Hz, 2H), 8.02 (dd, *J* = 8.7, 2.3 Hz, 2H), 7.28 (s, 1H), 7.26 (d, *J* = 0.4 Hz, 1H), 6.10 (t, *J* = 5.7 Hz, 2H), 4.61 (s, 4H), 3.45 (td, *J* = 7.3, 5.6 Hz, 4H), 1.66 – 1.59 (m, 4H), 1.42 – 1.24 (m, 36H), 0.90 – 0.85 (m, 6H). ^{13}C NMR (126 MHz, $CDCl_3$) δ 164.79, 153.90, 139.77, 133.15, 128.38, 124.43, 115.61, 68.86, 40.55, 32.07, 29.80, 29.78, 29.75, 29.69, 29.50, 29.46, 27.15, 22.84, 14.28; HRMS-DART: $[M+H]^+$ calcd for $C_{40}H_{63}N_4O_8$, 727.4646, found 727.4397.

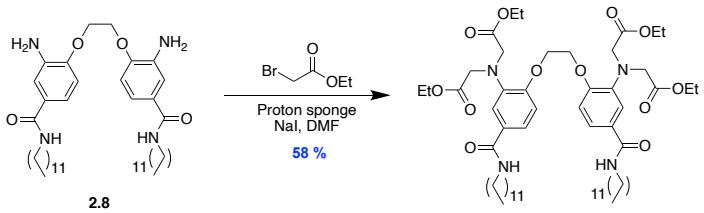


2.7 **2.8**

4,4'-(Ethane-1,2-diylbis(oxy))bis(3-amino-*N*-dodecylbenzamide) (2.8)

Compound **2.7** (0.2431 g, 0.334 mmol) and 10% Pd/C (0.0486 g, 20% weight of compound **2.7**) were added to a round bottom flask and dissolved in 20 mL ethyl acetate under argon. Then, argon was replaced by a hydrogen atmosphere using a balloon and the reaction mixture was further stirred under H_2 at room temperature for 12 hours. The Pd/C was carefully removed via a celite pad. After the removal of solvent under reduced pressure, the crude product was purified with column chromatography packed with alumina using eluant of 100% chloroform to 1% methanol-chloroform to afford compound **2.8** (130 mg, 0.195 mmol, 58%) as light yellow solid. R_f = 0.4 (7.5% methanol-chloroform).

^{1}H NMR (500 MHz, $CDCl_3$) δ 7.10 (d, *J* = 2.2 Hz, 2H), 7.05 (dd, *J* = 8.4, 2.2 Hz, 2H), 6.79 (d, *J* = 8.4 Hz, 2H), 6.55 (t, *J* = 5.7 Hz, 2H), 4.37 (s, 4H), 3.32 – 3.24 (m, 8H), 1.60 – 1.46 (m, 4H), 1.34 – 1.07 (m, 36H), 0.86 – 0.75 (m, 8H). ^{13}C NMR (126 MHz, $CDCl_3$) δ 167.42, 159.87, 153.89, 133.16, 124.44, 115.58, 111.39, 67.33, 40.56, 40.21, 32.07, 29.90, 29.86, 29.81, 29.78, 29.76, 29.72, 29.70, 29.50, 29.47, 27.19, 27.16, 22.85, 14.28. HRMS-DART: $[M+H]^+$ calcd for $C_{40}H_{66}N_4O_4$, 667.5162, found 667.4757.



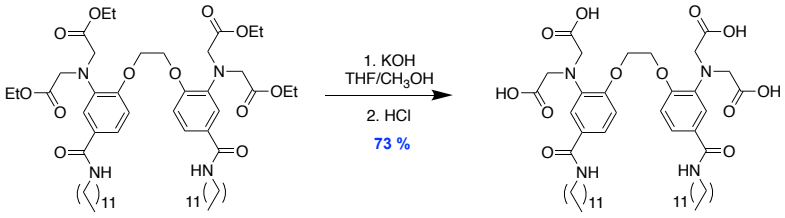
2.8 2.9

Tetraethyl 2,2',2'',2'''-(((ethane-1,2-diylbis(oxy))bis(5-(dodecylcarbamoyl)-2,1-phenylene))bis(azanetriyl))tetraacetate (2.9)

In a small vial, compound **2.8** (40 mg, 0.06 mmol), sodium iodide (47.7 mg, 0.318 mmol) and proton sponge (68.13 mg, 0.318 mmol) were dissolved in 1 mL DMF under argon. After addition of ethyl bromoacetate (53 μL, 0.318 mmol), the reaction mixture was stirred at 80 °C for 24 hours. After completion, DMF was removed under reduced pressure. The crude product was further purified by column chromatography using gradient elution of 100% chloroform to

6% methanol-chloroform and finally gave **2.9** as a brown solid (35 mg, 0.035 mmol, 58% yield). R_f = 0.3 (10% methanol-chloroform).

^{1}H NMR (500 MHz, $CDCl_3$) δ 7.32 (d, *J* = 2.2 Hz, 2H), 7.30 – 7.24 (m, 2H), 6.84 (d, *J* = 8.4 Hz, 2H), 6.03 (t, *J* = 5.7 Hz, 2H), 4.31 (s, 4H), 4.14 (s, 8H), 4.04 (q, *J* = 7.1 Hz, 8H), 3.41 (qd, *J* = 7.0, 2.9 Hz, 4H), 1.59 (qd, *J* = 8.6, 7.9, 4.5 Hz, 4H), 1.27 (d, *J* = 7.2 Hz, 36H), 1.16 (t, *J* = 7.2 Hz, 12H), 0.88 (t, *J* = 6.9 Hz, 6H). ^{13}C NMR (126 MHz, $CDCl_3$) δ 171.24, 166.95, 152.65, 139.41, 128.18, 120.63, 118.22, 112.32, 77.28, 77.03, 76.78, 67.17, 60.90, 53.50, 40.10, 31.92, 29.75, 29.66, 29.63, 29.61, 29.58, 29.56, 29.36, 29.35, 27.05, 27.03, 22.69, 14.18, 14.12, 14.07. HRMS-DART: $[M+H]^+$ calcd for $C_{56}H_{91}N_4O_{12}$, 1011.6634, found 1011.3491.



2.9 **2.5**

2,2',2'',2'''-(((Ethane-1,2-diylbis(oxy))bis(5-(dodecylcarbamoyl)-2,1-phenylene))bis(azanetriyl))tetraacetic acid (2.5•4H)

Compound **2.9** (20 mg, 0.0198 mmol) was dissolved in 800 μL THF and 200 μL MeOH mixture in a vial. After adding 150 μL 1M KOH, the reaction mixture was stirred at room temperature overnight. After completion, the solvent was removed under reduced pressure. 5 mL water was then added to dissolve the crude product. Finally, 4M HCl was added dropwise. When the pH reached 1, precipitate came out. Vacuum filtration was used to obtain **2.5•4H** as pale brown solid (13 mg, 0.014 mmol, 73% yield).

^{1}H NMR (500 MHz, 20% MeOD-$CDCl_3$) δ 7.35 – 7.29 (m, 2H), 7.27 (d, *J* = 2.0 Hz, 2H), 6.86 (dd, *J* = 8.3, 3.2 Hz, 2H), 4.29 (d, *J* = 3.1 Hz, 4H), 3.95 (d, *J* = 3.1 Hz, 8H), 3.34 – 3.23 (m, 4H), 1.52 (d, *J* = 8.2 Hz, 4H), 1.34 – 1.09 (m, 36H), 0.85 – 0.75 (m, 6H). ^{13}C NMR (126 MHz, 20% MeOD-$CDCl_3$) δ 174.25, 168.35, 153.14, 138.65, 128.17, 123.30, 118.16, 112.19, 77.80, 77.54, 77.28, 66.86, 55.20, 49.53, 49.36, 49.19, 49.02, 48.85, 48.68, 48.51, 40.46, 32.13, 29.88,

29.85, 29.82, 29.71, 29.62, 29.56, 27.30, 22.88, 14.17. ESI-MS: $[M-H]^-$ calcd for $C_{48}H_{73}N_4O_{12}$, 897.5225, found 897.4339.

Preparation of liposomes for Nile red release studies

Lipid **2.5**, PC and NR stock solutions were first prepared as follows: 5 mM NR stock solution was prepared by dissolving 4.41 mg NR in 2.77 mL chloroform, 32 mM PC stock solution was prepared by dissolving 25 mg PC with 1.014 mL chloroform, and for lipid **2.5**, a 5 mM stock solution was prepared by dissolving 2.6 mg of **2.5** in 580 µL of 50% methanol-chloroform. Next, proper volumes of each stock solution were pipetted into a clean vial to obtain the desired percentage of each component. As an example, to make 250 µL of a 2 mM liposome solution containing 10% of **2.5**, 13.3 µL PC (85%), 10 µL lipid **2.5** (10%) and 5 µL NR (5%) were combined in a vial. The solvents were then evaporated under nitrogen stream and the resulting solid was further dried under vacuum for at least two hours to yield a lipid film. After that, the lipid film was hydrated with MilliQ purified water (250 µL) at 50 °C for 3 sets of 10 mins with vortexing after each set. Freeze-thaw cycles (10 times) were done on the resulting liposome solution with dry/ice acetone bath and 50 °C water bath. Finally, the liposome solutions were extruded through a 200 nm polycarbonate membrane for 15 passes with a LiposoFast extruder (Avestin, Inc.). Other liposomes used for studies were produced in the same manner using different percentages of the lipid **2.5**.

Titrations of liposomes encapsulating Nile red with calcium chloride solutions

A 0.1 M Calcium chloride stock solution was made by dissolving calcium chloride into MilliQ purified water. A 100 µL aliquot of the 2 mM liposome solution prepared through the procedure above was added to a sub-micro quartz cuvette. The calcium chloride stock solution was added in 0.5 µL aliquots directly into the cuvette for each measurement in the titration (increment = ~0.5 mM) and the fluorescence intensity was then measured (excitation wavelength = 552 nm, excitation slit = 10 nm, emission slit = 5 nm). Since dilution effects will

also lower the fluorescence intensity, an additional control sample was run by instead adding 0.5 μL MilliQ water (no calcium) to a 100 μL solution of the same liposome. When processing the data, fluorescence intensities at 620 nm were selected and the intensity of the control sample was subtracted out to account for decreased signal resulting from dilution effect. Experiments were run at least 3 times each with different batches of liposomes, and averaged data were reported with error bars showing standard error.

Dynamic light scattering (DLS) liposome analysis during calcium addition

DLS measurements were carried out with a Malvern Zetasizer Nano ZS instrument equipped with a 4.0 mW laser operating at λ = 633 nm. Samples were prepared by diluting the liposome solutions before or after adding ions 10 times with MilliQ water. All samples were determined at a scattering angle of 173° at 25 °C. The data reported were the average of three tests with error bars showing standard error.

Metal comparison content release studies

Metal ion stock solutions (0.1 M) were prepared by dissolving their chloride salts ($ZnCl_2$, $MgCl_2$, $NiCl_2{\bullet}6H_2O$, $CoCl_2$, $FeCl_3$, NaCl, KCl, $CuCl_2$, or $MnCl_2$) in MilliQ water. For each metal study, take Zn^{2+} as an example, 5 μL of a 0.1 M Zn^{2+} stock solution was added to 50 μL of a 2 mM liposome containing 10% of **2.5** obtained from the procedure above (final concentration for $Zn^{2+} \approx 10$ mM). Fluorescence intensities were taken after 40 min incubation time with the same fluorescence detection method as titration. Studies with other ions were done in the same manner. A control experiment was also run by adding 5 μL MilliQ water to 50 μL of the same liposome to test the dilution effect. The same liposome solution was used for one set of comparison studies using each of the described metals. When processing the data, fluorescence intensities at 620 nm were selected and the intensity decrease caused by dilution effect was again subtracted out. The whole process was repeated 3 times with different batches of liposomes, and averaged data were reported with error bars showing standard error.

Preparation of liposomes encapsulating Sulforhodamine B

A 20 mM SRB stock solution was prepared by dissolving 0.2323 g SRB sodium salt in 20 mL MilliQ purified water. The lipid **2.5** and PC stock solutions were prepared as previously described in the NR release studies. Proper volumes of each stock solution were pipetted into a clean vial to obtain the desired percentage of each component. As an example, to make 200 µL of a 2 mM liposome solution containing 10% of **2.5**, 11.3 µL PC (90%) and 8 µL lipid **2.5** (10%) were combined in a vial. The solvents were then removed using rotary evaporation and the resulting solid was further dried under vacuum for at least two hours to yield a lipid film. After that, the lipid film was hydrated with 200 µL of the 20 mM SRB stock solution at 50 °C for 3 sets of 10 mins with vortexing after each set. Freeze-thaw cycles (10 times) were done on the resulting liposome solution with dry/ice acetone bath and 50 °C water bath. Then, the liposome solutions were extruded through a 200 nm polycarbonate membrane for 31 passes with a LiposoFast extruder (Avestin, Inc.). Finally, the unencapsulated dye was removed via a size exclusion column packed with Sephadex G-50 (pre-saturated with MilliQ water). Fractions were collected every ~1 mL and the second fraction was chosen to run further studies based on fluorescence increases observed when aliquots were treated with triton X-100.

Titrations of liposomes encapsulating Sulforhodamine B with $CaCl_2$ solutions

The calcium chloride stock solution that was used was the same as the NR release study (0.1 M). A solution of 10% Triton X-100 was prepared by dissolving 1 mL Triton X-100 into 10 mL MilliQ water. A 100 µL aliquot of the liposome solution prepared through the procedure above was added to a sub-micro quartz cuvette. The calcium chloride stock solution was added in 1.0 µL aliquots directly into the cuvette for each measurement in the titration (increment = ~1.0 mM) and the fluorescence intensity was then measured using an average of 3 scans. (Excitation wavelength = 550 nm, excitation slit = 7.5 nm, emission slit = 5.0 nm). After adding 20 mM Ca^{2+}, 2 µL of 10% Triton X-100 was added to trigger complete release. When

processing the data, fluorescence intensities at 585 nm were selected and fluorescence increases were reported as a percentage of the fluorescence after Triton X-100 treatment for each sample. Experiments were run at least 3 times each with different batches of liposomes, and averaged data were reported with error bars showing standard error.

STEM imaging of liposome samples

Liposome solutions (2 mM) consisting of only PC or 10% lipid **2.5** and 90% PC were prepared as previously described. As an example, to make 250 µL 10% liposomes, 14.1 µL PC (90%) and 10 µL lipid **2.5** were pipetted into a vial. After preparing the lipid films, 250 µL MilliQ water was added to hydrate, followed by 10 freeze-thaw cycles and extrusion through a 200 nm polycarbonate membrane. The formation of liposomes with desired size was confirmed by DLS. For STEM studies, a drop (5-10 µL) from each solution was immobilized onto a thin carbon film supported by a 200-mesh copper grid and then stained with a 0.5% (w/v) solution of phosphotungstic acid. After drying, the samples were stored in a desiccator overnight prior to examination. Images were collected using a Zeiss Auriga 40 microscope operating in scanning transmission (STEM) mode and a beam energy of 30 keV.

Chapter 3. Development of ATP-responsive liposomes

(The scientific data used in this Chapter has been published by the authors: Lou, Jinchao; Schuster, Jennifer A.; Barrera, Francisco N.; Best, Michael D., ATP-Responsive Liposomes via Screening of Lipid Switches Designed to Undergo Conformational Changes upon Binding Phosphorylated Metabolites, *J. Am. Chem. Soc.* **2022,** 144, 3746-3756.)

3.1. Project overview

In Chapter 2, we reported the development of a calcium-responsive liposome platform, where lipid switches were designed such that calcium binding induced a conformational change that was effective to drive the release of both hydrophobic and hydrophilic cargo.[88] While ions provided strategic targets for proof-of-concept, due to the existence of known sensors that exhibit high affinity and selectivity, this work showcased that molecular recognition principles can modulate liposome self-assembly properties. Small molecules, on the other hand, present unique challenges due to the dearth of clinically relevant host structures and the presence of multiple functional groups with varying three-dimensional presentation.

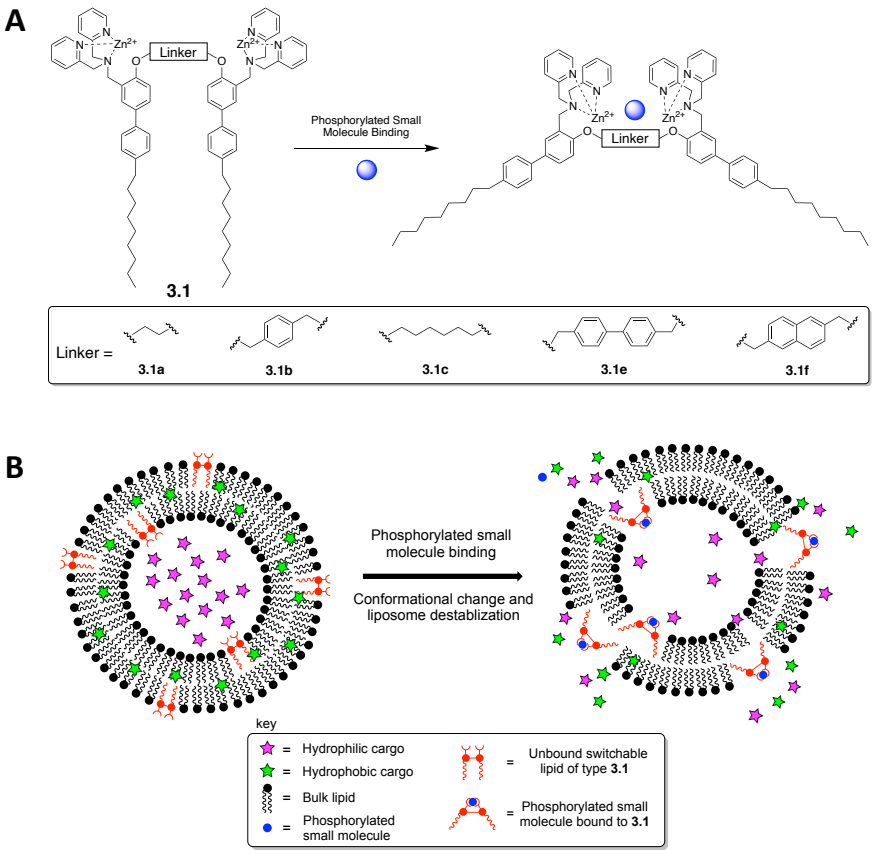
In this Chapter, we report an effort to achieve direct liposome triggered release driven by phosphorylated small molecules, which culminated in selective adenosine triphosphate-(ATP)-responsive liposomes. Phosphorylated metabolites are of particular interest since the introduction of phosphate groups into biomolecules is a critical means for regulating biological function.[151,152] ATP is an excellent target for metabolite-driven release due to its relatively high concentration and critical roles in biological systems. It is a universal energy source that controls vital biological processes, including signaling,[153,154] energy transduction,[155,156] regulation of cellular metabolism,[157,158] and DNA replication.[159,160] While ATP exhibits low concentrations in the extracellular space of healthy tissues (0.01-0.1 mM),[161] increases in ATP concentration up to the high mM range are associated with tumors resulting from conditions including inflammation, hypoxia and mechanical stresses.[162-164] Therefore, in the development

of platforms for drug release driven by the binding of small molecules, ATP provides an exciting prospective stimulus for liposome triggered release.

The concept of ATP-responsiveness has been validated using other delivery carriers featuring different mechanisms.[165-169] While most of the reported systems feature aptamer-based sensing mechanism, in a rare case employing liposomes, Gu and co-workers reported a co-delivery system employing a cell-penetrating peptide fusogenic shell and a core DNA-protein conjugate that is activated by supplemental liposome-encapsulated ATP.[170] While this elegant work confirmed that ATP-mediated delivery can enhance anti-cancer therapeutic efficacy, a direct approach in which liposome membrane properties are modulated via incorporated lipid switches, as presented herein, provides an efficient strategy that doesn't require multiple protein and DNA additives to trigger cargo escape.

3.2. Design and synthesis of the phosphorylated metabolites-responsive synthetic lipid switch

Building upon our calcium-responsive liposomes to develop liposomes that respond to phosphorylated small molecules, we initially designed artificial lipid switches of type **3.1** containing zinc(II) dipicolylamine (ZnDPA) groups, which culminated in the discovery of ATP-responsive properties. ZnDPA moieties were included since they effectively bind phosphorylated functional groups with high affinity.[171-174] Motivated by the success of our previous calcium responsive lipid switch, we mounted two ZnDPA groups onto rigid scaffolds (of type **3.1**, Scheme 3.1A), so that the resulting lipid can thus rest comfortably within liposomal membranes in the free form. Binding to phosphorylated small molecules was designed to induce a conformational change that produces lipid products exhibiting conical shapes. This was envisaged to disrupt membrane packing and trigger the release of encapsulated cargo by amplifying the properties of naturally existing non-bilayer lipids (Scheme 3.1B).[175]



Scheme 3.1. Design for phosphorylated metabolite-responsive liposomes. A. General structures of responsive lipids of type **3.1** bearing two ZnDPA units. These lipids are designed to adopt a cylindrical structure in the membrane prior to guest treatment. Chelation of a phosphorylated molecule is expected to lead to an increased cone angle and non-bilayer properties. **B.** Cartoon depiction of liposome release driven by phosphorylated metabolite addition. The conformational change upon guest molecule binding is expected to disrupt membrane integrity and trigger encapsulated cargo release.

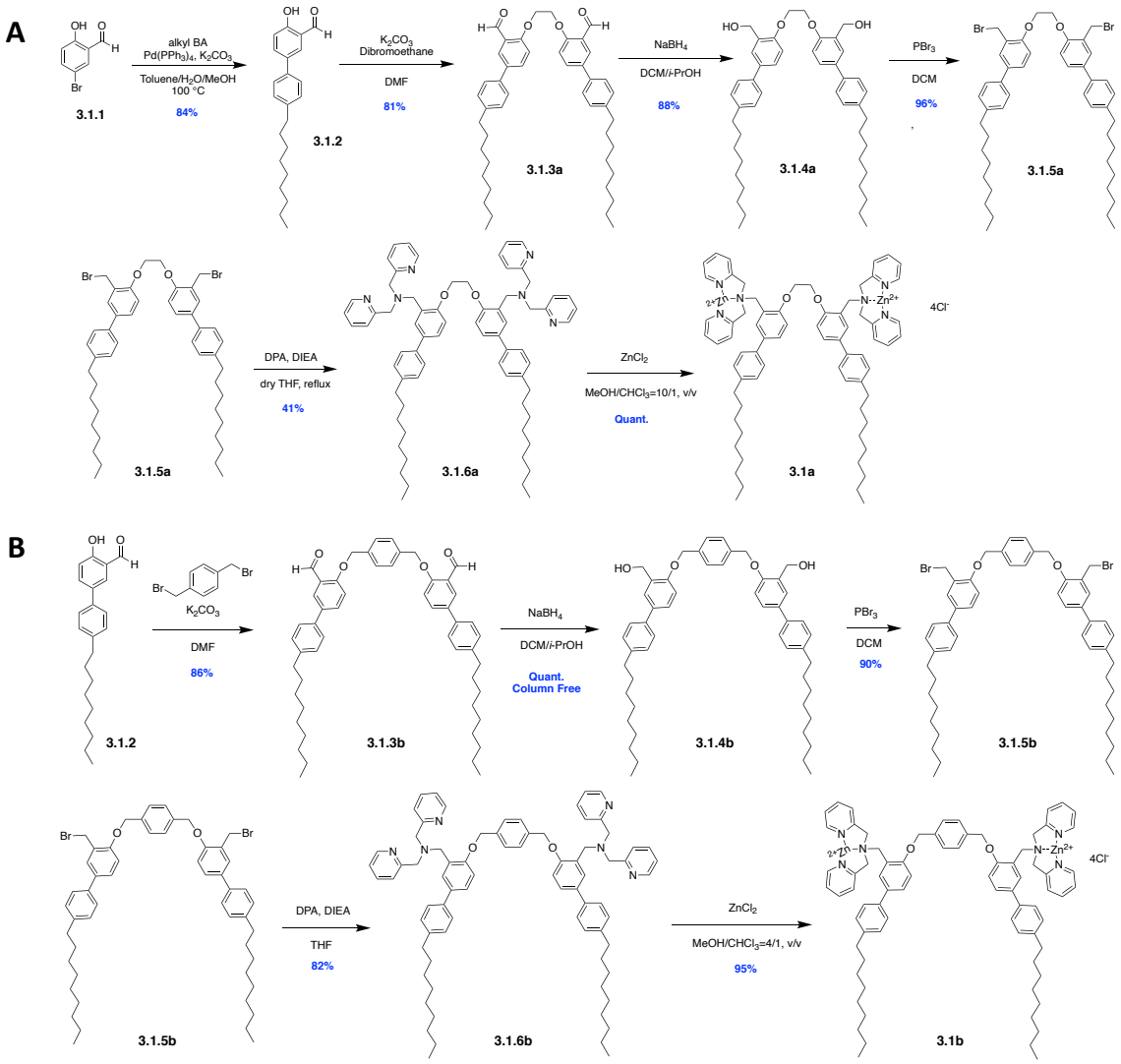
Since it is difficult to predict the exact host design and cavity size that would fit metabolite targets, we designed lipid structures bearing linkers of different length and rigidity between the two ZnDPA groups. Initial switches included a short ethylene linker (**3.1a**) and a slightly longer aromatic *p*-xylene linker **(3.1b**). The synthetic route to initial compounds **3.1a** and **3.1b** is shown in Scheme 3.2, which began with a Suzuki coupling reaction between 5-bromo-2-hydroxybenzaldehyde **3.1.1** and (4-nonylphenyl)boronic acid to add alkyl tails leading to **3.1.2**. This was next treated with either dibromoethane or *p*-xylene dibromide to produce dimeric products **3.1.3a** and **3.1.3b**, respectively, with different linker lengths of type **3.1.3**. These compounds were next subjected to aldehyde reduction to alcohols (**3.1.4a-b**), bromination to produce **3.1.5a-b**, and then treatment with dipicolylamine to afford compounds **3.1.6a-b** containing two DPA binding groups. The last step involved zinc chelation, which yielded the desired lipids of type **3.1** bearing two ZnDPA units.

3.3. Nile red-based dye release assays for phosphorylated small molecules

3.3.1. Phosphorylated metabolite selectivity screen

After we obtained the desired switchable lipids, we first employed fluorescence-based dye leakage assays to evaluate the efficacy of these compounds for triggering cargo release when incorporated into liposomes and subjected to different phosphorylated metabolites. Hydrophobic drugs generally benefit from inclusion within nanocarriers to improve pharmacokinetic properties and minimize off-target effects.[176] As a mimic of these drugs, we began by conducting hydrophobic dye release assays using the NR, which fluoresces when solubilized within membrane bilayers,[148] but for which fluorescence is diminished following release into aqueous media.[149] Thus, NR can not only mimic common hydrophobic drug cargo but also provides signal transduction for tracking release.

We began by incorporating **3.1a** at different percentages ranging from 0-20% within liposomes otherwise composed of phosphatidylcholine (PC, mixed isomers from egg) as a traditional



Scheme 3.2. Synthetic routes to bis-ZnDPA lipid structures 3.1a (A) and 3.1b (B). Compound **3.1.1** was coupled with (4-nonylphenyl)boronic acid to produce **3.1.2**, followed by dimerization using dibromoethane to **3.1.3a** or *p*-xylene dibromide to **3.1.3b**, aldehyde reduction and bromination to **3.1.5a-b**, introduction of the DPA units of **3.1.6a-b**, and finally zinc chelation to generate **3.1a-b**.

bilayer-forming lipid. These unilamellar liposomes were prepared using standard thin-film hydration techniques including film formation, hydration, freeze/thaw cycling as well as extrusion through a 200 nm membrane. The formation of stable liposomes was verified by dynamic light scattering (DLS) based on average particle sizes (*vide infra*). NR encapsulation efficiencies were determined for PC liposomes containing 0% or 10% **3.1a** using UV-Vis spectroscopy by constructing a NR calibration curve (Figure 3.1), which were calculated to be (29.30 ± 3.43)% and (21.23 ± 3.85)%, respectively.

We first screened release properties of liposomes containing metabolite-responsive lipid switch **3.1a** toward different phosphorylated compounds (Figure 3.2). A range of phosphate-containing metabolites were first screened, including inorganic phosphate (Pi), inorganic pyrophosphate (PPi), ATP, adenosine diphosphate (ADP), adenosine monophosphate (AMP), D-fructose-6-phosphate (FP) and D-fructose-1,6-bisphosphate (FBP). In these experiments, we observed that liposomes containing 20% of **3.1a** showed release only upon ATP and ADP addition among those guests, with slightly greater release in the presence of ATP (Figure 3.2A). Control PC liposomes did not show any background release. The observed selectivity of **3.1a** liposomes, ATP>ADP>AMP, could be attributed to the extent of negative charge in these guests. The variation we observed between ATP and ADP treatment led us to hypothesize that ATP/ADP selectivity could be fine-tuned by adjusting the percentage of lipid switch incorporation into liposomes. Specifically, by decreasing the percentage of **3.1a**, we expected that selectivity for ATP could be enhanced. To this end, we prepared liposomes containing 5% or 10% **3.1a** and screened them for NR release by phosphorylated metabolites. In line with our hypothesis, only ATP treatment induced significant amount of dye leakage among these analytes.

3.3.2. Triphosphate metabolite NR release screens

Having shown that **3.1a** liposomes effectively respond to ATP, we next screened NR release

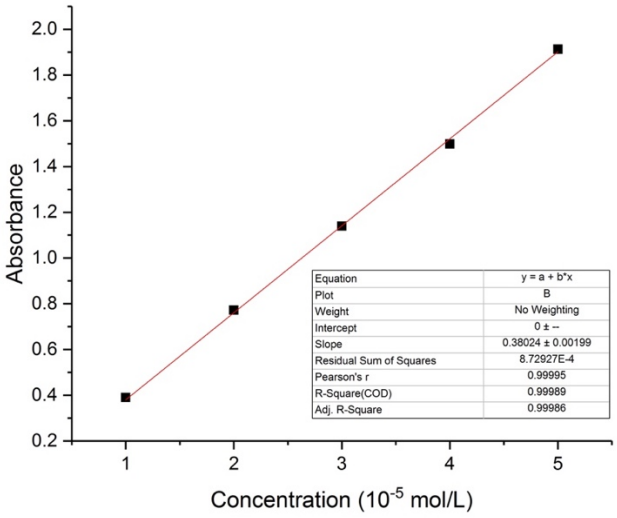


Figure 3.1. UV-Vis calibration curve for Nile red in chloroform used to measure encapsulation efficiency within liposomes. The plots were generated with three independent trials with error bars showing standard errors. The equation after linear fitting was determined to be y = (0.38024 ± 0.00199) x, with R^2 = 0.99986.

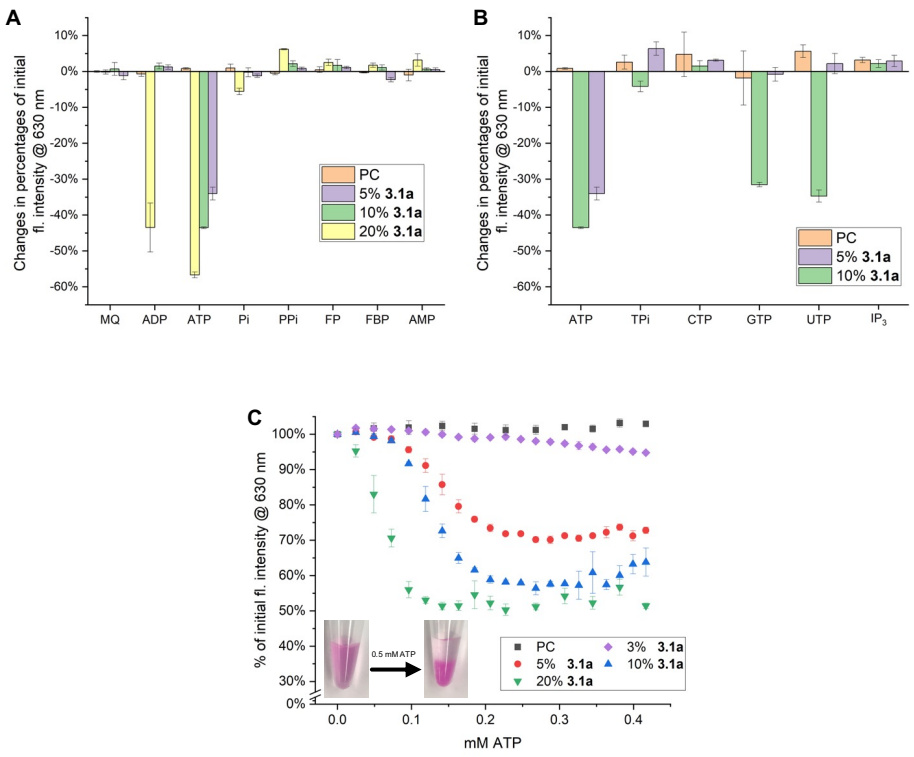


Figure 3.2. NR release results for liposomes containing lipid switch 3.1a. A. Selectivity of PC/**3.1a** liposomes towards different phosphorylated small molecules. While liposomes containing 20% **3.1a** released NR upon both ADP and ATP addition, decreasing incorporation to 10% or 5% resulted in liposomes that only respond to ATP. **B.** Selectivity of **3.1a** liposomes towards different triphosphates. Liposomes with 10% **3.1a** responded to both GTP and UTP, while 5% **3.1a** liposomes did not exhibit release for any nucleotide triphosphates other than ATP. **C.** ATP titration curves for **3.1a** liposomes show dose-dependent release correlating with the percentage of **3.1a**. Error bars denote standard errors from at least three independent studies. Insert: images of NR-encapsulated liposome solutions before and after ATP treatment. A pink precipitate was formed after 0.5 mM ATP addition.

upon treatment with other triphosphate-containing biomolecules including inorganic triphosphate (TPi), and the other nucleotide triphosphates (cytidine (CTP), guanidine (GTP), and uridine (UTP) triphosphate), which are structurally similar metabolites[177] that are also upregulated in tumor cells compared to normal cells,[178] as well as inositol-1,4,5-trisphosphate (IP_3), a key signaling molecule that releases calcium stores.[179-181]. As shown in Figure 3.2B, 10% **3.1a** liposomes showed release upon treatment with either GTP or UTP. We observed that CTP did not yield any release, which we were somewhat surprised about due to the similarity in structures among nucleotide triphosphates. However, among the different nucleotide triphosphates, CTP is known to be a weaker electron donor due to the presence of the pyrimidone functionality, which may negate release in this case.[182] Once again, we lowered the **3.1a** percentage within liposomes to determine if this would enhance selectivity. Accordingly, liposomes containing 5% **3.1a** exhibited selective NR-driven release by ATP over all other nucleotide triphosphates. These results indicate that designer lipid switch **3.1a** is effective for selective ATP-triggered liposome release over a range of similar phosphorylated metabolites, and that selectivity can be fine-tuned by incorporating different percentages of lipid switches within liposomes. Furthermore, ATP provides a particularly exciting target for metabolite-responsive liposome design due to its important biological roles and upregulation in diseased cells.

3.3.3. Expanded Nile red titration curves

A more detailed understanding of ATP-driven NR release using **3.1a** is showcased by the titration results in Figure 3.2C. Here, 2 mM PC liposomes doped with 0%, 3%, 5%, 10%, or 20% **3.1a** were titrated with ATP with fluorescence readings after each addition. The resulting titration curves showed dose-dependent decreases in NR fluorescence as a function of **3.1a** percentage with PC negative controls showing no non-specific release upon ATP treatment. Cargo release proceeded rapidly, as is shown in the kinetic curves shown in Figure 3.3. When

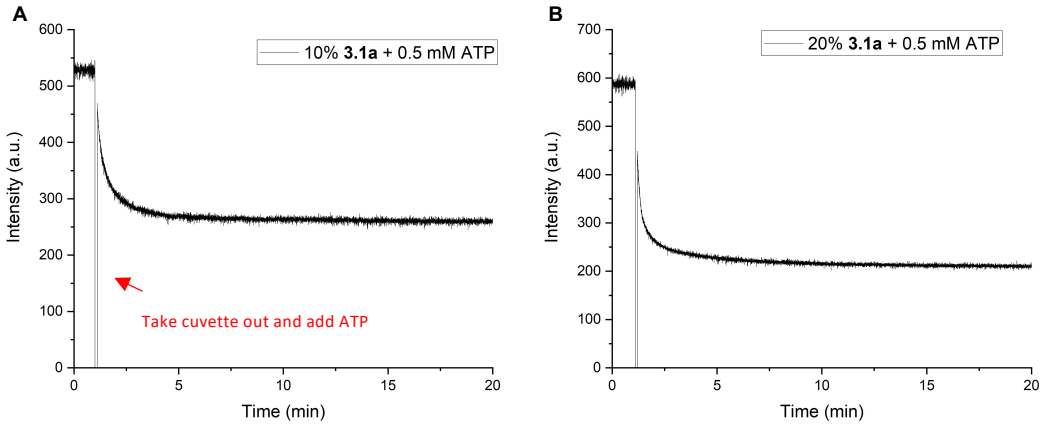


Figure 3.3. Kinetic curves of NR release from 2 mM 10% (A) and 20% (B) 3.1a/PC liposomes after adding ATP. In both cases, complete release was achieved within three minutes after treatment with 0.5 mM ATP.

treating 10% or 20% **3.1a** liposomes with 0.5 mM ATP, release reached a plateau within three minutes after ATP addition.

Dye release was also studied using lower concentrations of liposomes, which can provide insights into the release mechanism, for example, if fusion is occurring (less fusion expected at lower liposome concentration). For this purpose, we prepared 0.1 mM and 0.4 mM samples of 10% **3.1a** liposomes encapsulating NR and titrated them separately with ATP, with the results shown in Figure 3.4. Although dose-dependent release was still observed in both cases, the release percentage was diminished using the lower concentration of liposomes. Specifically, 0.4 mM 10% **3.1a** liposomes showed ~25% release, which was reduced to ~15% for 0.1 mM liposomes. Considering the fact that release was still observed after 5x and 20x decreases in liposome concentration, respectively, these results suggest that fusion is somewhat involved in the release process, but that leakage is not entirely driven by fusion.

Similar experiments were carried out with compound **3.1b**. As is shown in Figure 3.5A-B, for simple phosphorylated metabolites, 20% **3.1b** liposomes showed release for both ATP and ADP. However, when the percentage of this compound was decreased to 10%, **3.1b** liposomes could effectively distinguish between ATP and ADP, although with interference from GTP and slightly from UTP. From the titration profile outlined in Figure 3.5C, 20% and 10% **3.1b** liposomes functioned similarly compared to **3.1a** liposomes, with ~50% and ~40% release for 20% and 10% **3.1b** incorporation, respectively. Interestingly, when we reduced **3.1b** incorporation to 5% of liposome composition, ATP-driven release was almost completely abolished. This result indicates that the cavity present in compound **3.1a** with an ethyl linker provides an improved fit for ATP binding compared to **3.1b** (*p*-xylene tether). As a result, liposomes with lowered (5%) **3.1a** incorporation remain effective toward ATP-triggered release. The NR release kinetics of liposomes containing **3.1b** were also evaluated (Figure 3.6), which similarly showed that release reached a plateau within three minutes after treating 10% or 20%

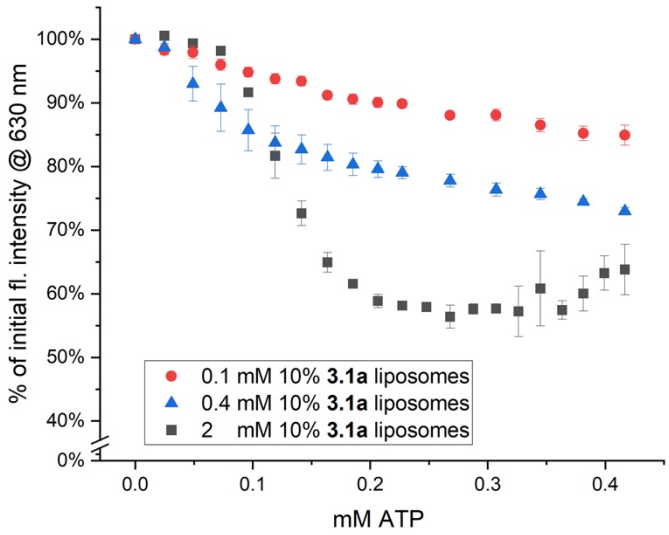


Figure 3.4. NR release profile using diluted 10% 3.1a/PC liposomes. When reducing liposome concentration from to 2 mM to 0.4 or 0.1 mM, diminished release was observed. Error bars denote standard errors from at least three studies.

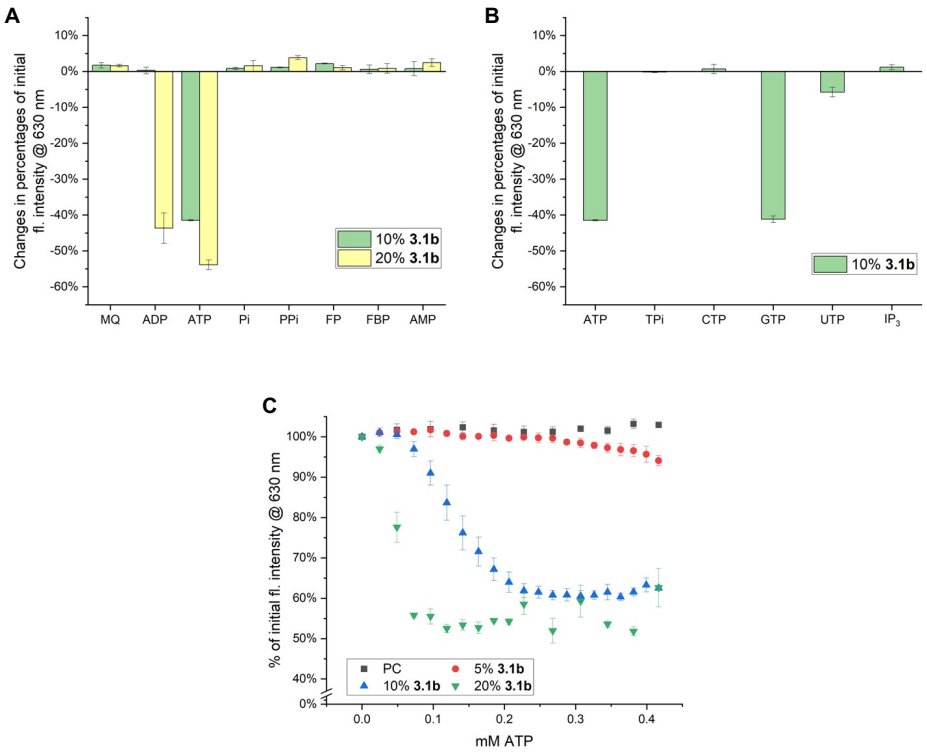


Figure 3.5. NR release results for liposomes containing 3.1b and PC. A. Phosphorylated metabolite selectivity screen with 10% and 20% **3.1b** /PC liposomes. While 20% liposomes showed release towards both ADP and ATP, 10% liposomes were only effective upon ATP treatment. **B.** Triphosphate selectivity screen with 10% **3.1b** liposomes. GTP showed interference among all triphosphates. **C.** NR release titration curve for PC liposomes containing 5%, 10%, or 20% **3.1b**. Dose-dependent release was observed for 10% and 20%, while 5% showed almost no release. Error bars denote standard errors from at least three studies.

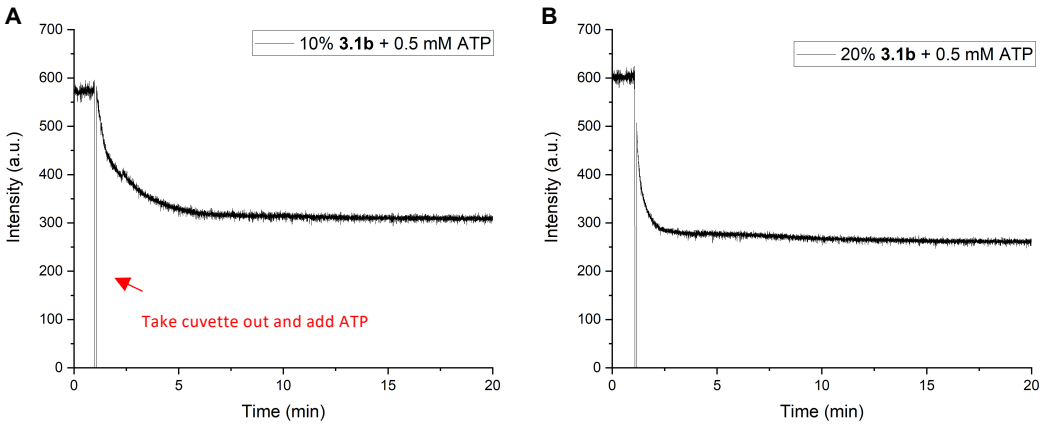


Figure 3.6. Kinetic curves of NR release from 2 mM 10% or 20% 3.1b/PC liposomes after adding ATP. In both cases, complete release was achieved within three minutes after adding 0.5 mM ATP.

3.1b liposomes with 0.5 mM ATP.

3.4. Dynamic light scattering studies

Triggered release is often accompanied by changes in liposome size and morphology, particularly when processes such as fusion or alterations to lipid self-assembly are involved. Therefore, we next probed potential changes in particle sizes through DLS experiments before and after triggered release. Here, PC liposomes containing 0%, 5%, 10%, or 20% **3.1a** were subjected to DLS analysis with and without ATP treatment. As can be seen in Figure 3.7A (grey bars), all samples showed uniform particle sizes with expected diameters (~140 nm) pre-ATP treatment, indicating stable liposomes were formed with up to at least 20% **3.1a** incorporation. Upon treatment with 0.5 mM ATP, PC-only negative control liposomes did not show any size change that would result from non-specific interactions. After ATP addition, however, all liposome samples containing **3.1a** showed size increases, and the average particle sizes post-ATP treatment correlated with the percentage of **3.1a** included within the formulation (red bars, Figure 3.7A). Raw distribution curves are included in Figure 3.7B-D.

Similar particle size changes were observed for PC/**3.1b** liposomes (Figure 3.8A-C). The previously described NR release results indicate that the selectivities of liposomes containing **3.1a**/**3.1b** toward ATP over ADP can be fine-tuned by adjusting percent incorporation. These data were further supported through DLS experiments. As shown in Figure 3.8D, uniform size particles were observed for 10% **3.1a**/**3.1b** liposomes after ADP treatment, indicating ADP did not induce significant morphology changes in these cases, in contrast to the dramatic changes observed upon ATP addition.

3.5. Transmission electron microscopy (TEM) and cryo-EM studies

Changes to lipid nanoparticles were further supported by EM experiments. PC liposomes after ATP addition did not show any change via TEM imaging using a negative staining technique

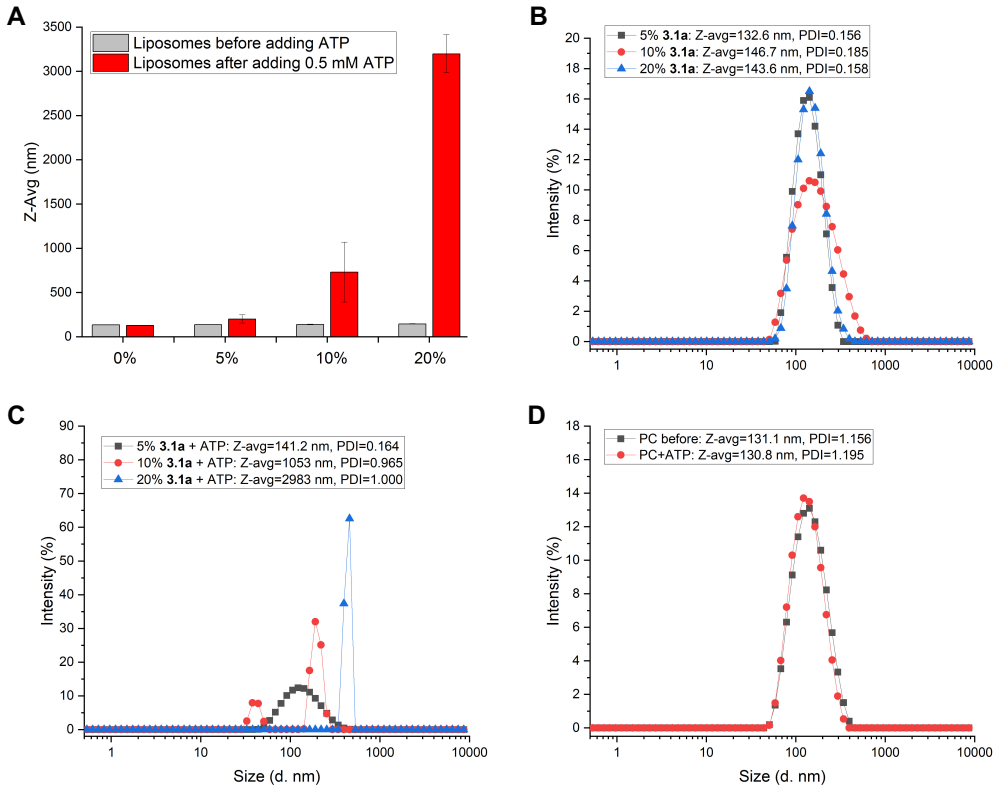


Figure 3.7. A. DLS analysis of PC-based liposomes containing different percentages of 3.1a encapsulating NR before and after ATP treatment. All samples showed uniformly sized particles pre-ATP addition. Increases in particle size were observed only for liposomes containing **3.1a** and the extent of increase correlated with the percentages of **3.1a** incorporated. Error bars indicate standard errors from at least three studies. **B**-**D**. DLS raw distribution curves of PC and **3.1a**/PC liposomes before and after ATP addition. Uniform size liposomes were formed in all cases before ATP treatment. After adding ATP, PC liposomes did not show any change, while significant changes were observed for 10% and 20% liposomes. Note: only representative sets of distribution curves are shown for liposomes after ATP treatment.

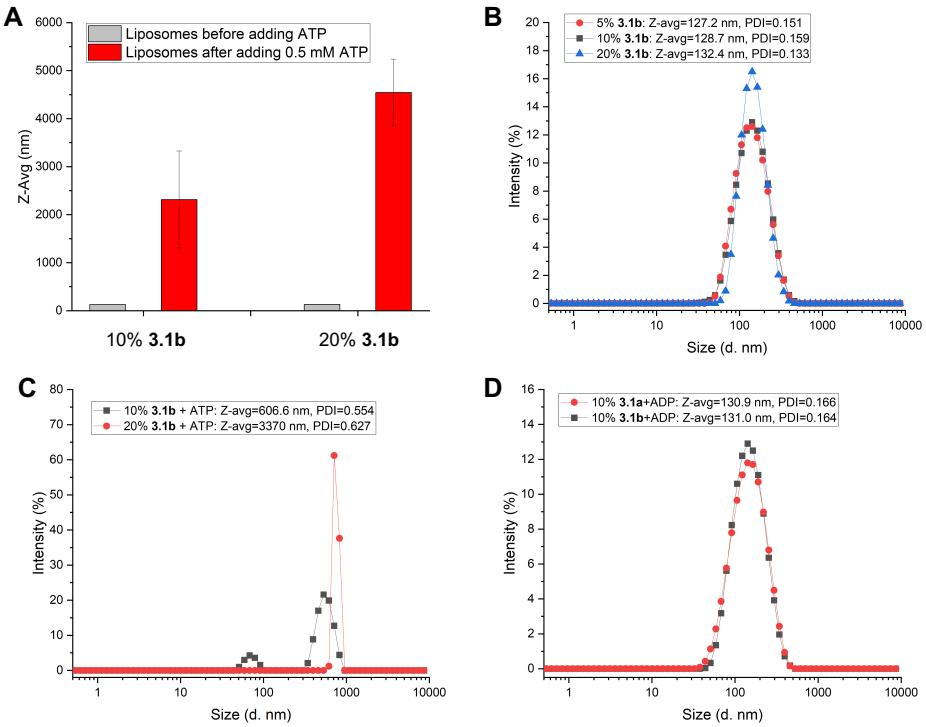


Figure 3.8. DLS results for liposomes containing 3.1b (A-C) and ADP selectivity for 3.1a or 3.1b liposomes (D). A. Grey bars indicate that uniformly sized 10% and 20% **3.1b** /PC liposomes were formed pre-ATP treatment. Dramatic size increases were observed after ATP addition. Error bars indicate standard errors from at least three studies. **B.** Raw distribution curves for 5%, 10%, and 20% **3.1b** liposomes before ATP treatment. **C.** Representative raw distribution curves for 10% and 20% **3.1b** liposomes after ATP treatment. Note: only representative distribution curves were shown for liposomes after ATP treatment. **D.** Raw distribution curves of 10% **3.1a**/PC and **3.1b**/PC liposomes upon ADP treatment. No changes in particle size were detected, indicating ADP did not induce a significant morphology change in these cases.

(Figure 3.9A). The morphology of **3.1a**/PC liposomes could not survive the negative stain treatment, which is likely due to the charge present on the membrane surface. As a result, we instead explored cryo-EM imaging, which verified the formation of stable unilamellar 10% **3.1a**/PC liposomes pre-ATP treatment (Figure 3.9B). Cryo-EM images for 10% liposomes after 1 minute ATP incubation showed drastic morphology changes (Figure 3.9 C-D) in which the original uniformly sized liposomes were replaced by multivesicular aggregates.

3.6. Fluorescence microscopy studies on liposome morphology changes

Since it is challenging to visualize particles with sizes in the micron range using EM techniques, we additionally implemented fluorescence microscopy to probe the formation of larger aggregates. In this experiment, PC liposomes containing 0 or 10% **3.1a** were labeled with 0.08% Rhodamine-PE (Rd-PE) and subjected to confocal fluorescence microscopy monitoring over time before and after ATP treatment. As can be seen in the captured images in Figure 3.10, while both liposomes initially showed very faint fluorescence (original liposome size below microscope resolution), only 10% **3.1a** liposomes generated highly fluorescent aggregates in the 2-3 μm size range after 15 minutes of ATP treatment. These results demonstrate changes in the physical properties of liposomes caused by the addition of ATP ligand, for which multiple plausible explanations exist. One possible reason for the size increases of lipid particles involves fusion of liposomes induced by changes in membrane packing. Additionally, changes in lipid structure could induce reorganization of lipids into alternate assemblies such as the inverted hexagonal phase.

3.7. Reversibility of NR release

Additionally, we pondered whether the NR release process might be a reversible phenomenon. To test this, ATPase enzyme was used to deplete ATP through hydrolysis into ADP and free phosphate ion. After adding ATP into 10% or 20% **3.1a** liposomes to trigger content release, ATPase was added, and fluorescence intensities were tracked over time. As is shown in Figure

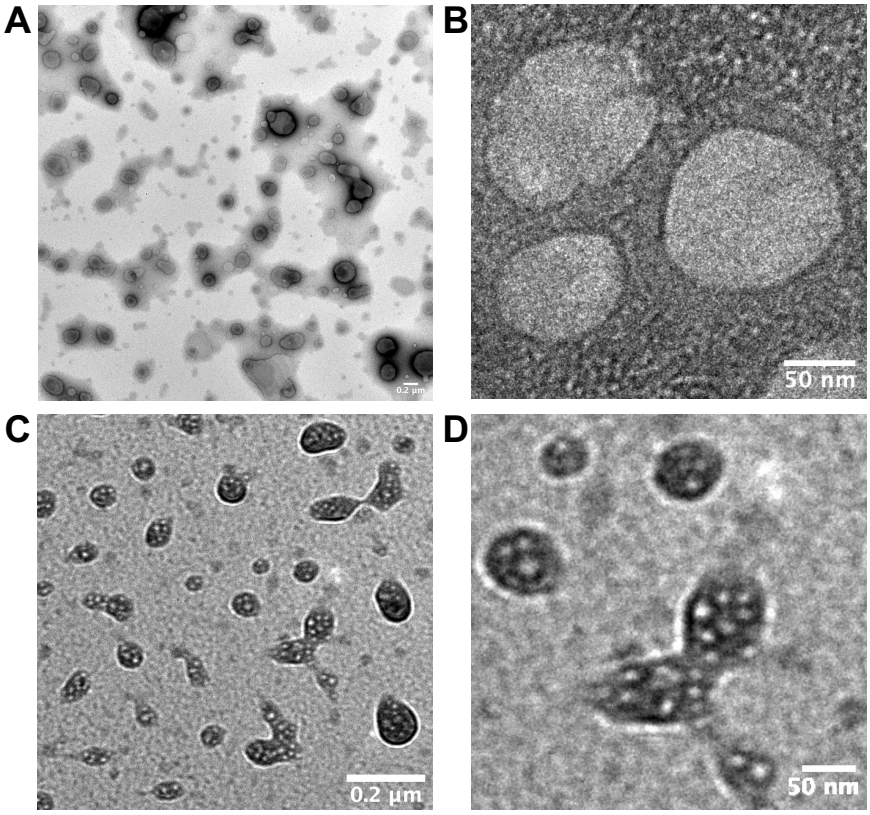


Figure 3.9. EM images of PC and 3.1a liposomes. A. TEM images of PC liposomes after ATP treatment stained with neutral phosphotungstic acid show intact liposomes. Scale bar denotes 200 nm. **B.** Cryo-EM image of 10% **3.1a**/PC liposomes before ATP addition. Unilamellar vesicles with expected diameters were observed under microscope. Scale bar denotes 50 nm. **C.** Cryo-EM image of 10% **3.1a** /PC liposomes after ATP addition, which instead showed complex multilamellar structures. Scale bar denotes 200 nm. **D.** Enlarged image from Figure 3.9C showing detailed structure of the aggregates. Scale bar denotes 50 nm.

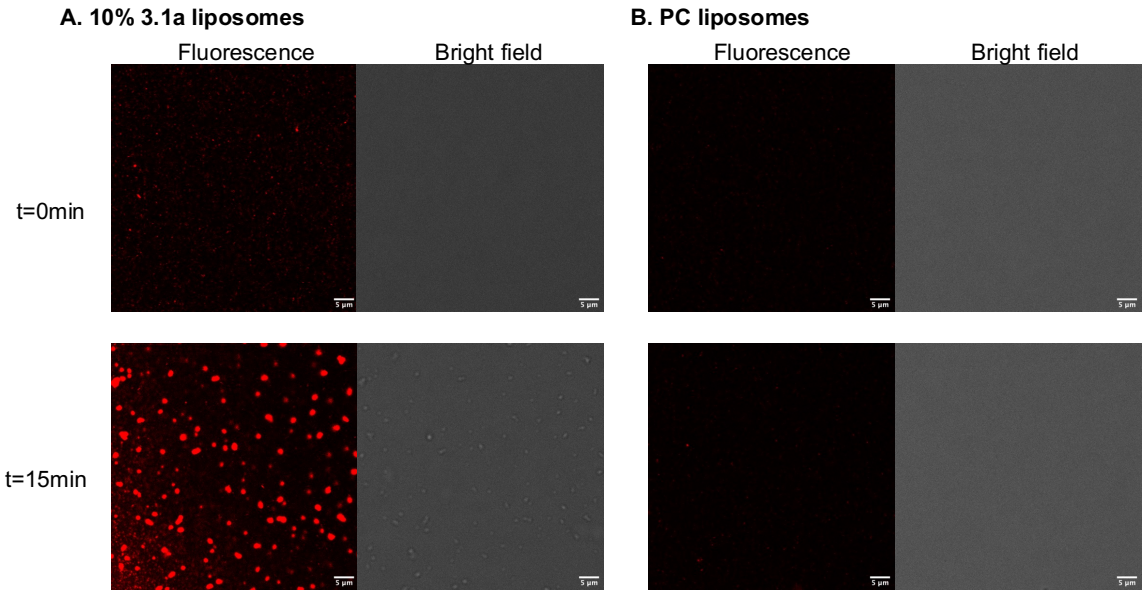


Figure 3.10. Fluorescence microscope images for 0% (B) or 10% 3.1a (A) liposomes labeled with Rd-PE before and after 15 minute incubation with 1 mM ATP. ATP treatment induced **3.1a** liposome aggregation and resulted in larger fluorescent particles under the microscope, while PC liposomes did not show aggregation after ATP incubation overtime. Scale bars denote 5 μm.

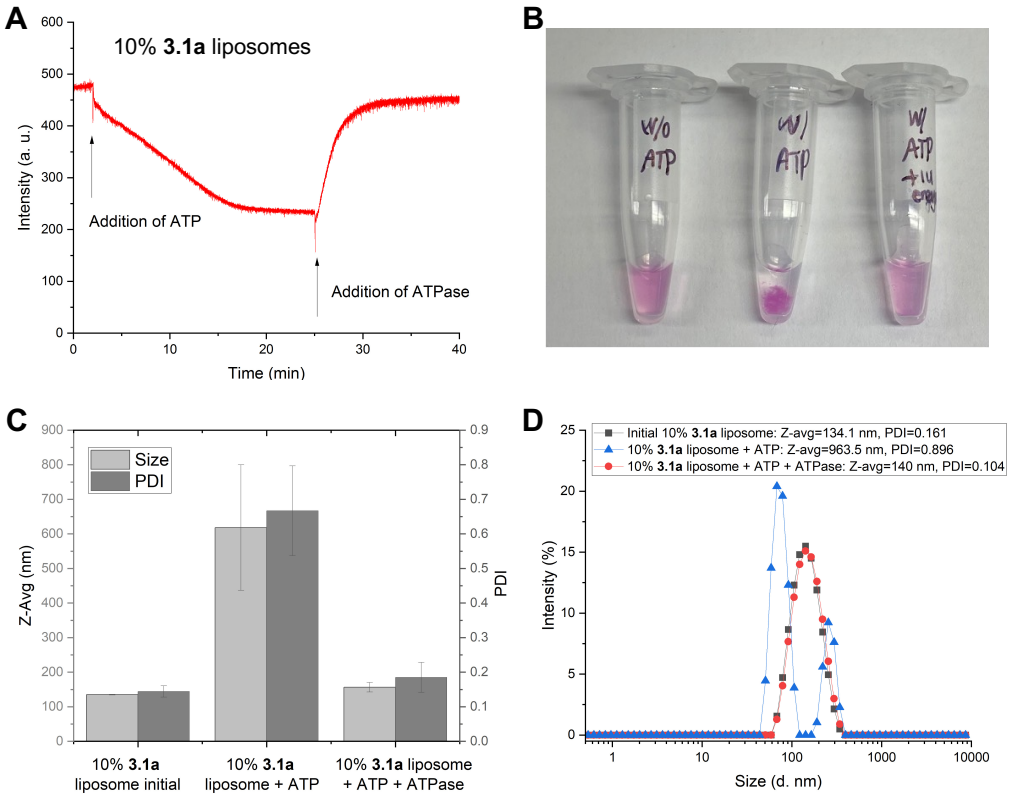


Figure 3.11. Reversibility test for Nile red release assay using 10% 3.1a liposomes. A. Kinetic curves for 10% **3.1a** liposomes treated with ATP followed by addition of ATPase. ATP addition induced NR release, while ATPase treatment completely restored NR fluorescence. **B.** Pictures for liposome solutions before and after ATP or ATP-ATPase treatment. From left to right: initial liposomes, liposomes after ATP treatment, liposomes after ATP and ATPase treatment. Pink precipitate was only observed at the bottom of the Eppendorf tube when liposomes were treated with ATP. **C.** DLS measurements for liposomes before and after ATP or ATP-ATPase treatment. ATP treatment resulted in increases in particle sizes, while subsequent ATPase treatment led to uniform size particles comparable to initial liposomes. **D.** Representative raw distribution curves for 10% **3.1a** liposomes before and after ATP or ATP-ATPase treatment.

3.11A, addition of ATPase to 10% liposomes post-ATP treatment completely restored NR fluorescence, and the pink precipitate observed after ATP treatment (Figure 3.11B) was re-dissolved, resulting in pink solutions. DLS experiments were again conducted to probe changes to self-assembly during this process and uniformly sized particles that were identical to initial liposomes were observed following ATPase (Figures 3.11C-D).

Interestingly, when the same experiments were conducted using 20% **3.1a** liposomes, only a partial restoration of original NR fluorescence was seen on the corresponding kinetic curve (Figure 3.12A), indicating that release from 20% **3.1a** liposomes is not completely reversible upon ATPase treatment. This was further supported by DLS analysis (Figures 3.12C-D), in which ATP treatment induced dramatic increases in particle sizes and subsequent ATPase addition only yielded partial decreases and did not result in particles with diameters comparable to initial liposomes. Additionally, pink precipitate could still be observed at the bottom of Eppendorf tubes after ATP and then ATPase addition (Figure 3.12B).

These reversibility results indicate that when lipid **3.1a** is incorporated at a low percentage (i.e., 10%), ATP treatment results in mild membrane reorganization that can be reversed when ATP in the system is consumed by ATPase enzyme. However, when **3.1a** is incorporated at a higher percentage (i.e., 20%), more significant changes in membrane packing likely occur that could lead to fusion, resulting in an irreversible release process. These results also match our ATP/ADP selectivity results. As previously discussed, when decreasing **3.1a** incorporation from 20% to 10%, we achieved selectivity for ATP over ADP and other phosphates (Figure 3.2). Therefore, ADP resulting from the hydrolysis of ATP by ATPase could still trigger content release for 20% **3.1a** liposomes, while that would not induce NR leakage from 10% **3.1a** liposomes. The ability to manipulate and reverse liposomal self-assembly properties is an exciting result that could be considered in the context of research investigating the origin of life and mimicking de novo membrane synthesis.[183]

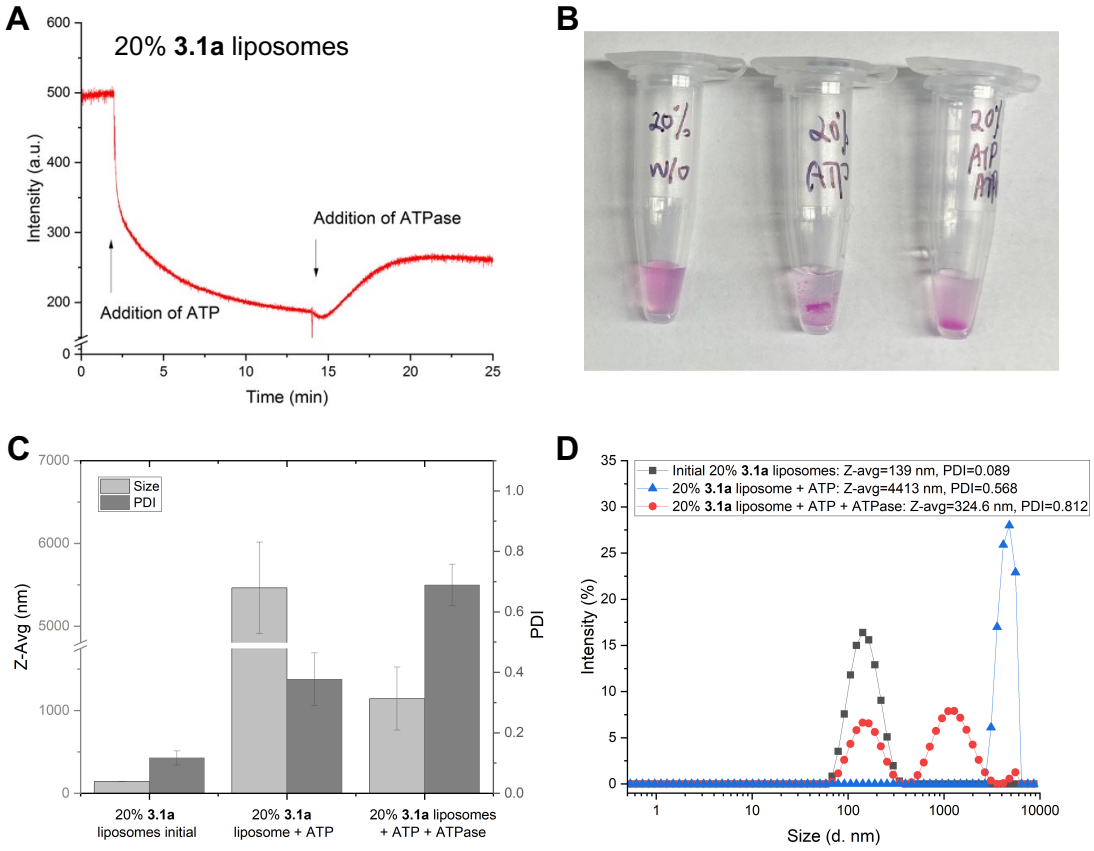


Figure 3.12. Reversibility test for Nile red release assay using 20% 3.1a liposomes. A. Kinetic curves for 20% **3.1a** liposomes treated with ATP followed by addition of ATPase. ATP addition induced NR release, and ATPase treatment only slightly restored NR fluorescence. **B.** Pictures for liposome solutions before and after ATP or ATP-ATPase treatment. From left to right: initial liposomes, liposomes after ATP treatment, liposomes after ATP and ATPase treatment. Pink precipitate was observed at the bottom of the Eppendorf tubes when liposomes were treated with ATP and ATP-ATPase. **C.** DLS measurements for liposomes before and after ATP or ATP-ATPase treatment. ATP treatment resulted in increases in particle sizes, and subsequent ATPase treatment did not result in uniform size particles comparable to initial liposomes. **D.** Representative raw distribution curves for 20% **3.1a** liposomes before and after ATP or ATP-ATPase treatment.

3.8. ATP triggered hydrophilic calcein release assay

Benefitting from the unique bilayer structure, liposomes are also capable of encapsulating and delivering hydrophilic cargo. Therefore, the release of polar contents from liposomes is also critical, particularly due to rapid recent advances in RNA therapies,[184,185] such as in recent COVID-19 vaccines, which are packaged in lipid nanocarriers. Therefore, we next studied the ATP-driven triggering of hydrophilic content release from PC liposomes containing **3.1a/3.1b**. For these investigations, we employed a calcein dye release assay, in which calcein fluorescence is initially quenched at high dye concentrations within liposomes, but is then restored upon release as it culminates in dilution.[186] Since calcein is non-specifically encapsulated within liposome interiors during preparation, size-exclusion chromatography (SEC) was performed after extrusion to remove unencapsulated dye. The formation of these calcein encapsulated liposomes was again supported by DLS (Figure 3.13). The results of this assay were calibrated through treatment with Triton X-100 detergent at the end of each titration to induce complete release. Data are reported as a percentage of the fluorescence intensity induced by Triton X-100 to show the percentage of total release and account for variations in dye inclusion among liposome samples. To evaluate ATP-responsive properties, we prepared calcein-encapsulated liposomes with 10% **3.1a** or **3.1b** in PC as well as control liposomes composed entirely of PC. As shown in the kinetic curves in Figure 3.14, PC liposomes containing 10% **3.1a** promoted ~70% calcein dye release within 30 min upon treatment with 10 mM ATP, while PC control liposomes lacking a lipid switch showed only minimal background release. Again, PC/**3.1b** liposomes showed comparable release efficacy (Figure 3.15). The potential reversibility of calcein release assay was also studied, but in this case ATPase treatment did not affect the kinetic release curve (Figure 3.16), indicating the hydrophilic content leakage is an irreversible process.

Polar calcein experiments were also carried out with diluted liposomes. To do so, purified 10% **3.1a**/PC liposomes post-SEC were further diluted 10X with isotonic buffer. Although release

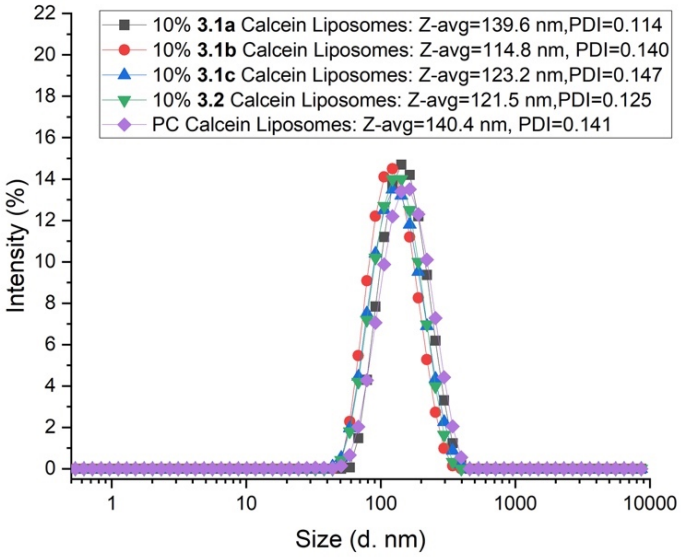


Figure 3.13. Raw distribution curves for calcein-encapsulated PC liposomes containing or lacking all lipid switches/controls studied herein. Stable and uniform liposomes were formed in all cases.

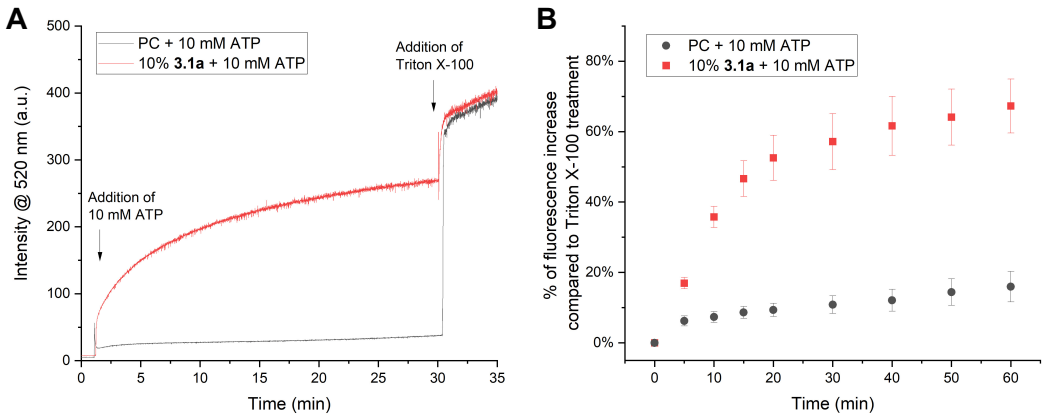


Figure 3.14. Calcein release results using 10% 3.1a/PC liposomes. A. Kinetic calcein release curves. Minimal increase in fluorescence intensity was observed for PC liposomes upon treatment with 10 mM ATP. After adding ATP to 10% **3.1a** /PC liposomes, significant increases in fluorescence were detected. Release was observed to be close to completion within 30 minutes. Triton X-100 detergent was added after fluorescence increases reached a plateau to induce 100% release and to calibrate this assay. One representative plot of at least three unique experiments is shown. **B.** Data are reported as percentages of fluorescence intensity increase relative to maximum fluorescence upon Triton X-100 treatment. More than ~70% release was observed within one hour. Error bars denote standard errors from at least three independent studies.

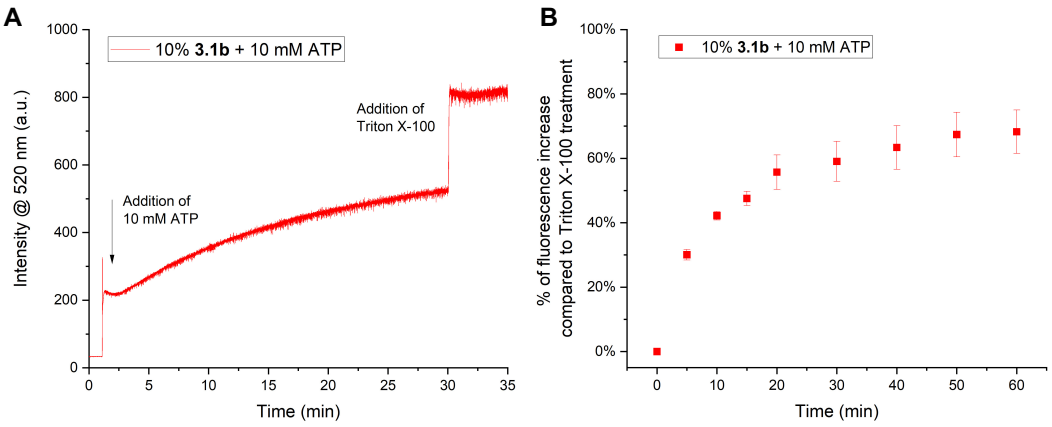


Figure 3.15. Calcein release results with 10% 3.1b/PC liposomes. A. Representative kinetic curve. An immediate increase in fluorescence was observed after adding 10 mM ATP. Triton X-100 was added at the end of the experiment to calibrate the assay and induce 100% release. **B.** Calcein release plots after data were converted to percentages of fluorescence intensity increase relative to maximum signal change upon Triton X-100 treatment. More than ~70% release was observed within one hour. Error bars denote standard errors from at least three independent studies

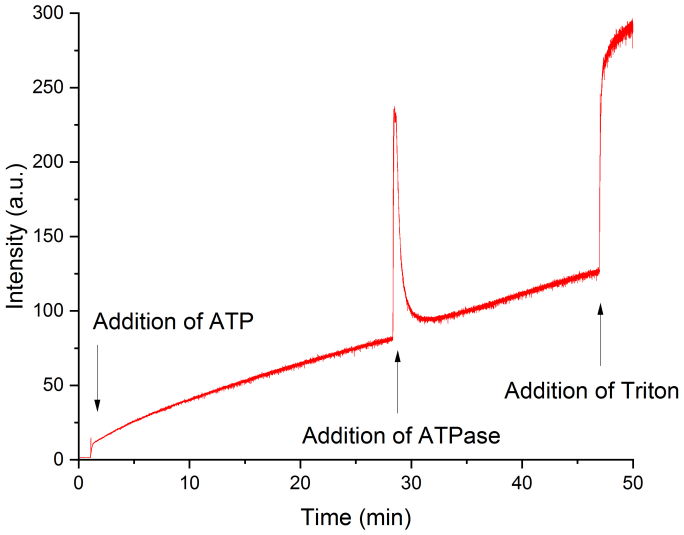


Figure 3.16. Reversibility test for calcein release assay using 10% 3.1a liposomes. ATPase addition did not affect the release process.

still occurred for diluted samples (Figure 3.17), only a slight drop in release percentages was observed (~50% compared to ~70%). This also suggests that fusion may be somewhat involved but is not a primary driving force for hydrophilic cargo release. Nevertheless, our results indicate that lipid switches **3.1a**-**3.1b** are effective for controlled release of both hydrophobic and hydrophilic cargo release triggered by ATP.

3.9. Techniques used to prove binding interactions between lipid switches and ATP

3.9.1. NMR titration and DOSY experiment

To explore whether liposome release is driven by binding interactions, the molecular recognition properties of the host switch **3.1a** towards ATP were next analyzed. First, ^{31}P NMR titration experiments were carried out to probe for spectral changes resulting from ATP binding.[187] To do so, **3.1a** was dissolved in *d*$_6$-DMSO in an NMR tube, which was subjected to titration with a solution of ATP in D_2O, with spectra recorded after each aliquot was added. After adding 1 mM ATP (traces A to B, Figure 3.18), an immediate shift in all three ^{31}P chemical shifts occurred, indicating binding interactions between **3.1a** and ATP. The greatest magnitude in shift change was observed for P_α and P_β, suggesting that these are closer in proximity to the binding interaction.

To investigate our proposed conformational change upon **3.1a**-ATP binding (Scheme 3.1), diffusion ordered spectroscopy (DOSY) experiments were conducted before and after addition of ATP in solution (Figure 3.19). We observed a decrease in diffusion coefficient, from (1.0793 ± 0.043) x 10^{-6} cm^2/s for **3.1a** and (1.142 ± 0.018) x 10^{-6} cm^2/s for ATP, to (0.987 ± 0.098) x 10^{-6} cm^2/s for **3.1a**-ATP. This result is in accordance with our model by indicating an increase in hydrodynamic radius per lipid molecule upon ATP binding. However, it should be noted that this experiment is performed in solution, and thus may not represent how **3.1a** behaves within the densely packed membrane environment.

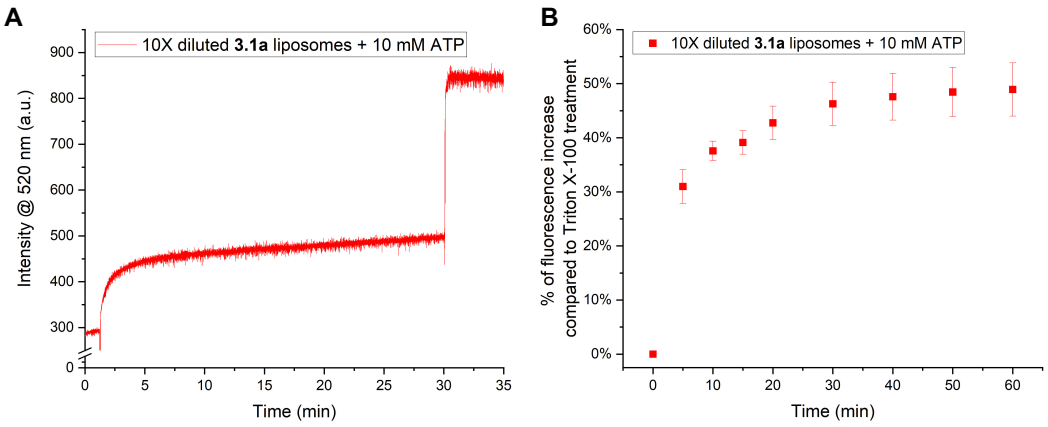


Figure 3.17. Calcein release results with 10X diluted 10% 3.1a/PC liposomes. A slight decrease in release percentage was observed. **A.** Representative kinetic curve. Immediate increase in fluorescence was observed after adding 10 mM ATP. Triton X-100 was added at the end to calibrate the assay and induce 100% release. **B.** Calcein release results after data were converted to percentages of fluorescence intensity increase relative to maximum signal change upon Triton X-100 treatment. ~50% release was observed within one hour. Error bars denote standard errors from at least three independent studies.

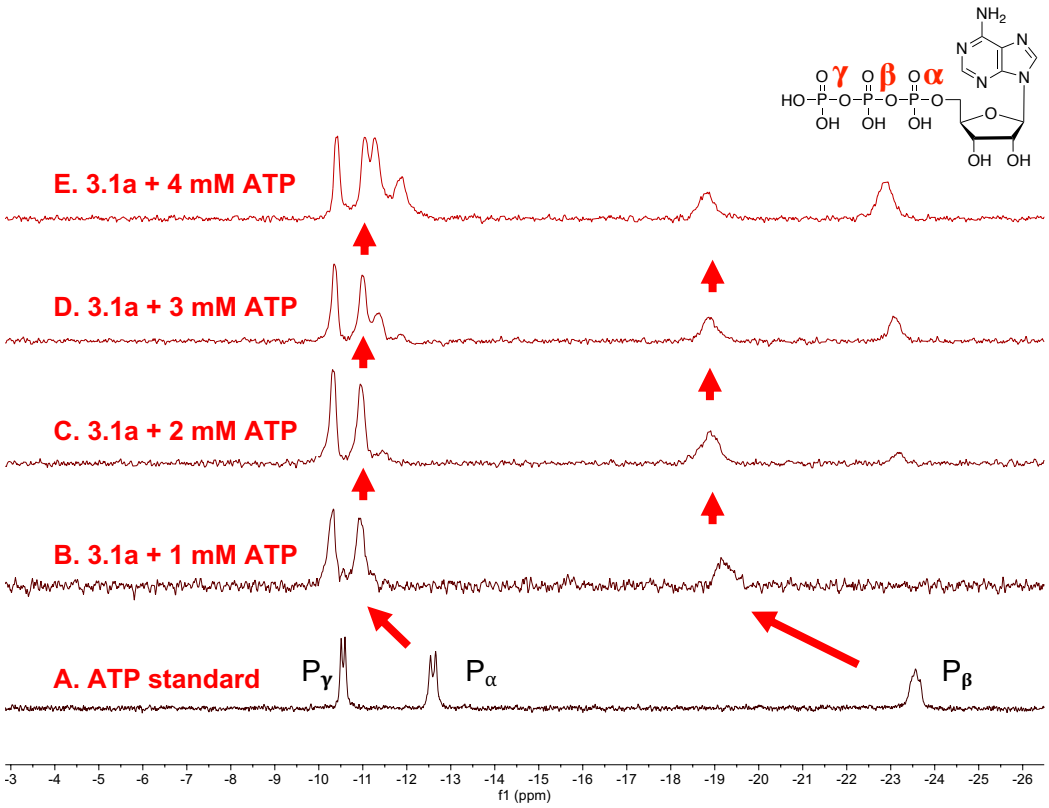


Figure 3.18. ^{31}P NMR spectra obtained from titration of free 3.1a lipid and ATP. Trace A. Free ATP. **Trace B-E:** 3 mM **3.1a** after adding 1-4 mM ATP. An immediate shift of P_α and P_β signals was observed after adding ATP to **3.1a**, indicating binding interactions between **3.1a** and ATP.

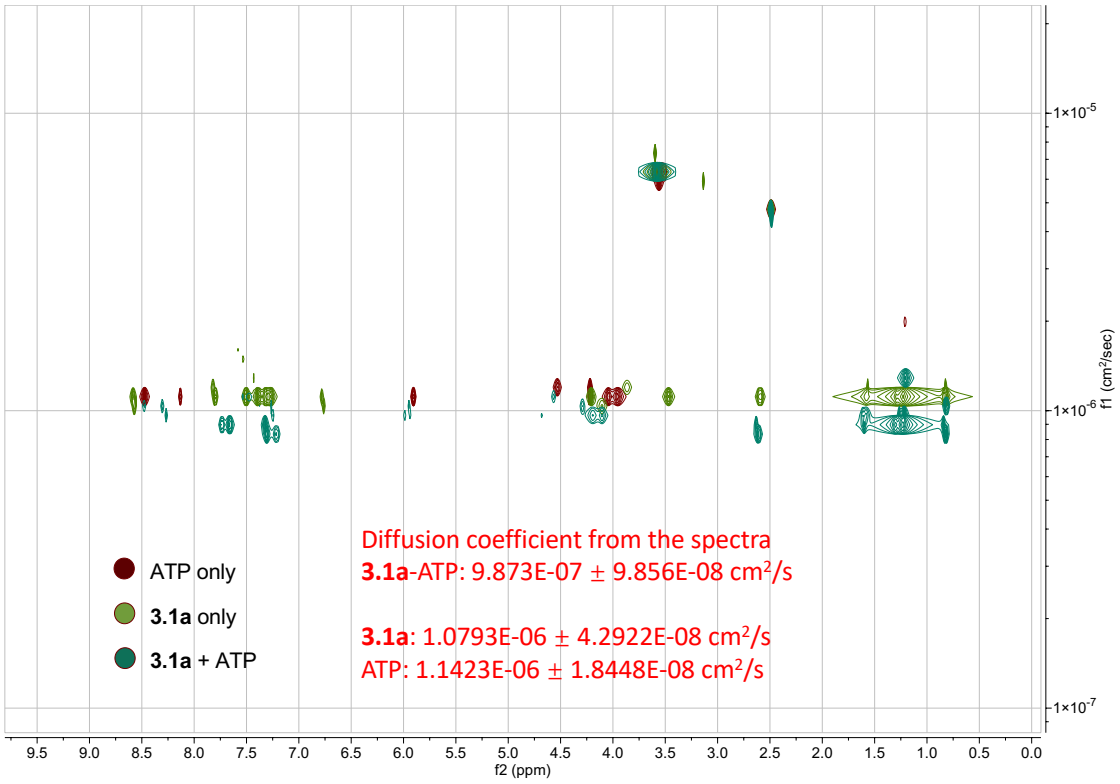


Figure 3.19. DOSY results for lipid 3.1a, ATP and 3.1a-ATP complex in *d*$_6$-DMSO containing 8% D_2O. 3.1a-ATP showed slightly lower diffusion coefficient, indicating an increase in area occupied per lipid molecule upon ATP binding.

3.9.2. UV-Vis titration experiment

UV-Vis titration experiments were also conducted to further probe binding. When compound **3.1a** in DMSO was titrated with ATP in H_2O, a decrease in absorbance along with a shift in λ_{max} was observed, further supporting direct **3.1a**-ATP binding (Figure 3.20). Attempts were made to eliminate ATP background absorbance by simultaneously titrating it into a separate reference cell, but this was complicated by the shifting of the host signal upon ATP binding (Figure 3.20A).

3.9.3. Zeta potential measurement

To probe binding interactions within a liposome environment, liposomes containing **3.1a** with and without ATP were evaluated by measuring zeta potential (ZP) values as an efficient means for analyzing surface charge. To do so, liposomes including 0%, 5%, or 10% of **3.1a** doped into PC were prepared and ZP values were measured before and after ATP treatment (Figure 3.21). Here, 100% PC liposomes initially showed slight negative charge, in agreement with literature,[188] and did not change much upon ATP incubation. For **3.1a**-liposomes, due to the presence of ZnDPA units on the lipid, initial liposomes were positively charged, and the degree of positive charge correlated with the percentage of **3.1a** present. After adding ATP, dramatic decreases in positive charge were detected, indicating that ATP is interacting with **3.1a** and counteracting the positive charge of the ZnDPA units of **3.1a**.

3.10. Development of alternative lipid structures to elucidate conformational changes

3.10.1. Design and synthesis of alternative lipid structures

Since we hypothesize that precise structural features are required to control conformational changes, we designed and synthesized additional lipid switches bearing different linkers and lipid chains (compounds **3.1c**-**d** and **3.2**, Figure 3.22) to determine effects on activity. Compared to **3.1a**, **3.1c** includes a longer and more flexible hexyl linker in between the two ZnDPA units, which was expected to diminish binding and release by increasing the cavity

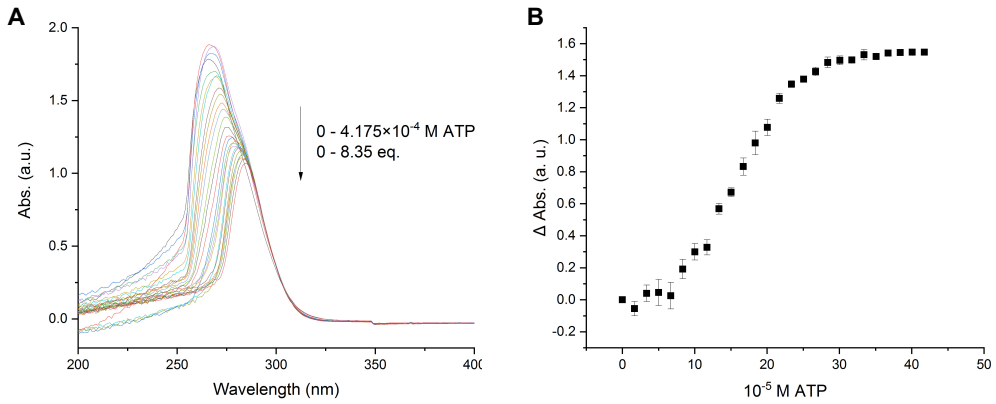


Figure 3.20. UV-Vis titration experiment with free 3.1a and ATP. Experiments were carried out in DMSO (**3.1a** concentration = 5×10^{-5} M). **A.** Raw absorbance spectra. After titrating ATP, **3.1a** showed a decrease in absorbance as well as a shift in its maximum absorbance peak. **B.** Binding isotherm for **3.1a**-ATP with absorbance changes at 265 nm plotted against amount of ATP added.

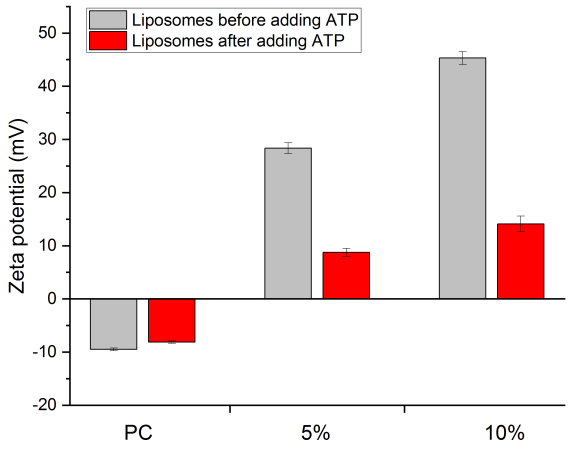


Figure 3.21. Zeta potential measurements for PC liposomes containing 0, 5%, or 10% 3.1a before and after adding ATP. Both 5% and 10% liposomes showed positive charge prior to ATP addition, with ATP addition yielding a reduction in positive charge. PC negative control liposomes showed only minimal ZP changes after ATP treatment.

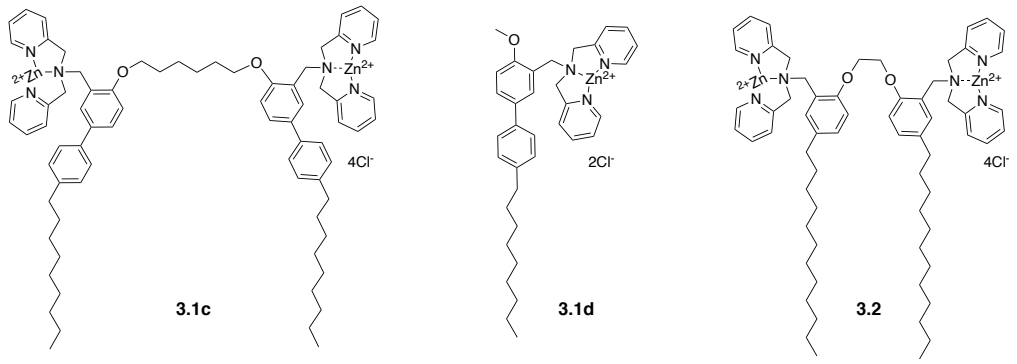
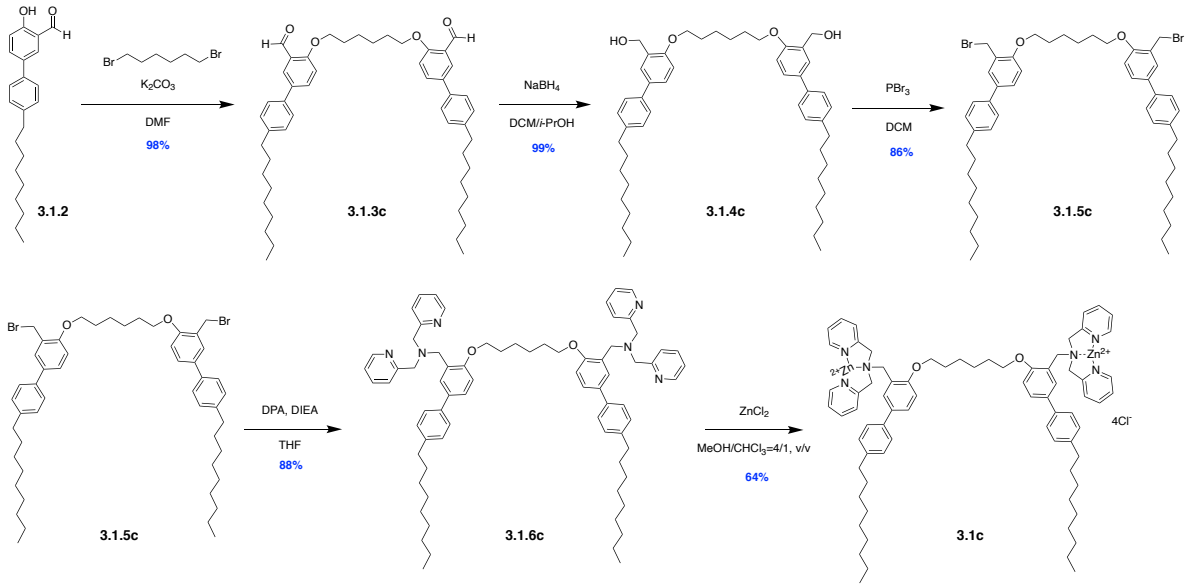


Figure 3.22. Structures of additional lipid switches designed to probe structural effects on activity. Compared to **3.1a**, **3.1c** bears a longer and more flexible hexyl linker. Compound **3.1d** contains only one ZnDPA binding unit. The rigidities of the lipid tails of **3.1a** were diminished by switching benzene rings to more flexible hydrocarbons in lipid switch **3.2**.

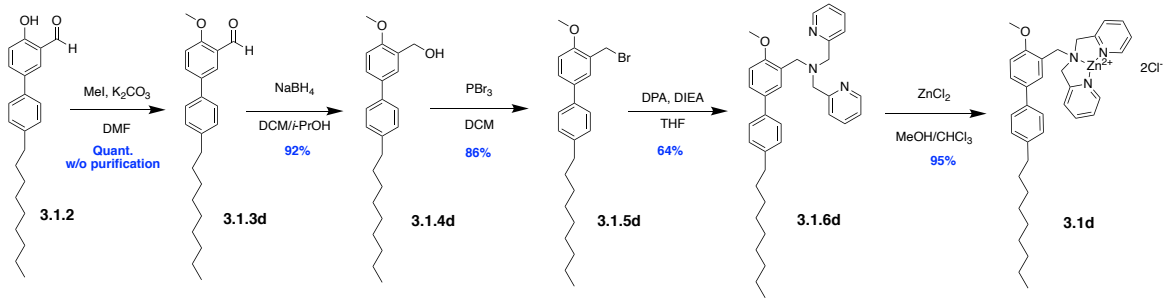
size and flexibility. Analog **3.1d** only contains one ZnDPA binding site. If we assume our lipid switches will be evenly distributed within liposomes comprised otherwise of PC, incorporating twice the percentage of **3.1d** compared to **3.1a** essentially mimics the longest and most flexible linker that is possible between ZnDPA units. Other than varying the linkers, compound **3.2** was modified within its lipid tails, in which we removed one aromatic ring (rigid) and replaced it with a more flexible C12 alkyl tail. The synthetic routes for these modified compounds are outlined in Schemes 3.3-3.5 which utilized similar strategies as were described for **3.1a** and **3.1b**.

3.10.2. Nile red release studies for all alternative lipids

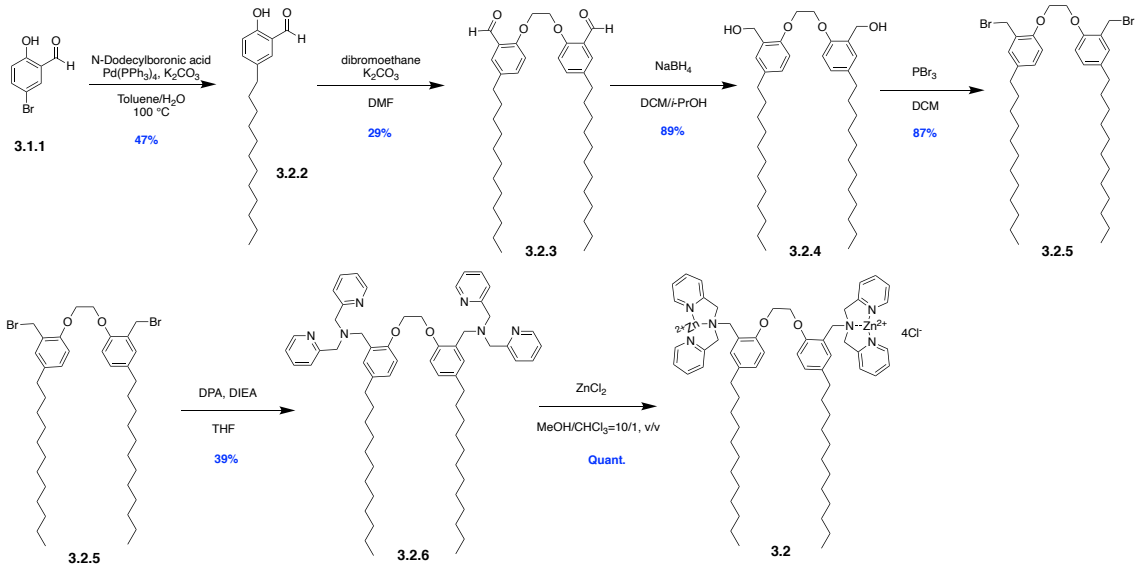
NR release efficacy and selectivity were next screened using PC-based liposomes doped with 10% or 20% **3.1c**-**d**/**3.2**. While these lipids generally remained effective for release upon ATP addition, as was expected, these compounds were overall less responsive. Compared to 10% **3.1a** liposomes, which showed release upon ATP, GTP as well as UTP addition, 10% **3.1c** liposomes exhibited reduced activity and responded only to ATP and GTP (Figure 3.23A-B). Similar results were observed for 20% **3.1d** liposomes, which contain the same number of ZnDPA binding sites on liposome surfaces as would 10% of **3.1a**-**c** (Figure 3.24A-B). Further decreasing **3.1d** incorporation to 10% completely abrogated release. Next, ATP-responsive properties of each compound were thoroughly evaluated by expanded NR release titration experiments using PC liposomes containing 5-20% of **3.1c**-**d**/**3.2** (Figures 3.23C-3.25C). While 10% **3.1a** and **3.1b** liposomes showed comparable ATP release properties, 10% **3.1c** liposomes exhibited much slower kinetics (Figure 3.23C), which were similar to 20% **3.1d** liposomes. Upon altering lipid chains, PC liposomes containing 10% **3.2** only responded to ATP among all the phosphorylated guest molecules we tested (Figure 3.25A-B). However, while 20% **3.1a**-**c** liposomes showed very fast release kinetics upon ATP binding, slightly slower release was observed for 20% **3.2** liposomes. In addition, 10% **3.2** liposomes showed an obvious longer induction period, indicating that rigidity within the tail also affects ATP binding/triggered release properties. Although π-π stacking interactions are known to be



Scheme 3.3. Synthetic route for alternative lipid switch 3.1c bearing a hexyl linker. A similar route was adapted from that of **3.1a-b**, except for the use of 1,6-dibromohexane to generate **3.1.3c**, which was followed by reduction to **3.1.4c**, bromination to **3.1.5c**, introduction of DPA units to **3.1.6c** and finally zinc chelation to **3.1c**.



Scheme 3.4. Synthetic route for alternative lipid switch 3.1d bearing only one ZnDPA binding unit. The alcohol group of **3.1.2** was methylated with iodomethane to generate **3.1.3d**, which was followed by reduction to **3.1.4d**, bromination to **3.1.5d**, introduction of DPA units to **3.1.6d** and finally zinc chelation to **3.1d**.



Scheme 3.5. Synthetic route for alternative lipid switch 3.2 bearing altered C12 alkyl tails. Compound **3.2.2** was first synthesized by Suzuki coupling between **3.1.1** and *N*-dodecylboronic acid. Next, a similar route was adapted from that of **3.1a-c**, including the use of 1,2-dibromoethane to generate **3.2.3**, which was followed by reduction to **3.2.4**, bromination to **3.2.5** introduction of DPA units to **3.2.6** and finally zinc chelation to **3.2**.

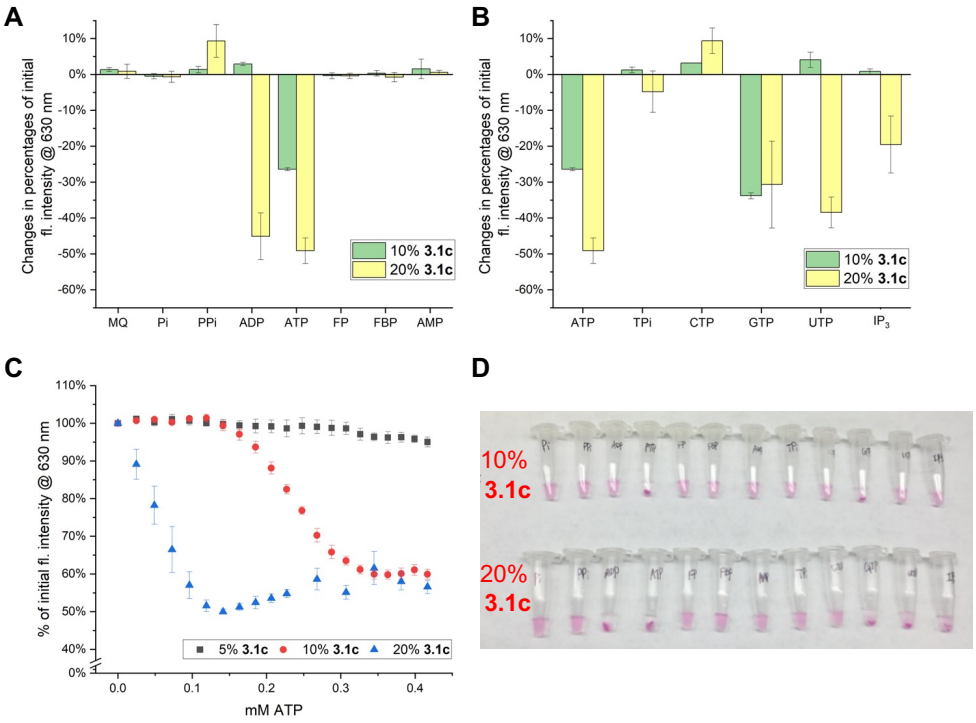


Figure 3.23. NR release results with liposomes composed of different percentages of 3.1c within PC. A. Phosphorylated metabolite selectivity screen results. 20% **3.1c** liposomes responded to ADP as well as ATP. By reducing **3.1c** incorporation to 10%, only ATP induced release. **B.** Triphosphate selectivity screen with 10% and 20% **3.1c** liposomes. While 20% liposomes showed release by ATP, GTP, UTP, and IP_3 treatment, 10% liposomes only released NR upon ATP and GTP addition. **C.** NR titration experiments using PC liposomes doped with 5%, 10% or 20% **3.1c**. Compared to **3.1a**, slower kinetics were observed for 10% **3.1c**/PC liposomes. **D.** Pictures taken from phosphorylated and triphosphate metabolite selectivity screens. In the cases where NR release occurred, pink precipitate could be observed at the bottoms of Eppendorf tubes. Top: 10% **3.1c** liposomes; Bottom: 20% **3.1c** liposomes. From left to right: Pi, PPi, ADP, ATP, FP, FBP, AMP, TPi, CTP, GTP, UTP, and IP_3.

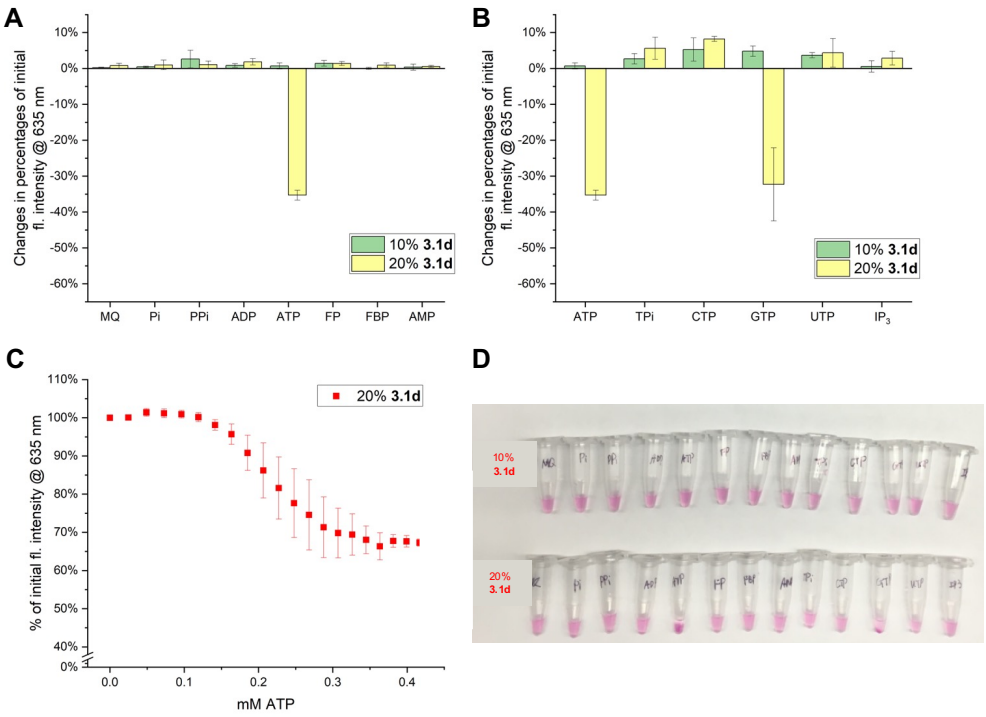


Figure 3.24. NR release results with liposomes composed of different percentages of 3.1d within PC. A. Phosphorylated metabolite selectivity screen results. 20% **3.1d** liposomes responded to ATP, while 10% did not respond to any phosphorylated metabolites tested. **B.** Triphosphate selectivity screen with 10% and 20% **3.1d** liposomes. While 20% liposomes showed release by ATP and GTP addition, reduction to 10%, again led to lack of release by any analyte tested. **C.** NR titration experiment with 20% **3.1d**/PC liposomes. Comparable release kinetics were observed compared to 10% **3.1c**/PC liposomes. **D.** Pictures taken from phosphorylated and triphosphate metabolite selectivity screens. In the cases where NR release occurred, pink precipitate could be observed at the bottoms of Eppendorf tubes. Top: 10% **3.1d** liposomes; Bottom: 20% **3.1d** liposomes. From left to right: MQ, Pi, PPi, ADP, ATP, FP, FBP, AMP, TPi, CTP, GTP, UTP, and IP_3.

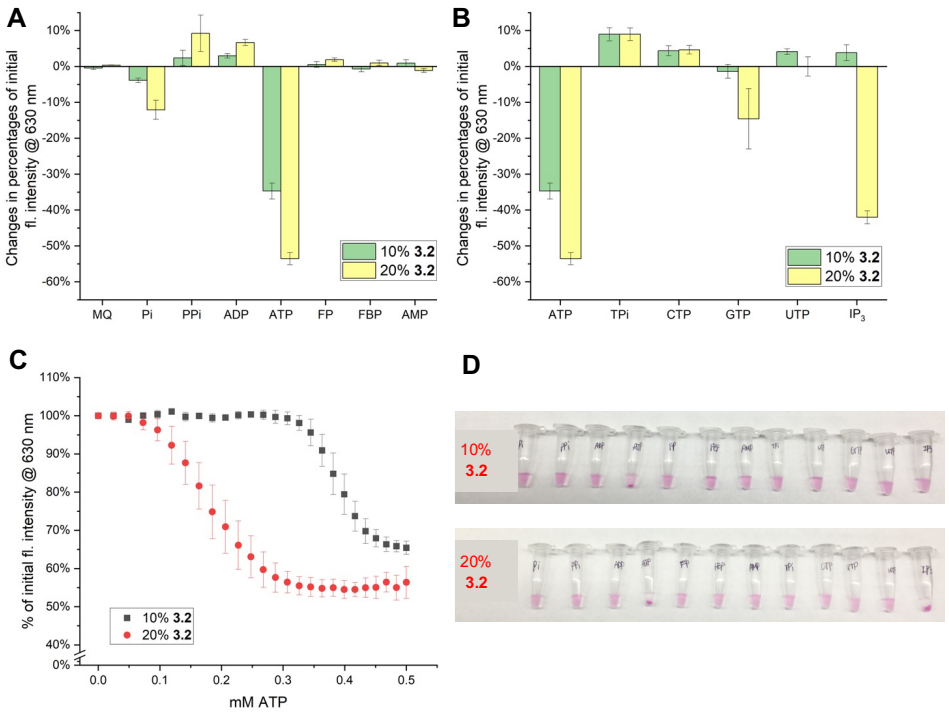


Figure 3.25. NR release results with liposomes composed of different percentages of 3.2 within PC A. Phosphorylated metabolite selectivity screen results. Both 10% and 20% **3.2** liposomes only responded to ATP. **B.** Triphosphate selectivity screen with 10% and 20% **3.2** liposomes. While 20% liposomes showed slight release by GTP and more IP_3 along with ATP treatment, 10% liposomes only responded to ATP. **C.** NR titration experiments with 10% and 20% **3.2**/PC liposomes. Compared to **3.1a**, much slower release kinetics were observed for both 10% and 20% **3.2** liposomes. **D.** Pictures taken from phosphorylated metabolite and triphosphate selectivity screens. In the cases where NR release occurred, pink precipitate could be observed at the bottoms of Eppendorf tubes. Top: 10% **3.2** liposomes; Bottom: 20% **3.2** liposomes. From left to right: Pi, PPi, ADP, ATP, FP, FBP, AMP, TPi, CTP, GTP, UTP, and IP_3.

involved in certain ATP sensors,[189] we don't expect a major contribution from this effect in our compounds, considering that these aromatic tails are far away from the binding sites, and are expected to be buried in the hydrophobic membrane, making them inaccessible to water-soluble ATP. Reductions in conformational changes induced by ATP binding provides a more reasonable explanation for the diminished release properties when switching rigid aromatic tails to more flexible aliphatic tails. NR release results using all lipid switches studied herein are summarized in Table 3.1.

3.10.3. DLS studies for all alternative lipids

DLS experiments were also carried out to probe size changes for liposomes containing different percentages of **3.1c** and **3.2** before and after adding ATP (Figures 3.26-3.27). These once again showed uniformly sized particles pre-ATP treatment with desired diameters, indicating stable liposome formation, followed by particle size increases post-ATP accompanied by precipitation (Figures 3.23D-3.25D).

3.10.4. Calcein release studies for all alternative lipids

Calcein release properties were also evaluated for 10% **3.1c** and **3.2** liposomes, with formation of uniformly sized particles verified by DLS analysis (Figure 3.13). Both of these compounds triggered ~60% calcein release upon 10 mM ATP treatment within 30 minutes, as is shown in the release curves as well as sample raw kinetic curves in Figures 3.28-3.29. These results indicate a slight decrease in the extent of release driven by **3.1c** and **3.2** compared to **3.1a** liposomes.

These results indicate that increasing flexibility in both the linker between ZnDPAs (**3.1c**) and in the lipid chains (**3.2**) indeed reduced liposome release via these lipid switches by ATP and other metabolites we tested. This also supports that maintaining a proper cavity size is critical for effective molecular recognition events and/or conformational changes that drive release.

Table 3.1. Summary of phosphorylated/triphosphate metabolite screen results using NR release assay with all lipid switches studied herein. Fluorescence readings were taken immediately after phosphorylated metabolites addition. For triphosphates, measurements were taken after 5 min incubation. ("--" denotes did not release; "NA" denotes did not test)

Entry	Liposome	Pi	PPi	ADP	ATP	FP	FBP	AMP	TPi	CTP	GTP	UTP	IP_3
1	PC	--	--	--	--	--	--	--	--	--	--	--	--
2	5% **3.1a**	--	--	--	~40%	--	--	--	--	--	--	--	--
3	10% **3.1a**	--	--	--	~40%	--	--	--	--	--	~40%	~40%,	--
4	20% **3.1a**	--	--	~40%	~60%	--	--	--	NA	NA	NA	NA	NA
5	10% **3.1b**	--	--	--	~40%	--	--	--	--	--	~40%	~5%	--
6	20% **3.1b**	--	--	~40%	~60%	--	--	--	NA	NA	NA	NA	NA
7	10% **3.1c**	--	--	--	~30%	--	--	--	--	--	~40%	--	--
8	20% **3.1c**	--	--	~40%	~40%	--	--	--	--	--	~50%	~40%	~30%
9	10% **3.1d**	--	--	--	--	--	--	--	--	--	--	--	--
10	20% **3.1d**	--	--	--	~40%	--	--	--	--	--	~40%	--	--
11	10% **3.2**	--	--	--	~40%	--	--	--	--	--	--	--	--
12	20% **3.2**	~10%	--	--	~60%	--	--	--	--	--	~15%	--	~40%

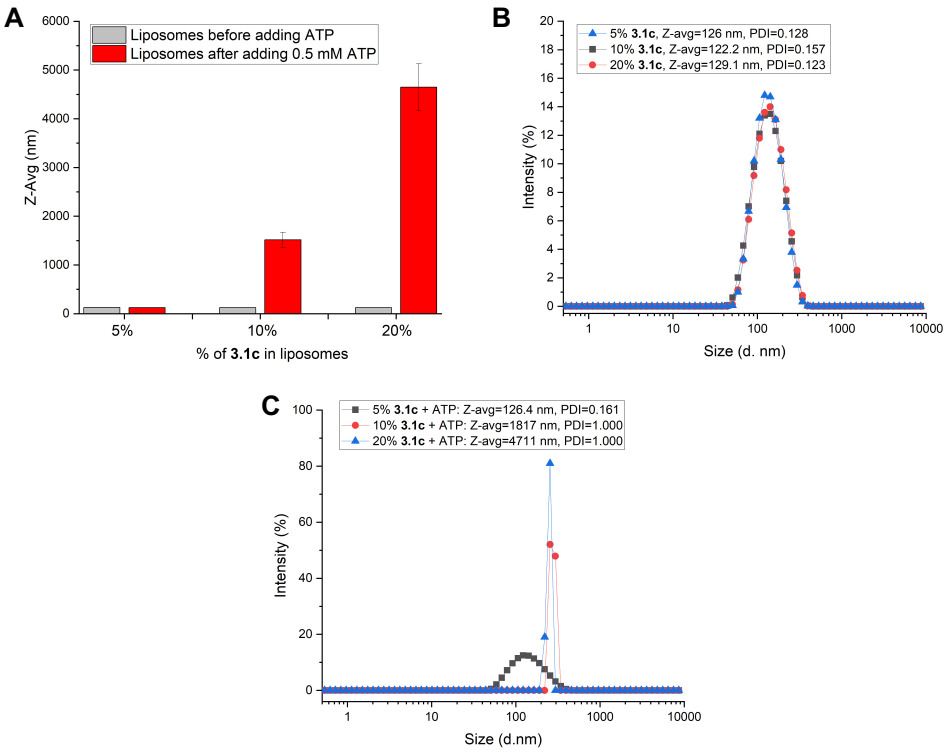


Figure 3.26. DLS results for liposomes containing 3.1c before and after ATP treatment. **A.** Grey bars indicate uniformly sized **3.1c** liposomes were formed pre-ATP treatment. Dramatic size changes were observed after ATP addition for 10% and 20% **3.1c** liposomes. Error bars indicate standard errors from at least three studies. **B.** Representative raw distribution curves for **3.1c** liposomes before ATP treatment. **C.** Representative raw distribution curves for **3.1c** liposomes after ATP treatment.

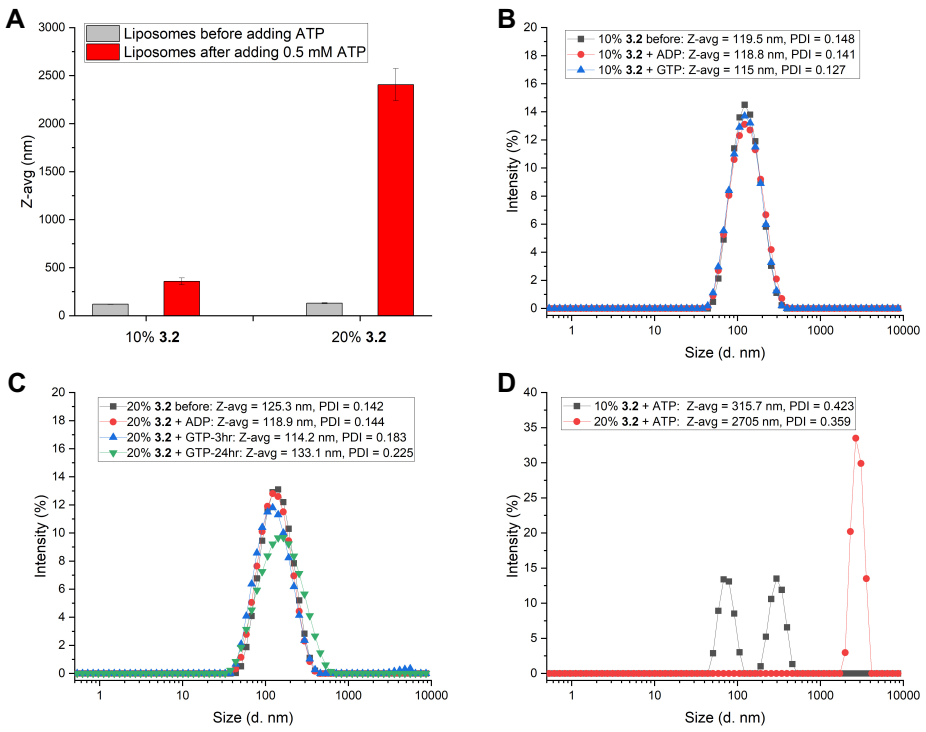


Figure 3.27. DLS results for liposomes containing 3.2 before and after ATP treatment. A. Grey bars indicate uniformly sized **3.2** liposomes were formed pre-ATP treatment. Dramatic size changes were observed after ATP addition. Error bars indicate standard errors from at least three studies. **B-C.** Representative raw distribution curves for **3.2** liposomes before ATP treatment and after ADP/GTP treatment. Uniformly sized particles were observed in all cases. **D.** Representative raw distribution curves for **3.2** liposomes after ATP treatment.

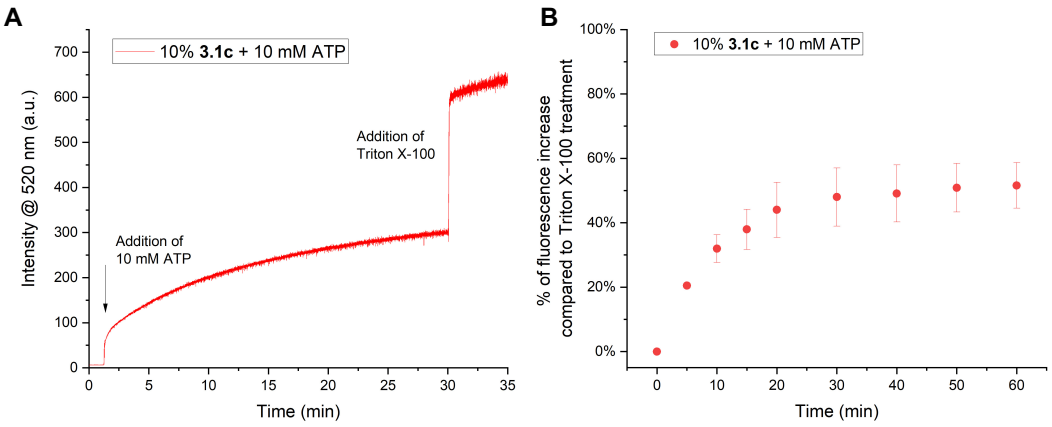


Figure 3.28. Calcein release results using 10% 3.1c/PC liposomes. A. Representative kinetic curve. Immediate increases in fluorescence were observed after adding 10 mM ATP. Triton X-100 was added at the end of experiments to calibrate the assay and induce total release. **B.** Data were converted to percentages of fluorescence intensity increases relative to maximum signal changes upon Triton X-100 treatment. More than ~50% release was observed within one hour. Error bars denote standard errors from at least three independent studies.

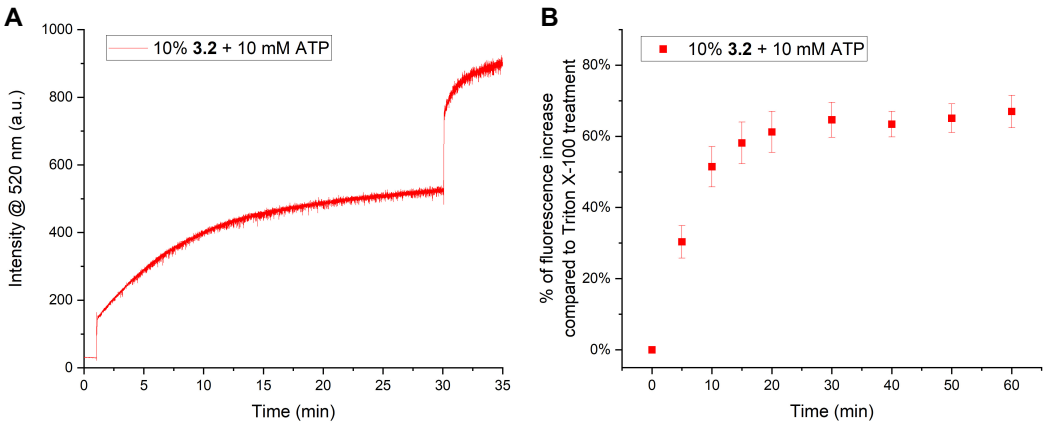


Figure 3.29. Calcein release results using 10% 3.2/PC liposomes. A. Representative kinetic curve. Immediate increases in fluorescence were observed after adding 10 mM ATP. Triton X-100 was added at the end to calibrate the assay and induce total release. **B.** Data were converted to percentages of fluorescence intensity increase relative to maximum signal change upon Triton X-100 treatment. More than ~60% release was observed within one hour. Error bars denote standard errors from at least three independent studies.

Further increasing the linker length beyond hexyl did not cause significant changes in activity. These results support our hypothesis that controlling the spacing of binding groups within lipid switches is critical for optimizing conformational changes that drive release. Furthermore, by diminishing general activity toward phosphorylated biomolecules, our results support that we achieved greater selectivity towards ATP, since activities toward other metabolites were decreased to a greater extent.

3.11. Cellular delivery studies

3.11.1. Delivery studies with untreated cells

After demonstrating the successful design of stimuli-responsive liposomes that selectively release contents in the presence of ATP, we next conducted fluorescence microscopy experiments to determine whether **3.1a** liposomes are a viable means to deliver encapsulated molecules to cells. Additionally, we determined if cargo release is controlled by ATP levels. These experiments were performed in collaboration with Dr. Francisco Barrera's lab in the UTK BCMB and led by graduate student Jennifer Schuster. For these experiments we employed PC-based liposomes containing 5% **3.1a**, a percentage determined to exhibit ATP-selectivity in release studies, which were also doped with 0.08% Rd-PE. This fluorescently tagged lipid enables facile detection of liposome cellular uptake using optical microscopy techniques. Liposomes were incubated with A375 melanoma cells for 30 minutes at 37 °C in a CO_2 environment, washed to remove unbound liposomes, labeled with DAPI (cell nuclei), fixed, and mounted on glass slides for imaging. In initial experiments, cells treated with 5% **3.1a** liposomes (Figure 3.30B) were compared to those subjected to PC control liposomes (Figure 3.30A), which showcased a drastic enhancement in Rd fluorescence resulting from cellular delivery. Corrected total cell fluorescence (CTCF) values showed a ~1,000-fold increase in cell delivery driven by **3.1a** (Figure 3.30C). These results indicate that **3.1a** is effective for driving liposomal cell entry.

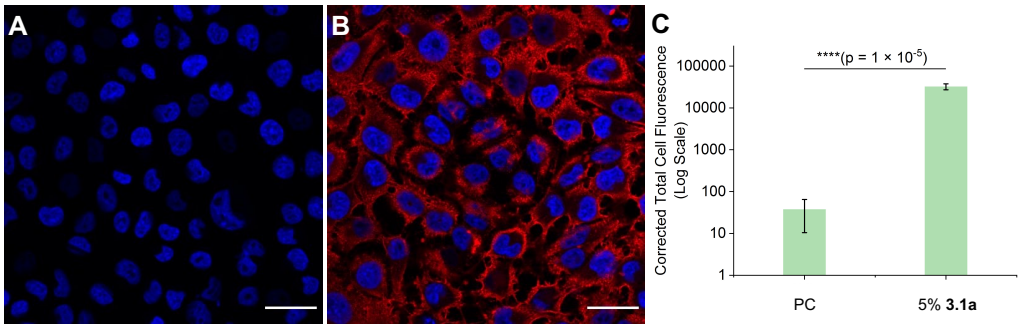


Figure 3.30 Fluorescence images of A375 cells treated with PC/Rd-PE liposomes (A) or 5% 1a/PC/Rd-PE liposomes (B) for 30 minutes. The presence of **3.1a** increases cellular uptake of liposomes while PC liposomes without **3.1a** showed minimal cellular infiltration. Blue: DAPI. Red: Rd-PE. Scale bars are 30 μm. **C.** Quantified corrected total cell fluorescence via ImageJ. Statistical analysis (t-test) indicates there is a significant increase ($p=1.7 \times 10^{-5}$) in uptake when 5% **3.1a** is present in PC liposomes. N=4. Error bars indicate standard deviation from the mean.

3.11.2. Delivery studies with inhibitor-treated cells for intracellular ATP manipulation

We next worked to ascertain the dependence of cellular delivery on ATP abundance, in which drugs were employed that modulate intracellular ATP biosynthesis. Specifically, combined treatment with Antimycin A (AA) and 2-deoxy-D-glucose (DG) was first conducted to inhibit mETC complex III and glycolysis, respectively, which decreases intracellular ATP levels.[190] Treatment with 5-aminoimidazole-4-carboxamide-1-ß-riboside (AICAR), on the other hand, increases intracellular ATP concentrations by activating AMPK.[191] Intracellular ATP concentrations upon inhibitor treatment were quantified using a commercially available luminescent ATP detection assay kit (Figure 3.31A).

Modulation of ATP concentrations led to profound effects on cellular delivery. Treatment with AA/DG to diminish intracellular ATP resulted in a significant decrease in cellular uptake (Figure 3.32C) compared to untreated cells (Figure 3.32A). Conversely, increase of ATP abundance using AICAR instead culminated in significantly increased uptake (Figure 3.32D). A control containing diluted DMSO (Figure 3.32B) was also run since AA was dissolved in DMSO. In all cases, fluorescence intensities were quantified, as indicated in Figure 3.32E. The data resulting from pharmacological ATP modification indicate that cellular delivery changes do not merely arise from different degrees of endocytosis. While cells with downregulated ATP resulting from treatment with AA/DG did yield some labeling, the minimal amount of delivery observed in these experiments may potentially result from the ability of ZnDPA groups to interact with cell surfaces by binding to anionic phospholipids.[171]

3.11.3. MTS assay

Cell viability in the presence of ATP-responsive liposomes was also measured using an MTS assay using 0% or 5% **3.1a**/PC liposomes and we did not observe any diminished cell growth for **3.1a** liposomes (Figure 3.33).

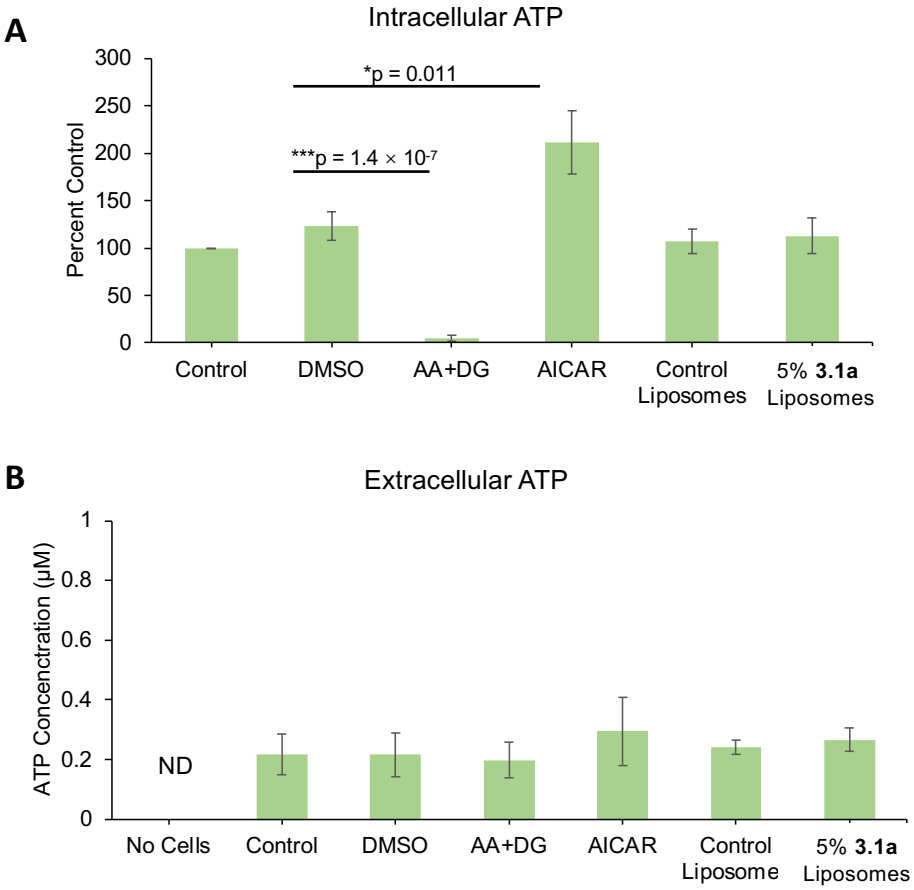


Figure 3.31. ATP assay of intracellular (A) and extracellular (B) ATP levels. A. Cells were treated with the vehicle control, DMSO, AA and DG simultaneously (1 hr), AICAR (3 hr), and liposomes with and without **3.1a** (30 minutes). Statistical analysis (one-way ANOVA ($p = 5.8 \times 10^{-13}$) with post hoc Dunnet T3) shows significant differences between DMSO and drug conditions, but no changes with liposomes. **B.** ATP levels were below the detection limit (ND) for media in the absence of cells. Low levels (~0.2 µM) of ATP were detected in media after cell incubation. There are no statistically significant ATP changes in any treatment conditions. N=3-5. Error bars indicate standard deviation from the mean.

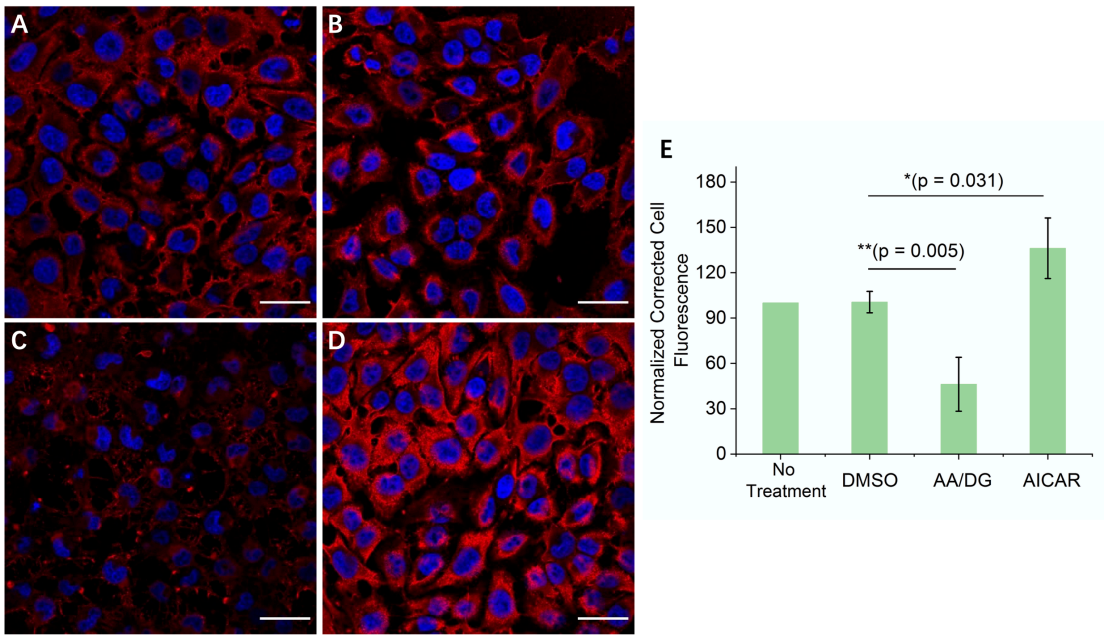


Figure 3.32. Fluorescence images of control cells (A), control cells including diluted DMSO (B), cells treated with AA/DG (C), or AICAR (D) followed by addition of PC/3.1a (5%)/Rd-PE liposomes for 30 minutes. Intracellular ATP modifications affect cellular uptake of vesicles containing lipid **3.1a**. Upregulating intracellular ATP increased liposome uptake, while down-regulating ATP level decreased uptake. Blue: DAPI. Red: Rd-PE. Scale bar is 30 μm. (**E**) CTCF values normalized to the untreated cell condition. One-way ANOVA (p=0.0003) with post-hoc Tukey showed a significant decrease in uptake when cells were pre-treated with AA/DG and a significant increase in uptake when cells were pretreated with AICAR. N=3-4. Error bars show the standard deviation from the mean.

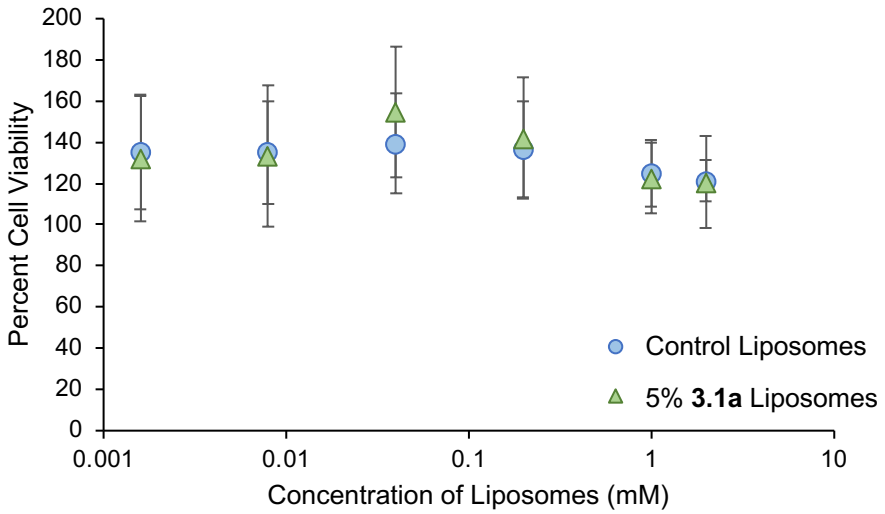


Figure 3.33. MTS assay indicating 3.1a does not affect cell viability. Cells were treated with Control (blue circle) or 5% **3.1a** (green triangle) liposomes at 2 mM, 1 mM, 200 μM, 40 μM, 8 μM, 1.6 μM, or 0 μM for 30 minutes and then washed and allowed to incubate for 24 hr, at which time MTS reagent was used to determine cell viability. 100% viability corresponds with cells treated with buffer only. N=3 and error bars denote standard deviation from the mean.

Overall, these results culminate in the conclusion that cellular delivery of **3.1a** liposomes is indeed driven by ATP and correlates with ATP concentrations. One potential explanation for this result involves literature evidence that intracellular ATP is released from cells through both active and passive pathways, especially in the case of dying or damaged cells.[192,193] Furthermore, **3.1a** liposomes can potentially interact with cell membranes and induce transient pore formation, which is a known mechanism by which cationic peptides and DNA/lipoplexes can induce intracellular ATP leakage.[194] To explore these possibilities, we measured extracellular ATP abundance and found that sub-micromolar levels were present in the cellular environment (Figure 3.31B). Since the results shown in Figure 3.2C indicate that release from liposomes containing **3.1a** requires significantly higher ATP concentrations, we therefore conclude that these low extracellular ATP levels are unlikely to play an important role in cellular delivery. Furthermore, we determined that **3.1a** liposomes do not promote ATP cellular leakage (Figure 3.31B). We instead propose that the higher levels of ATP contained within late endosomes may constitute the main source of ATP that drives liposome release. The notion that intracellular ATP is key for cargo release is supported by the results obtained with AA/DG and AICAR (Figure 3.32E). In accordance with these results, we propose that intracellular ATP compromises **3.1a** liposomes following their uptake into cells, resulting in their decomposition and release of contents.

3.11.4. Initial colocalization experiments

Fluorescence microscopy can also be used for probing the route by which liposome formulations deliver cargo to cells, which may proceed through multiple potential pathways. This may occur through traditional endocytosis mechanisms such as pinocytosis, after which liposomes would be expected to fuse to endosomes or lysosomes, which can be distinguished based on subcellular localization observed through fluorescence microscopy. Liposomes could also fuse to cell membranes causing direct release into the cytosol, in which case cargo will not be observed in endosomes or lysosomes. It is also possible that leakage may be triggered

by extracellular metabolites, causing release in the periphery of cells that can lead to uptake. By staining different cell compartments and colocalization techniques, we may determine the subcellular localization of the delivered fluorophores.

In preliminary experiments, we initiated fluorescence colocalization studies to determine the cargo delivery route using ATP-responsive lipid **3.1a**. Our initial studies focused on mitochondria since this organelle generates most cellular ATP, which was assessed by analyzing colocalization between red (Rd-PE from liposomes) and green (MitoTracker Deep Red-FM) channels using Coloc2 in ImageJ. As is indicated in the microscopy image shown in Figure 3.34, fluorescent liposomal components did not colocalize with mitochondria. The average Pearson's coefficient was calculated to be -0.208 (using 3 replicates), indicating negative correlation between Rd-PE and mitochondrial locations. Future works of performing systematic colocalization studies with other organelles to assess subcellular localization of liposome cargo are desired.

3.12. Miscellaneous experiments

3.12.1. Biphenyl- and naphthyl- linker compound synthesis

In this project, we intended to synthesize multiple targets by changing the linkers and lipid tails in order to tune the degree of confirmational changes. While we reported the synthesis and release properties for lipid switches **3.1a**-**3.1c** bearing ethyl, *p*-xylene and hexyl linkers, additional efforts have been made to further increase the linker length and rigidity. Synthetic attempts towards lipid switches bearing a biphenyl linker (**3.1e**) as well as a naphthyl linker (**3.1f**) (Scheme 3.1) were also made utilizing strategies similar to those described previously. Their synthetic routes are shown in Scheme 3.6. Different linkers were introduced by treating **3.1.2** with 4,4'-bis(bromomethyl)-1,1'-biphenyl or 2,6-bis(bromomethyl)naphthalene, leading to di-aldehyde compounds **3.1.3e-f**, which were reduced into primary alcohols **3.1.4e-f** with $NaBH_4$. However, when treating them with PBr_3, the reactions did not proceed as expected

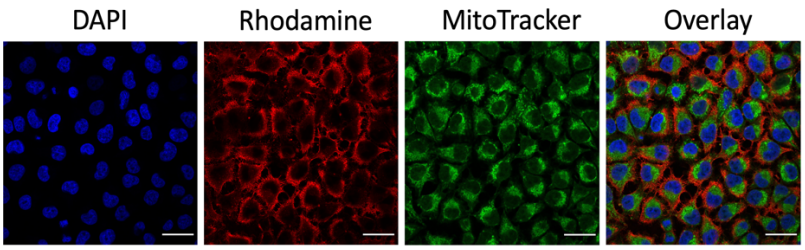
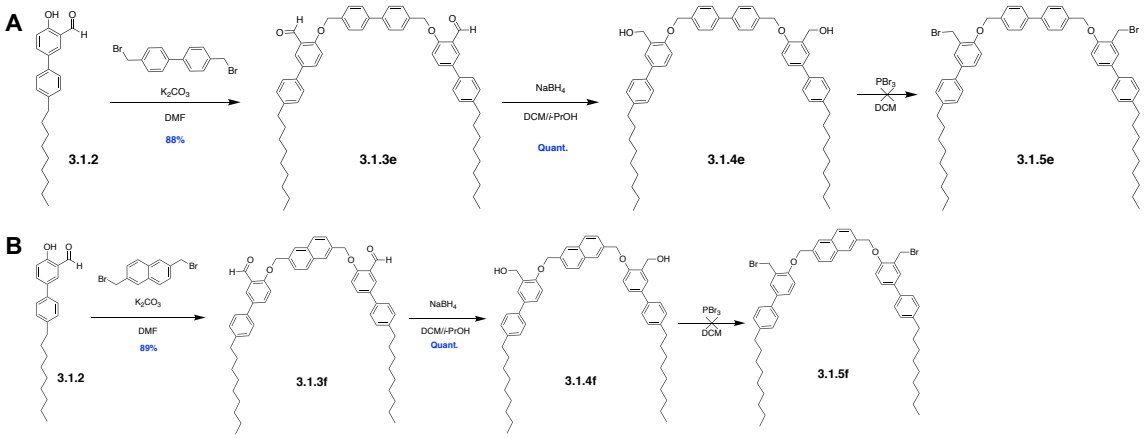


Figure 3.34. 3.1a liposomes do not colocalize with mitochondria. Blue = DAPI, Red = Rd-PE, Green = MitoTracker Deep Red-FM. Scale bar = 30 μm.



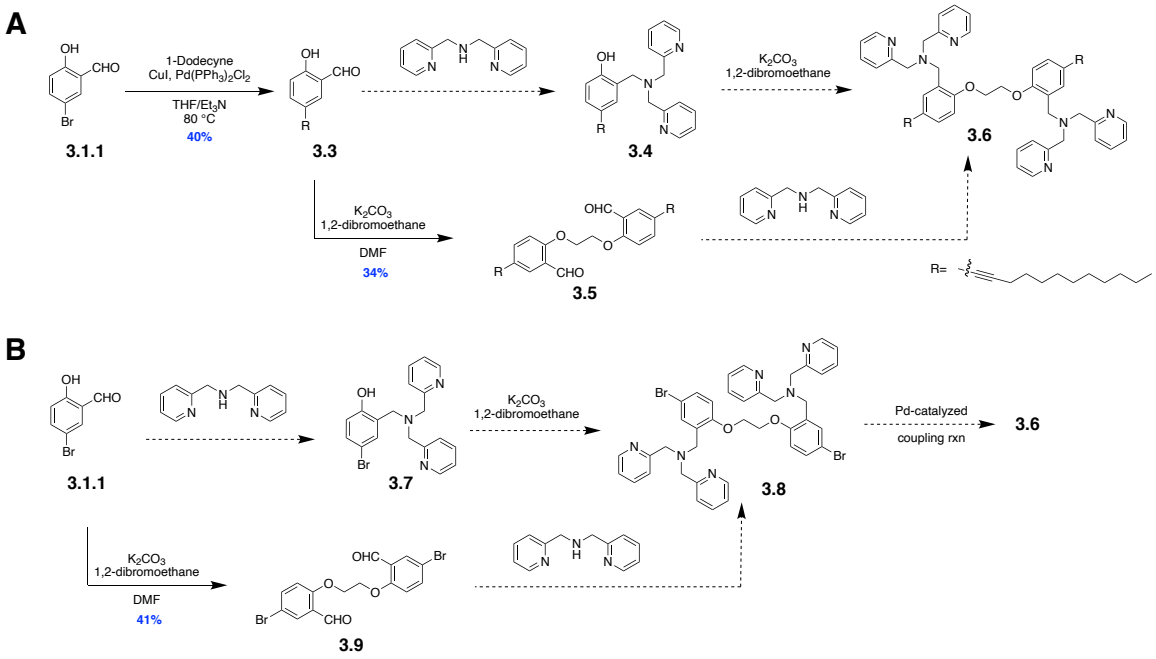
Scheme 3.6. Synthetic attempts made to make lipid switches bearing biphenyl linker (3.1e) as well as a naphthyl- linker (3.1f).

and turned out to be very messy. NMR analyses were inconclusive, but since we did not observe such problem with other linkers, we believe the presence of extended π-systems might account for these issues.

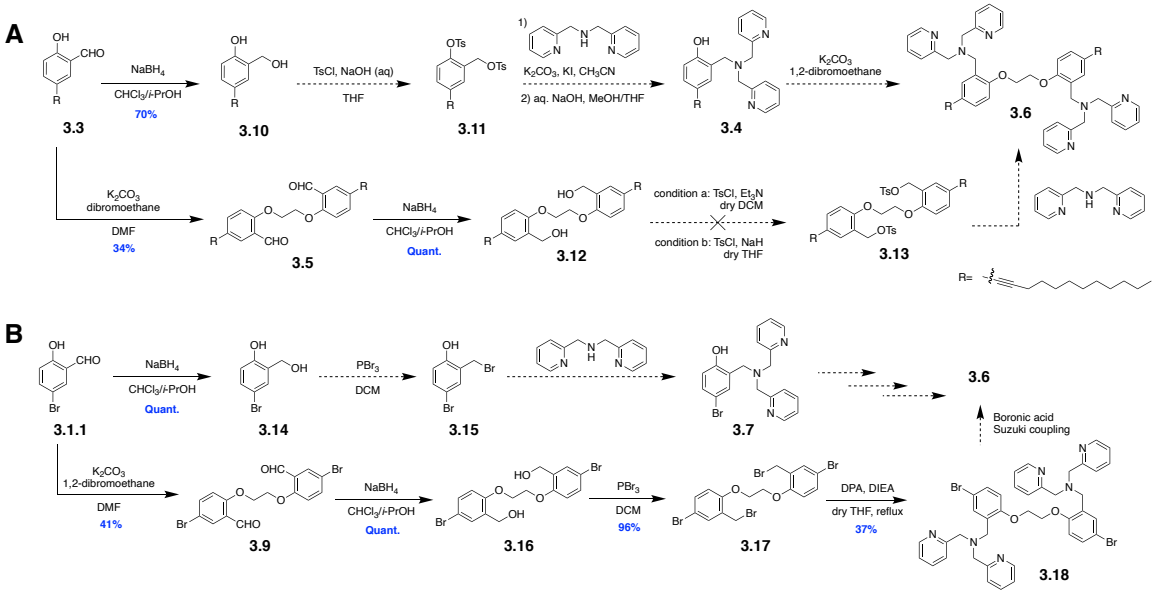
3.12.2. Initially designed synthetic route

In the initial synthetic design, we first made compound **3.3**, which has a rigid alkyne tail that was considered to be beneficial for programmed conformational changes. We also proposed to put the DPA units onto the switches through a one-step reductive amination reaction between aldehyde intermediates and dipicolylamine (Scheme 3.7). Once we obtained lipid **3.3**, we explored different conditions for reductive amination reaction. However, after trying multiple conditions for months (varying reducing reagents, reaction times, solvent systems, and pH), we were still not able to make this reaction work. Since we also wondered if it might be the substrate issue, and to expedite the synthesis, we pursued alternative routes at the same time by synthesizing dimerized intermediate **3.5**, or a direct reductive amination on commercially available **3.1.1** or dimerized intermediate **3.9**. Unfortunately, none of these worked for the reductive amination reactions under any conditions we tested.

To overcome this issue, we instead explored alkylation reactions to introduce the DPA binding sites (Scheme 3.8A). Again, two separate routes were pursued at the same time. We proposed to reduce the aldehyde groups of **3.3** or **3.5** first, and then put on tosyl groups that could be substituted by dipicolylamine. However, the tosylation reactions did not proceed well, possibly due to the steric interactions between bulky tosylates. In an alternative strategy, we proposed to synthesize the brominated intermediate instead of tosylates for alkylation. Due to synthetic concerns we have encountered when treating starting materials containing alkyne with PBr_3, we pursued an alternative route where we intended to add the alkyne tail at the late stage (Scheme 3.8B). After obtaining intermediates **3.14** and **3.16** containing primary alcohols, they were treated with PBr_3 for substitution reactions. Compound **3.15** was proven to be self-



Scheme 3.7. Initial designed synthetic route to switchable lipid 3.6 through reductive amination reactions.



Scheme 3.8. Initially designed synthetic route to switchable lipid through alkylation reactions.

immolative as it decomposed upon basic work-up; However, **3.17** was synthesized successfully as the phenol hydroxyl groups were masked with the ethyl linker. The subsequent alkylation reaction proceeded well and afforded **3.18** that could be purified with an alumina column. Although this route worked well so far, the final tail coupling was not successful, which is possibly due to the solubility of the DPA containing compounds. We made several synthetic attempts under varying conditions, but the reaction turned out messy in all the trials due to the presence of mono-tail byproduct. After realizing that lipid tails need to be coupled earlier in the synthesis and alkylation strategies work well, we ended up with the final synthesis plan as described earlier in this Chapter. Due to the concerns of the presence of functional groups present in the tail region that can potentially react with PBr_3, we started with lipid **3.1** series which have the rigid benzene tails, and later switched to a flexible C12 carbon tail for lipid **3.2** series.

3.12.3. Initial release studies with 3.1a

Once we obtained lipid switch **3.1a**, we worked on an initial screen of experimental conditions, such as buffer types. This could also shed a light on the general conditions needed for ion-responsive systems. Initial NR release studies focused on only two ions, Pi and PPi. Five different media were tested, including Milli-Q purified water, 1xTBS (pH=7.4), 1 mM HEPES (pH=7.4) and 1 mM HEPES (pH=7.4, 150 mM NaCl). 1xPBS (pH=7.4) was also tested, although we did not think it was ideal to use phosphate buffer in this case. Different formulations were formed, and NR fluorescence was measured. Results are summarized in Table 3.2.

After screening buffers with varying ionic strength and pH, we concluded that ionic strength (salt concentration or osmotic pressure) is more critical for ion/small molecule release systems compared to pH variations. For buffers with minimal ionic strength (MQ or 1 mM HEPES buffer; Entries 1-3 and 10-12), PC control liposomes exhibited background release for both Pi and

Table 3.2. Initial NR release studies with different buffer conditions.

Entry	Buffer	Comment	%PC	%**3.1a**	Stable?	Release Result
1	MQ	Minimal osmotic pressure, could not maintain pH	100	0	Yes	Background release for both Pi and PPi, ~20%
2			80	20	Yes	~20% background release for Pi, signal increased for PPi
3			50	50	No	--
4	1×PBS, pH 7.4	Phosphate buffer, not ideal	100	0	Yes	No background release
5			90	10	Yes	No release for Pi Signal increased for PPi
6			80	20	Yes	
7	1×TBS, pH 7.4	Minimal ion binding buffer, physiological osmotic pressure	100	0	Yes	No Background release
8			90	10	Yes	No release for Pi or PPi
9			80	20	Yes	~15% release for Pi, signal increased for PPi
10	1 mM HEPES, pH 7.4	Minimal ion binding buffer, minimal osmotic pressure	100	0	Yes	Background release for both Pi and PPi, ~20%
11			90	10	Yes	~20% background release for Pi, signal increased for PPi
12			80	20	Yes	
13	1 mM HEPES, 150 mM NaCl, pH=7.4	Minimal ion binding buffer, physiological osmotic pressure	100	0	Yes	No Background release
14			90	10	Yes	No release for Pi or PPi
15			80	20	Yes	~15% release for Pi, signal increased for PPi

PPi addition, while PC liposomes prepared with buffers with adjusted ionic strength showed no non-specific release. For calcium-responsive systems, we performed the release studies in MQ, which did not exhibit background release for PC liposomes upon treatment with calcium ion. While these two systems showed opposite properties, and we could not come to a definitive conclusion, it is obvious that ionic strength plays an important role in the ion-responsive systems. The buffer type for studies should be the first factor to consider for future ion/small molecule release projects.

Another interesting observation involved the fluorescence intensity changes upon analyte addition. While some of the liposomes containing **3.1a** showed fluorescence decreases upon Pi treatment, the NR fluorescence of 20% liposomes all went up after adding PPi. Possible explanations for this phenomenon would be that **3.1a** is interacting/binding with both Pi and PPi; however, they might affect the membrane in two different ways causing opposite fluorescence intensity changes.

3.13. Conclusions

We successfully developed small-molecule responsive liposomes that exhibit selectivity for ATP among a variety of phosphorylated metabolites using synthetic lipid switches that are driven by molecular recognition principles. This represents a new paradigm for controlled liposome release by exploiting as triggers critical and complex small molecule metabolites. Liposome delivery was achieved through the engineering of lipid structures to undergo binding interactions with specific guest molecules in a manner that modulates lipid self-assembly properties. Specifically, two phosphate-binding ZnDPA units were introduced within the rigid lipid scaffold of **3.1a**, such that ATP binding induces a conformational change within the lipid structure. This molecular arrangement promotes non-bilayer properties and disrupts membrane integrity to ultimately induce encapsulated cargo release. Our data show that **3.1a** is highly effective as a lipid switch for driving ATP-responsive liposome cargo release.

Furthermore, our results demonstrate that release properties can be fine-tuned to tailor selectivity towards ATP by modulating the percentage of **3.1a** within liposomes. Systematic evaluation of ATP binding properties, release of hydrophobic and hydrophilic cargoes, and lipid nanoparticle characteristics collectively showed that selective ATP-mediated liposome release was achieved through modulation of lipid self-assembly properties via ATP/lipid switch binding. By evaluating multiple alternative lipid switch structures with varying flexibility both in the linker between the ZnDPA units and within the lipid tails (**3.1a-d**/**3.2**), we showed that structural fit is critical for optimizing release properties. Finally, cellular fluorescence microscopy experiments demonstrated that **3.1a** liposomes are effective for cellular uptake controlled by intracellular ATP levels. This new direction offers an exciting avenue for enhancing control over liposome release by harnessing important biomolecules that are overabundant in disease. We envision that other aberrantly expressed biomolecules can act as targets for liposomal triggered release by designing complementary lipid switches using similar design strategies.

3.14. Synthesis and experimental procedure

General Experimental

Reagents and solvents were generally purchased from Sigma-Aldrich or Fisher Scientific and used without further purification. PC (L-α-Phosphatidylcholine, mixed isomers from chicken egg) was purchased from Avanti Polar Lipids, Inc (Alabaster, AL). Dry solvents were obtained from a Pure Solv MD-7 solvent purification system purchased from Innovative Technology, Inc (Newburyport, MA). Column chromatography was performed using 230-400 mesh silica gel purchased from Sorbent Technologies. NMR spectra were obtained using Varian 300 MHz or 500 MHz NMR spectrometers. Mass spectra were obtained with JEOL DART-AccuTOF and Waters Synapt G2-Si mass spectrometers (Milford, MA). Liposome extruder and polycarbonate membranes were obtained from Avestin (Ottawa, Canada) or Avanti Polar Lipids, Inc (Alabaster, AL). Ultrapure water was purified via a Millipore water system (≥ 18 MW·cm triple water purification system). Small quantities (< 5 mg) were weighed on a Mettler

Toledo XS105 dual range analytical balance. Osmotic pressure was measured with Wescor Vapor Pressure Osmometer 5520. Fluorescence studies were performed using a Cary Eclipse Fluorescence Spectrophotometer from Agilent Technologies. UV-Vis spectra were obtained using a Cary 5000 spectrophotometer. Plots were generated using Origin Pro 2019 or 2020. All error bars in plots indicate the standard errors of at least three experimental replicates.

Synthetic Procedures and Characterization Data

General procedure A, ether synthesis to **3.1.3** or **3.2.3**

Compound 3.1.2 or **3.2.2** and K_2CO_3 were dissolved in 10 mL dry DMF in a 100 mL RBF under Argon. After adding the appropriate dibromo reagent, the mixture was heated at 80 ºC. Reaction progress was monitored through TLC and the reaction was stopped when starting materials had been consumed. Next, the reaction mixture was poured into 100 mL 0.5 N HCl and extracted with 3 x 25 mL DCM. The combined organic layer was washed with 5 x 50 mL water and 1 x 50 mL brine. After being dried over Na_2SO_4, filtered, and concentrated under reduced pressure, the crude was purified via silica gel column chromatography using gradient elution from hexanes to 20% EtOAc in hexanes.

General procedure B, aldehyde reduction to **3.1.4a-d** or **3.2.4**

Dialdehyde **3.1.3a-d** or **3.2.3** was dissolved in 12 mL DCM/*i*-PrOH (3/1, v/v) under argon in a 50 mL RBF at 0 ºC. $NaBH_4$ (3 equiv.) was then added. Next, the reaction mixture was warmed up to rt and further stirred for 6h. After completion, the reaction mixture was brought back to 0 ºC with an ice bath and 10% citric acid was carefully added dropwise until no hydrogen gas was released, after which the reaction was further stirred for 20 min. The organic layer was collected, and the aqueous layer was further extracted with 2 x 25 mL DCM. The combined organic layer was washed with 1 x 50 mL water and 1 x 50 mL brine. After being dried over Na_2SO_4, filtered, and concentrated under reduced pressure, the crude was purified using column chromatography. Gradient elution from hexanes to 20% EtOAc in hexanes was

employed. For reactions run on a larger scale, DCM-hexanes eluant was used for silica gel column chromatography due to solubility issues.

General procedure C, bromination to **3.1.5a-d** or **3.2.5**

Di-alcohol **3.1.4a-d** or **3.2.4** was weighed into a 100 mL RBF under argon and dissolved with 20 mL dry DCM at 0 ºC. PBr_3 was next carefully added into the RBF dropwise. The reaction was warmed to rt and further stirred for six hours. After being cooled back to 0 ºC, MeOH was added dropwise to quench the unreacted PBr_3. The mixture was poured into 100 mL H_2O in a separatory funnel and the DCM layer was collected. The aqueous layer was further extracted with 2 x 20 mL DCM. The combined organic layer was washed with 1 x 50 mL H_2O and 1 x 50 mL brine before being dried over Na_2SO_4, filtered, and concentrated under reduced pressure. The crude was purified with a short column packed with silica gel using elution of 10% EtOAc in hexanes.

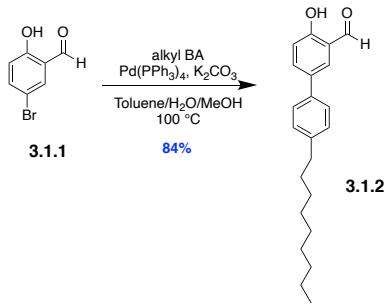
General procedure D, DPA introduction to **3.1.6a-d** or **3.2.6**

Dibromide **3.1.5a-d** or **3.2.5** was dissolved with 10 mL dry THF in a 50 mL RBF under Ar. *N,N*-Diisopropylethylamine (DIEA) and dipicolylamine (DPA) were next added, respectively. The reaction was refluxed at 70 ºC overnight, accompanied by a color change from colorless/pale yellow to brown. After evaporating the solvent under reduced pressure, the crude was subjected to neutral alumina column chromatography through gravity elution using 100% chloroform.

General procedure E, zinc chelation to **3.1a-d**, **3.2**

Bis-DPA precursor **3.1.6a-d** or **3.2.6** was dissolved with $CHCl_3$/MeOH (4/1, v/v for **3.1c-d**; 10/1, v/v for **3.1a-b**/**3.2**) in a 4 dr vial. Anhydrous $ZnCl_2$ was then added, and the reaction was stirred overnight. In some cases, products precipitated after overnight stirring, in which case the solid was collected via filtration. In the cases where products did not precipitate, the solvent was

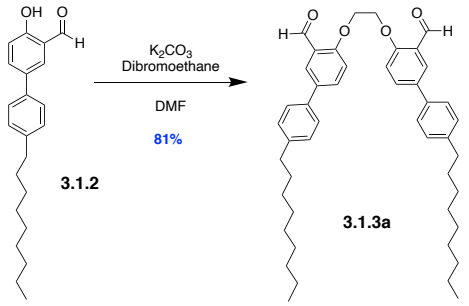
simply removed to yield the zinc-chelated product. The chelation was verified by ^{1}H NMR where a significant shift in the aromatic region was observed.



4-Hydroxy-4'-nonyl-[1,1'-biphenyl]-3-carbaldehyde (3.1.2)

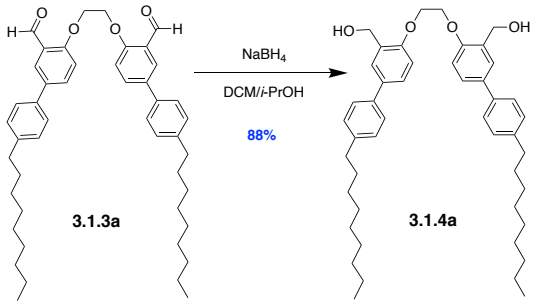
5-Bromo-2-hydroxybenzaldehyde (**3.1.1**, 0.729 g, 3.63 mmol), 4-(*n*-nonyl) benzeneboronic acid (1.08 g, 4.352 mmol), tetrakis(triphenylphosphine)palladium(0) (42 mg, 0.0363 mmol) as well as K_2CO_3 (0.752 g, 5.445 mmol) were combined in a 100 mL RBF under argon. After being dissolved with 25 mL toluene/H_2O/MeOH (2/2/1, v/v), the reaction mixture was heated at 100 ºC overnight. After completion, the reaction was cooled to rt and the solvent was removed using a rotary evaporator. The residue was re-dissolved in 25 mL DCM and washed with 50 mL water. The aqueous layer was extracted with 2 x 25 mL DCM. The combined organic layer was further washed with 1 x 50 mL water and 1 x 50 mL brine, respectively, before being dried over Na_2SO_4, filtered, and concentrated under reduced pressure. The crude was next loaded onto silica gel and subjected to column chromatography. Gradient elution from hexanes to 5% ethyl acetate in hexanes yielded the product as a slight yellow solid (0.9893 g, 3.049 mmol, 84% yield). R_f = 0.63 (10% EtOAc-hexanes).

^{1}H NMR (300 MHz, $CDCl_3$) δ 11.00 (s, 1H), 9.96 (s, 1H), 7.75 (d, *J* = 9.0 Hz, 2H), 7.47 (d, *J* = 7.8 Hz, 2H), 7.27 (d, *J* = 8.0 Hz, 2H), 7.06 (d, *J* = 8.4 Hz, 1H), 2.66 (t, *J* = 7.7 Hz, 2H), 1.67 (p, *J* = 7.1 Hz, 2H), 1.32 (d, *J* = 14.7 Hz, 12H), 0.91 (t, *J* = 6.5 Hz, 3H). ^{13}C NMR (75 MHz, $CDCl_3$) δ 196.68, 160.77, 142.32, 136.63, 135.60, 133.32, 131.61, 129.05, 126.42, 120.72, 118.04, 35.60, 31.92, 31.51, 29.59, 29.56, 29.37, 22.71, 14.14. HRMS-DART: $[M+H]^+$ calcd for $C_{22}H_{29}O_2$: 325.21656, Found: 325.1572



4,4''-(Ethane-1,2-diylbis(oxy))bis(4'-nonyl-[1,1'-biphenyl]-3-carbaldehyde) (3.1.3a)

General procedure A was followed. Compound **3.1.2** (0.15 g, 0.4623 mmol), K_2CO_3 (0.1916 g, 1.3869 mmol) and dibromoethane (19.92 µL 0.2311 mmol) were used. The product was obtained as a white solid (0.1265 g, 0.1874 mmol, 81% yield). R_f = 0.41 (25% EtOAc-hexanes). ^{1}H NMR (300 MHz, $CDCl_3$) δ 10.51 (s, 2H), 8.09 (d, *J* = 2.5 Hz, 2H), 7.81 (dd, *J* = 8.7, 2.5 Hz, 2H), 7.53 – 7.46 (m, 4H), 7.25 (d, *J* = 8.1 Hz, 4H), 7.14 (d, *J* = 8.7 Hz, 2H), 4.59 (s, 4H), 2.67 – 2.60 (m, 4H), 1.63 (q, *J* = 6.8 Hz, 4H), 1.30 (d, *J* = 18.0 Hz, 26H), 0.93 – 0.83 (m, 6H). ^{13}C NMR (75 MHz, $CDCl_3$) δ 189.47, 160.03, 142.54, 136.73, 134.82, 134.26, 129.11, 126.91, 126.72, 125.42, 113.33, 67.36, 35.73, 32.04, 31.63, 29.70, 29.67, 29.49, 29.48, 22.82, 14.26. HRMS-DART: $[M+H]^+$ calcd for $C_{46}H_{59}O_4$: 675.44135, Found: 675.35149

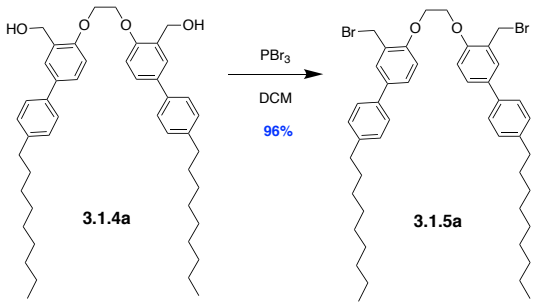


((Ethane-1,2-diylbis(oxy))bis(4'-nonyl-[1,1'-biphenyl]-4,3-diyl))dimethanol (3.1.4a)

General procedure B was followed. Compound **3.1.3a** (0.2 g, 0.296 mmol) and $NaBH_4$ (33 mg, 0.89 mmol) yielded the product as a white solid (0.176 g, 2.6 mmol, 88% yield). R_f = 0.3 (25% EtOAc-Hexanes).

^{1}H NMR (300 MHz, $CDCl_3$) δ 7.56 – 7.44 (m, 8H), 7.23 (d, *J* = 8.1 Hz, 4H), 7.01 (d, *J* = 8.4 Hz,

2H), 4.73 (s, 4H), 4.48 (s, 4H), 2.63 (dd, *J* = 8.8, 6.7 Hz, 4H), 1.64 (dd, *J* = 10.5, 4.7 Hz, 4H), 1.40 – 1.21 (m, 34H), 0.93 – 0.86 (m, 6H). ^{13}C NMR (75 MHz, $CDCl_3$) δ 155.86, 141.92, 137.96, 134.90, 130.12, 128.96, 128.42, 127.44, 126.81, 112.30, 67.20, 62.00, 35.74, 32.05, 31.67, 29.71, 29.69, 29.53, 29.49, 22.83, 14.27. HRMS-DART: HRMS-DART: $[M+H-H_2O]^+$ calcd for $C_{46}H_{61}O_3$: 661.4621, Found: 661.3605

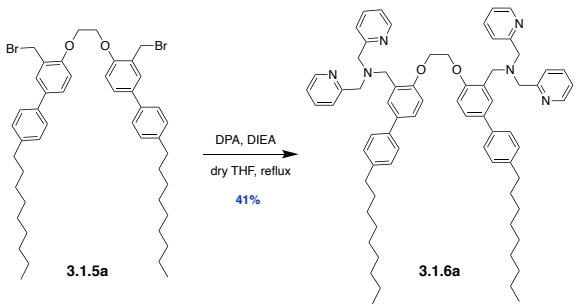


3.1.4a 3.1.5a

1,2-Bis((3-(bromomethyl)-4'-nonyl-[1,1'-biphenyl]-4-yl)oxy)ethane (3.1.5a)

General procedure C was followed. Compound **3.1.4a** (0.176 g, 0.259 mmol) and PBr_3 (0.74 mL, 7.78 mmol) were used. The product was obtained as a white solid (0.2 g, 0.249 mmol, 96% yield). R_f = 0.8 (25% EtOAc-Hexanes).

^{1}H NMR (500 MHz, $CDCl_3$) δ 7.57 (d, *J* = 2.3 Hz, 2H), 7.53 (dd, *J* = 8.5, 2.4 Hz, 2H), 7.47 (d, *J* = 7.7 Hz, 4H), 7.24 (d, *J* = 7.8 Hz, 4H), 7.06 (d, *J* = 8.5 Hz, 2H), 4.61 (s, 4H), 4.53 (s, 4H), 2.64 (t, *J* = 7.8 Hz, 4H), 1.64 (t, *J* = 7.5 Hz, 4H), 1.42 – 1.19 (m, 32H), 0.89 (t, *J* = 6.8 Hz, 6H). ^{13}C NMR (126 MHz, $CDCl_3$) δ 155.98, 142.03, 137.62, 134.61, 129.77, 128.99, 128.68, 127.02, 126.75, 112.76, 67.45, 35.74, 32.05, 31.67, 29.85, 29.71, 29.68, 29.51, 29.49, 29.27, 22.83, 14.27. HRMS-DART: $[M+2H-Br]^+$ calcd for $C_{46}H_{62}O_2Br$: 725.3933, Found: 725.2272

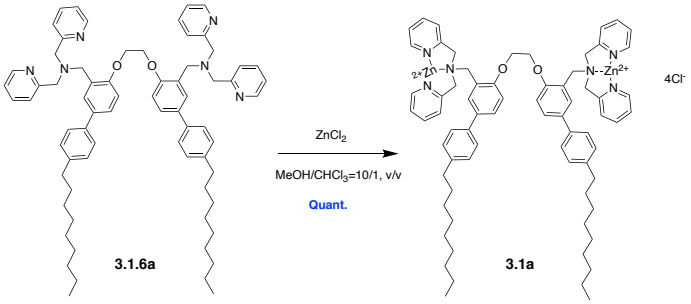


3.1.5a 3.1.6a

1,1'-((Ethane-1,2-diylbis(oxy))bis(4'-nonyl-[1,1'-biphenyl]-4,3-diyl))bis(*N*,*N*-bis(pyridin-2-ylmethyl)methanamine (3.1.6a)

General procedure D was followed. Compound **3.1.5a** (71 mg, 0.0882 mmol), DPA (36.54 µL, 0.203 mmol) and DIEA (35.36 µL, 0.203 mmol) yielded the product as a brown oil (37.8 mg, 0.0363 mmol, 41% yield). R_f = 0.42 (10% Methanol in chloroform).

^{1}H NMR (500 MHz, $CDCl_3$) δ 8.47 (dt, *J* = 4.8, 1.3 Hz, 4H), 7.81 (d, *J* = 2.4 Hz, 2H), 7.61 – 7.58 (m, 4H), 7.54 (td, *J* = 7.6, 1.8 Hz, 4H), 7.50 – 7.46 (m, 4H), 7.43 (dd, *J* = 8.5, 2.4 Hz, 2H), 7.24 (d, *J* = 8.2 Hz, 4H), 7.06 (ddd, *J* = 7.3, 4.8, 1.3 Hz, 4H), 6.92 (d, *J* = 8.5 Hz, 2H), 4.30 (s, 4H), 3.86 (s, 8H), 3.81 (s, 4H), 2.67 – 2.62 (m, 4H), 1.69 – 1.64 (m, 4H), 1.28 (qt, *J* = 8.3, 5.5 Hz, 30H), 0.90 – 0.87 (m, 6H). ^{13}C NMR (126 MHz, $CDCl_3$) δ 160.28, 156.38, 149.08, 141.64, 138.38, 136.46, 133.97, 129.15, 128.92, 126.79, 126.49, 122.62, 121.93, 111.95, 66.92, 60.54, 52.59, 35.76, 32.06, 31.72, 29.73, 29.71, 29.57, 29.50, 22.83, 14.27. HRMS-ESI: $[M+H]^+$ calcd for $C_{70}H_{85}N_6O_2$: 1041.6734, Found: 1041.6759

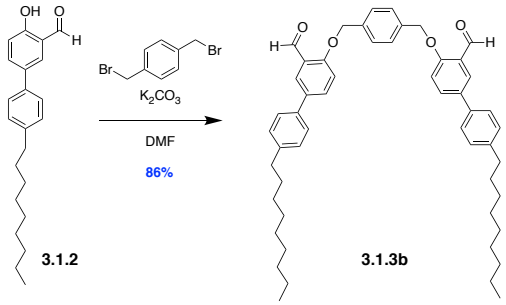


1,1'-((Ethane-1,2-diylbis(oxy))bis(4'-nonyl-[1,1'-biphenyl]-4,3-diyl))biszinc(*N*,*N*-bis(pyridin-2-ylmethyl)methanamine chloride (3.1a)

General procedure E was followed. Compound **3.1.6a** (23 mg, 0.0221 mmol) and $ZnCl_2$ (6.025 mg, 0.0442 mmol) yielded the product as a yellow solid (29.05 mg, 0.0221 mmol, quantitative yield).

^{1}H NMR (500 MHz, 50% $CD_3OD/CDCl_3$) δ 9.02 (dd, *J* = 5.4, 1.6 Hz, 4H), 7.90 (s, 4H), 7.72 (d, *J* = 8.2 Hz, 4H), 7.67 (dd, *J* = 8.5, 2.3 Hz, 2H), 7.59 – 7.56 (m, 4H), 7.50 (d, *J* = 2.4 Hz, 2H), 7.46 (d, *J* = 7.8 Hz, 4H), 7.29 (ddd, *J* = 7.5, 5.3, 1.1 Hz, 4H), 7.02 (d, *J* = 8.5 Hz, 2H), 4.48 (d,

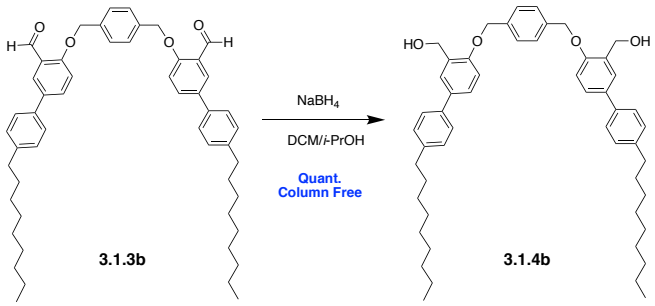
J = 16.2 Hz, 8H), 4.25 (d, *J* = 15.6 Hz, 4H), 3.78 (s, 4H), 2.99 – 2.92 (m, 4H), 2.00 – 1.87 (m, 4H), 1.69 – 1.46 (m, 36H), 1.18 – 1.09 (m, 6H).



4,4''-((1,4-Phenylenebis(methylene))bis(oxy))bis(4'-nonyl-[1,1'-biphenyl]-3-carbaldehyde) (3.1.3b)

General procedure A was followed. Compound **3.1.2** (0.15 g, 0.4623 mmol), K_2CO_3 (0.1916 g, 1.3869 mmol) and alpha,alpha′-dibromo-*p*-xylene (61 mg, 0.2311 mmol) were used. The product was obtained as a white solid (0.149 g, 0.1984 mmol, 86% yield). R_f = 0.61 (25% EtOAc-hexanes).

^{1}H NMR (300 MHz, $CDCl_3$) δ 10.73 (s, 2H), 8.23 (d, *J* = 2.5 Hz, 2H), 7.90 (dd, *J* = 8.6, 2.6 Hz, 2H), 7.68 – 7.54 (m, 8H), 7.37 (d, *J* = 7.8 Hz, 4H), 7.23 (s, 2H), 5.39 (s, 4H), 2.76 (t, *J* = 7.7 Hz, 4H), 1.77 (t, *J* = 7.7 Hz, 4H), 1.43 (d, *J* = 13.8 Hz, 25H), 1.25 – 0.79 (m, 6H). ^{13}C NMR (75 MHz, $CDCl_3$) δ 189.73, 160.23, 142.42, 136.78, 136.38, 134.37, 134.22, 129.07, 127.83, 126.72, 126.64, 125.38, 113.57, 70.42, 35.71, 32.03, 31.61, 29.69, 29.66, 29.47, 22.81, 14.25. HRMS-DART: $[M+H]^+$ calcd for $C_{52}H_{63}O_4$: 751.4726, Found: 751.3143

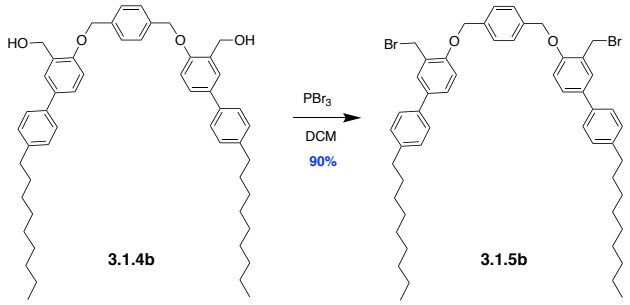


(((1,4-Phenylenebis(methylene))bis(oxy))bis(4'-nonyl-[1,1'-biphenyl]-4,3-

diyl))dimethanol (3.1.4b)

General procedure B was followed. Compound **3.1.3b** (0.1312 g, 0.175 mmol) and $NaBH_4$ (19.83 mg, 0.524 mmol) yielded the product as a white solid (0.132 g, 0.175 mmol, quantitative yield). R_f = 0.3 (25% EtOAc-Hexanes).

^{1}H NMR (500 MHz, $CDCl_3$) δ 7.56 (d, *J* = 2.3 Hz, 2H), 7.51 – 7.45 (m, 10H), 7.25 – 7.20 (m, 4H), 7.01 (d, *J* = 8.5 Hz, 2H), 5.18 (s, 4H), 4.80 (d, *J* = 4.2 Hz, 4H), 2.66 – 2.58 (m, 4H), 2.29 (d, *J* = 6.7 Hz, 2H), 1.68 – 1.59 (m, 4H), 1.42 – 1.19 (m, 26H), 0.88 (t, *J* = 6.9 Hz, 6H). ^{13}C NMR (126 MHz, $CDCl_3$) δ 155.95, 141.85, 138.04, 136.87, 134.41, 129.85, 128.96, 127.85, 127.69, 127.36, 126.77, 112.10, 70.07, 62.40, 35.74, 32.05, 31.67, 29.71, 29.69, 29.52, 29.49, 22.83, 14.27. HRMS-DART: $[M+H-H_2O]^+$ calcd for $C_{52}H_{65}O_3$: 737.4934, Found: 737.4126

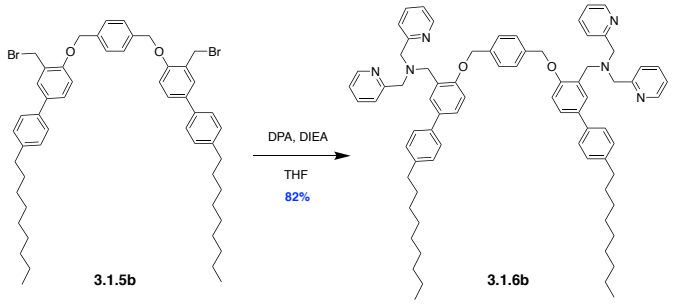


3.1.4b 3.1.5b

1,4-Bis(((3-(bromomethyl)-4'-nonyl-[1,1'-biphenyl]-4-yl)oxy)methyl)benzene (3.1.5b)

General procedure C was followed. Compound **3.1.4b** (0.1381 g, 0.183 mmol) and PBr_3 (0.52 mL, 5.49 mmol) were used. The product was obtained as a white solid (0.1447 g, 0.164 mmol, 90% yield). R_f = 0.7 (25% EtOAc-Hexanes).

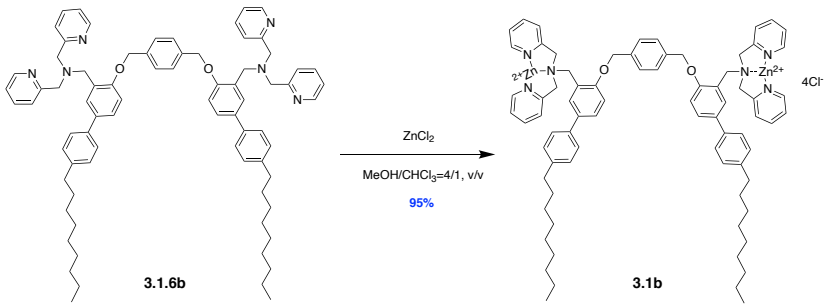
^{1}H NMR (500 MHz, $CDCl_3$) δ 7.58 (d, *J* = 2.4 Hz, 2H), 7.56 (s, 4H), 7.49 (dd, *J* = 8.5, 2.4 Hz, 2H), 7.47 – 7.44 (m, 4H), 7.23 (d, *J* = 8.2 Hz, 4H), 6.99 (d, *J* = 8.6 Hz, 2H), 5.22 (s, 4H), 4.68 (s, 4H), 2.66 – 2.59 (m, 4H), 1.68 – 1.60 (m, 4H), 1.40 – 1.22 (m, 28H), 0.88 (t, *J* = 6.9 Hz, 6H). ^{13}C NMR (126 MHz, $CDCl_3$) δ 155.93, 141.99, 137.64, 136.77, 134.35, 129.73, 128.99, 128.67, 127.60, 126.88, 126.73, 112.75, 70.17, 35.74, 32.05, 31.66, 29.71, 29.68, 29.51, 29.48, 29.36, 22.83, 14.27. HRMS-DART: $[M+NH_4+2]^+$ (+2 for bromine isotope pattern) calcd for $C_{52}H_{68}Br_2O_2N$: 898.36168, found: 898.6410.



1,1'-(((1,4-Phenylenebis(methylene))bis(oxy))bis(4'-nonyl-[1,1'-biphenyl]-4,3-diyl))bis(*N*,*N*-bis(pyridin-2-ylmethyl)methanamine) (3.1.6b)

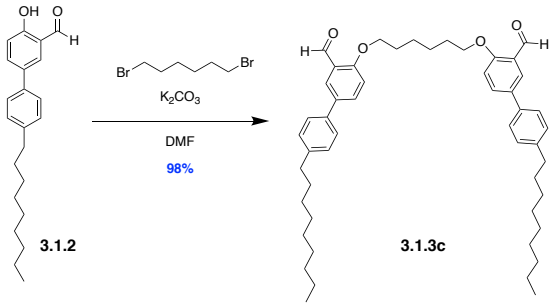
General procedure D was followed. Compound **3.1.5b** (30 mg, 0.034 mmol), DPA (14.1 µL, 0.0783 mmol) and DIEA (13.64 µL, 0.0783 mmol) yielded the product as a brown oil (31.3 mg, 0.028 mmol, 82% yield). R_f = 0.5 (10% Methanol in chloroform).

^{1}H NMR (500 MHz, $CDCl_3$) δ 8.49 (ddd, *J* = 4.8, 1.8, 0.9 Hz, 4H), 7.86 (d, *J* = 2.4 Hz, 2H), 7.62 (dt, *J* = 7.9, 1.2 Hz, 4H), 7.56 (td, *J* = 7.6, 1.8 Hz, 4H), 7.49 – 7.45 (m, 4H), 7.45 – 7.38 (m, 6H), 7.24 – 7.21 (m, 4H), 7.08 (ddd, *J* = 7.4, 4.9, 1.3 Hz, 4H), 6.95 (d, *J* = 8.5 Hz, 2H), 5.12 (s, 4H), 3.92 (s, 8H), 3.89 (s, 4H), 2.67 – 2.60 (m, 4H), 1.70 – 1.59 (m, 4H), 1.42 – 1.20 (m, 28H), 0.91 – 0.86 (m, 6H). ^{13}C NMR (126 MHz, $CDCl_3$) δ 160.22, 156.45, 149.08, 141.60, 138.40, 136.98, 136.49, 133.84, 128.98, 128.91, 127.82, 127.62, 126.75, 126.43, 122.67, 121.95, 112.17, 70.03, 60.61, 52.80, 35.75, 32.05, 31.70, 29.72, 29.70, 29.56, 29.49, 22.83, 14.26. HRMS-ESI: $[M+H]^+$ calcd for $C_{76}H_{89}N_6O_2$: 1117.7047, Found: 1117.7136



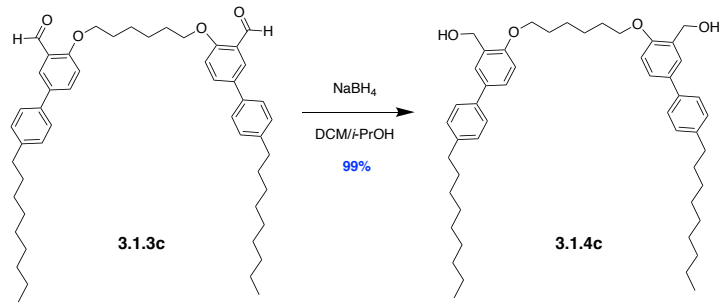
1,1'-(((1,4-Phenylenebis(methylene))bis(oxy))bis(4'-nonyl-[1,1'-biphenyl]-4,3-diyl))bis(*N*,*N*-biszinc(pyridin-2-ylmethyl)methanamine) chloride (3.1b)

General procedure E was followed. Compound **3.1.6b** (16 mg, 0.0143 mmol) and $ZnCl_2$ (3.9 mg, 0.0286 mmol) yielded the product as a white solid (18.98 mg, 0.01365 mmol, 95% yield). ^{1}H NMR (500 MHz, $CDCl_3$) δ 9.27 – 9.20 (m, 4H), 7.64 (td, *J* = 7.6, 1.7 Hz, 4H), 7.49 (dd, *J* = 8.5, 2.4 Hz, 2H), 7.40 – 7.36 (m, 4H), 7.31 (ddd, *J* = 7.4, 5.3, 1.2 Hz, 4H), 7.25 (d, *J* = 1.9 Hz, 4H), 7.16 (d, *J* = 2.5 Hz, 6H), 7.08 (dd, *J* = 7.8, 1.3 Hz, 4H), 7.03 (d, *J* = 8.7 Hz, 2H), 5.07 (s, 4H), 4.14 (s, 8H), 3.94 (s, 4H), 2.68 – 2.61 (m, 4H), 1.68 – 1.62 (m, 4H), 1.42 – 1.15 (m, 36H), 0.91 – 0.87 (m, 6H).



4,4''-(Hexane-1,6-diylbis(oxy))bis(4'-nonyl-[1,1'-biphenyl]-3-carbaldehyde) (3.1.3c)

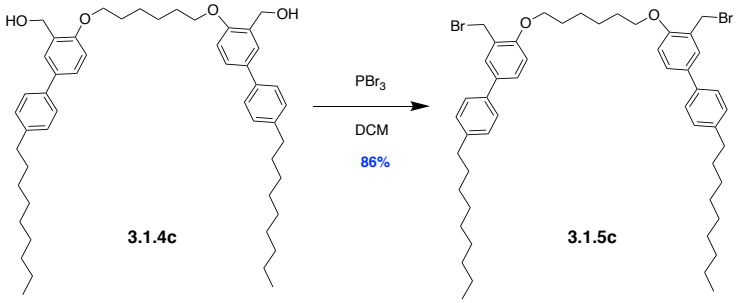
General procedure A was followed. Compound **3.1.2** (0.15 g, 0.4623 mmol), K_2CO_3 (0.1916 g, 1.3869 mmol) and 1,6-dibromohexane (36 µL, 0.2311 mmol) were used. The product was obtained as a white solid (0.1652 g, 0.226 mmol, 98 % yield). R_f = 0.42 (25% EtOAc-hexanes). ^{1}H NMR (500 MHz, $CDCl_3$) δ 10.56 (s, 2H), 8.06 (d, *J* = 2.5 Hz, 2H), 7.77 (dd, *J* = 8.6, 2.5 Hz, 2H), 7.49 (d, *J* = 8.0 Hz, 4H), 7.24 (d, *J* = 7.9 Hz, 4H), 7.05 (d, *J* = 8.7 Hz, 2H), 4.15 (t, *J* = 6.3 Hz, 4H), 2.64 (t, *J* = 7.8 Hz, 4H), 1.93 (t, *J* = 6.5 Hz, 4H), 1.64 (td, *J* = 7.8, 7.2, 4.8 Hz, 8H), 1.41 – 1.21 (m, 26H), 0.89 (t, *J* = 6.9 Hz, 6H). ^{13}C NMR (126 MHz, $CDCl_3$) δ 189.91, 160.79, 142.30, 136.93, 134.31, 133.82, 129.05, 126.62, 126.48, 125.07, 113.06, 68.58, 35.72, 32.03, 31.63, 29.70, 29.67, 29.49, 29.47, 29.20, 25.94, 22.82, 14.25. HRMS-DART: $[M+H]^+$ calcd for $C_{50}H_{67}O_4$: 731.5039, Found: 731.3751



((Hexane-1,6-diylbis(oxy))bis(4'-nonyl-[1,1'-biphenyl]-4,3-diyl))dimethanol (3.1.4c)

General procedure B was followed. Compound **3.1.3c** (0.1392 g, 0.19 mmol) and $NaBH_4$ (21.61 mg, 0.57 mmol) yielded the product as a white solid (0.1391 g, 0.189 mmol, 99% yield). R_f = 0.36 (25% EtOAc-Hexanes).

^{1}H NMR (500 MHz, $CDCl_3$) δ 7.51 (d, *J* = 2.4 Hz, 2H), 7.47 (dq, *J* = 8.5, 2.3 Hz, 6H), 7.24 – 7.21 (m, 4H), 6.93 (d, *J* = 8.5 Hz, 2H), 4.73 (s, 4H), 4.09 (t, *J* = 6.3 Hz, 4H), 2.63 (dd, *J* = 8.8, 6.8 Hz, 4H), 2.10 (s, 2H), 1.90 (dd, *J* = 7.9, 4.8 Hz, 4H), 1.68 – 1.58 (m, 8H), 1.40 – 1.23 (m, 26H), 0.92 – 0.86 (m, 6H). ^{13}C NMR (126 MHz, $CDCl_3$) δ 156.32, 141.72, 138.13, 133.88, 129.52, 128.93, 127.54, 127.30, 126.74, 111.52, 68.07, 62.49, 35.74, 32.05, 31.68, 29.71, 29.69, 29.53, 29.49, 29.37, 26.10, 22.83, 14.26. HRMS-DART: $[M+H]^+$ calcd for $C_{50}H_{71}O_4$: 735.5352 Found: 735.4180; $[M+H-H_2O]^+$ calcd for $C_{50}H_{69}O_3$: 717.5247, Found: 717.4163

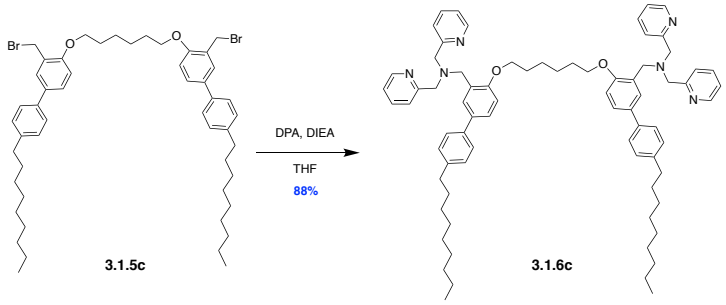


1,6-Bis((3-(bromomethyl)-4'-nonyl-[1,1'-biphenyl]-4-yl)oxy)hexane (3.1.5c)

General procedure C was followed. Compound **3.1.4c** (0.1066 g, 0.145 mmol) and PBr_3 (0.413 mL, 4.35 mmol) were used. The product was obtained as a white solid (0.1078 g, 0.125 mmol, 86% yield). R_f = 0.83 (50% DCM-Hexanes).

^{1}H NMR (500 MHz, $CDCl_3$) δ 7.55 (d, *J* = 2.3 Hz, 2H), 7.49 (dd, *J* = 8.5, 2.4 Hz, 2H), 7.47 –

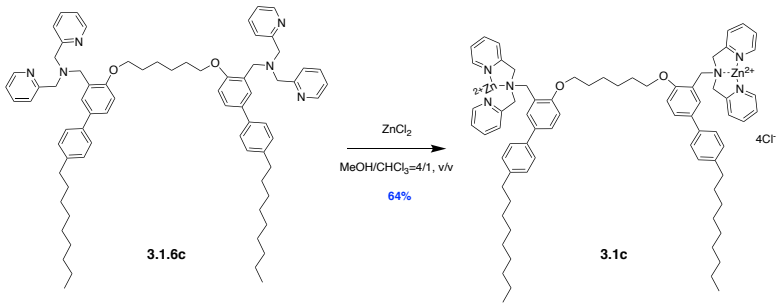
7.44 (m, 4H), 7.25 – 7.21 (m, 4H), 6.93 (d, *J* = 8.6 Hz, 2H), 4.62 (s, 4H), 4.11 (t, *J* = 6.3 Hz, 4H), 2.64 (dd, *J* = 8.8, 6.8 Hz, 4H), 1.93 (t, *J* = 6.3 Hz, 4H), 1.70 – 1.61 (m, 8H), 1.40 – 1.24 (m, 28H), 0.92 – 0.87 (m, 6H). ^{13}C NMR (126 MHz, $CDCl_3$) δ 156.40, 141.84, 137.77, 133.75, 129.57, 128.95, 128.64, 126.68, 126.52, 112.17, 68.29, 35.73, 32.04, 31.67, 29.85, 29.71, 29.68, 29.51, 29.48, 29.44, 29.35, 25.95, 22.83, 14.27. HRMS-DART: $[M+H-HBr]^+$ calcd for $C_{50}H_{68}BrO_2$: 779.4403, Found: 779.4280



1,1'-((Hexane-1,6-diylbis(oxy))bis(4'-nonyl-[1,1'-biphenyl]-4,3-diyl))bis(*N*,*N*-bis(pyridin-2-ylmethyl)methanamine) (3.1.6c)

General procedure D was followed. Compound **3.1.5c** (47.5 mg, 0.0552 mmol), DPA (22.8 µL, 0.127 mmol) and DIEA (22.12 µL, 0.127 mmol) yielded the product as a brown oil (53.6 mg, 0.0488 mmol, 88% yield). R_f = 0.5 (10% Methanol in chloroform).

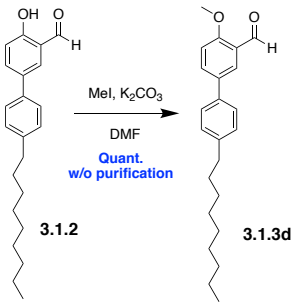
^{1}H NMR (500 MHz, $CDCl_3$) δ 8.54 – 8.47 (m, 4H), 7.83 (d, *J* = 2.4 Hz, 2H), 7.67 – 7.60 (m, 8H), 7.47 (d, *J* = 7.9 Hz, 4H), 7.41 (dd, *J* = 8.4, 2.5 Hz, 2H), 7.23 (d, *J* = 7.9 Hz, 4H), 7.11 (ddd, *J* = 6.8, 4.7, 1.6 Hz, 4H), 6.88 (d, *J* = 8.5 Hz, 2H), 3.98 (dd, *J* = 15.3, 8.8 Hz, 12H), 3.88 (s, 4H), 2.64 (t, *J* = 7.8 Hz, 4H), 1.81 (t, *J* = 6.6 Hz, 4H), 1.65 (p, *J* = 7.3 Hz, 4H), 1.55 – 1.49 (m, 4H), 1.39 – 1.23 (m, 30H), 0.89 (t, *J* = 6.7 Hz, 6H). ^{13}C NMR (126 MHz, $CDCl_3$) δ 156.79, 149.06, 141.47, 138.44, 136.54, 133.31, 128.86, 126.69, 126.51, 122.76, 122.02, 111.56, 68.14, 60.42, 52.57, 35.72, 32.02, 31.68, 29.82, 29.70, 29.67, 29.53, 29.46, 29.40, 26.06, 22.80, 14.24. HRMS-DART: $[M+H]^+$ calcd for $C_{74}H_{93}N_6O_2$: 1097.7360, Found: 1097.7063



1,1'-((Hexane-1,6-diylbis(oxy))bis(4'-nonyl-[1,1'-biphenyl]-4,3-diyl))bis(*N*,*N*-biszinc(pyridin-2-ylmethyl)methanamine) chloride (3.1c)

General procedure E was followed. Compound **3.1.6c** (39.4 mg, 0.036 mmol) and $ZnCl_2$ (9.8 mg, 0.072 mmol) yielded the product as a white solid (31.32 mg, 0.023 mmol, 64% yield).

^{1}H NMR (500 MHz, $CDCl_3$) δ 9.27 (dd, *J* = 5.3, 1.6 Hz, 4H), 7.78 (td, *J* = 7.6, 1.7 Hz, 4H), 7.44 – 7.38 (m, 6H), 7.34 – 7.28 (m, 4H), 7.23 (dd, *J* = 7.9, 5.8 Hz, 8H), 6.99 – 6.93 (m, 4H), 4.10 (s, 8H), 3.93 (t, *J* = 6.2 Hz, 4H), 3.69 (s, 4H), 2.69 – 2.62 (m, 4H), 1.67 (td, *J* = 9.4, 8.8, 4.8 Hz, 4H), 1.52 (t, *J* = 6.1 Hz, 4H), 1.43 – 1.23 (m, 28H), 1.06 (h, *J* = 3.7, 3.2 Hz, 4H), 0.92 – 0.84 (m, 6H).

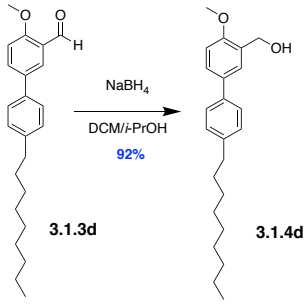


4-Methoxy-4'-nonyl-[1,1'-biphenyl]-3-carbaldehyde (3.1.3d)

General procedure A was followed with slight modification. Compound **3.1.2** (0.1 g, 0.308 mmol), K_2CO_3 (0.1278 g, 0.9246 mmol) and iodomethane (60 µL, 0.955 mmol) were used. The reaction proceeded at rt overnight. Following workup, the product was obtained as a white solid at a quantitative yield, which was passed along to next step without further purification. R_f = 0.42 (10% EtOAc-hexanes).

^{1}H NMR (300 MHz, $CDCl_3$) δ 10.55 (s, 1H), 8.10 (d, *J* = 2.5 Hz, 1H), 7.81 (dd, *J* = 8.6, 2.6 Hz,

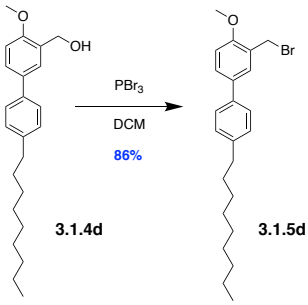
1H), 7.52 (d, *J* = 7.9 Hz, 2H), 7.27 (d, *J* = 7.9 Hz, 2H), 7.08 (d, *J* = 8.7 Hz, 1H), 3.99 (s, 3H), 2.73 – 2.54 (m, 2H), 1.67 (t, *J* = 7.5 Hz, 2H), 1.34 (d, *J* = 19.5 Hz, 12H), 0.92 (t, *J* = 6.6 Hz, 3H).



(4-Methoxy-4'-nonyl-[1,1'-biphenyl]-3-yl)methanol (3.1.4d)

General procedure B was followed. Compound **3.1.3d** (0.1184 g, 0.35 mmol) and $NaBH_4$ (40 mg, 1.05 mmol) yielded the product as a white solid (0.1094 g, 0.321 mmol, 92% yield). R_f = 0.27 (75% DCM-Hexanes).

^{1}H NMR (300 MHz, $CDCl_3$) δ 7.62 – 7.43 (m, 4H), 7.24 (d, *J* = 7.8 Hz, 2H), 6.95 (d, *J* = 8.3 Hz, 1H), 4.75 (s, 2H), 3.90 (s, 3H), 2.64 (t, *J* = 7.7 Hz, 2H), 2.26 (s, 1H), 1.67 (q, *J* = 7.2 Hz, 2H), 1.32 (d, *J* = 15.2 Hz, 12H), 0.90 (t, *J* = 6.5 Hz, 3H). ^{13}C NMR (75 MHz, $CDCl_3$) δ 156.90, 141.71, 138.09, 133.94, 129.39, 128.91, 127.58, 127.34, 126.73, 110.65, 62.38, 55.55, 35.72, 32.04, 31.66, 29.70, 29.68, 29.51, 29.47, 22.82, 14.25. HRMS-DART: $[M+H]^+$ calcld for $C_{23}H_{33}O_2$: 341.2480, Found: 341.2039.

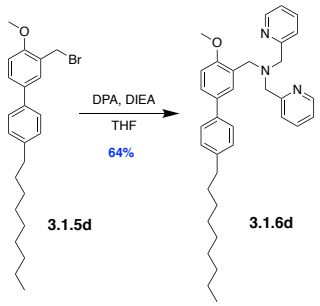


3-(Bromomethyl)-4-methoxy-4'-nonyl-1,1'-biphenyl (3.1.5d)

General procedure C was followed. Compound **3.1.4d** (0.1094 g, 0.321 mmol) and PBr_3 (0.457

mL, 4.82 mmol) were used. The product was obtained as a white solid (111.6 mg, 0.277 mmol, 86% yield). R_f = 0.46 (5% EtOAc-Hexanes).

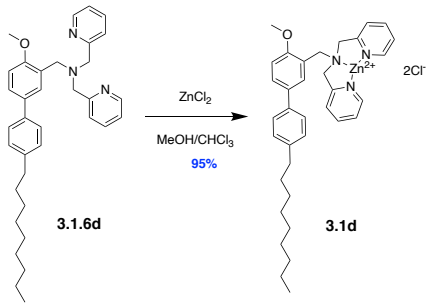
^{1}H NMR (500 MHz, $CDCl_3$) δ 7.58 (d, *J* = 2.3 Hz, 1H), 7.52 (dd, *J* = 8.5, 2.4 Hz, 1H), 7.49 – 7.46 (m, 2H), 7.26 – 7.23 (m, 2H), 6.95 (d, *J* = 8.5 Hz, 1H), 4.64 (s, 2H), 3.94 (s, 3H), 2.65 (dd, *J* = 8.7, 6.8 Hz, 2H), 1.70 – 1.62 (m, 2H), 1.41 – 1.23 (m, 12H), 0.91 (t, *J* = 6.9 Hz, 3H). ^{13}C NMR (126 MHz, $CDCl_3$) δ 156.88, 141.89, 137.68, 133.99, 129.63, 128.96, 128.95, 128.65, 126.68, 126.67, 126.43, 111.41, 55.89, 35.72, 32.04, 31.66, 29.71, 29.68, 29.50, 29.48, 29.22, 22.82, 14.26. HRMS-DART: $[M+H-HBr]^+$ calcld for $C_{23}H_{32}O$: 324.2453, Found: 324.2010.



1-(4-Methoxy-4'-nonyl-[1,1'-biphenyl]-3-yl)-*N*,*N*-bis(pyridin-2-ylmethyl)methanamine (3.1.6d)

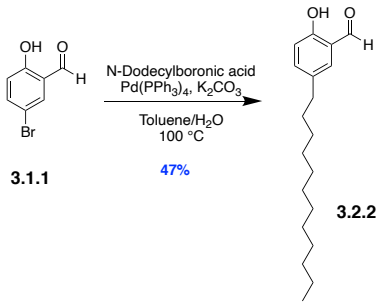
General procedure D was followed. Compound **3.1.5d** (40 mg, 0.1 mmol), DPA (20.7 µL, 0.115 mmol) and DIEA (20.03 µL, 0.115 mmol) yielded the product as a brown oil (33.6 mg, 0.064 mmol, 64% yield). R_f = 0.18 (5% Methanol in chloroform).

^{1}H NMR (500 MHz, $CDCl_3$) δ 8.52 (d, *J* = 4.8 Hz, 2H), 7.80 (d, *J* = 2.4 Hz, 1H), 7.71 – 7.58 (m, 4H), 7.49 – 7.40 (m, 3H), 7.22 (d, *J* = 7.9 Hz, 2H), 7.13 (ddd, *J* = 6.8, 4.8, 1.7 Hz, 2H), 6.89 (d, *J* = 8.4 Hz, 1H), 3.93 (s, 4H), 3.82 (s, 5H), 2.63 (t, *J* = 7.8 Hz, 2H), 1.65 (t, *J* = 7.6 Hz, 2H), 1.44 – 1.21 (m, 12H), 0.88 (t, *J* = 6.8 Hz, 3H). ^{13}C NMR (126 MHz, $CDCl_3$) δ 157.37, 149.08, 141.55, 136.55, 133.48, 128.90, 126.73, 122.79, 122.04, 110.69, 60.48, 55.51, 52.67, 35.74, 32.05, 31.70, 29.72, 29.69, 29.55, 29.48, 22.82, 14.26. HRMS-DART: $[M+H]^+$ calcd for $C_{35}H_{44}N_3O$: 522.3484, Found: 522.2514



1-(4-Methoxy-4'-nonyl-[1,1'-biphenyl]-3-yl)-*N*,*N*-biszinc(pyridin-2-ylmethyl)methanamine chloride (3.1d)

General procedure E was followed. Compound **3.1.6d** (18 mg, 0.0345 mmol) and $ZnCl_2$ (4.7 mg, 0.0345 mmol) yielded the product as a yellow solid (21.63 mg, 0.0329 mmol, 95% yield). ^{1}H NMR (500 MHz, $CDCl_3$) δ 9.21 – 9.02 (m, 2H), 7.82 (td, *J* = 7.7, 1.7 Hz, 2H), 7.43 (dd, *J* = 7.3, 5.6 Hz, 2H), 7.38 (dd, *J* = 8.3, 2.0 Hz, 3H), 7.26 (m, 5H), 6.77 (d, *J* = 8.6 Hz, 1H), 4.25 (s, 4H), 3.92 (s, 2H), 3.80 (s, 3H), 2.66 – 2.59 (m, 2H), 1.64 (t, *J* = 7.4 Hz, 2H), 1.40 – 1.18 (m, 16H), 0.88 (t, *J* = 6.8 Hz, 3H).



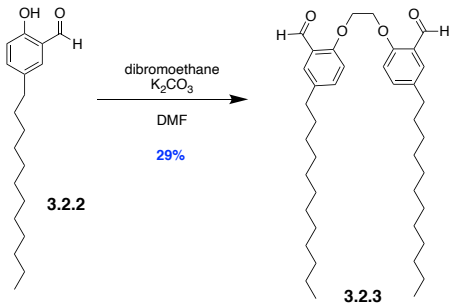
5-Dodecyl-2-hydroxybenzaldehyde (3.2.2)

5-Bromo-2-hydroxybenzaldehyde (**3.1.1**, 0.5 g, 2.49 mmol), *N*-dodecylboronic acid (0.8 g, 3.73 mmol), tetrakis(triphenylphosphine)palladium(0) (28.75 mg, 0.025 mmol) as well as K_2CO_3 (0.52 g, 3.73 mmol) were combined in a 100 mL RBF under argon. After being dissolved with 30 mL toluene/H_2O (2/1, v/v), the reaction mixture was heated at 100 ºC for 48 h. After completion, the reaction was cooled down to rt and the solvent was removed using a rotary evaporator. The residue was re-dissolved in 25 mL DCM and washed with 50 mL water. The aqueous layer was extracted with 2 x 25 mL DCM. The combined organic layer was further

washed with 1 x 50 mL water and 1 x 50 mL brine before being dried over Na_2SO_4, filtered, and concentrated under reduced pressure. The crude was next loaded onto silica gel and subjected to a column chromatography. Gradient elution from hexanes to 5% ethyl acetate in hexanes yielded the product as a white solid (0.34 g, 1.17 mmol, 47% yield). R_f = 0.78 (10% EtOAc-hexanes).

^{1}H NMR (300 MHz, $CDCl_3$) δ 10.85 (s, 1H), 9.86 (s, 1H), 7.34 (d, *J* = 7.5 Hz, 2H), 6.90 (d, *J* = 8.3 Hz, 1H), 2.58 (t, *J* = 7.7 Hz, 2H), 1.60 (t, *J* = 7.5 Hz, 2H), 1.33 (d, *J* = 3.9 Hz, 22H), 0.88 (t, *J* = 6.4 Hz, 3H). ^{13}C NMR (75 MHz, $CDCl_3$) δ 196.69, 159.85, 137.52, 134.43, 132.90, 120.49, 117.50, 34.83, 32.04, 31.53, 29.79, 29.77, 29.70, 29.59, 29.48, 29.25, 22.81, 14.23.

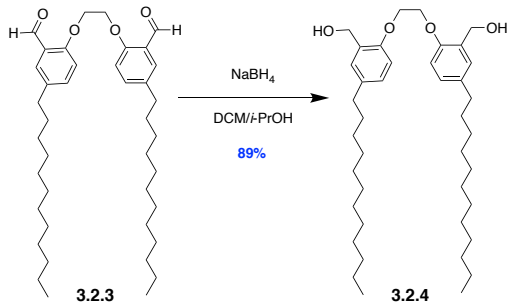
HRMS-DART: $[M+H]^+$ calcd for $C_{19}H_{31}O_2$: 291.2324, Found: 291.1524



6,6'-(Ethane-1,2-diylbis(oxy))bis(3-dodecylbenzaldehyde) (3.2.3)

General procedure A was followed. Compound **3.2.2** (0.35 g, 1.2 mmol), K_2CO_3 (0.497 g, 3.6 mmol) and dibromoethane (52 µL, 0.6 mmol) were used. The product was obtained as a white solid (0.106 g, 0.174 mmol, 29% yield). R_f = 0.63 (25% EtOAc-hexanes).

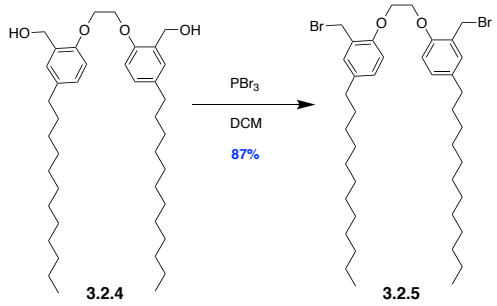
^{1}H NMR (500 MHz, $CDCl_3$) δ 10.42 (s, 2H), 7.65 (d, *J* = 2.4 Hz, 2H), 7.37 (dd, *J* = 8.5, 2.4 Hz, 2H), 6.97 (d, *J* = 8.5 Hz, 2H), 4.48 (s, 4H), 2.62 – 2.53 (m, 4H), 1.58 (d, *J* = 8.8 Hz, 6H), 1.41 – 1.18 (m, 43H), 0.88 (t, *J* = 6.9 Hz, 6H). ^{13}C NMR (126 MHz, $CDCl_3$) δ 189.75, 159.17, 136.27, 136.09, 128.15, 125.08, 112.90, 67.36, 34.96, 32.06, 31.52, 29.81, 29.79, 29.71, 29.61, 29.49, 29.32, 22.83, 15.65, 14.26. HRMS-DART: $[M+H]^+$ calcd for $C_{40}H_{63}O_4$: 607.4726, Found: 607.3618



((Ethane-1,2-diylbis(oxy))bis(5-dodecyl-2,1-phenylene))dimethanol (3.2.4)

General procedure B was followed. Compound **3.2.3** (64.4 mg, 0.106 mmol) and $NaBH_4$ (12 mg, 0.32 mmol) yielded product as a white solid (57.6 mg, 0.094 mmol, 89% yield). R_f = 0.45 (25% EtOAc-Hexanes).

^{1}H NMR (500 MHz, $CDCl_3$) δ 7.13 – 7.06 (m, 4H), 6.84 (d, *J* = 8.2 Hz, 2H), 4.63 (s, 4H), 4.38 (s, 4H), 2.54 (dd, *J* = 8.8, 6.7 Hz, 4H), 1.58 (t, *J* = 7.6 Hz, 4H), 1.36 – 1.22 (m, 40H), 0.89 (t, *J* = 6.9 Hz, 6H). ^{13}C NMR (126 MHz, $CDCl_3$) δ 154.62, 136.25, 129.82, 129.63, 128.66, 111.96, 67.22, 61.99, 35.23, 32.06, 31.82, 29.82, 29.78, 29.75, 29.67, 29.50, 29.46, 22.83, 14.26. HRMS-DART: $[M+H-H_2O]^+$ calcd for $C_{40}H_{65}O_3$: 593.4934, Found: 593.3863; $[M+H-2H_2O]^+$ calcd for $C_{40}H_{63}O_2$: 575.4828, Found: 575.3794

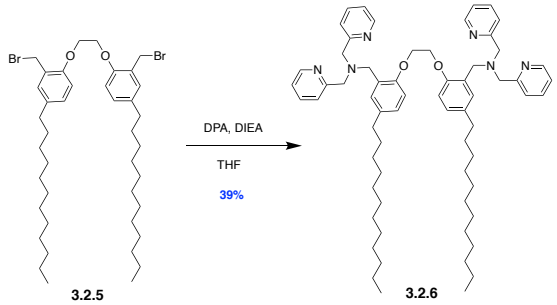


1,2-Bis(2-(bromomethyl)-4-dodecylphenoxy)ethane (3.2.5)

General procedure C was followed. Compound **3.2.4** (57.5 mg, 0.094 mmol) and PBr_3 (0.267 mL, 2.82 mmol) were used. The product was obtained as a white solid (60.6 mg, 0.082 mmol, 87% yield). R_f = 0.8 (25% EtOAc-Hexanes).

^{1}H NMR (500 MHz, $CDCl_3$) δ 7.15 (d, *J* = 2.3 Hz, 2H), 7.10 (dd, *J* = 8.4, 2.3 Hz, 2H), 6.89 (d, *J* = 8.3 Hz, 2H), 4.54 (s, 4H), 4.43 (s, 4H), 2.53 (dd, *J* = 8.8, 6.8 Hz, 4H), 1.64 – 1.55 (m, 4H),

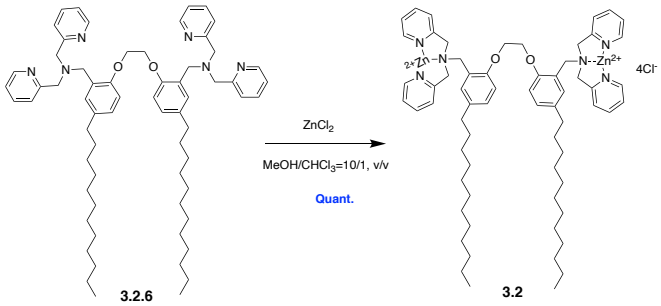
1.33 – 1.23 (m, 41H), 0.88 (t, *J* = 7.0 Hz, 6H). ^{13}C NMR (126 MHz, $CDCl_3$) δ 154.78, 135.93, 131.07, 130.06, 126.47, 112.46, 67.45, 35.10, 32.08, 31.73, 29.83, 29.82, 29.80, 29.75, 29.65, 29.51, 29.44, 22.84, 14.27. HRMS-DART: $[M+H-HBr]^+$ calcd for $C_{40}H_{64}BrO_2$: 655.4090 Found: 655.2601; $[M+H-2HBr]^+$ calcd for $C_{40}H_{63}O_2$: 575.4828, Found: 575.3531



1,1'-((Ethane-1,2-diylbis(oxy))bis(5-dodecyl-2,1-phenylene))bis(*N*,*N*-bis(pyridin-2-ylmethyl)methanamine) (3.2.6)

General procedure D was followed. Compound **3.2.5** (60.6 mg, 0.0823 mmol), DPA (34.05 µL, 0.189 mmol) and DIEA (33 µL, 0.189 mmol) yielded the product as a brown oil (31 mg, 0.032 mmol, 39% yield). R_f = 0.46 (10% Methanol in chloroform).

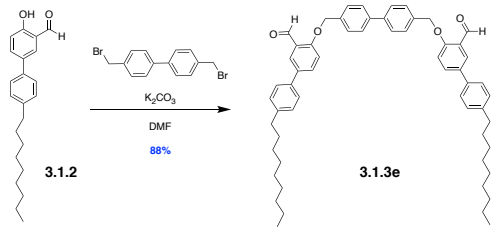
^{1}H NMR (500 MHz, $CDCl_3$) δ 8.46 (ddd, *J* = 5.1, 1.8, 0.9 Hz, 4H), 7.60 – 7.51 (m, 8H), 7.32 (d, *J* = 2.3 Hz, 2H), 7.06 (ddd, *J* = 7.2, 4.9, 1.5 Hz, 4H), 7.00 (dd, *J* = 8.3, 2.3 Hz, 2H), 6.77 (d, *J* = 8.2 Hz, 2H), 4.20 (s, 4H), 3.81 (s, 8H), 3.72 (s, 4H), 2.57 – 2.50 (m, 4H), 1.57 (p, *J* = 7.4 Hz, 4H), 1.35 – 1.17 (m, 42H), 0.88 (t, *J* = 7.0 Hz, 6H). ^{13}C NMR (126 MHz, $CDCl_3$) δ 160.41, 155.14, 149.00, 136.40, 135.30, 130.63, 127.83, 126.99, 122.62, 121.84, 111.69, 66.95, 60.47, 52.63, 35.31, 32.07, 31.85, 29.86, 29.85, 29.80, 29.73, 29.51, 29.48, 22.84, 14.27. HRMS-DART: $[M+H]^+$ calcd for $C_{64}H_{89}N_6O_2$: 973.7047, Found: 973.6695



1,1'-((Ethane-1,2-diylbis(oxy))bis(5-dodecyl-2,1-phenylene))bis(*N*,*N*-biszinc(pyridin-2-ylmethyl)methanamine) chloride (3.2)

General procedure E was followed. Compound **3.2.6** (31 mg, 0.0318 mmol) and $ZnCl_2$ (8.7 mg, 0.0637 mmol) yielded the product as a yellow solid (39.62 mg, 0.0318 mmol, quantitative yield).

^{1}H NMR (500 MHz, 20% CD_3OD-$CDCl_3$) δ 8.80 (d, *J* = 5.3 Hz, 4H), 7.61 (t, *J* = 8.1 Hz, 4H), 7.11 (dt, *J* = 28.8, 7.2 Hz, 8H), 6.92 (d, *J* = 2.7 Hz, 2H), 6.74 – 6.68 (m, 2H), 6.58 – 6.47 (m, 2H), 4.04 – 3.56 (m, 12H), 3.42 (d, *J* = 6.0 Hz, 4H), 2.46 – 2.37 (m, 4H), 1.51 (d, *J* = 8.2 Hz, 4H), 1.34 – 1.19 (m, 50H), 0.83 (t, *J* = 6.6 Hz, 6H).

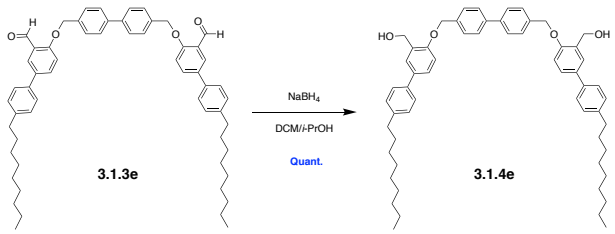


4,4''-(([1,1'-Biphenyl]-4,4'-diylbis(methylene))bis(oxy))bis(4'-nonyl-[1,1'-biphenyl]-3-carbaldehyde) (3.1.3e)

General procedure A was followed. Compound **3.1.2** (0.15 g, 0.4623 mmol), K_2CO_3 (0.1916 g, 1.3869 mmol) and 4,4'-bis(bromomethyl)-1,1'-biphenyl (78.58 mg, 0.2311 mmol) were used. The product was obtained as a white solid (0.1683 g, 0.2 mmol, 88% yield). R_f = 0.36 (75% DCM-hexanes).

^{1}H NMR (500 MHz, Chloroform-*d*) δ 10.63 (s, 2H), 8.11 (d, *J* = 2.5 Hz, 2H), 7.78 (dd, *J* = 8.7, 2.5 Hz, 2H), 7.66 (d, *J* = 8.1 Hz, 4H), 7.55 (d, *J* = 8.0 Hz, 4H), 7.50 (d, *J* = 8.0 Hz, 4H), 7.25

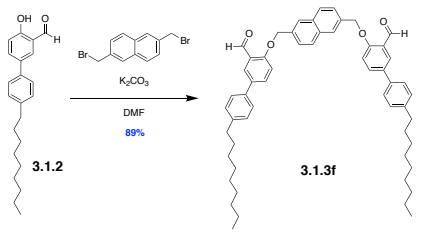
(d, *J* = 7.6 Hz, 4H), 7.15 (d, *J* = 8.7 Hz, 2H), 5.29 (s, 4H), 2.64 (t, *J* = 7.8 Hz, 4H), 1.64 (p, *J* = 7.4 Hz, 4H), 1.42 – 1.20 (m, 24H), 0.89 (t, *J* = 6.8 Hz, 6H). ^{13}C NMR (126 MHz, $CDCl_3$) δ 189.85, 160.36, 142.44, 140.79, 136.84, 135.50, 134.37, 134.26, 129.09, 128.01, 127.63, 126.74, 126.67, 125.42, 113.65, 70.55, 35.73, 32.04, 31.63, 29.71, 29.67, 29.50, 29.48, 22.83, 14.26. MS not detected on DART



((([1,1'-Biphenyl]-4,4'-diylbis(methylene))bis(oxy))bis(4'-nonyl-[1,1'-biphenyl]-4,3-diyl))dimethanol (3.1.4e)

General procedure B was followed. Compound **3.1.3e** (0.158 g, 0.191 mmol) and $NaBH_4$ (21.68 mg, 0.573 mmol) yielded the product as a white solid in a quantitative yield and used without purification. R_f = 0.38 (25% EtOAc-Hexanes).

^{1}H NMR (500 MHz, Chloroform-*d*) δ 7.71 – 7.61 (m, 4H), 7.59 (d, *J* = 2.3 Hz, 2H), 7.57 – 7.53 (m, 4H), 7.53 – 7.47 (m, 6H), 7.26 (d, *J* = 8.3 Hz, 4H), 7.06 (d, *J* = 8.5 Hz, 2H), 5.24 (s, 4H), 4.84 (s, 4H), 2.69 – 2.62 (m, 4H), 1.67 (t, *J* = 7.9 Hz, 4H), 1.43 – 1.23 (m, 28H), 0.91 (t, *J* = 6.8 Hz, 6H). ^{13}C NMR (126 MHz, $CDCl_3$) δ 156.03, 141.84, 140.72, 138.05, 136.09, 134.39, 129.86, 128.96, 128.00, 127.69, 127.60, 127.37, 126.78, 112.12, 70.14, 62.47, 35.74, 32.05, 31.67, 29.86, 29.71, 29.69, 29.53, 29.49, 22.83, 14.27. MS not detected on DART

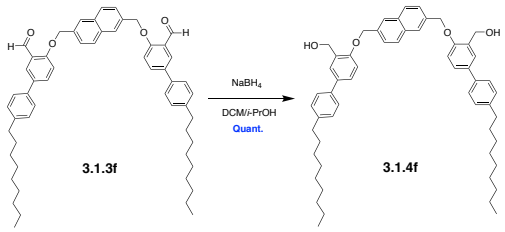


4,4''-((Naphthalene-2,6-diylbis(methylene))bis(oxy))bis(4'-nonyl-[1,1'-biphenyl]-3-

carbaldehyde) (3.1.3f)

General procedure A was followed. Compound **3.1.2** (0.15 g, 0.4623 mmol), K_2CO_3 (0.1916 g, 1.3869 mmol) and 2,6-bis(bromomethyl)naphthalene (72.6 mg, 0.2311 mmol) were used. The product was obtained as a white solid (0.1648 g, 0.2 mmol, 89% yield). R_f = 0.43 (75% DCM-hexanes).

^{1}H NMR (500 MHz, Chloroform-*d*) δ 10.65 (s, 2H), 8.11 (d, *J* = 2.4 Hz, 2H), 7.96 – 7.94 (m, 2H), 7.93 (d, *J* = 8.4 Hz, 2H), 7.77 (dd, *J* = 8.6, 2.5 Hz, 2H), 7.61 (dd, *J* = 8.4, 1.6 Hz, 2H), 7.51 – 7.47 (m, 4H), 7.26 – 7.23 (m, 4H), 7.16 (d, *J* = 8.7 Hz, 2H), 5.42 (s, 4H), 2.66 – 2.61 (m, 4H), 1.68 – 1.60 (m, 4H), 1.39 – 1.22 (m, 26H), 0.88 (t, *J* = 6.9 Hz, 6H). ^{13}C NMR (126 MHz, $CDCl_3$) δ 189.85, 160.35, 142.45, 136.83, 134.43, 134.30, 134.28, 133.17, 129.10, 128.91, 126.78, 126.68, 126.35, 125.72, 125.45, 113.70, 70.88, 35.73, 32.04, 31.63, 29.71, 29.67, 29.50, 29.48, 22.83, 14.26. HRMS-DART: $[M+H]^+$ calcd for $C_{56}H_{65}O_4$: 801.4883; Found: 801.4570.

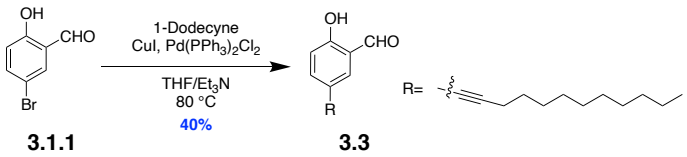


(((Naphthalene-2,6-diylbis(methylene))bis(oxy))bis(4'-nonyl-[1,1'-biphenyl]-4,3-diyl))dimethanol (3.1.4f)

General procedure B was followed. Compound **3.1.3f** (0.1472 g, 0.184 mmol) and $NaBH_4$ (37.83 mg, 0.5512 mmol) yielded the product as a white solid in a quantitative yield and passed along to the next step without purification. R_f = 0.3 (25% EtOAc-Hexanes).

^{1}H NMR (500 MHz, Chloroform-*d*) δ 7.94 – 7.87 (m, 4H), 7.58 (dd, *J* = 10.8, 2.1 Hz, 4H), 7.48 (dd, *J* = 8.4, 2.4 Hz, 6H), 7.25 – 7.21 (m, 4H), 7.05 (d, *J* = 8.5 Hz, 2H), 5.33 (s, 4H), 4.83 (s, 4H), 2.67 – 2.60 (m, 4H), 1.68 – 1.60 (m, 4H), 1.40 – 1.21 (m, 26H), 0.89 (t, *J* = 6.9 Hz, 6H). ^{13}C NMR (126 MHz, $CDCl_3$) δ 156.01, 141.83, 138.04, 134.81, 134.40, 133.14, 129.88, 128.95, 128.84, 127.66, 127.35, 126.77, 126.32, 125.76, 112.20, 70.51, 62.41, 35.74, 32.05, 31.67,

29.71, 29.69, 29.52, 29.49, 22.83, 14.26. HRMS-DART: $[M+H-H_2O]^+$ calcd for $C_{56}H_{67}O_3$: 787.5090; Found: 787.4271. $[M+H-2H_2O]^+$ calcd for $C_{56}H_{65}O_2$: 769.4984; Found: 769.4216

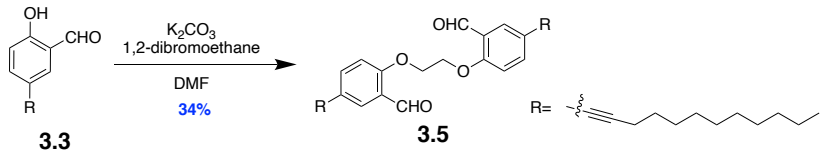


3.1.1 **3.3**

5-(Dodec-1-yn-1-yl)-2-hydroxybenzaldehyde (3.3)

5-Bromo-2-hydroxybenzaldehyde (**3.1.1**, 0.5 g, 2.48 mmol), bis(triphenylphosphine)palladium (II) chloride ($PdCl_2(PPh_3)_2$, 87.3 mg, 0.124 mmol) and CuI (23.7 mg, 0.124 mmol) were combined in a 50 mL RBF under nitrogen. After being dissolved with 15 mL DMF/TEA/THF (1/1/1, v/v) and the addition of 1-dodecyne (0.827 g, 1.06 mL, 4.97 mmol), the reaction mixture was refluxed for 30 hr. The reaction progress was tracked via TLC. After completion, the reaction was cooled to rt and the solvent was removed using a rotary evaporator. The residue was re-dissolved in 25 mL DCM and poured into 50 mL 0.5 N HCl in a separatory funnel. The DCM layer was collected, and the aqueous layer was extracted with 2 x 25 mL DCM. The combined organic layer was further washed with 1 x 50 mL water and 1 x 50 mL brine, respectively, before being dried over Na_2SO_4, filtered, and concentrated under reduced pressure. The crude was next loaded onto silica gel and subjected to column chromatography. Gradient elution from hexanes to 2% ethyl acetate in hexanes yielded the product as a dark brown oil (0.28 g, 1 mmol, 40% yield). R_f = 0.33 (5% EtOAc-hexanes).

^{1}H NMR (300 MHz, Chloroform-*d*) δ 11.02 (s, 1H), 9.84 (s, 1H), 7.60 (d, *J* = 2.1 Hz, 1H), 7.53 (dd, *J* = 8.6, 2.2 Hz, 1H), 6.91 (d, *J* = 8.6 Hz, 1H), 2.39 (t, *J* = 7.0 Hz, 2H), 1.63 – 1.55 (m, 2H), 1.49 – 1.39 (m, 2H), 1.34 – 1.21 (m, 16H), 0.90 – 0.85 (m, 3H). ^{13}C NMR (126 MHz, $CDCl_3$) δ 196.30, 160.96, 140.06, 136.79, 120.53, 117.98, 116.25, 90.14, 78.85, 32.07, 29.74, 29.69, 29.48, 29.31, 29.10, 28.86, 22.84, 19.48, 14.27.

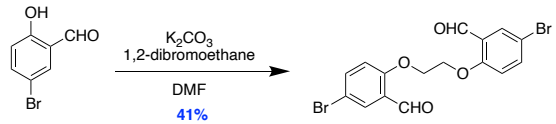


3.3 **3.5**

6,6'-(Ethane-1,2-diylbis(oxy))bis(3-(dodec-1-yn-1-yl)benzaldehyde) (3.5)

General procedure A was followed. **3.3** (47 mg, 0.164 mmol), K_2CO_3 (68 mg, 0.492 mmol) and dibromoethane (7.07 µL 0.082 mmol) were used. The product was obtained as a yellow oil (0.1265 g, 0.1874 mmol, 33% yield). R_f = 0.48 (25% EtOAc-hexanes).

^{1}H NMR (300 MHz, Chloroform-*d*) δ 10.39 (s, 2H), 7.87 (d, *J* = 2.2 Hz, 2H), 7.57 (dd, *J* = 8.6, 2.3 Hz, 2H), 6.97 (d, *J* = 8.7 Hz, 2H), 4.51 (s, 4H), 2.38 (t, *J* = 7.0 Hz, 4H), 1.63 – 1.53 (m, 6H), 1.48 – 1.37 (m, 4H), 1.28 (q, *J* = 5.0 Hz, 28H), 0.90 – 0.85 (m, 6H). ^{13}C NMR (126 MHz, $CDCl_3$) δ 188.69, 159.73, 138.75, 132.14, 125.09, 117.96, 112.79, 90.76, 78.99, 67.15, 32.06, 29.86, 29.75, 29.69, 29.48, 29.32, 29.09, 28.85, 22.84, 19.51, 14.27. HRMS-DART: $[M+H]^+$ calcd for $C_{40}H_{55}O_4$: 599.4100; Found: 599.3006.

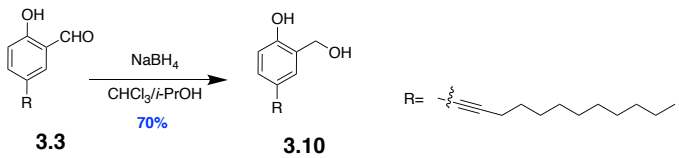


3.1.1 **3.9**

6,6'-(Ethane-1,2-diylbis(oxy))bis(3-bromobenzaldehyde) (3.9)

General procedure A was followed. 5-Bromo-2-hydroxybenzaldehyde (**3.1.1**, 1.0 g, 4.975 mmol), K_2CO_3 (1.97 g, 14.22 mmol) and dibromoethane (0.2 mL, 2.37 mmol) were used. The product was obtained as a white solid (0.4145 g, 0.97 mmol, 41% yield). R_f = 0.2 (25% EtOAc-hexanes); 0.61 (100% DCM).

^{1}H NMR (300 MHz, Chloroform-*d*) δ 10.36 (d, *J* = 0.8 Hz, 2H), 7.95 (dd, *J* = 2.6, 0.8 Hz, 2H), 7.66 (dd, *J* = 8.8, 2.6 Hz, 2H), 6.96 (dd, *J* = 8.9, 0.8 Hz, 2H), 4.51 (d, *J* = 0.9 Hz, 4H).

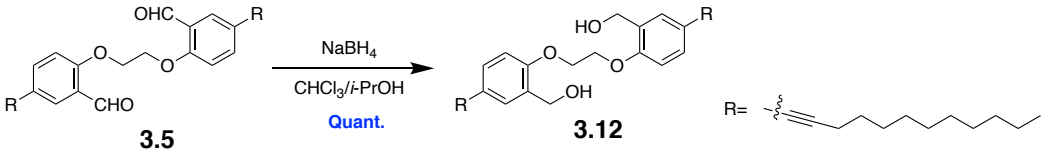


3.3 **3.10**

4-(Dodec-1-yn-1-yl)-2-(hydroxymethyl)phenol (3.10)

General procedure B was followed. **3.3** (0.1195 g, 0.417 mmol) and $NaBH_4$ (34.72 mg, 0.92 mmol) yielded the product as a slight yellow solid (81.5 mg, 0.283 mmol, 70% yield). R_f = 0.43 (25% EtOAc-hexanes).

^{1}H NMR (300 MHz, Chloroform-*d*) δ 7.42 (s, 1H), 7.28 – 7.18 (m, 1H), 7.08 (d, *J* = 2.1 Hz, 1H), 6.80 (d, *J* = 8.3 Hz, 1H), 4.83 (d, *J* = 3.2 Hz, 2H), 2.36 (t, *J* = 7.0 Hz, 2H), 2.23 (s, 1H), 1.56 (dd, *J* = 9.9, 4.7 Hz, 2H), 1.50 – 1.36 (m, 2H), 1.28 (q, *J* = 4.9, 4.0 Hz, 14H), 0.93 – 0.83 (m, 3H). ^{13}C NMR (126 MHz, $CDCl_3$) δ 155.87, 132.95, 131.08, 124.52, 116.81, 115.86, 88.95, 80.14, 64.69, 32.06, 29.75, 29.70, 29.48, 29.33, 29.09, 29.01, 22.84, 19.53, 14.27.

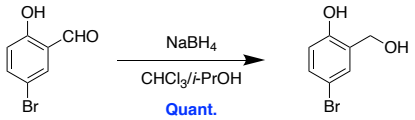


3.5 **3.12**

((Ethane-1,2-diylbis(oxy))bis(5-(dodec-1-yn-1-yl)-2,1-phenylene))dimethanol (3.12)

General procedure B was followed. **3.5** (16 mg, 0.027 mmol) and $NaBH_4$ (4.45 mg, 0.117 mmol) yielded the product as a yellow oil (16.2 mg, 0.027 mmol, quantitative yield). R_f = 0.42 (25% EtOAc-hexanes).

^{1}H NMR (500 MHz, Chloroform-*d*) δ 7.37 – 7.28 (m, 4H), 6.83 (d, *J* = 8.4 Hz, 2H), 4.60 (s, 4H), 4.39 (s, 4H), 2.37 (t, *J* = 7.1 Hz, 4H), 1.63 – 1.54 (m, 6H), 1.46 – 1.39 (m, 4H), 1.34 – 1.20 (m, 36H), 0.90 – 0.86 (m, 6H). ^{13}C NMR (126 MHz, $CDCl_3$) δ 155.83, 132.85, 132.33, 129.85, 117.49, 111.73, 89.56, 80.04, 66.98, 61.47, 32.06, 29.86, 29.75, 29.70, 29.48, 29.34, 29.10, 28.99, 22.84, 19.55, 14.27, 1.17. HRMS-DART: $[M+H]^+$ calcd for $C_{40}H_{59}O_4$: 603.4414; Found: 603.3863.

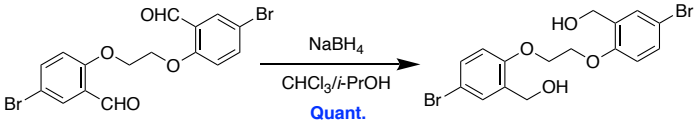


3.1.1 **3.14**

4-Bromo-2-(hydroxymethyl)phenol (3.14)

General procedure B was followed. 5-Bromo-2-hydroxybenzaldehyde (**3.1.1**, 0.1 g, 0.497 mmol), and $NaBH_4$ (41.4 mg, 1.1 mmol) yielded the product as a white solid in a quantitative yield without column chromatography purification. R_f = 0.5 (50% EtOAc-hexanes). Note: This compound has low solubility in chloroform; CD_3OD was needed when taking NMRs.

^{1}H NMR (300 MHz, $CDCl_3/CD_3OD$) δ 7.25 – 7.13 (m, 2H), 6.64 (dd, *J* = 8.3, 2.6 Hz, 1H), 4.62 (d, *J* = 2.4 Hz, 2H). ^{13}C NMR (75 MHz, $CDCl_3/CD_3OD$) δ 154.63, 131.35, 130.66, 128.32, 117.40, 111.47, 61.89.

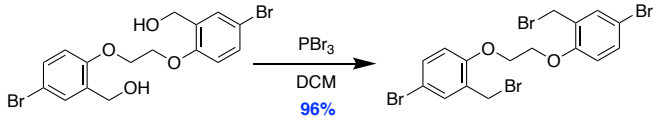


3.9 **3.16**

((Ethane-1,2-diylbis(oxy))bis(5-bromo-2,1-phenylene))dimethanol (3.16)

General procedure B was followed. **3.9** (0.1 g, 0.2336 mmol) and $NaBH_4$ (37.83 mg, 1.028 mmol) yielded the product as a white solid in a quantitative yield and was passed along to the next step without purification. R_f = 0.13 (25% EtOAc-Hexanes); 0.43 (50% EtOAc-Hexanes). Note: this compound has minimal solubility in DCM. Addition of MeOH could help shortly after making the product. However, it would not help after several days of preparation.

^{1}H NMR (300 MHz, Chloroform-*d*) δ 7.45 (dd, *J* = 2.6, 1.2 Hz, 2H), 7.38 (dd, *J* = 8.4, 2.5 Hz, 2H), 6.80 (dd, *J* = 8.7, 1.2 Hz, 2H), 4.61 (d, *J* = 1.1 Hz, 4H), 4.39 – 4.35 (m, 4H).

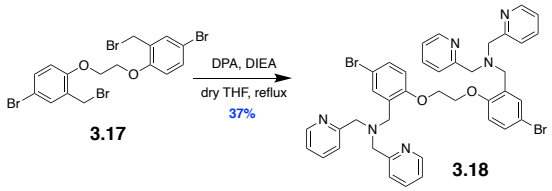


3.16 **3.17**

1,2-Bis(4-bromo-2-(bromomethyl)phenoxy)ethane (3.17)

General procedure C was followed. Compound **3.16** (0.2633 g, 0.472 mmol) and PBr_3 (1.36 mL, 14.16 mmol) were used. The product was obtained as a white solid (0.2534 g, 0.454 mmol, 96% yield). R_f = 0.8 (25% EtOAc-Hexanes).

^{1}H NMR (600 MHz, Chloroform-*d*) δ 7.46 (d, *J* = 2.5 Hz, 2H), 7.41 (dd, *J* = 8.7, 2.5 Hz, 2H), 6.86 (d, *J* = 8.7 Hz, 2H), 4.45 (s, 4H), 4.44 (s, 4H). ^{13}C NMR (151 MHz, $CDCl_3$) δ 155.70, 133.76, 132.91, 128.89, 114.11, 113.44, 67.45, 27.71. HRMS-DART: $[M+H]^+$ calcd for $C_{16}H_{14}Br_4O_2$: 553.7727; Found: 553.7512.



1,1'-((Ethane-1,2-diylbis(oxy))bis(5-bromo-2,1-phenylene))bis(*N*,*N*-bis(pyridin-2-ylmethyl)methanamine) (3.18)

General procedure D was followed. Compound **3.17** (100 mg, 0.18 mmol), DPA (45 µL, 0.414 mmol) and DIEA (72.1 µL, 0.414 mmol) yielded the product as a pale yellow solid (53 mg, 0.067 mmol, 37% yield). R_f = 0.24 (5% Methanol in DCM).

^{1}H NMR (300 MHz, Chloroform-*d*) δ 8.48 (ddd, *J* = 4.9, 1.8, 0.9 Hz, 4H), 7.69 – 7.49 (m, 10H), 7.29 (dd, *J* = 8.7, 2.6 Hz, 2H), 7.09 (ddd, *J* = 6.9, 5.0, 1.4 Hz, 4H), 6.72 (d, *J* = 8.7 Hz, 2H), 4.19 (s, 4H), 3.80 (s, 8H), 3.68 (s, 4H). ^{13}C NMR (75 MHz, $CDCl_3$) δ 159.53, 155.79, 148.94, 136.41, 132.82, 130.62, 129.73, 122.58, 121.93, 113.51, 113.28, 66.85, 60.31, 51.70. HRMS-DART: $[M+H]^+$ calcd for $C_{40}H_{39}Br_2O_2N_6$: 793.1501; Found: 793.0636.

Liposome preparation and Assays

Preparation of liposomes for Nile red release assays

Stock solutions of 5 mM lipid switches **3.1a-d/3.2** were prepared in $CHCl_3$/MeOH solution (1/1, v/v). 32.46 mM PC and 5 mM NR stock solutions were prepared in chloroform. All the stock solutions were kept in a -20 ºC freezer after preparation. Proper volumes of each stock solution were pipetted into a 1 dr vial to reach a total lipid concentration of 2 mM, 0.4 mM or 0.1 mM with desired percentages of each lipid composition. NR was added as an extra 5% of the total lipid content. The organic solvents were next evaporated under a nitrogen stream, and the

resulting lipid films were kept under vacuum for at least one hour. After that, the films were hydrated with proper volumes of 1×TBS buffer (pH=7.4, containing 25 mM Tris/Tris HCl, 0.13 M NaCl, 0.0027 M KCl) in a 60 ºC water bath for 1 hr. The vials were taken out and vortexed every 20 min. Next, ten freeze-thaw cycles were performed with a dry ice-acetone bath and 60 ºC water bath. Finally, the liposome solutions were extruded through a 200 nm polycarbonate membrane for 19 passes with an extruder purchased from either Avestin or Avanti. The resulting liposomes were stored at 4 ºC and were studied within a maximum of 48 hours.

Phosphorylated metabolite selectivity screen for liposome Nile red release

50 mM stock solutions stock solutions of each phosphorylated metabolite were prepared by dissolving the appropriate salts (sodium phosphate dibasic heptahydrate (Pi, $Na_2HPO_4{\cdot}7H_2O$); Sodium pyrophosphate dibasic (PPi, $Na_2H_2P_2O_7$); Adenosine 5'-diphosphate sodium salt (ADP); Adenosine 5'-triphosphate disodium salt, hydrate (ATP); D-Fructose-6-phosphate disodium salt (FP); D-Fructose-1,6-bisphosphate trisodium salt (FBP); Sodium tripolyphosphate (TPi); Cytidine-5'-triphosphate disodium salt (CTP); Guanosine-5'-triphosphate trisodium salt (GTP); Uridine 5′-triphosphate trisodium salt hydrate (UTP); D-*myo*-inositol-1,4,5-triphosphate sodium salt (IP_3)) with MilliQ water. Adenosine 5′-monophosphate monohydrate (AMP) was prepared as 25 mM stock solutions in MilliQ water due to solubility issue. For each study, 50 µL of liposome solution encapsulating NR was first added into a sub-micro quartz cuvette. After an initial scan, 1 µL of 50 mM stock solutions of the phosphorylated metabolite under study was added to the cuvette (final concentration = 1 mM, 2 µL for AMP), and the fluorescence intensities were recorded immediately (for typical phosphorylated metabolites) or after incubation for 5 min (for triphosphates) (excitation wavelength = 552 nm, excitation slit = 5 nm, emission slit = 5 nm). Control experiments were run by adding 1 or 2 µL MilliQ water. When processing the data, the fluorescence intensities at 630 nm were selected (635 nm for **3.1d**) and converted to percentage of initial fluorescence before phosphorylated

metabolite addition. Experiments were run at least three times with different batches of liposomes. Averaged data were reported with error bars denoting standard error.

ATP titration Nile red release assay

ATP stock solutions (2.5 mM) were prepared by diluting the previously prepared 50 mM ATP stock solution 20× with MilliQ water. A 100 μL aliquot of 2 mM liposomes encapsulating NR prepared through the procedure described above was added into a sub-micro quartz cuvette. After an initial scan, 1 μL of 2.5 mM ATP stock solution was added directly into the cuvette for each measurement in the titration, and the fluorescence intensities were measured using the same detection method as described above. When processing the data, the fluorescence intensities at 630 nm were selected (635 nm for **3.1d**) and converted to percentage of initial fluorescence before ATP addition. Experiments were run at least three times with different batches of liposomes. Averaged data were reported with error bars denoting standard errors. Kinetic experiments were run on a Cary Eclipse Fluorescence Spectrophotometer using kinetic mode. The excitation wavelength was set to 552 nm, and the fluorescence intensities at 630 nm were constantly collected over time. For NR release experiments containing diluted liposomes, 0.4 mM or 0.1 mM liposomes were prepared using the same preparation method described above except the total lipid content was cut down during film preparation. The same excitation and emission wavelengths were used. For 0.4 mM, Ex/Em slits were set to be 5/10 nm, and Ex/Em slits were set to be 10/10 nm for 0.1 mM liposomes.

Preparation of liposomes for calcein release assays

The same stock solutions of **3.1a-d/3.2** and PC prepared for NR release assay were used. 50 mM calcein stock solutions were prepared by dissolving calcein with 25 mM Tris-HCl buffer and the pH was then adjusted to 7.4 by adding 1 N NaOH. The osmolality of the solution was determined to be 255 mOsm/kg. Proper volumes of each lipid stock solution were pipetted into a clean 1 dr vial to reach a total lipid content of 5 mM scale with desired percentages of each

lipid composition. The organic solvents were next removed with a nitrogen stream and the resulting lipid films were further dried under vacuum for at least 1 hr. The films were next hydrated with 50 mM calcein solution at 60 ºC in a water bath for four sets of 15 min with vortexing after each set. Next, the solutions were subjected to ten freeze-thaw cycles with a dry ice-acetone bath and a 60 ºC water bath, followed by extrusion through a 200 nm polycarbonate membrane for 21 passes with an extruder purchased from either Avestin or Avanti. Finally, the unencapsulated calcein dye was removed by size-exclusive chromatography. To do so, a micro-column was first packed with Sephadex G-50 (pre-saturated with isotonic TBS buffer). The fractions were next collected every ~1 mL from the column and the second fraction showing significant turbidity was collected. The presence of liposomes was further verified by treating liposomes with Triton X-100 detergent, where an increase in fluorescence intensity was observed.

Calcein release assays via ATP treatment

An aliquot of 100 μL liposomes encapsulating calcein prepared through the procedure described above was added into a sub-micro quartz cuvette. After an initial scan, 25 μL of a 50 mM ATP stock solution in MilliQ water was added into the cuvette (final concentration = 10 mM), and the fluorescence intensities were recorded over time (λ_{ex}=490 nm, λ_{em}=520 nm, Ex/Em slit=10/2.5 nm). After completion, the assay was calibrated by adding 1 μL of 20% Triton X-100 detergent to lyse the liposomes and induce 100% release. When processing the data, fluorescence intensities at 520 nm were selected and reported as a percentage of the fluorescence after Triton X-100 treatment for each sample. For release studies with diluted liposomes, liposomes were prepared using the same method and then further diluted 10× with isotonic buffer. The same amount of ATP addition and detection methods were used. Experiments were run at least three times with different batches of liposomes. Averaged data were reported with error bars denoting standard errors. Kinetic experiments were run on a Cary Eclipse Fluorescence Spectrophotometer using kinetic mode. The excitation wavelength

was set to 490 nm and the fluorescent intensities at 520 nm were constantly collected overtime.

DLS analysis of liposomes before and after triggered release

DLS analyses were carried out with a Malvern Zetasizer Nano ZS instrument equipped with a 4.0 mW laser operating at l = 633 nm. Samples were prepared by diluting the liposomes before and after triggered release 10× with proper buffer. All measurements were taken at a scattering angle of 173º at 20 ºC. Bar graphs were generated by the average of at least three experiments with error bars denoting standard error.

Nile red encapsulation efficiency

UV/vis scans before and after liposome formulation were used to assess cargo encapsulation. The NR calibration curve in chloroform was first generated. The same PC-based liposomes containing 0% or 10% **3.1a** used in NR release assays were prepared as described previously. After liposome formation, an aliquot of 300 µL of liposomes was transferred into a 4 dr vial and water was removed under reduced pressure. The resulting film was kept under vacuum for five hours before being re-dissolved with 3 mL chloroform and sonication to dissolve all components. The resulting solution was filtered through a 0.2 µm PTFE filter and transferred into a quartz cuvette for UV-Vis measurements. The absorbance peaks at 540 nm were used to calculate the NR encapsulation efficiency.

Calcein encapsulation efficiency

The same PC-based liposomes containing 0% or 10% **3.1a** used in calcein release assays were prepared according to the previously described procedure. After liposome formation, an aliquot of 30 µL of liposomes was transferred into a disposable cuvette and diluted into 3 mL with MilliQ purified water. An aqueous solution of 10% Triton X-100 (2 µL) was added before acquiring UV-Vis spectra. The absorbance peaks at 495 nm were used to calculate calcein encapsulation efficiency using the previously reported method ($\varepsilon_{495,free}=\varepsilon_{495,encapsulated}=7.0 \times 10^4$

M^{-1} cm^{-1} for calcein and an estimated bilayer thickness=4 nm, cross-sectional area of lipids=0.7 nm^2 and [encapsulated calcein]=5 × 10^{-2} M).[195]

Reversibility of Nile red release assay and calcein release assay

PC-based liposomes containing 10% or 20% **3.1a** encapsulating NR or calcein were prepared as previously described. 100 Unit/mL apyrase from potatoes (Sigma-Aldrich, A6535) stock solutions were prepared in 1XTBS (pH=7.4, containing 5 mM $CaCl_2$ for activation). For NR kinetic analysis, the excitation wavelength was set to be 552 nm and the fluorescence intensities at 630 nm were constantly collected over time. For calcein release assays, excitation and emission wavelengths were set at 490 nm and 520 nm, respectively. For NR assays, a 50 µL aliquot of liposomes was first added into a sub-micro quartz cuvette. ATP (2 µL of a 50 mM stock solution for a final concentration = 2 mM) in MQ was added into the cuvette. Once the fluorescence intensity plateaued, 5 µL ATPase enzyme (0.5 U) was added. For calcein assays, ATP (12.5 µL of 50 mM stock solution for a final concentration = 10 mM) in MQ was added into the cuvette instead. 5 µL ATPase enzyme (0.5 U) was then added. DLS measurements were acquired as previously described.

DOSY NMR Experiments to determine diffusion coefficients

Lipid **3.1a** and ATP were dissolved in 0.5 mL d_6-DMSO containing 8% D_2O at a concentration of 3 mM and 4 mM, respectively, in two separate NMR tubes. In a third NMR tube, 3 mM lipid **3.1a** and 4 mM ATP were co-dissolved in the same solution to keep consistency. DOSY spectra were recorded and analyzed by MestReNova. Experiments were performed in triplicate and diffusion coefficients are reported as an average over three trials with standard deviations reported.

Electron Microscope (EM) analysis

1 mM solutions of liposomes containing 100% PC or 10% **3.1a** in PC without any dye

encapsulation were prepared using the standard procedure described above. For samples after triggered release, 1 μL of 50 mM ATP stock solution was added into a solution of 100 μL liposomes in a vial.

For regular transmission EM (TEM) studies, one drop (5-10 μL) of each sample was immobilized (for 1 min) onto a thin carbon film supported by 200 mesh copper grid and then stained (for 1 min) with a 1.0% (w/v) solution of neutral phosphotungstic acid. After drying, the samples were stored in a desiccator overnight prior to imaging. Images were taken using a JOEL 1400 Flash microscope operating with a beam energy of 80 keV. Images were taken using a Gatan One View camera and processed with ImageJ software.

For cryo-EM studies, a drop (2-3 μL) of each sample was deposited onto a thin carbon film supported by 300 mesh copper grid and then vitrified with liquid propane. Grids were stored in liquid nitrogen prior to imaging. Images were taken using a Zeiss libra 200 HT FE MC microscope. Images were taken with a Gatan One View camera and processed with ImageJ software.

Fluorescence microscopy studies for liposome aggregation after ATP treatment

1 mM solutions of 0% and 10% **3.1a** liposomes in PC labeled with 0.08% rhodamine L-α-phosphatidylethanolamine (Rd-PE) in 1×TBS buffer (pH=7.4, containing 25 mM Tris/Tris HCl, 0.13 M NaCl, 0.0027 M KCl) were prepared using the previously described thin-film hydration procedures.

An aliquot of the liposome solution (100 μL) was first added into a FluoroDish Cell Culture Dish (WPI Inc.) and allowed to settle for 15 min before imaging using a 63x 1.4NA oil objective on a Leica SP8 White Light Laser Confocal Microscope (Wetzlar, Germany). Rd-PE was excited by using a 561 nm laser line and the emission was collected between 566-620 nm.

^{31}P NMR titration binding experiment

Lipid **3.1a** was first dissolved in d_6-DMSO at a concentration of 4 mg/mL (~3 mM) in a vial. Then, 0.5 mL of the solution was transferred into an NMR tube. A 50 mM ATP stock solution was prepared in D_2O. In a separate NMR tube containing 0.5 mL d_6-DMSO, 40 µL of ATP stock solution was added (final conc. = 4 mM, 8% D_2O in d_6-DMSO) to generate the ATP standard. ^{31}P NMR analysis of the ATP standard sample was first performed. To the NMR tube containing **3.1a**, 10 µL of ATP stock solution was added each time, and ^{31}P NMR were recorded immediately after each addition (increment = 1 mM ATP, 2% D_2O). The spectra were processed using MestReNova.

Zeta potential measurements of 1a liposomes before and after adding ATP

Zeta potential values were also measured with a Malvern Zetasizer Nano ZS instrument equipped with a 4.0 mW laser operating at l = 633 nm. A 1 mM solution of PC-based liposomes containing 0%, 5% and 10% **3.1a** without dye encapsulation were prepared in 1 mM HEPES (pH=7.4, containing 30 mM NaCl). A 200 µL aliquot of liposomes was diluted with 800 µL buffer before addition of 5 µL of 50 mM ATP (conc of liposomes = 0.2 mM, conc of ATP = 0.25 mM). The solutions were next transferred into an DTS1070 folded capillary cell ready for measurement. All measurements were taken at 20 ºC. Data were generated with at least three replicates.

UV-Vis titration 3.1a-ATP binding experiment

5 mM **3.1a** stock solutions in MeOH/$CHCl_3$ and 50 mM ATP in MilliQ water that were prepared for previous release studies were used. 30 µL of **3.1a** stock solution was added into 3 mL DMSO in a quartz cuvette (final **3.1a** concentration = 5×10^{-5} M). Another quartz cuvette containing 3 mL DMSO and 30 µL MeOH/$CHCl_3$ was prepared as a reference cell. 1 µL of ATP solution was added into both cuvettes at the same time using a glass syringe and the spectra

were recorded after each addition (increment = 1.67×10^{-5} M). When processing the data, the intensities at 265 nm were selected. The decreases in absorbance were plotted against concentrations of ATP added.

Cellular delivery experiments

Cell Culture

A375 cells were purchased from ATCC and maintained in Dulbecco's Modified Eagle Medium (DMEM) (Gibco 11-995-073) containing 10% Fetal Bovine Serum (FBS) and 100 U/mL penicillin/streptomycin (Gibco 15-140-122) at 37ºC with 5% CO_2. Cells were passed at approximately 80% confluency and were not used for more than 30 passes.

Fluorescence Microscopy

2 mM solutions of 0% and 5% **3.1a** liposomes in PC containing 0.08% rhodamine L-α-phosphatidylethanolamine (Rd-PE) in 1×TBS buffer (pH=7.4, containing 25 mM Tris/Tris HCl, 0.13 M NaCl, 0.0027 M KCl) were prepared using the previously described thin-film hydration procedures.

1.2×10^5 A375 cells were plated per well of a 12-well plate containing sterile #1.5 12 mm round glass coverslips 48 hours before treatment and media was changed 24 hours before treatment. Cells were treated with 1 mM of PC liposomes containing 0.08% Rd-PE with (study liposomes) or without (control liposomes) 5% **3.1a** for 30 min at 37ºC. Cells were then washed four times with PBS containing 1 mM $MgCl_2$ and 100 mM $CaCl_2$ (PBS^{++}), fixed for 15 min in 4% paraformaldehyde at 37ºC and stained with DAPI. Coverslips were then mounted on microscope slides using Prolong Diamond Antifade Mountant (Invitrogen) and allowed to cure for 24 h before imaging using a 63x 1.4NA oil objective on a Leica SP8 White Light Laser Confocal Microscope. Images were the product of 3-fold line averaging. Three to five images were taken per coverslip and fluorescence was measured for 6 cells per image via ImageJ.

Cell Viability Assay

PC liposomes (4 mM) containing 0% (PC control) or 5% **3.1a** without any content encapsulation were prepared using the standard liposome preparation procedure described above.

2 x 10^4 A375 cells were plated per well of a clear flat bottom 96 well plate and allowed to adhere and incubate for 24 hours. Cells were then treated with 2 mM, 1 mM, 200 μM, 40 μM, 8 μM, 1.6 μM, or 0 μM liposomes (Control and 5% **3.1a**) in a 1:1 solution of serum free media and TBS for 30 minutes. Cells were then washed with PBS^{++} and incubated in 100 μL phenol free DMEM containing 10% FBS for 24 hours. Finally, 10 μL MTS reagent (Promega G3582) was added to the wells, incubated for 1.5 hr, and 490 nm absorbance was measured using a Biotek Cytation V microplate reader with Gen5 software.

Intracellular ATP Modification

Prior to treatment with study or control liposomes, cells were washed twice and incubated with the following ATP modifying drug treatments: 1 μM antimycin-A (AA) and 250 mM 2-deoxy-D-glucose (DG), or 500 mM AICAR in glucose-free DMEM (Gibco 11-966-025) at 37 ºC for 1 hr (AA/DG) or 3 hr (AICAR).

ATP Quantification

For ATP quantification, 4 x 10^4 cells were plated per well of a white opaque 96-well plate 48 hours before treatment, and media was changed 24 hours before treatment. Cells were treated for ATP modification using the above protocol. Cells were then washed 2 times with PBS^{++}, and ATP was quantified using a luminescent ATP detection assay kit from Abcam (ab113849) according to manufacturer's protocols. Briefly, 100 μL glucose-free DMEM was added to cells, followed by 50 μL of detergent addition, and the plate was shaken on an orbital shaker for 5

min to lyse the cells. 50 µL of substrate was added and the plate was again shaken for 5 min. The plate was then equilibrated in the dark for 10 min before luminescence reading were acquired using a Biotek Cytation V microplate reader with Gen5 software. A fresh standard curve of ATP was prepared each day and the experiment was performed in triplicate.

Chapter 4. Development of IP_3-responsive liposomes

(The scientific data used in this Chapter has been published by the authors: Bottcher, Sydney E.;‡ Lou, Jinchao;‡ Best, Michael D.; Liposome Triggered Content Release Through Molecular Recognition of Inositol Trisphosphate. *Chem. Comm.* **2022**, *58*, 4520-4523.)

4.1. Project overview

To expand the limited toolbox designed for triggering release, we have continued to explore a unique approach for achieving targeted liposomal cargo release by leveraging the molecular recognition of biomolecules that are upregulated in disease states.[90,106] These innovative strategies culminated in more pronounced disruptions to membrane packing, thereby triggering cargo release with high specificity and efficiency.[27] Following the successful demonstration of calcium- and ATP-responsive liposomes described in earlier Chapters, we continued constructing novel switchable lipid scaffolds that can undergo major structural alterations upon binding to other important aberrant metabolites.

Herein, we selected another phosphorylated small molecule target, inositol 1,4,5-trisphosphate (IP_3), due its key roles in regulating biological processes. Although IP_3 is a key signaling molecule that releases calcium stores,[179-181] less is known about IP_3 concentrations since this is a challenging analytical target. Fluctuations in concentration from low nM to μM have been reported resulting from hydrolysis of the lipid phosphatidylinositol-4,5-bisphosphate ($PI(4,5)P_2$) by phospholipase C.[196-198] Response to IP_3 would also need to be differentiated from other phosphorylated carbohydrates such as D-fructose-1,6-bisphosphate (FBP), a glycolysis intermediate.[199] Thus, IP_3 provides a challenging but exciting target for liposomal triggering release platforms.

4.2. Design and synthesis of the IP_3-responsive lipid switch

Building on our ATP-responsive system described in Chapter 3, we hypothesized that we may alter selectivity properties to develop an IP_3-responsive platform by modulating structural

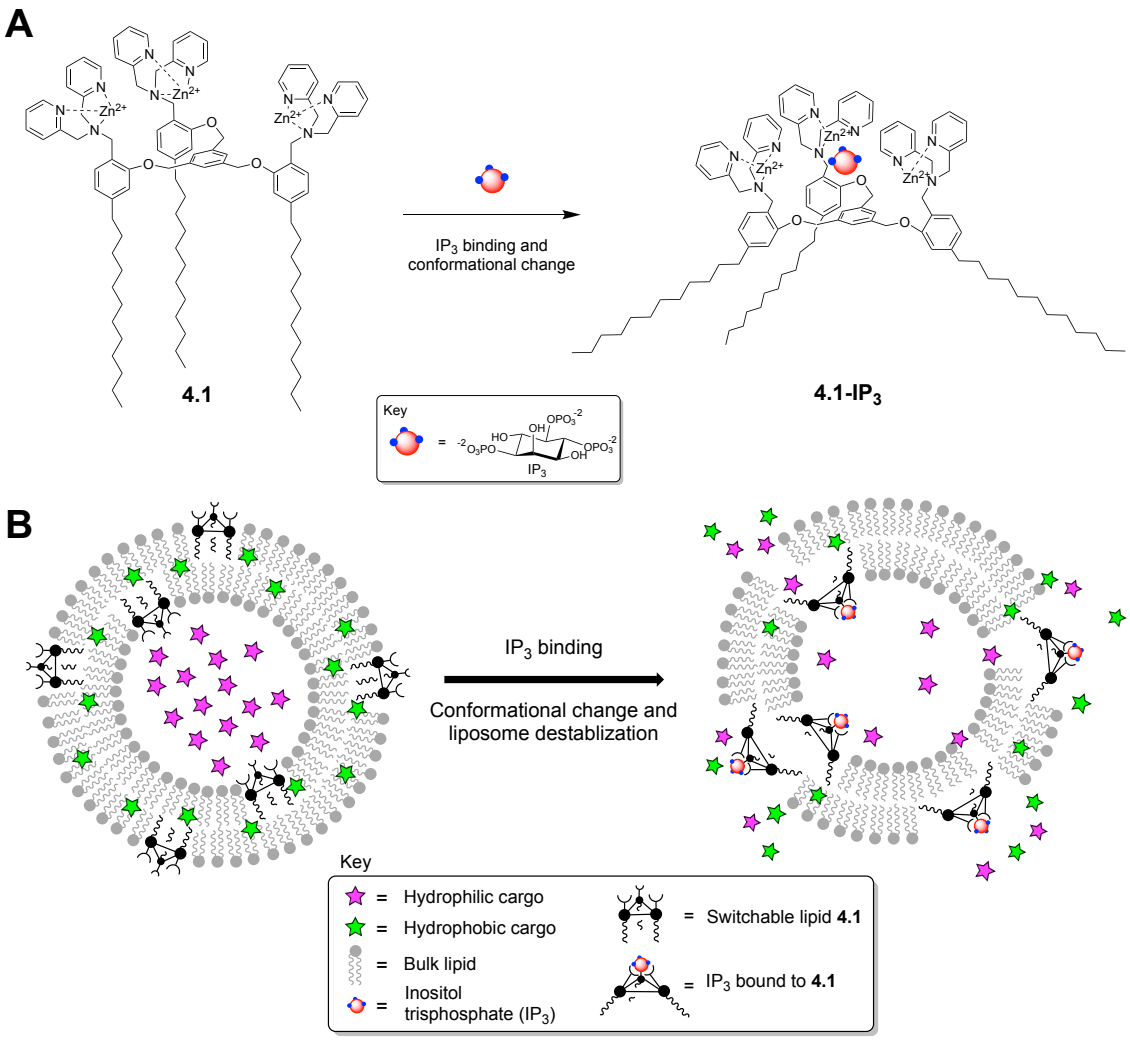
features of the lipid switches. Based on IP_3 supramolecular hosts that we and others have reported,[200-202] we designed switch **4.1** containing three ZnDPA moieties to accommodate the three phosphates of IP_3 (Scheme 4.1A). The binding domains are installed onto rigid lipid scaffolds containing a C12 alkyl chain, which are expected to adopt a cylindrical lipid shape that favors formation of bilayer lipid membranes in the unbound form. However, **4.1**-IP_3 binding is envisioned to cause tris-ZnDPA headgroup constriction that can induce a conical shape known to perturb bilayers and thereby drive encapsulated cargo release (Scheme 4.1B).[25] We began with the lipid bearing C12 alkyl chains based on the observations in Table 3.1, where compound **3.2** showed enhanced release towards IP_3 treatment compared to other switches containing a rigid aromatic ring in the tail region (entry 12). This project was completed through approximately equal contributions with REU student Sydney Bottcher.

The synthesis of lipid **4.1** is outlined in Scheme 4.2, which began with a Suzuki coupling reaction between 5-bromo-2-hydroxybenzaldehyde and *N*-dodecylboronic acid to **3.2.2** to install the lipid tails. Three equivalents of **3.2.2** was then reacted with 1,3,5-tris(bromomethyl)benzene to form the trimerized switch scaffold through ether coupling reaction to produce **4.2**. Next, this compound was reduced by sodium borohydride to generate **4.3**, followed by treatment with phosphorus tribromide to **4.4**. Subsequent coupling with dipicolylamine afforded **4.5**, which was finally subjected to zinc chelation to produce lipid switch **4.1** bearing three ZnDPA units.

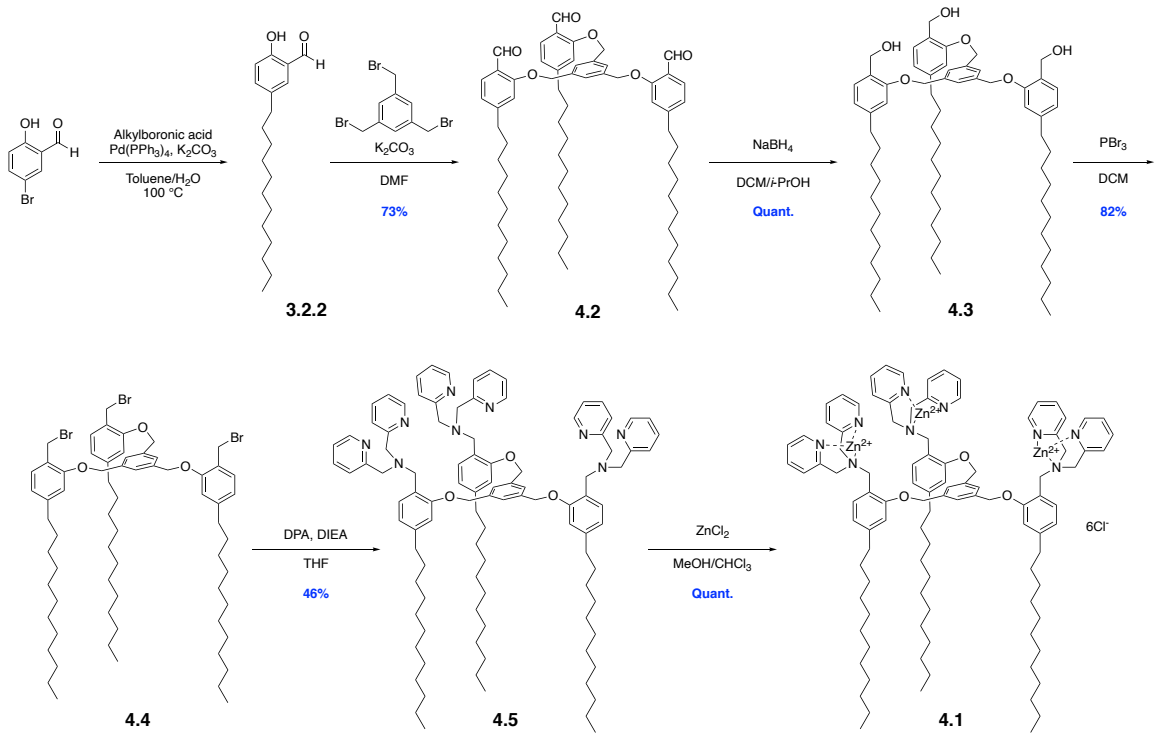
4.3. Nile red-based dye release assays

4.3.1. Phosphorylated metabolite selectivity screen

Once we obtained the desired switch, we set out to evaluate the triggered release properties with liposomes containing **4.1** utilizing fluorescence-based dye release assays. We began by hydrophobic content release assay employing the NR dye. We first prepared 2 mM unilamellar NR liposomes composed primarily of L-α-phosphatidylcholine (PC, mixed isomers from egg)



Scheme 4.1. Design for IP_3-responsive liposomes. A. Structure for lipid switch **4.1** and hypothesized conformational changes upon IP_3 binding. The three ZnDPA units on **4.1** are introduced to effectively bind to IP_3, leading to a cone-shaped non-bilayer forming lipid. **B.** Cartoon illustration of liposome cargo release triggered by IP_3 addition. The binding interactions between **4.1** and IP_3 are envisaged to induce a conformational change that results in membrane disruption and content release.



Scheme 4.2. Synthetic route to lipid switch 4.1. 5-Bromo-2-hydroxybenzaldehyde was coupled with *N*-dodecylboronic acid to produce **3.2.2,** followed by trimerization using 1,3,5-tris(bromomethyl)benzene to **4.2**, aldehyde reduction to **4.3**, bromination to **4.4**, introduction of the DPA units of **4.5**, and finally zinc chelation to generate **4.1**.

doped with 0-20% lipid **4.1**. A standard thin-film hydration method was used including film formation, hydration, freeze-thaw cycling and extrusion through 200 nm polycarbonate membranes. To test our hypothesis that **4.1** is IP_3 responsive, we began with a selectivity screen using a wide variety of phosphorylated small molecule metabolites, including inorganic phosphate (Pi), inorganic pyrophosphate (PPi), adenosine diphosphate (ADP), adenosine monophosphate (AMP), D-fructose-6-phosphate (FP), D-fructose-1,6-bisphosphate (FBP), inorganic triphosphate (TPi) and the nucleotide triphosphates (ATP, cytidine (CTP), guanidine (GTP), and uridine (UTP) triphosphate).

Liposomes containing 20% of compound **4.1** were first tested. After an initial scan, different analytes (1 mM) were added into the liposomes and incubated for five minutes before taking another reading. As shown in Figure 4.1A, IP_3 treatment induced the greatest amount of content release as indicated by an ~45% decrease in NR fluorescence, with inorganic phosphate additionally yielding ~20% signal decrease. When we reduced the **4.1** percentage to 10%, the resulting liposomes showed excellent selectivity towards IP_3 among other eleven phosphorylated metabolites. Only IP_3 addition induced ~20% content release, while others showed minimal background leakage (< 5%). Control experiments were also carried out with liposomes composed of 100% PC (Figure 3.2) or titrating MilliQ purified water (MQ) into the **4.1**-liposomes (Figure 4.1A), none of which showed significant background release. These results demonstrated that liposomes containing **4.1** are sensitized to IP_3 and that the selectivity can be tuned by adjusting the percentage of **4.1** incorporated within the membrane.

4.3.2. Expanded Nile red titration experiments

To obtain a more detailed understanding of IP_3-induced NR release, we next carried out expanded titration experiments. PC-based liposomes containing 0%, 5%, 10%, 15% or 20% lipid **4.1** (2 mM) were prepared and subjected to IP_3 titration. As is shown in the curves detailed in Figure 4.1B, dose-dependent NR release was observed when **4.1** is present at more than

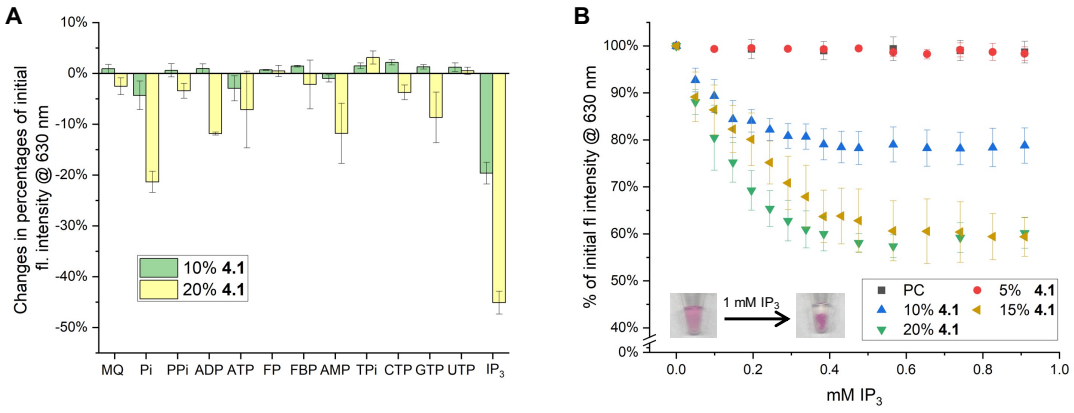


Figure 4.1. Results from NR release assay using PC-based liposomes containing lipid switch 4.1. A. Phosphorylated metabolite screen experiments for 10% and 20% **4.1**/PC liposomes. 20% Liposomes exhibited selectivity towards IP_3 (~45% fluorescence decrease) with inorganic phosphate showing ~20% release. 10% Liposomes showed significant content release only upon IP_3 addition. **B.** Expanded IP_3 titration curves for liposomes containing **4.1**. Dose-dependent release correlating with the percentages of **4.1** was observed upon IP_3 addition. Error bars denote standard errors from at least three independent trials.

10% within the membrane bilayer. Specifically, 10% **4.1** liposomes showed an ~20% decrease in fluorescence intensity, while that was increased to ~40% for 15% **4.1** liposomes. Further increasing **4.1** percentage to 20% did not improve release. Pink precipitate was observed when liposomes containing 15% or 20% **4.1** after IP_3 addition. PC control liposomes did not show any background release and the same result was observed for 5% **4.1** liposomes. We also treated 5% **4.1**-liposomes with up to >5 mM IP_3 (Figure 4.2), and <5% release was observed, indicating that excess IP_3 did not yield activity. The correlations between release extent and the percentages of **4.1** incorporation show that compound **4.1** is necessary for driving release, and sufficient **4.1** is required for effective content leakage. The release kinetics were also studied by tracking fluorescence intensities over time. As shown in Figure 4.3, release with both 10% and 20% **4.1** liposomes plateaued within ten minutes, indicating release process proceeded fast.

The stabilities of 0-20% **4.1**-liposomes encapsulating NR were also tested by measuring fluorescence over time. These were generally stable at 4 °C for five days, although minor decreases in fluorescence were observed (Figure 4.4).

4.4. DLS studies on morphology changes

Next, we probed changes in particle sizes during the release process using dynamic light scattering (DLS). PC liposomes containing various percentages of **4.1**, ranging from 0% to 25% were prepared and their sizes were measured before and after IP_3 treatment. As is indicated by the grey bars in Figure 4.5A (representative raw distribution curves for all DLS measurements are included in Figure 4.6.), all the liposomes pre-IP_3 addition showed uniform size particles with desired diameters around 200 nm, suggesting the initial liposomes were stable and **4.1** could be incorporated up to at least 25%. After IP_3 treatment, minimal changes in particle sizes were observed for PC control liposomes and 5% **4.1** liposomes. However, for 15%-25% **4.1** liposomes, dramatic increases in particle sizes were observed (Figure 4.5A, red

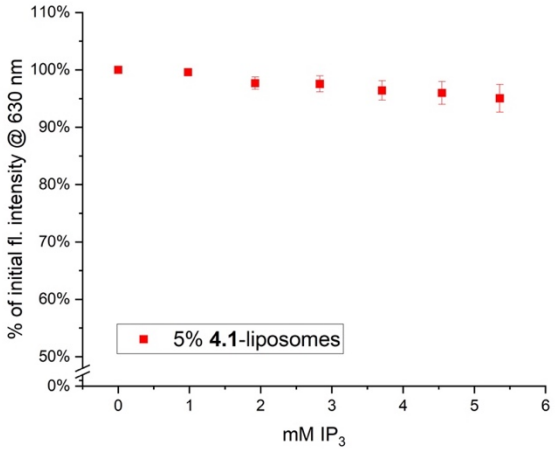


Figure 4.2. NR release titration curve for 5% 4.1-liposomes by titrating with IP_3 to an excess amount (> 5 mM). Less than 5% background leakage was observed, indicating that higher amounts of IP_3 did not further affect release. Error bars denote standard errors from three replicates.

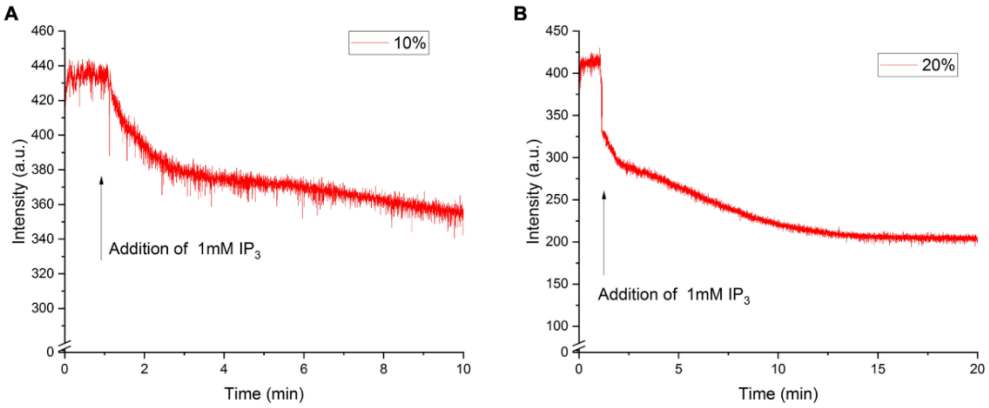


Figure 4.3. Kinetic curves of NR release from 2 mM 10% and 20% 4.1/PC liposomes after adding IP_3. NR release is tracked over time by decreases observed in fluorescence intensities. In both cases, release began immediately after treatment and plateaued within ten minutes after adding 1 mM IP_3.

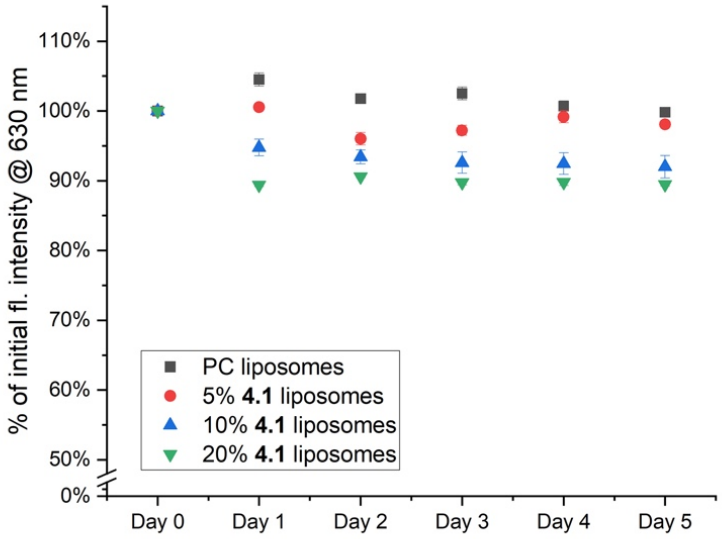


Figure 4.4. Liposome stability test for NR encapsulated PC-based liposomes containing 0-20% lipid 4.1. All liposomes generally showed only minor fluctuations in fluorescence over time, although these were greater for 10% and 20% **4.1**-liposomes, which showed ~10% fluorescence decreases over five days. Error bars denote standard errors from at least three replicates.

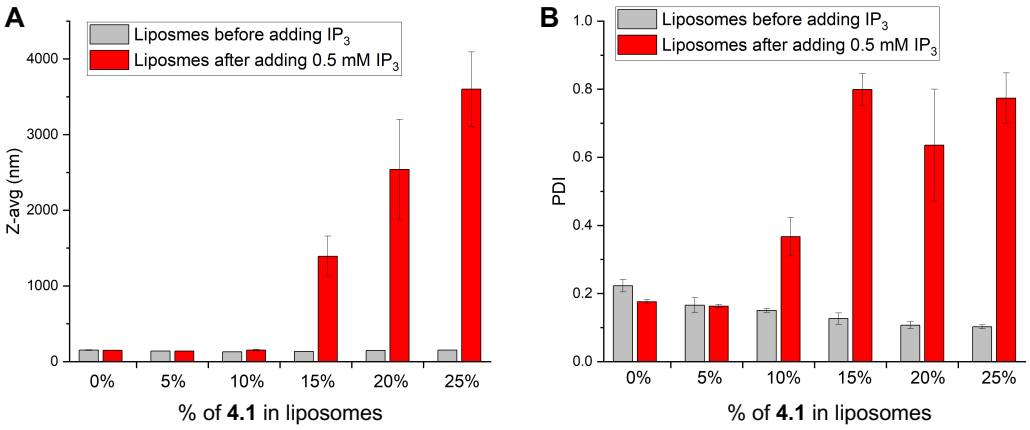


Figure 4.5. DLS results for 0-25% 4.1/PC liposomes before (grey) and after (red) IP_3 treatment. A. Z-average results. Uniformly sized particles with desired diameters were initially formed in all cases. Upon IP_3 addition, liposomes containing 0%, 5% and 10% **4.1** did not show increases in particle sizes, while dramatic increases in particle sizes were observed for those containing 15%, 20% and 25% **4.1**. **B.** Polydispersity index (PDI) results. While 0% and 5% **4.1** liposomes remained uniform in size upon IP_3 addition, 10%-25% **4.1** liposomes all showed dramatic changes in PDI, indicating variations in particle sizes. Error bars denotes standard errors from at least three replicates.

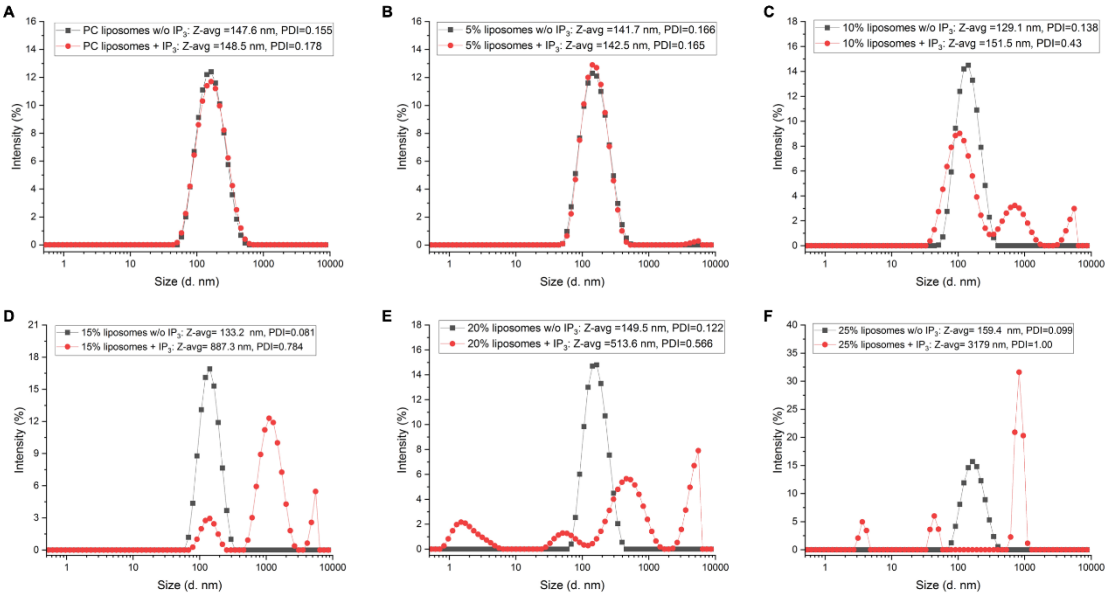


Figure 4.6. DLS raw distribution curves for PC and 5-25% 4.1/PC liposomes before and after IP_3 addition. Uniform size liposomes were formed in all cases before IP_3 treatment. After adding IP_3, PC and 5% **4.1** liposomes did not show any change, while significant changes were observed for 10-25% **4.1** liposomes. Note: only a representative set of distribution curves is shown for 10-25% **4.1** liposomes after IP_3 treatment.

bars), and the increase correlated with the percentages of **4.1** within the membrane. Although 10% **4.1** liposomes post-IP_3 addition did not show obvious average size changes, the corresponding polydispersity indeces (PDIs) of the samples increased significantly (Figure 4.5B), indicating changes in morphology. These results are in line with previous NR release observations that ~10% of **4.1** in liposomes is needed to induce significant cargo leakage. Nevertheless, we demonstrated changes in nanoparticle structure driven by IP_3 treatment when **4.1** is present, which could be explained by alterations in self-assembly structures (i.e., bilayer to inverted hexagonal phase) or fusion.

4.5. Fluorescence microscopy studies on liposome morphology changes

Our DLS data suggested processes such as fusion that would generate larger particles. We additionally implemented confocal fluorescence microscopy as an alternate technique to probe the formation of larger aggregates over time. To do so, 1 mM 0% or 20% **4.1**/PC liposomes labeled with 0.08% Rd-PE were prepared and imaged before and after IP_3 addition. As shown in Figure 4.7, both liposomes exhibited minimal initial fluorescence as their sizes were below the resolution limit of the microscope. After IP_3 treatment, the formation of ~2-3 μm aggregates was only seen for 20% **4.1**-liposomes.

4.6. Zeta potential measurements

The binding interactions between lipid **4.1** and IP_3 within the membrane environment were successfully characterized using zeta potential (ZP) analysis, which can effectively measure particle surface charge. PC liposomes doped with 0%, 10% or 20% **4.1** were prepared and their ZP values were measured before and after IP_3 addition (Figure 4.8). PC liposomes were slightly negatively charged, which is in line with previously reported literature.[188] IP_3 addition did not cause any ZP change to these negative controls. Both 10% and 20% **4.1** liposomes were positively charged initially due to the presence of ZnDPA binding units, and the extent of positive charges correlated with the percentages of **4.1** incorporation. However, after IP_3

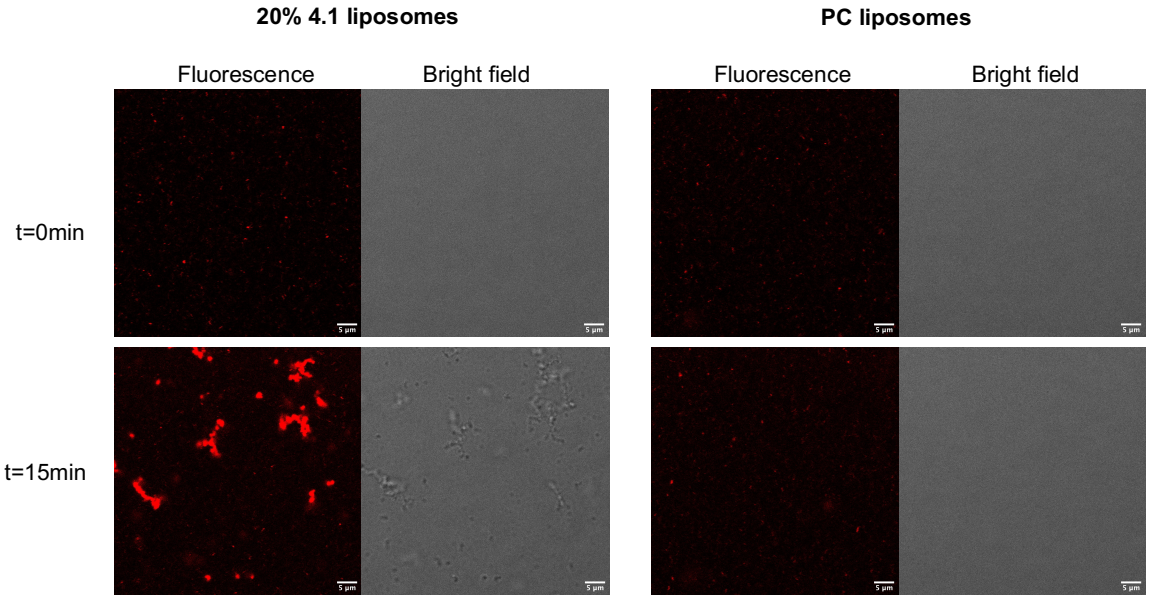


Figure 4.7. Fluorescence microscopy images for Rd-PE labeled 0% (B) and 20% (A) 4.1-liposomes (1 mM) before and after 15 minute 1 mM IP_3 incubation. IP_3 treatment resulted in aggregation of **4.1** liposomes, indicated by the larger fluorescent particles under the microscope. No aggregation was observed for PC liposomes after IP_3 treatment over time. Scale bars denote 5 μm.

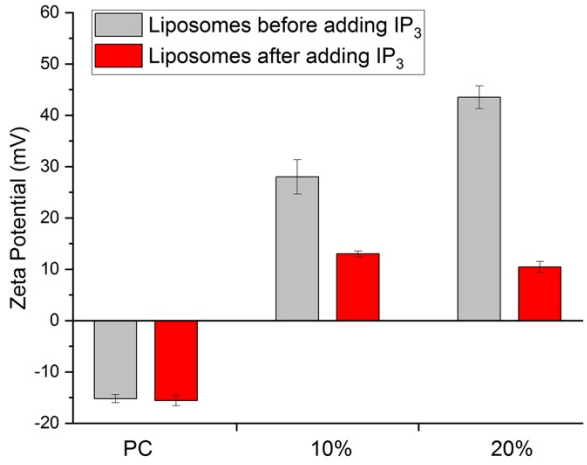


Figure 4.8. Zeta potential measurements for PC liposomes containing 0, 10%, or 20% 4.1 before and after adding IP_3. Both 10% and 20% **4.1** liposomes showed positive charge prior to IP_3 addition, with IP_3 treatment yielding a reduction in positive charge. PC control liposomes showed only minimal ZP changes after IP_3 treatment. Error bars denote standard errors from three replicates.

incubation, we observed a significant decrease in ZP, indicating binding interactions between negatively charged IP_3 and the ZnDPA membrane surface, counteracting the positive charges from initial **4.1**-liposomes.

4.7. Sulforhodamine B release studies

Liposomes are also capable of encapsulating hydrophilic content in their aqueous core benefitting from their unique structures.[203] However, it is usually very challenging to release hydrophilic contents considering that these are encapsulated within the inner core and thus more dramatic membrane disruption is required to trigger cargo release. We next moved to evaluate the hydrophilic content release abilities of liposomes containing **4.1**. The dye SRB, as described in Chapter 2, was employed as the water-soluble fluorescent cargo, which was encapsulated at high concentration such that its fluorescence is initially quenched due to collisional effect.[204] Once the SRB escapes from the membrane bilayer and is diluted by media, its fluorescence will be activated. Since the dyes were non-specifically encapsulated, SEC was again employed to remove unencapsulated dye. Here, we doped 10% **4.1** into 1,2-dipalmitoyl-*sn*-glycero-3-phosphocholine (DPPC) and DOPE liposomes. DOPE is a well-known non-bilayer lipid that can be incorporated within the bilayer membrane up to a certain percentage. This serves to destabilize the initial membrane to bring this close to the threshold for release, which we found to be necessary to drive cargo release upon IP_3 treatment.[27] The formation of stable liposomes was characterized with DLS, as shown in Figure 4.9.

After an initial fluorescence scan, IP_3 was titrated into liposome solutions. After the signal plateaued, the detergent Triton X-100 was added into the solution to lyse the liposomes and trigger complete content release to normalize the release assay. When reporting the data, the extent of fluorescence increase is plotted as a percentage of each liposome's maximum fluorescence following Triton treatment. As can be seen in Figure 4.10 (representative raw spectra in Figure 4.11), liposomes containing 10% **4.1** showed ~40% dye release upon 10 mM

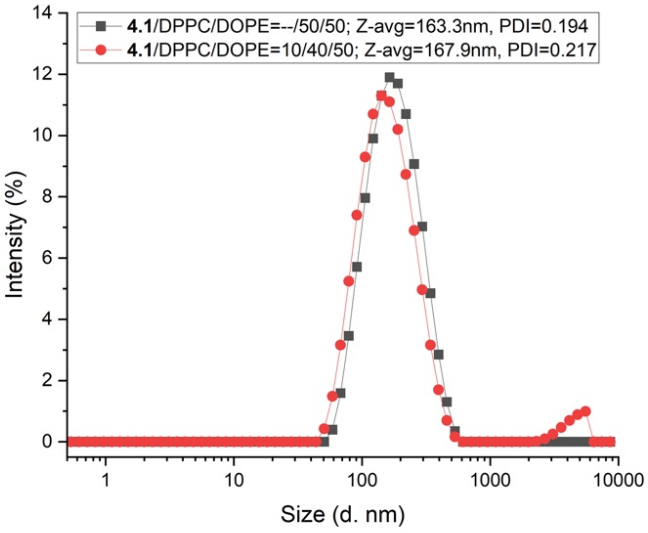


Figure 4.9. DLS raw distribution curves for SRB-encapsulated DPPC/DOPE liposomes containing or lacking lipid 4.1. Stable and uniform liposomes were formed in both cases.

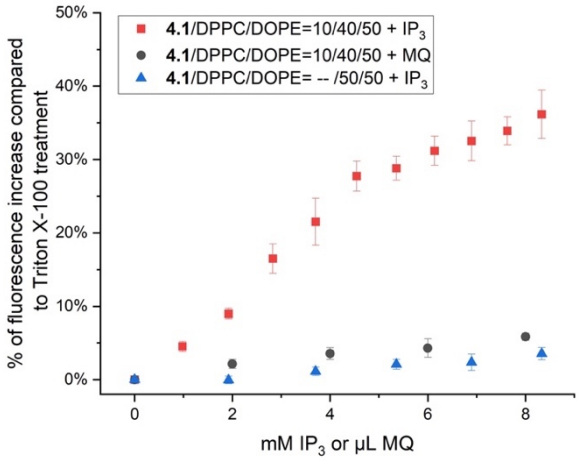


Figure 4.10. SRB release results for DPPC/DOPE liposomes containing or lacking lipid switch 4.1 upon IP_3 treatment. Release was only observed for liposomes containing 10% **4.1**, 40% DPPC, and 50% DOPE after IP_3 titration, while negative control liposomes containing only DPPC and DOPE or **4.1**-liposomes titrated with MQ did not show background release. Error bars were standard errors generated from three independent trials.

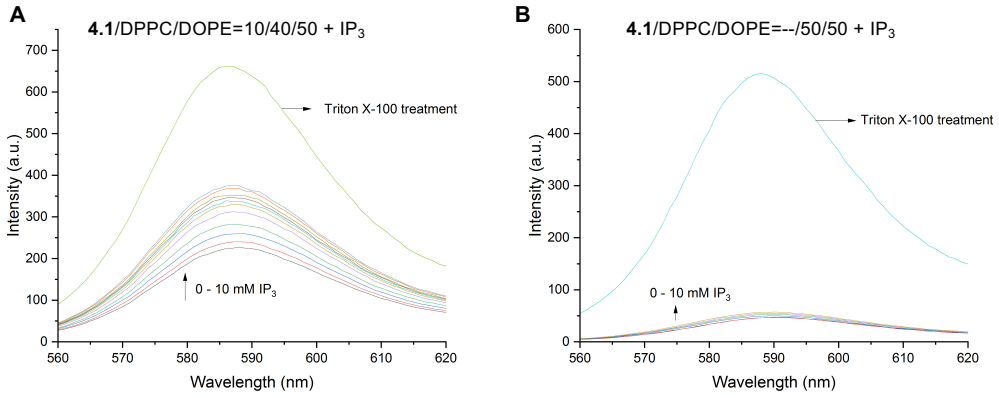


Figure 4.11. Sample raw fluorescence emission spectra for liposomes containing 0 or 10% lipid 4.1, 50% or 40% DPPC and 50% DOPE used in SRB release assay. Fluorescence intensities were recorded after each addition (λ_{ex} = 550 nm, Ex/Em slit = 10/2.5 nm).

IP_3 addition, while the control liposomes lacking **4.1** treated with IP_3 or the same liposomes treated with MQ both showed minimal background release. Our data showcase that liposomes containing **4.1** are also effective for driving release of hydrophilic cargo upon IP_3 addition.

4.8. Attempts at NMR and UV-Vis titrations

Attempts to study the binding interactions between lipid switch **4.1** and IP_3 were made using the protocols described in Chapter 3. NMR titration experiments were first attempted. However, we were not able to find a solvent mixture that could dissolve **4.1** and IP_3 at the same time. Compound **4.1** (2 mM) could not dissolve in the 8% D_2O in *d_6*-DMSO mixture that worked well for lipid **3.1a**. Although **4.1** could dissolve in 100% DMSO, it precipitated out with 8% H_2O addition. While IP_3, on the other hand, is more likely to dissolve in H_2O instead of DMSO, a 4 mM IP_3 solution in 8% D_2O in *d_6*-DMSO appeared hazy. Since such experiments require a high concentration/amount of IP_3, which is expensive, we did not proceed to explore more possible solvent conditions.

For UV-Vis titration experiments, we encountered a different problem. When using the same concentrations described for **3.1a** (5×10^{-5} M for **4.1** and 1.67×10^{-5} M increment for each IP_3 addition), the absorbance maximum at 263 nm kept increasing and never plateaued even after 3.5×10^{-4} M IP_3 addition, as is shown in Figures 4.12A-B. Data were processed anyways to produce a mole fraction graph (Figure 4.12C) by plotting absorbance intensities at 263 nm over [**4.1**]/([**4.1**]+[IP_3]). Two separate linear fittings were conducted on the mole fraction graph. Although the resulting R^2 value was only around 0.9, the data suggested a 1:1 binding mode between **4.1** and IP_3.

4.9. Miscellaneous experiments

Similar to the ATP-responsive liposomes, we also wondered if the selectivity and sensitivity of our lipid target towards IP_3 can be fine-tuned by adjusting the compound design. We attempted

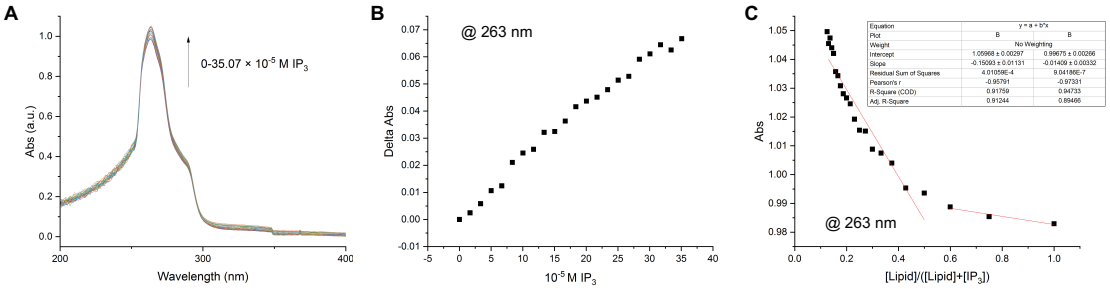
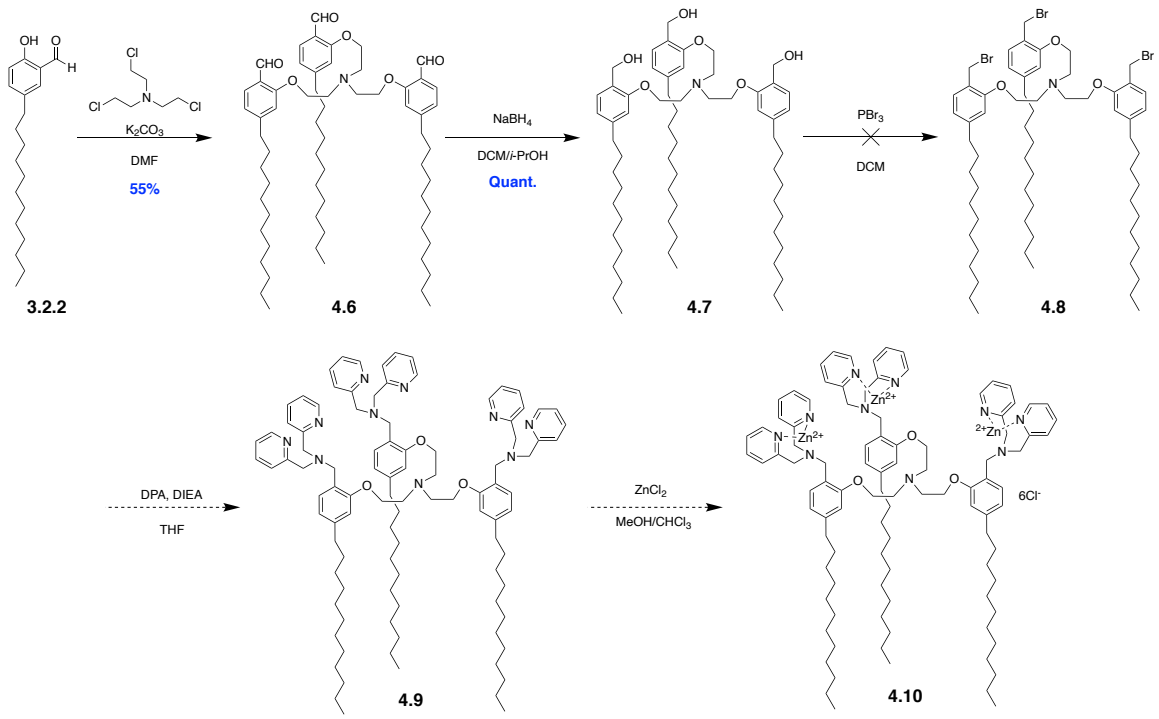


Figure 4.12. UV-Vis titration results. A. Raw absorbance spectra for lipid **4.1** before and after IP_3 titration. **B.** Increases in absorbance intensities at 263 nm over concentrations of IP_3 added. The host absorbance kept increasing. **C.** Mole fraction graph of the titration experiment. Linear fitting indicated an approximately 1:1 binding mode with R^2 of 0.9.

to switch the 1,3,5-trismethylbenzene linker of lipid **4.1** into a triethylamine linker. The synthetic route for the resulting lipid **4.10** is shown in Scheme 4.3, utilizing similar strategies. Intermediate **3.2.2** was first subjected to a trimerization reaction using tris(2-chloroethyl)amine hydrochloride to **4.6**, followed by sodium borohydride reduction to obtain tris-alcohol compound **4.7**. However, when **4.7** was treated with phosphorus tribromide, we did not observe the formation of the desired product **4.8**. The presence of the amine group in the linker could be responsible for the failure of this reaction.

4.10. Conclusions

In conclusion, we designed and synthesized lipid **4.1** as an effective lipid switch for IP_3-responsive liposomes. Building up from our previous ATP-responsive liposomes, lipid **4.1** contains three ZnDPA units that can selectively target IP_3 by manipulating the display of binding groups within lipid switches. Upon IP_3 treatment, **4.1** is designed to undergo a conformational change that results in non-bilayer properties that can disrupt membrane integrity and trigger encapsulated content release. Our data show that **4.1**-liposomes were able to release both hydrophobic and hydrophilic content upon IP_3 addition. We also demonstrated that the selectivity towards IP_3 could be tuned by adjusting percentages of **4.1** incorporation with NR release assay. This work further proved that targeted liposomal cargo release could be achieved by leveraging the molecular recognition of biomolecules that are upregulated in disease states. We also envision other aberrantly expressed metabolites could be targeted with the same strategy presented herein. Finally, IP_3 remains a difficult target to detect and quantify in biological systems. While conventional sensors suffer from poor sensitivity,[200-202] the major signal amplification caused by dye release could position the proposed liposomes as effective sensors for these molecules.



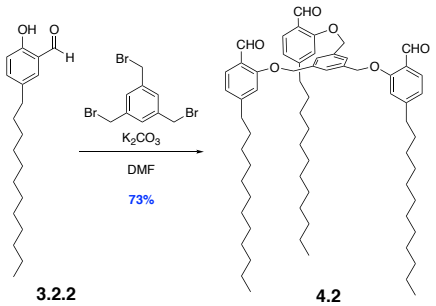
Scheme 4.3. Synthetic route to lipid 4.10 bearing a triethylamine linker.

4.11. Synthesis and experimental procedure

General Experimental

Reagents and solvents were generally purchased from Sigma-Aldrich or Fisher Scientific and used without further purification. PC (L-α-Phosphatidylcholine, mixed isomers from chicken egg), 1,2-dipalmitoyl-*sn*-glycero-3-phosphocholine (DPPC), 18:1 Lissamine Rhodamine PE (Rd-PE, 1,2-dioleoyl-*sn*-glycero-3-phosphoethanolamine-*N*-(lissamine rhodamine B sulfonyl) (ammonium salt)) and 1,2-dioleoyl-*sn*-glycero-3-phosphoethanolamine (DOPE) was purchased from Avanti Polar Lipids, Inc (Alabaster, AL). D-*myo*-Inositol-1,4,5-triphosphate (sodium salt, IP_3, item # 10008205) was purchased from Cayman Chemical. Dry solvents were obtained from a Pure Solv MD-7 solvent purification system purchased from Innovative Technology, Inc (Newburyport, MA). Column chromatography was performed using 230-400 mesh silica gel purchased from Sorbent Technologies. NMR spectra were obtained using Varian 300 MHz or 500 MHz NMR spectrometers. Mass spectra were obtained with JEOL DART-AccuTOF and Waters Synapt G2-Si mass spectrometers (Milford, MA). Liposome extruder and polycarbonate membranes were obtained from Avestin (Ottawa, Canada) or Avanti Polar Lipids, Inc (Alabaster, AL). Ultrapure water was purified via a Millipore water system (≥ 18 MW·cm triple water purification system). Small quantities (< 5 mg) were weighed on a Mettler Toledo XS105 dual range analytical balance. Fluorescence studies were performed using a Cary Eclipse Fluorescence Spectrophotometer from Agilent Technologies. DLS analyses were carried out with a Malvern Zetasizer Nano ZS instrument equipped with a 4.0 mW laser operating at l = 633 nm. Plots were generated using Origin Pro 2021b. All error bars in plots indicate the standard errors of at least three experimental replicates.

Synthesis

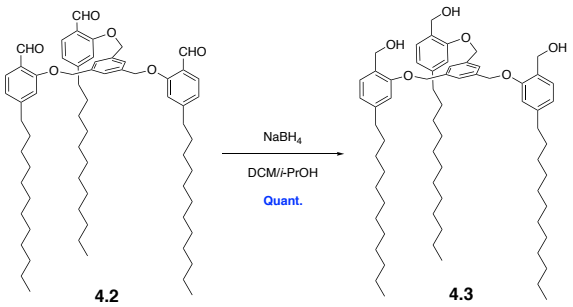


3.2.2 4.2

2,2',2''-((Benzene-1,3,5-triyltris(methylene))tris(oxy))tris(4-dodecylbenzaldehyde) (4.2)

Compound **3.2.2** (155.5 mg, 0.535 mmol), potassium carbonate (665 mg, 4.82 mmol) and 1,3,5-tris(bromomethyl)benzene (63.5 mg, 0.178 mmol) were dissolved in 10 mL dry *N*,*N*-dimethylformamide in a 100 mL RBF under Argon and the mixture was heated at 110 ºC overnight. After completion, the reaction was cooled to rt and the solvent was removed using a rotary evaporator. The residue was re-dissolved in 25 mL methylene chloride and washed with 50 mL water. The aqueous layer was extracted with 2 x 25 mL methylene chloride. The combined organic layer was further washed with 1 x 50 mL water and 1 x 50 mL brine, respectively, before being dried over sodium sulfate, filtered, and concentrated under reduced pressure. The crude was purified via silica gel column chromatography using gradient elution from hexanes to 70% methylene chloride in hexanes. The product was obtained as a brown solid (0.128 g, 0.130 mmol, 73% yield). R_f = 0.25 (75% methylene chloride-hexanes).

^{1}H NMR (500 MHz, $CDCl_3$) δ 10.52 (s, 3H), 7.67 (d, *J* = 2.3 Hz, 3H), 7.51 (d, *J* = 3.4 Hz, 3H), 7.37 – 7.33 (m, 3H), 6.96 (d, *J* = 8.5 Hz, 3H), 5.21 (s, 6H), 2.63 – 2.54 (m, 6H), 1.58 (d, *J* = 7.5 Hz, 6H), 1.27 (m, 54H), 0.88 (t, *J* = 7.0 Hz, 9H). ^{13}C NMR (126 MHz, $CDCl_3$) δ 189.84, 159.11, 137.73, 136.13, 136.03, 128.23, 125.83, 125.01, 113.06, 70.25, 34.94, 32.03, 31.49, 29.78, 29.77, 29.76, 29.70, 29.59, 29.47, 29.32, 22.81, 14.24. ESI-MS: $[M+H]^+$ calcd for $C_{66}H_{96}O_6$: 985.7285; Found: 985.7243.

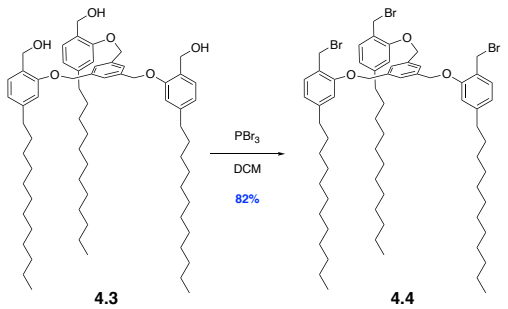


4.2 4.3

(((Benzene-1,3,5-triyltris(methylene))tris(oxy))tris(4-dodecylbenzene-2,1-diyl))trimethanol (4.3)

Compound **4.2** (0.105 g, 0.106 mmol) was dissolved in 12 mL methylene chloride/isopropanol (3/1, v/v) under argon in a 50 mL RBF at 0 ºC. Sodium borohydride (20.1 mg, 0.531 mmol) was then added. Next, the reaction mixture was warmed up to rt and further stirred for 6h. After completion, the reaction mixture was brought back to 0 ºC with an ice bath and 10% citric acid was carefully added dropwise until no hydrogen gas was released, after which the reaction was further stirred for 20 min. The organic layer was collected, and the aqueous layer was further extracted with 2 x 25 mL methylene chloride. The combined organic layer was washed with 1 x 50 mL water and 1 x 50 mL brine. After being dried over sodium sulfate, filtered, and concentrated under reduced pressure, the product was obtained as a white solid in a quantitative yield (0.1057 g, 0.106 mmol). R_f = 0.45 (25% ethyl acetate-hexanes).

^{1}H NMR (500 MHz, $CDCl_3$) δ 7.44 (s, 3H), 7.15 (d, *J* = 2.1 Hz, 3H), 7.05 (dd, *J* = 8.3, 2.2 Hz, 3H), 6.83 (d, *J* = 8.3 Hz, 3H), 5.12 (s, 6H), 4.71 (s, 6H), 2.58 – 2.51 (m, 6H), 1.62 – 1.55 (m, 6H), 1.29 (m, 54H), 0.89 (t, *J* = 7.0 Hz, 9H). ^{13}C NMR (126 MHz, $CDCl_3$) δ 154.46, 138.27, 135.83, 129.24, 129.20, 128.58, 125.25, 111.68, 69.80, 61.96, 35.25, 32.06, 31.85, 29.82, 29.78, 29.76, 29.68, 29.49, 22.83, 14.26. ESI-MS: $[M+Na]^+$ calcd for $C_{66}H_{102}O_6Na$:1013.7574; Found: 1013.7584.

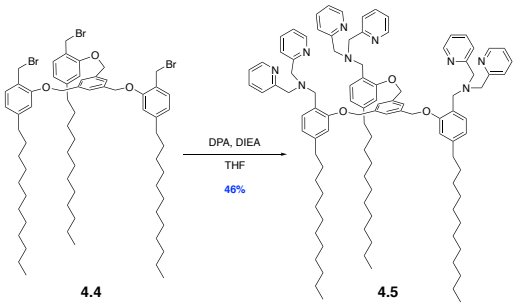


4.3 4.4

1,3,5-Tris((2-(bromomethyl)-5-dodecylphenoxy)methyl)benzene (4.4)

Tris-alcohol **4.3** (90.4 mg, 0.091 mmol) was weighed into a 100 mL RBF under argon and dissolved with 20 mL dry methylene chloride at 0 ºC in an ice bath. Phosphorus tribromide (0.386 mL, 4.10 mmol) was next carefully added into the RBF dropwise. The reaction was warmed to rt and further stirred for six hours. After being cooled back to 0 ºC, methanol was added dropwise to quench the unreacted PBr_3. The mixture was poured into 100 mL water in a separatory funnel and the methylene chloride layer was collected. The aqueous layer was further extracted with 2 x 20 mL methylene chloride. The combined organic layer was washed with 1 x 50 mL water and 1 x 50 mL brine before being dried over sodium sulfate, filtered, and concentrated under reduced pressure. The crude was purified with a short column packed with silica gel using elution of 10% ethyl acetate in hexanes as a brown oil (0.0882 g, 0.0747 mmol, 82% yield). R_f = 0.36 (5% EtOAc-hexanes).

^{1}H NMR (500 MHz, $CDCl_3$) δ 7.60 (s, 3H), 7.17 (d, *J* = 2.2 Hz, 3H), 7.06 (dd, *J* = 8.4, 2.2 Hz, 3H), 6.84 (d, *J* = 8.4 Hz, 3H), 5.18 (s, 6H), 4.61 (s, 6H), 2.57 – 2.51 (m, 6H), 1.61 – 1.55 (m, 6H), 1.29 (m, 54H), 0.89 (t, *J* = 7.0 Hz, 9H). ^{13}C NMR (126 MHz, $CDCl_3$) δ 154.65, 138.07, 135.69, 131.02, 130.07, 126.29, 125.55, 112.45, 70.11, 35.10, 32.07, 31.71, 30.11, 29.83, 29.82, 29.80, 29.76, 29.74, 29.66, 29.51, 29.47, 22.84, 14.27. ESI-MS: $[M+K]^+$ calcd for $C_{66}H_{99}Br_3O_3K$: 1215.4781; Found: 1215.6144.

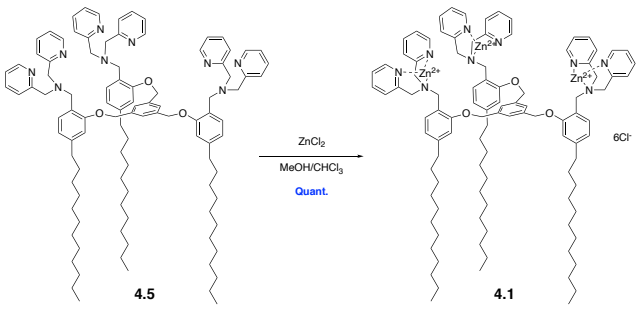


4.4 4.5

1,1',1''-(((Benzene-1,3,5-triyltris(methylene))tris(oxy))tris(4-dodecylbenzene-2,1-diyl))tris(*N*,*N*-bis(pyridin-2-ylmethyl)methanamine) (4.5)

Compound **4.4** (43.4 mg, 0.0368 mmol) was dissolved with 10 mL dry tetrahydrofuran in a 50 mL RBF under Ar. *N,N*-Diisopropylethylamine (DIEA, 21.1 µL, 0.121 mmol) and dipicolylamine (DPA, 21.8 µL, 0.121 mmol) were next added, respectively. The reaction was refluxed at 70 ºC overnight, accompanied by a color change from pale yellow to brown. After evaporating the solvent under reduced pressure, the crude was subjected to neutral alumina column chromatography through gravity elution using 100% chloroform. Product **4.5** was obtained as a brown oil (25.9 mg, 0.0168 mmol, 46% yield). R_f = 0.5 (10% methanol in chloroform).

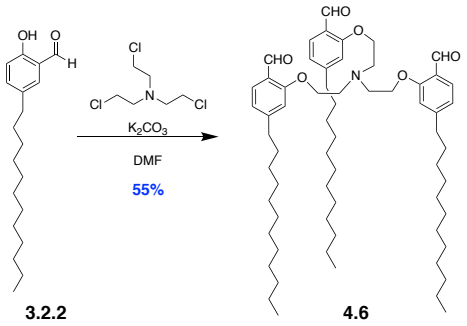
^{1}H NMR (500 MHz, $CDCl_3$) δ 8.44 (d, *J* = 4.1 Hz, 6H), 7.56 (d, *J* = 7.8 Hz, 6H), 7.48 (td, *J* = 7.7, 1.7 Hz, 6H), 7.39 – 7.32 (m, 6H), 7.05 – 6.99 (m, 6H), 6.96 (dd, *J* = 8.3, 2.1 Hz, 3H), 6.77 (d, *J* = 8.4 Hz, 3H), 5.00 (s, 6H), 3.84 (s, 12H), 3.78 (s, 6H), 2.60 – 2.49 (m, 6H), 1.55 (q, *J* = 7.1 Hz, 6H), 1.26 (m, 54H), 0.87 (t, *J* = 7.0 Hz, 9H). ^{13}C NMR (126 MHz, $CDCl_3$) δ 160.28, 155.22, 148.99, 138.33, 136.36, 135.24, 130.63, 127.87, 127.06, 125.76, 122.67, 121.84, 111.99, 70.20, 60.46, 52.87, 35.32, 32.07, 31.84, 29.87, 29.85, 29.81, 29.74, 29.51, 22.84, 14.27. ESI-MS: $[M+2H]^{2+}$ calcd for $C_{102}H_{137}N_9O_3$: 768.0422; Found: 768.0386. $[M+3H]^{3+}$ calcd for $C_{102}H_{138}N_9O_3$: 512.3641; Found: 512.3618.



1,1',1''-(((Benzene-1,3,5-triyltris(methylene))tris(oxy))tris(4-dodecylbenzene-2,1-diyl))triszinc(*N*,*N*-bis(pyridin-2-ylmethyl)methanamine) chloride (4.1)

Compound **4.5** (16.1 mg, 0.01 mmol) was dissolved with 2.2 mL chloroform/methanol (10/1, v/v) in a 4 dr vial. Anhydrous $ZnCl_2$ (4.29 mg, 0.031 mmol) was then added, and the reaction was stirred overnight. Next, the solvent was moved under nitrogen flow and the product was obtained as a brown solid in a quantitative yield.

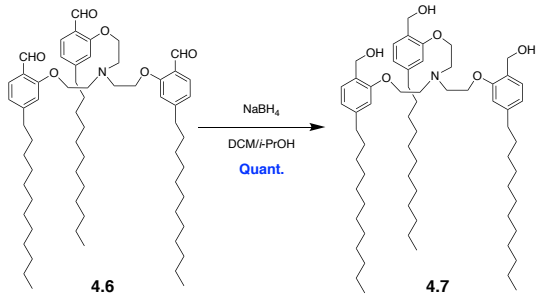
^{1}H NMR (500 MHz, 10% CD_3OD-$CDCl_3$) δ 8.86 (d, J = 5.0 Hz, 6H), 7.58 – 7.53 (m, 6H), 7.24 – 7.19 (m, 6H), 7.07 (d, J = 7.8 Hz, 6H), 6.98 – 6.92 (m, 6H), 6.76 (d, J = 8.5 Hz, 3H), 6.70 (d, J = 1.7 Hz, 3H), 4.90 (s, 6H), 4.17 (s, 6H), 3.76 (s, 12H), 2.45 – 2.32 (m, 6H), 1.44 (s, 6H), 1.19 (m, 54H), 0.77 (t, J = 6.9 Hz, 9H).



2,2',2''-((Nitrilotris(ethane-2,1-diyl))tris(oxy))tris(4-dodecylbenzaldehyde) (4.6)

Compound **3.2.2** (108.8 mg, 0.375 mmol), K_2CO_3 (155.3 mg, 1.124 mmol) and tris(2-chloroethyl)amine hydrochloride (30.09 mg, 0.125 mmol) were dissolved in 10 mL dry DMF in a 100 mL RBF under Argon. Next, the mixture was heated at 110 ºC overnight. After completion, the reaction was cooled to rt and the solvent was removed using a rotary evaporator. The residue was re-dissolved in 25 mL DCM and washed with 50 mL water. The aqueous layer

was extracted with 2 x 25 mL DCM. The combined organic layer was further washed with 1 x 50 mL water and 1 x 50 mL brine, respectively, before being dried over Na_2SO_4, filtered, and concentrated under reduced pressure. The crude was purified via silica gel column chromatography using gradient elution from hexanes to 25% EtOAc in hexanes. The product was obtained as a brown solid (67 mg, 0.069 mmol, 55% yield). R_f = 0.3 (25% EtOAc-hexanes). ^{1}H NMR (500 MHz, $CDCl_3$) δ 10.42 (s, 3H), 7.59 (d, *J* = 2.3 Hz, 3H), 7.32 (dd, *J* = 8.5, 2.3 Hz, 3H), 6.87 (t, *J* = 9.0 Hz, 3H), 4.17 (t, *J* = 4.8 Hz, 6H), 3.22 (d, *J* = 5.0 Hz, 6H), 2.58 – 2.51 (m, 6H), 1.60 – 1.53 (m, 6H), 1.27 (d, *J* = 19.2 Hz, 60H), 0.88 (t, *J* = 7.0 Hz, 9H). ^{13}C NMR (126 MHz, $CDCl_3$) δ 189.83, 159.28, 136.21, 135.73, 128.19, 124.79, 112.70, 67.94, 54.58, 34.93, 32.06, 31.52, 29.80, 29.78, 29.73, 29.62, 29.49, 29.35, 22.83, 14.26.



(((Nitrilotris(ethane-2,1-diyl))tris(oxy))tris(4-dodecylbenzene-2,1-diyl))trimethanol (4.7)

Tris-aldehyde **4.6** (52.3 mg, 0.054 mmol) was dissolved in 12 mL DCM/*i*-PrOH (3/1, v/v) under argon in a 50 mL RBF at 0 ºC. $NaBH_4$ (12.3 mg, 0.32 mmol) was then added. Next, the reaction mixture was warmed up to rt and further stirred for 6h. After completion, the reaction mixture was brought back to 0 ºC with an ice bath and 10% citric acid was carefully added dropwise until no hydrogen gas was released, after which the reaction was further stirred for 20 min. The organic layer was collected, and the aqueous layer was further extracted with 2 x 25 mL DCM. The combined organic layer was washed with 1 x 50 mL water and 1 x 50 mL brine. After being dried over Na_2SO_4, filtered, and concentrated under reduced pressure, the product was obtained as a white solid in a quantitative yield and did not require further purification. R_f = 0.45 (50% EtOAc-hexanes).

^{1}H NMR (500 MHz, $CDCl_3$) δ 7.07 – 6.96 (m, 6H), 6.77 (d, *J* = 8.2 Hz, 3H), 4.52 (s, 6H), 4.18 (s, 6H), 2.54 – 2.45 (m, 6H), 1.58 – 1.49 (m, 6H), 1.27 (d, *J* = 14.8 Hz, 64H), 0.88 (t, *J* = 7.0 Hz, 9H). ^{13}C NMR (126 MHz, $CDCl_3$) δ 154.81, 135.89, 129.90, 128.76, 112.02, 61.89, 54.60, 35.23, 32.07, 31.82, 29.84, 29.80, 29.77, 29.69, 29.51, 22.84, 14.27.

Preparation of liposomes for Nile red release assay

Stock solutions of 5 mM lipid switch **4.1** were prepared in chloroform/methanol solution (1/1, v/v). Stock solutions of 32.46 mM PC and 5 mM NR were prepared in chloroform. All the stock solutions were kept in a -20 ºC freezer after preparation. Proper volumes of each stock solution were pipetted into a 1 dr vial to reach a total lipid concentration of 2 mM with desired percentages of each lipid composition. NR was added as an extra 5% of the total lipid content. The organic solvents were next evaporated under a nitrogen stream, and the resulting lipid films were kept under vacuum for at least one hour. After that, the films were hydrated with proper volumes of 1×TBS buffer (pH 7.4, containing 25 mM Tris/Tris HCl, 0.13 M NaCl, 0.0027 M KCl) in a 60 ºC water bath for 1 hr. The vials were taken out and vortexed every 20 min. Next, ten freeze-thaw cycles were performed with a dry ice-acetone bath and 60 ºC water bath. Finally, the liposome solutions were extruded through a 200 nm polycarbonate membrane for 19 passes with an extruder purchased from either Avestin or Avanti. The resulting liposomes were stored at 4 ºC and were studied immediately after preparation.

Phosphorylated metabolite selectivity screen for liposome Nile red release

Stock solutions (50 mM) of each phosphorylated metabolite were prepared by dissolving the appropriate salts (sodium phosphate dibasic heptahydrate (Pi, $Na_2HPO_4{\cdot}7H_2O$); sodium pyrophosphate dibasic (PPi, $Na_2H_2P_2O_7$); adenosine 5’-diphosphate sodium salt (ADP); adenosine 5’-triphosphate disodium salt, hydrate (ATP); D-fructose-6-phosphate disodium salt (FP); D-fructose-1,6-bisphosphate trisodium salt (FBP); sodium tripolyphosphate (TPi); cytidine-5'-triphosphate disodium salt (CTP); guanosine-5’-triphosphate trisodium salt (GTP);

uridine 5′-triphosphate trisodium salt hydrate (UTP); and D-*myo*-inositol-1,4,5-triphosphate sodium salt (IP_3)) with MilliQ water. Adenosine 5′-monophosphate monohydrate (AMP) was prepared as 25 mM stock solutions in MilliQ water due to solubility issue. For each study, 50 μL of liposome solution encapsulating NR was first added into a sub-micro quartz cuvette. After an initial scan, 1 μL of a 50 mM stock solution of the phosphorylated metabolite under study was added to the cuvette (final concentration = 1 mM, 2 μL for AMP), and the fluorescence intensities were recorded after incubation for 5 min (excitation wavelength = 552 nm, excitation slit = 5 nm, emission slit = 5 nm). Control experiments were run by adding 1 or 2 μL MilliQ water. When processing the data, the fluorescence intensities at 630 nm were selected and converted to percentage of initial fluorescence before phosphorylated metabolite addition. Experiments were run at least three times with different batches of liposomes. Averaged data were reported with error bars denoting standard error.

Expanded IP_3 titration experiment using Nile red release assay

IP_3 stock solutions (10 mM) were prepared by diluting the previously prepared 50 mM IP_3 stock solution 5× with MilliQ water. A 100 μL aliquot of 2 mM liposomes encapsulating NR prepared through the procedure described above was added into a sub-micro quartz cuvette. After an initial scan, 0.5 μL of 10 mM IP_3 stock solution was added directly into the cuvette for each measurement in the titration, and the fluorescence intensities were measured using the same detection method as described above. When processing the data, the fluorescence intensities at 630 nm were selected and converted to percentage of initial fluorescence before IP_3 addition. Experiments were run at least three times with different batches of liposomes. Averaged data were reported with error bars denoting standard errors. Kinetic experiments were run on a Cary Eclipse Fluorescence Spectrophotometer using kinetic mode. The excitation wavelength was set to 552 nm, and the fluorescence intensities at 630 nm were constantly collected over time.

Liposome stability test

The same PC liposome samples containing 0-20% lipid **4.1** for NR release studies were prepared as previously described. The stability and dye retention properties of these liposomes were tracked by measuring NR fluorescence. When not taking measurements, liposomes were stored in a 4 °C fridge. Fluorescence intensity was measured every 24 hours (excitation wavelength = 552 nm, excitation slit = 5 nm, emission slit = 5 nm). When processing the data, fluorescence intensities at 630 nm were selected. Experiments were run with three different batches of liposomes, and averaged data are reported with error bars denoting standard error.

Preparation of liposomes for SRB release assay

The same stock solutions of **4.1** and PC prepared for NR release assay were used. Stock solutions of 33.6 mM DOPE and 34.1 mM DPPC were prepared in chloroform. SRB stock solutions (20 mM) were prepared by dissolving SRB with 1 × TBS (pH 7.4, containing 25 mM Tris/Tris HCl, 0.13 M NaCl, 0.0027 M KCl). Proper volumes of each lipid stock solution were pipetted into a clean 1 dr vial to reach a total lipid content of 5 mM scale with desired percentages of each lipid composition. The organic solvents were next removed with a nitrogen stream and the resulting lipid films were further dried under vacuum for at least 1 hr. The films were next hydrated with 20 mM SRB solution at 60 ºC in a water bath for four sets of 15 min with vortexing after each set. Next, the solutions were subjected to ten freeze-thaw cycles with a dry ice-acetone bath and a 60 ºC water bath, followed by extrusion through a 200 nm polycarbonate membrane for 21 passes with an extruder purchased from either Avestin or Avanti. Finally, the unencapsulated dye was removed by size-exclusive chromatography. To do so, a micro-column was first packed with Sephadex G-50 (pre-saturated with isotonic TBS buffer). The fractions were next collected every ~1 mL from the column and the second fraction showing significant turbidity was collected. The presence of liposomes was further verified by treating liposomes with Triton X-100 detergent, where an increase in fluorescence intensity was observed.

SRB release assay upon IP_3 treatment

An aliquot of 50 μL liposomes encapsulating SRB prepared through the procedure described above was added into a sub-micro quartz cuvette. After an initial scan, 1 μL of a 50 mM IP_3 stock solution in MilliQ water was added into the cuvette each time, and the fluorescence intensities were recorded after each addition (λ_{ex} = 550 nm, Ex/Em slit = 10/2.5 nm). After completion, the assay was calibrated by adding 1 μL of 10% Triton X-100 detergent to lyse the liposomes and induce 100% release. When processing the data, fluorescence intensities at 585 nm were selected and reported as a percentage of the fluorescence after Triton X-100 treatment for each sample. Experiments were run at least three times with different batches of liposomes. Averaged data were reported with error bars denoting standard errors.

Dynamic light scattering experiment

Samples were prepared by diluting the liposomes before and after triggered release 10× with proper buffer. All measurements were taken at a scattering angle of 173º at 20 ºC. Bar graphs were generated by the average of at least three experiments with error bars denoting standard error.

Zeta potential measurement of 4.1-liposomes before and after adding IP_3

Zeta potential values were also measured with a Malvern Zetasizer Nano ZS instrument equipped with a 4.0 mW laser operating at l = 633 nm. A 1 mM solution of PC-based liposomes containing 0%, 10% and 20% **4.1** without dye encapsulation were prepared in 1 mM HEPES (pH 7.4, containing 30 mM NaCl). 2.5 μL of 50 mM IP_3 was added into a 100 μL aliquot of liposomes before being diluted with 900 μL buffer (conc of liposomes = 0.1 mM, conc of IP_3 = 0.125 mM). The solutions were next transferred into an DTS1070 folded capillary cell ready for measurement. All measurements were taken at 20 ºC. Data were generated with at least three replicates.

Fluorescence microscopy studies for liposome aggregation after ATP treatment

Solutions of 0% and 20% **4.1** liposomes in PC (1 mM) labeled with 0.08% Rd-PE in 1×TBS buffer (pH=7.4, containing 25 mM Tris/Tris HCl, 0.13 M NaCl, 0.0027 M KCl) were prepared using the previously described thin-film hydration procedures.

An aliquot of the liposome solution (100 μL) was first added into a FluoroDish Cell Culture Dish (WPI Inc.) and allowed to settle for 15 min before imaging using a 63x 1.4NA oil objective on a Leica SP8 White Light Laser Confocal Microscope (Wetzlar, Germany). 4.2 μL of a 25 mM IP_3 stock solution was added into the liposomes (final concentration = 1 mM), and the images were taken over time. Rd-PE was excited by using 561 nm laser line and the emission was collected between 566-620 nm.

Chapter 5. A general strategy to develop enzyme-responsive liposomes

(The scientific data used in this Chapter has been published by the authors: Lou, Jinchao; Best, Michael D., A general approach to enzyme-responsive liposomes, *Chem. Eur. J.* **2020**, *26*, 8597-8607.)

5.1. Project overview

Diseased cells normally exhibit upregulated enzyme concentrations, providing another exciting stimulus for smart liposome development. However, most reported enzyme-responsive liposome systems have focused on the lipid-modifying enzyme, such as phospholipases. In this Chapter, we present a general approach to enzyme-responsive liposomes, targeting esterases, phosphatases and galactosidases, all of which are associated with certain diseases. Instead of leveraging conformational changes, we adapted a different design strategy where enzyme-responsive headgroups are appended onto a self-immolative linker (SIL) connected to a DOPE scaffold. Upon trigger headgroup removal and the release of DOPE, this non-bilayer forming lipid can disrupt the membrane and drive the release of encapsulated content. Liposome dye leakage assays demonstrated that each enzyme-responsive lipid yielded significant content release upon enzymatic treatment compared to minimal release in negative controls. Results also showed that fine-tuning liposome composition was critical for controlling release. DLS analysis showed particle size increases in the cases of esterase- and β-galactosidase-responsive lipids, supporting alterations to membrane properties. These results showcase an effective modular strategy that can be tailored to target different enzymes, providing another promising new avenue for advancing liposomal drug delivery.

5.1.1. Introduction to previous enzyme-responsive liposomes

Among the potential stimuli for triggered release, the targeting of enzymes is particularly promising due to the significant overexpression of enzyme abundance commonly associated with diseased cells. Despite this potential, the development of enzyme-responsive liposomes

has received less attention than other strategies, and has been limited to a small group of enzyme targets.[87,205-207] Most previously reported enzyme-responsive systems have targeted matrix metalloproteinase (MMP),[208,209] cholinesterase[210] or phospholipase enzymes.[211-213] The latter approach has exploited the fact that phospholipase enzymes directly modify lipids that compose the liposome. As an example, the Andresen group[211] developed a class of prodrugs incorporated within lipid scaffolds (lipid **5.1**, Figure 5.1A), for which drug release is driven by lipid hydrolysis catalyzed by secretory phospholipase A_2 (sPLA2). These prior studies support the hypothesis that enzymatic reactions can be harnessed to drive liposome release. However, there are many other enzymes that are significantly overexpressed in different types of cancerous and otherwise diseased cells that provide exciting targets. In addition, the Szoka group developed a cholesterol-based phosphate lipid analog (**5.2**, Figure 5.1B), which was able to stabilize the DOPE bilayer.[214] Addition of alkaline phosphatase and hydrolysis of the phosphate headgroup disrupted the bilayer and caused encapsulated cargo release.

5.1.2. Introduction of enzymes in biology and disease

In this work, we report a general, modular strategy for developing liposomal drug delivery platforms that is effective for targeting a range of enzymes that exhibit dramatic upregulation in diseases such as cancer, including esterases, phosphatases, and β-galactosidases. Esterase concentrations have been reported to be enhanced by two to three orders of magnitude in cancer cells,[215-217] and these enzymes have been implicated in other diseases such as neuronal,[218] liver[219] and Alzheimer's diseases.[220] Overabundance of multiple phosphatase enzymes, such as alkaline phosphatase, has also been correlated with cancer[221-223] as well as liver,[224,225] cardiovascular[226] and kidney diseases.[227] β-Galactosidases are also overexpressed in cancer, and thus have been targeted for cancer imaging.[228-231] Glycosidase enzymes in general are involved in numerous diseases including diabetes, cancer, viral infections such as HIV, and lysosomal storage disorders.[232] These particular enzyme targets have been the subject of few studies. In a rare example, the ganglioside GM1 has been

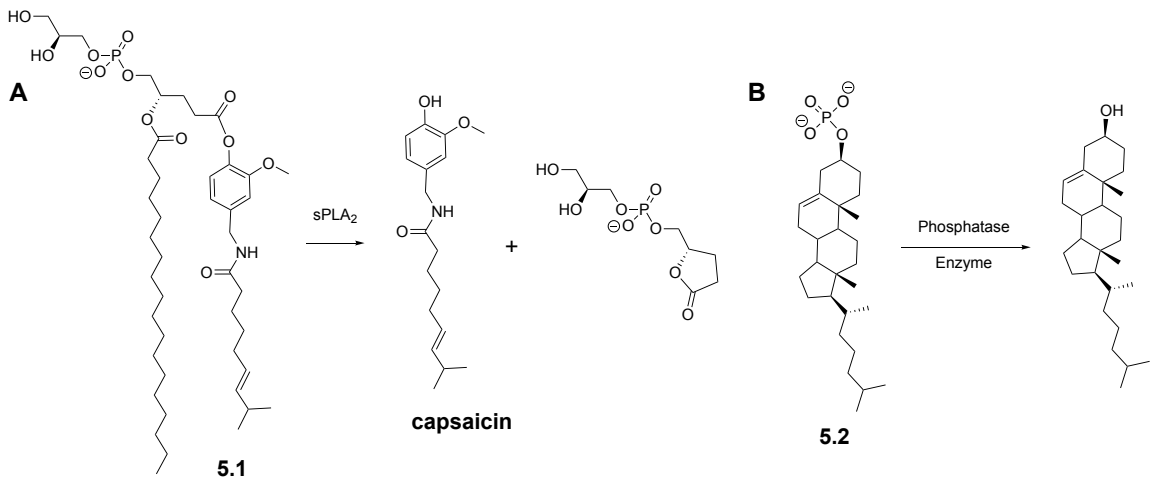


Figure 5.1. Representative previous reported enzyme-responsive liposomes. A. PG analogue developed by the Andresen group. sPLA2 hydrolysis released a capsaicin prodrug embedded within the lipid scaffold. **B.** Cholesterol analogue developed by the Szoka group, which can be hydrolyzed by addition of phosphatase enzymes.

reported for triggered release using β-galactosidase based on the modulation of membrane properties upon truncation of the carbohydrate headgroup.[233] While this is an elegant strategy, it relies upon a complex glycolipid structure for release.

5.1.3. Structure of DOPE and its self-assembly properties

An introductory review of lipid packing parameters was provided in Chapter 1. Developing of different strategies to modulate lipid packing properties is the key foundation to triggering the release of encapsulated contents from liposomes. Besides the novel mechanisms introduced in Chapters 2-4, a more traditional strategy has entailed modification of well-known non-bilayer lipids to add stimuli-responsive moieties, so that the resulting lipids will prefer to form a bilayer assembly initially. Upon the addition of certain stimuli and removal of trigger groups, a non-bilayer lipid that can disrupt the membrane is produced. The most common non-bilayer lipid explored for this purpose is DOPE. It is well-known to prefer hexagonal phase (H_{II}) lipid assemblies in aqueous solution at physiological conditions due to the small head-to-tail volume ratio.[234] DOPE is also a convenient synthetic building block for stimuli-responsive lipid development through acylation of the amino group, which can result in increased size of the headgroup, leading to DOPE-conjugates that can significantly stabilize membrane bilayers.[235,236]

5.1.4. Headgroup-modified DOPE based release systems

Due to the special properties of DOPE, a common strategy has been to design stimuli-responsive lipids modified at the headgroup. Earlier work on elastase-responsive liposomes based on DOPE scaffold was reported by Meers and co-workers. Lipid **5.3** was produced by attaching an *N*-acylated dialanine peptide to DOPE (Figure 5.2).[237] A FRET mixing assay was conducted to verify that elastase enzyme actives vesicle fusion. This system was further modified by switching the headgroup into *N*-methoxysuccinyl-Ala-Ala-Pro-Val, leading to lipid **5.4** with greater sensitivity and selectivity for elastase.[238] Similar approaches have also been

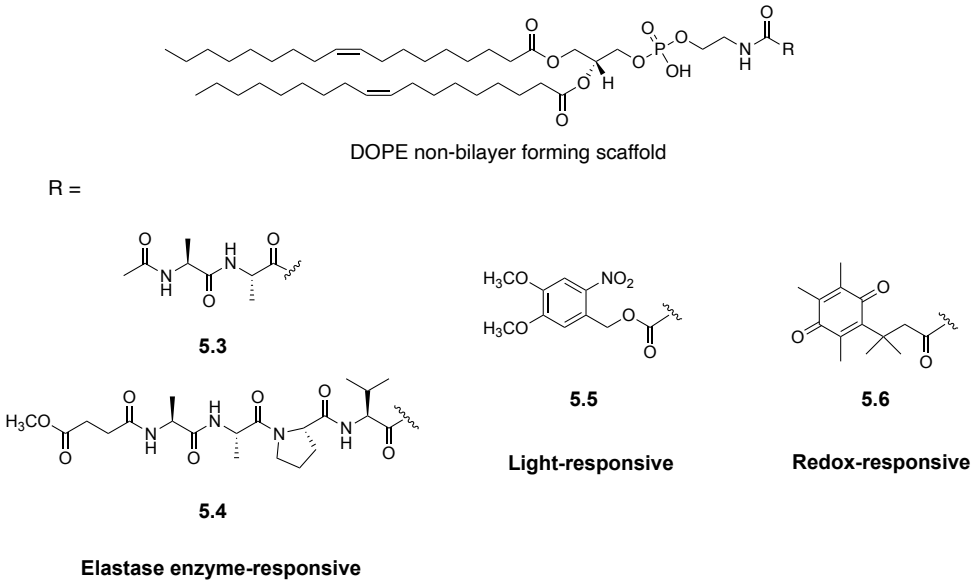


Figure 5.2. Lipids designed for triggered release through the production of natural non-bilayer lipid DOPE product.

used in developing liposomes that could respond to other stimuli. Smith and co-workers developed photoactivatable liposomes by conjugating the nitroveratrylcarbonyl group onto DOPE to form compound **5.5**.[239] UV irradiation of liposomes composed of 50% **5.5** in egg PE led to 90% uncaging of this compound and release of ~50% of encapsulated calcein dye. In addition, McCarley and colleagues developed liposomes that respond to a reducing environment using quinone-DOPE conjugate **5.6**.[195,240] This compound was designed such that quinone reduction produces a phenoxide intermediate known as the trimethyl lock (TML) that is known to undergo fast kinetics for lactonization via intramolecular cyclization.[241,242]

5.1.5. Introduction to self-immolative linkers

Self-immolation chemistry focuses on the study of cascading decomposition reactions triggered by addition of certain stimuli to ultimately release appended constituents, such as small molecule drugs or fluorophores.[243,244] This type of chemistry has been widely explored in the area of nanomedicine and sensor development.[244,245] A general self-immolative system design is illustrated in Figure 5.3A, in which molecules contain a stimuli-responsive headgroup, an SIL and a reporter moiety. The stimulus treatment initiates the electronic cascade reactions that break the chemical bond between the headgroup and linker, which ultimately leads to the release of reporter groups. Self-immolation processes are normally considered driven by a combination of the increases in entropy as well as the formation of thermodynamically stable products.[246] They can be generally classified into two major categories, including 1,4/1,6-elimination or cyclization. Representative examples are showcased in Figure 5.3B-C, including a 1,4-quinone-methide (QM) elimination and the trimethyl lock (TML, *o*-hydroxydihydrocinnamic acid) cyclization. Both the TML[241,242,247-249] and QM[250,251] moieties are well known for fast kinetics of decomposition upon trigger removal.

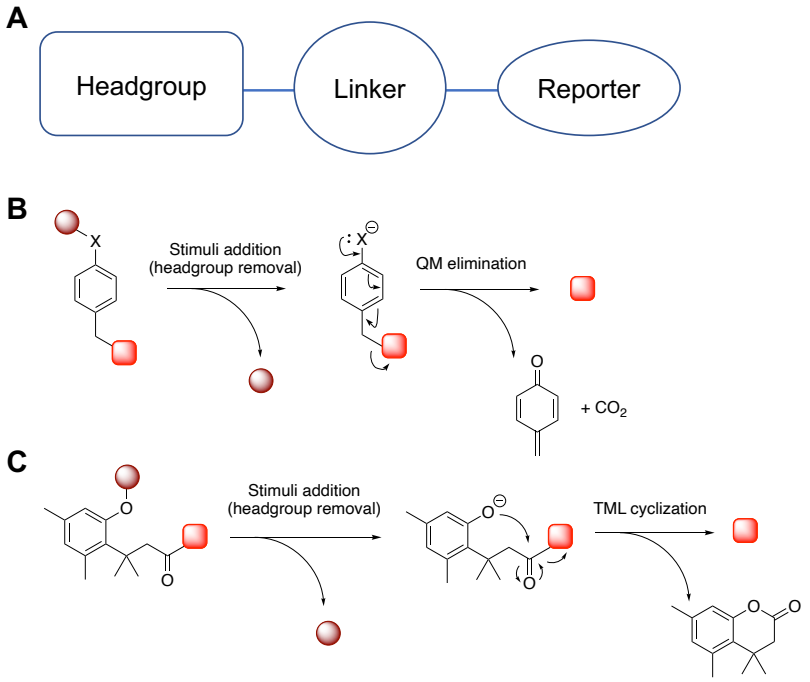
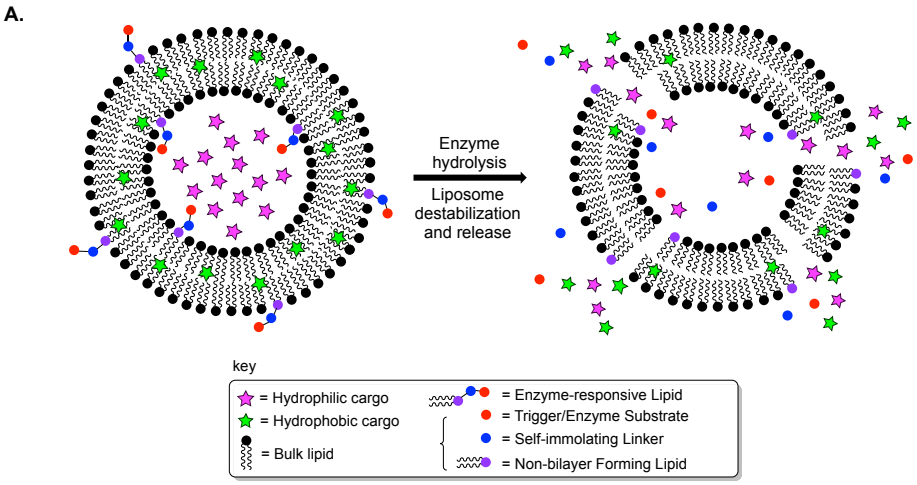


Figure 5.3. Design for general self-immolative systems and examples for self-immolative linkers. A. General design for self-immolative systems bearing trigger, linker and reporter groups. **B.** Sample 1,4-QM-elimination reaction and its immolation mechanism. **C.** Sample TML cyclization reaction and its immolation mechanism.

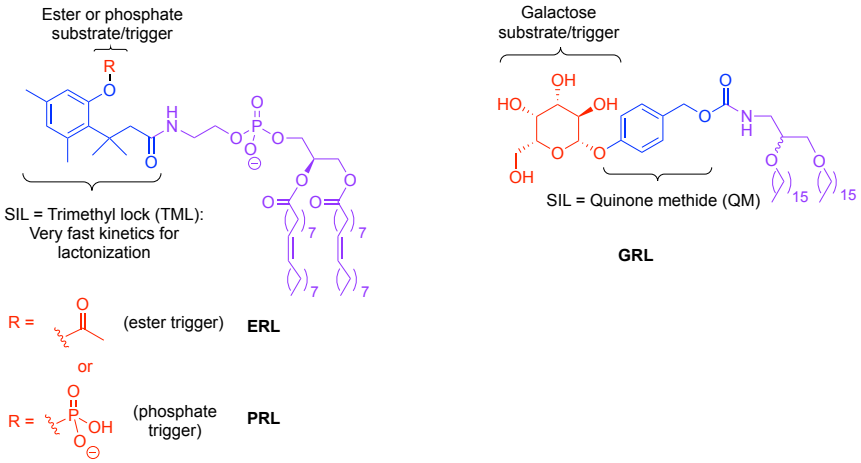
5.2. Design and synthesis of enzyme-responsive lipids

In this Chapter, we report a versatile stimuli-responsive lipid design by exchanging appended substrate moieties to target multiple enzymes that are commonly overexpressed in cancer cells. The design strategy is shown in Scheme 5.1. Each lipid analog contains three functional regions. First, a variable substrate moiety corresponding to each target enzyme is included that acts as the trigger for liposome release. This includes an ester that can be cleaved by an esterase (esterase-responsive lipid (**ERL**)), a phosphate group that is hydrolyzed by a phosphatase (phosphatase-responsive lipid (**PRL**)) or a β-galactose moiety for enzymatic cleavage by a β-galactosidase (galactosidase-responsive lipid (**GRL**)). Secondly, an SIL is present in between the trigger headgroup and the lipid scaffold to be released. Upon trigger removal, the SIL is designed to quickly undergo a disassembly reaction that results in release of an appended leaving group. Specifically, the SILs for our responsive lipids include TML for **ERL** and **PRL** or the QM-elimination reaction for **GRL**. Finally, these responsive lipids are designed to form stable liposome membranes that are perturbed upon enzymatic removal of the trigger, in this case through the release of a non-bilayer lipid that will destabilize the membrane and trigger release of liposome contents. The lipids DOPE and aminodialkylglycerol were employed for this purpose, with the latter selected to avoid synthetic challenges associated with introduction of the sugar headgroup of **GRL**. Our systems are designed such that enzymatic removal of trigger groups will stimulate decomposition of the SIL to produce non-bilayer lipids that disrupt the membrane and release encapsulated cargo.

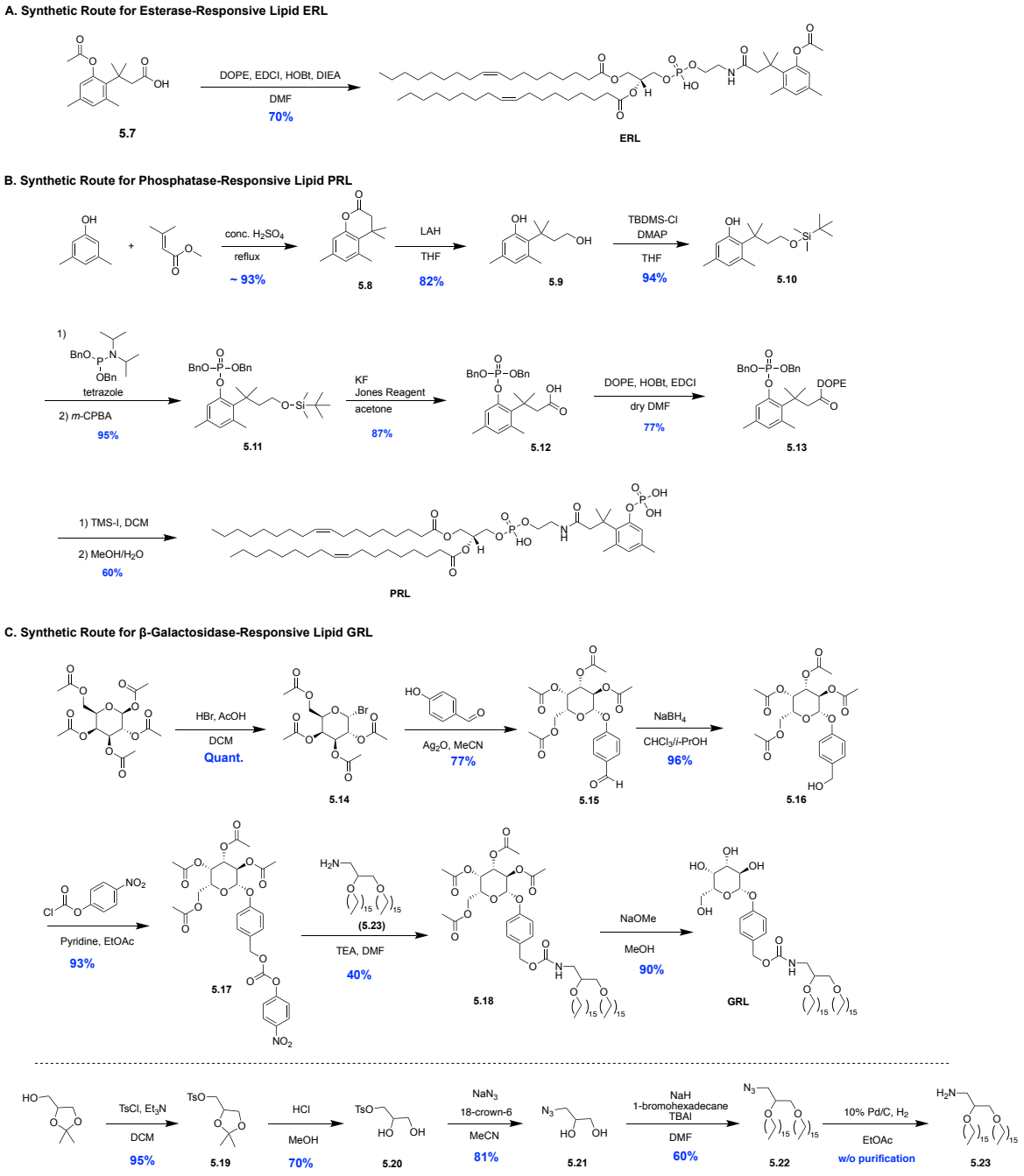
The synthetic routes used to access the three enzyme-responsive lipids are shown in Scheme 5.2. The synthesis of **ERL** benefitted from commercially available esterified TML-carboxylic acid **5.7**, which allowed for convenient access to this product through a one-step amide-bond coupling reaction with DOPE (Scheme 5.2A). To access **PRL**, compounds **5.8**-**5.10** were synthesized from 3,5-dimethylphenol as previously reported[252,253] through a Michael addition with methyl 3-methylbut-2-enoate, spontaneous lactonization to **5.8**, reductive ring opening to



B. Structures of Enzyme-Responsive Lipids



Scheme 5.1. Design of enzyme-responsive liposomes. A. Cartoon depicting hypothetical model for liposome release. Enzyme-responsive lipids contain three major regions including enzyme substrate headgroup, SIL, and a non-bilayer lipid scaffold. After hydrolysis of the substrate by the appropriate enzyme, SIL decomposition will cause the release of a non-bilayer lipid to disrupt membrane integrity and release of encapsulated cargo. **B.** Structures of enzyme-responsive lipids. Esterase- and phosphatase-responsive lipids (**ERL** and **PRL**, respectively) include TML as the SIL and DOPE as the lipid scaffold. β-Galactosidase-responsive lipid **GRL** instead bears a QM-generating SIL and an aminodialkylglycerol analogue as the lipid scaffold.



Scheme 5.2. Synthetic routes developed to access ERL (A) PRL (B) and GRL (C).

5.9, and silyl protection to **5.10**. Phosphoramidite chemistry was next performed to produce the phosphodiester of **5.11**, followed by Jones oxidation and simultaneous silyl deprotection to afford **5.12**.[252] Finally, an amide coupling reaction with DOPE yielding **5.13** was followed by benzyl deprotection to produce **PRL**. For **GRL**, the design and synthetic route were different, as shown in Scheme 5.2C. As discussed above, to overcome synthetic issues associated with the use of acetyl protecting groups, 4-hydroxy benzyl alcohol was instead used as the SIL and dialkylglycerol as the non-bilayer forming lipid scaffold. Compounds **5.14**-**5.17** were synthesized from β-D-galactose pentaacetate as previously reported by Toth et al[254] through hydrobromic acid treatment to form α-D-galactopyranosyl bromide (**5.14**), glycosylation with 4-hydroxyl benzaldehyde to produce **5.15**, aldehyde reduction to **5.16**, and conversion of the resulting alcohol to *p*-nitrophenyl carbonate **5.17**. Dialkyl aminoglycerol lipid **5.23** was synthesized from solketal in five steps, similar to strategies we previously reported[89,255] through tosylate introduction to **5.19**, acetonide deprotection to **5.20**, substitution of tosylate with azide to **5.21**, Williamson ether synthesis to introduce lipid alkyl chains to **5.22**, and reduction of azide to the primary amine **5.23** (bottom of Scheme 5.2C). Amine **5.23** and carbonate **5.17** were combined to produce the carbamate moiety of protected lipid **5.18**, followed by deprotection of the acetyl groups on galactose to access **GRL**.

5.3. TLC analysis of enzyme-mediated cleavage of free lipid ERL

Following the successful synthesis of all three lipids, we first tested their enzyme-responsive properties. Considering the accessibility of **ERL** compared to the other two lipids, we initiated studies with this compound to determine conditions for liposomal release. Prior to incorporating this compound into liposomes, we set out to evaluate esterase hydrolysis of the free lipid using a TLC assay in a manner similar to a previous report.[237] For this experiment, 2 µg of **ERL** was dissolved in 50 µL of TBS buffer and was then incubated with 0.45 U of commercially available porcine liver esterase at room temperature for three hours. After this, the reaction mixture was spotted on a silica gel TLC plate, which was run with 20% MeOH-chloroform as eluant and

visualized with potassium permanganate stain.[256] As is shown in Figure 5.4, this plate indicated complete disappearance of the **ERL** spot in the product coupled with the appearance of a new spot attributed to DOPE. This result indicates that **ERL** acts as an appropriate substrate and provided evidence that the esterase hydrolyzed only the TML headgroup while leaving the DOPE fatty acid ester chains intact. In addition, the catalytic activities of phosphatase and β-galactosidase enzymes were confirmed via colorimetric assays using *p*-nitrophenylphosphate and *p*-nitrophenylgalactose, respectively, in which the yellow color of *p*-nitrophenoxide was observed upon enzymatic hydrolysis (Figure 5.5).

5.4. Fluorescence-based dye release assays and DLS studies

5.4.1. Nile red release assay

With evidence that **ERL** acts as a substrate for esterase enzyme, we next moved on to evaluate liposome triggered release properties using fluorescence-based dye leakage assays. These assays can be used to evaluate the release of either hydrophobic or hydrophilic dyes encapsulated within the membrane bilayer or aqueous core, respectively, as judged by changes in dye emission properties. The first assay we pursued utilized the hydrophobic dye NR. We incorporated responsive lipids at varying percentages into liposomes primarily composed of bulk lipids including PC and DOPE. Other lipid additives such as DOTAP and PA were also included to probe their effects on liposome membrane stability before and after enzyme treatment. Unilamellar liposomes were prepared using standard thin-film hydration methods including lipid film preparation, hydration, freeze-thaw cycles and extrusion through 200 nm polycarbonate membranes. Dynamic light scattering (DLS) experiments were performed to verify the successful formation of the stable liposome vesicles, as will be later discussed.

During the course of these studies, we systematically varied lipid composition to analyze liposomes containing a wide range of percentages of different mixtures of PC, DOPE, DOTAP

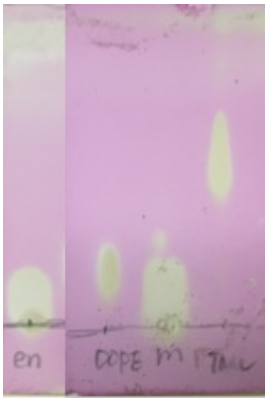


Figure 5.4. TLC analysis of free ERL as an esterase substrate. Lane 1: esterase enzyme, Lane 2: DOPE, Lane 3: Reaction mixture, Lane 4: **ERL** standard. All **ERL** was converted into DOPE upon three-hour esterase treatment.

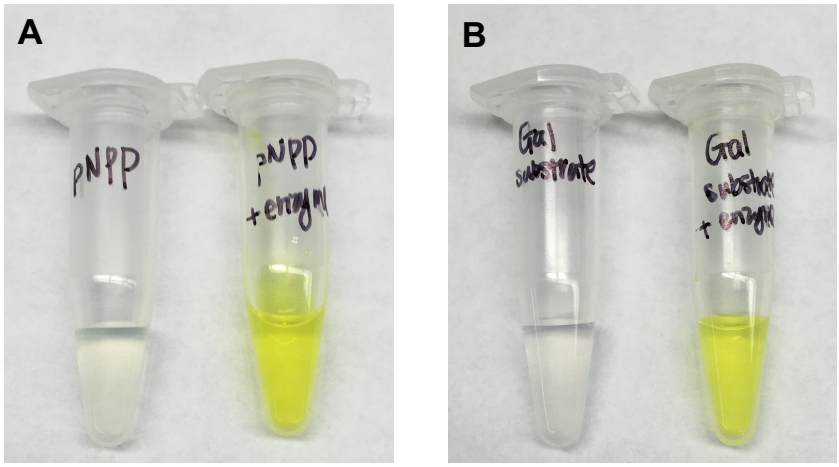


Figure 5.5. Photos of colorimetric assays testing enzyme activity. A. Alkaline phosphatase. treatment of a colorless solution of 60 mM *p*-nitrophenylphosphate (pNPP) in TBS buffer (left) with 0.35 U phosphatase (right) led to the immediate appearance of the yellow color of the nitrophenol hydrolysis product. **B.** A similar result was observed when a 66 mM solution of 4-nitrophenyl β-D-galactopyranoside in TBS buffer (left) was treated with 0.55 U of galactosidase.

and PA. The results of these studies are summarized in Table 5.1. Many of these liposome formulations were found to not release contents or to not be sufficiently stable before enzyme treatment, indicating that the stability of the liposomes before and after enzymatic release needs to be carefully fine-tuned. We will note that we did not observe these same issues in the development of ion- and metabolite-responsive liposomes in the prior three chapters, which we attribute to those compounds undergoing more dramatic structural changes upon stimulus introduction.

Our initial success in esterase-responsive liposome release was achieved using liposomes composed of PC, DOPE, and DOTAP. DOTAP is a cationic lipid that is widely used in transfection[257] and has been reported to render membranes more fusogenic, which is why we began introducing this compound into liposomes in an effort to induce cargo release.[237] After screening a variety of different lipid mixtures, liposomes composed of 30% **ERL**, 50% DOPE, 10% PC and 10% DOTAP treated with 0.45 U of porcine liver esterase and incubated in a 30 °C water bath in between measurements showed an ~30% decrease in fluorescent intensity upon esterase treatment within 40 minutes (Figure 5.6A and Table 5.1, Entry 1). We have previously found that heating of liposomes can be necessary to achieve effects such as liposome fusion.[258] Different control sets were also tested using the exact same liposome formulation by treating with only buffer or with heat-denatured enzyme, leading to diminished fluorescence changes (background release ranging from ~8-12%, Figure 5.6A). Similar results were also observed for liposomes lacking **ERL** in which this lipid was replaced by PC. To drive home the sensitive nature of liposome composition, we will note that liposomes containing 30% **ERL**, 50% DOPE, 15% PC, and 5% DOTAP showed almost the same fluorescence intensity decrease (~10%) as the control sets, indicating that trading only 5% of DOTAP for PC was sufficient to stabilize the membrane and shut down release of encapsulated dye. On the other hand, liposomes containing 30% **ERL**, 50% DOPE, 5% PC, and 15% DOTAP only showed ~15% release. In this way, the liposome composition needed to be carefully fine-tuned in order

Table 5.1. Summary of formulations explored for triggered release using ERL containing different percentages of PC, DOPE, DOTAP or PA.

Entry	Comments	% ERL	% Egg PC	% DOTAP	% DOPE	% PA	Outcome
1	Ref. set for DOTAP addition	30	10	10	50	--	~ 30% release
2	Varying DOTAP and DOPE	30	10	20 ↑	40 ↓	--	Did not produce stable liposomes.
3				30 ↑	30 ↓	--	Did not produce stable liposomes.
4	Varying egg PC and DOPE	30	20	10	40	--	Minimal release.
5			30		30	--	
6			40		20	--	
7	Varying egg PC and DOTAP	30	5 ↓	15 ↑	50	--	~ 20% release.
8			15 ↑	5 ↓		--	Minimal release.
9	Varying **ERL** and DOPE	40	10	10	40	--	Minimal release.
10		50			30	--	~20% release.
11	Varying **ERL** and DOTAP	20 ↓	10	20 ↑	50	--	Did not produce stable liposomes.
12		40 ↑		0 ↓		--	Minimal release.
13	Without Egg PC	40	0	10	50	--	Did not produce stable liposomes.
14	Without DOTAP	30	20	0	50	--	Minimal release.
15	Ref. set for PA addition	30	10	--	50	10	~ 60% release within 6 hours.
16	Varying PA and DOTAP	30	10	5	50	5	~ 35% release within 6 hours.
17	Varying PA and DOPE	30	10	--	40	20	35% release over 20 hours.

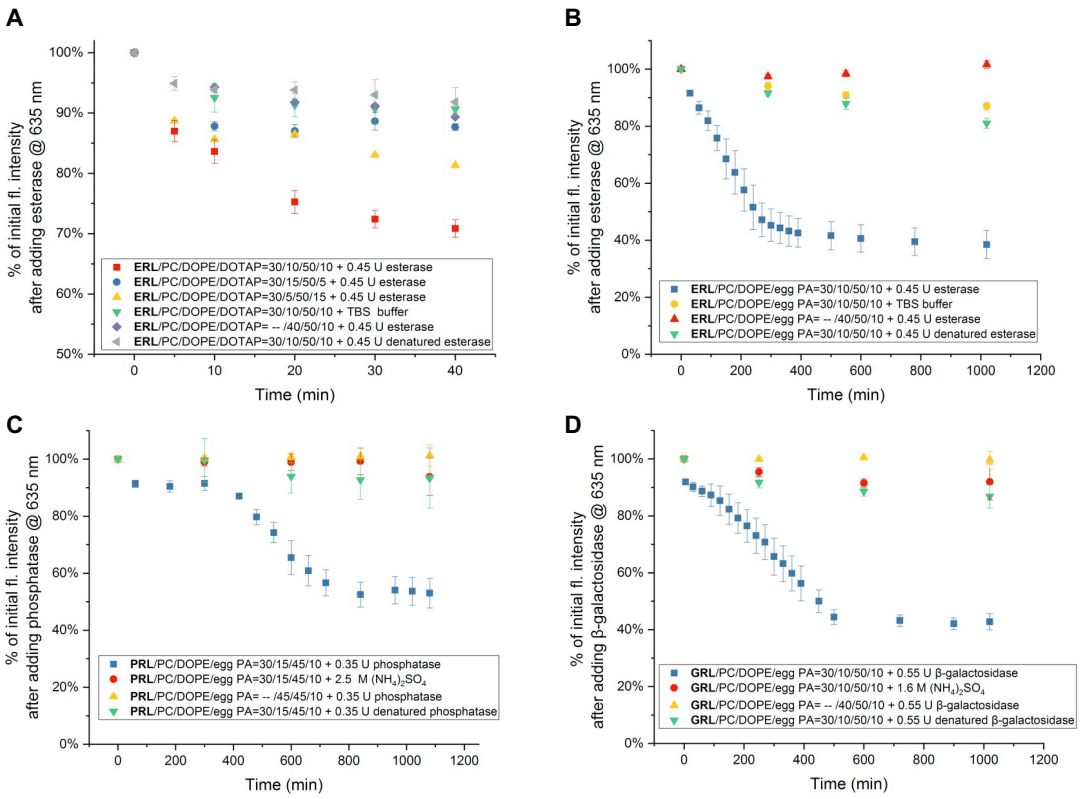


Figure 5.6. Release of NR over time from different formulations of enzyme-responsive liposomes. A. Data for **ERL** liposomes composed of 30% **ERL**, 50% DOPE and varying percentage of PC or DOTAP addition. **B.** Data for **ERL**-containing liposomes containing PA. A 30/10/50/10 ratio of **ERL**/PC/DOPE/PA yielded ~60% release over time upon esterase treatment. **C.** Data for **PRL**-containing liposomes. A 30/15/45/10 ratio of **PRL**/PC/DOPE/PA gave ~50% release overtime upon phosphatase treatment. **D.** Data for **GRL**-containing liposomes. A 30/10/50/10 ratio of **GRL**/PC/DOPE/PA resulted in ~60% release overtime upon galactosidase treatment. Control experiments involving treatment with buffer or heat-denatured enzyme, along with removal of responsive lipid, did not show significant fluorescent decrease in all cases. Error bars indicate standard errors from at least three studies.

to optimize release properties.

The sensitive nature of DOTAP-containing liposomes led us to next explore another lipid additive, PA. PA is an ionic lipid that is known to exaggerate the non-bilayer properties of DOPE within membranes.[259] After evaluating different lipid percentages (Table 5.1, Entries 15-17), we identified that the formulation in which DOTAP was simply replaced by PA showed significantly enhanced activity (30% **ERL**, 10% PC, 50% DOPE and 10% egg PA). NR release curves for these experiments are shown in Figure 5.6B. Upon treatment with esterase and heating at 30 °C in between measurements, the fluorescence intensity gradually decreased by ~60%, although this process took a significantly longer time (approximately five hours) to run to completion. Control experiments were also done as before, either treating the exact same liposome solution with buffer or heat denatured esterase or by treating liposomes in which **ERL** was replaced by PC with esterase. All of these, again, showed only minimal background release. We will also note that the percent change in fluorescence may not indicate the total percentage of dye release, for example since the released hydrophobic dye may be re-encapsulated into other lipid assembly structures after being initially released. These results indicate that **ERL** enables effective enzyme-responsive liposome properties for the release of hydrophobic cargo.

To pursue our goal of developing a general strategy that could be adapted to target different enzymes, we next evaluated triggered release conditions driven by **PRL** and **GRL**. For the former, we again tested different formulations (Table 5.2) and arrived at an effective composition of 30% **PRL**, 15% PC, 45% DOPE and 10% PA. After adding 0.35 U alkaline phosphatase from *Escherichia coli* and incubating at 30 °C in between measurements, a fluorescence intensity decrease of ~50% was observed after about thirteen hours, as is shown Figure 5.6C. Interestingly, this release curve appeared to exhibit an induction period of approximately 5 hours before a steeper drop in fluorescence intensity. This result was only

Table 5.2. Summary of formulations explored for forming stable PRL liposomes containing different percentages of PC, DOPE, DOTAP or PA.

Entry	Comments	% PRL	% Egg PC	% DOPE	% PA	% DOTAP	Outcome
1	Fix 30% **PRL** and 10% PA. Varying egg PC and PA.	30	10	50	10	--	Did not produce stable liposomes.
2		30	15	45	10	--	Stable liposomes. ~50% release within 13 hours.
3		30	20	40	10	--	Stable liposomes. Minimal release.
4	Fix 30% **PRL** and 10% DOTAP. Varying egg PC and DOPE.	30	10	50	--	10	Did not produce stable liposomes.
5		30	20	40	--	10	Did not produce stable liposomes.

observed with **PRL**, and since this is the only anionic enzyme-responsive lipid tested, it is possible that the altered charge of the membrane affects enzymatic modification and/or release properties. Also, as mentioned above, a key point we encountered with each of these responsive systems is that initial and final stability of the membrane must be carefully tuned to maximize release. In this case, this was done by dropping the percentage of DOPE from 50% for **ERL** to 45% for **PRL**, which was perhaps needed to compensate for the introduction of the negatively charged **PRL** lipid.

GRL exhibited release properties that were quite similar to **ERL**, despite being composed of entirely different structural attributes (altered enzymatic substrate, SIL, and lipid scaffold that is released). Again, different formulations were screened (Table 5.3), and a 30/10/50/10 ratio of **GRL**/PC/DOPE/PA resulted in an ~60% decrease in fluorescent intensity within nine hours upon addition of β-galactosidase from *Escherichia coli* (Figure 5.6D). For both **PRL and GRL**, multiple control experiments were again carried out. Liposomes containing responsive lipids didn't show significant release upon treatment with either buffer or heat-denatured enzyme addition. Similar results were again observed for liposomes in which responsive lipids were replaced by PC and treated with enzyme. These dye release results showcase that these enzyme-responsive liposome systems are effective for controlling the release of encapsulated contents in a manner driven by enzyme treatment. These also indicate that our design indeed provides a general strategy for targeting different enzymes by simply exchanging the enzymatic substrate trigger incorporated into the headgroups of enzyme-responsive lipid structures.

The stability of liposomes formed by all these three responsive lipids as well as PA in formulation were tested via tracking encapsulated NR fluorescence over time (Figure 5.7). All of them were stable for at least three days when being kept at 4 °C.

Table 5.3. Summary of formulation explored for triggered release using GRL containing different percentages of PC, DOPE, DOTAP or PA

Entry	Comments	% GRL	% Egg PC	% DOPE	% DOTAP	% PA	Outcome
1	**GRL**/PC based liposomes	20	80	--	--	--	Stable liposomes. Minimal release.
2		50	50	--	--	--	Stable liposomes. Minimal release.
3		75	25	--	--	--	Stable liposomes. Minimal release.
4	**GRL**/PC/DOPE based liposomes	50	40	10	--	--	Stable liposomes. Minimal release.
5		50	25	25	--	--	Stable liposomes. Minimal release.
6	**GRL**/PC/DOTAP based liposomes	20	70	--	10	--	Stable liposomes. Minimal release.
7		30	60	--	10	--	Stable liposomes. Minimal release.
8		50	40	--	10	--	Stable liposomes. Minimal release.
9	Fix 30% DOPE and 10% DOTAP. Varying **GRL** and PC.	20	40	30	10	--	Stable liposomes. Minimal release.
10		30	30	30	10	--	Stable liposomes. Minimal release.
11	Fix 30% **GRL** and 10% DOTAP. Varying egg PC and DOPE.	30	20	40	10	--	Did not produce stable liposomes.
12		30	10	50	10	--	Did not produce stable liposomes.
13	Fix 30% **GRL** and 10% PA. Varying egg PC and DOPE.	30	20	40	--	10	Stable liposomes. Minimal release.
14		30	10	50	--	10	Stable liposomes. ~60% release within 9 hours

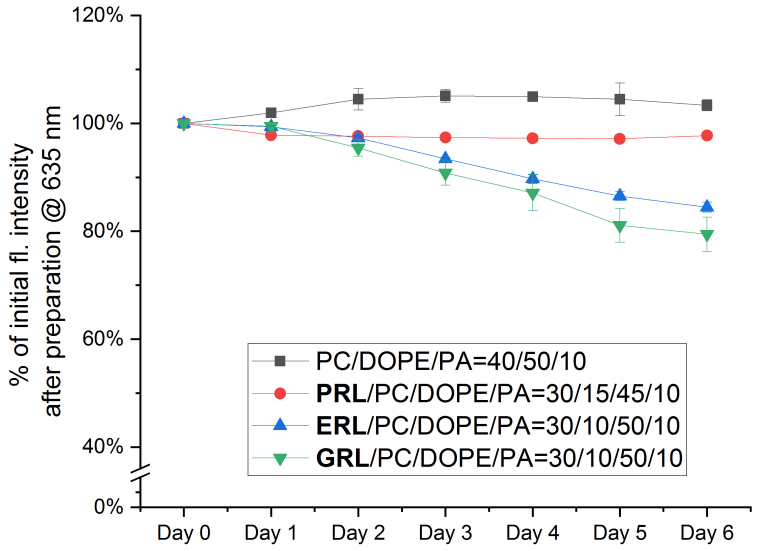


Figure 5.7. Liposome stability test for NR-encapsulated PA-containing liposomes with all three enzyme-responsive lipids. Control liposomes as well as **PRL**-containing liposomes were stable for six days, while **ERL**- and **GRL**- containing liposomes showed gradual degradation, particularly after three days.

5.4.2. DLS studies

In order to evaluate potential structural changes to self-assembled lipid structures caused by the introduction of enzymatic stimuli, we next performed DLS studies using each system. For these experiments, liposome formulations that yielded optimal NR release results in the prior studies were analyzed by DLS before and after enzyme treatment, with results shown in Figure 5.8. In all cases, the original liposome samples prior to enzyme treatment showed uniform vesicle sizes with average diameters ranging from 150 nm - 200 nm, which is expected for particles prepared via extrusion by passing through membranes of 200 nm. This indicates that these formulations containing responsive lipids form stable liposomes. As can be seen in Figure 5.8A (raw distribution curves are included in Figure 5.9), incubation of **ERL** containing liposomes with esterase resulted in a dramatic increase in average particle size. In the corresponding control experiments, liposomes containing **ERL** but instead treated with TBS buffer or liposomes without **ERL** subjected to esterase only showed minimal changes. These results are in line with previous stimuli-responsive liposomes we have developed,[88,89] and indicate that liposomes underwent structural changes upon esterase treatment. Possible explanations include that lipids adopt different assembly properties after enzyme modification such as the inverted hexagonal phase, which is favored by DOPE at physiological conditions.[234] Considering the complicated lipid composition, another reasonable explanation would be that after enzyme treatment, the membrane was destabilized, ultimately leading to fusion and concomitant release of encapsulated cargo.

Liposomes containing **GRL** yielded comparable increases in average particle sizes after adding β-galactosidase and null results in controls (Figure 5.8C, raw distribution curves are included in Figure 5.10), suggesting that this system underwent alterations to lipid self-assembly properties that were similar to **ERL** liposomes. However, somewhat surprisingly, **PRL** liposomes did not yield any significant size changes in any of these experiments, suggesting that **PRL**-containing liposomes did not undergo significant changes in lipid

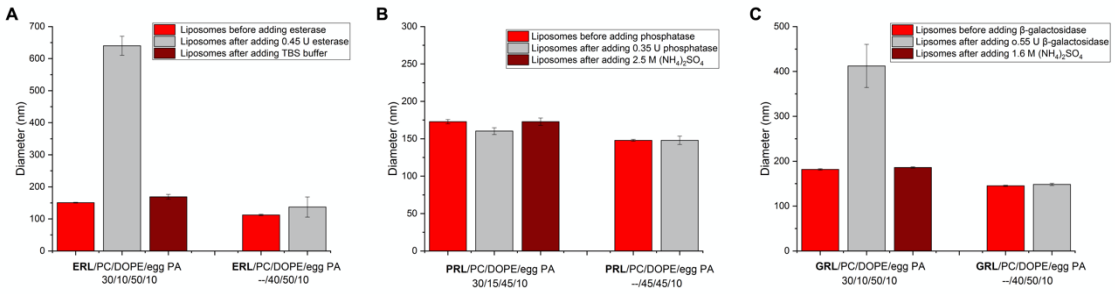


Figure 5.8. DLS results from enzyme-responsive liposomes used in NR release experiments. Data for **ERL**-containing liposomes (**A**) and **GRL**-containing liposomes (**C**) yielded significant increases in average particle sizes upon esterase or β-galactosidase treatment, respectively. For **PRL**-containing liposomes (**B**), minimal changes were observed under any conditions. Control experiments in all three cases did not show any significant change. Error bars indicate standard errors from at least three studies.

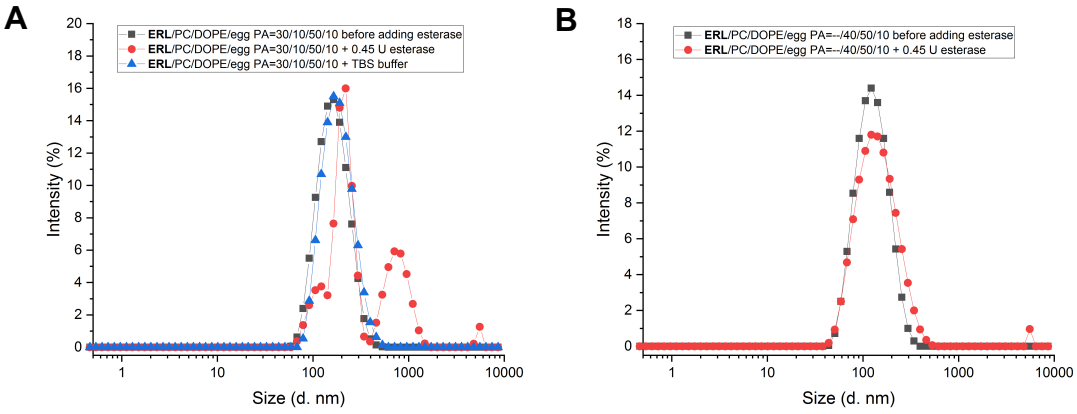


Figure 5.9. Raw DLS size distribution plots for A. ERL-containing liposomes before and after esterase/buffer treatment, and B. control liposomes without ERL before and after esterase addition.

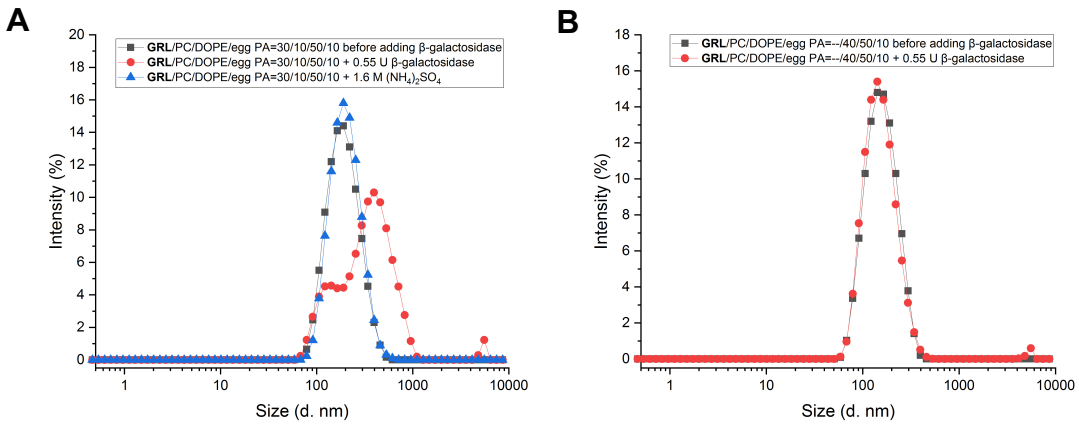


Figure 5.10. Raw DLS size distribution plots for A. GRL-containing liposomes before and after β-galactosidase/buffer treatment, and B. control liposomes without GRL before and after β-galactosidase addition.

assembly properties (Figure 5.8B and Figure 5.11). While **PRL** liposomes did exhibit NR release, the response curve was unique from the others since it showed an induction period and it ultimately yielded less of a decrease in percentage of fluorescence. Again, the most significant difference in this compound is the presence of the charged phosphate group, which may impact either liposome membrane packing or the interaction of phosphatase enzyme with the liposomes. Nevertheless, we have previously observed similar results in which a light-triggered release liposomal platform yielded significant NR released but no size changes were detected via DLS.[104]

5.4.3. SRB release assay

To evaluate the hydrophilic content release properties for our systems, we again selected SRB release assays. When preparing these liposomes, similar methods were used that were modified by the addition of purification through SEC, which is needed after extrusion to remove unencapsulated dye. The successful preparation of liposomes was again determined by DLS.

To assess the hydrophilic cargo release properties of esterase-responsive liposomes, SRB was encapsulated within liposomes containing 30% **ERL**, 10% PC, 50% DOPE and 10% PA as well as control liposomes containing 30% DPPC, 10% egg PC, 50% DOPE and 10% PA. After treating with esterase and incubating in a 30 °C water bath for 17 hours when not performing measurements, the detergent Triton X-100 was added into the liposome solution as a measure of the total release of encapsulated contents. The normalized results are reported for each point as a percentage of fluorescent increase compared to Triton X-100 treatment. As is shown in Figure 5.12, liposomes containing **ERL** exhibited a significant increase in fluorescence compared to negative control experiments in which liposomes containing **ERL** were instead treated with buffer or liposomes without **ERL** were subjected to enzyme, which both showed minimal fluorescence change. These results showcase that enzyme-responsive systems are also capable of releasing hydrophilic contents.

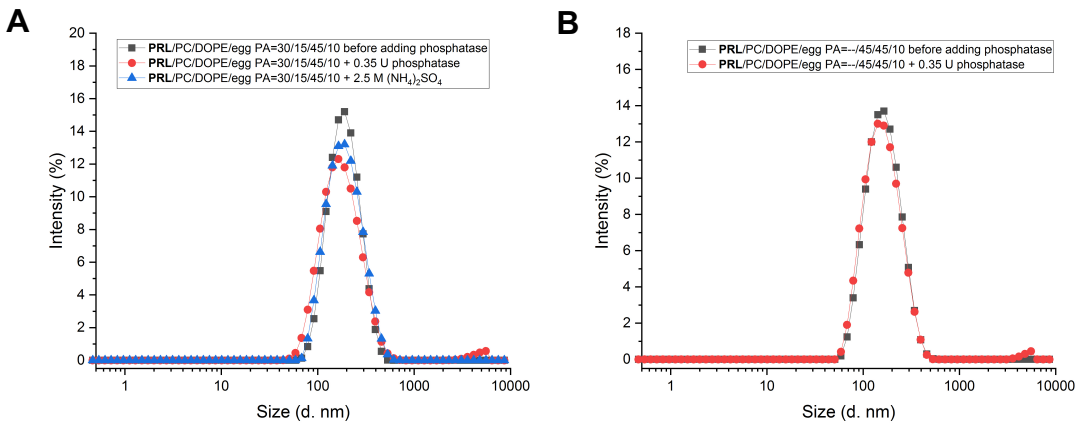


Figure 5.11. Raw DLS size distribution plots for A. PRL-containing liposomes before and after phosphatase/buffer treatment, and B. control liposomes without PRL before and after phosphatase addition.

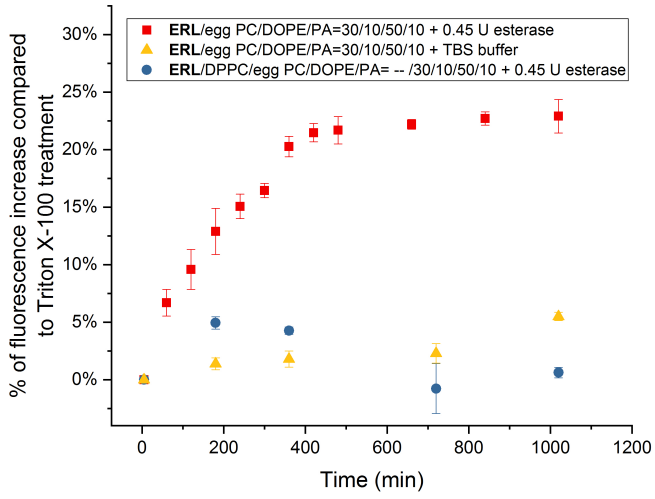


Figure 5.12. SRB release data over time upon esterase addition to liposomes containing 30% ERL, 50% DOPE, 10% PC and 10% PA or control experiments of buffer treatment or liposomes lacking ERL. Only liposomes containing **ERL** with esterase treatment showed significant fluorescence increases. Error bars indicate standard errors from at least three studies.

5.5. Miscellaneous experiments

5.5.1. ERL related attempts

5.5.1.1. TML-ester-acid 5.7 synthesis

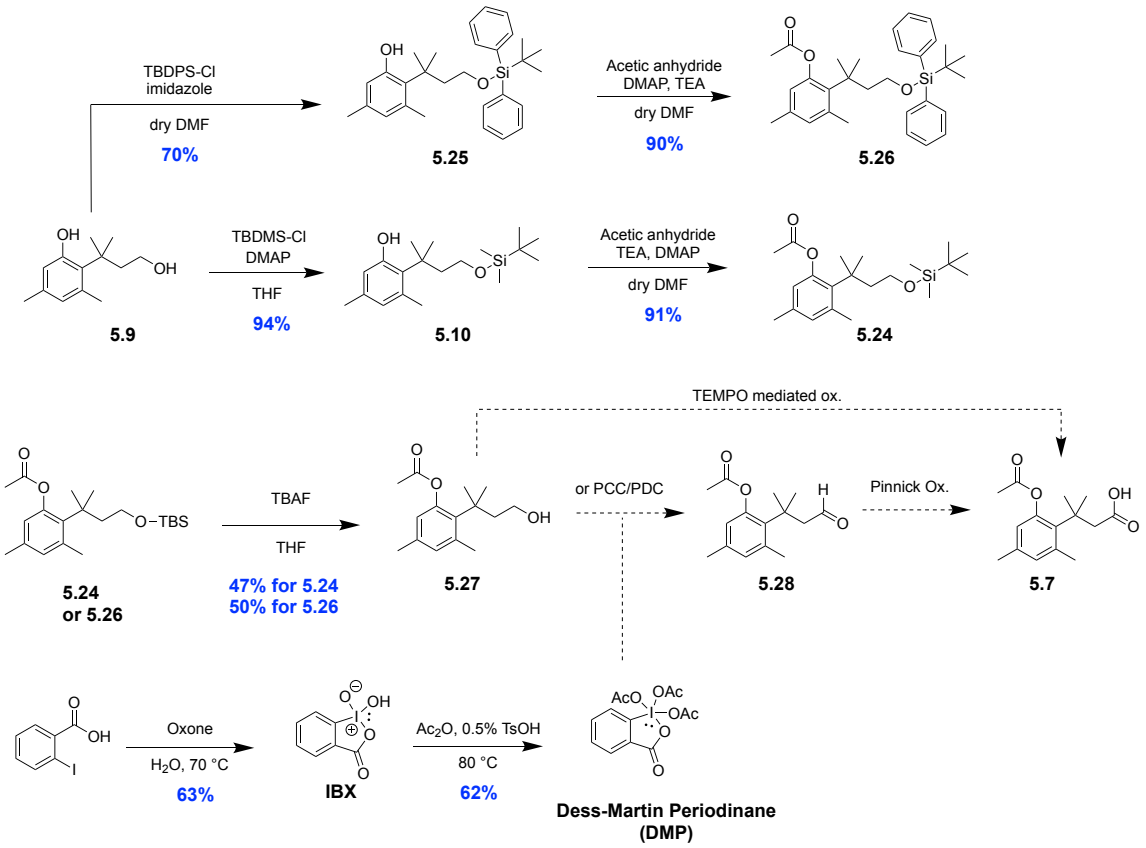
At the early stage of this project, synthetic attempts were made prior to purchasing the commercially available **5.7**. The route is illustrated in Scheme 5.3. Esterification of the phenol group on **5.10** followed by TBDMS deprotection resulted in the primary alcohol **5.27**, which was ready for the subsequent oxidation reactions to afford **5.7**. TBDPS protected versions of **5.25** and **5.26** were also made. Various oxidative conditions were next explored, including PCC/PDC oxidation, TEMPO-mediated oxidation, and Dess-Martin oxidation using periodinane. However, none of them led to the desired product **5.7**.

5.5.1.2. Initial ERL lipid 5.29 based on POPE lipid backbone

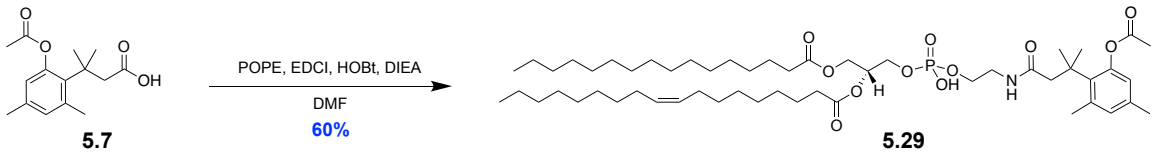
For our initial design, we began by using POPE-based enzyme-responsive lipids. Synthesis of the POPE version esterase-responsive lipid **5.29** is shown in Scheme 5.4, which involves one-step amide coupling reaction from commercially available **5.7**.

Preliminary release studied were primarily conducted by previous group member Sara Barker. After serval months of exploration, we determined that modifications were required for this system to work. The first possible reason for those failures might be that POPE, although belongs to the PE family, does not provide enough membrane destabilization once it is released within bilayer compared to DOPE. As is pointed out by Boyd et al (Figure 5.13),[26] the packing parameter for POPE is around 1, indicating POPE favors bilayer assemblies instead of hexagonal assemblies at physiological conditions.

The most stable conformational configurations of POPE and DOPE were predicted with ChemBioDraw 3D using MM2 energy minimization method. As is shown in Figure 5.14, one extra double bond in the tail provides DOPE a much greater area in its tail region compared to



Scheme 5.3. Synthetic route and attempts to make commercially available intermediate 5.7.



Scheme 5.4. Synthesis of POPE version esterase-responsive lipid 5.29.

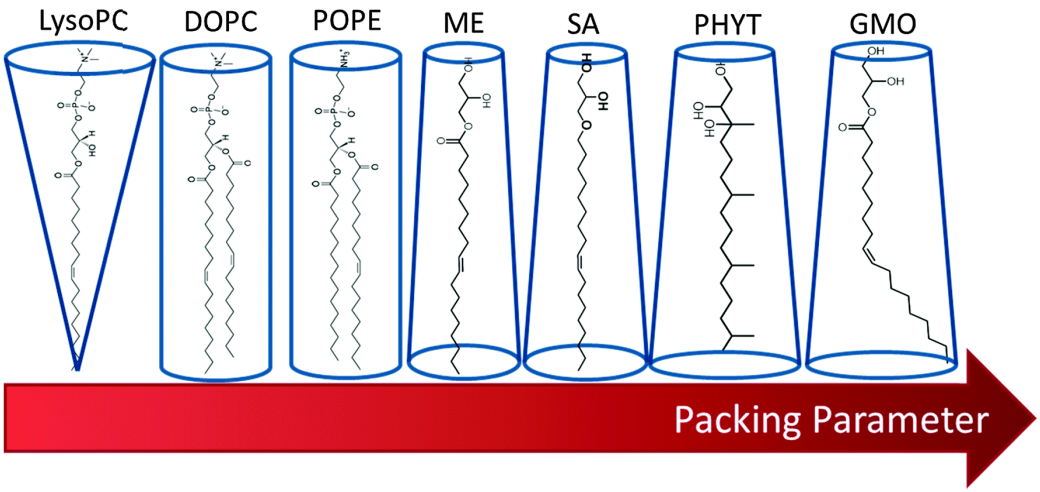


Figure 5.13. Packing parameters of certain membrane lipids. POPE, unlike DOPE, is actually a cylindric lipid similar to DOPC. Figure adapted with permission from ref [26], Copyright 2014, Royal Society of Chemistry.

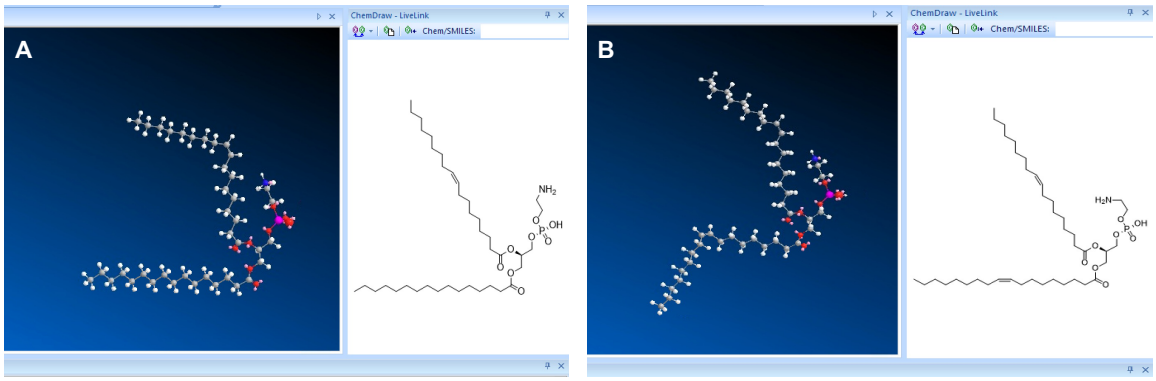


Figure 5.14. ChemBioDraw 3D prediction of POPE (A) and DOPE (B) conformation. One extra double bond in the tail region makes DOPE a more cone-shaped lipid compared to POPE.

its headgroup, leading to a cone-shaped non-bilayer lipid. Such difference in packing parameter can result in more significant membrane disruption once the lipid scaffold is released within the bilayer.

5.5.1.3. STEM and Cryo-EM attempts

Attempts to obtain STEM images of esterase-responsive liposomes using **ERL** were made, which might give us a better understanding of the morphology changes during the release processes. Images were taken for liposomes before and after esterase addition. For the samples post enzyme treatment, the prepared liposomes were incubated with esterase for 17 hours before taking STEM images. Different negative staining techniques were explored. Initial attempts were made with uranyl acetate stain, which has a pH of 3. As shown in Figure 5.15A-B, although liposomes were not stained well pre-enzyme treatment, significant changes were observed after enzyme treatment. Small particles with diameters smaller than 20 nm could be seen under the microscope, which is too small for STEM to visualize their detailed structural features. Since uranyl acetate stain has a pH around 3 and our liposomes were prepared with pH 8 buffer, liposomes might be destroyed during the sample preparation process. To obtain better images for the initial liposomes, we switched to neutral phosphotungstic acid staining with pH adjusted to 7. As shown in Figure 5.15C-D, liposomes were stained much better. After adding enzyme, similar changes were observed. Only particles less than 20 nm could be seen under the microscope.

Since we need to carefully tune the stability of our initial liposome formulations to the right threshold so that slight disruption could drive significant cargo release, we ended up with ~60% non-bilayer forming lipids in our initial formulation. This could cause problems for the negative staining technique, which was necessary for the (S)TEM imaging. To avoid potential interactions between the staining reagents and our liposomes, extra efforts were made to obtain cryo-TEM images, which not only do not require staining but can also provide better

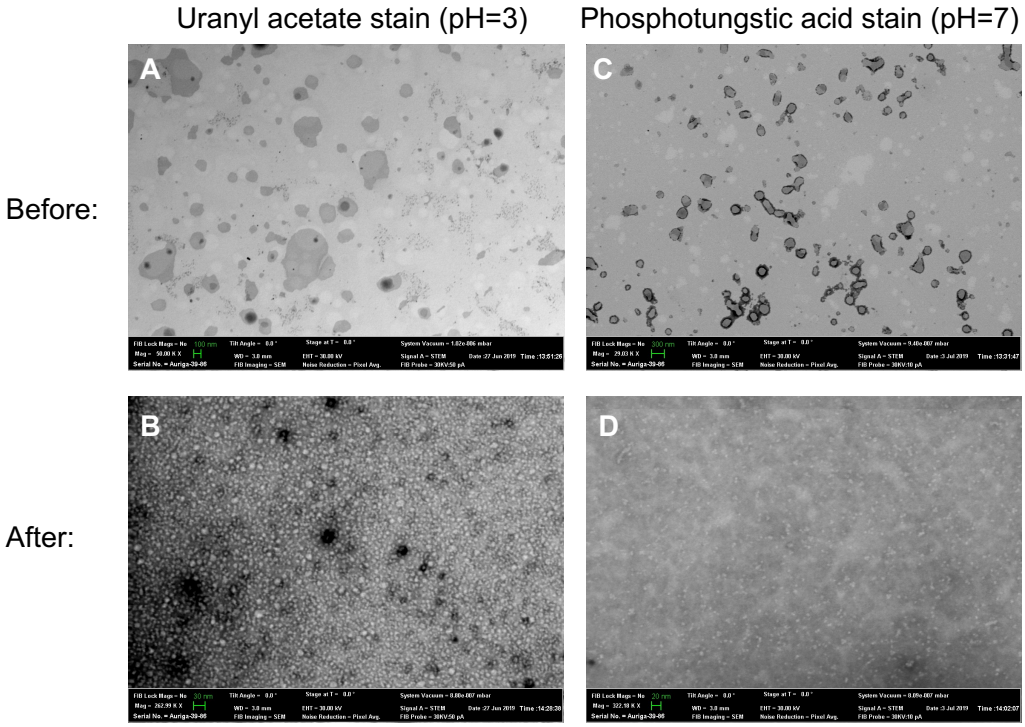


Figure 5.15. Attempts to acquire STEM images of esterase-responsive lipid ERL. Liposomes containing 30% **ERL**, 50% DOPE, 10% PA and 10% PC were used. Different negative staining reagents were used, including acidic uranyl acetate stain (**A** and **B**) and neutral phosphotungstic acid (**C** and **D**). Scale bars denote 100 nm, 30 nm, 300 nm and 20 nm in the images.

resolution compared to STEM. Liposomes prior to enzyme treatment were loaded onto the grid, frozen by liquid ethane and subjected to electron microscopy. We tried more than four times but only ended up with one image, as is shown in Figure 5.16. Although bilayer structures could be observed, the grid was covered by ice, which was formed when the samples were injected into the instrument. Another major issue we encountered was that the vesicles disappeared after being exposed to the electron beam, which might still be due to the instability of the initial liposomes.

5.5.1.4. Cell studies attempts with ERL lipid

After we obtained promising release study results for **ERL**, we collaborated with Dr. Barrera in UTK BCMB department for cellular delivery studies. Treatment conditions with varying liposome concentrations and incubation times were screened with representative data shown in Figure 5.17. The results were discouraging, possibly since the formulations we used were at the threshold and were not very stable. We observed significant levels of liposome uptake in the control conditions. In addition, the liposomes seem to stick to the plastic plate, since deposition as “spots” in the areas without cells could be seen. Most importantly, we did not clearly see better accumulation in the two conditions (with **ERL**, without or with enzyme treatment).

5.5.2. PRL related attempts

5.5.2.1. Synthesis of initial PRL lipid 5.33 based on POPE scaffold

Similar to compound **5.29** described above, the initial version of phosphatase-responsive lipid was also based on POPE scaffold. The synthetic route is shown in Scheme 5.5A. **5.12** was coupled with POPE via a one-step amide coupling reaction to **5.30**. Subsequent deprotection of the phosphotriester benzyl ester groups afforded the POPE version of phosphatase-responsive lipid **5.33**. Multiple synthetic attempts were made for this final deprotection reaction, as is outlined in Scheme 5.5B. Commonly used reductive debenzylation condition with

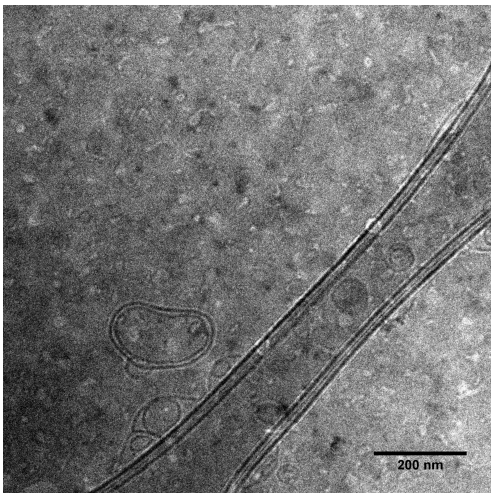


Figure 5.16. Cryo-EM image of liposomes containing 30% ERL, 50% DOPE, 10% PA and 10% PC. Scale bar denotes 200 nm.

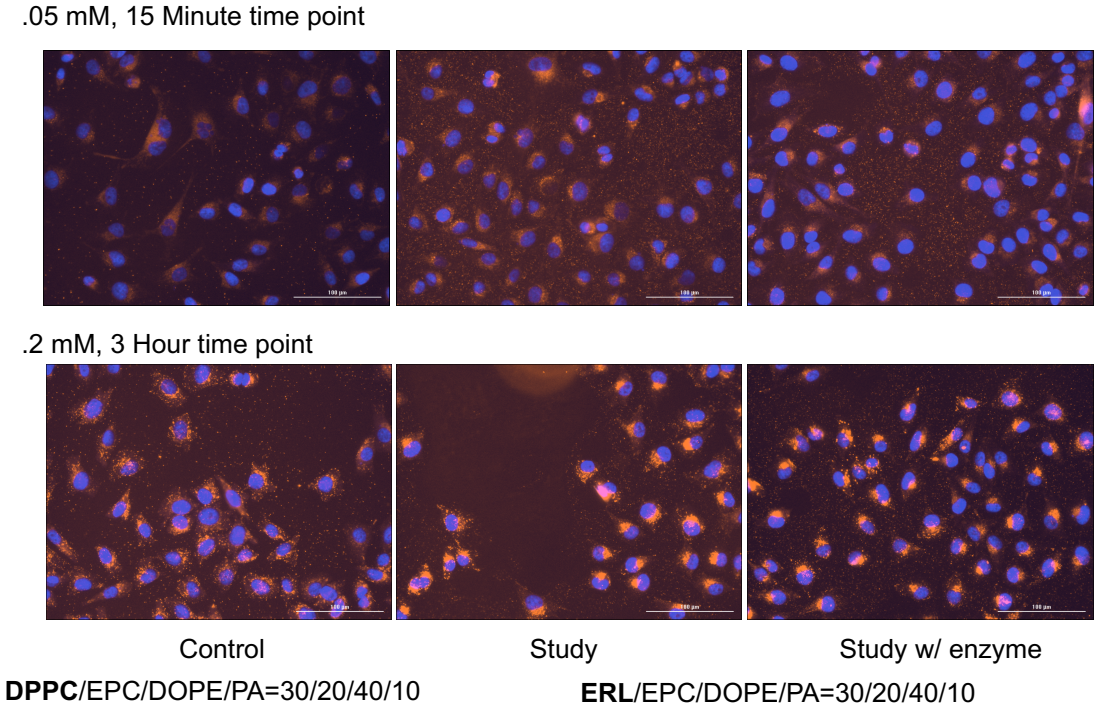
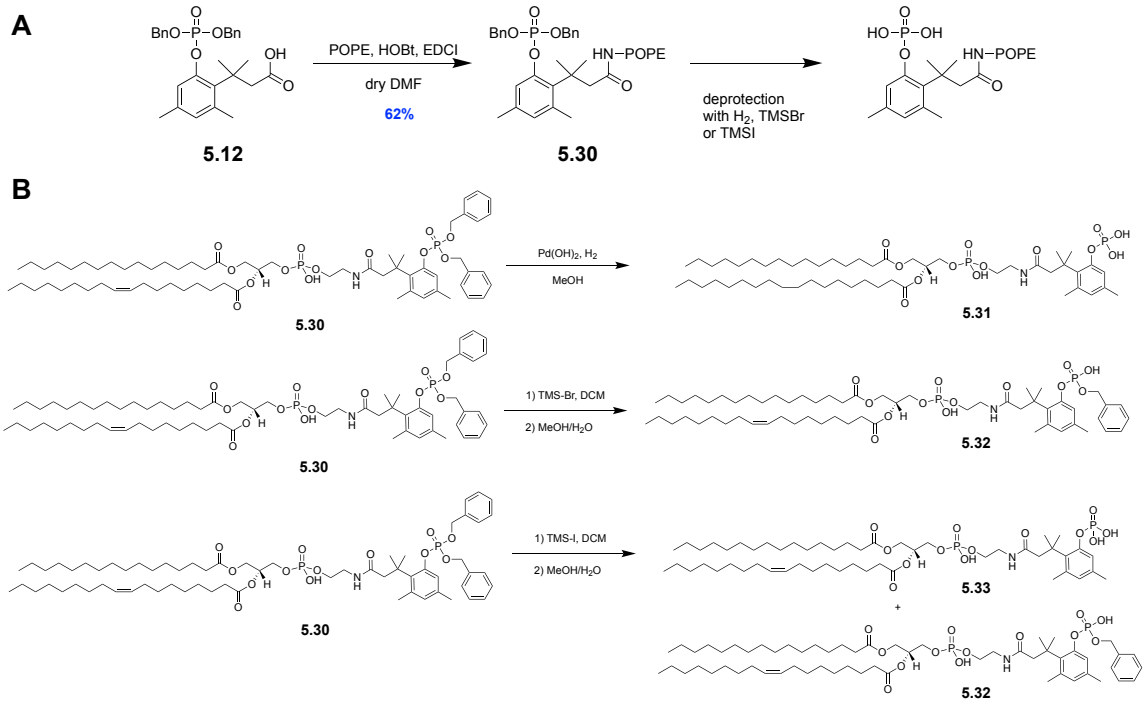


Figure 5.17. Cellular delivery studies using liposomes containing ERL. Significant background delivery was observed, and there was no obvious difference between study and control conditions.



Scheme 5.5. Synthetic route and attempts to make the POPE version of phosphatase-responsive lipid 5.33. A. Route overview. **B.** Debenzylation attempts to make the final lipid.

hydrogen gas reduced the double bond in the tail at the same time, leading to product **5.31**. An alternative method employed cleavage with bromotrimethylsilane, followed by hydrolysis with methanol/water. However, this only gave mono-debenzylated product **5.32**. Further modification using iodotrimethylsilane ultimately resulted in the desired product **5.33** as well as the mono-debenzylated by product **5.32**, which could be easily separated via flash column chromograph.

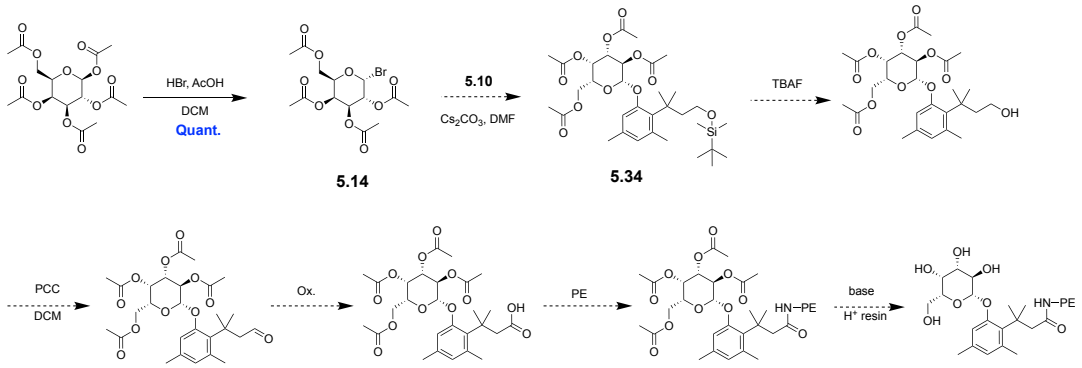
5.5.3. GRL related attempts

5.5.3.1. Initial GRL design and synthetic attempts

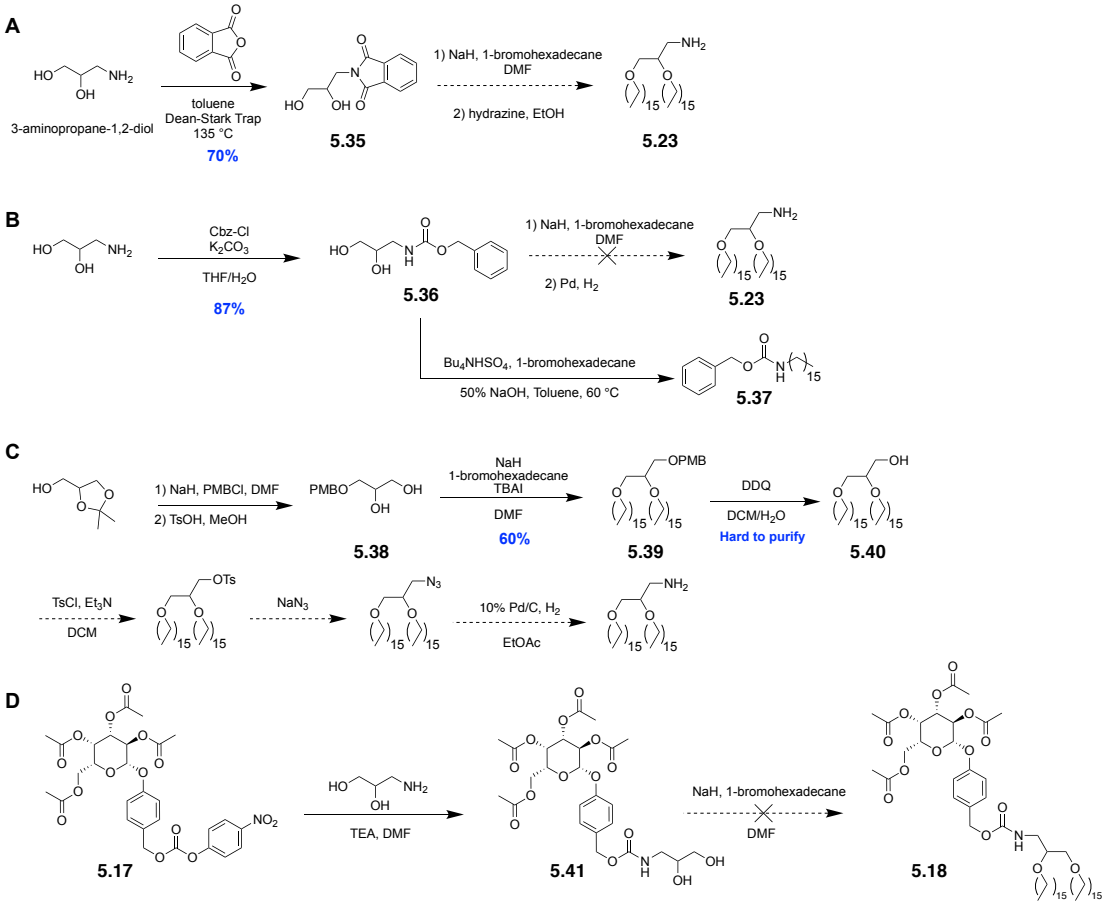
Our initial design for galactosidase-responsive lipids was based on the TML SIL, similar to **PRL** and **ERL**. The proposed synthetic route is shown in Scheme 5.6. However, we became stuck on the glycosylation reaction between **5.14** and **5.10**. Reaction did not proceed in DMF using cesium carbonate as the base at room temperature. When increasing the reaction temperature to 80 °C, the silyl protecting group fell off; all we recycled from this reaction was **5.9**. Further evaluations of this proposed route arose other concerns. For example, we wondered whether the galactose sugar headgroup could survive the subsequent oxidation reaction. In addition, the ester groups presented on the PE tail region might be cleaved as well in the final acetyl deprotection step in the presence of the strong base (i.e., sodium ethoxide). Taking all these potential pitfalls into consideration, we came up with the alternative version of **GRL** described earlier in this Chapter, including a QM SIL and an amino dietherglycerol lipid scaffold.

5.5.3.2. Synthetic attempts for amino dietherglycerol lipid backbone 5.23

We encountered several synthetic issues when trying to synthesize the amino dietherglycerol lipid backbone **5.23** for the final **GRL** lipid. Initial attempts involved a three-step route described by Zhang et al from 3-aminopropane-1,2-diol, as is shown in Scheme 5.7A,[89] including phthalic anhydride protection of the free amine group to **5.35**, ether coupling to install the alkyl tails,



Scheme 5.6. Initial design and proposed synthetic route for trimethyl lock-based galactosidase-responsive lipid.



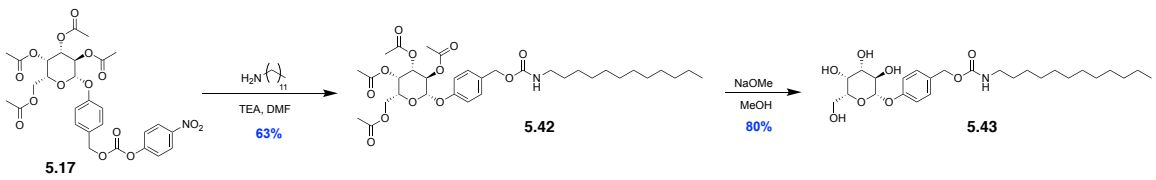
Scheme 5.7. Synthetic attempts to the make the lipid scaffold of GRL lipid (A-C) and alternative route for direct coupling to make GRL (D).

and the deprotection of the phthalic anhydride group. Multiple attempts were made for the final deprotection step, all of which resulted in purification problems. An alternative route using CBz as the protecting group was explored, as shown in Scheme 5.7B. However, alkylation of **5.36** using sodium hydride resulted in a very messy reaction mixture, which might be due to the presence of the carbamate proton that could be potentially removed by hydride treatment. Another ether coupling protocol with milder conditions was followed; however, it only resulted in undesired rearranged by product **5.37** through unknown mechanisms. Scheme 5.7C presents the third route we attempted. PMB protection followed by acetal deprotection afforded **5.38**. When we were trying to deprotect the alkylated **5.39**, we figured that deprotected PMB byproduct co-eluted with desired product **5.40**, causing purification issues. Although the final synthetic route presented earlier in this Chapter (Scheme 5.2C) contains more synthetic steps, all the reactions proceeded successfully even at large scales (the largest scale we ran resulted in 0.5 gram final lipid). It is worth noting that the primary amine was produced by an efficient azide reduction reaction in the final route, in which we could obtain the pure product simply after the Pd catalyst removal. During the process of working out the aminodietherglycerol lipid synthesis, we attempted a separate alternative route (Scheme 5.7D), where we directly coupled 3-aminopropane-1,2-diol with **5.17**. However, the intermediate **5.41** has the same carbamate proton as **5.36**, and we were not able to install the ether tails of **5.18** in the presence of strong base.

5.5.3.3. Synthesis and studies for alternative GRL 5.43 with dodecyl tail

To figure out the carbamate coupling conditions and explore the possibilities to obtain more alternative responsive targets, we synthesized lipid **5.43** by reacting **5.17** with dodecylamine, followed by acetyl deprotection, as is shown in Scheme 5.8.

Preliminary NR release assays were conducted with lipid **5.43**. As is shown in Figure 5.18, when we diluted the initial 2 mM liposomes into 40 μL, we observed significant and random



Scheme 5.8. Synthesis of an alternative galactosidase-responsive lipid 5.43, bearing a dodecylamine lipid chain as the scaffold.

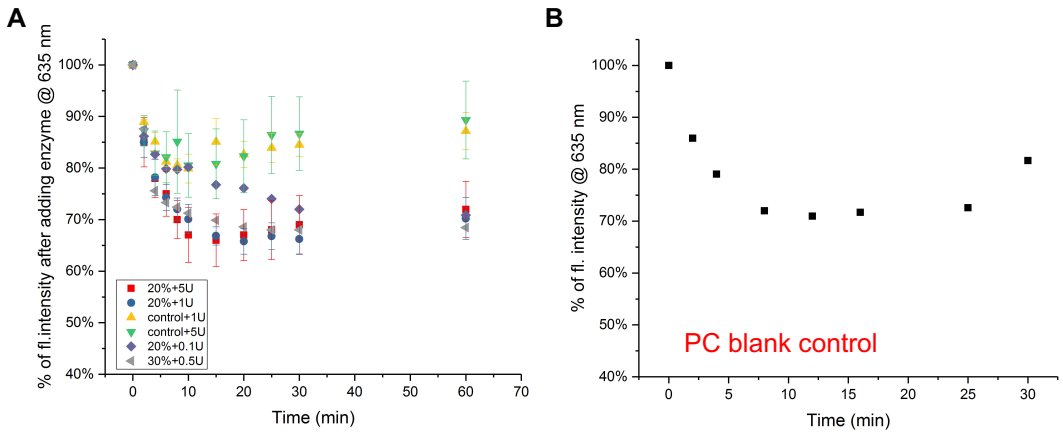


Figure 5.18. Preliminary NR release assays with lipid 5.43 at 40 μM liposome concentrations. Random background release was observed overtime after diluting 2 mM liposomes into 40 μM.

background leakage. This was the first time we realized that liposomes encapsulated with NR could not undergo significant dilution, which most likely due to the fact that hydrophobic dyes are encapsulated within the bilayer, and it is easier for them to leak out. From our previous experimental attempts, we observed that NR-encapsulated liposomes could only undergo mild dilution (i.e., 2X), but that greater dilution (i.e., 10X) resulted in significant background release. However, we did not observe the same phenomenon for liposomes encapsulating hydrophilic cargo. Even though SEC was included during preparation, which may result in significant liposome dilution, the cargo could still be effectively retained. In later studies, if we needed to conduct NR release assays at lower liposome concentrations, we had to cut down the concentrations from film preparation instead of diluting the concentrated liposomes.

5.5.3.4. Lectin binding experiments with GRL lipid

GRL lipid is a slightly more exciting target compared to other enzyme-responsive lipids, since its galactose headgroup can effectively bind to cell surface carbohydrate receptors, providing this lipid with the potential for active targeting functions.[260] Unconjugated *Erythrina Cristagalli* lectins, which are highly specific carbohydrate-binding proteins for galactoses, were explored for such purpose. We again employed the NR release assay and representative raw data are presented in Figure 5.19 with Figure 5.19A showing titration, and Figure 5.19B for time-dependent release. However, none of these showed release/decreases in fluorescence intensities. This is not too surprising, considering the fact that lectins may not be a great candidate for multivalent binding and triggering release due to the presence and presentation of their binding sites. More conditions with varying liposome formulations or lectin concentrations could be explored if we want to further study this direction.

5.5.4. Chain extension attempts

5.5.4.1. Overview

Once we obtained **ERL** and screened preliminary release conditions, we did not observe any

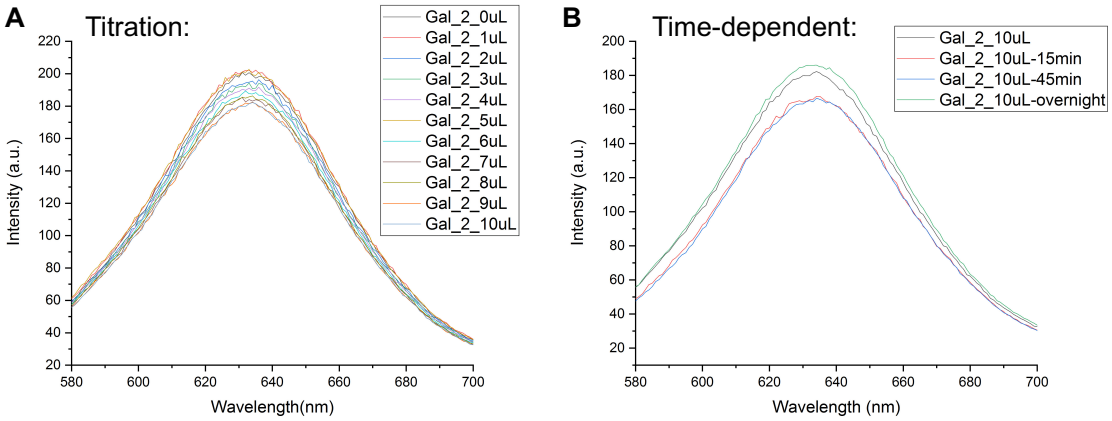


Figure 5.19. Raw data for GRL lectin binding and release experiments. A. Dose-dependent titration curves. **B.** Time-dependent release curves. None of these show changes upon lectin treatment.

promising results in numerous initial studies. Other than continuing to explore different formulations, another possible reason we came up with was the steric hindrance between the enzyme and liposomes. For enzymatic reactions to work, the substrate must bind with enzyme's active site, which may be deeply buried inside the enzyme, causing accessibility issues, especially for giant substrates such as liposomes. As is illustrated in Figure 5.20, this is a well-known issue in the drug delivery field.[261] This could explain why enzyme-responsive liposome release proceeded very slowly and required heating. To make the substrates more accessible to the enzyme, a common resolution was to put a self-immolative polymer (SIP) between the substrate and drug. After the headgroup is removed by a trigger, the linker will automatically fall apart through electronic cascade reactions. In addition, the SIP is also hypothesized to provide the benefit of replacing polymers (i.e., PEG) that are typically grafted onto liposomes to shield their surfaces and thereby enhance circulation time and avoid clearance by the reticuloendothelial system (RES).[63,262-264]

As an initial step in extending the spacer in our system, we propose to add an extra QM SIL in between the TML ester headgroup and the non-bilayer forming DOPE scaffold, as shown in Scheme 5.9A-B. When these polymer lipids will be incorporated into membrane bilayers, the ester trigger headgroup is expected to be far from the liposome surface while still capable of inducing membrane destabilization through cascading depolymerization reactions upon removal.

The polymer synthesis will be discussed in the next section. However, when there is only one repeating unit (n = 1, Scheme 5.9C), the resulting lipid **5.46** can be potentially obtained via stepwise synthesis, as is indicated in Scheme 5.10. The QM immolative unit was installed through an amide coupling reaction between TML acid **5.7** and 4-aminobenzyl alcohol to **5.44**. To conjugate the POPE lipid scaffold, **5.44** was treated with 4-nitrophenol chloroformate first to afford **5.45** before reacting with POPE.

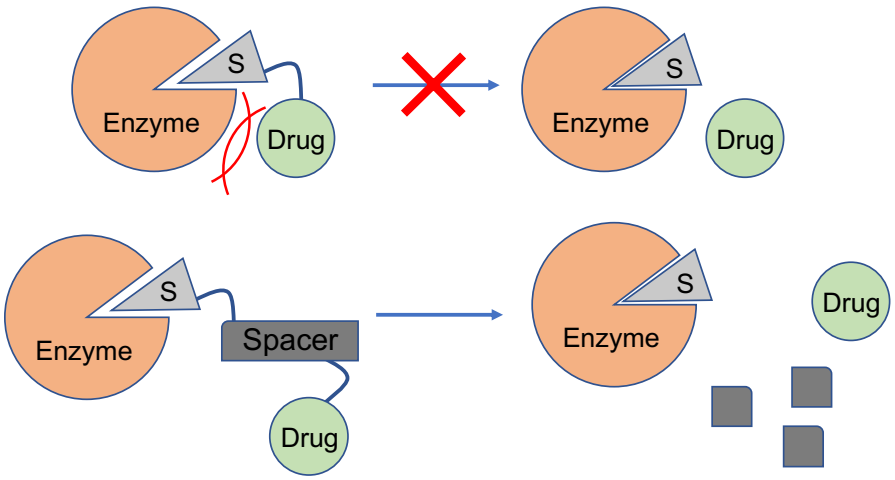
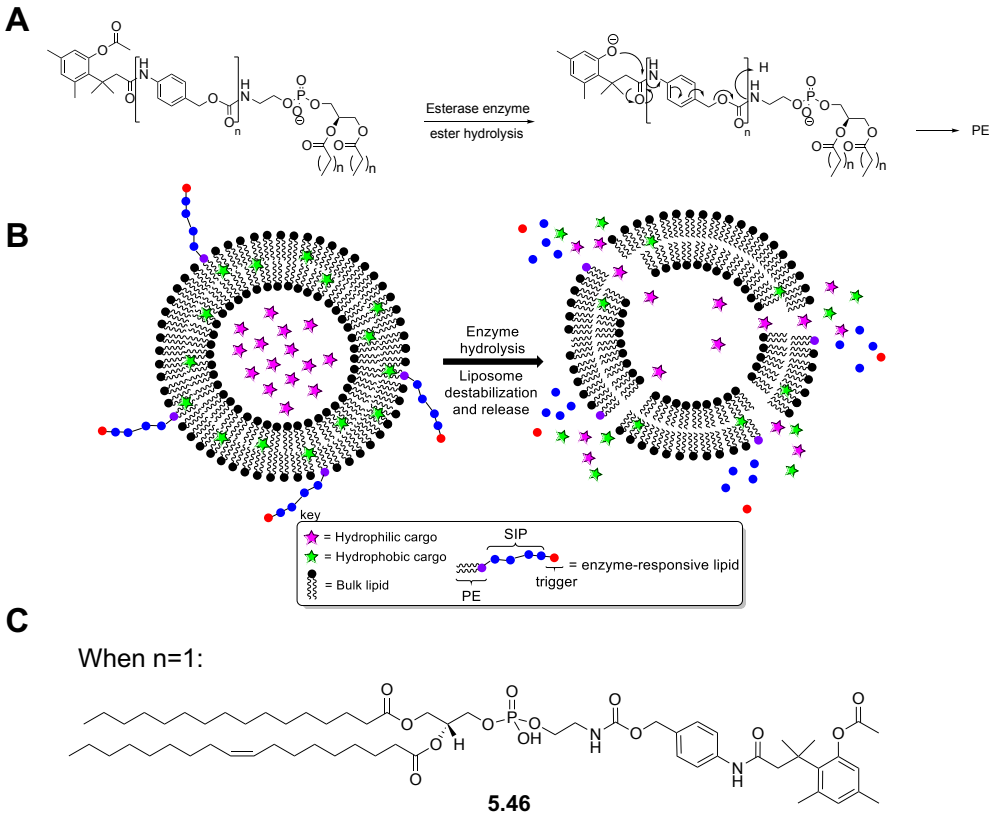
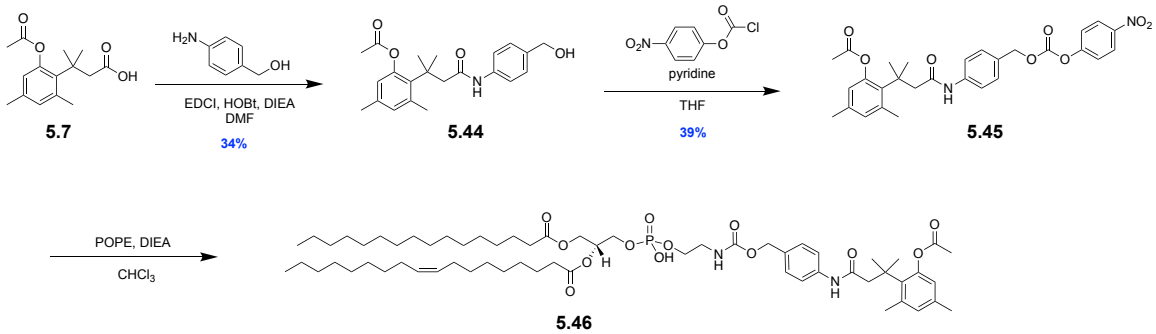


Figure 5.20. Substrate accessibility is a common problem in drug delivery research area.



Scheme 5.9. Self-immolative polymer (SIP) lipid design. A. Structure for esterase-responsive SIP lipid and its depolymerization mechanism upon trigger headgroup removal. **B.** Cartoon illustration for liposomes containing SIP lipid. The trigger headgroups are expected to be far away from the liposome surface, providing enough accessibility for enzymatic reactions. **C.** Structure for SIP lipid **5.46** containing only one QM repeating self-immolative unit.

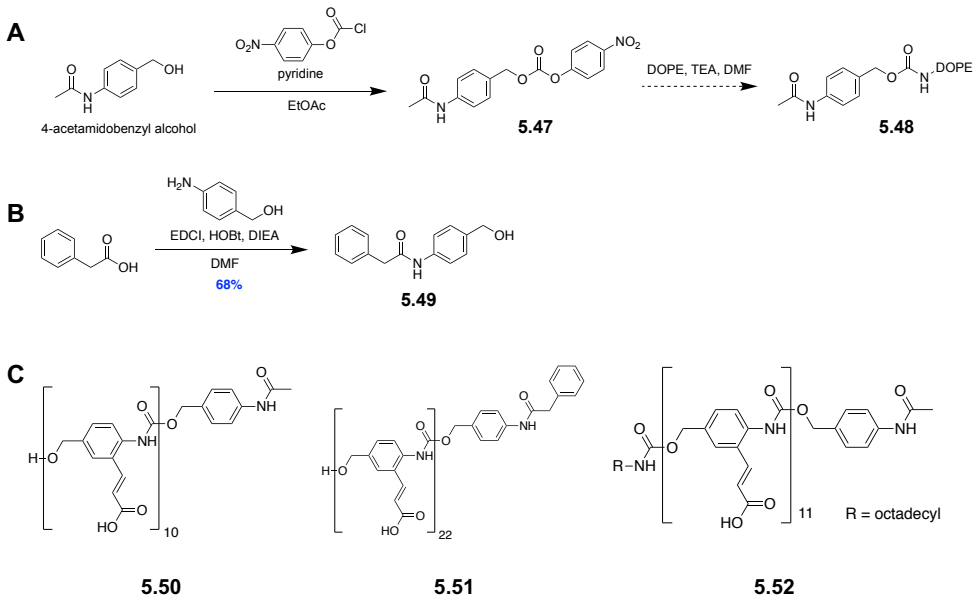


Scheme 5.10. Synthetic route for SIP lipid 5.46 with one QM immolating unit.

5.5.4.2. Synthesis and studies for self-immolative polymer (SIP)

The SIP lipid synthesis involving polymerization was carried out by Cameron Workman in Dr. Brain Long's lab in UTK Chemistry department. Due to the synthetic concerns involving the potential interactions between metal catalyst DBTL used in the polymerization and ester/carbohydrate headgroups, we avoided using substrates containing these functional groups. Instead, we explored two new trigger headgroup containing amide bond, methyl acetamide-based version for AADAC enzymes and phenylacetamide version for penicillin G amidase (PGA) enzymes. The key headgroup intermediate synthesis is shown in Schemes 5.11A-B. Compound **5.49** that we synthesized and commercially available 4-acetamidobenzyl alcohol were passed along to the Long lab for polymerization reactions. Attempts to synthesize DOPE version of acetamide lipid **5.48** were also made, including a carbonate formation reaction to **5.47**, followed by treatment of DOPE scaffold.

Two polymer intermediates **5.50** and **5.51** without the tail addition were received from the Long lab, as shown in Scheme 5.11C and Figure 5.21. Initial enzyme mediated depolymerization studies were conducted, with representative results shown in Figure 5.21A-D. The results were overall disappointing. For both of the polymers, they exhibited stronger fluorescence intensities at lower polymer concentrations (Figure 5.21A and C). It is worth noting that, the peaks ~550 nm belong to the depolymerized SI units, which was obvious for both of the polymers. For polymer **5.50**, addition of AADAC enzymes seemed to induce depolymerization, as judged by the increases in intensities at 550 nm. However, such increases happened immediately after enzyme treatment without showing any further change overtime, which was concerning. For polymer **5.51** intended for PGA enzyme, the enzyme itself has fluorescence emission at 550 nm that can interfere with the detection of depolymerization process. Polymer **5.52** containing an octadecyl tail and a methyl acetamide headgroup was also synthesized by Cameron. However, this polymer could not be incorporated within the PC membrane at various percentages (10%-50%) using traditional thin-film hydration techniques. Other liposome



Scheme 5.11. Polymer SIP lipid related synthesis. A. Methyl acetamide-based DOPE version responsive lipid for AADAC enzymes. **B.** Phenylacetamide headgroup synthesis for PGA enzymes. **C.** Polymers received from the Long lab.

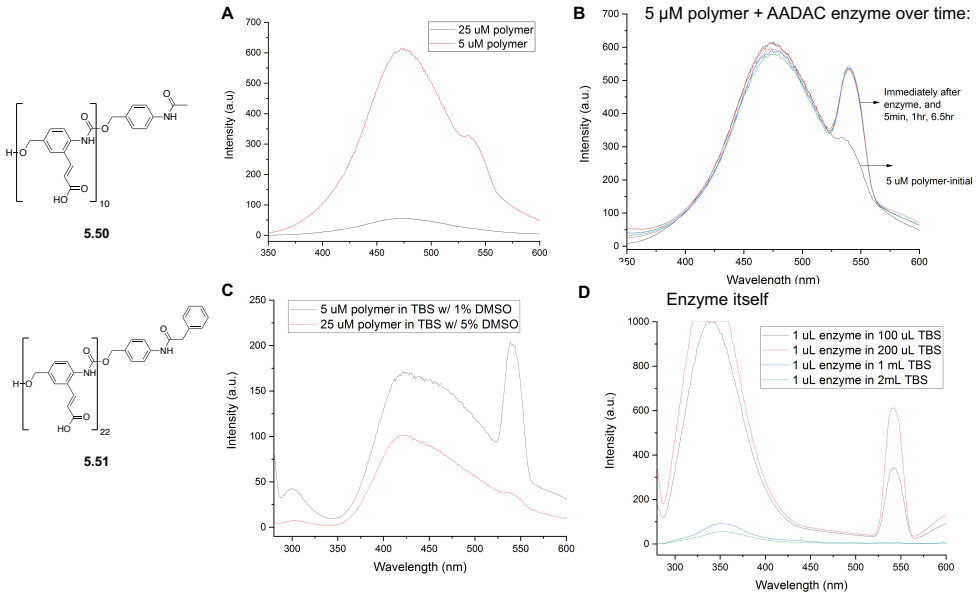


Figure 5.21. Initial enzyme mediated depolymerization studies with two polymer intermediates 5.50 and 5.51.

preparation techniques could be explored in the future, such as ethanol ejection or post insertion method. In addition, structural modifications of the polymer design would be beneficial. For example, dual tail lipid scaffolds (i.e., **5.23**) could be considered.

5.6. Conclusions

In conclusion, we have designed and synthesized three enzyme-responsive lipids targeting unique enzyme families that are commonly aberrant in disease, including esterase, phosphatase and β-galactosidase. These lipids shared similar design strategies including an enzyme substrate/trigger at the headgroup, a self-immolating linker, and a non-bilayer forming lipid scaffold. These novel lipids were incorporated into liposomes, and after careful fine-tuning of membrane stability based on composition, each compound was found to be successful for achieving triggered release of the hydrophobic dye NR upon treatment with the appropriate enzyme. These results showcase that this approach provides a general strategy for enzyme-responsive liposomes in which different enzymes can be targeted by modifying the substrate trigger displayed at the lipid headgroup. However, despite the generality of this approach, there were differences observed in release properties based on structural nuances. In particular, **PRL** was found to exhibit NR release curves (less release and induction period) and DLS results (no observed change) that were different from **ERL** and **GRL**, despite the fact that the structures of **ERL** and **PRL** only differ by one functional group, and indeed they are expected to produce the same lipid product upon release. This exception indicates that response properties can vary based on changes to the structures, in this case most likely due to the charge of the resulting enzyme-responsive liposomes. Finally, **ERL**-containing liposomes also showed the ability to release hydrophilic cargo. Enzymes provide exciting targets for controlling release of encapsulated drugs from nanocarriers using stimuli-responsive materials since these are commonly overexpressed in many diseases. However, the existence of numerous families of enzymes that catalyze wide-ranging reactions by which varying substrates are modified provides a grand challenge for exploring different potential therapeutic targets. The

modular strategy reported herein provides an efficient approach to overcoming this barrier as an initial step for advancing enzyme-responsive liposomal therapeutics.

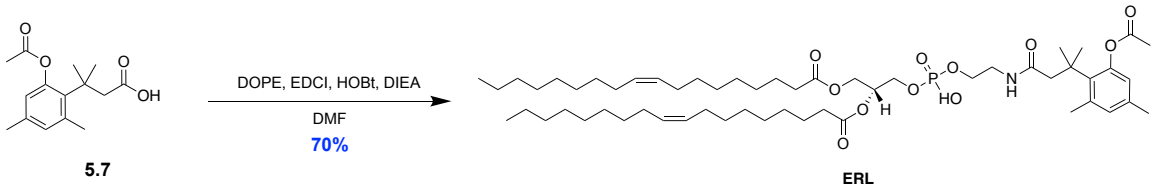
5.7. Synthesis and experimental procedure

General experimental

Reagents and solvents were generally purchased from Acros, Sigma-Aldrich, or Fisher Scientific and used without further purification. PC (L-α-Phosphatidylcholine, mixed isomers from chicken eggs), PA (L-α-phosphatidic acid sodium salt from chicken eggs), DOPE (1,2-dioleoyl-*sn*-glycero-3-phosphoethanolamine), DPPC (1,2-dipalmitoyl-*sn*-glycero-3-phosphocholine) and DOTAP (1,2-dioleoyl-3-trimethylammonium-propane, chloride salt) were purchased from Avanti Polar Lipids, Inc (Alabaster, AL). Esterase from porcine liver was purchased from Sigma-Aldrich (lyophilized powder, ≥15 units/mg solid, SKU: E3019). β-Galactosidase from *Escherichia coli* was purchased from Abnova (in 1.6 M ammonium sulfate, Catalog #: P5270). Alkaline phosphatase from *Escherichia coli* was purchased from Sigma-Aldrich (in 2.5 M ammonium sulfate, SKU: P4252). β-Galactosidase substrate, 4-nitrophenyl β-D-galactopyranoside was purchased from Carbosynth. Phosphatase substrate, 4-nitrophenyl phosphate disodium salt hexahydrate (pNPP) was purchased from Sigma-Aldrich (5 mg tablet, SKU S0942). Compounds **5.10**,[252,253] and **5.16**[254] were synthesized as previously reported with matching characterization data. Dry solvents were obtained from a Pure Solv MD-7 solvent purification system purchased from Innovative Technology, Inc (Newburyport, MA). Column chromatography was performed using 230-400 mesh silica gel purchased from Sorbent Technologies. NMR spectra were obtained using Varian 300 MHz, 500 MHz or 600 MHz spectrometers. Mass spectra were obtained with JEOL DART-AccuTOF and Waters Synapt G2-Si mass spectrometers (Milford, MA). Liposome extruder and polycarbonate membranes were obtained from Avestin (Ottawa, Canada). Ultrapure water was purified via a Millipore water system (≥ 18 MW·cm triple water purification system). Small quantities (< 5 mg) were weighed on an OHRUS analytical-grade mass balance. Fluorescence studies were

performed using a Cary Eclipse Fluorescence Spectrophotometer from Agilent Technologies. Plots were generated using Origin Pro 2018. All error bars in plots show the standard errors of at least three experimental replicates.

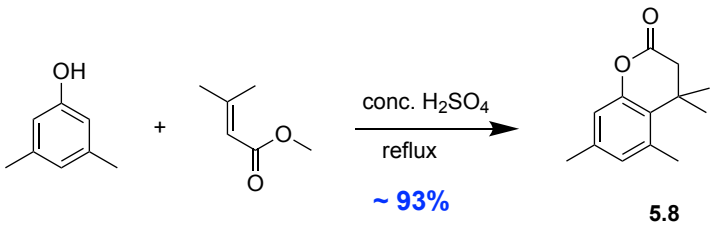
Synthesis



ERL

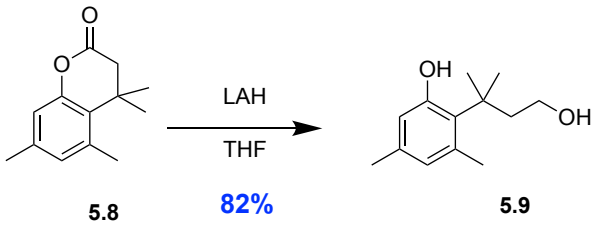
DOPE (100 mg, 0.1344 mmol), compound **5.7** (42.63 mg, 0.1613 mmol) and hydroxybenzotriazole (HOBt, 24.7 mg, 0.1613 mmol) were added into a small vial under N_2. Then, 1 mL dry DMF was added into the vial and the reaction mixture was cooled to 0 °C. After being stirred for 5 min, 1-Ethyl-3-(3-dimethylaminopropyl)carbodiimide (EDCI, 30.92 mg, 0.1613 mmol) and *N*,*N*-Diisopropylethylamine (DIEA, 55 µL, 0.336 mmol) were added. The reaction was then stirred at rt for 5 h before being quenched by pouring into 100 mL 1 M HCl. The aqueous layer was extracted three times with 25 mL chloroform. The combined organic layer was washed with 20 mL water five times and once with 20 mL brine. After being dried over Na_2SO_4, filtered, and concentrated, the crude was subjected to column chromatography using gradient elution from 100% chloroform to 20% methanol-chloroform, which yielded **ERL** as a colorless oil (123 mg, 0.124 mmol, 92 % yield). R_f = 0.48 (10% methanol-chloroform). ^{1}H NMR (300 MHz, Chloroform-*d*) δ 6.80 (s, 1H), 6.55 (d, *J* = 2.0 Hz, 1H), 5.37 – 5.29 (m, 4H), 5.20 (s, 1H), 4.36 (d, *J* = 11.8 Hz, 1H), 4.11 (dd, *J* = 12.2, 7.2 Hz, 1H), 3.89 (s, 2H), 3.68 (s, 2H), 3.33 (d, *J* = 10.6 Hz, 2H), 2.52 (d, *J* = 25.0 Hz, 5H), 2.33 – 2.23 (m, 8H), 2.21 (s, 3H), 2.00 (q, *J* = 6.6 Hz, 8H), 1.56 (s, 10H), 1.37 – 1.20 (m, 46H), 0.91 – 0.84 (m, 6H). ^{13}C NMR (75 MHz, $CDCl_3$) δ 173.70, 173.32, 171.29, 149.50, 138.23, 136.49, 133.45, 132.50, 129.89, 129.51, 129.49, 123.11, 70.24, 63.62, 62.48, 39.69, 39.39, 34.06, 33.91, 31.76, 31.28, 29.60, 29.37, 29.17, 29.01, 27.06, 27.03, 24.75, 22.52, 13.84. ^{31}P NMR (121 MHz, $CDCl_3$) δ 1.46.

ESI-MS: $[M-H]^-$ calcd for $C_{56}H_{95}NO_{11}P$, 988.6643, found 988.6609.



4,4,5,7-Tetramethylchroman-2-one (5.8)

3,5-Dimethylphenol (0.5 g, 4.09 mmol) and methyl 3-methylbut-2-enoate (0.83 g, 5.73 mmol) were dissolved with 20 mL benzene in a 100 mL RBF. Concentrated H_2SO_4 (0.5 mL) was then added. The reaction mixture was heated under reflux for two hours to afford a dark yellow solution. After completion, solvent was removed under reduced pressure. The residual was redissolved with 50 mL EtOAc and washed with 50 mL H_2O, 50 mL saturated $NaHCO_3$, and 50 mL brine, respectively. The organic layer was collected, dried with Na_2SO_4, filtered, and concentrated under vacuum. A yellow oil was obtained, which crystalized later at room temperature. Compound **5.8** was used without further purification.

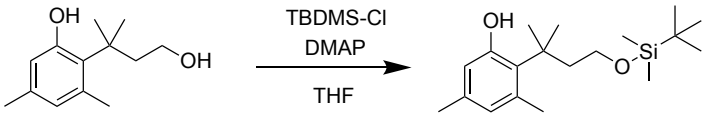


2-(4-Hydroxy-2-methylbutan-2-yl)-3,5-dimethylphenol (5.9)

Compound **5.8** (0.509 g, 2.5 mmol) was weighed into a 100 mL RBF under nitrogen. 20 mL dry THF was used to dissolve **5.8** and the reaction mixture was cooled down to 0 °C with an ice bath. $LiAlH_4$ (0.759 g, 20 mmol) was then carefully added into the reaction flask portion wise. The reaction was allowed to warm up to room temperature and further stirred for 2 hours before being carefully quenched by adding 1 M HCl. The insoluble solid was removed via vacuum filtration through a celite pad and the filtrate was concentrated under reduced pressure.

The residue was redissolved with 50 mL EtOAc and the organic layer was washed with 50 mL water and 50 mL brine before being dried over Na_2SO_4. After removal of the solvent, the crude was subjected to silica gel column chromatography. Gradient elution from 5% EtOAc-hexanes to 40% EtOAc-hexanes was used to obtain **5.9** as a white solid (0.43 g, 2.06 mmol, 82% yield). R_f = 0.17 (25% EtOAc-hexanes)

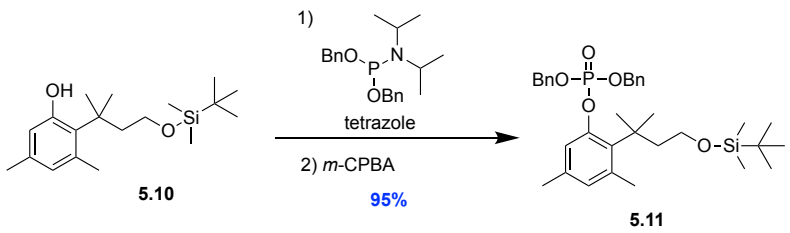
^{1}H NMR (300 MHz, Chloroform-*d*) δ 6.49 (s, 1H), 6.33 (s, 1H), 3.62 (t, *J* = 7.1 Hz, 2H), 2.47 (s, 3H), 2.24 (t, *J* = 7.1 Hz, 2H), 2.16 (d, *J* = 0.7 Hz, 3H), 1.55 (s, 6H). ^{13}C NMR (75 MHz, $CDCl_3$) δ 155.63, 137.90, 136.22, 128.70, 126.99, 116.40, 61.57, 45.06, 39.64, 31.98, 25.70, 20.34. HRMS-DART: $[M+H]^+$ calcd for $C_{13}H_{21}O_2$, 209.1542, found 209.1609.



5.9 **5.10**

2-(4-((*tert*-Butyldimethylsilyl)oxy)-2-methylbutan-2-yl)-3,5-dimethylphenol (5.10)

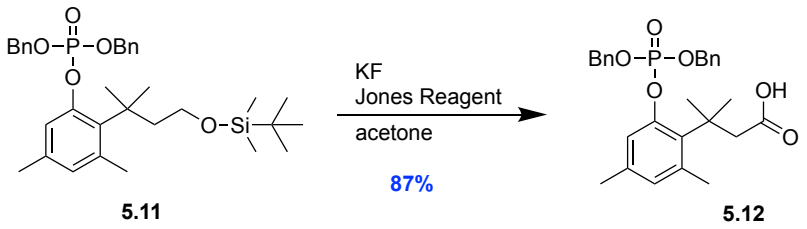
In a 100 mL RBF, **5.9** (2.89 g, 13.86 mmol) and DMAP (2.708 g, 22.17 mmol) were dissolved with 20 mL dry THF at 0 °C in an ice bath under nitrogen. TBDMSCl (2.3 g, 15.24 mmol) was then added into the flask and the reaction was stirred overnight. The reaction was quenched by addition of water and THF was removed by rotary evaporation. $CHCl_3$ (3 × 50 mL) was used to extract the aqueous layer and the combined organic layer was washed with water and brine. After drying with Na_2SO_4 and filtering, the solvent was removed under vacuum. Silica gel column chromatography using gradient elution with DCM to 2% MeOH-DCM was needed to obtain **5.10** as a white solid. (4.188 g, 12.98 mmol, 94% yield). R_f = 0.77 (25% EtOAc-hexanes). ^{1}H NMR (300 MHz, Chloroform-*d*) δ 6.58 – 6.47 (m, 1H), 6.40 (d, *J* = 2.0 Hz, 1H), 6.01 (d, *J* = 1.2 Hz, 1H), 3.63 (t, *J* = 7.2 Hz, 2H), 2.48 (s, 3H), 2.27 – 2.06 (m, 5H), 1.57 (s, 6H), 0.91 (s, 9H), 0.06 (s, 6H). ^{13}C NMR (75 MHz, $CDCl_3$) δ 155.71, 137.73, 135.98, 129.15, 126.84, 116.78, 62.00, 45.10, 39.50, 32.17, 26.12, 25.67, 20.36, 18.47, -5.13.



Dibenzyl (2-(4-((*tert*-butyldimethylsilyl)oxy)-2-methylbutan-2-yl)-3,5-dimethylphenyl) phosphate (5.11)

Compound **5.10**[252,253] (0.1 g, 0.31 mmol) was dissolved in 4 mL dry DCM under nitrogen followed by addition of tetrazole (2.1 mL, 0.93 mmol, 0.45 M in MeCN). The reaction mixture was cooled down to 0 °C and then dibenzyl *N*,*N*-diisopropylphosphoramidite (0.155 mL, 0.456 mmol) was added. After the reaction was allowed to warm up to rt and further stirred for 1.5 h, it was brought back to 0 °C again. *m*-CPBA (0.281 g, 0.93 mmol, 57% purity) was added and the reaction was stirred for another 1.5 h. After completion, the reaction was quenched by adding 100 mL saturated $NaHCO_3$ and the aqueous phase was extracted three times with 25 mL $CHCl_3$. The combined organic layer was then washed with 50 mL water, 50 mL brine, and dried over Na_2SO_4. After being filtered, and concentrated under reduced pressure, the crude was purified through silica gel column chromatography using gradient elution from hexanes to 20% EtOAc-hexanes. Compound **5.11** was obtained as a yellow oil (0.1714 g, 0.3 mmol, 95% yield). R_f = 0.24 (10% EtOAc-hexanes).

^{1}H NMR (300 MHz, Chloroform-*d*) δ 7.43 – 7.26 (m, 10H), 7.11 (d, *J* = 2.1 Hz, 1H), 6.75 – 6.69 (m, 1H), 5.12 (d, *J* = 8.2 Hz, 4H), 3.49 (dd, *J* = 7.9, 6.9 Hz, 2H), 2.50 (s, 3H), 2.18 (s, 3H), 2.13 – 2.05 (m, 2H), 1.53 (d, *J* = 0.8 Hz, 6H), 0.84 (d, *J* = 0.8 Hz, 9H), -0.04 (d, *J* = 0.8 Hz, 6H). ^{13}C NMR (75 MHz, $CDCl_3$) δ 150.44, 150.35, 138.66, 136.21, 135.82, 135.73, 132.86, 132.75, 131.09, 128.62, 128.59, 128.04, 118.95, 118.93, 69.80, 69.73, 61.11, 45.91, 39.63, 32.24, 26.05, 25.69, 20.42, 18.31, -5.22. ^{31}P NMR (121 MHz, $CDCl_3$) δ -6.98. HRMS-DART: $[M+H]^+$ calcd for $C_{33}H_{48}O_5PSi$: 583.3009, found: 583.2745.

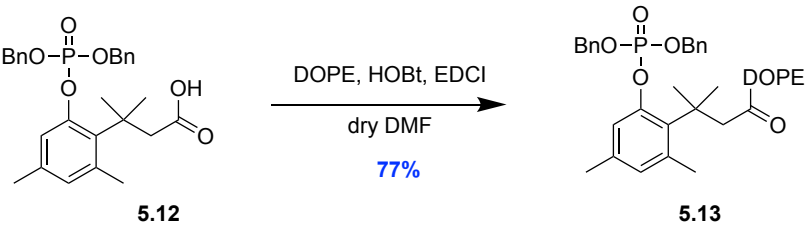


5.11 **5.12**

3-(2-((Bis(benzyloxy)phosphoryl)oxy)-4,6-dimethylphenyl)-3-methylbutanoic acid (5.12)

Compound **5.11** (0.43 g, 0.74 mmol) was dissolved with 4 mL acetone in a 50 mL RBF followed by addition of KF (47.34 mg, 0.815 mmol) and stirred briefly before being cooled down to 0 °C. Jones reagent (~1 mL, containing 1 mL H_2O, 0.23 mL concentrated H_2SO_4 and 0.27 g CrO_3) was then added dropwise to obtain a clear orange solution. The reaction was allowed to warm up to rt and further stirred for 3 h. After this time, the reaction mixture was filtered through a column packed with florisil and the filtrate was concentrated under reduced pressure. The crude was loaded onto silica gel and subjected to column chromatography. Gradient elution from DCM to 5% MeOH-DCM containing 1 drop of acetic acid was used to obtain **5.12** as a yellow oil. (0.31 g, 0.64 mmol, 87% yield). R_f = 0.4 (5% MeOH-DCM)/0.625 (50% EtOAc-hexanes).

^{1}H NMR (300 MHz, Chloroform-*d*) δ 7.31 (t, *J* = 1.8 Hz, 10H), 7.05 (d, *J* = 1.9 Hz, 1H), 6.72 – 6.68 (m, 1H), 5.12 (s, 2H), 5.09 (s, 2H), 2.89 (s, 2H), 2.50 (s, 3H), 2.13 (s, 3H), 1.59 (s, 6H). ^{13}C NMR (126 MHz, $CDCl_3$) δ 150.13, 150.08, 138.72, 136.68, 135.53, 135.48, 132.08, 132.02, 131.56, 128.77, 128.71, 128.18, 128.17, 119.13, 119.11, 70.17, 70.12, 47.50, 39.39, 31.79, 29.84, 25.69, 20.43. ^{31}P NMR (202 MHz, $CDCl_3$) δ -6.77. HRMS-DART: $[M+H]^+$ calcd for $C_{27}H_{32}O_6P$, 483.1936, found 483.1644

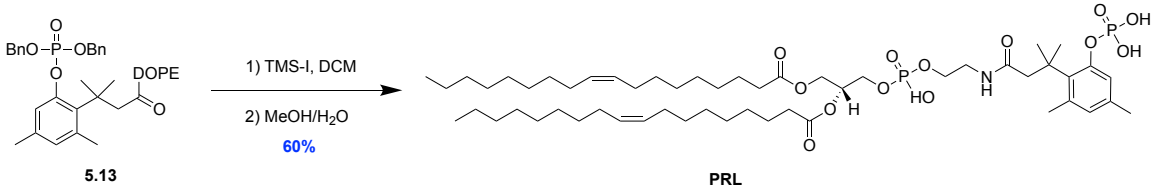


5.12 **5.13**

(2*R*)-3-(((2-(3-(2-((Bis(benzyloxy)phosphoryl)oxy)-4,6-dimethylphenyl)-3-methylbutanamido)ethoxy)(hydroxy)phosphoryl)oxy)propane-1,2-diyl dioleate (5.13)

DOPE (29.9 mg, 0.04 mmol) and HOBt (7.35 mg, 0.048 mmol) were dissolved in 0.8 mL of dry DMF containing **5.12** (23.16 mg, 0.048 mmol) in a small vial. The reaction was cooled down to 0 °C and stirred for 5 min followed by addition of EDCI (9.2 mg, 0.048 mmol) and DIEA (17 µL, 0.1 mmol). The mixture was stirred overnight before being quenched by pouring into 100 mL 1 M HCl. The aqueous layer was extracted three times with 20 mL chloroform. The combined organic layer was washed five times with 50 mL water, once with 50 mL brine, dried with Na_2SO_4, filtered, and concentrated under reduced pressure. Silica gel column chromatography using gradient elution from chloroform to 10% MeOH-chloroform was needed to obtain **5.13** as a yellow oil. (37.22 mg, 0.03 mmol, 77% yield). R_f = 0.18 (10% MeOH-chloroform).

^{1}H NMR (300 MHz, Chloroform-*d*) δ 7.27 (s, 11H), 6.84 (s, 1H), 6.65 (s, 1H), 5.38 – 5.29 (m, 5H), 5.14 (d, *J* = 8.4 Hz, 6H), 4.29 (d, *J* = 12.1 Hz, 1H), 4.03 (s, 1H), 3.88 (s, 2H), 3.77 – 3.59 (m, 2H), 3.29 (s, 2H), 2.70 (s, 2H), 2.47 (s, 4H), 2.26 – 2.10 (m, 5H), 2.09 – 1.92 (m, 14H), 1.27 (h, *J* = 9.3, 8.3 Hz, 57H), 0.86 (d, *J* = 6.9 Hz, 6H). ^{31}P NMR (121 MHz, $CDCl_3$) δ -3.98, -9.02.



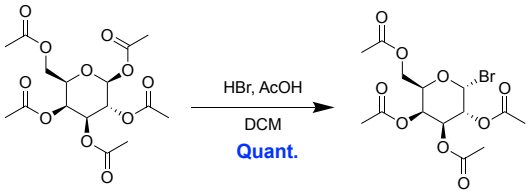
5.13 **PRL**

PRL

Compound **5.13** (34.4 mg, 0.0285 mmol) was dissolved in 1 mL dry DCM in a small vial at 0 °C. TMS-I (10.2 µL, 0.0712 mmol) was then added. The reaction was stirred for 40 min followed by removal of the solvent under reduced pressure. After further drying under high vacuum for 30 min, 2 mL of MeOH/H_2O (95/5, v/v) was added into the vial and the reaction was stirred for another one hour. Upon removal of the solvent, the crude was subjected to

silica gel column chromatography. Gradient elution from chloroform to 30% methanol-chloroform and final elution with MeOH/chloroform/H_2O (25/65/4, v/v) was performed to purify **PRL** as a yellow oil. (17.6 mg, 0.0171 mmol, 60% yield).

^{1}H NMR (300 MHz, 20% CD_3OD-$CDCl_3$) δ 6.42 (m, 2H), 5.21 – 5.17 (m, 4H), 5.01 (s, 1H), 4.19 (d, J = 11.5 Hz, 2H), 3.72 (d, J = 33.7 Hz, 6H), 2.29 (s, 4H), 2.12 (t, J = 15.6 Hz, 8H), 1.86 (d, J = 6.2 Hz, 8H), 1.44 (s, 4H), 1.13 (t, J = 6.0 Hz, 46H), 0.75 – 0.69 (m, 6H). ^{31}P NMR (121 MHz, 20% CD_3OD-$CDCl_3$) δ 0.63, -4.55. ESI-MS: $[M-H]^-$ calcd for $C_{54}H_{94}NO_{13}P_2$, 1026.6200, found 1026.6173. $[M-2H]^{2-}$ calcd for $C_{54}H_{93}NO_{13}P_2$, 512.8061, found 512.8077. $[M+I]^-$ calcd for $C_{54}H_{95}NO_{13}P_2I$, 1154.5323, found 1154.5304.



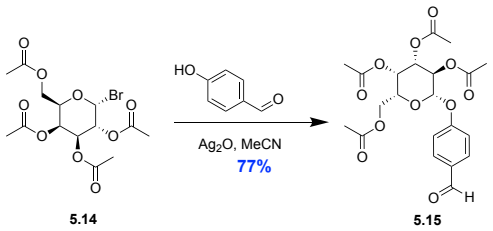
5.14

α-D-Galacopyranosyl bromide (5.14)[265]

β-D-Galactose pentaacetate (5 g, 12.81 mmol) was weighed out in a 100 mL round-bottom flask. 30 mL HBr in AcOH (33%) was then added and the reaction was stirred at room temperature for 40 min. After completion, the reaction mixture was diluted with DCM and transferred into a separatory funnel containing ice. The organic layer was washed with ice-cold water until the aqueous layer reached neutral pH. After the final wash with brine, the organic layer was collected, dried over Na_2SO_4, and concentrated to afford **5.14** as a yellow oil in a quantitative yield.

^{1}H NMR (300 MHz, Chloroform-*d*) δ 6.60 (dd, *J* = 3.9, 0.6 Hz, 1H), 5.41 (dd, *J* = 3.4, 1.3 Hz, 1H), 5.33 – 5.24 (m, 1H), 4.93 (dd, *J* = 10.6, 3.9 Hz, 1H), 4.39 (dddd, *J* = 6.9, 6.3, 1.4, 0.7 Hz, 1H), 4.14 – 3.91 (m, 2H), 2.04 (s, 3H), 2.00 (s, 3H), 1.94 (s, 3H), 1.89 (s, 3H). ^{13}C NMR (75 MHz, $CDCl_3$) δ 170.04, 169.78, 169.67, 169.49, 88.20, 70.98, 67.81, 67.60, 66.83, 60.70, 20.56, 20.45, 20.39, 20.37. HRMS-DART: $[M+H]^+$ calcd for $C_{14}H_{20}O_9Br$: 411.0291, found:

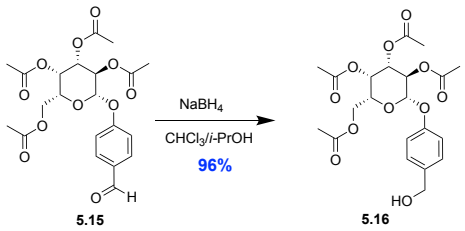
411.03705



(2*R*,3*S*,4*S*,5*R*,6*S*)-2-(Acetoxymethyl)-6-(4-formylphenoxy)tetrahydro-2*H*-pyran-3,4,5-triyl triacetate (5.15)[254]

α-D-Galacopyranosyl bromide (**5.14**) (1 g, 2.43 mmol), 4-hydroxybenzaldehyde (0.326 g, 2.67 mmol) and Ag_2O (1.13 g, 4.86 mmol) were weighed out in a 100 mL round-bottom flask under nitrogen and dissolved with 25 mL dry MeCN. The reaction was stirred in the dark overnight. After removing Ag_2O with vacuum filtration through a celite pad, the filtrate was concentrated and subjected to a silica gel column. Gradient elution from hexanes to 50% ethyl acetate-hexanes afforded **5.15** as a fluffy white solid (0.8421 g, 1.86 mmol, 77% yield). R_f = 0.4 (50% EtOAc-hexanes).

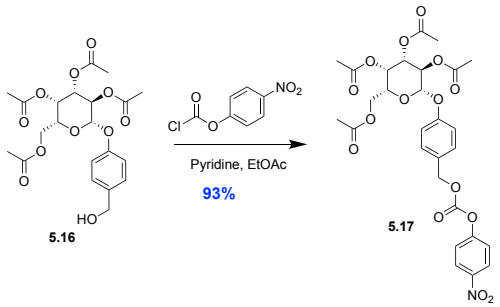
^{1}H NMR (300 MHz, Chloroform-*d*) δ 9.90 (s, 1H), 7.82 (dt, *J* = 6.7, 1.7 Hz, 2H), 7.13 – 7.04 (m, 2H), 5.54 – 5.42 (m, 2H), 5.19 – 5.09 (m, 2H), 4.25 – 4.02 (m, 3H), 2.16 (s, 3H), 2.01 (m, 9H). ^{13}C NMR (75 MHz, $CDCl_3$) δ 190.77, 170.37, 170.23, 170.12, 169.37, 161.36, 131.87, 131.87, 116.82, 116.81, 98.65, 71.40, 70.73, 68.49, 66.84, 61.44, 20.72, 20.70, 20.63, 20.62. HRMS-DART: $[M+H]^+$ calcd for $C_{21}H_{25}O_{11}$: 453.1397, found: 453.0938. $[M+NH_4]^+$ calcd for $C_{21}H_{28}O_{11}N$: 470.1662, found: 470.1156.



(2*R*,3*S*,4*S*,5*R*,6*S*)-2-(Acetoxymethyl)-6-(4-(hydroxymethyl)phenoxy)tetrahydro-2*H*-pyran-3,4,5-triyl triacetate (5.16)

Compound **5.15** (0.4928 g, 1.09 mmol) was dissolved with $CHCl_3$/*i*-PrOH (25 mL/8 mL) at 0 °C in a 100 mL round-bottom flask under nitrogen. $NaBH_4$ (91 mg, 2.398 mmol) was then quickly added into the flask. The reaction mixture was allowed to warm up to room temperature and further stirred for 3 hours before being quenched by adding 25 mL 10% citric acid (w/w). After being stirred for 20 minutes, the reaction mixture was extracted with 3 x 25 mL chloroform. The combined organic layer was then washed twice with 50 mL 50% $NaHCO_3$ solution, once with 50 mL brine, dried over Na_2SO_4, and concentrated under vacuum. The crude was purified via silica gel column chromatography using gradient elution from 10% EtOAc-hexanes to 70% EtOAc-hexanes to afford **5.16** as a fluffy white solid (0.475 g, 1.04 mmol, 96% yield). R_f = 0.23 (50% EtOAc-hexanes).

^{1}H NMR (300 MHz, Chloroform-*d*) δ 7.29 (d, *J* = 8.5 Hz, 2H), 6.99 (d, *J* = 8.6 Hz, 2H), 5.53 – 5.42 (m, 2H), 5.11 (dd, *J* = 10.4, 3.4 Hz, 1H), 5.04 (d, *J* = 7.9 Hz, 1H), 4.62 (s, 2H), 4.19 (qd, *J* = 11.2, 6.6 Hz, 2H), 4.07 (ddd, *J* = 7.1, 6.0, 1.1 Hz, 1H), 2.18 (s, 3H), 2.06 (s, 3H), 2.05 (s, 3H), 2.01 (s, 3H). ^{13}C NMR (75 MHz, $CDCl_3$) δ 170.45, 170.34, 170.20, 169.49, 156.42, 136.08, 128.46, 117.01, 99.74, 71.03, 70.85, 68.72, 66.93, 64.59, 61.40, 20.77, 20.69, 20.61. HRMS-DART: $[M+H]^+$ calcd for $C_{21}H_{27}O_{11}$: 455.1553, found: 455.1072.

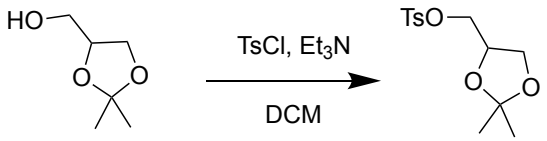


(2*R*,3*S*,4*S*,5*R*,6*S*)-2-(Acetoxymethyl)-6-(4-((((4-nitrophenoxy)carbonyl)oxy)methyl)phenoxy)tetrahydro-2*H*-pyran-3,4,5-triyl triacetate (5.17)

To a 100 mL round-bottom flask, **5.16** (0.1 g, 0.22 mmol) was added under nitrogen and 5 mL

EtOAc was used to dissolve the starting material. After the solution was cooled down to 0 °C, pyridine (53 μL, 0.66 mmol) was added and the reaction mixture was stirred for 30 min before 4-nitrobenzyl chloroformate (0.133 g, 0.66 mmol) was added into the flask. The reaction was further stirred at room temperature for 20 hours before being diluted with DCM. The organic layer was washed twice with 50 mL saturated $NaHCO_3$, and once with 50 mL water and 50 mL brine before being dried over Na_2SO_4, and concentrated under reduced pressure. Silica gel chromatography was performed using gradient elution from 10% EtOAc-hexanes to 50% EtOAc-hexanes. **5.17** was obtained as a faint yellow fluffy solid (0.126 g, 0.2 mmol, 93% yield). R_f = 0.6 (50% EtOAc-hexanes).

^{1}H NMR (300 MHz, Chloroform-*d*) δ 8.30 – 8.21 (m, 2H), 7.43 – 7.31 (m, 4H), 7.07 – 6.98 (m, 2H), 5.55 – 5.41 (m, 2H), 5.24 (s, 2H), 5.16 – 5.04 (m, 2H), 4.26 – 4.05 (m, 3H), 2.18 (d, *J* = 0.7 Hz, 3H), 2.06 (dd, *J* = 1.6, 0.8 Hz, 6H), 2.03 – 2.00 (m, 3H). ^{13}C NMR (75 MHz, $CDCl_3$) δ 170.40, 170.28, 170.17, 169.42, 157.49, 155.56, 152.49, 145.48, 130.61, 129.15, 125.37, 121.83, 117.13, 99.42, 71.18, 70.82, 70.56, 68.66, 66.91, 61.42, 20.81, 20.73, 20.65. HRMS-DART: $[M+H]^+$ calcd for $C_{28}H_{30}O_{15}N$: 620.1615, found: 620.0971. $[M+NH_4]^+$ calcd for $C_{28}H_{33}O_{15}N_2$: 637.1881, found: 637.1205.



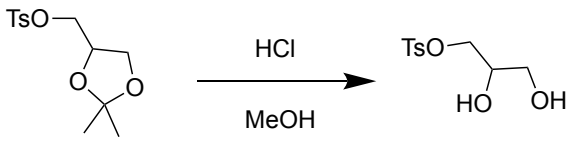
5.19

(2,2-Dimethyl-1,3-dioxolan-4-yl)methyl 4-methylbenzenesulfonate (5.19)

Solketal (2 mL, 18.2 mmol) was dissolved with 30 mL dry DCM in a 100 mL RBF under nitrogen. Et_3N (3.14 mL, 22.5 mmol) and 4-toluenesulfonyl chloride (4.30 g, 22.5 mmol) were then added into the flask. The reaction was run overnight before being quenched by pouring into 150 mL 0.75 N HCl. The organic layer was collected and the residual aqueous layer was extracted one more time with DCM. The combined organic layer was then washed with water and brine, dried over Na_2SO_4, and concentrated under reduced pressure. Silica gel column chromatography

was performed using gradient elution from 100% hexanes to 25% EtOAc-hexanes to yield **5.19** as a colorless oil (4.37 g, 15.3 mmol, 95% yield). R_f = 0.41 (25% EtOAc-hexanes).

^{1}H NMR (300 MHz, Chloroform-*d*) δ 7.80 (ddt, *J* = 10.5, 8.5, 1.9 Hz, 2H), 7.44 – 7.31 (m, 2H), 4.34 – 4.22 (m, 1H), 4.18 – 3.87 (m, 4H), 3.77 (ddd, *J* = 11.3, 8.3, 5.2 Hz, 1H), 2.48 (s, 3H), 1.33 (dd, *J* = 10.4, 8.2 Hz, 6H). ^{13}C NMR (75 MHz, $CDCl_3$) δ 145.17, 132.76, 130.06, 130.03, 128.11, 110.15, 73.03, 69.62, 66.31, 26.77, 25.29, 25.26, 21.80. HRMS-DART $[M+H]^+$ calcd for $C_{13}H_{19}O_5S$: 287.0953, found: 287.0699

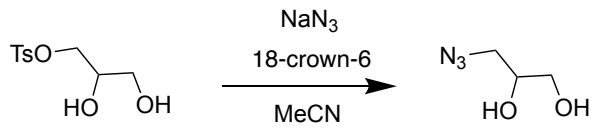


5.19 **70%** **5.20**

2,3-Dihydroxypropyl 4-methylbenzenesulfonate (5.20)

Compound **5.19** (4.37 g, 15.25 mmol) was dissolved with 40 mL MeOH followed by addition of 50 mL 0.5 N HCl. The reaction was stirred at room temperature overnight. After completion, the reaction was quenched by adding saturated $NaHCO_3$ and MeOH was removed under reduced pressure. Aqueous residual was extracted three times with DCM and the combined organic layer was washed with water and brine. After drying with Na_2SO_4, filtering and removal of the solvent, the crude was purified with silica gel column chromatography using gradient elution from 50% EtOAc-hexanes to 100% EtOAc. The product was obtained as a yellow oil which crystallized over time. (2.62 g, 10.6 mmol, 70% yield). R_f = 0.5 (100% EtOAc)

^{1}H NMR (300 MHz, Chloroform-*d*) δ 7.78 – 7.71 (m, 2H), 7.31 (d, *J* = 8.2 Hz, 2H), 4.00 (dd, *J* = 5.3, 2.4 Hz, 2H), 3.89 (q, *J* = 5.1 Hz, 1H), 3.55 (qd, *J* = 11.6, 4.3 Hz, 2H), 2.40 (s, 3H). ^{13}C NMR (75 MHz, $CDCl_3$) δ 145.26, 132.27, 130.05, 127.97, 70.86, 69.69, 62.78, 53.55, 21.66, 21.64. HRMS-DART: $[M+H]^+$ calcd for $C_{10}H_{15}O_5S$: 247.0640, found: 247.0407.



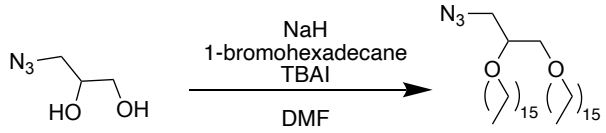
5.20 **81%** **5.21**

3-Azidopropane-1,2-diol (5.21)

Compound **5.20** (1.1757 g, 4.77 mmol), NaN_3 (0.93 g, 14.3 mmol) and 18-crown-6 (0.125 g, 0.477 mmol) were weighed into a 100 mL RBF under argon and then dissolved with 25 mL MeCN. The reaction was stirred for two days under reflux before being allowed to cool down to room temperature. The solid left in the round-bottomed flask was filtered off through a celite pad and the filtrate was concentrated under vacuum. The resulting crude was subjected to silica gel column chromatography and gradient elution from 25% EtOAc-hexanes to 100 % EtOAc was used to yield **5.21** as a colorless oil (0.4525 g, 3.86 mmol, 81% yield). R_f = 0.5 (100% EtOAc).

Note: this reaction was initially done in DMF/NaN_3/90 °C. However, we ended up with less than 10% yield, which was probably because **5.21** could be removed under vacuum when removing DMF using a rotary evaporator. Switching to MeCN and careful controlling of the temperature could effectively avoid such problem.

^{1}H NMR (300 MHz, Chloroform-*d*) δ 3.88 (tdd, *J* = 6.2, 4.8, 3.5 Hz, 1H), 3.78 – 3.53 (m, 2H), 3.51 – 3.30 (m, 2H), 3.21 – 2.80 (m, 2H). ^{13}C NMR (75 MHz, $CDCl_3$) δ 71.04, 64.12, 53.61. HRMS-DART $[M+H]^+$ calcd for $C_3H_8O_2N_3$: 118.0616, found: 118.0250; $[M+H-N_2]^+$ calcd for $C_3H_8O_2N$: 90.0555, found: 90.0203



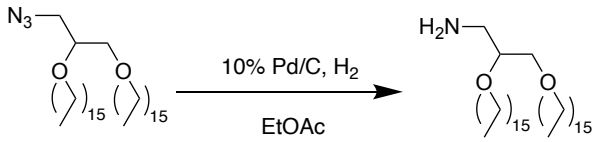
5.21 **60%** **5.22**

1-(3-Azido-2-(hexadecyloxy)propoxy)hexadecane (5.22)

Compound **5.21** (50.8 mg, 0.43 mmol) was weighed into a 50 mL RBF under nitrogen. 3 mL dry DMF was used to dissolve the starting material followed by addition of NaH (0.104 g, 2.604

mmol, 60% dispersion in mineral oil). The mixture was stirred at 0 °C for 30 min before adding 1-bromohexadecane (0.531 mL, 1.74 mmol) and TBAI (5 mg, 10% w/w of diol). After leaving the reaction running overnight, it was carefully quenched by adding water. The reaction mixture was extracted three times with EtOAc. The combined organic layer was washed with water five times, once with brine, dried and concentrated. Silica gel column chromatography using gradient elution from 100% hexanes to 5% EtOAc-hexanes yielded **5.21** as a white solid (0.1488 g, 0.26 mmol, 61% yield). R_f = 0.46 (5% EtOAc-hexanes)

^{1}H NMR (300 MHz, Chloroform-*d*) δ 3.60 – 3.51 (m, 3H), 3.50 – 3.38 (m, 4H), 3.33 (dd, *J* = 5.0, 3.5 Hz, 2H), 1.56 (tt, *J* = 12.7, 4.5 Hz, 4H), 1.26 (s, 57H), 0.93 – 0.83 (m, 6H). ^{13}C NMR (75 MHz, $CDCl_3$) δ 78.06, 71.91, 70.79, 70.27, 52.22, 32.09, 30.18, 29.86, 29.83, 29.77, 29.62, 29.53, 26.25, 26.18, 22.85, 14.26. HRMS-DART: $[M+H]^+$ calcd for $C_{35}H_{72}O_2N_3$: 566.5624, found: 566.5190. $[M+H-N_2]^+$ calcd for $C_{35}H_{72}O_2N$: 538.5563, found: 538.5150.



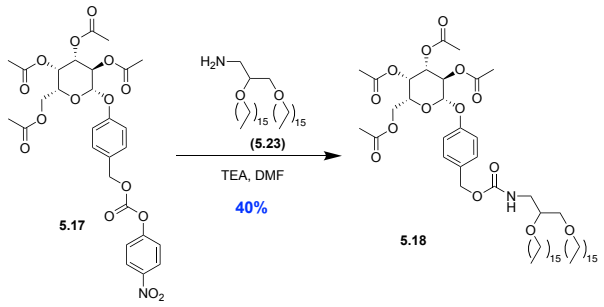
5.22 **5.23**

2,3-Bis(hexadecyloxy)propan-1-amine (5.23)

Compound **5.22** (0.133 g, 0.235 mmol) was weighed into a 50 mL RBF under nitrogen. Pd/C (30 mg, ~20% wt of starting material) was added into the flask carefully. 10 mL EtOAc was used to dissolve starting material and the nitrogen atmosphere was then replaced with hydrogen. The reaction was monitored by TLC until there was no starting material left. Pd/C catalyst was carefully removed through a celite pad and the solvent was removed under reduced pressure to yield **5.23** in a quantitative yield as a white solid. **5.23** was used without further purification. R_f = 0.41 (10% MeOH-DCM).

^{1}H NMR (300 MHz, Chloroform-*d*) δ 3.62 – 3.35 (m, 7H), 2.90 – 2.67 (m, 2H), 1.59 – 1.48 (m, 6H), 1.25 (s, 58H), 0.93 – 0.83 (m, 6H). ^{13}C NMR (75 MHz, $CDCl_3$) δ 96.26, 80.08, 71.86, 71.40, 70.53, 43.73, 32.08, 30.34, 29.85, 29.83, 29.78, 29.65, 29.51, 26.32, 26.29, 22.84,

14.27. HRMS-DART: $[M+H]^+$ calcd for $C_{35}H_{74}O_2N$: 540.5720, found: 540.5024.



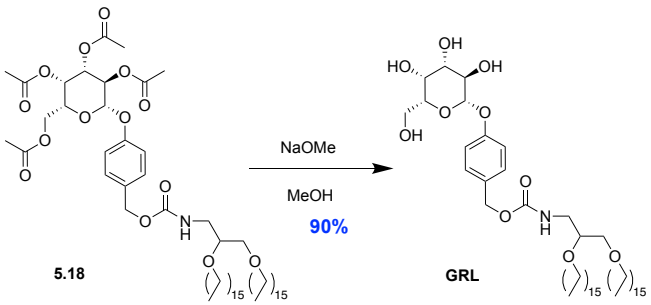
(2*R*,3*S*,4*S*,5*R*,6*S*)-2-(Acetoxymethyl)-6-(4-((((2,3-bis(hexadecyloxy) propyl)carbamoyl)oxy)methyl)phenoxy)tetrahydro-2*H*-pyran-3,4,5-triyl triacetate (**5.18**)

In a 50 mL RBF, **5.17** (172 mg, 0.278 mmol), and **5.23** (125 mg, 0.23 mmol) were added under nitrogen and the flask was cooled down to 0 °C in an ice bath. 2 mL DMF containing triethylamine (96.2 µL, 0.69 mmol) was then added into the flask. After overnight stirring, the reaction was quenched by pouring into 100 mL water. The aqueous layer was extracted three times with 25 mL chloroform. After washing the combined organic layer with 50 mL water five times, and 50 mL brine once, the resulting solution was dried over Na_2SO_4, filtered, and concentrated under vacuum, the crude was purified by silica gel column chromatography using gradient elution from 10% EtOAc-hexanes to 40% EtOAc-hexanes to yield **5.18** as a white solid (174 mg, 0.17 mmol, 74% yield). R_f = 0.7 (50% EtOAc-hexanes).

^{1}H NMR (300 MHz, Chloroform-*d*) δ 7.34 – 7.28 (m, 2H), 7.04 – 6.92 (m, 2H), 5.55 – 5.41 (m, 2H), 5.16 – 4.98 (m, 5H), 4.28 – 3.99 (m, 3H), 3.60 – 3.36 (m, 8H), 3.29 – 3.17 (m, 1H), 2.18 (s, 3H), 2.06 (s, 6H), 2.01 (s, 3H), 1.54 (t, *J* = 7.3 Hz, 4H), 1.25 (s, 56H), 0.93 – 0.84 (m, 6H).

^{13}C NMR (75 MHz, $CDCl_3$) δ 170.46, 170.37, 170.25, 169.49, 156.95, 156.56, 131.81, 129.94, 117.06, 99.81, 71.96, 71.29, 71.20, 70.96, 70.41, 68.76, 67.02, 66.97, 66.27, 61.49, 42.60, 32.07, 30.18, 29.85, 29.81, 29.77, 29.63, 29.51, 26.24, 22.84, 20.87, 20.82, 20.74, 14.27.

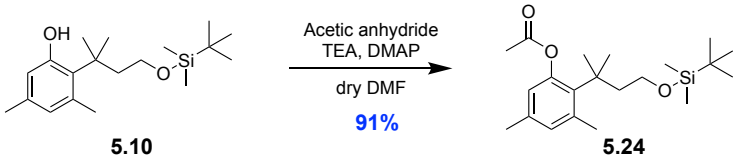
HRMS-DART: $[M+H]^+$ calcd for $C_{57}H_{98}O_{14}N$: 1020.6987, found: 1020.6404.



GRL

Compound **5.18** (20 mg, 0.0196 mmol) was dissolved in 2 mL MeOH in a large 4 dr vial at 0 °C. NaOMe (27 µL, 0.1176 mmol, 4.375 M in MeOH) was next added slowly. The reaction mixture immediately turned yellow and was stirred overnight before being neutralized with 1 N HCl. The solvent was evaporated, and the crude was purified via silica gel column chromatography using gradient elution from 100% chloroform to 30% MeOH-chloroform. **GRL** was obtained as a white solid (15 mg, 0.0176 mmol, 90% yield). R_f = 0.2 (10% MeOH-chloroform).

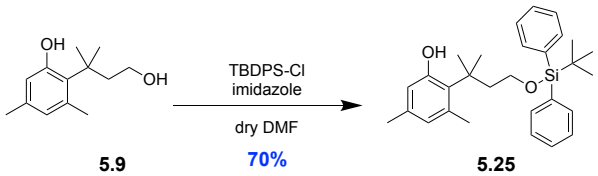
^{1}H NMR (600 MHz, 20% CD_3OD-Chloroform-*d*) δ 7.12 (d, *J* = 7.9 Hz, 2H), 6.92 – 6.86 (m, 2H), 4.92 – 4.83 (m, 2H), 4.70 (dd, *J* = 7.7, 1.9 Hz, 1H), 3.80 (t, *J* = 2.6 Hz, 1H), 3.70 – 3.59 (m, 3H), 3.49 (t, *J* = 6.1 Hz, 1H), 3.46 – 3.38 (m, 2H), 3.38 – 3.20 (m, 7H), 3.05 (dd, *J* = 14.3, 6.1 Hz, 1H), 1.39 (q, *J* = 6.6 Hz, 4H), 1.09 (d, *J* = 2.0 Hz, 58H), 0.71 (td, *J* = 7.0, 2.0 Hz, 6H). ^{13}C NMR (126 MHz, 20% CD_3OD-Chloroform-*d*) δ 157.21, 156.88, 130.45, 129.43, 116.56, 101.18, 77.36, 76.97, 75.00, 73.33, 71.69, 70.88, 70.23, 68.53, 66.22, 61.07, 49.24, 49.13, 49.07, 48.96, 48.90, 48.78, 48.73, 48.69, 48.61, 48.56, 48.44, 48.27, 48.10, 41.93, 31.75, 29.79, 29.52, 29.50, 29.48, 29.46, 29.39, 29.30, 29.18, 25.90, 25.87, 22.49, 13.79. ESI-MS: $[M+H]^+$ calcd for $C_{49}H_{90}O_{10}N$: 852.6565, found 852.6561, $[M+NH_4]^+$ calcd for $C_{49}H_{93}O_{10}N_2$: 869.6830, found: 869.6847. $[M+Na]^+$ calcd for $C_{49}H_{89}O_{10}NNa$:874.6384, found: 874.6409.



2-(4-((*tert*-Butyldimethylsilyl)oxy)-2-methylbutan-2-yl)-3,5-dimethylphenyl acetate (5.24)

Compound **5.10** (100 mg, 0.31 mmol) as well as DMAP (9.7 mg, 0.08 mmol) were combined in a 50 mL RBF under nitrogen. 1 mL dry DMF was added, followed by addition of acetic anhydride (58.6 µL, 0.62 mmol) and TEA (87 µL, 0.62 mmol). The reaction was stirred at room temperature overnight before being poured into 100 mL water. The aqueous phase was extracted with 3×25 mL chloroform. The combined organic layer was washed with 5×30 mL water and 30 mL brine. After being dried over Na_2SO_4, filtered, and concentrated under reduced pressure, the crude was purified via silica gel column chromatography using gradient elution from hexanes to 10% EtOAc-hexanes to yield the product as a colorless oil (103.1 mg, 0.283 mmol, 91% yield). R_f = 0.5 (10% EtOAc-Hexanes).

^{1}H NMR (300 MHz, Chloroform-*d*) δ 6.81 (dq, *J* = 2.1, 0.7 Hz, 1H), 6.62 – 6.54 (m, 1H), 3.54 – 3.44 (m, 2H), 2.52 (s, 3H), 2.26 (dd, *J* = 12.9, 0.6 Hz, 6H), 2.05 (dd, *J* = 8.0, 7.1 Hz, 2H), 1.48 (s, 6H), 0.86 (d, *J* = 0.5 Hz, 9H), -0.01 (d, *J* = 0.5 Hz, 6H). ^{13}C NMR (75 MHz, $CDCl_3$) δ 170.21, 149.76, 138.51, 136.05, 134.19, 132.48, 132.45, 123.25, 123.20, 60.89, 46.14, 39.15, 31.89, 29.84, 26.07, 25.41, 21.98, 20.33, 18.36, -5.19.



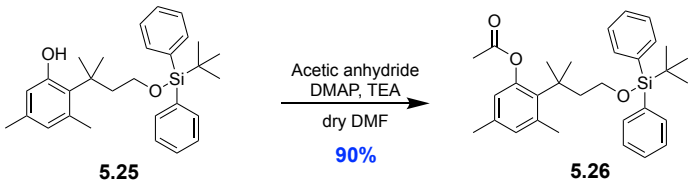
5.9 **5.25**

2-(4-((*tert*-Butyldiphenylsilyl)oxy)-2-methylbutan-2-yl)-3,5-dimethylphenol (5.25)

Compound **5.9** (72 mg, 0.346 mmol) and imidazole (61.2 mg, 0.8987 mmol) were combined in a 50 mL RBF under nitrogen. 3 mL dry DMF was used to dissolve the starting materials at 0 °C. After adding TBDPSCl (90 µL, 0.346 mmol), the resulting mixture was stirred at room temperature overnight. After completion, the reaction was quenched by pouring into 100 mL water, which was next extracted with 3×20 mL chloroform. The combined organic layer was next washed with 5×50 mL water and 50 mL brine. After being dried under Na_2SO_4, filtered, and concentrated under reduced pressure, the crude was purified with a column packed with

SiO_2 using gradient elution from hexanes to 10% EtOAc-hexanes to yield the product as a colorless oil (108.2 mg, 0.242 mmol, 70% yield). R_f = 0.76 (25% EtOAc-Hexanes).

^{1}H NMR (300 MHz, Chloroform-*d*) δ 7.65 – 7.59 (m, 4H), 7.46 – 7.32 (m, 6H), 6.47 (dd, *J* = 2.2, 1.0 Hz, 1H), 6.27 (d, *J* = 1.9 Hz, 1H), 4.79 (s, 1H), 3.61 (t, *J* = 7.1 Hz, 2H), 2.41 (s, 3H), 2.26 – 2.14 (m, 5H), 1.50 (s, 6H), 1.03 (s, 9H). ^{13}C NMR (75 MHz, $CDCl_3$) δ 155.14, 137.98, 135.92, 135.83, 134.13, 129.57, 129.21, 127.66, 116.68, 62.57, 45.22, 39.59, 32.10, 27.01, 25.63, 20.34, 19.19.

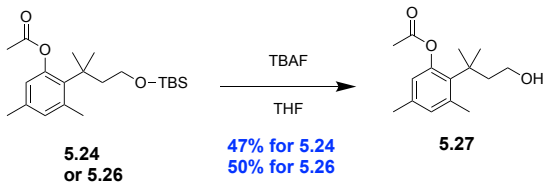


5.25 **5.26**

2-(4-((*tert*-Butyldiphenylsilyl)oxy)-2-methylbutan-2-yl)-3,5-dimethylphenyl acetate (5.26)

Compound **5.25** (59 mg, 0.132 mmol) as well as DMAP (4.2 mg, 0.034 mmol) were combined in a 50 mL RBF under nitrogen. 1 mL dry DMF was added, followed by addition of acetic anhydride (25 µL, 0.264 mmol) and TEA (37 µL, 0.264 mmol). The reaction was stirred at room temperature for extra three hours before being poured into 100 mL water. The aqueous phase was extracted with 3×25 mL chloroform. The combined organic layer was washed with 5×30 mL water and 30 mL brine. After being dried over Na_2SO_4, filtered, and concentrated under reduced pressure, the crude was purified via silica gel column chromatography using gradient elution from hexanes to 10% EtOAc-hexanes to yield **5.26** as a colorless oil (58.1 mg, 0.119 mmol, 90% yield). R_f = 0.76 (25% EtOAc-Hexanes, same as SM; formation of product confirmed by mass spectrometry).

^{1}H NMR (300 MHz, Chloroform-*d*) δ 7.70 – 7.57 (m, 4H), 7.50 – 7.29 (m, 8H), 6.81 – 6.73 (m, 1H), 6.57 – 6.47 (m, 1H), 3.61 – 3.49 (m, 2H), 2.41 (s, 3H), 2.22 (d, *J* = 0.9 Hz, 6H), 2.14 – 2.01 (m, 2H), 1.41 (d, *J* = 0.8 Hz, 6H), 1.32 – 1.19 (m, 3H), 1.00 (d, *J* = 0.9 Hz, 9H).

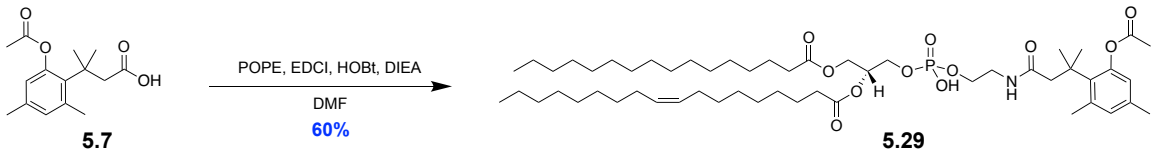


5.24 or 5.26 **5.27**

2-(4-Hydroxy-2-methylbutan-2-yl)-3,5-dimethylphenyl acetate (5.27)

Compound **5.26** (20 mg, 0.041 mmol) was dissolved in THF in a 50 mL RBF under nitrogen, followed by addition of TBAF (50 µL, 1 M in THF). The reaction was stirred overnight before being quenched by pouring into 100 mL water. The aqueous phase was extracted with 3×25 mL chloroform. The combined organic layer was washed by 50 mL water and 50 mL brine. After being dried over Na_2SO_4, filtered, and concentrated under reduced pressure, the crude was purified with silica gel column chromatography using gradient elution from 100% hexanes to 20% EtOAc-hexanes to yield a colorless oil (5.13 mg, 0.0205 mmol, 50% yield). R_f = 0.5 (25% EtOAc-hexanes, $KMnO_4$ active). Same reaction was performed using TBDMS-protected **5.24** as the starting material, where 0.4537 g, 1.244 mmol **5.24** was used. The yield was calculated to be 47% (0.144 g, 0.575 mmol).

^{1}H NMR (300 MHz, Chloroform-*d*) δ 6.48 (d, *J* = 2.7 Hz, 1H), 6.32 (t, *J* = 2.6 Hz, 1H), 4.74 (d, *J* = 3.1 Hz, 1H), 3.97 (td, *J* = 7.6, 3.4 Hz, 2H), 2.46 (d, *J* = 3.2 Hz, 3H), 2.27 (dt, *J* = 7.4, 3.7 Hz, 2H), 2.17 (d, *J* = 3.2 Hz, 3H), 1.93 (d, *J* = 3.4 Hz, 3H). ^{13}C NMR (126 MHz, $CDCl_3$) δ 171.42, 154.92, 138.27, 136.29, 128.30, 127.58, 116.35, 63.41, 41.64, 41.05, 39.72, 32.08, 31.81, 29.86, 25.67, 22.85, 21.17, 20.32, 14.27. ESI-MS (positive mode): $[M+Na]^+$ calcd for $C_{15}H_{22}O_3Na$, 273.1467, found 273.1604.

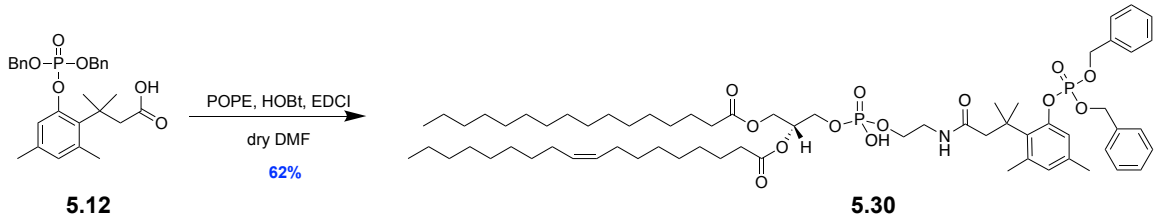


5.7 **5.29**

(2*R*)-1-(((2-(3-(2-Acetoxy-4,6-dimethylphenyl)-3-methylbutanamido)ethoxy)(hydroxy) phosphoryl)oxy)-3-(palmitoyloxy)propan-2-yl oleate (5.29)

POPE (10 mg, 0.014 mmol), **5.7** (4.42 mg, 0.0167 mmol) and hydroxybenzotriazole (HOBt,

2.56 mg, 0.0167 mmol) were dissolved with 1 mL dry DMF in a small vial under N_2. The reaction mixture was then cooled to 0 °C and further stirred for 5 minutes. Then, 1-ethyl-3-(3-dimethylaminopropyl)carbodiimide (EDCI, 3.2 mg, 0.0167 mmol) was added into the vial and followed by *N*, *N*-diisopropylethylamine (DIEA, 5.75 µL, 0.0348 mmol). The reaction was then stirred at room temperature for 5 hours before being quenched by pouring into 100 mL 1 M HCl. The aqueous layer was extracted three times with chloroform. The combined organic layer was washed with water five times and once with brine. After being dried over Na_2SO_4 and concentrated under vacuum, the crude was purified with silica gel column chromatography using gradient elution from 100% chloroform to 30% methanol-chloroform. **5.29** was obtained as a pale yellow oil (8.04 mg, 8.35 µmol, 60% yield). R_f = 0.67 (30% methanol-chloroform). ^{1}H NMR (500 MHz, 20%-CD_3OD/Chloroform-*d*) δ 6.73 (s, 1H), 6.69 (s, 1H), 6.43 (s, 1H), 5.19 (q, *J* = 5.3 Hz, 2H), 5.05 (s, 1H), 4.25 – 4.15 (m, 1H), 3.99 (dd, *J* = 11.9, 6.7 Hz, 1H), 3.77 (s, 2H), 3.57 (s, 2H), 3.14 (d, *J* = 5.8 Hz, 2H), 2.44 (s, 2H), 2.37 (s, 3H), 2.22 – 2.12 (m, 7H), 2.09 (s, 3H), 1.87 (q, *J* = 5.9 Hz, 4H), 1.44 (s, 11H), 1.21 – 1.01 (m, 51H), 0.73 (t, *J* = 6.8 Hz, 6H). ^{13}C NMR (151 MHz, 20%-CD_3OD/Chloroform-*d*) δ 173.73, 173.31, 171.24, 149.51, 138.23, 136.48, 133.48, 132.51, 129.89, 129.50, 123.11, 77.37, 77.33, 77.16, 76.95, 70.24, 63.64, 62.45, 62.45, 51.42, 39.40, 38.14, 37.75, 37.30, 34.07, 31.78, 31.29, 29.55, 29.38, 29.18, 29.01, 27.07, 25.10, 24.76, 24.73, 22.53, 21.52, 19.91, 19.69, 13.86, 13.82. ^{31}P NMR (202 MHz, 20%-CD_3OD/Chloroform-*d*) δ 1.08. ESI-MS (negative mode): $[M-H]^-$ calcd for $C_{54}H_{93}NO_{11}P$, 962.6486, found 962.7045.

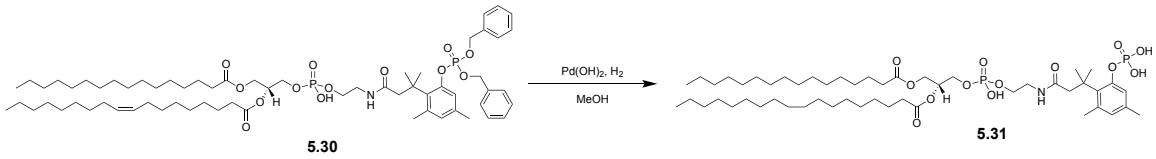


5.12 **5.30**

(2*R*)-1-(((2-(3-(2-((Bis(benzyloxy)phosphoryl)oxy)-4,6-dimethylphenyl)-3-methylbutanamido)ethoxy)(hydroxy)phosphoryl)oxy)-3-(palmitoyloxy)propan-2-yl oleate (5.30)

POPE (25 mg, 0.035 mmol) and HOBt (6.432 mg, 0.042 mmol) were weighed in a 50 mL RBF under nitrogen. 1 mL dry DMF containing **5.12** (20.26 mg, 0.042 mmol) was then added into the RBF at 0 °C. After being stirred for five minutes, EDCI (8.05 mg, 0.042 mmol) was added, followed by addition of DIEA (15 µL, 0.087 mmol). The reaction was further stirred for six hours at room temperature before being quenched by pouring into 100 mL of 1 N HCl. The aqueous phase was extracted with 3×25 mL chloroform. The combined organic layer was washed with 5×50 mL water and 50 mL brine. After being dried over Na_2SO_4, filtered, and concentrated under reduced pressure, the crude was purified with silica gel column chromatography using gradient elution from chloroform to 10% methanol in chloroform to yield the product as a yellow oil (25.5 mg, 0.0216 mmol, 62 % yield). R_f = 0.18 (10% MeOH-chloroform).

^{1}H NMR (500 MHz, 20% CD_3OD/Chloroform-*d*) δ 7.26 – 7.13 (m, 10H), 6.80 (s, 1H), 6.60 (d, *J* = 1.8 Hz, 1H), 5.22 (dd, *J* = 5.4, 4.2 Hz, 2H), 5.02 (qt, *J* = 11.6, 6.4 Hz, 5H), 4.21 (dd, *J* = 12.1, 3.0 Hz, 1H), 3.98 (dd, *J* = 12.0, 6.8 Hz, 1H), 3.51 (dt, *J* = 10.5, 6.1 Hz, 2H), 3.24 (p, *J* = 1.6 Hz, 2H), 3.14 – 3.04 (m, 2H), 2.49 (s, 2H), 2.36 (s, 3H), 2.18 – 2.11 (m, 4H), 2.01 (s, 3H), 1.88 (q, *J* = 6.7 Hz, 4H), 1.47 (s, 11H), 1.27 – 1.06 (m, 54H), 0.76 (t, *J* = 6.9 Hz, 6H). ^{13}C NMR (126 MHz, CD_3OD/Chloroform-*d*) δ 173.70, 173.28, 172.91, 149.85, 138.77, 136.61, 134.96, 134.90, 132.19, 131.50, 129.93, 129.56, 128.84, 128.63, 128.61, 128.57, 128.06, 128.04, 128.00, 118.77, 70.38, 70.33, 63.46, 62.48, 49.33, 49.30, 49.16, 49.14, 49.10, 48.99, 48.97, 48.93, 48.82, 48.80, 48.76, 48.65, 48.63, 48.59, 48.48, 48.46, 48.42, 48.30, 48.25, 39.96, 39.56, 34.08, 33.96, 31.83, 31.81, 31.71, 29.66, 29.61, 29.60, 29.57, 29.55, 29.43, 29.27, 29.22, 29.17, 29.07, 29.04, 29.01, 27.12, 27.09, 25.38, 24.79, 24.76, 22.58, 22.52, 20.03, 13.92. ^{31}P NMR (121 MHz, CD_3OD/Chloroform-*d*) δ 1.51, -3.59.



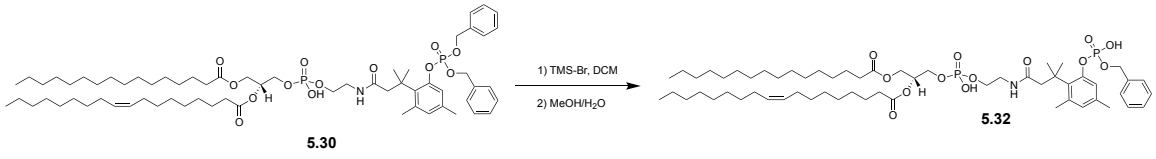
5.30 5.31

(2*R*)-1-(((2-(3-(2,4-Dimethyl-6-(phosphonooxy)phenyl)-3-methylbutanamido)ethoxy)(hydroxy)phosphoryl)oxy)-3-(palmitoyloxy)propan-2-yl stearate (5.31)

Compound **5.30** (12 mg, 0.01 mmol) was weighed in a 50 mL RBF under nitrogen. $Pd(OH)_2$ on charcoal (4 mg, 30% weight of SM) was weighed out quickly and carefully transferred into the RBF. 5 mL MeOH was used to dissolve the reaction mixture. Then, the nitrogen atmosphere was replaced by a hydrogen balloon, and the reaction was stirred vigorously overnight. After completion, the catalyst was carefully removed via vacuum filtration through a celite pad. The filtrate was concentrated under reduced pressure and the product was obtained as a yellow oil in a quantitative yield without further purification.

From its corresponding NMR, benzyl groups were gone but double bonds were also reduced. Alkyl regions were off. Playing around with CD_3OD percentage didn't help.

^{1}H NMR (500 MHz, 40% CD_3OD/Chloroform-*d*) δ 7.11 (s, 1H), 6.61 – 6.55 (m, 1H), 6.20 (s, 1H), 4.92 (d, *J* = 6.8 Hz, 1H), 4.10 (dd, *J* = 12.0, 3.1 Hz, 1H), 3.86 (dd, *J* = 12.0, 6.8 Hz, 1H), 3.63 (q, *J* = 5.3, 4.8 Hz, 2H), 3.55 (s, 1H), 3.49 – 3.36 (m, 3H), 2.92 (q, *J* = 5.2 Hz, 2H), 2.56 (s, 2H), 2.14 (s, 3H), 2.08 – 1.98 (m, 5H), 1.91 (s, 6H), 1.63 (s, 1H), 1.33 (d, *J* = 29.0 Hz, 14H), 1.02 (d, *J* = 51.6 Hz, 101H), 0.57 (q, *J* = 10.4, 8.6 Hz, 18H). ^{31}P NMR (202 MHz, 40% CD_3OD/$CDCl_3$) δ 6.30, 4.69. HRMS-ESI: $[M-H]^-$ calcd for $C_{52}H_{94}O_{13}NP_2$, 1002.6200, found 1002.6200.

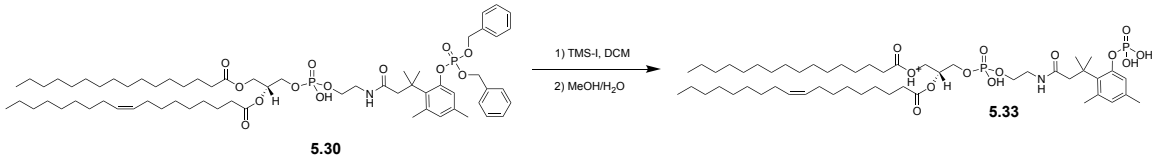


5.30 5.32

(2*R*)-1-(((2-(3-(2-(((Benzyloxy)(hydroxy)phosphoryl)oxy)-4,6-dimethylphenyl)-3-methylbutanamido)ethoxy)(hydroxy)phosphoryl)oxy)-3-(palmitoyloxy)propan-2-yl oleate (5.32)

Compound **5.30** (12 mg, 0.01 mmol) was dissolved with 1 mL dry DCM in a 4 dr vial under N_2 at 0 °C. TMS-Br (6.7 µL, 0.05 mmol) was added and the reaction mixture was allowed to warm up to room temperature. After being stirred for one extra hour, the solvent was removed under reduced pressure and the resulting mixture was placed under vacuum for six hours to remove any volatile by products. Next, the orange solid was re-dissolved in a methanol/water mixture (1 mL, 95/5, v/v). After being stirred for one hour, all the orange solids turned white. The solvent was removed directly with a rotary evaporator and the vial was kept under vacuum overnight. The crude was subjected to a column packed with silica gel. Gradient elution using chloroform to 20 % MeOH in chloroform and a final elution with chloroform/methanol/water 65/25/4 (v/v) was needed to obtain the product as a slight yellow oil (3.8 mg, 0.0035 mmol, 35% yield). R_f = 0.67 (chloroform/methanol/water=65/25/4, v/v, phospray active).

^{1}H NMR (500 MHz, 20% CD_3OD/Chloroform-*d*) δ 7.23 – 7.04 (m, 5H), 7.00 (d, *J* = 2.0 Hz, 1H), 6.43 (d, *J* = 1.9 Hz, 1H), 5.17 (qd, *J* = 4.3, 2.6 Hz, 2H), 5.03 – 4.97 (m, 1H), 4.86 (d, *J* = 5.9 Hz, 2H), 4.16 (dd, *J* = 12.0, 3.2 Hz, 1H), 3.93 (dd, *J* = 12.0, 6.8 Hz, 1H), 3.82 (dd, *J* = 5.8, 2.4 Hz, 1H), 3.76 – 3.68 (m, 2H), 3.56 (dt, *J* = 11.7, 5.6 Hz, 2H), 3.12 (t, *J* = 5.8 Hz, 2H), 2.65 (s, 2H), 2.30 (s, 3H), 2.19 – 2.06 (m, 5H), 1.98 (s, 3H), 1.93 – 1.80 (m, 4H), 1.54 – 1.34 (m, 12H), 1.27 – 0.99 (m, 59H), 0.77 – 0.61 (m, 10H). Integrations in alkyl regions were high. ^{31}P NMR (202 MHz, 20% CD_3OD/$CDCl_3$) δ 1.01, -4.34.



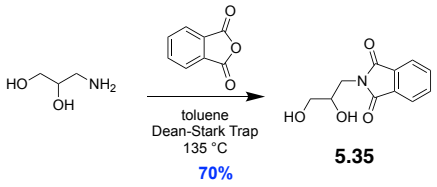
5.30 5.33

((2*R*)-3-(((2-(3-(2,4-Dimethyl-6-(phosphonooxy)phenyl)-3-methylbutanamido)ethoxy)(hydroxy)phosphoryl)oxy)-2-(oleoyloxy)propyl)(palmitoyl)oxonium (5.33)

Compound **5.30** (13.5 mg, 0.0114 mmol) was dissolved with 1 mL dry DCM in a 4 dr vial under

nitrogen at 0 °C. TMS-I (4.06 µL, 0.05 mmol) was added and the reaction mixture immediately turned yellow. After being stirred for 40 minutes at 0 °C, the solvent was removed under reduced pressure and the resulting mixture was placed under vacuum for 20 minutes to remove any volatile by products. Next, the crude was re-dissolved in a methanol/water mixture (1 mL, 95/5, v/v). After being stirred for one hour, the solvent was again removed directly with a rotary evaporator. The crude was subjected to a column packed with silica gel. Both Gradient elution using chloroform to 20 % MeOH in chloroform and a final elution with chloroform/methanol/water 65/25/4 (v/v) was needed to obtain the product **5.33** as a slight yellow oil (5.7 mg, 0.0057 mmol, 50 % yield). R_f = 0.32 (chloroform/methanol/water=65/25/4, v/v, phospray active).

^{1}H NMR (500 MHz, 20% CD_3OD/Chloroform-*d*) δ 6.46 (s, 1H), 5.19 (p, *J* = 5.2 Hz, 2H), 5.07 – 4.95 (m, 2H), 4.20 (d, *J* = 11.9 Hz, 2H), 3.77 (s, 3H), 3.67 (s, 2H), 2.73 (s, 1H), 2.32 (s, 3H), 2.14 (t, *J* = 7.6 Hz, 6H), 2.02 (d, *J* = 25.9 Hz, 6H), 1.87 – 1.79 (m, 6H), 1.45 (s, 16H), 1.11 (d, *J* = 7.3 Hz, 106H), 0.72 (t, *J* = 6.8 Hz, 17H). Integrations in alkyl regions were high. ESI-MS: $[M-H]^-$ calcd for $C_{52}H_{92}O_{13}NP_2$, 1000.6044, found 1000.6044.



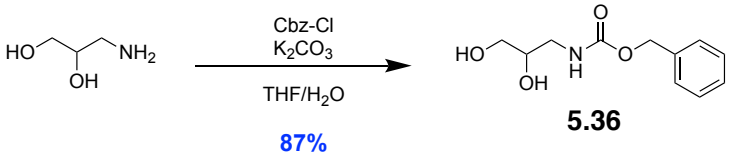
5.35

2-(2,3-Dihydroxypropyl)isoindoline-1,3-dione (5.35)

3-Aminopropane-1,2-diol (1.45 g, 15.9 mmol) and phthalic anhydride (2.6 g, 17.55 mmol) were combined in a 200 mL RBF. 50 mL toluene was then added, and the reaction was heated at 135 °C with a Dean-Stark trap overnight. After completion, the reaction was allowed to cool down to room temperature before being poured into 100 mL saturated $NaHCO_3$ solution. The mixture was extracted with 3×30 mL chloroform. The combine organic layer was washed with 50 mL sat. $NaHCO_3$ and 50 mL brine. Pure product was obtained as a white solid after being dried over Na_2SO_4, filtered, and concentrated under reduced pressure, as indicated from TLC

(2.52 g, 11.375 mmol, 70% yield). R_f = 0.2 (50% EtOAc-hexanes). Note: Solid precipitated out immediately after reaction completion, which was removed from filtration since this solid did not dissolve in chloroform. However, it was confirmed to be product later. Also, the product has poor solubility in chloroform at room temperature. To acquire an NMR, heating was required to dissolve the compound in $CDCl_3$.

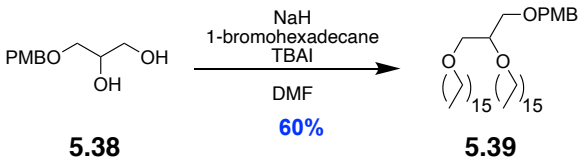
^{1}H NMR (300 MHz, Chloroform-*d*) δ 7.86 (ddd, *J* = 5.4, 2.9, 0.7 Hz, 2H), 7.74 (ddd, *J* = 5.2, 3.3, 0.7 Hz, 2H), 4.03 – 3.93 (m, 1H), 3.92 – 3.78 (m, 2H), 3.64 (qd, *J* = 11.8, 4.5 Hz, 2H). ^{13}C NMR (75 MHz, $CDCl_3$) δ 169.18, 134.44, 131.96, 123.70, 70.43, 63.93, 40.61.



Benzyl (2,3-dihydroxypropyl)carbamate (5.36)[266]

3-Amino-1,2-propandiol (1.87 g, 20.52 mmol) was weighed in a 200 mL RBF and dissolved with 105 mL THF/water mixture (2/1, v/v). After adding potassium carbonate (8.5 g, 61.5 mmol), the reaction mixture was cooled down to 0 °C. Cbz-Cl (~3mL, 20.52 mmol) was added dropwise. Next, the reaction mixture was allowed to warm up to room temperature and further stirred for extra three hours. After completion, the reaction was extracted with 3×20 mL EtOAc. The combined organic layer was washed with 50 mL brine and dried over Na_2SO_4. After being filtered, the solvent was removed under reduced pressure. The resulting oily crude was added into hexanes. White precipitate was observed after five minutes and was collected via vacuum filtration with a Buchner funnel (4.02 g, 17.85 mmol, 87% yield).

^{1}H NMR (300 MHz, Chloroform-*d*) δ 7.44 – 7.28 (m, 5H), 5.22 (s, 1H), 5.11 (s, 2H), 3.76 (dt, *J* = 5.9, 4.9 Hz, 1H), 3.59 (qd, *J* = 11.5, 4.8 Hz, 2H), 3.41 – 3.24 (m, 2H), 2.40 (s, 2H). ^{13}C NMR (75 MHz, $CDCl_3$) δ 136.29, 128.73, 128.44, 128.28, 71.31, 67.34, 63.83, 43.43.

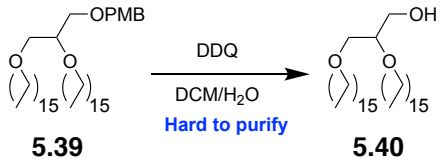


5.38 **5.39**

1-((2,3-Bis(hexadecyloxy)propoxy)methyl)-4-methoxybenzene (5.39)

Compound **5.38** (synthesized with the same protocol as **8.8** in Chapter 8, 1.021 g, 4.81 mmol) was dissolved with 3 mL dry DMF in a 50 mL RBF under nitrogen at 0 °C. NaH (1.15 g, 28.86 mmol, 60% dispersion in mineral oil) was added carefully. The reaction mixture was stirred for 30 min before addition of TBAI (0.1021 g, 10% w/w of diol) and 1-bromohexadecane (5.89 mL, 19.24 mmol). Next, the reaction was allowed to warm up to room temperature and further stirred overnight before being quenched by addition of water. 3×25 mL EtOAc was used to extract the aqueous residual. The combined organic layer was washed with 5×50 mL water and 50 mL brine. After being dried over Na_2SO_4, filtered, and concentrated under reduced pressure, the crude was purified with silica gel column chromatography using gradient elution from hexane to 10% EtOAc in hexanes as a white solid (1.48 g, 2.24 mmol, 40% yield). R_f = 0.45 (10% EtOAc-hexanes).

^{1}H NMR (300 MHz, Chloroform-*d*) δ 7.29 – 7.22 (m, 2H), 6.89 – 6.84 (m, 2H), 4.48 (s, 2H), 3.80 (d, *J* = 1.2 Hz, 3H), 3.60 – 3.53 (m, 4H), 3.53 – 3.44 (m, 4H), 3.41 (d, *J* = 6.6 Hz, 2H), 1.55 (q, *J* = 6.4 Hz, 6H), 1.26 (s, 65H), 0.91 – 0.85 (m, 6H). ^{13}C NMR (75 MHz, $CDCl_3$) δ 159.10, 130.52, 129.18, 113.67, 77.93, 72.99, 71.63, 70.79, 70.57, 69.95, 55.24, 55.18, 31.92, 30.10, 29.70, 29.66, 29.51, 29.36, 26.13, 26.10, 22.68, 14.11.



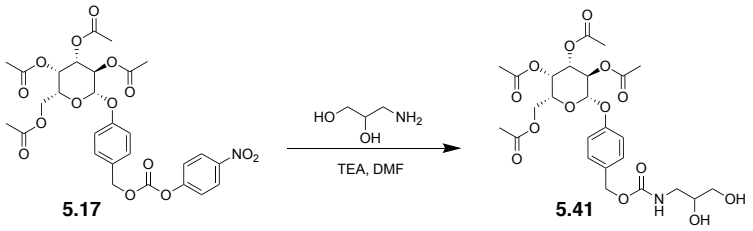
5.39 **5.40**

2,3-Bis(hexadecyloxy)propan-1-ol (5.40)

Compound **5.39** (0.7407 g, 1.12 mmol) and DDQ (0.51 g, 2.24 mmol) were combined in a 100 mL RBF. 22 mL DCM/H_2O (10/1, v/v) was added, and the reaction was stirred vigorously at room temperature for six hours. After completion, the reaction was quenched by adding 100

mL saturated sodium bicarbonate. The mixture was extracted with 3×50 mL DCM. The combined organic layer was washed with 100 mL water and 100 mL brine, respectively. After being dried over Na_2SO_4, filtered, and concentrated under reduced pressure, the crude was purified with silica gel column chromatography using gradient elution from hexanes to 25% EtOAc-hexanes to yield the product as a white solid. Yield was not calculated since only one clean fraction was obtained via column. It turned out that the by-product PMB aldehyde co-eluted with product. We could try to run the column slower and see if they could be separated. R_f = 0.6 (25% EtOAc-hexane).

^{1}H NMR (300 MHz, Chloroform-*d*) δ 3.74 – 3.36 (m, 9H), 1.57 (p, *J* = 5.8 Hz, 4H), 1.26 (s, 56H), 0.94 – 0.78 (m, 6H). ^{13}C NMR (126 MHz, $CDCl_3$) δ 78.39, 72.01, 71.99, 71.83, 71.07, 70.55, 69.63, 63.28, 32.08, 30.24, 29.85, 29.84, 29.83, 29.82, 29.78, 29.77, 29.71, 29.63, 29.52, 26.26, 22.85, 14.27.



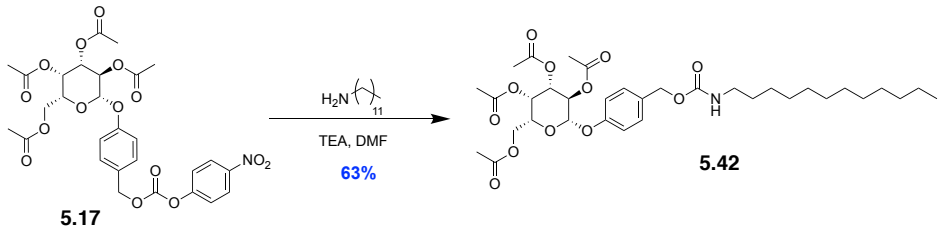
5.17 **5.41**

(2*R*,3*S*,4*S*,5*R*,6*S*)-2-(Acetoxymethyl)-6-(4-((((2,3-dihydroxypropyl)carbamoyl)oxy) methyl)phenoxy)tetrahydro-2*H*-pyran-3,4,5-triyl triacetate (5.41)

Compound **5.17** (50 mg, 0.081 mmol) was dissolved with 1 mL dry DMF in a 50 mL RBF under nitrogen. 3-Amino-1,2-propandiol (5.2 µL, 0.0673 mmol) and TEA (28 µL, 0.2 mmol) were dissolved with 2 mL dry DMF in a small vial and then added into the reaction mixture. After being stirred overnight, the reaction was quenched by pouring into 150 mL water. The resulting aqueous solution was extracted with 3×25 mL chloroform. The combined organic phase was washed with 5×50 mL water and 50 mL brine. After being dried with Na_2SO_4, filtered, and concentrated under reduced pressure, the crude was subjected to silica gel column chromatography. Gradient elution from DCM to 10% methanol in DCM was needed to yield

the product as a colorless oil (43.8 mg, 0.077 mmol, 95% yield based on **5.17** since amine was too sticky and hard to weigh). R_f = 0.2 (5% MeOH in DCM).

^{1}H NMR (300 MHz, Chloroform-*d*) δ 7.33 – 7.27 (m, 2H), 7.01 – 6.95 (m, 2H), 5.53 – 5.41 (m, 2H), 5.20 (s, 1H), 5.14 – 5.00 (m, 4H), 4.18 (qd, *J* = 11.2, 6.6 Hz, 2H), 4.05 (t, *J* = 6.5 Hz, 1H), 3.76 (s, 1H), 3.58 (d, *J* = 12.8 Hz, 2H), 3.32 (s, 2H), 2.32 (s, 2H), 2.19 – 2.15 (m, 3H), 2.05 (d, *J* = 0.9 Hz, 6H), 2.02 – 1.99 (m, 3H).



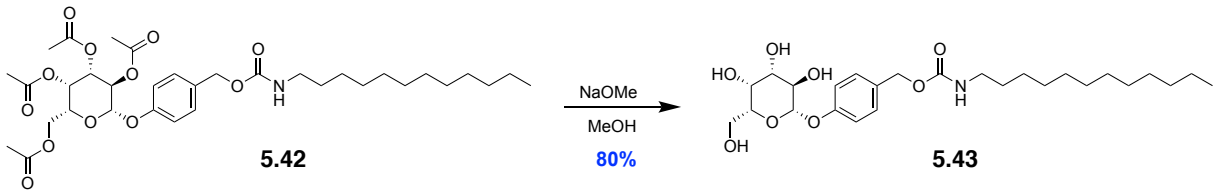
5.17 **5.42**

(2*R*,3*S*,4*S*,5*R*,6*S*)-2-(Acetoxymethyl)-6-(4-(((dodecylcarbamoyl)oxy)methyl)phenoxy)tetrahydro-2*H*-pyran-3,4,5-triyl triacetate (5.42)

Compound **5.17** (50 mg, 0.081 mmol) was weighed into a 50 mL RBF under nitrogen. 0.5 mL dry DMF was added, and the reaction mixture was stirred at 0 °C. Dodecylamine (12.46 mg, 0.067 mmol) and triethylamine (28 µL, 0.201 mmol) were dissolved with 2 mL dry DMF in a separate vial and then injected into the RBF. The reaction was stirred overnight before being quenched by pouring into 200 mL water. The aqueous solution was extracted with chloroform three times. The combined organic layer was then washed with water five times, brine once, dried over Na_2SO_4, and concentrated under reduced pressure. The crude was purified via silica gel column chromatography using gradient elution from 100% hexanes to 30% EtOAc-hexanes. **5.42** was obtained as a white solid (28.1 mg, 0.042 mmol, 63% yield). R_f = 0.4 (35% EtOAc-hexanes)

^{1}H NMR (300 MHz, Chloroform-*d*) δ 7.35 – 7.27 (m, 2H), 7.05 – 6.94 (m, 2H), 5.58 – 5.36 (m, 2H), 5.16 – 4.97 (m, 4H), 4.69 (s, 1H), 4.19 (qd, *J* = 11.3, 6.6 Hz, 2H), 4.11 – 4.00 (m, 1H), 3.16 (q, *J* = 6.7 Hz, 2H), 2.18 (s, 3H), 2.06 (s, 6H), 2.01 (s, 3H), 1.46 (d, *J* = 7.2 Hz, 2H), 1.26 (d, *J* = 7.3 Hz, 20H), 0.91 – 0.84 (m, 3H). ^{13}C NMR (75 MHz, $CDCl_3$) δ 170.47, 170.36, 170.24,

169.49, 156.92, 156.43, 131.83, 129.94, 117.05, 99.75, 71.18, 70.96, 68.76, 66.96, 66.15, 61.49, 41.27, 32.04, 30.09, 29.76, 29.70, 29.67, 29.47, 29.40, 26.87, 22.82, 20.81, 20.78, 14.25. HRMS-DART: $[M+NH_4]^+$ calcd for $C_{34}H_{55}O_{12}N_2$: 683.3755, found: 683.3210.

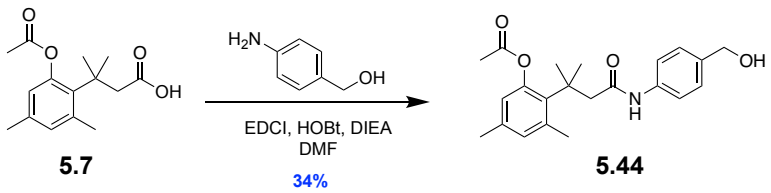


5.42 **5.43**

4-(((2*S*,3*R*,4*S*,5*R*,6*R*)-3,4,5-Trihydroxy-6-(hydroxymethyl)tetrahydro-2*H*-pyran-2-yl)oxy)benzyl dodecylcarbamate (5.43)

Compound **5.42** (16.7 mg, 0.025 mmol) was dissolved in 2 mL MeOH in a small vial at 0 °C. NaOMe (34.3 µL, 0.15 mmol, 4.375 M in MeOH) was added into the vial. The reaction mixture immediately turned yellow. After being stirred overnight, the reaction was quenched by neutralizing with 1 N HCl until the mixture showed a color change from yellow to colorless. Then, the solvent was evaporated under reduced pressure and the crude was subjected to silica gel column chromatography. Compound **5.43** was obtained using gradient elution from 100% chloroform to 20% MeOH-$CHCl_3$ as a white solid (10 mg, 0.02 mmol, 80% yield). R_f = 0.2 (10% MeOH-$CHCl_3$).

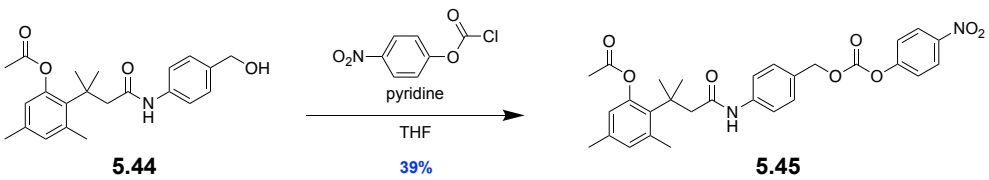
^{1}H NMR (500 MHz, 20% MeOD-Chloroform-*d*) δ 7.14 – 7.09 (m, 2H), 6.92 – 6.86 (m, 2H), 4.84 (s, 2H), 4.70 (d, *J* = 7.7 Hz, 1H), 3.80 (dd, *J* = 3.4, 1.1 Hz, 1H), 3.70 – 3.60 (m, 3H), 3.52 – 3.41 (m, 2H), 3.19 (p, *J* = 1.6 Hz, 1H), 2.96 (t, *J* = 7.2 Hz, 2H), 1.32 (t, *J* = 7.1 Hz, 2H), 1.19 – 0.94 (m, 20H), 0.71 (t, *J* = 6.9 Hz, 3H). ^{13}C NMR (126 MHz, 20% MeOD-$CDCl_3$) δ 157.16, 156.94, 130.57, 129.40, 116.54, 101.17, 77.36, 75.01, 73.33, 70.88, 68.55, 66.04, 61.09, 40.80, 31.76, 31.74, 29.66, 29.51, 29.46, 29.44, 29.41, 29.38, 29.16, 29.13, 26.60, 22.48, 13.78, 13.77. HRMS-DART: $[M+H]^+$ calcd for $C_{26}H_{44}O_8N$: 498.3067, found: 498.2650. $[M+NH_4]^+$ calcd for $C_{26}H_{47}O_8N_2$: 515.3332, found: 515.2980.



2-(4-((4-(Hydroxymethyl)phenyl)amino)-2-methyl-4-oxobutan-2-yl)-3,5-dimethylphenyl acetate (5.44)

Compound **5.7** (30 mg, 0.1135 mmol), 4-aminobenzyl alcohol (15.4 mg, 0.125 mmol), as well as HOBt (17.4 mg, 0.1135 mmol) were combined in a 50 mL RBF under nitrogen. 1 mL dry DMF was used to dissolve all the starting materials at 0 °C. After being stirred for 5 min, EDCI (22 mg, 0.1135 mmol) was added, followed by addition of DIEA (50 µL, 0.29 mmol). The reaction mixture was allowed to warm to room temperature and stirred overnight before being quenched by pouring into 100 mL of 1 M HCl. The aqueous solution was extracted with 3×25 mL chloroform. The combined organic layer was further washed with 5×50 mL water and 50 mL brine. After being dried over Na_2SO_4, filtered, and concentrated under reduced pressure, the resulting crude was purified through silica gel column chromatography using gradient elution from hexanes to 50% ethyl acetate-hexanes to yield the product as a yellow oil (14.2 mg, 0.0384 mmol, 34% yield). R_f = 0.27 (50% EtOAc-hexanes).

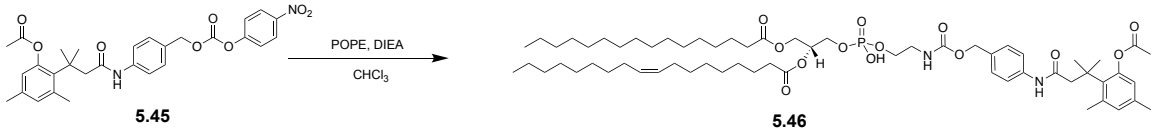
^{1}H NMR (500 MHz, Chloroform-*d*) δ 7.17 (tdd, *J* = 8.7, 6.1, 2.5 Hz, 4H), 6.81 – 6.77 (m, 1H), 6.67 – 6.62 (m, 1H), 4.59 (d, *J* = 3.5 Hz, 2H), 2.56 (d, *J* = 3.4 Hz, 2H), 2.40 (dd, *J* = 14.0, 3.7 Hz, 6H), 2.25 (d, *J* = 3.6 Hz, 3H), 1.69 (t, *J* = 2.5 Hz, 6H). ^{13}C NMR (126 MHz, $CDCl_3$) δ 172.18, 169.73, 150.27, 149.83, 140.37, 139.34, 137.84, 137.34, 137.28, 136.26, 133.24, 127.71, 123.57, 119.78, 65.22, 51.20, 40.59, 32.37, 29.85, 25.69, 22.10, 20.32. HRMS-DART: $[M+H]^+$ calcd for $C_{22}H_{22}O_4N$, 370.2018, found 370.2142.



3,5-Dimethyl-2-(2-methyl-4-((4-((((4-nitrophenoxy)carbonyl)oxy)methyl)phenyl)amino)-4-oxobutan-2-yl)phenyl acetate (5.45)

Compound **5.44** (14 mg, 0.038 mmol) was dissolved with dry THF in a 50 mL RBF under nitrogen. Next, pyridine (anhydrous, 7.63 µL, 0.095 mmol) was added. 4-Nitrophenol chloroformate (15.3 mg, 0.076 mmol) was then added after the reaction mixture was brought down to 0 °C with ice bath. The reaction was further stirred at room temperature overnight (color change from light orange to yellow was observed) before being diluted with 100 mL chloroform. The organic residue was washed with 100 mL 1 M $KHSO_4$ and 100 mL brine. After being dried over Na_2SO_4, filtered, and concentrated under reduced pressure, the crude was purified with silica gel column chromatography twice using gradient elution from 100% DCM to 2% methanol in DCM. After the second round of column, there was still pyridinium impurities in the product. The separated product was used directly in the next step without further purification (7.9 mg, 39% yield based on NMR). R_f = 0.58 (5% MeOH-DCM).

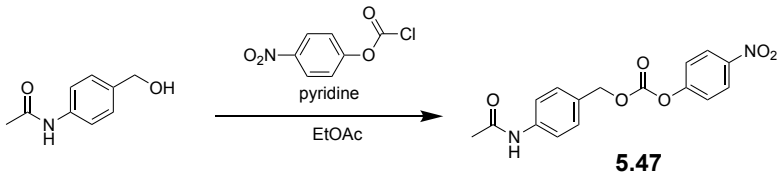
^{1}H NMR (300 MHz, Chloroform-*d*) δ 8.27 (d, *J* = 9.1 Hz, 2H), 8.18 – 8.12 (m, 3H), 7.49 (s, 1H), 7.41 – 7.33 (m, 2H), 7.32 – 7.26 (m, 2H), 7.20 (d, *J* = 8.5 Hz, 2H), 6.96 – 6.86 (m, 4H), 6.86 – 6.76 (m, 3H), 6.65 (d, *J* = 2.0 Hz, 1H), 5.20 (s, 2H), 2.58 (s, 2H), 2.41 (d, *J* = 4.3 Hz, 6H), 2.25 (s, 3H), 1.70 (s, 7H). Extra peaks in aromatic region are from pyridinium salts. HRMS-DART: $[M+H]^+$ calcd for $C_{29}H_{31}N_2O_8$, 535.2080, found 535.3512.



(2*R*)-1-(((2-((((4-(3-(2-Acetoxy-4,6-dimethylphenyl)-3-methylbutanamido)benzyl)oxy) carbonyl)amino)ethoxy)(hydroxy)phosphoryl)oxy)-3-(palmitoyloxy)propan-2-yl oleate (5.46)

Compound **5.45** (7.9 mg, 0.01478 mmol, with impurities) was dissolved with 3 mL chloroform (sieve-dried) in a 50 mL RBF under nitrogen at 0 °C. POPE (7.2 mg, 0.01 mmol) as well as DIEA (4.95 µL, 0.03 mmol) were dissolved with 1 mL dry chloroform and then added into the reaction mixture. After being allowed to warm to room temperature, the reaction was further

stirred for 3 hours before being diluted with 50 mL chloroform. The organic phase was washed with 100 mL 5% $NaHCO_3$ solution, 100 mL 1 N HCl and 100 mL brine, respectively. The organic solvent was evaporated under reduced pressure and put under high vacuum for several hours to avoid drying step. The resulting crude was subjected to a micro-column packed with silica gel. Gradient elution from chloroform to 30% methanol in chloroform was needed to obtain the product as a light-yellow oil (6 mg, 0.0054 mmol, 54% yield). R_f = 0.75 (30% MeOH-chloroform). ^{1}H NMR (300 MHz, 20% CD_3OD/Chloroform-*d*) δ 7.10 (s, 4H), 6.71 (d, *J* = 2.1 Hz, 1H), 6.55 (d, *J* = 2.1 Hz, 1H), 5.28 – 5.22 (m, 2H), 5.08 (d, *J* = 24.2 Hz, 1H), 4.90 (s, 2H), 4.25 (s, 1H), 4.05 (s, 1H), 3.84 (s, 4H), 2.51 (s, 2H), 2.35 (s, 3H), 2.29 (s, 4H), 2.24 – 2.14 (m, 9H), 1.97 – 1.87 (m, 6H), 1.59 (s, 6H), 1.50 (s, 8H), 1.33 – 1.01 (m, 85H), 0.85 – 0.73 (m, 14H). Alkyl region a bit high. ESI-MS (negative mode): $[M-H]^-$ calcd for $C_{62}H_{100}N_2O_{13}P$: 1111.6963, found: 1111.8591



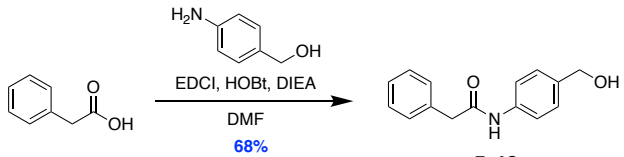
5.47

4-Acetamidobenzyl (4-nitrophenyl) carbonate (5.47)

4-Acetamidobenzyl alcohol (0.1 g, 0.605 mmol) was dissolved with 5 mL EtOAc (sieve-dried) under nitrogen in a 50 mL RBF at 0 °C. Pyridine (0.146 mL, 1.82 mmol) was then added, followed by addition of *p*-nitrophenol chloroformate (0.393 g, 1.82 mmol). The reaction was stirred overnight before being diluted with 100 mL DCM. The resulting mixture was further washed with 100 mL saturated $NaHCO_3$ solution, 100 mL water as well as 100 mL brine. The collected organic phase was dried over Na_2SO_4, filtered, and concentrated under reduced pressure. Solid started to precipitate out during rotary evaporation, which has poor solubility in DCM but was confirmed to be the desired product later. The crude was loaded onto silica gel (considering its solubility) and subjected to silica gel column chromatography. Gradient elution from hexanes to 50% EtOAc in hexanes was needed to yield the product as a pale-

yellow solid (0.1 g, 0.3 mmol, 50% yield). R_f = 0.25 (50% EtOAc-hexanes). The product has low solubility in chloroform and only ^{1}H NMR was obtained.

^{1}H NMR (300 MHz, Chloroform-*d*) δ 8.35 – 8.20 (m, 2H), 7.55 (d, *J* = 8.3 Hz, 2H), 7.47 – 7.31 (m, 4H), 5.25 (s, 2H), 2.20 (s, 3H).



5.49

***N*-(4-(Hydroxymethyl)phenyl)-2-phenylacetamide (5.49)**

Phenyl acetic acid (0.5 g, 3.67 mmol), 4-aminobenzyl alcohol (0.497 g, 4.04 mmol), and HOBt (0.561 g, 3.67 mmol) were combined in a 50 mL RBF under argon. 5 mL dry DMF was used to dissolve all the starting material. After cooling down to 0 °C, EDCI (0.7035 g, 3.67 mmol) as well as DIEA (1.52 mL, 9.175 mmol) were added. The reaction was stirred overnight at room temperature before being quenched by pouring into 150 mL 1 N HCl. 3×50 mL EtOAc was used to extract the aqueous phase. The combined organic layer was further washed with 5×100 mL water and 100 mL brine. After being dried over Na_2SO_4, filtered, and concentrated under reduced pressure, the crude was loaded onto silica gel and subjected to silica gel column chromatography. Gradient elution from hexanes to 100% EtOAc was needed to yield the product as a yellow solid (0.65 g, 2.69 mmol, 73%). R_f = 0.45 (75% EtOAc-hexanes).

^{1}H NMR (500 MHz, 20% CD_3OD/Chloroform-*d*) δ 7.38 – 7.33 (m, 2H), 7.31 – 7.15 (m, 7H), 4.49 (s, 2H), 3.61 (s, 2H). ^{13}C NMR (126 MHz, 20% CD_3OD/$CDCl_3$) δ 170.15, 137.18, 137.06, 134.74, 129.28, 128.89, 127.58, 127.31, 120.14, 64.21, 44.21, 41.19.

Preparation of liposomes for Nile red (NR) release studies

Enzyme-responsive lipids, bulk lipids and NR stock solutions were prepared in either chloroform or MeOH/chloroform mix and stored in -20 °C freezer. Proper volumes of each stock solution were pipetted into a small vial to obtain the desired percentage of each lipid. NR

was added as 5% of the total lipid content. The solvents were then evaporated under nitrogen stream and the resulting lipid film was further dried under vacuum for at least one hour. After that, the appropriate buffer or water was added into the vial. For **ERL** and **GRL** containing liposomes, 1×TBS (pH=8, containing 25 mM Tris/Tris HCl, 0.13 M NaCl, 0.0027 M KCl) was used. For **PRL** containing liposomes, 1×TBS with cation activators (pH=8, containing 25 mM Tris/Tris HCl, 0.13 M NaCl, 0.0027 M KCl, 0.25 mM $MgCl_2$ and 0.25 mM $ZnCl_2$) was used. The concentration of the total lipid content used in this release assay was 2 mM. The film was hydrated in a 60 °C water bath for 4 sets of 15 min with vortexing after each set, followed by ten freeze-thaw cycles using a dry ice-acetone bath and 60 °C water bath. Finally, the solutions were extruded through a 200 nm polycarbonate membrane for 15 passes with a LiposoFast extruder (Avestin, Inc.). The resulting liposomes were stored at 4 °C and were used up within two days.

Enzyme stock preparation

The esterase stock solution was prepared in 1×TBS (pH=8, containing 25 mM Tris/Tris HCl, 0.13 M NaCl, 0.0027 M KCl) at a concentration of 3 mg/mL. According to LOT bioactivity analysis and unit definition provided by Sigma-Aldrich, the unit concentration was ~45 U/mL. The stock solutions were divided into small aliquots in Eppendorf tubes and stored in a -20 °C freezer until their use. Alkaline phosphatase was used directly after purchasing. According to the LOT bioactivity analysis, the unit concentration was 350 U/mL. The solution was stored in a 4 °C fridge. β-Galactosidase was also used directly after purchasing. According to the LOT bioactivity analysis, the unit concentration was 550 U/mL. The solution was stored in 4 °C fridge. Denatured enzyme solutions were prepared by heating the above-mentioned stock solutions in a 60 °C water bath for one hour and then slowly cooling back down to room temperature.

Nile red release studies with enzyme addition

A 100 μL aliquot of the prepared 2 mM liposome solution was added into a sub-micro quartz cuvette. Enzyme was added directly into the cuvette (esterase: 10 μL enzyme stock (0.45 U), β-galactosidase: 1 μL enzyme stock (0.55 U), alkaline phosphatase: 1 μL enzyme stock (0.35 U)). The cuvettes were heated in a 30 °C water bath in between measurements. Buffer control sets were also done by switching enzyme solution into either TBS or ammonia sulfate buffer based on the buffers used for the different enzymes used in study. Fluorescence intensity was then measured over time (excitation wavelength=552 nm). For **GRL** and **ERL**, spectrometer settings were: excitation slit=5 nm, emission slit=5 nm. For **PRL**, these were: excitation slit=5 nm, emission slit=10 nm. When processing the data, fluorescence intensities at 635 nm were selected. Experiments were run at least 3 times, each with different batches of liposomes, and averaged data were reported with error bars showing standard error.

Preparation of liposomes for sulforhodamine B (SRB) studies

The same lipid stocks prepared for NR study were used. SRB sodium salt was dissolved with 1×TBS (pH=8, containing 25 mM Tris/Tris HCl, 0.10 M NaCl, 0.0027 M KCl) to produce a 20 mM solution. Proper volumes of each stock solution were pipetted into a small vial to obtain the desired percentage of each lipid. The solvents were evaporated under nitrogen stream and the resulting lipid film was further dried under vacuum for at least one hour. After that, the lipid film was hydrated with 20 mM SRB stock solution in a 60 °C water bath for 4 sets of 15 min with vortexing after each set, followed by ten freeze-thaw cycles in a dry ice-acetone bath and a 60 °C water bath. Then, the solutions were extruded through a 200 nm polycarbonate membrane for 15 passes with a LiposoFast extruder (Avestin, Inc.). Finally, the unencapsulated dye was removed with a size exclusive column (SEC). Sephadex G-50 used for SEC was pre- equilibrated with 1×TBS (pH=8, containing 25 mM Tris/Tris HCl, 0.13 M NaCl, 0.0027 M KCl) for at least one hour prior to use. A micro-column was used for separation and gravity elution was sufficient for separation. Fractions were collected every ~1mL, and the first

fraction showing pink color was usually the liposome solution, which was further checked by adding Triton X-100 under a UV lamp, after which an increase in fluorescent intensity was observed denoting the release of encapsulated dye.

SRB release assays with esterase addition

A 100 μL aliquot of the prepared liposome solution was added into a sub-micro quartz cuvette. Esterase stock solution (10 μL, 3 mg/mL, 0.45 U) was added directly into the cuvette to a final concentration of 0.27 mg/mL. The cuvette was heated in a 30 °C water bath in between measurements. Buffer control sets were also performed by switching enzyme solution into TBS buffer and performing the same readings. Fluorescence intensity was then measured over time (excitation wavelength=550 nm, excitation slit=10 nm, emission slit=2.5 nm). After completion, 1 μL of an aqueous 20% Triton X-100 solution was added to trigger complete release. When processing the data, fluorescence intensities at 590 nm were selected and fluorescence increases were reported as a percentage of the fluorescence after triton X-100 treatment for each sample. Experiments were run at least 3 times each with different batches of liposomes, and averaged data were reported with error bars showing standard error.

DLS analysis of particle sizes before and after the enzyme treatment

DLS measurements were carried out with a Malvern Zetasizer Nano ZS instrument equipped with a 4.0 mW laser operating at λ=633 nm. Samples were prepared by diluting the liposome solutions before or after adding enzyme by 10x with the proper matching buffer. As an example, a 5 μL of the liposome solution was added into 45 μL of proper buffer in a micro cuvette for measurement. All samples were determined at a scattering angle of 173° at 25 °C. The reported data were the average of three tests with error bars showing standard error.

TLC analysis of esterase modification of free ERL

ERL stock solution (1 μL of a 5 mM solution, ~2 μg lipid) was pipetted into a small Eppendorf

tube and the solvent was removed under nitrogen flow. After further drying under high vacuum for 15 min, 50 μL TBS buffer was added into the Eppendorf tube. Vigorous vortexing for 10 minutes was performed to ensure that all of the **ERL** was dissolved. Next, 0.45 U esterase (10 μL, 45 U/mL) was added, and the reaction mixture was left at room temperature for three hours. After that time, the reaction mixture, and separate standards for enzyme stock, DOPE and **ERL** were spotted onto a normal aluminum backed TLC plate. To make sure all of the solvent was removed, the plate was placed under vacuum for 15 minutes before developing with 20% MeOH-$CHCl_3$ as eluant. The plate was visualized with $KMnO_4$ stain after developing.

Colorimetric assay of enzyme activities

Colorimetric assays were performed for galactosidase and phosphatase using commercially available 4-nitrophenyl β-D-galactopyranoside and 4-nitrophenyl phosphate disodium salt hexahydrate (pNPP). For galactosidase, a 66 mM solution of 4-nitrophenyl β-D-galactopyranoside was prepared in 1×TBS, pH=8. To 100 μL of substrate solution, 1 μL galactosidase (0.55 U/μL in 1.6 M $(NH_4)_2SO_4$) was added. The color change from colorless to bright yellow was observed with the bare eye immediately after enzyme addition (Figure 5.5B). For phosphatase, 60 mM phosphatase substrate was also prepared in 1×TBS, pH=8. To 100 μL substrate solution, 1 μL phosphatase was added (0.35 U/μL in 2.5 M $(NH_4)_2SO_4$). The color change from colorless to bright yellow was also determined with bare eye immediately after enzyme addition as is shown in Figure 5.5A.

Liposome stability test

The same liposome samples containing egg PA in formulations used for NR release studies were prepared as previously described. The stability and dye retention properties of the liposomes were tracked by measuring the encapsulated NR fluorescence. When not taking measurements, liposomes were stored in a 4 °C fridge. Fluorescence intensity was measured every 24 hours (excitation wavelength = 552 nm, excitation slit = 5 nm, emission slit = 5 nm).

When processing the data, fluorescence intensities at 635 nm were selected. Experiments were run with three different batches of liposomes, and averaged data were reported with error bars denoting standard error.

Chapter 6. Development of ROS-responsive liposomes

(The scientific data used in this Chapter has been published by the authors: Lou, Jinchao; Best, Michael D., Reactive oxygen species-responsive liposomes via boronate-caged phosphatidylethanolamine. *Bioconjugate Chem.* **2020,** 31, 2220−2230.)

6.1. Project overview

Although a number of stimuli have been explored for triggering liposomal release, reactive oxygen species (ROS), which have received significantly less attention, provide excellent targets due to their key roles in biology and overabundance in diseased cells. In this Chapter, we report a ROS-responsive liposome platform through the inclusion of lipid **6.1** bearing a boronate ester headgroup and a quinone-methide (QM)-generating SIL attached onto a DOPE lipid scaffold. Fluorescence-based dye release assays validated that this system enables release of both hydrophobic and hydrophilic contents upon hydrogen peroxide (H_2O_2) addition. Details of the release process were carefully studied, and data showed that oxidative removal of the boronate headgroup is sufficient to result in hydrophobic content release, while production of DOPE is needed for hydrophilic cargo leakage. These results showcase that lipid **6.1** can serve as a promising ROS-responsive liposomal delivery platform for controlled release.

6.1.1. Introduction of ROS and ROS-responsive nanocarriers

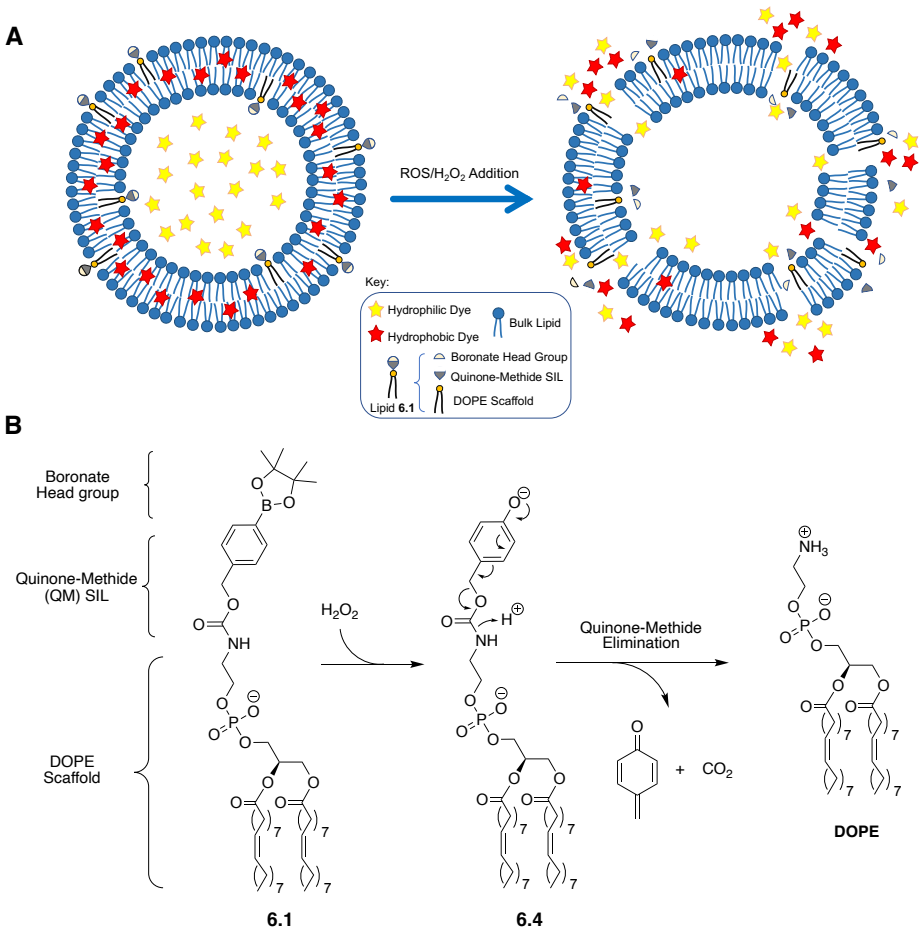
Typical ROS include hydrogen peroxide (H_2O_2), singlet oxygen ($^1O_2$), superoxide ($O_2^{\cdot-}$) and hydroxyl radicals ($HO^{\cdot}$), all of which are single electron reduction products from oxygen and normally interchangeable within biological systems through a series of cascade reactions.[267] ROS play crucial roles in metabolism,[268] regulation of various biological and physiological processes,[269] and are normally maintained at low levels by reduction-oxidation balance.[270] Upregulated ROS, however, produce oxidative stress, which can irreversibly damage cellular compartments resulting in numerous pathological conditions including aging, cancer,

inflammation, etc.[271-273] It has been shown that cancer cells have ROS concentrations that are about two orders of magnitude higher than those in normal cells (~100 μM compared to ~20 nM).[274] Thus, ROS provide an exciting target for triggered release drug delivery platforms.

Outside of liposomes, different ROS-responsive nanocarriers have been developed based on various oxidation mechanisms exploiting different functional groups.[275,276] However, reports of ROS-responsive liposomes remain sparse. There is one recent example reported by the Li group, which utilized thioether-functionalized phosphatidylcholine liposomes that can form stable bilayers.[277] Upon addition of H_2O_2, the hydrophobic thioethers are oxidized into hydrophilic sulfoxides/sulfones, altering the membrane properties and ultimately causing the release of encapsulated hydrophilic doxorubicin (DOX). In sensor development, arylboronic acid/ester moieties have been applied for ROS-responsive materials due to their fast degradation kinetics upon H_2O_2 contact.[278,279]

6.2. Design and synthesis of the ROS-responsive lipid 6.1

In this Chapter, we report a ROS-responsive liposome system exploiting lipid **6.1**, containing a H_2O_2-responsive arylboronic ester headgroup attached to DOPE, as shown in Scheme 6.1. The arylboronic ester is included since this moiety can undergo oxidization by H_2O_2 through insertion of an oxygen atom into the carbon-boron bond leading to phenol intermediate **6.4**. This phenol was designed as part of a quinone methide- (QM-) generating functionality linked via a carbamate group that acts as a SIL, which is a strategy widely used in nanomedicine and sensor development.[244,245] Upon the cleavage of trigger groups, SILs undergo fast decomposition to release caged moieties such as fluorophores or drugs. In our specific case, boronate oxidative cleavage was designed to trigger QM elimination and decarboxylation to release DOPE.



Scheme 6.1. Design strategy for ROS-responsive liposomes. A. Cartoon illustration of liposomal release driven by ROS/ H_2O_2 addition. **B.** Structure of ROS-responsive lipid **6.1** and its decomposition mechanism upon stimulus addition. The boronate headgroup of **6.1** is expected to be oxidatively cleaved by H_2O_2, leading to SIL breakdown, which releases the non-bilayer forming lipid DOPE that can disrupt membrane integrity and trigger encapsulated cargo release.

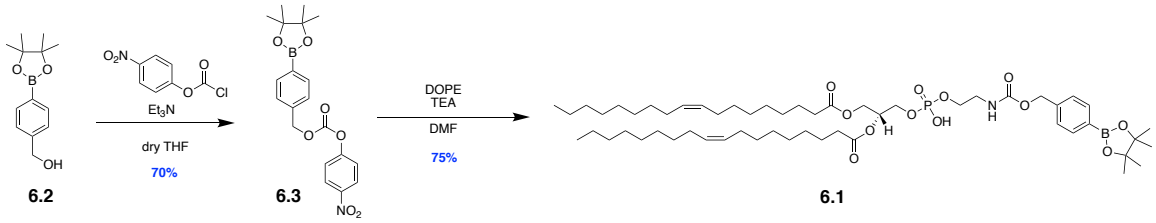
To realize the goal of encapsulated cargo release, robust liposomes that are sufficiently stable to survive circulation can be designed to undergo significant alterations to lipid packing properties upon encountering the desired stimulus. Adapting a similar strategy as described in Chapter 5, lipid **6.1** was designed to form stable liposomes prior to trigger removal. After the addition of H_2O_2, the formation of the non-bilayer lipid DOPE was designed to disrupt membrane and cause the release of the encapsulated liposomal contents. Multiple successful examples of stimuli-responsive liposomes have been reported in which the generation of DOPE is harnessed to drive release in the presence of stimuli including reduction conditions,[195] light[239] and enzymes,[280] which is showcased in Chapter 5.

The synthetic route to lipid **6.1** is shown in Scheme 6.2, which involves an efficient two-step synthesis. *p*-Nitrophenol carbonate compound **6.3** was first synthesized by treating commercially available compound **6.2** with 4-nitrophenol chloroformate,[281] which was then treated with DOPE to form the desired product **6.1**.

6.3. Hydrophobic release assays using Nile red

6.3.1. Initial studies

Upon successful synthesis of the desired trigger lipid, we next moved to evaluate its release properties with fluorescence-based dye release assays. The first assay involved lipophilic dye NR. The NR release properties of liposomes containing different percentages of **6.1** (0-100%) mixed with the remaining percentage of PC (egg, mixed isomers) were first investigated (Figure 6.1). We prepared these NR-encapsulated unilamellar liposomes with standard liposome preparation methods including lipid film formation, hydration, freeze-thaw, and extrusion through 200 nm polycarbonate membranes. The formation of stable liposomes with desired diameters was also confirmed by dynamic light scattering (DLS) analysis, which will be discussed later in this Chapter. After an initial scan, each liposome sample was treated with H_2O_2 and the fluorescence intensities were measured over time at room temperature. As is



Scheme 6.2. Synthetic route developed to produce ROS-responsive lipid 6.1. Compound **6.2** was reacted with *p*-nitrophenol chloroformate to form **6.3**, which was next treated with DOPE to afford **6.1**.

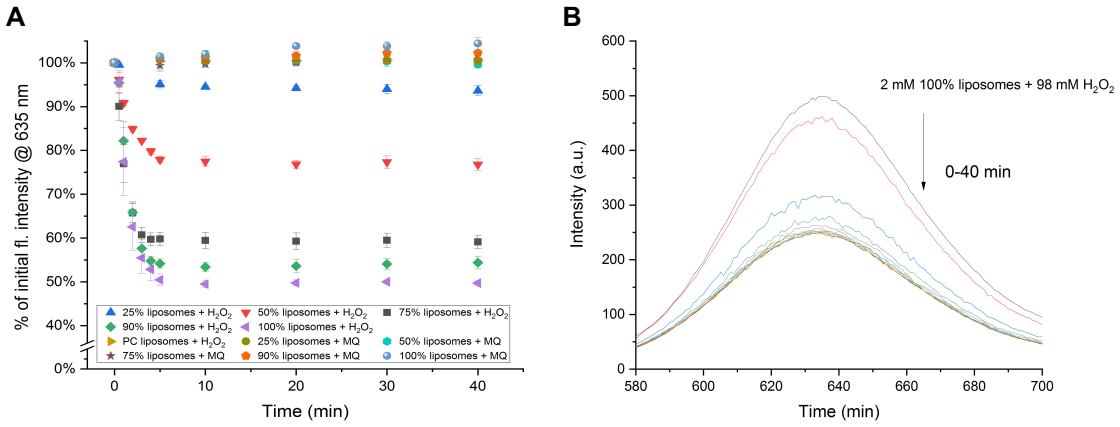


Figure 6.1. Nile red release profiles for liposomes containing various percentages (0-100%) of lipid 6.1 mixed with PC as the remaining percentage after adding 98 mM H_2O_2. **A**. Dose-dependent release curve showing that the extent of release is dependent on the percentage of lipid **6.1**. When more than 75% lipid **6.1** was present, over 40% release was observed within five minutes after adding H_2O_2. Minimal release was seen for all control experiments. All data represent the averages of at least three replicates with error bars denoting standard errors. **B.** Sample raw fluorescence emission spectra for 2 mM NR-containing liposomes composed of 100% lipid **6.1** after adding 98 mM H_2O_2. Fluorescence intensities were recorded over time. (Ex. Wavelength=552 nm, ex. Slit=5 nm, em. Slit=5 nm)

shown in Figure 6.1A (sample raw spectra in Figure 6.1B), we observed an immediate drop in NR fluorescence after adding H_2O_2 only when lipid **6.1** was present within the liposome bilayer. While inclusion of 25% of lipid **6.1** within PC liposomes only led to an ~5% fluorescence decrease attributed to release, dose-dependent release was observed depending on this percentage. Specifically, fluorescence decreases upon H_2O_2 addition were enhanced to ~25% with 50% lipid **6.1**, and a steep drop of ~40% was observed when 75% lipid **6.1** was incorporated. Further increasing the percentage of lipid **6.1** to 90% or 100% improved the release to ~45% and 50%, respectively. One interesting note is that these release processes all showed fast kinetics, particularly compared to other liposome release strategies. In all cases, release reached a plateau within five minutes after H_2O_2 addition. Negative control experiments were also done by adding H_2O_2 into 100% PC (egg, mixed isomers) liposomes or simply adding MilliQ purified water (MQ) into lipid **6.1** containing liposomes. In all the control experiments, no background release was observed over time.

To verify that the fluorescent decrease is indeed caused by NR release rather than bleaching from H_2O_2, additional control experiments were carried out. As is shown in Figure 6.2, no obvious intensity decrease could be observed when NR alone was treated with H_2O_2 in MeOH or MeOH/H_2O. Also, NR fluorescence could be fully restored when liposomes that had undergone triggered release were subjected to Triton X-100 detergent (Figure 6.3). These results showcase that liposomes containing ROS-responsive lipid **6.1** serve as effective carriers and triggered release systems for hydrophobic contents driven by H_2O_2 addition. Furthermore, the extent of release can be carefully tuned based on the percentage of **6.1** in the membrane.

6.3.2. NR release with different concentrations of peroxide

The NR release properties were further investigated by treating 2 mM samples of liposomes containing 75% of ROS-responsive lipid **6.1** and 25% PC with different concentrations of

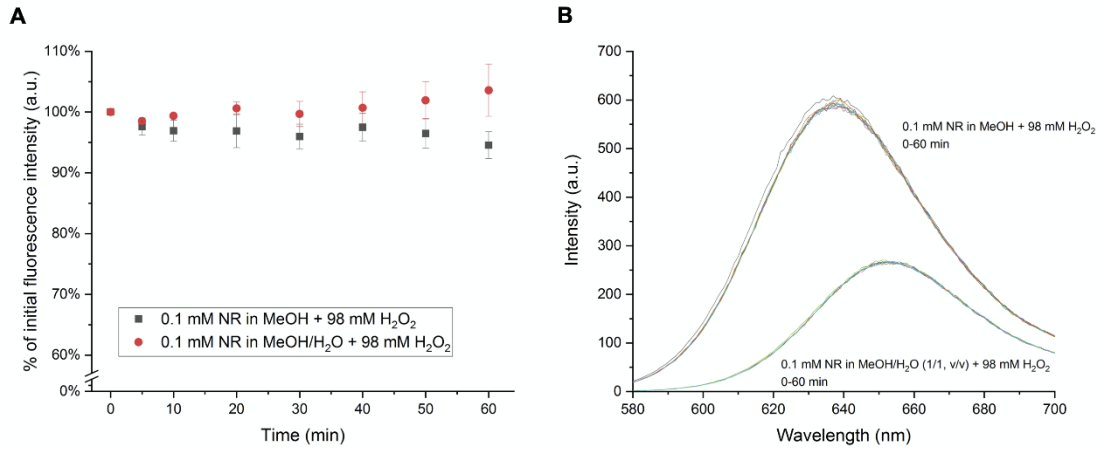


Figure 6.2. NR fluorescence intensity change over time when treating NR with excess H_2O_2 in MeOH or MeOH/H_2O. A. No significant intensity decrease could be observed within 60 min. Error bars indicate standard errors from three experiments. **B.** Sample raw fluorescence emission spectra (Ex. Wavelength=530 nm, ex. Slit=5 nm, em. Slit=5 nm).

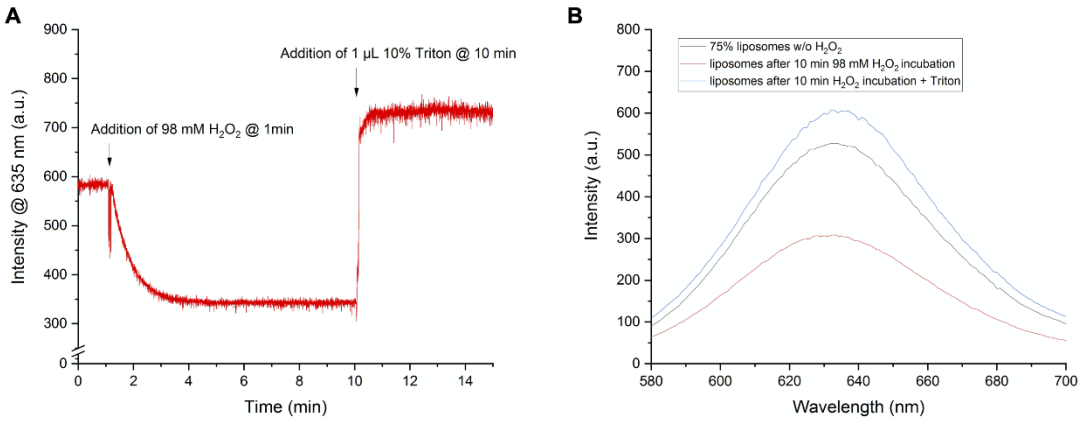


Figure 6.3. Triton addition to liposomes post NR release. A. Kinetic curve of NR fluorescence in liposomes at 635 nm after adding H_2O_2 and then later Triton X-100. PC liposomes containing 75% **6.1** were first treated with H_2O_2 to trigger content release as is indicated by decrease in NR fluorescence. After plateauing, Triton X-100 was added to re-dissolve NR, which restored its fluorescence. **B.** Full fluorescence emission spectra before release, after H_2O_2 addition and after Triton X-100 addition. (Ex. Wavelength=552 nm, ex. Slit=5 nm, em. Slit=5 nm)

hydrogen peroxide (ranging from 0-98 mM). The results indicate the sensitivity towards H_2O_2 and are shown in Figure 6.4 (sample raw fluorescence spectra in Figure 6.4B), in which the release properties correlated with the amount of peroxide added. For samples in which an excess amount of H_2O_2 was added (3.27 mM and 98 mM), the same ending point was observed at 40% release, with the latter case exhibiting faster kinetics. In addition, lowering the H_2O_2 concentration below that of lipid **6.1** was observed to minimize the extent of release. For example, when the amount of H_2O_2 added (0.98 mM) fell to ~60% of the amount of lipid **6.1** present, the extent of release dropped to ~25%. Further lowering the H_2O_2 concentration to 0.196 mM lowered the content release to 6%. These results again indicate ROS responsive lipid **6.1** plays an important role in hydrophobic content release. As previously discussed, certain cancer cells have been shown to contain overabundant ROS concentrations (~100 μM) compared to healthy cells (~20 nM).[274] The results shown in Figure 6.4 indicate that liposomes containing 75% of **6.1** begin to show a small amount of release in the former concentration range. While this would need to be improved for clinical viability by developing liposomes tuned to maximize content release at upregulated ROS concentrations while minimizing release at normal ROS levels, the current work is nevertheless an important step towards ROS-responsive delivery systems.

6.3.3. NR release with diluted liposomes

Liposome release was also studied using samples with lower liposome concentrations to further probe for potential release properties involving interactions between liposomes, such as fusion (Figure 6.5A, sample raw spectra in Figure 6.5B). In these experiments, release was still observed when the liposome concentration was lowered from 2 mM to 0.1 mM. Specifically, upon treatment with 3.27 mM of H_2O_2, 2 mM liposomes showed ~40% release compared to ~25% release from 0.1 mM liposomes. Control experiments were also performed by treating 0.1 mM liposomes with MQ water. No decrease in fluorescence intensity was observed, indicating that these liposomes are stable at least within the release time period. This is also

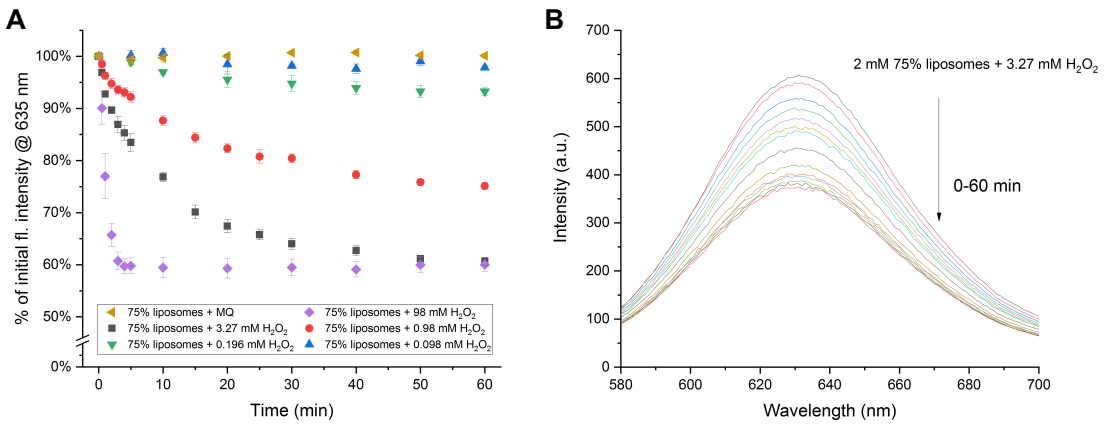


Figure 6.4. Nile red release profiles for PC liposomes containing 75% of lipid 6.1 after addition of varying concentrations of H_2O_2. A. Dose-dependent release curve. The extent of release is dependent on the amount of H_2O_2 added. When excess peroxide was added (3.27 mM or 98 mM), ~40% release was observed over time. Further lowering H_2O_2 concentration led to diminished release. All data represent the averages of at least three replicates with error bars denoting standard errors. **B.** Sample raw fluorescence emission spectra for 2 mM PC-based liposomes encapsulating NR containing 75% lipid **6.1** after adding 3.27 mM H_2O_2. Fluorescence intensities were recorded over time. (Ex. Wavelength=552 nm, ex. Slit=5 nm, em. Slit=5 nm)

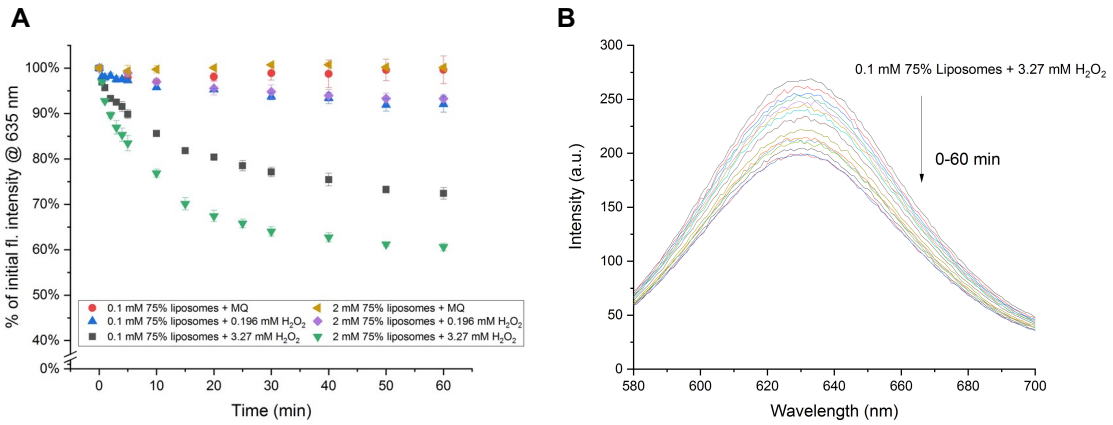


Figure 6.5. Nile red release profiles using different concentrations of PC-based liposomes containing 75% of 6.1. A. 0.1 mM liposomes showed comparable results to 2 mM liposomes when being treated with 0.196 mM H_2O_2, while slightly less release was observed when these were treated with 3.27 mM H_2O_2. Control experiments in which 2 mM and 0.1 mM liposomes were treated with MQ did not show background release. Error bars denote standard errors from at least three independent experiments. **B.** Sample raw fluorescence emission spectra for 0.1 mM PC-based liposomes encapsulating NR containing 75% lipid **6.1** after adding 3.27 mM H_2O_2. Fluorescence intensities were recorded over time. (Ex. Wavelength=552 nm, ex. Slit=5 nm, em. Slit=10 nm)

supported by DLS experiments showing liposomes of the expected sizes were formed at these low liposome concentrations (Figure 6.6). Minimal changes in particle size were observed for these samples before and after release as well. Although slight decreases in release extent were observed, the modest changes in NR release properties upon a dramatic reduction in liposome concentration, combined with the lack of changes in DLS before and after peroxide treatment, provide further evidence that release is not entirely driven by processes involving contact between liposomes such as fusion.

6.4. Dynamic light scattering studies

During these studies, we probed potential changes in liposome particle sizes by conducting DLS experiments before and after content release (Figure 6.7, raw distribution curves in Figure 6.8). All the liposomes used in this study initially showed uniform sizes at ~150 nm pre H_2O_2 treatment (grey bars, Figure 6.7), which is expected since all the samples were extruded through 200 nm membrane during preparation. However, following H_2O_2 addition, we did not observe any significant changes in particle sizes in any of these cases (red bars, Figure 6.7).

6.5. Transmission electron microscopy studies

The lack of changes to liposome structures was further supported by TEM experiments performed by negative staining of PC-based liposomes containing 0% or 75% of lipid **6.1** with neutral phosphotungstic acid. As is shown in Figure 6.9, in both of these cases intact liposomes were observed after at least 2-hr hydrogen peroxide treatment. These results indicate that the change in membrane properties is not significant enough to cause reorganization of lipids into different assemblies or induce processes such as fusion. In fact, this result is likely preferable for drug delivery applications compared to radical changes that commonly lead to larger and aggregated lipid self-assemblies that are likely problematic *in vivo*. We have previously observed that the extent of liposome size changes varies among different triggered release systems. Specifically, we developed light-[104] and phosphatase-responsive liposomes (Chapter

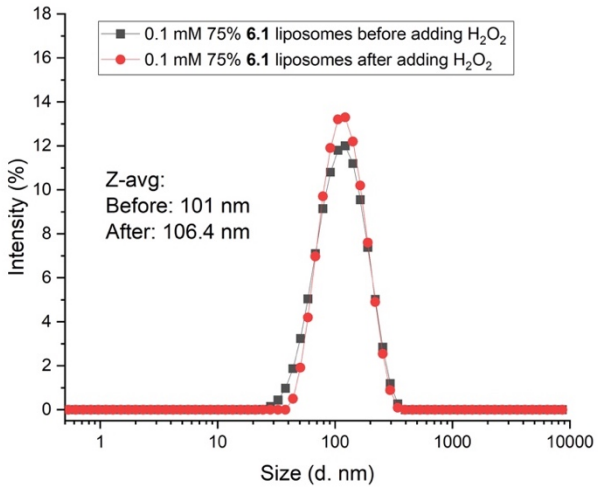


Figure 6.6. DLS size distribution plots for 0.1 mM PC-based liposomes containing 75% 6.1 before and after H_2O_2 addition. Stable liposomes were formed and no obvious changes in particle size could be observed after H_2O_2 treatment.

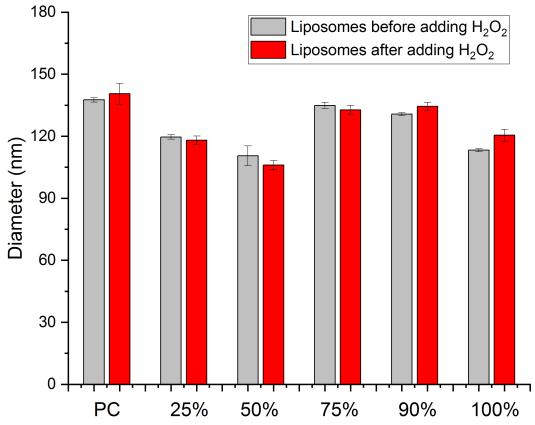


Figure 6.7. DLS analysis of NR-encapsulated liposomes containing different percentages of lipid 6.1 (0-100%) mixed with the remaining percentage of PC before and after H_2O_2 addition. All of these formed stable and uniform liposomes before H_2O_2 treatment. Minimal changes in particle size were observed after triggering release in each case. Error bars presented indicate standard errors from at least three studies.

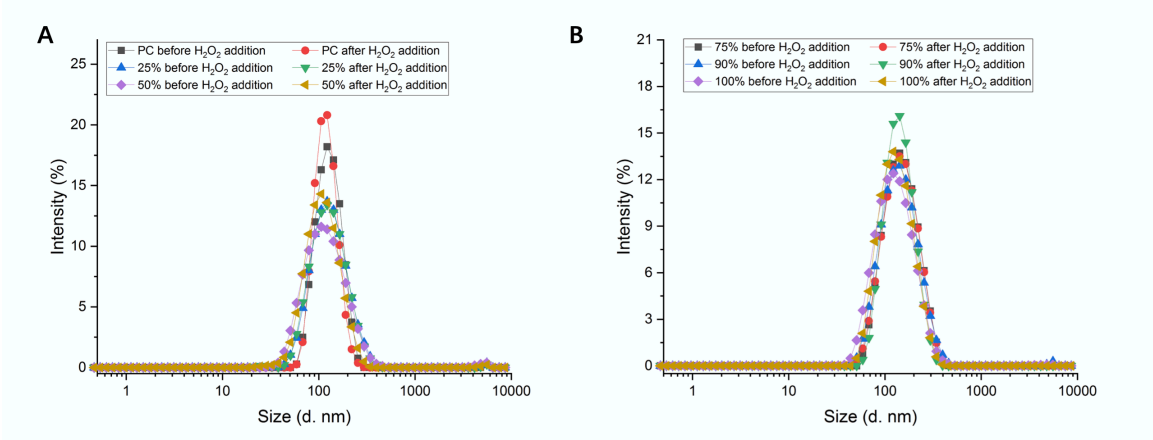


Figure 6.8. Raw DLS size distribution plots for liposomes containing 6.1 used in NR release assays. A. PC based liposomes containing 0, 25% and 50% lipid **6.1** before and after adding H_2O_2. **B.** PC based liposomes containing 75%, 90% and 100% lipid **6.1** before and after adding H_2O_2. Samples are separated for the sake of clarity.

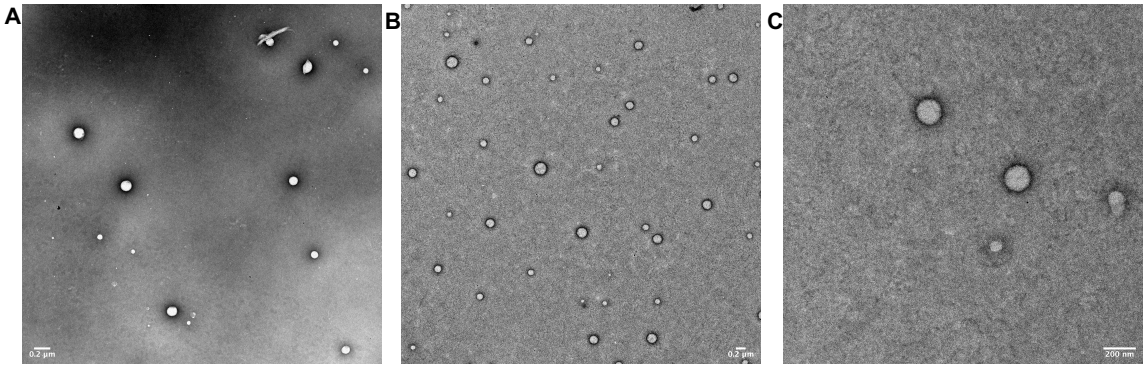


Figure 6.9. TEM images of A. liposomes composed of 100% PC after H_2O_2 treatment, and B. and C. liposomes containing 75% of lipid 6.1 and 25% PC after H_2O_2 incubation. Liposomes were stained with a 1.0% (w/v) solution of neutral phosphotungstic acid. In all cases, traditional circular liposome cross-section structures were observed under the microscope. Scale bars denote 200 nm.

5)[280] that both resulted in a significant amount of NR release despite minimal changes in particle size observed by DLS, which is similar to the results observed in this ROS-responsive system.

6.6. Hydrophilic dye release assay with ANTS/DPX

Benefitting from their unique structure, liposomes can not only encapsulate hydrophobic drugs, but are also able to transport hydrophilic drugs within their aqueous core. We next performed a FRET-based dye leakage assay to evaluate the hydrophilic content release behavior of liposomes containing **6.1**. This assay utilizes the FRET pair of 8-aminonaphthalene-1,3,6-trisulfonic acid (ANTS) as well as the quencher *p*-xylene-bis-pyridinium bromide (DPX), which is widely used in assessing liposome permeability.[282] Both of the dyes are co-encapsulated within the aqueous core leading to initially quenched fluorescence. After membrane disruption and release of the encapsulated contents, an increase in ANTS fluorescence is observed upon release due to dilution that diminishes the quenching effect of DPX. Since the dyes are non-specifically encapsulated, it is necessary to perform a SEC following normal liposome preparation procedures to remove any unencapsulated dye.

Our initial attempts at ANTS/DPX release, which utilized the same PC-based liposomes containing different percentages of **6.1** previously described for NR release, turned out to be unsuccessful. This was our first inkling that the process by which polar dyes were released may be different than that of non-polar dye leakage. As a result, we experimented with different formulations other than **6.1**/PC for polar content release. This was done by pursuing different lipid mixtures to tune liposome stability such that these would be stable enough to retain the encapsulated content but could be destabilized by modifying membrane properties upon stimulus treatment. Ultimately, we settled on a formulation in which ANTS and DPX were co-encapsulated within liposomes containing 30% lipid **6.1**, 10% egg PC, 50% DOPE as well as 10% phosphatidic acid (PA), which is a mixture we showed to be effective for cargo release

previously through systematic studies of liposome formulations for various enzyme-responsive liposomal systems in Chapter 5.[280] After adding H_2O_2 into these liposomes, the fluorescence intensities were measured over time at room temperature. At the end of the release process, Triton X-100 was used to lyse the liposomes and induce complete release of contents. When reporting the data, the results were normalized as a percentage of fluorescent increase compared to Triton X-100 treatment. As can be seen in Figure 6.10 (sample raw spectra in Figure 6.11), liposomes containing lipid **6.1** showed a significant fluorescent increase after H_2O_2 addition within five hours. Similarly, control experiments were also conducted by replacing lipid **6.1** with DPPC or instead titrating MilliQ purified water (MQ) into liposomes containing lipid **6.1**. Minimal release was observed for both of the control experiments.

Once again, the successful formation of stable membranes was demonstrated by DLS analysis (Figure 6.12, raw distribution curves in Figure 6.13) and we did not observe significant changes in liposome particle sizes despite release. Nevertheless, these results demonstrate that **6.1** is effective for developing ROS responsive liposomes that can encapsulate and release either hydrophobic or hydrophilic dyes.

Similar to the NR release studies, the ANTS/DPX assay was also carried out with liposomes at lower concentrations. Liposomes diluted 10X showed comparable release properties, as is shown in Figure 6.14, which again argues against cargo escape driven by inter-liposome processes such as fusion or contact-mediate lysis.

6.7. Mechanistic studies

6.7.1. Evidence for the formation of DOPE

6.7.1.1. Time-dependent NMR titration experiment

At this point we were intrigued by the different properties we observed for **6.1**-containing liposomes in terms of hydrophobic and hydrophilic content release behavior, and particularly

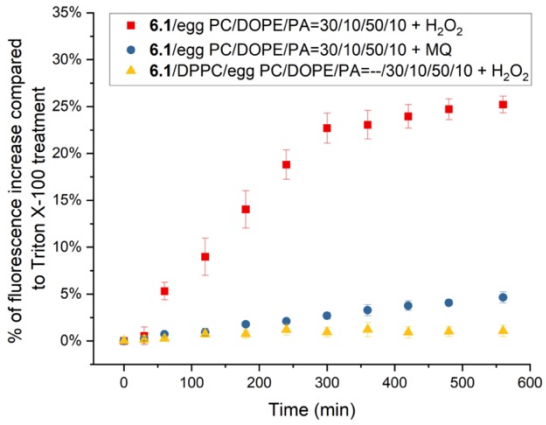


Figure 6.10. Hydrophilic dye release results using liposomes containing 30% lipid 6.1, 50% DOPE, 10% PC and 10% PA utilizing an ANTS/DPX leakage assay. Increases in ANTS fluorescence, reported relative to maximum fluorescence upon Triton X-100 addition, were only observed for liposomes containing **6.1** with H_2O_2 treatment. Error bars indicate standard errors from at least three experiments.

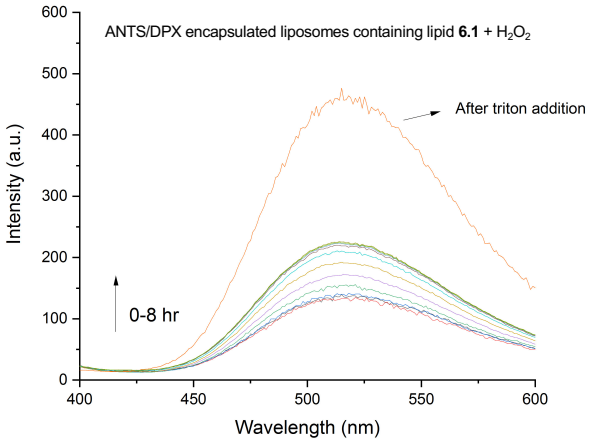


Figure 6.11. Sample raw fluorescence emission spectra for liposomes containing 30% lipid 6.1, 10% egg PC, 50% DOPE and 10% PA used in ANTS/DPX release assay after H_2O_2 addition. Fluorescence intensities were recorded over time. (Ex. Wavelength=350 nm, ex. Slit=10 nm, em. Slit=10 nm)

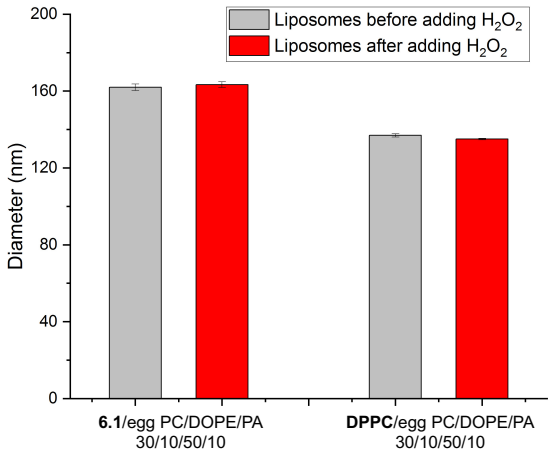


Figure 6.12. DLS results using liposomes containing 30% lipid 6.1, 50% DOPE, 10% PC and 10% PA before and after release via the ANTS/DPX assay. Uniformly sized stable liposomes were initially formed. Minimal changes in particle sizes were observed after adding H_2O_2. Error bars presented indicate standard errors from at least three studies.

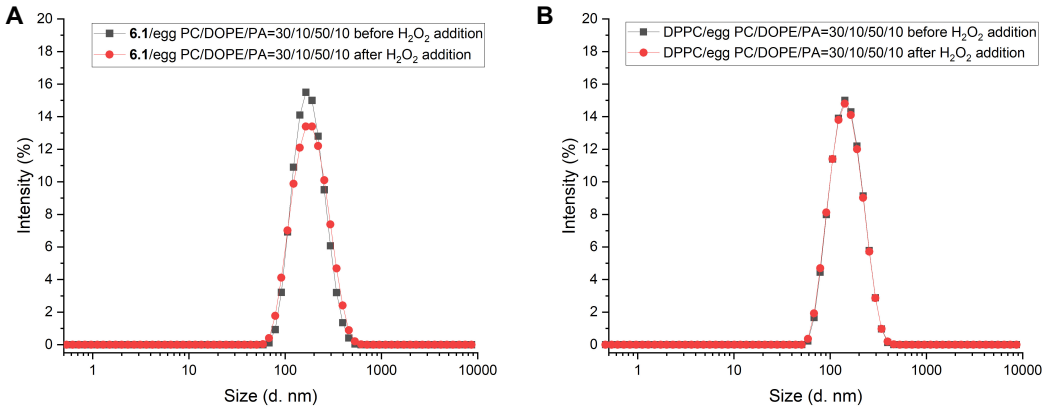


Figure 6.13. Raw DLS size distribution plots for liposomes used in ANTS/DPX release assays. A. Liposomes containing 30% lipid **6.1**, 10% egg PC, 50% DOPE, and 10% PA before and after adding H_2O_2. **B**. Control liposomes containing 30% DPPC, 10% egg PC, 50% DOPE and 10% PA before and after adding H_2O_2. Samples are separated for the sake of clarity.

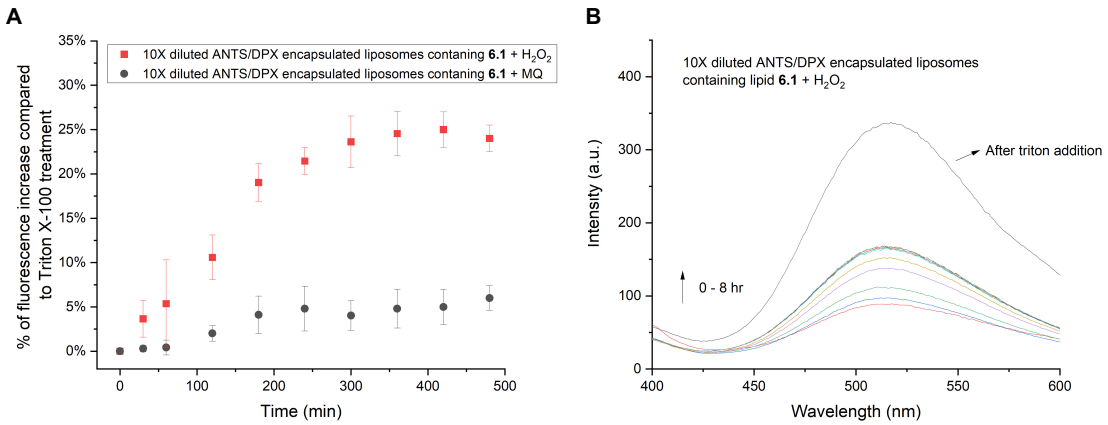


Figure 6.14. ANTS/DPX release profile for 10X diluted liposomes containing 30% lipid 6.1, 50% DOPE, 10% PC and 10% PA. A. Time-dependent release curve showing comparable increases in fluorescence were observed, indicating concentration does not affect release extent. **B.** Sample raw fluorescence emission spectra. Fluorescence intensity was recorded over time (Ex. Wavelength=350 nm, ex. Slit=20 nm, em. Slit=20 nm).

the dramatic discrepancy in the time scale needed for release, which prompted us to further investigate the release mechanism. We began by studying the end products resulting from oxidation of free lipid **6.1**, which was initially studied by time-dependent NMR analysis. To do so, compound **6.1** was dissolved in $CDCl_3/CD_3OD/D_2O$=65/25/4 (v/v) in an NMR tube, and after an initial scan and addition of H_2O_2, spectra were taken over time. As is shown in Figure 6.15, oxidative cleavage of the boronate headgroup of **6.1** took place immediately after treatment with hydrogen peroxide, as is indicated by a significant and complete signal shift for aromatic protons from ~7.6 and ~7.15 ppm to ~6.9 and ~6.6 ppm within 5 min (Figure 6.15, trace A and B). The benzylic methylene peak also showed a slight shift from ~4.9 ppm to ~4.77 ppm during this time. After 25 min incubation, a new peak at ~2.95 ppm appeared, which corresponds to the methylene peak next to the amino moiety of the headgroup of DOPE (Figure 6.15, trace B, C and H). The shifted benzylic methylene signal also completely disappeared after 2 hours and no further decomposition occurred after 3 days of incubation (Figure 6.15, trace E to G). No change was observed for the DOPE alkene peaks at ~5.2 ppm, indicating that peroxide does not oxidize the double bonds on the lipid tails under these conditions. When no peroxide was added, compound **6.1** was stable in the NMR tube for more than three months when being kept in a -20 °C freezer (20% $CD_3OD/CDCl_3$, data not shown).

6.7.1.2. TLC analysis and Mass spectrometry evidence of DOPE formation

The ultimate production of DOPE was further supported by thin-layer chromatography (TLC) as well as mass spectrometry (MS). In TLC plates run before and after this process (Figure 6.16), a new spot appeared upon H_2O_2 incubation that has the same R_f value as DOPE. In MS experiments (Figure 6.17), the DOPE peak could be clearly observed when lipid **6.1** was treated with H_2O_2.

6.7.1.3. Zeta potential measurement

Zeta potential (ZP) values were also measured for PC liposomes composed of 0% and 75%

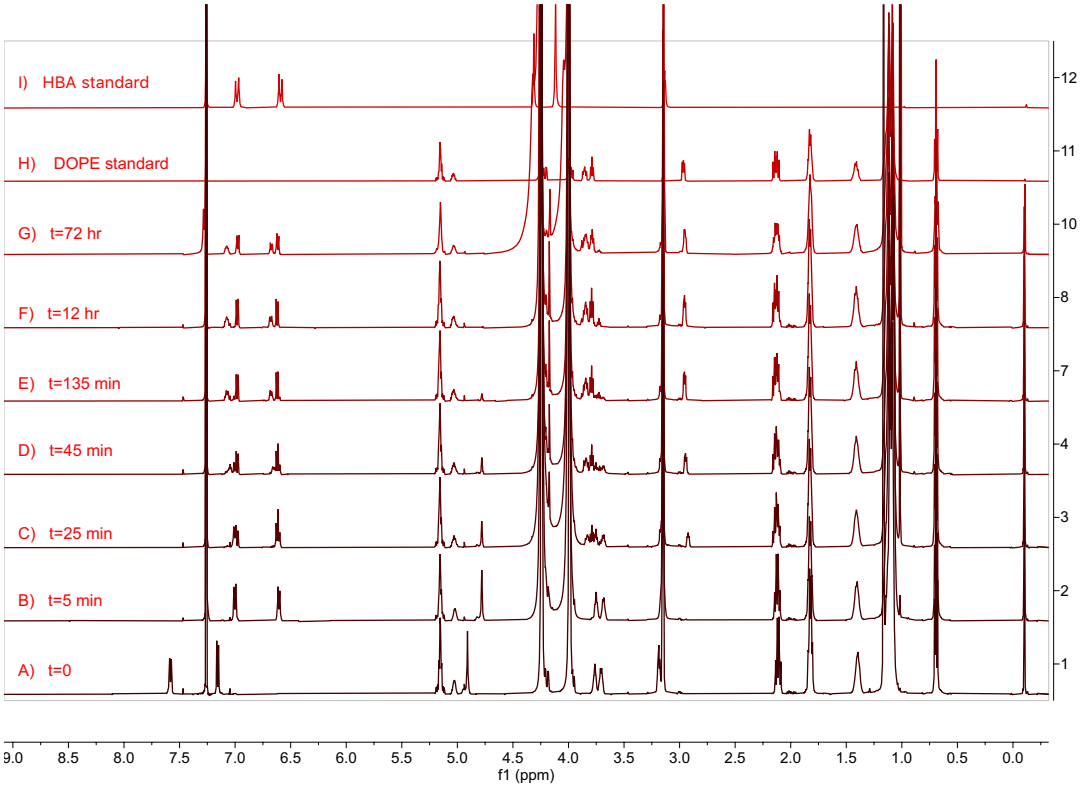


Figure 6.15. Time-dependent NMR analysis for lipid 6.1 in $CDCl_3/CD_3OD/D_2O$=65/25/4 (v/v) upon treatment with hydrogen peroxide. Trace A: lipid **6.1** before adding H_2O_2. Trace B to G: spectra for lipid **6.1** upon H_2O_2 treatment, which were taken over time. Trace H: DOPE standard. Trace I: 4-hydroxybenzyl alcohol (HBA) standard.

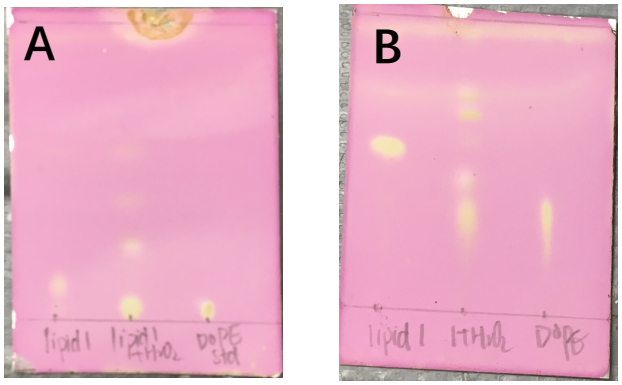


Figure 6.16. TLC analysis of free lipid 6.1 after adding H_2O_2. Plates were developed in **A.** 10% $CH_3OH/CHCl_3$, **B.** 20% $CH_3OH/CHCl_3$. Lane 1: lipid **6.1** standard; Lane 2: lipid **6.1** + H_2O_2; Lane 3: DOPE standard. After H_2O_2 incubation, a new spot appeared with the same R_f value as DOPE.

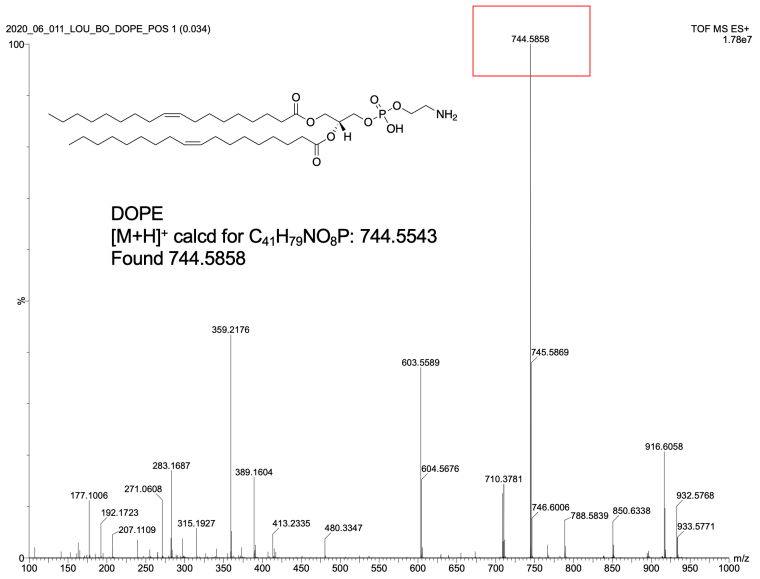


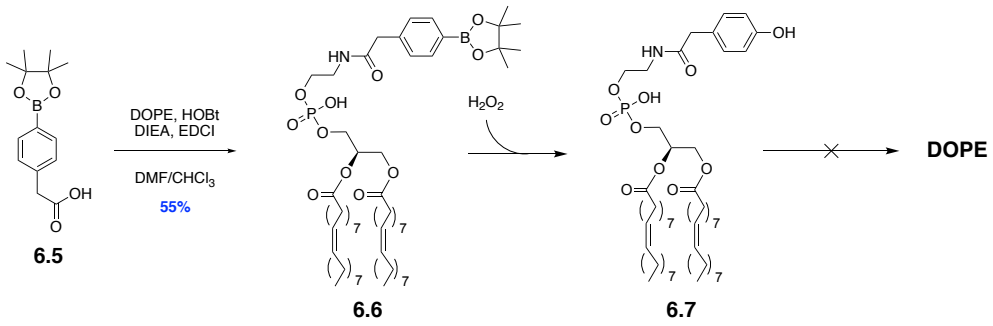
Figure 6.17. Mass spectrum including a peak matching DOPE after treating free lipid 6.1 with hydrogen peroxide.

lipid **6.1** before and after triggered release. For PC control liposomes, ZP values before and after peroxide treatment were measured to be (-2.63 ± 0.19) mV and (-2.42 ± 0.27) mV. For 75% liposomes before and after adding peroxide, they were determined to be (-28.47 ± 0.21) mV and (-27.77 ± 1.27) mV, respectively. When negatively charged lipid **6.1** decomposes into zwitterionic DOPE, one might expect the ZP value to change more than we observed here. However, several groups have reported that DOPE liposomes exhibit surprisingly negative surface charges compared to PC liposomes,[283,284] indicating ZP measurements may not be an ideal method to probe changes in this case. This may be exacerbated by the unusual electronics of the boronate moiety of lipid **6.1**. Overall, these results demonstrate the release of DOPE upon oxidation of **6.1** and the NMR results in particular differentiate the timescales of oxidative deborylation vs. QM self-immolation to produce DOPE.

6.7.2. Additional compound to elucidate release mechanism

6.7.2.1. Design and synthesis

From the NMR titration results, we noted that the oxidative cleavage of the boronate headgroup takes place immediately after addition of hydrogen peroxide; however, the QM self-immolation process and release of DOPE is much slower. It occurred to us that these results correlated with the different kinetics we observed for hydrophobic (fast) and hydrophilic (slow) dye release. As a result, we hypothesized that the faster release of NR may result solely from the oxidative cleavage of the boronate headgroup. This could be explained since hydrophobic content leaks more readily and may only require minimal modulation to the membrane, while hydrophilic cargo is retained more effectively by liposomes, and thus production of DOPE within the bilayer may be needed to provide more significant membrane disruption. To investigate this hypothesis, control lipid **6.6** was designed and synthesized, where the carbamate moiety of **6.1** was replaced by an amide group (Scheme 6.3), essentially subtracting one oxygen from **6.1**. By doing so, the boronate headgroup of **6.6** is still available for oxidative cleavage by addition of H_2O_2; however, since the self-immolative unit is changed,



Scheme 6.3. Design and synthetic route for control lipid 6.6. The arylboronate headgroup is connected to DOPE through a single step amide coupling reaction between commercially available **6.5** and DOPE. The headgroup of **6.6** is also expected to be oxidatively cleaved upon addition of hydrogen peroxide to produce **6.7**, which is designed to avoid subsequent decomposition into DOPE.

6.6 is designed to resist further decomposition into DOPE.

6.7.2.2. Fluorescence-based release studies of control lipid 6.6

Next, NR release assays were performed with PC based liposomes containing 50% or 75% of **6.6** using the same experimental procedures as previously described for PC/ **6.1** liposomes. As shown in Figure 6.18A (sample raw spectra in Figure 6.19A), both of these samples showed similar release results including comparable fast kinetics compared to corresponding liposomes containing lipid **6.1** after addition of H_2O_2. Specifically, PC liposomes containing 50% or 75% of **6.6** showed ~30% and ~40% release, respectively, within 5 min after peroxide addition. We then turned our attention to conduct the ANTS/DPX release assay using liposomes containing control lipid **6.6**. Here, the same formulation was adopted that was previously found to be successful using **6.1**, which in this case included 30% **6.6**, 10% egg PC, 50% DOPE as well as 10% PA. As is shown in Figure 6.18B (sample raw spectra in Figure 6.19B), only less than 5% background release was observed after 10 hours of hydrogen peroxide incubation for this experiment.

For both the NR and ANTS/DPX assays using compound **6.6**, DLS was also used to analyze particle sizes before and after H_2O_2 treatment (Figure 6.20). Similar to lipid **6.1**, stable membranes were formed initially, and no significant change was observed in particle sizes after triggered release. The non-polar/polar release profiles of lipid **6.6** are in agreement with our hypothesis that rapid NR release can be achieved solely by boronate ester oxidative removal, but that production of DOPE is necessary for hydrophilic content release.

6.7.3. Membrane asymmetry in the release process

Another interesting question we considered is whether membrane asymmetry is involved in the release process. To address this, NMR analysis was performed using samples derived from liposomes composed of 100% lipid **6.1** without dye encapsulation. These liposomes were treated with H_2O_2 for 5 min at room temperature before thiosulfate was added to quench

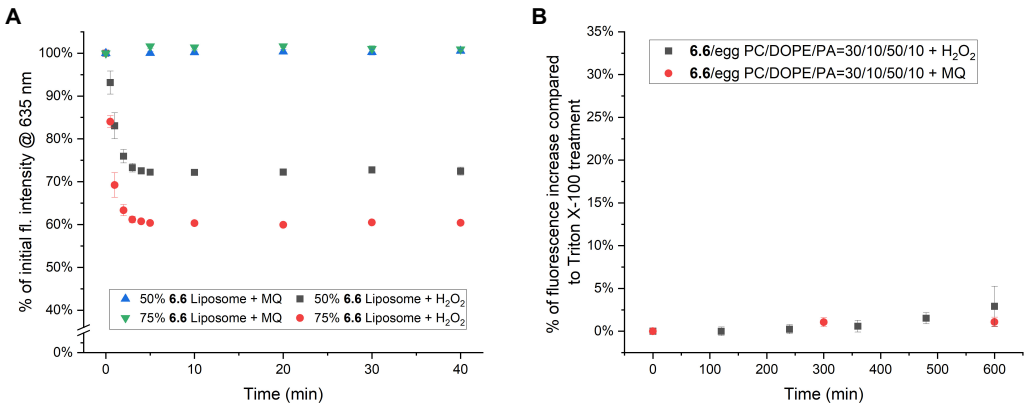


Figure 6.18. Release profiles of liposomes containing control lipid 6.6. A. NR release profiles for **6.6**/PC liposomes. Both 50% and 75% liposomes showed comparable release kinetics and results compared to **6.1**/PC liposomes. **B.** ANTS/DPX release profile of **6.6**-containing liposomes, where minimal increase in fluorescence was observed after incubation of H_2O_2. Error bars are from at least three different experiments denoting standard error.

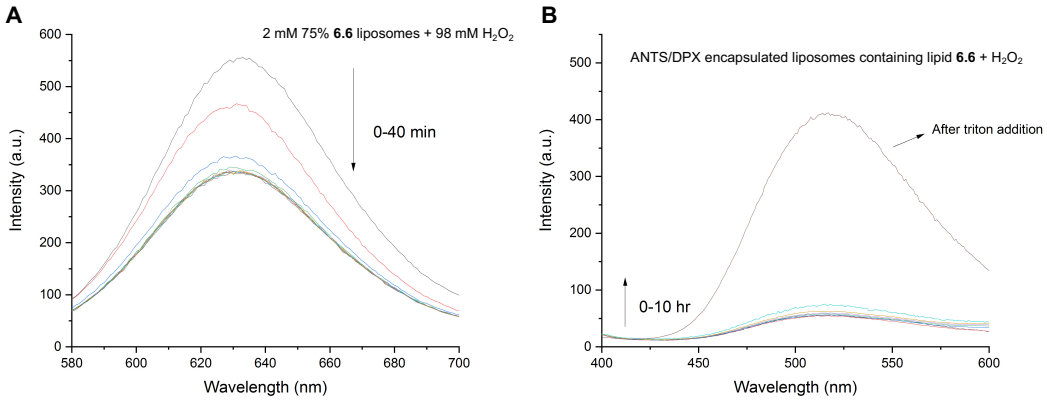


Figure 6.19. Sample raw fluorescence emission spectra for 6.6 liposomes. A. NR release for 2 mM 75% **6.6** liposomes upon H_2O_2 treatment. Fluorescence intensities were recorded over time. (Ex. Wavelength=552 nm, ex. Slit=5 nm, em. Slit=5 nm) **B.** ANTS/DPX assay with liposomes containing 30% lipid **6.6**, 10% egg PC, 50% DOPE and 10% PA after H_2O_2 addition. Fluorescence intensity was recorded over time. (Ex. Wavelength=350 nm, ex. Slit=10 nm, em. Slit=10 nm)

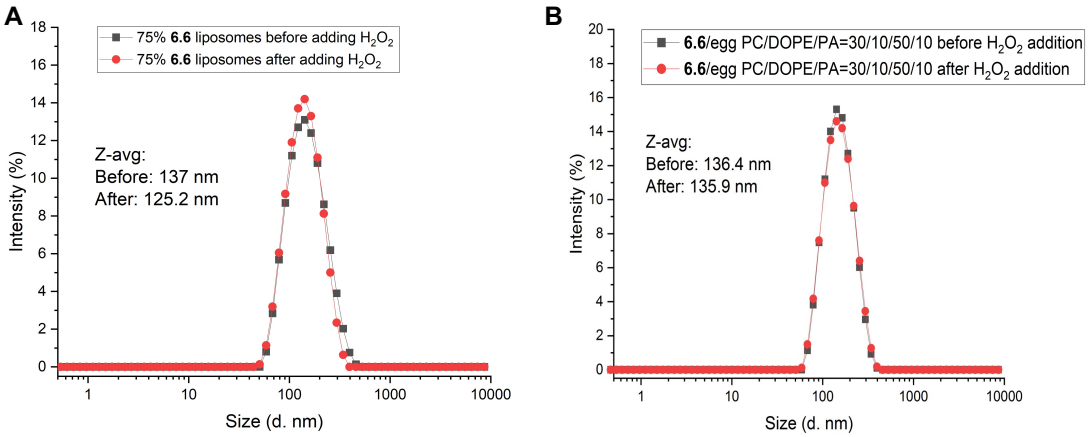


Figure 6.20. DLS size distribution plots for 6.6 liposomes. A. 75% **6.6** liposomes used in NR release assays before and after H_2O_2 addition. No significant change was observed in particle size after H_2O_2 treatment. **B.** DLS size distribution plots for ANTS/DPX-encapsulated **6.6** liposomes containing 30% **6.6**, 10% egg PC, 50% DOPE and 10% PA before and after H_2O_2 addition. Minimal changes were observed in particle sizes.

excess hydrogen peroxide. After the aqueous solvent was removed by rotary evaporation, the resulting mixture was re-dissolved in 20% $CD_3OD/CDCl_3$ and subjected to NMR analysis. As is shown in Figure 6.21, all boronate headgroups were removed from lipid **6.1** after only five minutes of hydrogen peroxide incubation, as judged by the significant peak shift within the aromatic region. This result provides evidence that molecules of lipid **6.1** on both leaflets of the bilayer can be successfully oxidized by peroxide within a very short time period. We do have to note here that, although the distinct DOPE characteristic peak at ~2.95 ppm could be observed in the spectrum, it could not be unambiguously determined in this case that DOPE was generated at this point since heating was used when removing water from liposomes, which can facilitate the immolation process. Indeed, from NMR titrations of free lipid **6.1** (Figure 6.15), DOPE is not released until after 25 min H_2O_2 incubation. With this result, we can also reasonably postulate that boronate removal occurs very quickly within several minutes on both leaflets of ANTS/DPX-encapsulated liposomes. Formation of DOPE will next take place on both leaflets concomitantly, which argues against the involvement of membrane asymmetry in content release for the formulations studied herein.

Taken as a whole, our data support that oxidation of boronate-lipids **6.1** and **6.6** is sufficient to drive release of the non-polar dye NR, while further decomposition to DOPE is needed for leakage of the polar dyes ANTS/DPX. The former result is not too surprising since non-polar dye release generally requires less membrane perturbation and the oxidation reaction results in a significant change to the size and electronic state of the headgroups of **6.1** and **6.6** by converting a pinacol boronate into a lone hydroxyl group. While DOPE production being necessary for polar release makes sense, it is somewhat surprising that we did not observe DLS changes in any of these liposomes during dye release studies. A plausible explanation for this would be that although production of DOPE may result in local changes to membrane properties that alter permeability, such disruption appears to not be sufficient to induce membrane fusion or drive other significant morphology changes in these cases.

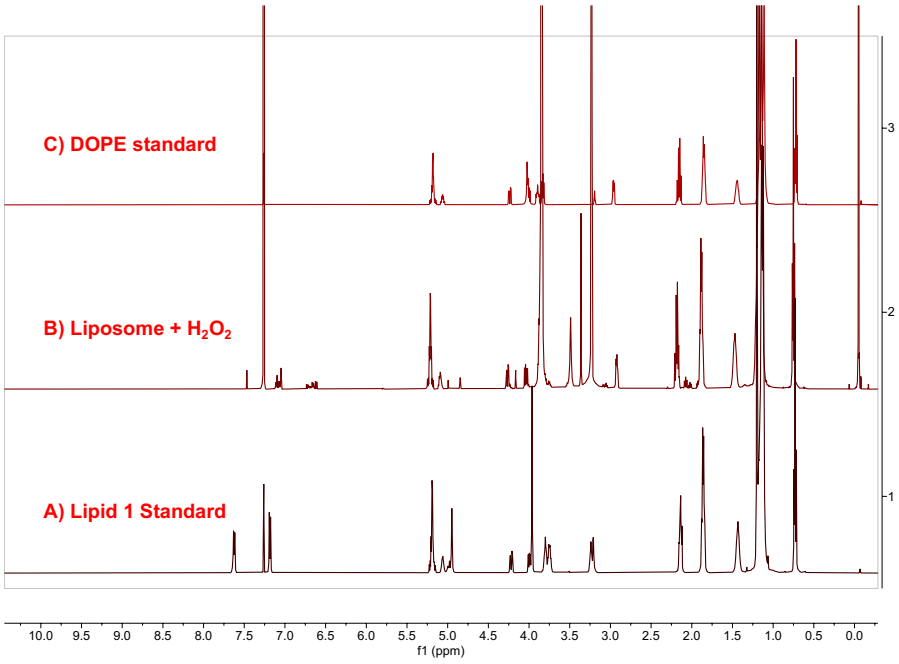


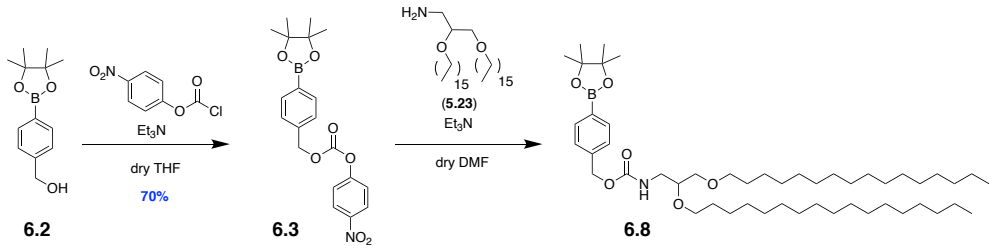
Figure 6.21. NMR analysis for liposomes composed of 100% lipid 6.1 after treatment with H_2O_2 for five minutes. Excess H_2O_2 was quenched and water was removed before re-dissolving the mixture in 20% $CD_3OD/CDCl_3$ for NMR analysis. All lipid **6.1** was oxidized within five minutes. Trace A: lipid **6.1** standard; Trace B: 100% liposome after 5 min H_2O_2 incubation; Trace C: DOPE standard.

6.8. Miscellaneous experiments

6.8.1. Alternative designs

The first ROS-responsive lipid target we synthesized for this project was based on the amino dietherglycerol lipid scaffold **5.23** through a two-step synthesis similar to lipid **6.1** (Scheme 6.4). This lipid shares the same design strategies, which contains a H_2O_2-responsive headgroup, a QM SIL and a non-bilayer forming lipid backbone.

While initial release studies looked promising, they proved to not be reproducible. One possible reason we came up was that lipid **6.8** is overall too hydrophobic, which may limit its inclusion or alter the boronate headgroup presentation in membrane bilayers. To overcome this issue, we proposed lipid **6.1** based on a DOPE scaffold (Figure 6.22A), as is described earlier in this Chapter. The presence of DOPE not only provided enough membrane disruption for cargo release upon ROS treatment, but also increased the hydrophilicity of the molecule by the introduction of an anionic phosphodiester group, which could aid lipid inclusion. Another possible reason could be that the membrane disruption upon the release of the amino dietherglycerol lipid **5.23** was not significant enough to drive release. Upon ROS incubation, **5.23** could still be stably incorporated within the bilayer. To enhance the degree of membrane disruption, we additionally designed lipids **6.9**-**6.11**, which contain ester or carbonate groups in their tail region. For lipid **6.9** containing esters, upon H_2O_2 addition and immolation, the resulting amino DAG lipid can undergo a migration reaction. While we expect such migration can enhance the disruption, dual tail lipid products will still present, which can possibly be trapped within the membrane. This could be fixed by switching the ester functionality into a carbonate group, in which case the released primary amine group can attack the carbonate group in the tail and release a long chain alcohol. Acyl chain migrations have proven to be problematic for lipid synthesis by yielding undesired byproducts,[285,286] but here we propose to exploit this inherent reactivity for liposome destabilization. The ultimate design we proposed was lipid **6.11**, which contains two boronate triggers to promote a greater change in structure



Scheme 6.4. Structure and synthetic route for initially designed ROS-responsive lipid target 6.8. 6.3 was treated with the amino dietherglycerol lipid scaffold **5.23** to afford **6.8**.

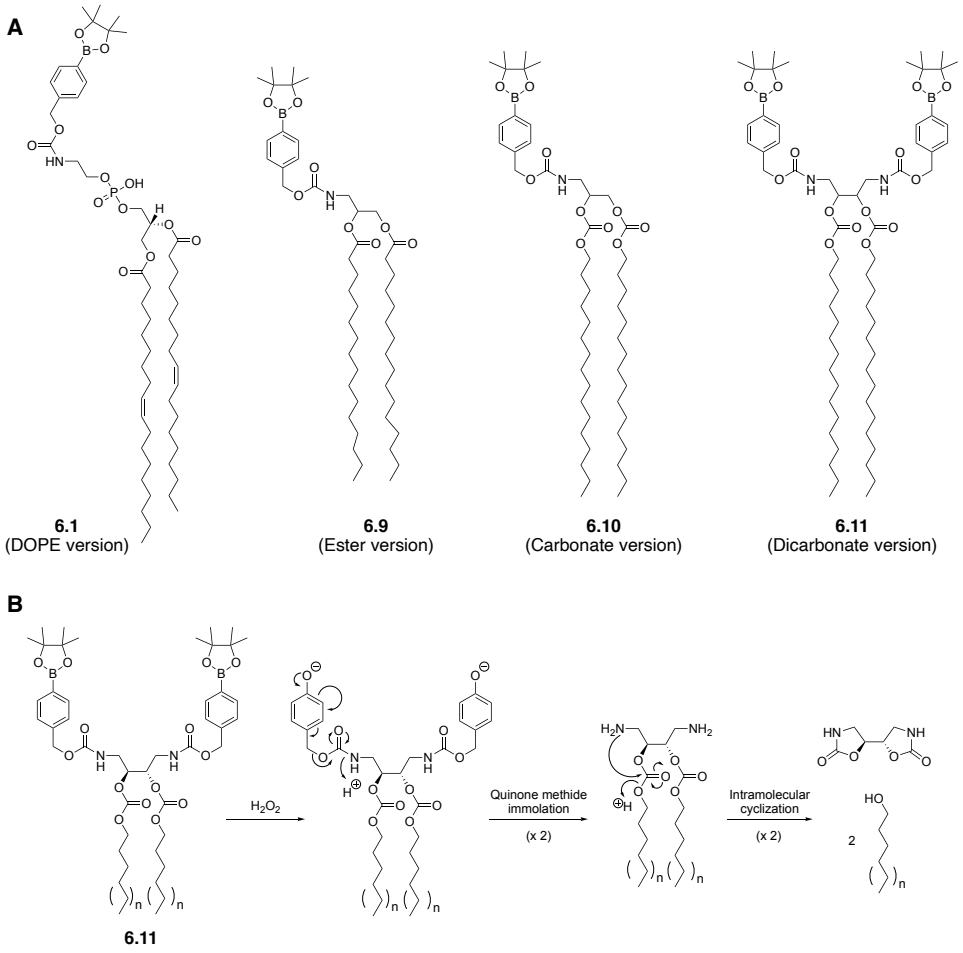


Figure 6.22. A. Alternative designs for ROS-responsive lipids 6.1 and 6.9-6.11. B. Proposed decomposition mechanism for lipid 6.11 upon H_2O_2 addition. ROS oxidation is expected to yield dual QM decomposition, leading to a diamine product that can undergo two intramolecular cyclization reactions and release the attached alcohols.

post ROS treatment and thereby magnify release. For this specific switch, ROS oxidation is expected to yield dual QM decomposition. The resulting diamine product is then designed to undergo two intramolecular cyclization reactions, wherein the two amines engage in nucleophilic attacks of proximal carbonyl groups, as shown in Figure 6.22B.

6.8.1.1. Synthetic efforts made for lipid 6.9 and 6.10

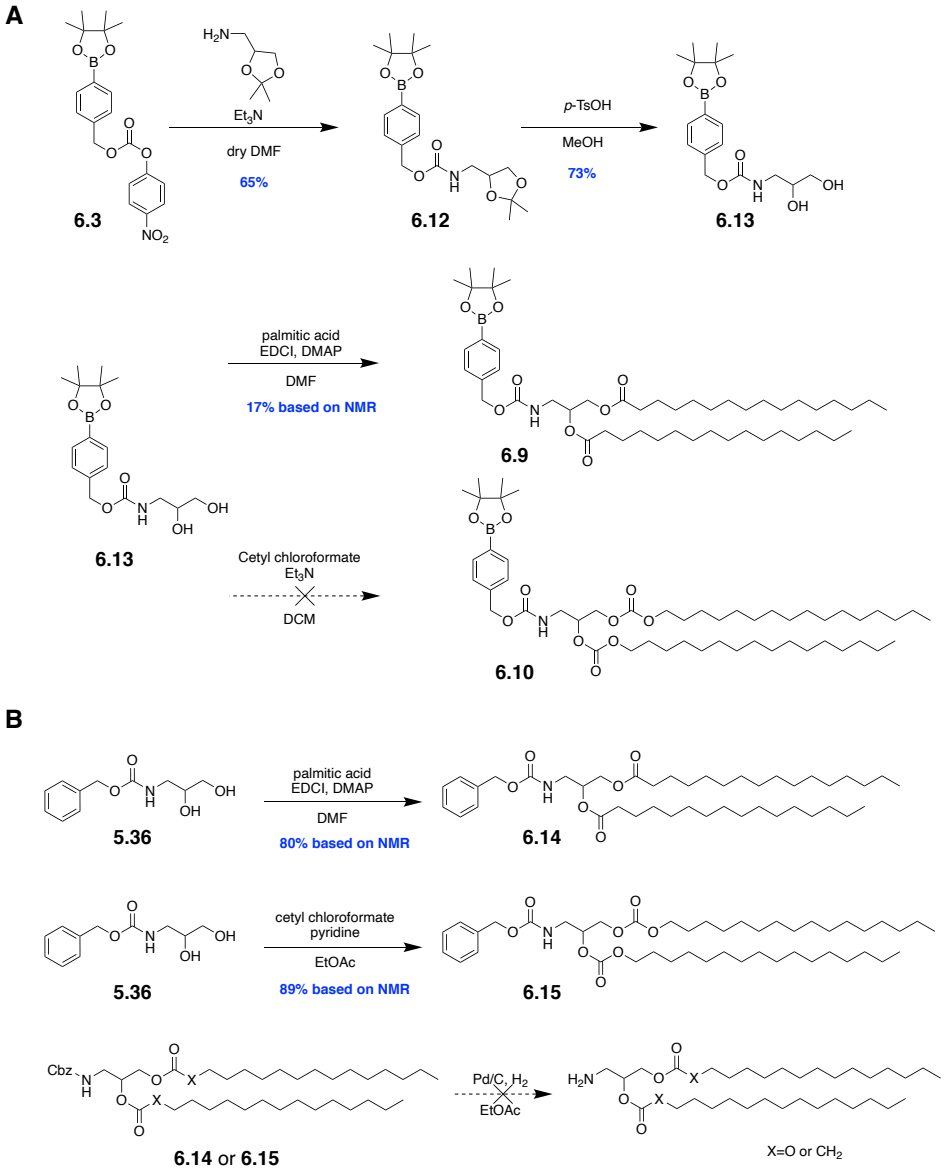
Two routes to these structures were pursued simultaneously. As shown in Scheme 6.5A, **6.3** was first reacted with acetal protected 3-amino-1,2-propanediol to form **6.12**, followed by deprotection of the acetal to **6.13**. Tails with either ester or carbonate functionalities can next be installed with palmitic acid for alkyl chloroformate to form the desired lipid product. Ester version **6.9** was synthesized successfully but we were not able to synthesize the carbonate version **6.10**. In a separate route shown in Scheme 6.5B, we intended to form the lipid scaffold first, which could then react with **6.3**. Compound **5.36** was treated with palmitic acid or cetyl chloroformate to attach the tails with desired functional groups of **6.14** and **6.15**. Although **6.14** and **6.15** were successfully synthesized, subsequent CBz deprotection with hydrogen and Pd/C only resulted in migrated product.

6.8.1.2. Synthesis for lipid di-carbonate immolative lipid 6.11

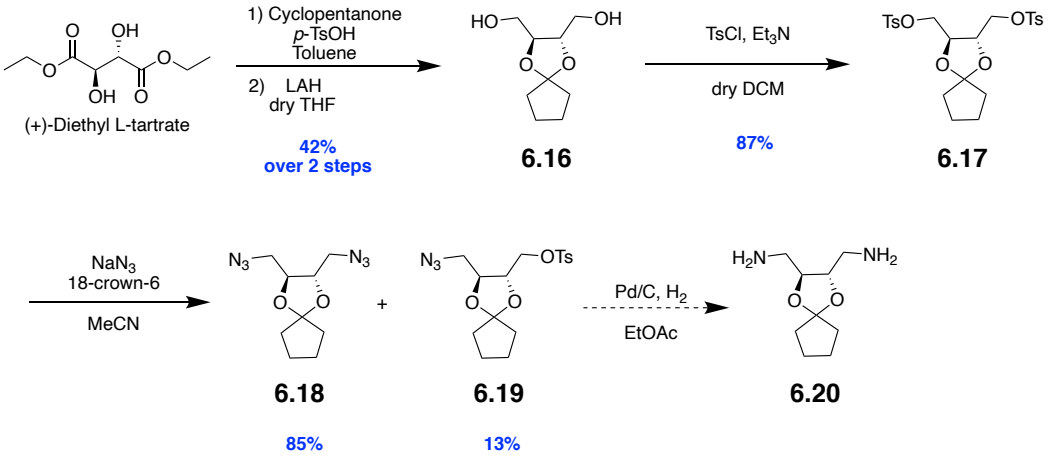
The key to synthesize the designed lipid **6.11** is to obtain the diamine scaffold **6.20** (Scheme 6.6), which can then be coupled to the boronate headgroup as well as the desired lipid tails. The route started with an acetal protection of (+)-diethyl L-tartrate with cyclopentanone, followed by lithium aluminum hydride reduction to diol compound **6.16**, tosylation to **6.17**, azide substitution to **6.18** as well as mono-substituted by-product **6.19**. Initial attempts to reduce **6.19** to diamine compound **6.20** proved unsuccessful, possibly due to solubility issues.

6.8.2. Synthesis and release studies of alternate control lipid 6.22

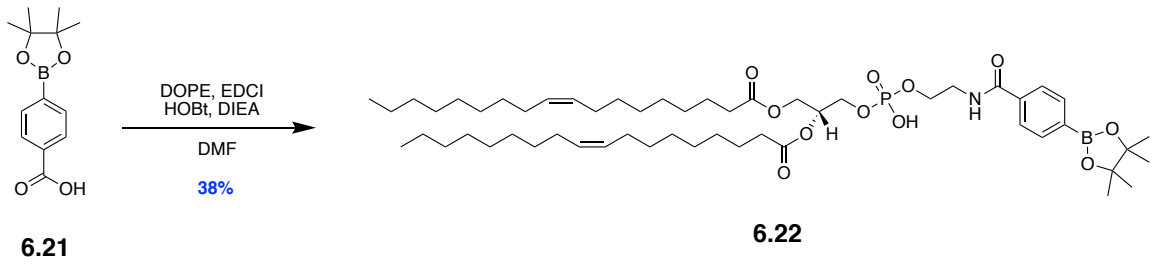
Another control lipid **6.22** (Scheme 6.7) was synthesized through a one-step amide coupling



Scheme 6.5. Proposed synthetic route to ester and carbonate version of ROS-responsive lipid 6.9 and 6.10. Two separate routes were pursued including building up the molecules from the headgroups (**A**) or synthesizing the tail scaffold first (**B**).



Scheme 6.6. Synthetic route for the key building block of di-carbonate immolative lipid 6.11.



Scheme 6.7. Synthetic route to control lipid 6.22. One-step amide coupling reaction between **6.21** and DOPE afforded **6.22**.

reaction between **6.21** and DOPE. Similar to lipid **6.6**, this control lipid is designed to resist further decomposition into DOPE. Fluorescence-based dye release assays results were determined to be comparable to lipid **6.6**. As shown in Figure 6.23A, 50% and 75% **6.22** liposomes showed ~20% and ~30% NR release within 5 min upon addition of H_2O_2. However, diminished hydrophilic dye release was observed through ANTS/DPX assay (Figure 6.23B-C), which could be attributed to the replacement of the self-immolative functionalities that ultimately prevented the formation of non-bilayer DOPE lipid. NMR titration experiment by dissolving **6.22** in chloroform/MeOH/H_2O with the incubation of H_2O_2 (Figure 6.24) further confirmed that DOPE was not released in this case. However, it is interesting to note that changing the immolative connection also affected the reaction time required for boronate oxidation. For lipid **6.1**, oxidative cleavage completed within five minutes after H_2O_2 treatment (Figure 6.15). However, the oxidative cleavage of lipid **6.22** did not complete after three hours of H_2O_2 incubation. The changes in the SIL may alter the electronic effect of the boronate headgroup, which ultimately affects the reaction time of oxidation.

6.8.3. Alternative ROS-responsive lipids based on poly-unsaturated PE scaffold

Although **6.1** was shown to be effective for both hydrophilic and hydrophobic cargo release, we hypothesized that this system can potentially be improved if we manage to further destabilize the membrane during the release process. Instead of a DOPE scaffold, which has only one *cis* double bond in its acyl chain, we installed the boronate trigger headgroup onto poly-unsaturated PE scaffolds. Lipids **6.23** (based on 18:2 PE scaffold) and **6.24** (based on 18:3 PE scaffold) were synthesized, which contain multiple *cis* double bonds in their tail region. By introducing more kinks into the hydrophobic area, we expect these poly-unsaturated lipids can exhibit more dramatic non-bilayer properties after triggering release. Their structures and synthetic routes are shown in Scheme 6.8. We also synthesized an additional control lipid **6.25** based on 18:1 trans PE, which could potentially shed light on how the *cis* and *trans* double bond in the tails could affect the membrane packing properties.

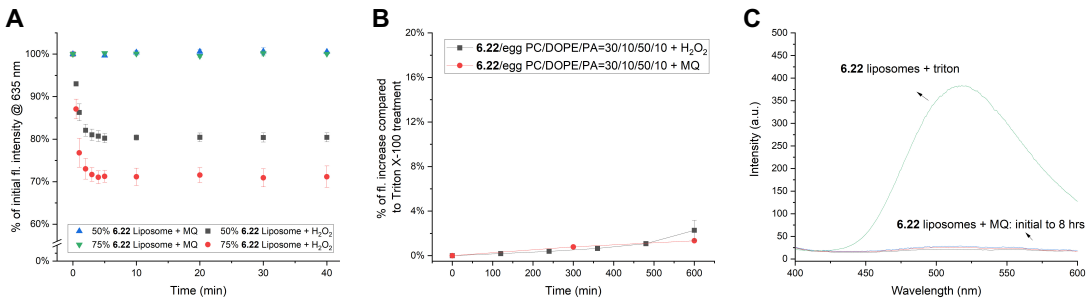


Figure 6.23. Release studies for lipid 6.22. A. NR release assay. H_2O_2 addition induced ~20% and ~30% release for 50% and 75% **6.22** liposomes, respectively. **B.** ANTS/DPX assay release assay. Liposomes containing **6.22** did not exhibit dye leakage upon H_2O_2 incubation for 10 hours. **C.** Representative raw fluorescence curve for ANTS/DPX release assay shown in Figure 6.23B.

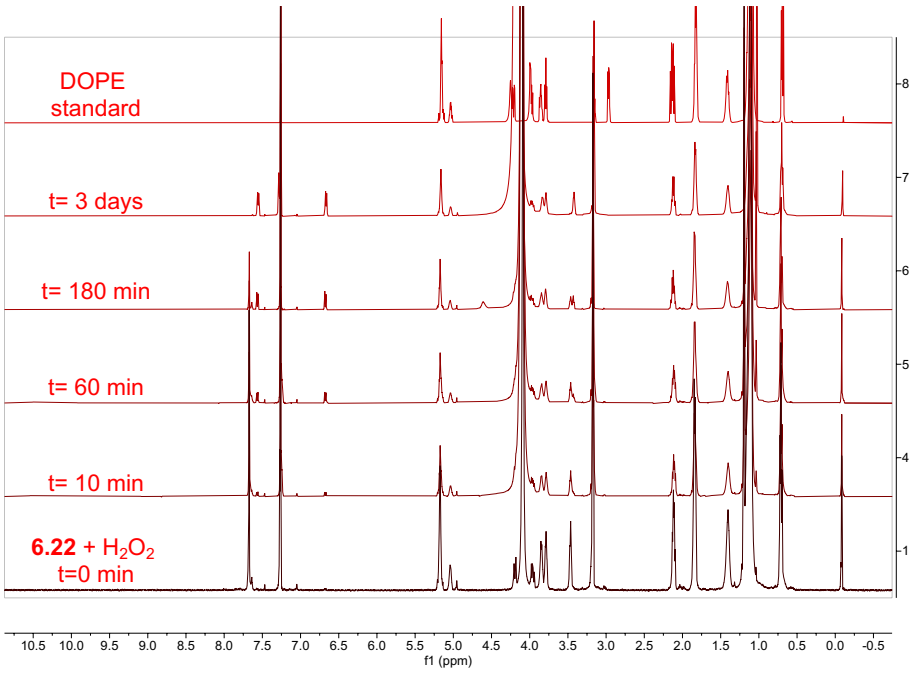
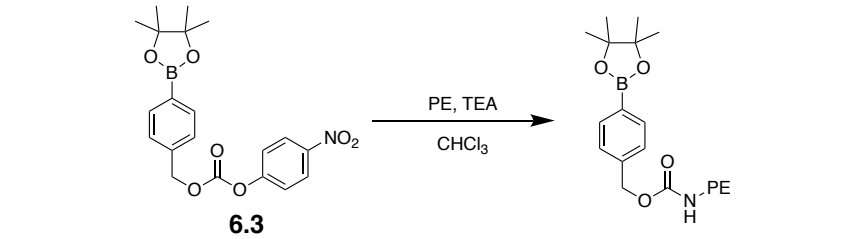
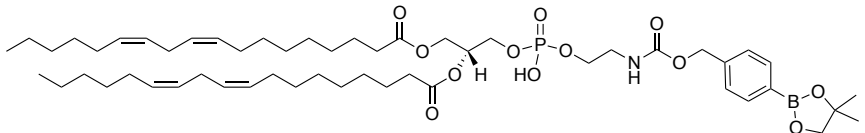


Figure 6.24. NMR titration of lipid 6.22 upon treatment of H_2O_2. 6.22 was dissolved in $CHCl_3$/MeOH/H_2O. No further decomposition to DOPE was observed after three days of H_2O_2 treatment.

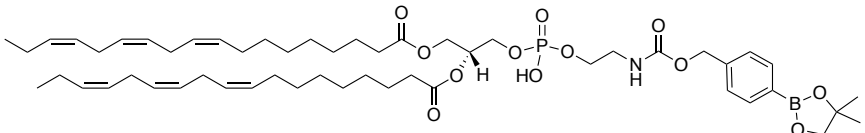


6.3



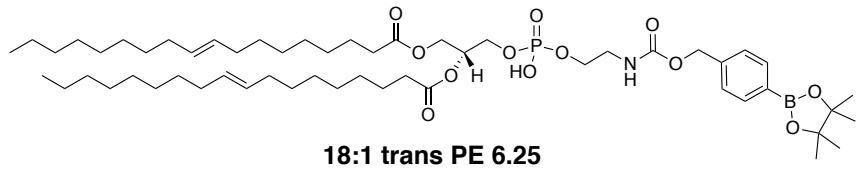
18:2 PE 6.23

69%



18:3 PE 6.24

43%



18:1 trans PE 6.25

79%

Scheme 6.8. Structures and synthetic route to alternative ROS-responsive lipids based on poly-unsaturated PE scaffolds. Similar synthetic strategies to obtain lipid **6.1** were used.

Since poly-unsaturated lipids can be easily oxidized, we quickly moved onto fluorescence-based assays to evaluate their release properties once we synthesized the target molecules. However, the results were surprising. As always, we conducted hydrophobic NR release assays first. As shown in Figures 6.25A-B, no matter how we varied liposome compositions, trans PE-based lipid **6.25** showed the greatest changes in NR fluorescence compared to 18:2 PE-based lipid **6.23** and 18:3 PE-based lipid **6.24**. Next, hydrophilic ANTS/DPX assays were conducted utilizing the same experimental conditions described earlier for lipid **6.1**. As shown in Figures 6.25C-D, similar to the NR release assay, 18:1 PE version **6.25** worked best. Considering the fact that only liposomes containing **6.25** showed a significant amount of fluorescence increase after Triton X-100 treatment, **6.23** and **6.24** might not be forming stable liposomes under the current conditions.

From the experimental data, we conclude that poly-unsaturated PE scaffolds may not be as effective as we previously thought. For lipids including DOPE, monounsaturated acyl chains have one single optimal conformation, and can only move along with x,y axis. However, for these poly-unsaturated acyl chains, besides the x,y axis, they can also be moved along z axis, which means they can be either extended or bent without much energetic penalty. By doing so, they can soften various molecular stresses in the hydrophobic core of the membrane.[287] Thus, our initial hypothesis may not be reasonable, since the presence of multiple double bonds could result in more fluid membrane that can easily compensate the disruption caused by our synthetic lipids.

6.9. Conclusion

In conclusion, we developed a ROS-responsive liposome platform containing synthetic lipid **6.1**, which exhibited content release properties for both hydrophilic and hydrophobic cargo upon H_2O_2 addition. Lipid **6.1** contains three major structural parts including an H_2O_2-responsive boronate ester headgroup, a QM-generating SIL and a non-bilayer forming DOPE

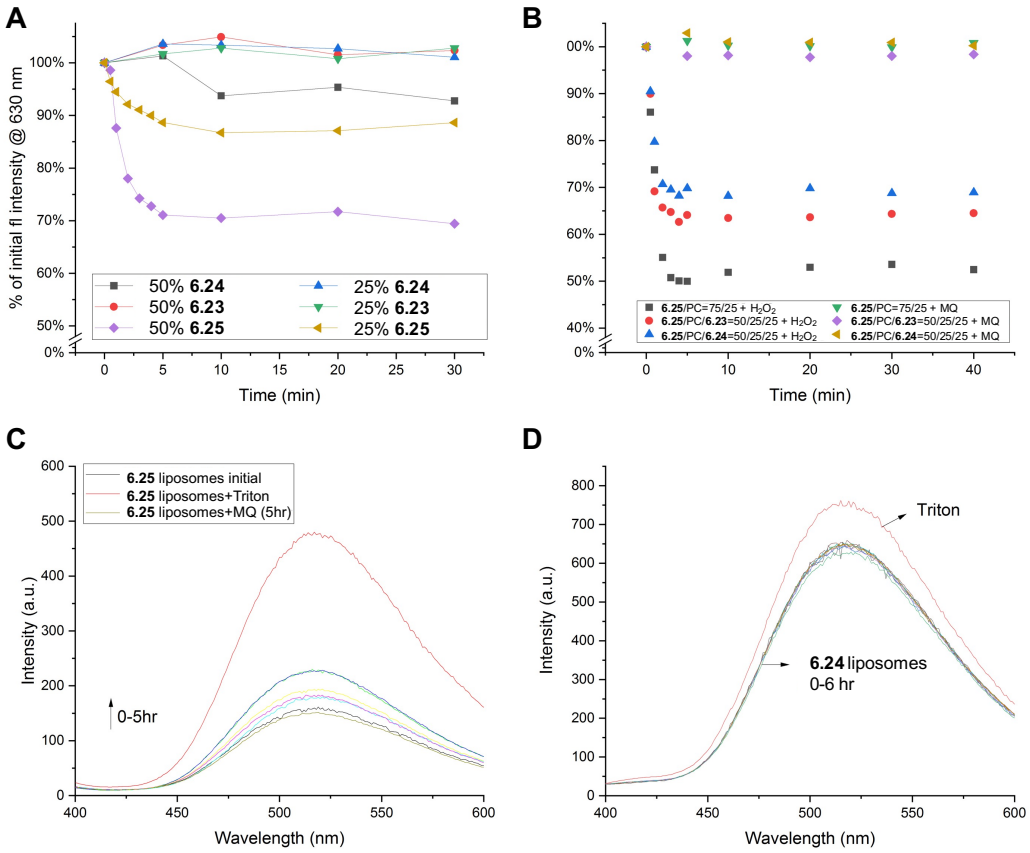


Figure 6.25. Fluorescence-based assays to evaluate the release properties for poly-unsaturated lipids 6.23-6.25. A. NR release assay for PC based liposomes containing 25% and 50% lipids **6.23**-**6.25**. While 25% and 50% **6.25** liposomes showed comparable cargo release compared to lipid **6.1**, lipids **6.23** and **6.24** did not show cargo leakage upon H_2O_2 treatment. **B.** NR release assays with liposomes containing 25% PC, 50% **6.25** and otherwise composed of **6.23**-**6.25**. Similarly, **6.25** showed best NR release. **C-D.** ANTS/DPX release assay for liposomes containing 50% DOPE, 10% PA, 10% PC and 30% **6.25**.

lipid scaffold. The mechanism for release was also studied in detail, and the data shows that oxidative cleavage of the boronate headgroup alone is sufficient to result in rapid release of the hydrophobic dye NR, while further decomposition and release of DOPE is required to achieve sufficient membrane disruption for leakage of the hydrophilic content ANTS/DPX, despite the fact that changes in liposomal particle sizes were not observed by DLS or TEM. Though they have not been explored to a great extent in liposomal research, ROS provide exciting targets for triggered release considering their overabundance in diseased cells compared to normal cells. We also envision that other aberrantly expressed biomolecules can serve as promising targets utilizing similar design strategies in developing liposomal release platforms for controlled release.

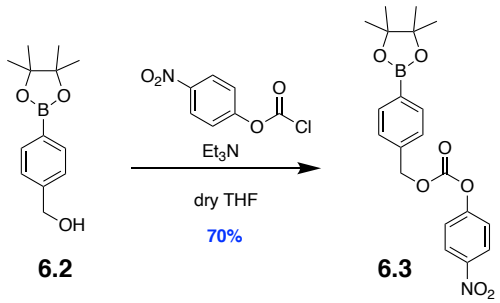
6.10. Synthesis and experimental procedure

General experimental

Reagents and solvents were generally purchased from Sigma-Aldrich or Fisher Scientific and used without further purification. PC (L-α-Phosphatidylcholine, mixed isomers from chicken eggs), PA (L-α-phosphatidic acid sodium salt from chicken eggs), DOPE (1,2-dioleoyl-*sn*-glycero-3-phosphoethanolamine), and DPPC (1,2-dipalmitoyl-*sn*-glycero-3-phosphocholine) were purchased from Avanti Polar Lipids, Inc (Alabaster, AL). Dry solvents were obtained from a Pure Solv MD-7 solvent purification system purchased from Innovative Technology, Inc (Newburyport, MA). Column chromatography was performed using 230-400 mesh silica gel purchased from Sorbent Technologies. NMR spectra were obtained using Varian 300 MHz or 500 MHz NMR spectrometers. Mass spectra were obtained with JEOL DART-AccuTOF and Waters Synapt G2-Si mass spectrometers (Milford, MA). Liposome extruder and polycarbonate membranes were obtained from Avestin (Ottawa, Canada). Ultrapure water was purified via a Millipore water system (≥ 18 MW·cm triple water purification system). Osmotic pressure was measured with a Wescor Vapor Pressure Osmometer 5520. Small quantities (< 5 mg) were weighed on a Mettler Toledo XS105 dual range analytical balance. Fluorescence

studies were performed using a Cary Eclipse Fluorescence Spectrophotometer from Agilent Technologies. Plots were generated using Origin Pro 2019. All error bars in plots show the standard errors of at least three experimental replicates.

Synthesis

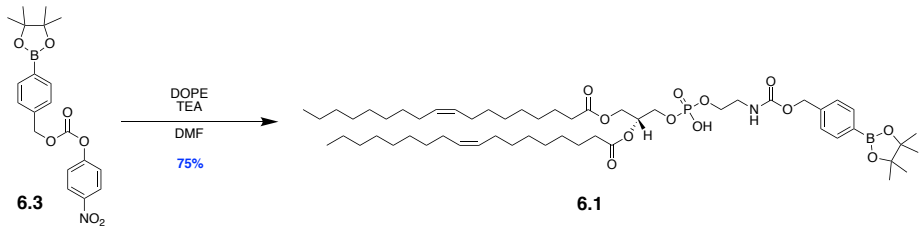


6.2 **6.3**

(4-Nitrophenyl (4-(4,4,5,5-tetramethyl-1,3,2-dioxaborolan-2-yl)benzyl) carbonate) (6.3)[281]

4-(Hydroxymethyl)phenylboronic acid pinacol ester (**6.2**, 0.5 g, 2.1 mmol) was weighed in a 50 mL RBF under Argon. Next, 5 mL dry THF was used to dissolve the starting material at 0 °C. Triethylamine (0.6 mL, 4.3 mmol) was then added into the reaction flask, followed by addition of 4-nitrophenyl chloroformate (0.47 g, 2.3 mmol). The reaction mixture was further stirred for three hours before being diluted with 100 mL DCM. The organic layer was washed with 100 mL saturated $NaHCO_3$ solution and the aqueous layer was further extracted with 2 x 25 mL DCM. The combined organic layer was then washed with 100 mL water and then 100 mL brine. After being dried over Na_2SO_4 and filtered, and concentrated under reduced pressure, the crude reaction mixture was purified via silica gel column chromatography using gradient elution from 100% hexane to 30% ethyl acetate-hexanes to afford the product as a white solid (0.587 g, 1.47 mmol, 70% yield). R_f = 0.61 (25% EtOAc/Hexanes).

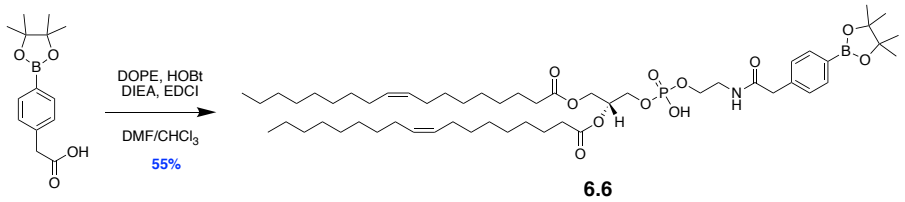
^{1}H NMR (300 MHz, Chloroform-*d*) δ 8.33 – 8.21 (m, 2H), 7.91 – 7.81 (m, 2H), 7.47 – 7.34 (m, 4H), 5.31 (s, 2H), 1.35 (d, *J* = 0.6 Hz, 12H). ^{13}C NMR (75 MHz, $CDCl_3$) δ 155.49, 152.39, 145.37, 137.07, 135.17, 127.60, 125.26, 121.76, 83.97, 70.76, 24.86. HRMS-DART: $[M+NH_4]^+$ calcd for $C_{20}H_{26}BO_7N_2$: 417.1833, found: 417.1144



(2*R*)-3-((Hydroxy(2-((((4-(4,4,5,5-tetramethyl-1,3,2-dioxaborolan-2-yl)benzyl)oxy)carbonyl)amino)ethoxy)phosphoryl)oxy)propane-1,2-diyl dioleate (6.1)

DOPE (100 mg, 0.1344 mmol) and **6.3** (64.4 mg, 0.1613 mmol) were combined in a 50 mL RBF under an Ar atmosphere. Dry DMF (3 mL) was then added to dissolve the starting materials at 0 °C. After adding triethylamine (56 µL, 0.4032 mmol), the reaction was stirred overnight before being quenched by pouring into 100 mL of 0.5 N HCl. The aqueous layer was extracted with 3×25 mL chloroform. The combined organic layer was washed with 5×100 mL water and once with brine. The collected organic phase was dried over Na_2SO_4, filtered, and concentrated under reduced pressure. The resulting crude was subjected to silica gel column chromatography. Gradient elution from 100% chloroform to 20% MeOH in chloroform was needed to purify the product as a white solid (101.2 mg, 0.1008 mmol, 75 % yield). R_f = 0.45 (20% MeOH-chloroform).

^{1}H NMR (500 MHz, 20% $CD_3OD/CDCl_3$) δ 7.62 (d, *J* = 7.6 Hz, 2H), 7.18 (d, *J* = 7.7 Hz, 2H), 5.25 – 5.14 (m, 4H), 5.06 (qd, *J* = 5.4, 3.0 Hz, 1H), 4.98 (s, 2H), 4.22 (dd, *J* = 12.0, 3.2 Hz, 1H), 4.04 – 3.97 (m, 1H), 3.83 – 3.71 (m, 4H), 3.24 (t, *J* = 5.6 Hz, 2H), 2.14 (dq, *J* = 10.4, 4.0 Hz, 4H), 1.90 – 1.82 (m, 8H), 1.44 (tq, *J* = 9.5, 6.3, 5.1 Hz, 4H), 1.22 – 1.10 (m, 55H), 0.73 (t, *J* = 6.9 Hz, 6H). ^{13}C NMR (126 MHz, 20% $CD_3OD/CDCl_3$) δ 173.73, 173.38, 157.10, 139.49, 134.76, 129.87, 129.53, 129.51, 126.74, 83.88, 70.29, 70.22, 66.43, 64.39, 63.50, 62.47, 41.33, 34.05, 33.89, 31.77, 29.61, 29.60, 29.53, 29.38, 29.17, 29.13, 29.10, 29.03, 29.02, 28.99, 28.96, 27.07, 27.04, 24.75, 24.69, 24.58, 22.52, 13.85. ^{31}P NMR (121 MHz, 20% $CD_3OD/CDCl_3$) δ 0.99. ^{11}B NMR (160 MHz, 20% $CD_3OD/CDCl_3$) δ 30.77, 18.38. ESI-MS [M-H]$^-$ calcd for $C_{55}H_{94}BNO_{12}P$: 1002.6607, found: 1002.6715.



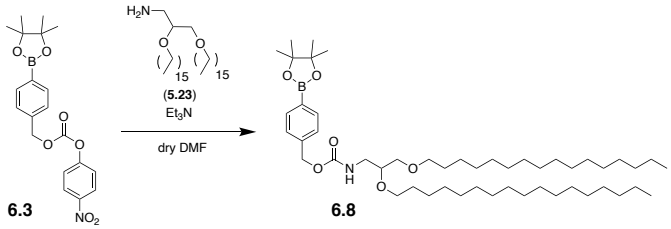
6.5 6.6

(2*R*)-3-((Hydroxy(2-(2-(4-(4,4,5,5-tetramethyl-1,3,2-dioxaborolan-2-yl)phenyl)acetamido)ethoxy)phosphoryl)oxy)propane-1,2-diyl dioleate (6.6)

4-(Carboxymethyl)phenylboronic acid pinacol ester (**6.5,** 42.3 mg, 0.1613 mmol), DOPE (100 mg, 0.1314 mmol) as well as hydroxybenzotriazole (HOBt, 24.7 mg, 0.1613 mmol) were combined in a 50 mL RBF under Argon. Dry DMF/$CHCl_3$ (6 mL, 1/1, v/v) was used to dissolve the starting materials at 0 °C. Next, 1-ethyl-3-(3-dimethylaminopropyl)carbodiimide (EDCI, 30.92 mg, 0.1613 mmol) was added into the reaction followed by *N*,*N*-diisopropylethylamine (DIEA, 56 µL, 0.336 mmol). The reaction was allowed to warm up to room temperature and further stirred for six hours before being quenched by pouring into 100 mL 1 N HCl. The aqueous layer was then extracted with 3×25 mL $CHCl_3$. The combined organic layer was next washed with 50 mL water five times and once with 50 mL brine. After being dried over Na_2SO_4, filtered, and concentrated under reduced pressure, the crude was subjected to silica gel column chromatography. Gradient elution from chloroform to 15% methanol in chloroform was needed to obtain **6.6** as a pale-yellow wax (73.43 mg, 0.074 mmol, 55% yield). R_f = 0.47 (20% MeOH/$CHCl_3$).

^{1}H NMR (500 MHz, 20% CD_3OD/$CDCl_3$) δ 7.59 (d, *J* = 7.9 Hz, 2H), 7.15 (d, *J* = 7.7 Hz, 2H), 5.24 – 5.15 (m, 4H), 5.06 (qd, *J* = 5.4, 3.0 Hz, 1H), 4.21 (dd, *J* = 12.1, 3.2 Hz, 1H), 4.00 (m, 1H), 3.83 – 3.76 (m, 2H), 3.72 (dt, *J* = 8.9, 5.7 Hz, 2H), 3.40 (s, 2H), 3.27 (t, *J* = 5.6 Hz, 2H), 2.15 (ddd, *J* = 9.9, 5.7, 2.2 Hz, 4H), 1.86 (q, *J* = 6.4 Hz, 8H), 1.43 (td, *J* = 10.2, 8.9, 5.7 Hz, 4H), 1.21 – 1.09 (m, 58H), 0.73 (t, *J* = 6.8 Hz, 6H). ^{13}C NMR (126 MHz, 20% CD_3OD/$CDCl_3$) δ 173.76, 173.42, 172.35, 138.25, 134.95, 129.87, 129.54, 129.52, 128.42, 83.81, 70.31, 70.25, 63.94, 63.90, 63.48, 62.53, 43.06, 40.13, 34.05, 33.90, 31.76, 29.61, 29.59, 29.53, 29.38, 29.17, 29.13, 29.10, 29.03, 29.02, 28.99, 28.96, 27.06, 27.04, 24.75, 24.70, 24.56,

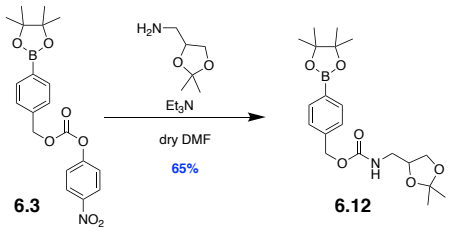
22.52, 13.84. ^{31}P NMR (202 MHz, 20% $CD_3OD/CDCl_3$) δ -2.58. ^{11}B NMR (160 MHz, 20% $CD_3OD/CDCl_3$) δ 27.21. ESI-MS $[M-H]^-$ calcd for $C_{55}H_{94}BNO_{11}P$: 986.6658, found: 986.6659



4-(4,4,5,5-Tetramethyl-1,3,2-dioxaborolan-2-yl)benzyl (2-(heptadecyloxy)-3-(hexadecyloxy)propyl)carbamate (6.8)

In a 50 mL RBF, **6.3** (110.7 mg, 0.2773 mmol), and **5.23** (124 mg, 0.23 mmol) were combined under nitrogen and the flask was cooled down to 0 °C in an ice bath. 2 mL DMF containing triethylamine (96.6 µL, 0.6932 mmol) was then added into the flask. After overnight stirring, the reaction was quenched by pouring into 200 mL water. The aqueous layer was extracted three times with 25 mL chloroform. After washing the combined organic layer with 50 mL water five times, and 50 mL brine once, the resulting solution was dried over Na_2SO_4, filtered, and concentrated under vacuum, the crude was purified through silica gel column chromatography using gradient elution hexanes to 15% EtOAc-hexanes to yield **6.8** as a white solid (50 mg, 0.061 mmol, 26% yield). R_f = 0.76 (25% EtOAc-hexanes).

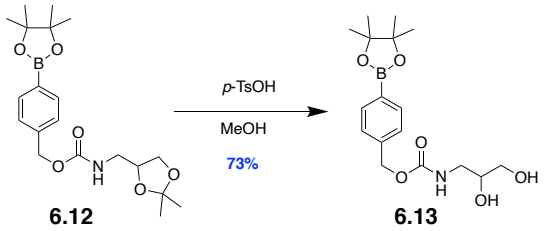
^{1}H NMR (300 MHz, Chloroform-*d*) δ 7.79 (d, *J* = 7.7 Hz, 2H), 7.35 (d, *J* = 7.7 Hz, 2H), 5.11 (s, 2H), 3.61 – 3.51 (m, 1H), 3.51 – 3.19 (m, 9H), 1.55 (s, 6H), 1.34 (d, *J* = 0.6 Hz, 12H), 1.25 (s, 55H), 0.98 – 0.75 (m, 6H). ^{13}C NMR (126 MHz, $CDCl_3$) δ 156.39, 139.69, 134.93, 127.04, 83.78, 76.88, 71.79, 71.19, 70.26, 66.46, 42.45, 31.91, 30.01, 29.69, 29.66, 29.65, 29.62, 29.60, 29.46, 29.35, 26.09, 26.07, 24.83, 22.67, 14.18, 14.10. HRMS-DART: $[M+H]^+$ calcd for $C_{49}H_{91}BO_6N$: 800.6939; Found: 800.6457.



4-(4,4,5,5-Tetramethyl-1,3,2-dioxaborolan-2-yl)benzyl ((2,2-dimethyl-1,3-dioxolan-4-yl)methyl)carbamate (6.12)

Compound **6.3** (100 mg, 0.25 mmol) was dissolved with 1 mL dry DMF in a 50 mL RBF under nitrogen. (2,2-Dimethyl-1,3-dioxolan-4-yl)methanamine (39 μL, 0.3 mmol) and TEA (100 μL, 0.75 mmol) were dissolved with 2 mL dry DMF in a small vial and then added into the reaction mixture. After being stirred overnight, the reaction was quenched by pouring into 150 mL water. The resulting aqueous solution was extracted with 3×25 mL EtOAc. The combined organic phase was washed with 5×50 mL water and 50 mL brine. After being dried with Na_2SO_4, filtered, and concentrated under reduced pressure, the crude was subjected to silica gel column chromatography. Gradient elution from hexanes to 25% EtOAc in hexanes was needed to yield the product as a colorless oil (64 mg, 0.164 mmol, 65%). R_f = 0.21 (25% EtOAc-hexanes).

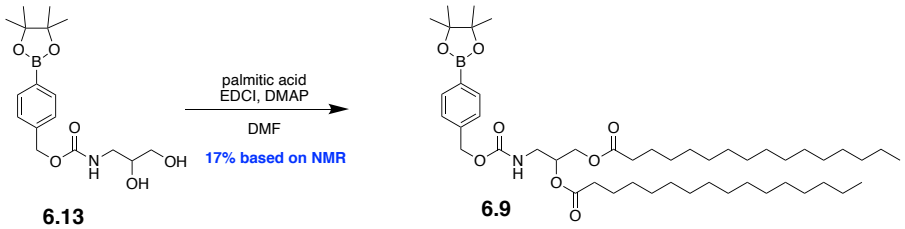
^{1}H NMR (300 MHz, Chloroform-*d*) δ 7.79 (dt, *J* = 7.4, 1.0 Hz, 2H), 7.34 (ddd, *J* = 7.6, 1.2, 0.6 Hz, 2H), 5.12 (s, 2H), 4.32 – 4.11 (m, 1H), 4.03 (dd, *J* = 8.3, 6.3 Hz, 1H), 3.65 (ddd, *J* = 8.4, 6.4, 1.0 Hz, 1H), 3.53 – 3.34 (m, 1H), 3.25 (dtd, *J* = 14.0, 5.9, 1.0 Hz, 1H), 1.41 (t, *J* = 0.9 Hz, 3H), 1.34 (d, *J* = 1.0 Hz, 15H). ^{13}C NMR (126 MHz, $CDCl_3$) δ 156.90, 139.85, 135.37, 127.48, 109.81, 84.23, 75.10, 67.10, 66.97, 43.69, 27.16, 25.62, 25.25.



4-(4,4,5,5-Tetramethyl-1,3,2-dioxaborolan-2-yl)benzyl (2,3-dihydroxypropyl)carbamate (6.13)

Compound **6.12** (64 mg, 0.1635 mmol) was dissolved with 3 mL MeOH in a 4 dr vial followed by addition of *p*-TsOH (2.8 mg, 0.0164 mmol). The reaction was stirred at room temperature. TLC indicated the reaction completed after two hours. After completion, the reaction was quenched by adding 3 mg solid $NaHCO_3$, and MeOH was removed under reduced pressure. The crude was purified through silica gel column chromatography using gradient elution from 25% EtOAc-hexanes to 100% EtOAc. The product was obtained as a yellow oil (42.2 mg, 0.12 mmol, 73% yield). R_f = 0.45 (100% EtOAc).

^{1}H NMR (300 MHz, Chloroform-*d*) δ 7.79 (d, *J* = 7.9 Hz, 2H), 7.32 (d, *J* = 7.9 Hz, 2H), 5.42 (s, 1H), 5.10 (s, 2H), 3.74 (s, 1H), 3.55 (d, *J* = 15.1 Hz, 2H), 3.42 – 2.91 (m, 4H), 1.33 (d, *J* = 1.9 Hz, 12H). ^{13}C NMR (126 MHz, $CDCl_3$) δ 157.55, 139.23, 134.97, 127.08, 83.85, 71.12, 66.91, 63.72, 43.27, 24.82.



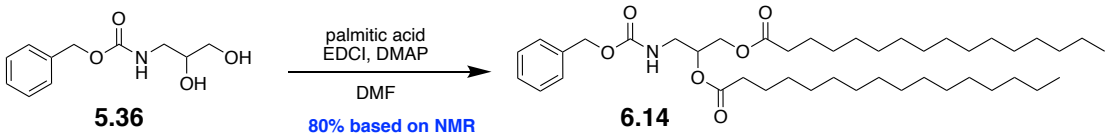
6.13 **6.9**

3-((((4-(4,4,5,5-Tetramethyl-1,3,2-dioxaborolan-2-yl)benzyl)oxy)carbonyl)amino)propane-1,2-diyl dipalmitate (6.9)

Compound **6.13** (43.6 mg, 0.124 mmol), palmitic acid (95.4 mg, 0.372 mmol), 4-dimethylaminopyridine (DMAP, 6.1 mg, 0.05 mmol), and 1-ethyl-3-(3-dimethylaminopropyl)carbodiimide (EDCI, 57.75 mg, 0.372 mmol) were dissolved with 3 mL dry DMF in a 50 mL RBF under Argon. After stirring at room temperature overnight, the reaction mixture was poured into a separatory funnel containing 100 mL H_2O. The aqueous layer was extracted with 3 × 25 mL EtOAc, and the combined organic layer was further washed with 5 × 50 mL H_2O and 1 × 50 mL brine. After being dried over Na_2SO_4, filtered, and concentrated under reduced pressure, the crude was purified with a column packed with silica gel using gradient elution from hexanes to 25% EtOAc in hexanes. Compound **6.9** was obtained as a

white solid after two columns (17.3 mg, 0.021 mmol, 17% yield based on NMR). R_f = 0.54 (25% EtOAc-Hexanes). NOTE: Separated compound has impurities in the alkyl region (possibly palmitic acid). Yield was calculated based on NMR integrations.

^{1}H NMR (500 MHz, Chloroform-*d*) δ 7.80 (d, *J* = 7.5 Hz, 2H), 7.34 (d, *J* = 7.6 Hz, 2H), 5.11 (s, 2H), 4.99 (t, *J* = 6.2 Hz, 1H), 4.20 (ddd, *J* = 74.4, 12.1, 4.8 Hz, 2H), 3.43 (dp, *J* = 27.5, 7.7, 6.4 Hz, 2H), 2.32 (dt, *J* = 28.1, 7.6 Hz, 6H), 1.68 – 1.56 (m, 7H), 1.34 (s, 13H), 1.25 (s, 78H), 0.88 (t, *J* = 6.7 Hz, 9H).

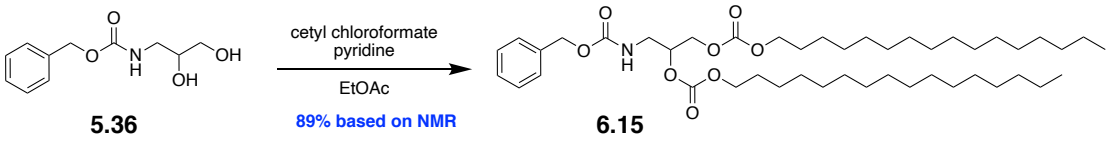


5.36 **6.14**

3-(((Benzyloxy)carbonyl)amino)propane-1,2-diyl dipalmitate (6.14)

Compound **5.36** (0.1 g, 0.444 mmol), palmitic acid (0.341 g, 1.332 mmol), 4-dimethylaminopyridine (DMAP, 21.75 mg, 0.178 mmol) and 1-ethyl-3-(3-dimethylaminopropyl)carbodiimide (EDCI, 0.206 g, 1.332 mmol) were dissolved with 5 mL dry DMF in a 50 mL RBF under Argon. After stirring at room temperature overnight, the reaction mixture was poured into a separatory funnel containing 100 mL H_2O. The aqueous layer was extracted with 3 × 25 mL EtOAc, and the combined organic layer was further washed with 5 × 50 mL H_2O and 1 × 50 mL brine. After being dried over Na_2SO_4, filtered, and concentrated under reduced pressure, the crude was purified with a column packed with silica gel using gradient elution from hexanes to 20% EtOAc in hexanes. **6.14** was obtained as a white solid (0.25 g, 0.35 mmol, 80% yield based on NMR). R_f = 0.54 (25% EtOAc-Hexanes). NOTE: Separated compound has impurities in the alkyl region (possibly palmitic acid). Yield was calculated based on NMR integrations.

^{1}H NMR (300 MHz, Chloroform-*d*) δ 7.43 – 7.28 (m, 5H), 5.17 – 5.07 (m, 3H), 5.02 (t, *J* = 6.2 Hz, 1H), 4.20 (ddd, *J* = 45.7, 12.0, 5.0 Hz, 2H), 3.54 – 3.30 (m, 2H), 2.31 (ddd, *J* = 12.3, 8.9, 6.0 Hz, 6H), 1.71 – 1.51 (m, 6H), 1.26 (s, 74H), 0.93 – 0.79 (m, 8H). HRMS-DART: $[M+H]^+$ calcd for $C_{43}H_{76}NO_6$: 702.5673; Found: 702.5433.

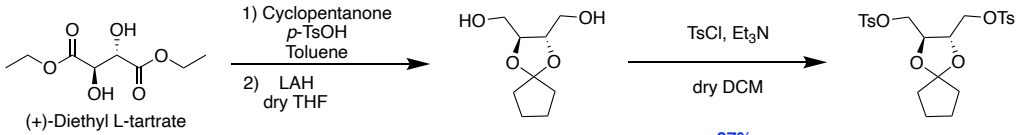


5.36 **6.15**

Benzyl (2,3-bis(((hexadecyloxy)carbonyl)oxy)propyl)carbamate (6.15)

Compound **5.36** (0.1 g, 0.444 mmol) was weighed in a 100 mL RBF under Argon. Next, 5 mL dry EtOAc was used to dissolve the starting material at 0 °C. Pyridine (0.22 mL, 2.664 mmol) was then added into the reaction flask, followed by addition of cetyl chloroformate (0.812 g, 2.664 mmol). The reaction mixture was further stirred overnight before being diluted with 100 mL DCM. The organic layer was washed with 100 mL saturated $NaHCO_3$ solution and the aqueous layer was further extracted with 2 x 25 mL DCM. The combined organic layer was then washed with 100 mL water and then 100 mL brine. After being dried over Na_2SO_4 and filtered, and concentrated under reduced pressure, the crude reaction mixture was purified via silica gel column chromatography using gradient elution from 100% hexanes to 25% ethyl acetate-hexanes to afford the product as a white solid (0.28 g, 0.376 mmol, 89% yield based on NMR). R_f = 0.54 (25% EtOAc-Hexanes). NOTE: Separated compound has impurities in the alkyl region (possibly cetyl alcohol). Yield was calculated based on NMR integrations.

^{1}H NMR (300 MHz, Chloroform-*d*) δ 7.44 – 7.29 (m, 5H), 5.11 (s, 3H), 4.96 (q, *J* = 5.1 Hz, 1H), 4.31 (ddd, *J* = 53.9, 12.1, 4.6 Hz, 2H), 4.16 – 4.06 (m, 4H), 3.69 – 3.36 (m, 4H), 1.61 (dp, *J* = 27.1, 6.7 Hz, 6H), 1.26 (s, 77H), 0.98 – 0.84 (m, 8H).

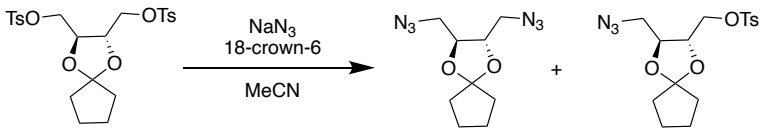


6.16 **6.17**

((2*S*,3*S*)-1,4-Dioxaspiro[4.4]nonane-2,3-diyl)bis(methylene) bis(4-methylbenzenesulfonate) (6.17)

Compound **6.16** was synthesized following the protocol reported by previous group member

Matthew Smith.[288] The characterizations of purified product matched the reported values. Compound **6.16** (1.03 g, 5.45 mmol) was dissolved with 20 mL dry DCM in a 100 mL RBF under argon. Et_3N (2.28 mL, 16.36 mmol) and *p*-TsCl (3.12 g, 16.36 mmol) were then added into the flask. The reaction was run overnight before being quenched by pouring into 150 mL 0.75 N HCl. The organic layer was collected and the residual aqueous layer was extracted one more time with DCM. The combined organic layer was then washed with water and brine, dried over Na_2SO_4, and concentrated under reduced pressure. Silica gel column chromatography was performed using gradient elution from 100% hexanes to 25% EtOAc-hexanes to yield **6.17** as a white needle-like solid (2.3445 g, 4.72 mmol, 87% yield). R_f = 0.3 (25% EtOAc-hexanes) ^{1}H NMR (300 MHz, Chloroform-*d*) δ 7.82 – 7.75 (m, 4H), 7.39 – 7.33 (m, 4H), 4.08 – 4.03 (m, 4H), 4.00 – 3.93 (m, 2H), 2.46 (s, 6H), 1.74 – 1.56 (m, 8H). ^{13}C NMR (126 MHz, $CDCl_3$) δ 145.37, 132.63, 130.14, 128.17, 120.89, 75.14, 68.69, 37.31, 23.55, 21.84.



6.17 **6.18** **6.19**

85% 13%

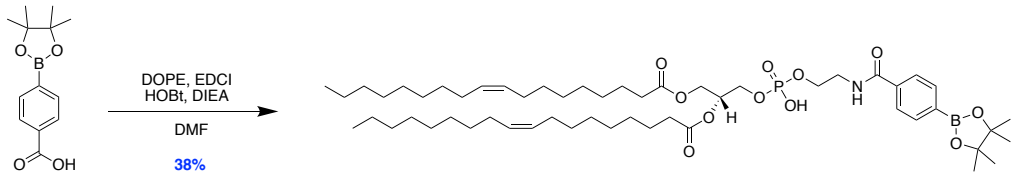
(2*S*,3*S*)-2,3-Bis(azidomethyl)-1,4-dioxaspiro[4.4]nonane (6.18)

Compound **6.17** (2.1335 g, 4.3 mmol), NaN_3 (1.676 g, 25.7 mmol) and 18-crown-6 (0.227 g, 0.86 mmol) were weighed into a 100 mL RBF under argon and then dissolved with 30 mL MeCN. The reaction was stirred for two days under reflux before being allowed to cool down to rt. The solid left in the round bottom flask was filtered off through celite pad and the filtrate was concentrated under vacuum. The resulting crude was subjected to silica gel column chromatography and gradient elution from hexanes to 25% EtOAc-hexanes was used to yield **6.18** as a white solid (0.8691 g, 3.64 mmol, 85% yield). R_f = 0.75 (25% EtOAc-hexanes). ^{1}H NMR (500 MHz, Chloroform-*d*) δ 3.95 (p, *J* = 1.8 Hz, 2H), 3.46 (dd, *J* = 13.2, 3.8 Hz, 2H), 3.33 (ddd, *J* = 13.0, 3.3, 1.6 Hz, 2H), 1.86 – 1.79 (m, 4H), 1.67 (tdt, *J* = 11.5, 5.9, 3.1 Hz, 4H).

^{13}C NMR (126 MHz, $CDCl_3$) δ 120.26, 76.92, 51.83, 37.20, 23.39. HRMS-DART: $[M\text{-}N_2+H]^+$ calcd for $C_9H_{15}N_4O_2$: 211.1195; Found: 211.0962.

Mono-tosylated by-product **6.19** was also separated from the same column as a white solid (0.2074 g, 13% yield). R_f = 0.6 (25% EtOAc-hexanes).

^{1}H NMR (500 MHz, Chloroform-*d*) δ 7.86 – 7.72 (m, 2H), 7.49 – 7.30 (m, 2H), 4.14 – 4.06 (m, 2H), 4.05 – 3.91 (m, 2H), 3.48 (dd, *J* = 13.1, 4.0 Hz, 1H), 3.32 (dd, *J* = 13.1, 5.1 Hz, 1H), 2.46 (s, 3H), 1.87 – 1.59 (m, 8H). ^{13}C NMR (126 MHz, $CDCl_3$) δ 145.37, 132.65, 130.09, 128.13, 120.62, 76.97, 75.24, 68.83, 51.90, 37.39, 37.19, 23.60, 23.46, 21.81. HRMS-DART: $[M\text{-}N_2+H]^+$ calcd for $C_{16}H_{22}NSO_5$: 340.1219; Found: 340.0885.



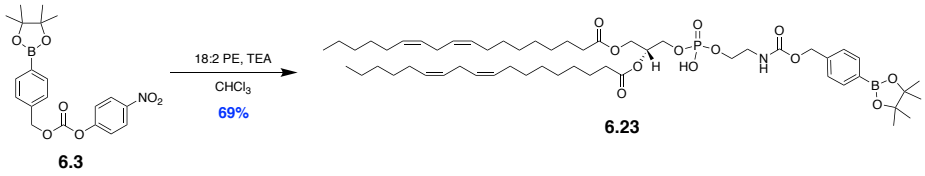
6.21 **6.22**

(2*R*)-3-((Hydroxy(2-(4-(4,4,5,5-tetramethyl-1,3,2-dioxaborolan-2-yl)benzamido)ethoxy)phosphoryl)oxy)propane-1,2-diyl dioleate (6.22)

4-(4,4,5,5-Tetramethyl-1,3,2-dioxaborolan-2-yl)-benzoic acid (**6.21**, 40 mg, 0.1613 mmol), DOPE (100 mg, 0.1344 mmol) and HOBt (24.7 mg, 0.1613 mmol) were dissolved with 3 mL dry DMF in a 50 mL RBF under Argon at 0 °C. After being stirred for five minutes, EDCI (30.92 mg, 0.1613 mmol) as well as DIEA (55 µL, 0.336 mmol) were added. The reaction was stirred at room temperature overnight before being quenched by pouring into 100 mL 1 N HCl. 3×25 mL $CHCl_3$ was used to extract the aqueous layer. Next, the combined organic layer was further washed by 5×50 mL water and once with 50 mL brine. After being dried over Na_2SO_4, filtered, and concentrated under reduced pressure, the crude was purified through silica gel column chromatography. Gradient elution from chloroform to 15% MeOH in chloroform was used to yield **6.22** as a light yellow wax (50.1 mg, 0.0513 mmol, 38% yield). R_f = 0.55 (20%

MeOH/$CHCl_3$).

^{1}H NMR (500 MHz, 20% $CD_3OD/CDCl_3$) δ 8.20 (t, *J* = 5.6 Hz, 1H), 7.70 (s, 4H), 5.20 (dt, *J* = 6.4, 4.5 Hz, 4H), 5.06 (tt, *J* = 8.9, 4.3 Hz, 1H), 4.21 (dd, *J* = 12.0, 3.3 Hz, 1H), 3.98 (dd, *J* = 12.0, 6.7 Hz, 1H), 3.89 – 3.84 (m, 2H), 3.81 (t, *J* = 6.2 Hz, 2H), 3.50 (q, *J* = 5.4 Hz, 2H), 2.14 (td, *J* = 8.1, 7.6, 2.2 Hz, 4H), 1.87 (q, *J* = 6.5 Hz, 8H), 1.44 (dd, *J* = 9.2, 5.8 Hz, 4H), 1.22 (s, 12H), 1.21 – 1.07 (m, 46H), 0.74 (t, *J* = 6.8 Hz, 6H). ^{13}C NMR (126 MHz, 20% $CD_3OD/CDCl_3$) δ 174.02, 173.68, 168.73, 136.34, 134.91, 130.14, 129.81, 126.52, 98.10, 84.40, 70.53, 70.47, 64.24, 63.79, 62.68, 40.94, 34.31, 34.16, 32.03, 29.88, 29.86, 29.80, 29.64, 29.44, 29.37, 29.35, 29.28, 29.24, 29.21, 27.33, 27.30, 24.99, 24.95, 24.88, 22.79, 14.12. ^{31}P NMR (121 MHz, 20% $CD_3OD/CDCl_3$) δ -1.49. ^{11}B NMR (160 MHz, 20% $CD_3OD/CDCl_3$) δ 30.69.

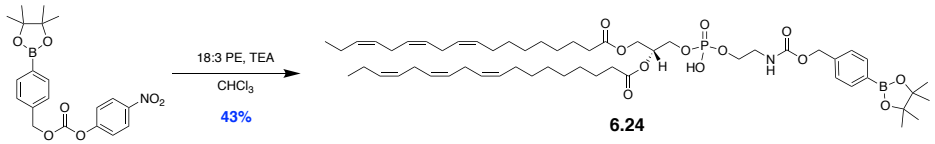


(2*R*)-3-((Hydroxy(2-((((4-(4,4,5,5-tetramethyl-1,3,2-dioxaborolan-2-yl)benzyl)oxy)carbonyl)amino)ethoxy)phosphoryl)oxy)propane-1,2-diyl (9*Z*,9'*Z*,12*Z*,12'*Z*)-bis(octadeca-9,12-dienoate) (6.23)

18:2 PE (25 mg, 0.0337 mmol) and **6.3** (16.2 mg, 0.0405 mmol) were dissolved with 5 mL dry $CHCl_3$ at 0 °C in a 50 mL RBF under Ar protection. After adding triethylamine (14.12 μL, 0.101 mmol), the reaction was stirred overnight before being quenched by pouring into 100 mL of 0.5 N HCl. The aqueous layer was extracted with 3×25 mL chloroform. The combined organic layer was washed with 5×100 mL water and once with brine. The collected organic phase was dried over Na_2SO_4, filtered, and concentrated under reduced pressure. The resulting crude was subjected to silica gel column chromatography. Gradient elution from 100% chloroform to 10% MeOH in chloroform was needed to purify the product as a colorless oil (23.2 mg, 0.0232 mmol, 69% yield). R_f = 0.42 (20% MeOH-chloroform).

^{1}H NMR (500 MHz, 20% CD_3OD-$CDCl_3$) δ 7.60 (d, *J* = 7.7 Hz, 2H), 7.16 (d, *J* = 7.9 Hz, 2H),

5.27 – 5.10 (m, 8H), 5.09 – 4.99 (s, 1H), 4.94 (d, *J* = 13.8 Hz, 2H), 4.20 (dd, *J* = 12.0, 3.0 Hz, 1H), 3.97 (dd, *J* = 12.0, 6.8 Hz, 1H), 3.83 – 3.68 (m, 4H), 3.20 (d, *J* = 10.5 Hz, 2H), 2.59 (t, *J* = 6.5 Hz, 4H), 2.17 – 2.08 (m, 4H), 1.88 (q, *J* = 6.8 Hz, 8H), 1.46 – 1.36 (m, 4H), 1.22 – 1.06 (m, 48H), 0.72 (t, *J* = 6.9 Hz, 6H). ^{13}C NMR (126 MHz, 20% CD_3OD-$CDCl_3$) δ 173.80, 173.44, 157.18, 139.55, 134.80, 130.09, 129.85, 127.98, 127.78, 126.78, 83.94, 70.31, 66.46, 64.46, 63.56, 62.50, 55.77, 41.38, 34.07, 33.92, 31.41, 29.53, 29.23, 29.15, 29.12, 29.04, 29.00, 28.98, 27.07, 25.50, 24.77, 24.72, 24.59, 22.44, 13.82. ^{31}P NMR (202 MHz, 20% CD_3OD-$CDCl_3$) δ -2.66. ^{11}B NMR (160 MHz, 20% CD_3OD-$CDCl_3$) δ 30.74. ESI-MS: $[M-H]^-$ calcd for $C_{55}H_{90}BNO_{12}P$: 998.6294; Found: 998.6536.



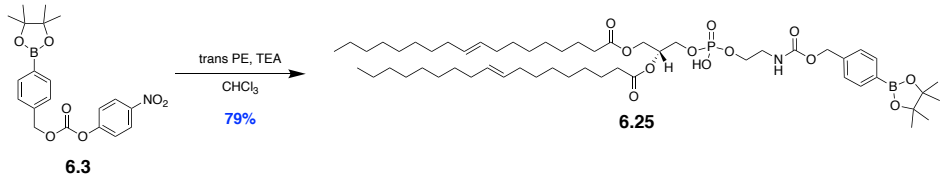
6.3 **6.24**

(2*R*)-3-((Hydroxy(2-((((4-(4,4,5,5-tetramethyl-1,3,2-dioxaborolan-2-yl)benzyl)oxy)carbonyl)amino)ethoxy)phosphoryl)oxy)propane-1,2-diyl (9*Z*,9'*Z*,12*Z*,12'*Z*,15*Z*,15'*Z*)-bis(octadeca-9,12,15-trienoate) (6.24)

18:3 PE (25 mg, 0.034 mmol) and **6.3** (16.3 mg, 0.041 mmol) were dissolved with 5 mL dry $CHCl_3$ at 0 °C in a 50 mL RBF under Ar protection. After adding triethylamine (14.2 µL, 0.102 mmol), the reaction was stirred overnight before being quenched by pouring into 100 mL of 0.5 N HCl. The aqueous layer was extracted with 3×25 mL chloroform. The combined organic layer was washed with 5×100 mL water and once with brine. The collected organic phase was dried over Na_2SO_4, filtered, and concentrated under reduced pressure. The resulting crude was subjected to silica gel column chromatography. Gradient elution from 100% chloroform to 10% MeOH in chloroform was needed to purify the product as a colorless oil (14.7 mg, 0.0148 mmol, 43% yield). R_f = 0.43 (20% MeOH-chloroform).

^{1}H NMR (600 MHz, 20% CD_3OD-$CDCl_3$) δ 7.59 (d, *J* = 7.7 Hz, 2H), 7.15 (d, *J* = 7.7 Hz, 2H), 5.25 – 5.06 (m, 12H), 5.03 (s, 1H), 4.92 (s, 2H), 4.19 (dd, *J* = 11.9, 2.9 Hz, 1H), 3.96 (dd, *J* =

12.0, 6.8 Hz, 1H), 3.81 – 3.68 (m, 4H), 3.21 (d, *J* = 2.7 Hz, 2H), 2.62 (t, *J* = 6.1 Hz, 8H), 2.16 – 2.08 (m, 4H), 1.88 (dt, *J* = 14.5, 7.3 Hz, 8H), 1.40 (s, 4H), 1.24 – 1.02 (m, 42H), 0.79 (t, *J* = 7.5 Hz, 6H). ^{13}C NMR (126 MHz, 20% CD_3OD-$CDCl_3$) δ 173.97, 173.60, 157.36, 139.72, 134.95, 132.60, 131.96, 130.22, 130.20, 128.34, 128.32, 128.26, 128.25, 127.83, 127.82, 127.16, 126.93, 116.36, 84.11, 75.04, 70.46, 66.61, 64.65, 63.74, 62.63, 55.91, 41.52, 34.22, 34.07, 31.96, 29.70, 29.67, 29.65, 29.30, 29.27, 29.20, 29.19, 29.15, 29.13, 27.24, 25.64, 25.54, 24.92, 24.87, 24.73, 24.38, 22.70, 20.56, 14.17, 14.16, 13.98. ^{31}P NMR (202 MHz, 20% CD_3OD-$CDCl_3$) δ -2.44. ^{11}B NMR (160 MHz, 20% CD_3OD-$CDCl_3$) δ 31.81. ESI-MS: $[M-H]^-$ calcd for $C_{55}H_{86}BNO_{12}P$: 994.5981; Found: 994.6401.



(2*R*)-3-((Hydroxy(2-((((4-(4,4,5,5-tetramethyl-1,3,2-dioxaborolan-2-yl)benzyl)oxy)carbonyl)amino)ethoxy)phosphoryl)oxy)propane-1,2-diyl (9*E*,9'*E*)-bis(octadec-9-enoate) (6.25)

18:1 trans PE (25 mg, 0.0336 mmol) and **6.3** (15.97 mg, 0.04 mmol) were dissolved with 5 mL dry $CHCl_3$ at 0 °C in a 50 mL RBF under Ar protection. After adding triethylamine (14.05 µL, 0.1 mmol), the reaction was stirred overnight before being quenched by pouring into 100 mL of 0.5 N HCl. The aqueous layer was extracted with 3×25 mL chloroform. The combined organic layer was washed with 5×100 mL water and once with brine. The collected organic phase was dried over Na_2SO_4, filtered, and concentrated under reduced pressure. The resulting crude was subjected to silica gel column chromatography. Gradient elution from 100% chloroform to 10% MeOH in chloroform was needed to purify the product as a colorless oil (26.8 mg, 0.0267 mmol, 79 % yield). R_f = 0.45 (20% MeOH-chloroform).

^{1}H NMR (500 MHz, 20% CD_3OD/$CHCl_3$) δ 7.62 (d, *J* = 7.6 Hz, 2H), 7.18 (d, *J* = 7.7 Hz, 2H), 5.22 (t, *J* = 4.8 Hz, 4H), 5.06 (s, 1H), 4.96 (d, *J* = 13.5 Hz, 2H), 4.21 (d, *J* = 9.8 Hz, 1H), 3.77

(d, *J* = 22.7 Hz, 4H), 3.23 (s, 2H), 2.14 (td, *J* = 7.7, 3.6 Hz, 4H), 1.86 – 1.75 (m, 8H), 1.43 (s, 4H), 1.23 – 1.03 (m, 64H), 0.72 (d, *J* = 7.0 Hz, 6H). ^{13}C NMR (126 MHz, 20% $CD_3OD/CHCl_3$) δ 173.76, 173.41, 157.11, 139.51, 134.75, 130.35, 130.03, 130.01, 126.74, 83.89, 70.24, 66.41, 64.47, 63.53, 62.41, 55.74, 45.29, 41.36, 34.04, 33.89, 32.44, 32.42, 31.75, 29.50, 29.48, 29.46, 29.33, 29.16, 29.03, 28.96, 28.93, 28.88, 28.86, 24.73, 24.69, 24.56, 24.22, 22.51, 13.82. ^{11}B NMR (160 MHz, 20% $CD_3OD/CHCl_3$) δ 30.82. ESI-MS: $[M-H]^-$ calcd for $C_{55}H_{94}BNO_{12}P$: 1002.6607; Found: 1002.6474.

Preparation of liposomes for Nile red release assays

A stock solution of 25 mM lipid **6.1** was prepared in a mixture of methanol and chloroform, while NR and PC stock solutions were prepared in chloroform. All the stock solutions were stored in -20 °C freezer after preparation. Proper volumes of each stock solution were pipetted into a small vial to obtain a mixture of 2 mM/or 0.1 mM of total lipid content with the desired percentage of each lipid. NR was added as an extra 5% of the total lipid content. The organic solvents were then evaporated under a nitrogen stream and the resulting lipid film was further dried under vacuum for at least one hour. The film was then hydrated with 1×TBS (pH=7.4, containing 25 mM Tris/Tris HCl, 0.13 M NaCl, 0.0027 M KCl) at 60 °C water bath for 3 sets of 20 min with vortexing after each set. After ten freeze-thaw cycles with dry ice-acetone bath and 60 °C water bath, the solutions were extruded through a 200 nm polycarbonate membrane for 15 passes with a LiposoFast extruder (Avestin, Inc.). The resulting liposomes were stored at 4 °C and were used up within two days. NR encapsulated **6.6**-containing liposomes were prepared with the exact same procedure.

Preparation of liposomes for ANTS/DPX release assays

The same stock solutions of lipid **6.1** and PC prepared for NR study were used as well as PA, DPPC and DOPE stock solutions prepared in either chloroform or MeOH/chloroform mix. 12.5 mM ANTS and 45 mM DPX were co-dissolved with 20 mM HEPES buffer (pH=7.4, osmotic

pressure of final stock solution was adjusted to 344 mOsm/kg by addition of solid NaCl). Proper volumes of each stock solution were pipetted into a small vial to obtain the desired percentage of each lipid at a 5 mM total lipid content scale. The solvents were evaporated under nitrogen stream and the resulting lipid film was further dried under vacuum for at least one hour. After that, the lipid film was hydrated with the ANTS/DPX stock solution at 60 °C water bath for 4 sets of 15 min with vortexing after each set, followed by ten freeze-thaw cycles with dry ice-acetone bath and 60 °C water bath. The resulting liposome solutions were then extruded through a 200 nm polycarbonate membrane for 21 passes with a LiposoFast extruder (Avestin, Inc.). Finally, the unencapsulated dye was removed via a size exclusion column packed with Sephadex G-50 (pre-saturated with isotonic 20 mM HEPES buffer, pH=7.4). Fractions were collected every ~1 mL and the second fraction showing significant turbidity was chosen to run further release studies, where fluorescence increases were observed when aliquots were treated with triton X-100. **6.6** containing liposomes encapsulating ANTS/DPX were prepared with the exact same procedure.

Nile red release studies with hydrogen peroxide addition

100 μL of the prepared 2 mM NR-encapsulated liposome solution was added into a sub-micro quartz cuvette. 1 μL of 30% H_2O_2 solution was then added into the cuvette. Fluorescence intensities of the resulting solution were measured over time at room temperature (excitation wavelength=552 nm, excitation slit=5 nm, emission slit=5 nm). Control experiments were also done by adding MilliQ water into the lipid **6.1** containing liposomes or adding H_2O_2 into liposomes without lipid **6.1**. When processing the data, intensities at 635 nm were selected and converted into percentage of initial fluorescence intensity before adding stimuli. Experiments were run at least 3 times with different batches of liposomes. Averaged data were reported with error bars denoting standard error. **6.6** liposomes were tested with same method.

For NR release studies with different concentrations of H_2O_2, 2 mM PC-based liposome

samples containing 75% lipid **6.1** encapsulating NR were used. Different concentrations of H_2O_2 stock solutions were prepared by diluting 30% H_2O_2 with MilliQ purified water. Aliquots of 1 μL of different concentrations of H_2O_2 stock solution were then added into 100 μL liposome solutions in the sub-micro quartz cuvette. The same fluorescence detection and data analysis method was used as described above.

For NR release studies with diluted liposomes containing 75% lipid **6.1**, 0.1 mM liposomes were prepared using same thin film-hydration method by cutting total lipid concentration down during the lipid film preparation. The same hydrogen peroxide stock solutions were used. Aliquots of 1 μL of different concentration of H_2O_2 stock solution were then added into 100 μL solutions in the cuvette. Fluorescence intensities of the resulting solutions were measured over time at room temperature (excitation wavelength=552 nm, excitation slit=5 nm, emission slit=10 nm).

ANTS/DPX release assays with hydrogen peroxide addition

A 100 μL aliquot of the prepared liposome solution was added into a sub-micro quartz cuvette. 1 μL 30% of H_2O_2 stock solution was added directly into the cuvette. Fluorescence intensities were then measured over time at room temperature (excitation wavelength=350 nm, excitation slit=10 nm, emission slit=10 nm). After completion, 1 μL 20% Triton X-100 was added to lyse the liposomes. Control experiments were also done by switching H_2O_2 into MilliQ water. When processing the data, fluorescence intensities at 510 nm were selected and fluorescence increases were reported as a percentage of the fluorescence after triton X-100 treatment for each sample. **6.6** liposomes were tested with the same method. For release studies with 10X diluted liposomes containing **6.1**, liposomes were first prepared using the same method, and then they were diluted 10X with isotonic buffer. The same experimental and detection methods were used except for switching of the Ex/Em slits to 20/20 nm. Experiments were run at least 3 times with different batches of liposomes. Averaged data were reported with error bars

showing standard error.

Dynamic light scattering (DLS) and zeta potential (ZP) analysis of liposome size before and after release

DLS measurements were carried out with a Malvern Zetasizer Nano ZS instrument equipped with a 4.0 mW laser operating at l=633 nm. Samples were prepared by diluting the liposome solutions before or after release 10 times with proper buffer. All samples were determined at a scattering angle of 173° at 20 °C. The data reported were the average of three tests with error bars indicating standard error. ZP values for PC liposomes and liposomes containing 75% lipid **6.1** in PC before and after H_2O_2 addition were also measured on the Malvern Zetasizer Nano ZS instrument. The liposome solutions were diluted 10 times with proper buffer and added into a DTS1070 folded capillary cell before measurement.

Transition electron microscope (TEM) analysis

0.5 mM PC liposomes and 75% lipid **6.1** in PC liposomes without any dye encapsulation were prepared according to the above-mentioned standard liposome preparation procedure. To 100 μL liposomes in a vial, 0.5 μL of 30% H_2O_2 was added and the samples were incubated at room temperature for at least 2 hours before TEM analysis. For TEM studies, a drop (5–10 μL) from each solution was immobilized (for 1 minute) onto a thin carbon film supported by a 200-mesh copper grid and then stained (for one minute) with a 1.0% (w/v) solution of neutral phosphotungstic acid. After drying, the samples were stored in a desiccator overnight prior to examination. Images were collected using a JEOL 1400 Flash microscope operating with a beam energy of 80 keV. Images were collected using a Gatan One View camera and processed with ImageJ software. Scale bars on images denote 200 nm.

TLC analysis of free lipid 6.1 after treatment of hydrogen peroxide

1 μL of 30% H_2O_2 was added to 0.5 mL of a 1 mg/mL stock solution of lipid **6.1** in 50%

methanol/chloroform and incubated at room temperature for 2 hours. The reaction mixture, alongside separate standards for lipid **6.1** as well as DOPE were spotted onto a normal aluminum-backed silica gel TLC plate. The plates were developed with 10% or 20% MeOH-$CHCl_3$ as eluant and were visualized with $KMnO_4$ stain after developing.

Mass spectrometry analysis of free lipid 6.1 after hydrogen peroxide treatment

For free lipid **6.1**, 1 μL of 30% H_2O_2 was added into 30 μL of a 25 mM stock solution lipid **6.1** in 50% methanol/chloroform. The mixture was next diluted into 5 mL with methanol before being subjected to the mass spectrometer. The final concentration was ~150 μM. ESI positive mode was used for detection.

NMR analysis of free lipid 6.1 or liposomes containing 6.1 after treatment of hydrogen peroxide

For analysis of free lipid, compound **6.1** was dissolved in a mixture of $CDCl_3/CD_3OD/D_2O$=65/25/4 (v/v) at a concentration of 2 mg/mL. A 0.5 mL solution was transferred into an NMR tube for analysis. After taking an initial reading, 1 μL of 30% H_2O_2 was added directly into the NMR tube and the mixture was mixed well by gentle shaking. NMR spectra were recorded over time and analyzed by MestReNova.

For NMR analysis of liposomes, 2 mM liposomes composed of 100% lipid **6.1** without dye encapsulation were prepared. 5 μL of 30% H_2O_2 was added into 500 μL liposome solution. After being incubated at room temperature for five minutes, excess peroxide was quenched by adding 50 μL 1 M thiosulfate followed by vigorous vortexing. Next, water was removed under reduced pressure and the vial was placed under vacuum for an extra one hour. NMR samples were prepared by dissolving the residue in 0.6 mL 20% $CDCl_3/CD_3OD$ (v/v).

Evaluation of potential NR bleaching by H_2O_2

NR (0.1 mM) solutions were prepared in both methanol and 50% methanol in water (v/v), and then 100 µL was transferred into a sub-micro cuvette. After taking an initial reading, 1 µL 30% H_2O_2 was added into the cuvette (final concentration = 98 mM). The fluorescence intensities were measured over time (Ex. Wavelength = 530 nm, Ex/Em slit = 5/5 nm, Em. Wavelength = 635 (MeOH) or 655 (MeOH/H_2O)). Cuvettes were sealed during measurement to prevent solvent evaporation.

Restoration of NR fluorescence after liposome release using Triton X-100

For liposome studies, 2 mM PC-based liposomes containing 75% **6.1** were used. Kinetic curves were taken on a Cary Eclipse fluorometer using kinetic mode. Liposomes (100 µL) were first added into a sub-micro cuvette. The excitation wavelength was set to be 552 nm and intensities at 635 nm were recorded over time. 1 µL 30% H_2O_2 was added at 1 min, and 1 µL 10% Triton X-100 was added at 10 min.

Chapter 7. Development of ROS-responsive caged guanidine lipids for targeted delivery

(The scientific data used in this Chapter was included in the manuscript by the authors: Lou, Jinchao; Qualls, Megan L.; Hudson, Macy M.; McBee Dillon P.; Baccile, Joshua A.; Best, Michael D., Reactive Oxygen Species (ROS) Activated Liposomal Cell Delivery using a Boronate-Caged Guanidine Lipid, in submission)

7.1. Project overview

In Chapters 2-6, we present multiple triggered release systems that can enhance therapeutic cargo release in a controlled manner upon treatment of various disease-related metabolites. Other than triggering release, liposomal delivery platforms can also take advantage of active targeting strategies that allow precise delivery of cargo to the specific disease site. Cell-penetrating peptides (CPPs) exhibit exceptional cell delivery properties by leveraging repeating cationic units such as arginine (presenting positively charged guanidinium moieties at physiological pH) to bind and traverse lipid membranes. However, their drawback is the lack of selectivity toward diseased cells. Due to the excellent potential of ROS-mediated drug delivery strategies, in this Chapter, we report a boronate-caged guanidine-lipid **7.1** for enhancing liposome cellular delivery mediated driven by reactive oxygen species (ROS). These liposomes are designed to mimic the exceptional cell delivery properties of CPPs. Furthermore, the inclusion of the boronate cage is designed to enhance selectivity such that cell entry will only be activated in the presence of ROS. Boronate uncaging by hydrogen peroxide was verified by mass spectrometry and zeta potential (ZP) measurements. A microplate-based fluorescence assay, as well as dynamic light scattering (DLS) analysis, were employed to study the ROS-mediated vesicle interactions between **7.1**-liposomes and anionic membranes. Cellular delivery studies utilizing fluorescence microscopy demonstrated significant enhancements in cell infiltration only when **7.1**-liposomes were incubated with hydrogen peroxide. Our results showcase that lipid **7.1** exhibits strong potential as an ROS-responsive liposomal platform for targeted drug delivery applications.

7.1.1. Liposome targeting and cell penetrating peptides

Liposomes are effective drug delivery nanocarriers; however, smart liposomes containing caged targeting moieties or triggered release mechanisms can enhance diseased-cell specificity and drug release/potency.[109,289-291] The selective targeting of liposomes to diseased cells is a key aspect that requires improvement. While moieties including antibodies and small molecules (i.e., folate, peptides) enhance delivery to diseased cells by binding to overexpressed cell-surface receptors, these are not economically feasible or tunable to different cell types, respectively. Cell-penetrating peptides (CPPs), polycationic peptide sequences inspired by the HIV tat protein,[292] have emerged as powerful transport vectors for intracellular delivery.[293-295] Despite their great potential in clinical uses and the fact that numerous CPPs have entered clinical trials since the late 1980s, none of these have been approved by FDA for clinical use.[295] Typical CPPs possess positively charged amino acid sequences that bind to negatively charged cell membranes through electrostatic interactions at physiological pH and leverage these associations to traverse cell membranes.[292] As a result, most of these do not exhibit cell type or tissue specificity. Non-specific CPP-mediated cell-penetration into normal tissues can result in reduced therapeutic efficacy and increased toxicity, which limits applicability.[296,297]

7.1.2. Introduction to activable cell penetrating peptide

To address this problem, smart delivery systems utilizing activable CPPs have been developed, which are designed to be responsive to a certain stimulus that can enhance the selectivity of CPPs towards certain diseased cells.[298,299] External stimuli such as light have been widely used via the development of photocleavable CPPs.[300-302] Pathophysiological conditions of diseased cells, including enhanced acidity[303-305] and aberrant enzyme expression[208,306,307] have been harnessed for targeted delivery. For example, the Rodosz group reported pH activable CPP **7.2** (Figure 7.1A) that can be potentially applied in tumor-targeted delivery.[16] They chose a well-known TAT peptide sequence and chemically masked the primary amine

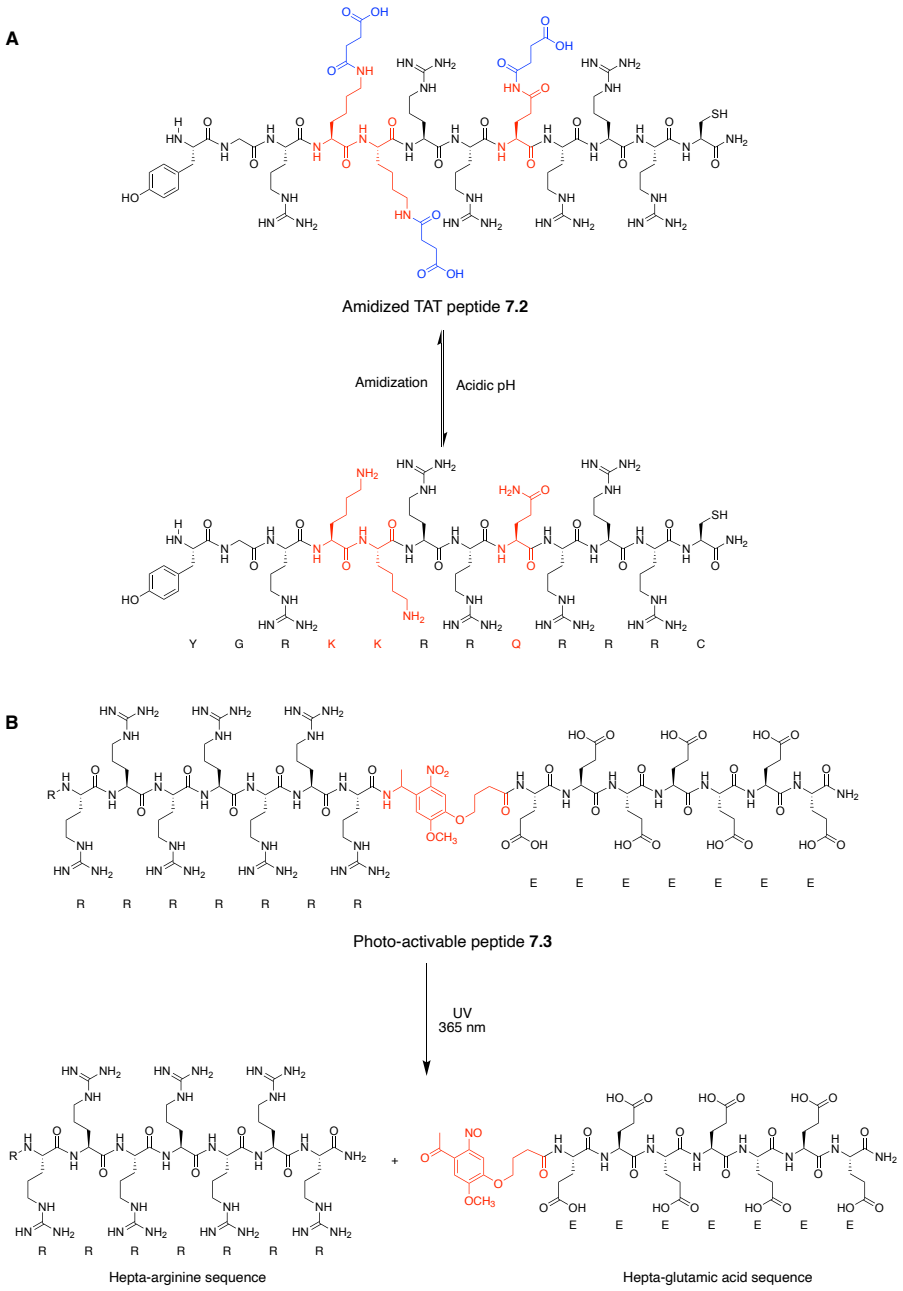


Figure 7.1. Representative activable CPPs that show cellular uptake only upon treatment of a desired stimulus. A. pH activable peptide **7.2** based on a TAT peptide. The primary amines on the side chains are masked with succinyl amide, which could be removed in an acidic environment. **B.** Photo-activable peptide **7.3** combining CPP R7 and hepta-glutamic acid peptide with a photo-cleavable linker. UV irradiation resulted in a free R7 peptide that could increase cellular uptake.

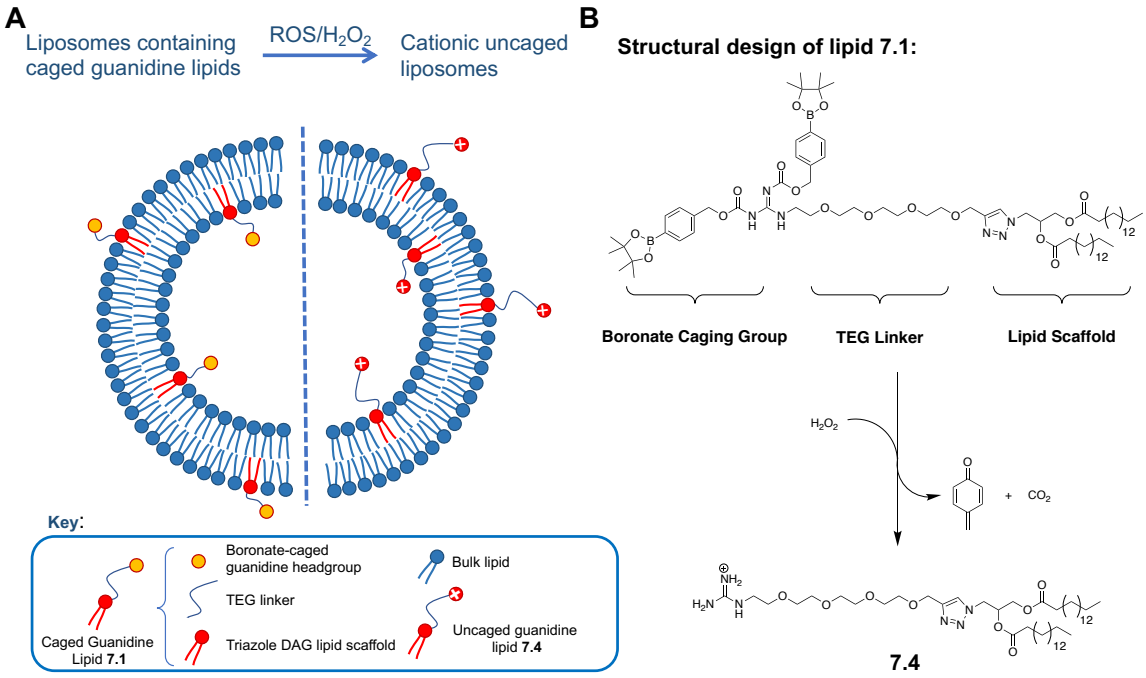
residues through the formation of succinyl amides. The amidized peptide **7.2** could be activated in more acidic tumor environment due to the rapid hydrolysis of the succinyl amide cages and the unveiling of positive charges. Regarding external stimuli, the Stevens group developed photo-caged peptide **7.3** (Figure 7.1B) by connecting the well-known positively charged CPP hepta-arginine (R7) and negatively charged hepta-glutamic acid (E7) together with a photo-sensitive linker.[300] Upon UV irradiation and the cleavage of the linker, the resulting CPP R7 could effectively enter cells. They demonstrated that this strategy could be utilized to deliver a wide variety of molecular cargo, including small molecules, proteins, and nanoparticles.

Although clever strategies have been developed over the years, and they have proven to be effective for enhanced cellular uptake, internal stimuli are hindered by minimal differences between healthy and diseased cells (i.e., pH ~6.5-6.7 (cancer) vs. ~7.2-7.4 (healthy)),[308] providing a narrow window for differentiation. The delivery of external stimuli to the desired diseased sites is also problematic, exemplified by UV light irradiation exhibiting limited tissue penetration abilities and can cause damage to healthy tissue.[309] As described in Chapter 6, ROS has been significantly underexplored as a trigger for liposome activation, which are known to be upregulated and closely related to diseases such as cancer,[271] Alzheimer's disease,[310,311] atherosclerosis,[312] hypertension,[313] diabetic nephropathy,[314] and lung fibrosis.[272,273] One rare H_2O_2-activated CPP example was reported by Tsien et al.,[315] where they incorporated a boronic acid-containing cleavable linker between polycationic and polyanionic CPPs separately labeled with a FRET pair. This system selectively reacts with endogenous H_2O_2, acting effectively as a H_2O_2 sensor for cellular targeting and imaging purposes. While this elegant design showcased that ROS could be applied to activable CPP design, reports of liposomal delivery platforms using similar strategies remain sparse.

7.2. Design and synthesis of the ROS-responsive caged guanidine lipids

In this Chapter, we report the development of a smart liposomal delivery system containing masked lipid **7.1** bearing boronate-caged guanidinium headgroups to activate cell entry only in the presence of ROS. This provides a key advancement in which neutral, latent liposomes will circulate, while encountering of upregulated ROS will unveil cationic groups to promote cell entry (Scheme 7.1A). The polycationic characteristics of typical CPPs result from the inclusion of arginine or lysine, which contain a guanidine and an amine group, respectively. Although they carry the same net charge under physiological conditions, the guanidine groups can interact more effectively with cell membranes due to hydrogen bonding interactions with phosphate and sulfate moieties presented on the cell surface, leading to enhanced internalization.[316-318] For example, Aida and co-workers developed dendritic photoactivable guanidinium molecular glues that could efficiently adhere to anionic biomolecules, such as DNA and phospholipid membranes, upon light irradiation.[319]

The structural design for lipid **7.1** is shown in Scheme 7.1B. The guanidium headgroup of lipid **7.1** is masked using arylboronic ester groups, which have been widely applied in ROS-responsive materials due to their fast degradation kinetics upon H_2O_2 contact.[278] Similar to the strategies we presented in Chapter 6, lipid **7.1** can be specifically oxidized by H_2O_2. After the oxidative cleavage, the remaining structure undergoes a QM elimination reaction that releases cationic guanidium lipid **7.4** designed to turn on cell entry. Since CPPs typically contain several cationic groups such as arginine residues, it is noteworthy that our compound contains only one caged guanidine. This is because it was envisioned that liposome membranes would provide a fluid multivalent environment in which multiple individual guanidinium-lipid conjugates would conspire to mimic CPP structures. Furthermore, the density of charged moieties can be modulated based on the percentage of **7.1** that is incorporated within the liposomes. Lipid **7.1** also contains a tetra ethylene glycol (TEG) linker between the caged guanidinium headgroup and the lipid backbone to prevent the headgroups from being buried



Scheme 7.1. Design for caged guanidine liposomes containing lipid 7.1 for ROS-mediated targeted delivery. A. Cartoon depicting uncaging when lipid **7.1** is incorporated in the membrane. Positively charged membranes will be generated in the presence of H_2O_2. **B.** Structure of caged guanidinium lipid **7.1** and the uncaging mechanism after adding H_2O_2. The addition of H_2O_2 cleaves the boronate ester headgroup, leading to a QM self-immolation process that ultimately produces cationic guanidinium lipid **7.4**.

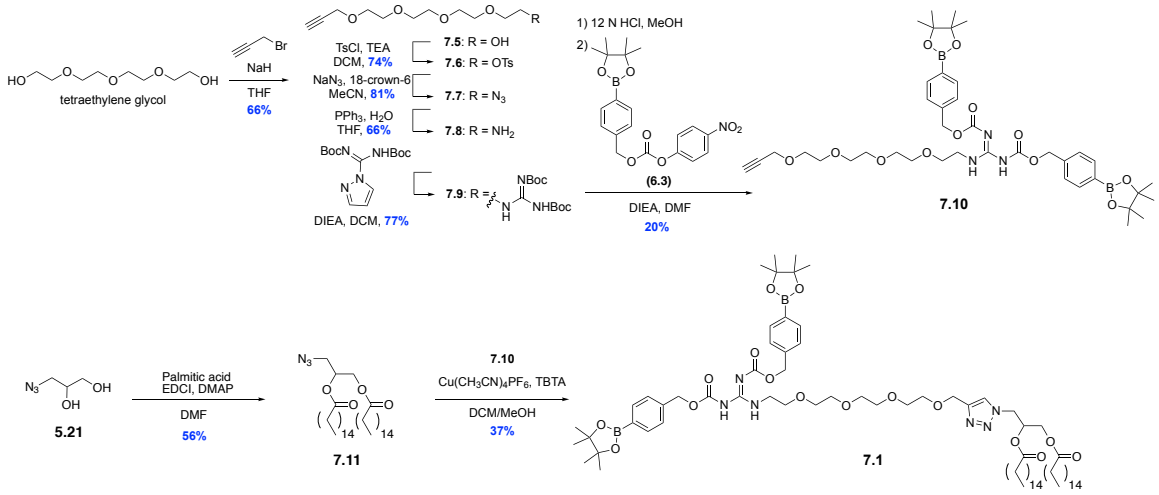
inside the membrane bilayer and thus inaccessible to react with added H_2O_2. Furthermore, a key triazole functionality is included as a lipid headgroup mimetic since this polar moiety is known to prefer the aqueous interface rather than the hydrophobic membrane environment.[320] This also facilitates synthesis of **7.1** by exploiting the copper-catalyzed azide-alkyne cycloaddition (CuAAC) reaction.

The synthetic route to compound **7.1** is detailed in Scheme 7.2. Amino and alkynyl functionalized TEG linker **7.8** was first synthesized in four steps from tetra ethylene glycol, including mono-ether coupling with propargyl bromide to **7.5**, alcohol tosylation to **7.6**, substitution with azide to **7.7**, and a Staudinger reduction to reduce the azide into the amine group of **7.8** without reducing the alkyne group.[321] Compound **7.8** was next reacted with *N*,*N*′-di-Boc-1H-pyrazole-1-carboxamidine to introduce the Boc-protected guanidine headgroups of **7.9**. Deprotection of the Boc groups with concentrated hydrochloric acid followed by coupling to arylboronate ester *p*-nitrophenol carbonate compound **6.3**[281,322] resulted in boronate caged guanidine intermediate **7.10**, which was reacted via CuAAC with azido-lipid **7.11**[255,258] to produce boronate-caged guanidine lipid **7.1**.

7.3. Verification of lipid uncaging

7.3.1. Mass spectrometry analysis

Once we obtained ROS-responsive caged guanidine lipid **7.1**, we first verified that the uncaging process occurred upon H_2O_2 addition using high-resolution mass spectrometry (HRMS). Lipid **7.1** was dissolved in a chloroform/methanol mixture and incubated with H_2O_2 for 1 hour before HRMS analysis. Direct infusion positive mode electrospray ionization (ESI^+) HRMS showed successful boronate uncaging and formation of positively charged guanidinium lipid **7.4** based on the presence of expected mass peaks for this product (Figure 7.2).



Scheme 7.2. Synthetic route to caged guanidine lipid 7.1. Alkynyl and amino functionalized TEG intermediate **7.8** was synthesized in four steps from tetraethylene glycol, including alkylation with propargyl bromide, tosylation, azide substitution, and Staudinger reduction, which was followed by guanidinylation to introduce the Boc-protected guanidine headgroups of **7.9**. Boc deprotection, boronate caging group introduction, and CuAAC with azido-lipid **7.11** yielded the final caged guanidine lipid **7.1**.

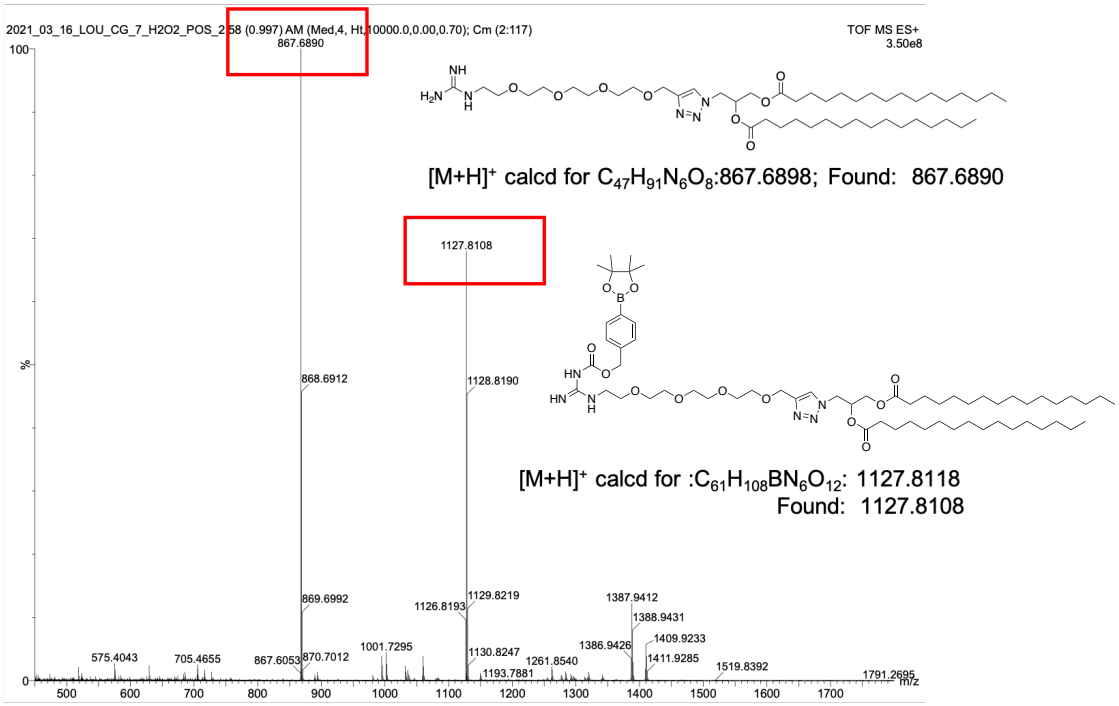


Figure 7.2. High-resolution mass spectrometry analysis of lipid 7.1 after H_2O_2 treatment.

Expected uncaged products were detected after H_2O_2 incubation.

7.3.2. Zeta potential analysis of lipid uncaging

Next, to study uncaging and guanidinium formation within a membrane environment, zeta potential (ZP) measurements were conducted to verify the expected introduction of positive charge within liposomes. Unilamellar liposomes containing 0-20% of lipid **7.1** and otherwise composed of PC (mixed isomers from chicken egg) were prepared using standard thin-film hydration methods, including lipid film preparation, hydration, freeze-thaw cycling, and extrusion through 200 nm polycarbonate membranes. The formation of uniform liposomes with desired diameters was determined by dynamic light scattering (DLS), with details discussed in later sections. ZP values were first measured for PC liposomes including 0%, 10%, or 20% of **7.1** before and after ~25 mM H_2O_2 incubation for one hour. As shown in Figure 7.3A, 100% PC liposomes initially showed a slight negative charge, in agreement with literature,[188] and did not change upon H_2O_2 incubation. For **7.1**-liposomes, dramatic increases in positive charge were detected that correlated with the percentages of **7.1** within liposomes. These results show that compound **7.1** is successfully uncaged by H_2O_2 to produce the positively charged lipid product, as expected.

Next, a detailed study of ZP changes upon H_2O_2 treatment over time was conducted by treating liposomes containing 20% **7.1** with 0.1 mM, 0.5 mM, or 1 mM H_2O_2. As shown in Figure 7.3B, increasingly positive ZP values were observed over time for liposomes treated with 0.5 mM or 1 mM H_2O_2, with 1 mM H_2O_2 showing slightly faster kinetics. Whereas PC liposomes treated with 1 mM H_2O_2 showed minimal changes in ZP values. Interestingly, 20% liposomes incubated with 0.1 mM H_2O_2 also only exhibited a modest increase in ZP values. Considering that oxidative cleavage of the boronate headgroups requires stoichiometric amounts of peroxide, insufficient H_2O_2 could lead to incomplete uncaging, resulting in limited changes to liposome surface charge that could affect subsequent cellular entry. These results show that 20% **7.1**-liposomes begin to produce cationic liposomes when subjected to ROS concentrations in the range previously cited for cancer cells (~100 μM), although the response

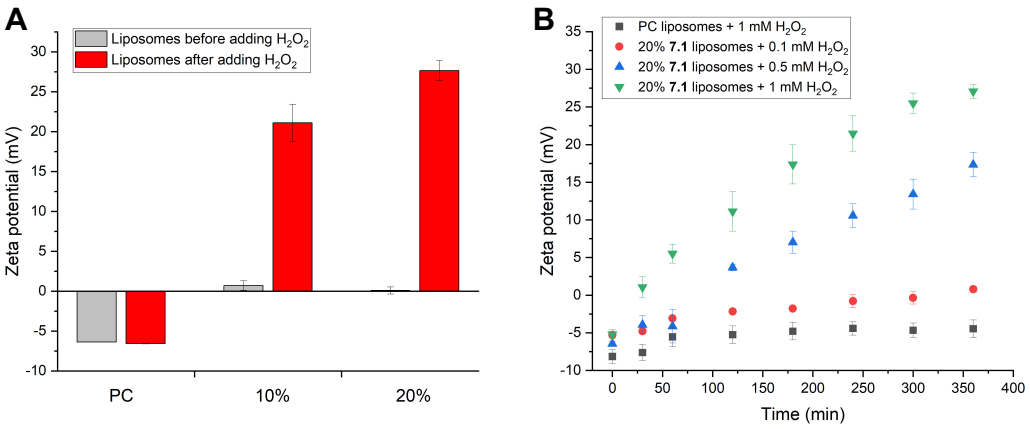


Figure 7.3. Zeta potential measurements for liposomes containing 0%, 10%, and 20% lipid 7.1 before and after H_2O_2 addition. A. End point studies indicate strongly positively charged liposomes were generated after H_2O_2-induced uncaging, while 100% PC control liposomes did not show any changes in ZP values. **B.** Time-dependent ZP analysis for PC-based liposomes containing 0% or 20% **7.1** after adding 0.1 mM, 0.5 mM, or 1 mM H_2O_2. **7.1**-Liposomes treated with 0.5 mM or 1 mM H_2O_2 both showed increases in ZP values over time, while 0.1 mM H_2O_2 treatment only resulted in a slight ZP increase. Error bars denote standard errors from at least three independent trials.

is fairly weak at this level. Further optimization would be beneficial to increase activity at lower H_2O_2 concentrations. Nevertheless, these results support uncaging of **7.1** and confirm the generation of cationic liposomes.

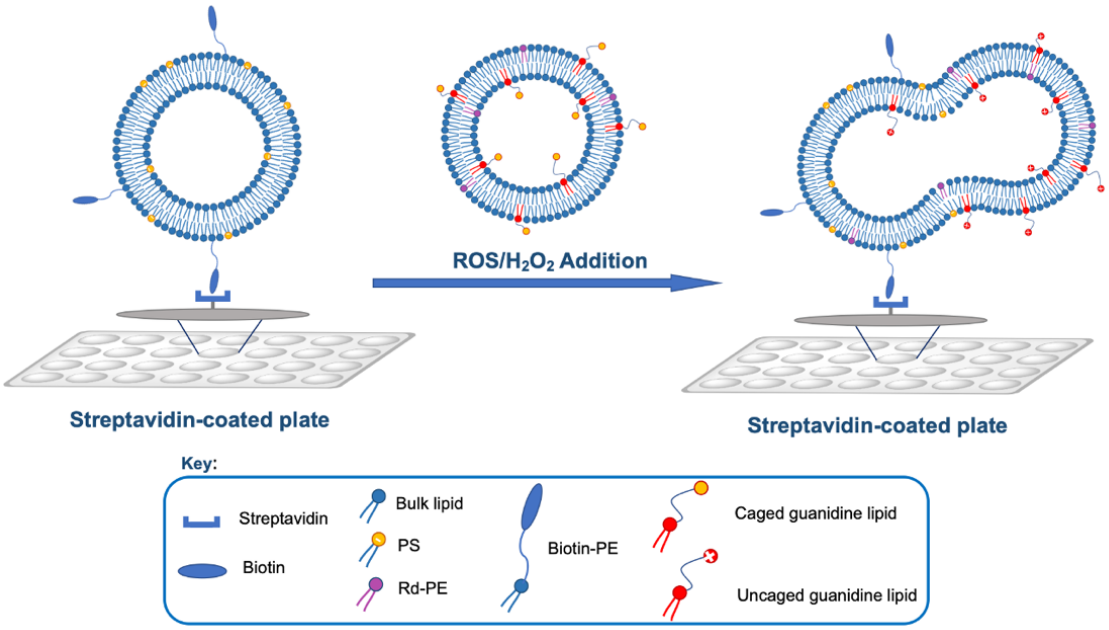
7.4. Microplate-based liposome assay to detect binding/fusion driven by uncaging

7.4.1. Assay overview

To study interactions involving anionic membranes after boronate uncaging, we developed a fluorescence-based microplate vesicle binding/fusion assay by modifying protocols for immobilizing intact liposomes that we reported previously.[255,323,324] This assay provides an effective model system for gauging cell entry by determining the extent to which the presence of uncaged **7.1** promotes liposome binding/fusion. Anionic liposomes targeted for binding/fusion contained phosphatidylserine (PS), which is of particular interest since cancer cells are known to overexpress this negatively charged lipid on the outer leaflets of their cell membranes, which could be exploited for promoting cell entry.[23,325] This approach analyzes the binding and/or fusion of two different samples of liposomes, as shown in Scheme 7.3. The first batch of liposomes was immobilized onto 96-well streptavidin-coated microplates by including biotin-PE (1%) within a PC formulation doped with PS. The resulting functionalized microplate surfaces were next treated with a second liposome batch that includes a varying percentage of **7.1** and a fluorescently labeled lipid, rhodamine-L-α-phosphatidylethanolamine (Rd-PE), for detection purposes. Washes were performed after each step to remove liposomes that did not interact with the surface or with immobilized liposomes, respectively. Next, microplate fluorescence readings were acquired to evaluate binding/fusion based on expected fluorescence enhancements.

7.4.2. Microplate binding/fusion assay results

Initially, we sought to show that liposomes were successfully immobilized onto microplates, for which experiments only required one batch of liposomal samples. To do so, we prepared PC-



Scheme 7.3. Cartoon illustration for fluorescence-based microplate binding assays. Anionic PS liposomes containing biotin-PE are first immobilized onto a streptavidin-coated plate. The second batch of liposomes containing lipid **7.1** and labeled with Rd-PE either treated with H_2O_2 or untreated was then added, with washes used to remove non-interacting liposomes. Increased fluorescence is expected to result from **7.1** uncaging that activates fusion/binding to immobilized liposomes (fusion is depicted in the cartoon).

based liposomes doped with 5% PS and 1% biotin-PE that were fluorescently labeled with 1% Rd-PE. After treating each well with different concentrations of these samples, and conducting washes to remove unbound liposomes, microplate fluorescence readings were acquired. As shown in Figure 7.4, we observed a dose-dependent increase in Rd-PE fluorescence, indicating that liposomes were successfully immobilized. Liposomes without biotin-PE only resulted in minimal fluorescence changes, acting as effective negative controls. Undergraduate student Macy Hudson assisted with this assay.

To apply microplate functionalization for a vesicle binding/fusion assay, the first batch of liposomes composed of PC doped with 5% PS and 1% biotin-PE were immobilized onto streptavidin-coated microplates. The resulting microplate wells were then treated with the second batch of samples. These consisted of PC liposomes containing 0%, 10%, or 20% **7.1** along with 1% Rd-PE in which half of the samples were treated with 10 mM H_2O_2, while the other half were untreated controls. The resulting liposomes were incubated for 3 hours with the previously functionalized microplates to interact with immobilized liposomes and unbound fluorescent liposomes were removed via washing with TBS buffer. Fluorescence analysis then showed that **7.1**-liposomes yielded a significant dose-dependent increase in fluorescence (Figure 7.5), with 20% liposomes showing greater enhancements compared to 10% liposomes. In negative control experiments, **7.1**-liposomes not treated with H_2O_2, PC liposomes lacking **7.1**, or only buffer addition to immobilized liposomes all yielded minimal fluorescence signal changes.

A positive control experiment was also performed by treating 5% PS liposome-functionalized microplate surfaces with Rd-PE-labeled PC liposomes containing 10% or 20% of DOTAP, which is a cationic lipid widely used in cell transfection.[257] Since DOTAP carries the same net charge as uncaged lipid **7.1**, this experiment serves as an ideal positive control that mimics the expected endpoint conditions of the previous assay. We again observed increases in Rd-

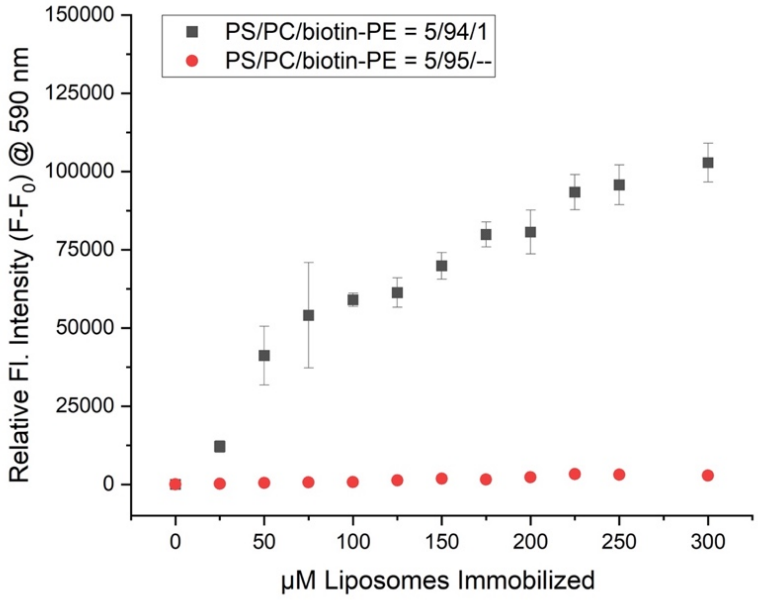


Figure 7.4. Evidence of successful immobilization of anionic PS liposomes onto streptavidin-coated microplates containing 5% PS, 1% biotin-PE and 1% Rd-PE. Dose-dependent increases were observed for liposomes labeled with biotin-PE, while those without biotin-PE incorporation showed minimal fluorescence enhancements. Error bars denote standard errors from at least three independent trials.

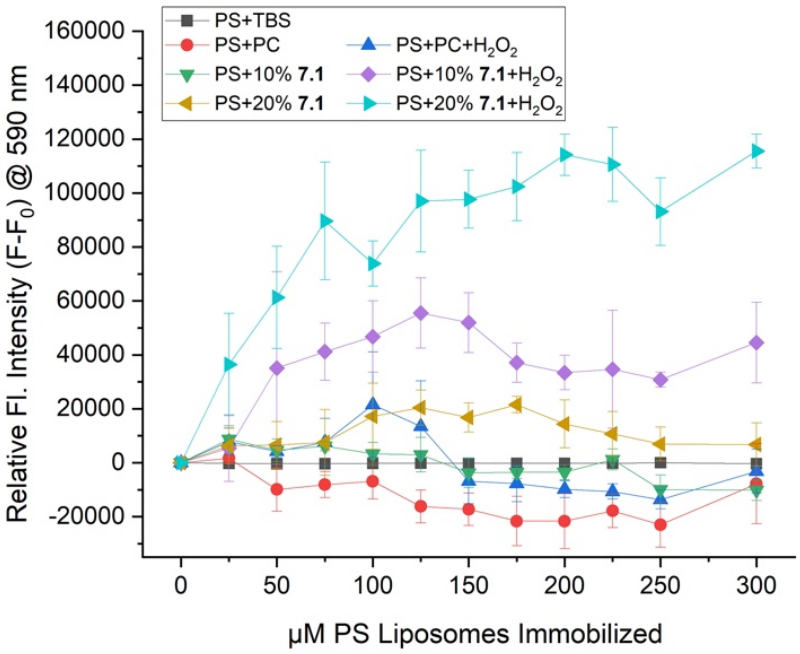


Figure 7.5. Results for microplate-based binding/fusion assay. Dose-dependent fluorescence increases were observed only when 10% or 20% **7.1**/PC liposomes were incubated with 5% PS/PC liposomes after treatment with H_2O_2. Minimal changes were observed without H_2O_2, when PS/PC liposomes were treated with liposomes lacking **7.1**, or with just TBS buffer addition. Error bars depict the standard errors of at least three readings.

PE fluorescence that correlated with DOTAP percentages, which also match well with the experimental data obtained from liposomes containing **7.1** with H_2O_2 incubation (Figure 7.6). These results support that ROS treatment leads to uncaging of **7.1**-liposomes, which promotes association with anionic liposomes that are in this case immobilized on microplate surfaces.

7.5. Dynamic light scattering studies

These conclusions were further evidenced by DLS analysis, in which our data support that 20% **7.1**/PC formulations form stable liposomes and that H_2O_2 treatment does not alter their morphology (raw distribution curves in Figure 7.7). However, when these liposomes were incubated with 10% PS/PC or 10/40/50 PA/PC/DOPE liposomes along with H_2O_2, increases in particle sizes were observed that we attribute to liposome fusion and/or binding. As shown in Figure 7.8 (raw distribution curves in Figure 7.9), particles with larger diameters and greater polydispersity indices (PDI) were only detected after H_2O_2 incubation. In contrast, negative control experiments in which liposomes were incubated with TBS buffer showed minimal changes in particle sizes. Here, the addition of DOPE appears to result in the production of particles with larger sizes, which likely results enhanced fusion due to the non-bilayer properties of this lipid.

7.6. Cellular delivery studies

After the successful demonstration of H_2O_2-mediated uncaging of lipid **7.1** and subsequent interactions with anionic membranes elucidated via microplate binding assays, we moved on to fluorescence microscopy studies to evaluate whether **7.1**-liposomes enhance the cellular delivery of liposomal cargo in the presence of H_2O_2. These experiments were performed in collaboration with Dr. Joshua Baccile's lab in UTK Chemistry. Graduate students Dillon McBee from the Baccile group and Megan Qualls from the Best lab led these studies.

For these experiments, we prepared 20% **7.1**/PC liposomes labeled with 0.08% Rd-PE, which

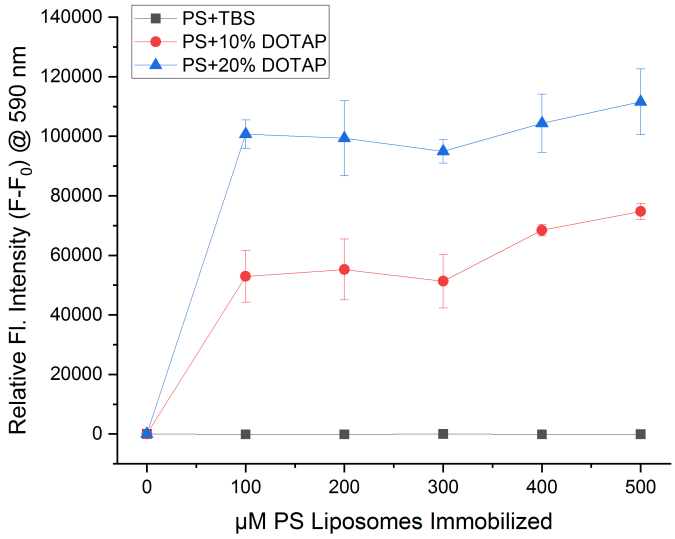


Figure 7.6. Microplate-based binding assay using 10% or 20% DOTAP liposomes. Increases in fluorescence were observed for liposomes containing 10% and 20% DOTAP, which correlated with the percentages of DOTAP incorporation and are comparable to the results of uncaged **7.1**-liposomes. Error bars denote standard errors from at least three independent trials.

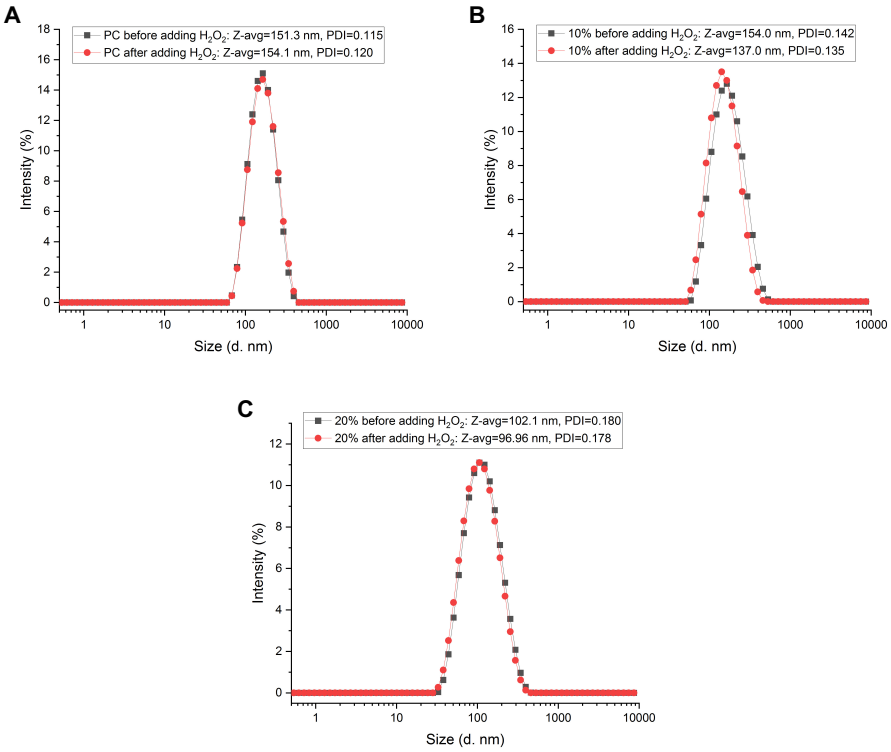


Figure 7.7. DLS raw distribution curves for PC liposomes containing 0%, 10%, or 20% lipid 7.1 before and after H_2O_2 incubation. Uniform vesicles with desired diameters were formed prior to H_2O_2 addition in all cases. No changes in particle sizes were observed after H_2O_2 treatment.

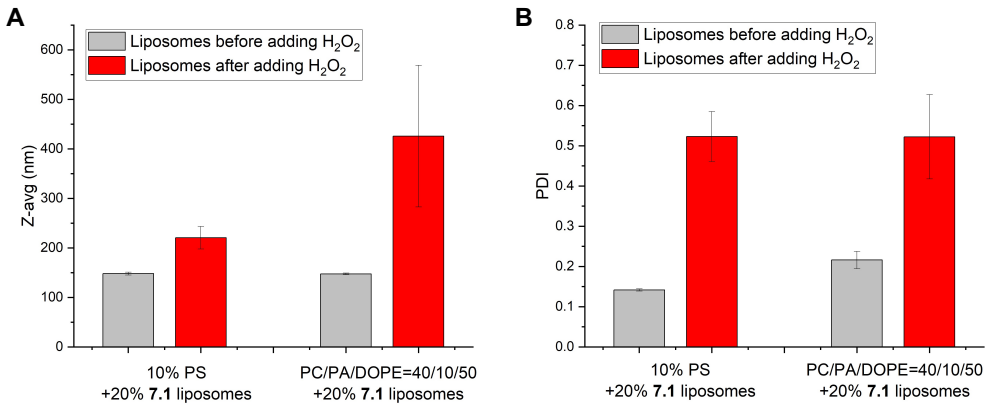


Figure 7.8. DLS results for 20% 7.1/PC liposomes mixed with 10% PS/PC or PA/PE/PC=10/50/40 liposomes before and after addition of H_2O_2. A. Z-avg results. Larger particles were detected upon H_2O_2 treatment in both cases. **B.** Polydispersity index (PDI) changes for 20% **7.1**-liposomes treated with 10% PS or PC/PA/DOPE=40/10/50 liposomes with or without H_2O_2 treatment. Error bars denote standard errors from at least three different batches of liposomes.

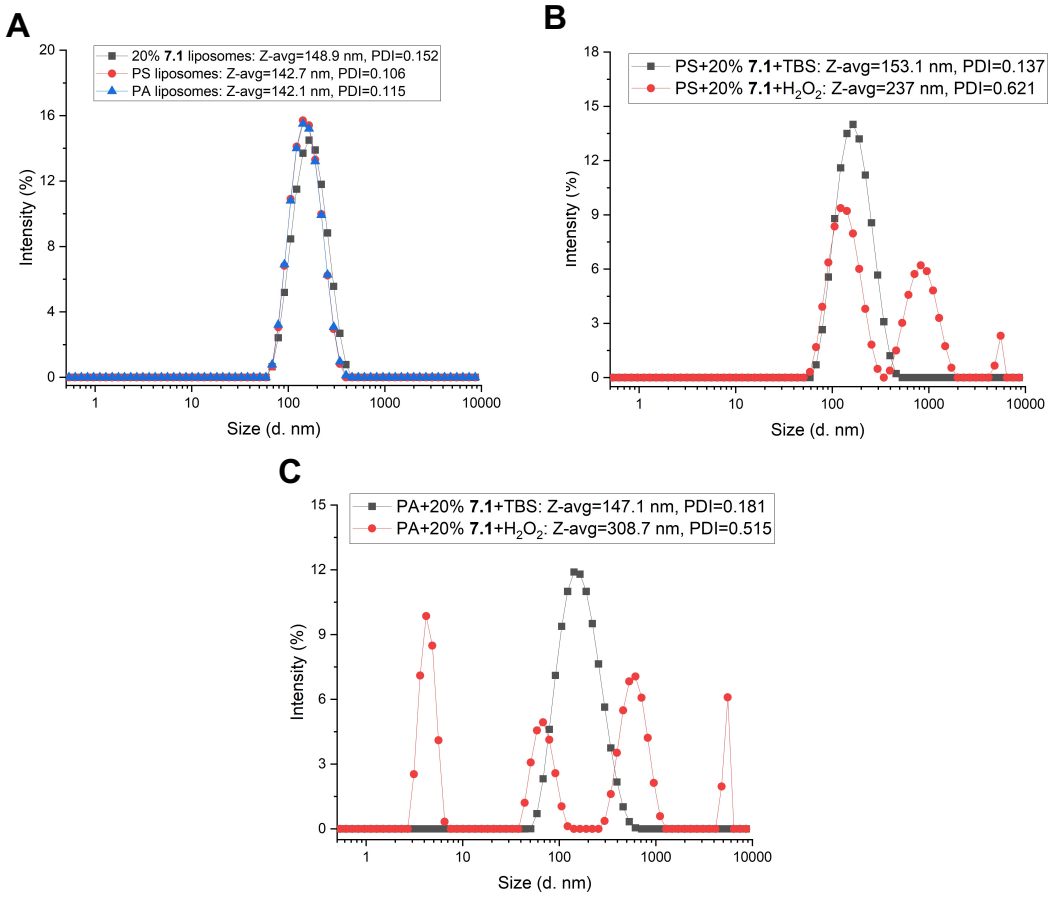


Figure 7.9. Raw distribution curves for all liposomes analyzed in this experiment. For liposomes with low PDI (pre-mixing or TBS addition), distribution curves were averaged from multiple samples using Zetasizer Software. For those after H_2O_2 addition, only one representative distribution curve from one sample is shown.

enables detection of cellular infiltration by liposomes through microscopy analysis. These study liposomes (2 mM) were pre-incubated with 1 mM H_2O_2 for uncaging at room temperature for six hours before being diluted with buffer to 1 mM (H_2O_2 concentration = 0.5 mM) and subjected to human epithelial breast cancer cells (MDA-MB-231) in a 96-well plate. After 1 hour incubation at 37 °C in a CO_2 environment, liposome solutions were removed, and cells were washed, fixed, labeled with DAPI, and imaged with fluorescence microscopy. A significant increase in Rd-PE fluorescence was observed for cells incubated with H_2O_2 pre-treated 20% **7.1**/PC liposomes (Figure 7.10F) compared to those treated with only 20% **1**/PC liposomes (Figure 7.10E). Negative control experiments were also conducted with PC liposomes with and without H_2O_2 incubation. Additionally, the cells were treated with PBS^{++} buffer or 0.5 mM H_2O_2 in the absence of any liposome solutions as alternate negative controls. As shown in Figures 7.10A-D, minimal Rd-PE fluorescence could be seen in all cases, indicating no non-specific cell entry under these conditions. 4X Images were captured (Figure 7.11A-F) and the Rd-PE fluorescence intensities were quantified with Gen5 software. The result shown in Figure 7.11G indicates a ~400-fold increase in cellular delivery when the cells were treated with uncaged 20% **7.1** liposomes.

The same experiment was conducted with a slightly different protocol where the liposomes were diluted with media before incubation with cells, since the excess H_2O_2 could potentially be quenched by the catalase from fetal bovine serum. As shown in Figures 7.12-7.13, comparable results were observed in which only uncaged **7.1**-liposomes enhanced cellular entry.

The same experiments were also conducted with 10% **7.1**-liposomes (Figures 7.14-7.15). These liposomes with lower percentages of uncaged **7.1** did not lead to significant cell delivery, which matched the vesicle assays (Figure 7.5). Nevertheless, these results demonstrated that **7.1**-liposomes yield dramatic enhancements in cellular delivery only in the presence of H_2O_2,

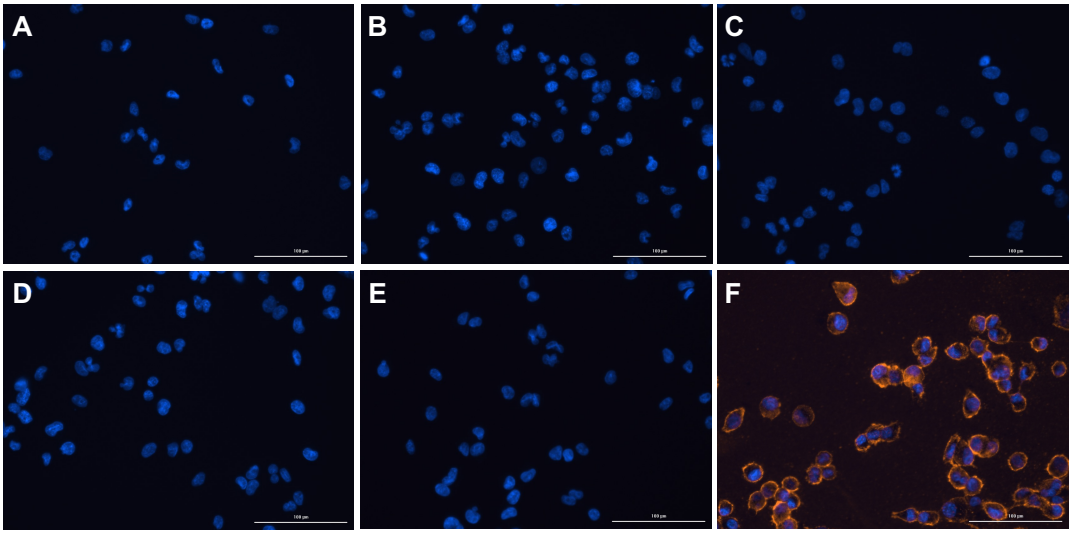


Figure 7.10. Fluorescence images indicating enhanced liposomal delivery to MDA-MB-231 cells with liposomes containing 20% H_2O_2-uncaged 7.1 under buffer dilution conditions. Representative 20X images of cells treated with (**A**) PBS^{++} buffer, (**B**) 0.5 mM H_2O_2, (**C**) PC/Rd-PE liposomes, (**D**) PC/Rd-PE liposomes pre-incubated with H_2O_2, (**E**) **7.1**/PC/Rd-PE liposomes, (**F**) **7.1**/PC/Rd-PE liposomes pre-incubated with H_2O_2. Blue: DAPI; red: Rd-PE. Scale bar, 100 μm.

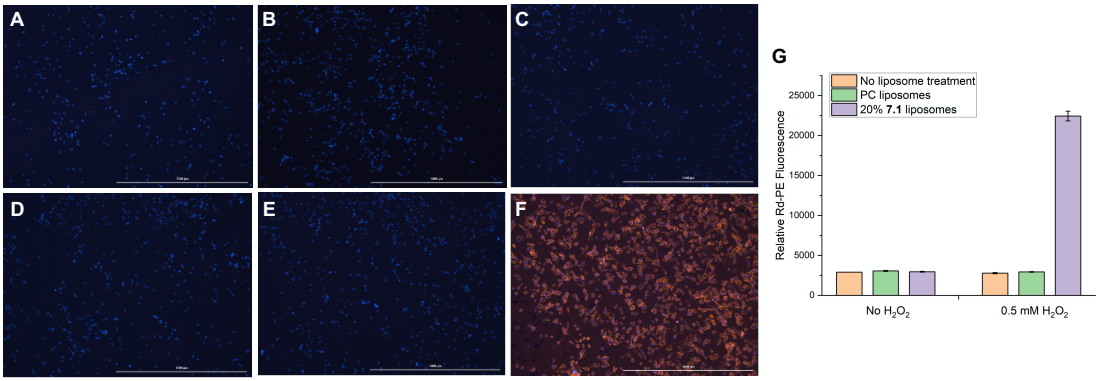


Figure 7.11. Representative 4X fluorescence images indicating enhanced liposomal delivery to MDA-MB-231 cells with liposomes containing 20% H_2O_2-uncaged 7.1 under buffer dilution conditions. Images are from cells treated with (**A**) PBS^{++} buffer, (**B**) 0.5 mM H_2O_2, (**C**) PC/Rd-PE liposomes, (**D**) PC/Rd-PE liposomes pre-incubated with H_2O_2, (**E**) **7.1**/PC/Rd-PE liposomes, (**F**) **7.1**/PC/Rd-PE liposomes pre-incubated with H_2O_2. Blue: DAPI; red: Rd-PE. Scale bar, 1000 μm. (**G**) Quantified Rd-PE fluorescence intensities with 4X images. A significant increase in Rd-PE fluorescence could only be seen for cells treated with H_2O_2-uncaged **7.1**-liposomes. Error bars represent standard errors of at least three replicates.

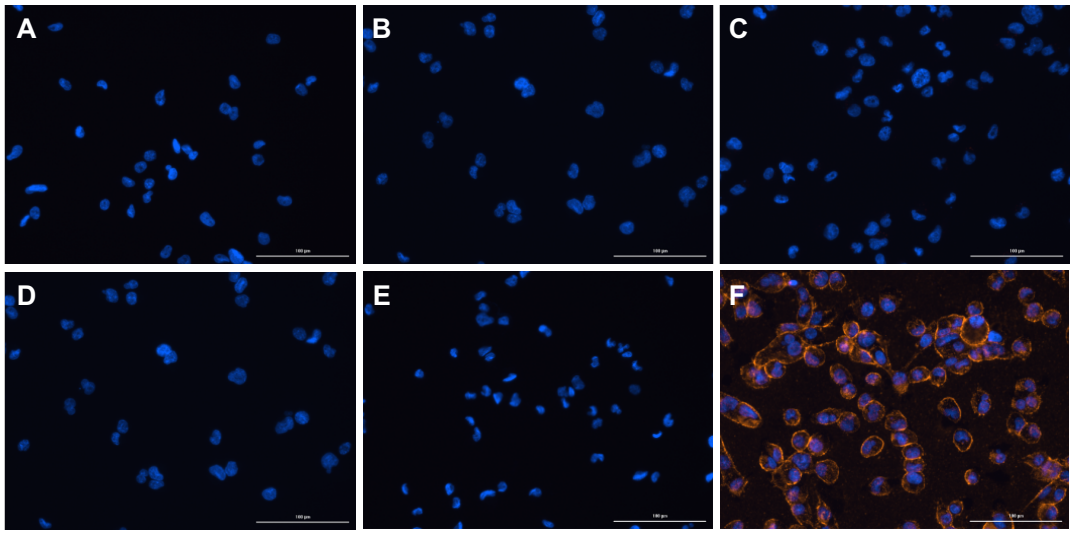


Figure 7.12. Fluorescence images indicating enhanced liposomal delivery to MDA-MB-231 cells with liposomes containing 20% H_2O_2-uncaged 7.1 under media dilution conditions. Representative 20X images of cells treated with (**A**) media, (**B**) 0.5 mM H_2O_2, (**C**) PC/Rd-PE liposomes, (**D**) PC/Rd-PE liposomes pre-incubated with H_2O_2, (**E**) **7.1**/PC/Rd-PE liposomes, (**F**) **7.1**/PC/Rd-PE liposomes pre-incubated with H_2O_2. Blue: DAPI; red: Rd-PE. Scale bar, 100 μm.

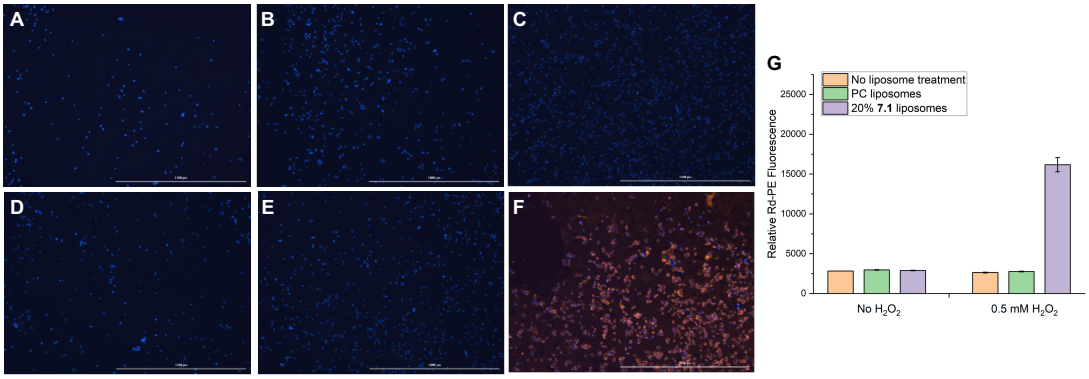


Figure 7.13. Representative 4X fluorescence images indicating enhanced liposomal delivery to MDA-MB-231 cells with liposomes containing 20% H_2O_2-uncaged 7.1 under media dilution conditions. Images are from cells treated with (**A**) media, (**B**) 0.5 mM H_2O_2, (**C**) PC/Rd-PE liposomes, (**D**) PC/Rd-PE liposomes pre-incubated with H_2O_2, (**E**) **7.1**/PC/Rd-PE liposomes, (**F**) **7.1**/PC/Rd-PE liposomes pre-incubated with H_2O_2. Blue: DAPI; red: Rd-PE. Scale bar, 1000 μm. (**G**) Quantified Rd-PE fluorescence intensities with 4X images. A significant increase in Rd-PE fluorescence was only seen for cells treated with H_2O_2-uncaged **7.1**-liposomes. Error bars represent standard errors of at least three replicates.

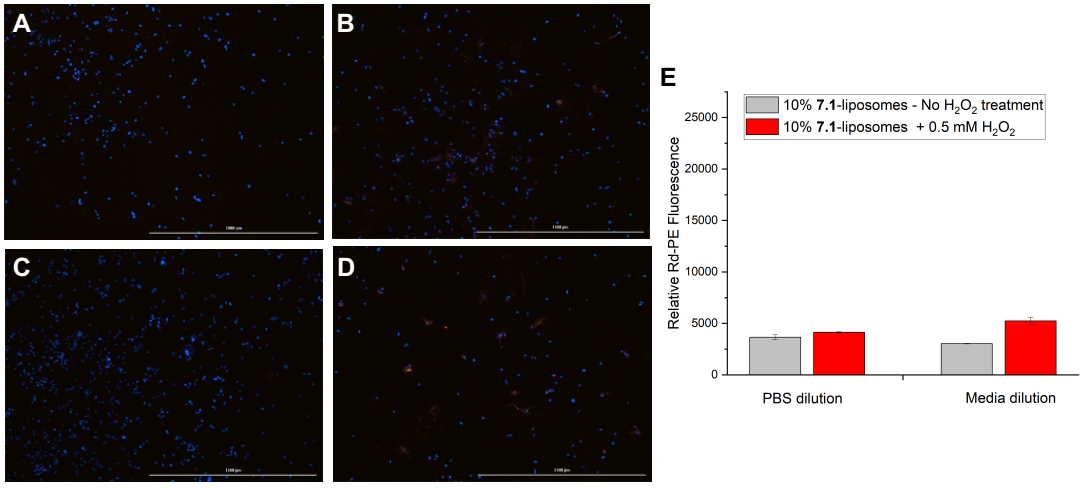


Figure 7.14. Representative 4X fluorescence images for MDA-MB-231 cells treated with liposomes containing 10% H_2O_2-uncaged 7.1 under PBS^{++} or media dilution conditions. Images are from cells treated with (**A**) PBS^{++} diluted 10% **7.1**-liposomes, (**B**) PBS^{++} diluted 10% **7.1**-liposomes pre-incubated with 0.5 mM H_2O_2, (**C**) media diluted 10% **7.1**-liposomes, (**D**) media diluted 10% **7.1**-liposomes pre-incubated with 0.5 mM H_2O_2. Blue: DAPI; red: Rd-PE. Scale bar, 1000 μm. (**E**) Quantified Rd-PE fluorescence intensities with 4X images. These liposomes did not yield significant cell infiltration. Error bars denote standard errors from at least three independent trials.

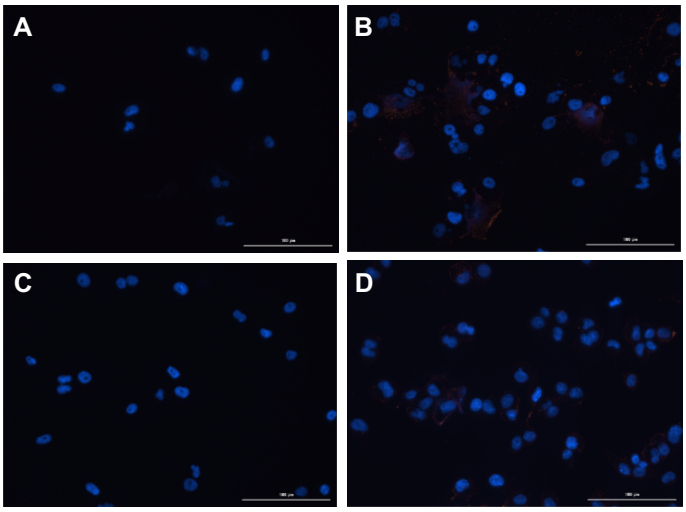


Figure 7.15. Representative 20X fluorescence images for MDA-MB-231 cells treated with liposomes containing 10% H_2O_2-uncaged 7.1 under PBS^{++} or media dilution conditions. Images are from cells treated with (**A**) PBS^{++} diluted 10% **7.1**-liposomes, (**B**) PBS^{++} diluted 10% **7.1**-liposomes pre-incubated with 0.5 mM H_2O_2, (**C**) media diluted 10% **7.1**-liposomes, (**D**) media diluted 10% **7.1**-liposomes pre-incubated with 0.5 mM H_2O_2. Blue: DAPI; red: Rd-PE. Scale bar, 1000 μm.

showcasing their potential in the ROS-mediated liposomal target delivery.

7.7. Conclusions

In conclusion, we developed a ROS-responsive liposome platform for targeted delivery with boronate-caged guanidine lipid **7.1**. This compound contains three major structural components, including a H_2O_2-responsive boronate ester-caged guanidinium headgroup bearing a QM SIL, a hydrophilic TEG linker, and a triazole lipid anchor. Upon H_2O_2 incubation, lipid **7.1** undergoes decomposition to unveil guanidinium-containing cationic lipid product **7.4**. Mass spectrometry as well as ZP measurements verified the expected uncaging processes in the presence of H_2O_2 in the solution state and within a membrane environment, respectively. Liposomes containing **7.1** could efficiently fuse/bind to anionic membranes, as demonstrated by a microplate-based fluorescence assay as well as DLS analyses. Cellular fluorescence microscopy experiments verified enhanced cellular delivery with **7.1**-liposomes pre-treated with H_2O_2. Our data showcase a smart delivery system where liposomes are designed to initially be neutral and inactive, while encountering upregulated ROS unveils cationic characteristics that promote cell entry. This approach shows strong prospects for enhancing the targeting of liposomes to diseased rather than healthy cells in a manner mediated by local ROS abundance.

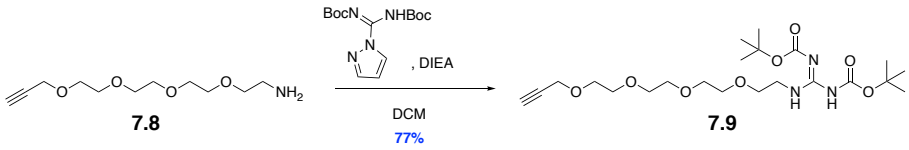
7.8. Synthesis and experimental procedure

General experimental

Reagents and solvents were generally purchased from Sigma-Aldrich or Fisher Scientific and used without further purification. PC (L-α-phosphatidylcholine, mixed isomers from chicken eggs), PA (L-α-phosphatidic acid sodium salt from chicken eggs), DOPE (1,2-dioleoyl-*sn*-glycero-3-phosphoethanolamine), 18:1 biotinyl cap PE (biotin-PE, 1,2-dioleoyl-*sn*-glycero-3-phosphoethanolamine-*N*-(cap biotinyl) (sodium salt)), 18:1 Liss Rhod PE (Rd-PE, 1,2-dioleoyl-*sn*-glycero-3-phosphoethanolamine-*N*-(lissamine rhodamine B sulfonyl) (ammonium salt)) and

DOTAP (1,2-dioleoyl-3-trimethylammonium-propane) were purchased from Avanti Polar Lipids, Inc (Alabaster, AL). Dry solvents were obtained from a Pure Solv MD-7 solvent purification system purchased from Innovative Technology, Inc (Newburyport, MA). Column chromatography was performed using 230-400 mesh silica gel purchased from Sorbent Technologies. NMR spectra were obtained using Varian 300 MHz or 500 MHz NMR spectrometers. Mass spectra were obtained with JEOL DART-AccuTOF and Waters Synapt G2-Si mass spectrometers (Milford, MA). Liposome extruder and polycarbonate membranes were obtained from Avestin (Ottawa, Canada). Ultrapure water was purified via a Millipore water system (≥ 18 MW·cm triple water purification system). Small quantities (< 5 mg) were weighed on a Mettler Toledo XS105 dual range analytical balance. Fluorescence readings of microplate-based assays were recorded with a BioTek Synergy 2 Multi-Detection Microplate Reader with absorbance, fluorescence, polarization and time-resolved capabilities. Dynamic light scattering (DLS) and zeta potential (ZP) measurements were carried out with a Malvern Zetasizer Nano ZS instrument equipped with a 4.0 mW laser operating at l=633 nm. Plots were generated using Origin Pro 2021b. All error bars in plots show the standard errors of at least three experimental replicates. Fluorometric analysis was performed using Gen5 software and cytation 1 cell imaging multimode microplate reader (BioTek Instruments, Winooski, VT) with an RFP filter (Ex 531 / Em 593 nm) and DAPI filter (Ex 377 / Em 447 nm).

Synthesis



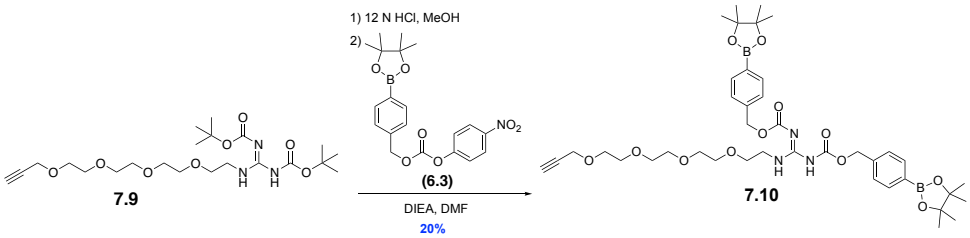
7.8 **7.9**

1,2-Bis(*tert*-butoxycarbonyl)-3-(3,6,9,12-tetraoxapentadec-14-yn-1-yl)guanidine (7.9)

Compound **7.8**[321] (51 mg, 0.221 mmol) and *N*,*N*′-bis(*tert*-butoxycarbonyl)-1H-pyrazole-1-carboxamidine (75.25 mg, 0.243 mmol) were dissolved in 10 mL dry dichloromethane in a 50 mL RBF under Argon. After adding *N*,*N*-diisopropylethylamine (DIEA, 115 µL, 0.663 mmol), the reaction was stirred at rt overnight. Upon completion, the reaction was poured into 100 mL

1 N hydrochloric acid, and the organic layer was collected. The aqueous layer was further extracted with 2 × 25 mL dichloromethane, and the combined organic layer was washed with 1 × 50 mL water and 1 × 50 mL brine. After being dried over sodium sulfate, filtered, and concentrated under reduced pressure, the crude was purified via silica gel column using gradient elution from hexanes to 50% ethyl acetate in hexanes. Compound **7.9** was obtained as a yellow oil (80 mg, 0.17 mmol, 77% yield). R_f = 0.28 (50% Ethyl acetate-Hexanes).

^{1}H NMR (500 MHz, $CDCl_3$) δ 11.46 (s, 1H), 8.61 (s, 1H), 4.19 (d, *J* = 2.4 Hz, 2H), 3.65 (m, 16H), 2.43 (t, *J* = 2.4 Hz, 1H), 1.49 (s, 9H), 1.48 (s, 9H). ^{13}C NMR (126 MHz, $CDCl_3$) δ 163.62, 156.38, 153.10, 83.06, 79.80, 79.39, 74.65, 70.82, 70.80, 70.73, 70.61, 70.56, 69.46, 69.25, 58.54, 40.81, 28.44, 28.21. HRMS-DART: $[M+H]^+$ calcd for $C_{22}H_{40}O_8N_3$: 474.2815; Found: 474.2481.

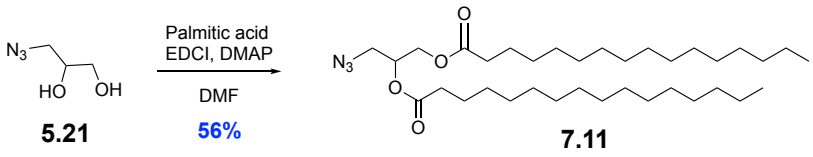


1,2-Bis(4-(4,4,5,5-tetramethyl-1,3,2-dioxaborolan-2-yl)benzyl)oxy)carbonyl)-3-(3,6,9,12-tetraoxapentadec-14-yn-1-yl)guanidine (7.10)

Compound **7.9** (80 mg, 0.17 mmol) was dissolved with 3 mL methanol in a 50 mL RBF under Argon. After adding 3 mL 12 N hydrochloric acid, the reaction mixture showed a color change from colorless to yellow and was stirred at rt for 20 h. Next, the solvent was removed under reduced pressure. Compound **6.3** (0.27 g, 0.676 mmol) was then added into the RBF under Argon, followed by addition of 5 mL dry dimethylformamide and *N*,*N*-diisopropylethylamine (0.24 mL, 1.352 mmol). The reaction was heated at 65 ºC for 60 h. Upon completion, the solvent was removed under reduced pressure. The residual was re-dissolved with 20 mL dichloromethane and 20 mL water and transferred into a separatory funnel. The dichloromethane layer was collected and the aqueous layer was further extracted with 2 × 10

mL dichloromethane. The combined dichloromethane layer was washed with 1 × 50 mL water and 1 × 50 mL brine. After being dried over sodium sulfate, filtered, and concentrated under reduced pressure, the crude was subjected to silica gel column chromatography. Gradient elution from hexanes to 50% ethyl acetate-hexanes was used to obtain the product as a yellow oil (26.9 mg, 0.034 mmol, 20% yield). R_f = 0.4 (50% Ethyl acetate-Hexanes).

^{1}H NMR (500 MHz, $CDCl_3$) δ 9.42 (s, 1H), 9.23 (s, 1H), 7.85 – 7.75 (m, 4H), 7.38 (d, *J* = 7.9 Hz, 4H), 5.23 (s, 2H), 5.15 (s, 2H), 4.22 (t, *J* = 5.8 Hz, 2H), 4.18 (d, *J* = 2.3 Hz, 2H), 3.71 – 3.49 (m, 14H), 2.42 (t, *J* = 2.4 Hz, 1H), 1.36 – 1.32 (m, 24H). ^{13}C NMR (126 MHz, $CDCl_3$) δ 163.88, 160.68, 156.11, 140.29, 137.79, 135.27, 135.02, 127.52, 127.07, 84.07, 83.99, 83.89, 79.84, 74.63, 70.72, 70.68, 70.51, 70.42, 69.23, 68.93, 66.99, 58.51, 43.94, 29.83, 24.99. ESI-MS: $[M+H]^+$ calcd for $C_{40}H_{58}B_2N_3O_{12}$: 794.4207; Found: 794.4188

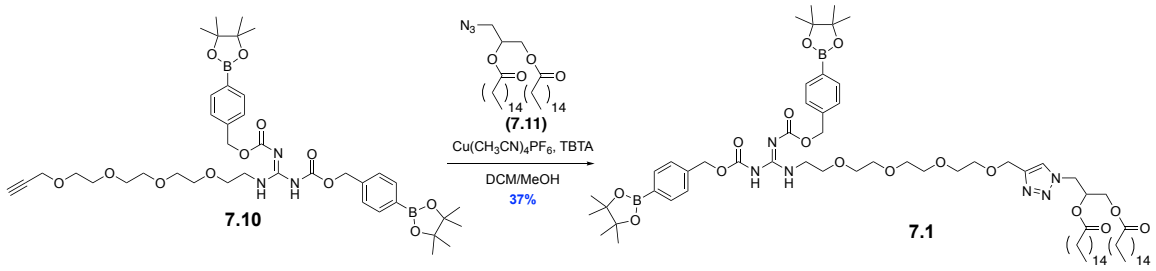


3-Azidopropane-1,2-diyl dipalmitate (7.11)

Compound **5.21**[280] (0.1345 g, 1.149 mmol), palmitic acid (0.8846 g, 3.447 mmol), 4-dimethylaminopyridine (DMAP, 70.19 mg, 0.5745 mmol) and 1-ethyl-3-(3-dimethylaminopropyl)carbodiimide (EDCI, 0.5351 g, 3.447 mmol) were dissolved with 10 mL dry dimethylformamide in a 100 mL RBF under Ar. After stirring at rt overnight, the reaction mixture was poured into a separatory funnel containing 100 mL water. The aqueous layer was extracted with 3 × 25 mL ethyl acetate, and the combined organic layer was further washed with 5 × 50 mL water and 1 × 50 mL brine. After being dried over sodium sulfate filtered, and concentrated under reduced pressure, the crude was purified with a column packed with silica gel using gradient elution from hexanes to 10% ethyl acetate in hexanes. Compound **7.11** was obtained as a white solid (0.381 g, 0.64 mmol, 56% yield). R_f = 0.4 (10% Ethyl acetate-Hexanes).

^{1}H NMR (500 MHz, $CDCl_3$) δ 5.19 – 5.14 (m, 1H), 4.28 (dd, *J* = 11.9, 4.5 Hz, 1H), 4.14 (dd, *J*

= 11.9, 5.7 Hz, 1H), 3.51 – 3.38 (m, 2H), 2.32 (dt, *J* = 17.1, 7.6 Hz, 4H), 1.66 – 1.54 (m, 4H), 1.25 (s, 48H), 0.87 (t, *J* = 7.0 Hz, 6H). ^{13}C NMR (126 MHz, $CDCl_3$) δ 173.28, 172.92, 70.00, 62.40, 51.01, 34.30, 34.15, 32.05, 29.83, 29.81, 29.79, 29.74, 29.60, 29.49, 29.39, 29.38, 29.24, 29.19, 24.98, 24.94, 22.81, 14.22. HRMS-DART: $[M+H]^+$ calcd for $C_{35}H_{68}N_3O_4$: 594.5210; Found: 594.4256. $[M+H-N_2]^+$ calcd for $C_{35}H_{68}NO_4$: 566.5148; Found: 566.4205.



(*E*)-3-(4-(3-Oxo-5-((((4-(4,4,5,5-tetramethyl-1,3,2-dioxaborolan-2-yl)benzyl)oxy)carbonyl)amino)-1-(4-(4,4,5,5-tetramethyl-1,3,2-dioxaborolan-2-yl)phenyl)-2,9,12,15,18-pentaoxa-4,6-diazanonadec-4-en-19-yl)-1*H*-1,2,3-triazol-1-yl)propane-1,2-diyl dipalmitate (7.1)

Compounds **7.10** (26.9 mg, 0.0339 mmol) and **7.11** (22.15 mg, 0.0373 mmol), tris(benzyltriazolylmethyl)amine (TBTA, 1.8 mg, 0.0034 mmol)[326] and tetrakis(acetonitrile)copper(I) hexafluorophosphate ($Cu(CNCH_3)_4PF_6$, 1.27 mg, 0.0034 mmol) were combined in a 50 mL RBF under Ar. After adding 5 mL methanol/dichloromethane (1:1, v/v), the reaction mixture was stirred overnight. Next, the solvent was removed under reduced pressure, and the crude was purified via silica gel column chromatography using gradient elution from hexanes to 75% ethyl acetate in hexanes. **7.1** was obtained as a yellow oil (17.6 mg, 0.0127 mmol, 37%). R_f = 0.6 (75% Ethyl acetate-Hexanes).

^{1}H NMR (500 MHz, Chloroform-*d*) δ 9.42 (s, 1H), 9.24 (s, 1H), 7.79 (dd, *J* = 17.2, 8.0 Hz, 4H), 7.60 (s, 1H), 7.41 – 7.34 (m, 4H), 5.37 (p, *J* = 5.1, 4.7 Hz, 1H), 5.23 (s, 2H), 5.15 (s, 2H), 4.66 (s, 2H), 4.57 (d, *J* = 6.3 Hz, 2H), 4.31 (dd, *J* = 12.1, 4.3 Hz, 1H), 4.21 (t, *J* = 5.4 Hz, 2H), 4.06 (dd, *J* = 12.1, 5.3 Hz, 1H), 3.67 – 3.49 (m, 14H), 2.36 – 2.25 (m, 4H), 1.71 – 1.51 (m, 8H), 1.33 (d, *J* = 4.1 Hz, 24H), 1.25 (s, 48H), 0.88 (t, *J* = 6.9 Hz, 6H). ^{13}C NMR (126 MHz, $CDCl_3$) δ

173.27, 172.72, 163.77, 160.80, 156.05, 145.61, 140.26, 137.74, 135.29, 135.13, 135.04, 127.56, 127.04, 123.56, 84.09, 83.92, 70.49, 70.27, 69.73, 69.48, 69.00, 66.98, 64.65, 62.15, 56.12, 50.19, 44.06, 34.17, 34.13, 32.07, 29.85, 29.82, 29.80, 29.80, 29.78, 29.64, 29.62, 29.60, 29.59, 29.58, 29.56, 29.51, 29.43, 29.41, 29.28, 29.18, 25.01, 25.00, 24.99, 24.89, 22.83, 14.26. ESI-MS: $[M+H]^+$ calcd for $C_{75}H_{125}B_2N_6O_{16}$: 1387.9338; Found: 1387.9325

Liposome preparation for binding assay

Stock solutions of 5 mM lipid **7.1** and DOTAP were prepared in a mixture of methanol and chloroform, while PC, biotin-PE, Rd-PE, PA, and DOPE stock solutions were prepared in chloroform. All stock solutions were stored in a -20 °C freezer after preparation. Proper volumes of each stock solution were pipetted into a small vial to obtain a mixture of 1 mM of total lipid content with the desired percentages of each lipid. The organic solvents were then evaporated under a nitrogen stream, and the resulting lipid film was further dried under vacuum for at least one hour. The film was then hydrated with 1×TBS (pH=7.4, containing 25 mM Tris/Tris HCl, 0.13 M NaCl, 0.0027 M KCl) in a 60 °C water bath for three sets of 20 min with vortexing after each set. After ten freeze-thaw cycles with a dry ice-acetone bath and a 60 °C water bath, the solutions were extruded through a 200 nm polycarbonate membrane for 15 passes with a LiposoFast extruder (Avestin, Inc.). The resulting liposomes were stored at 4 °C and were used up within two days.

Microplate-based PS liposome immobilization assay

Two batches of 1 mM PC liposomes containing 5% PS, 1% Rd-PE with and without 1% bio-PE anchor were prepared in 1×TBS buffer (pH=7.4) and diluted to 0.5 mM before use. Experimental wells on a streptavidin-coated microplate were washed with 1×TBS buffer for 30 min under low vortex. After removing the wash buffer, each well was incubated with different concentrations of PS liposomes (100 μL total volume, diluted from 1 mM liposomes) for 1 h at rt. Next, the liposome solutions were removed, and the wells were further washed with 3 x 250

μL wash buffer. The microplate was placed under low vortex for three min during each wash. After the final wash, 100 μL TBS buffer was added to each well, and the fluorescence readings were measured with a plate reader. The data was reported as the fluorescence intensities for each well (F) subtracting the initial background fluorescence intensities for each set of the experiment (F_0, wells without Rd-PE labeled liposome treatment) at 590 nm. Experiments were run at least three times with different batches of liposomes. Averaged data were reported with error bars denoting standard errors.

Microplate-based fluorescent assay to study vesicle interactions

Solutions (1.35 mL of 1 mM 5% PS/PC liposomes containing 1% biotin-PE) were prepared in 1×TBS buffer (pH=7.4) and diluted to 0.5 mM before use. A second batch of 1.35 mL of 1 mM PC liposomes containing 0%, 10% and 20% lipid **7.1** was prepared using the same method described above. Half of these liposomes were diluted to 0.5 mM with TBS buffer before use. Solutions of 20 mM H_2O_2 were prepared by diluting 9.8 M concentrated H_2O_2 with TBS buffer. A certain number of wells on a streptavidin-coated microplate were washed with 1×TBS buffer for 30 min under low vortex. After removing the wash buffer, each well was incubated with different concentrations of PS liposomes (100 μL total volume, diluted from 0.5 mM liposomes) for 1 h at rt. Next, PS liposome solutions were removed, and the wells were further washed with 3 x 250 μL wash buffer. The microplate was placed under low vortex for three minutes during each wash. After the final wash, the PS-functionalized wells were treated with 0.5 mM liposomes containing 0-20% lipid **7.1** in the presence of H_2O_2. Control experiments without H_2O_2 addition were conducted at the same time. For the wells without H_2O_2 treatment, 100 μL of 0.5 mM diluted **7.1**-liposome solutions were added. For the well with H_2O_2 treatment, 50 μL undiluted 1 mM **7.1**-liposomes were first added, followed by the addition of 50 μL 20 mM H_2O_2 solutions (final H_2O_2 concentrations = 10 mM). After three hours of incubation, all the solutions were removed, and the wells were further washed with 1 x 250 μL wash buffer. The microplate was placed under low vortex for three minutes during the wash. After that, 100 μL TBS buffer

was added to each well, and the fluorescence readings were measured with the plate reader. The data was reported as the fluorescence intensities for each well (F) subtracting the initial background fluorescence intensities for each set of the experiment (F_0, wells without Rd-PE labeled liposome treatment) at 590 nm. Experiments were run at least three times with different batches of liposomes. Averaged data were reported with error bars denoting standard errors. For DOTAP positive control experiments, the same protocol was used, except for switching the **7.1**-liposomes into Rd-PE labeled PC liposomes containing 10% and 20% DOTAP.

Mass spectrometry analysis of free lipid 7.1 after hydrogen peroxide treatment

For free lipid **7.1**, 0.5 μL of 30% H_2O_2 (9.8 M) was added into 20 μM lipid **7.1** in 5 mL 50% methanol/chloroform (v/v). After 1 hr incubation, excess H_2O_2 was quenched by adding 3 M thiosulfate solutions in case it would damage the mass spectrometer. ESI positive mode was used for detection.

DLS analysis of liposome size before and after treatment with H_2O_2

Liposomes were prepared using the same procedure described above. For liposomes after H_2O_2 treatment, 1 μL of 9.8 M H_2O_2 was added into 100 μL liposomes and incubated for 2 h before taking DLS readings. Samples were prepared by diluting the liposome solutions before or after H_2O_2 addition 10 times with TBS buffer. All samples were determined at a scattering angle of 173° at 20 °C. The data reported are the averages of three tests with error bars indicating standard errors.

To analyze vesicle sizes change during fusion/binding interactions, 2 mM 20% **7.1**-liposomes, 10% PS/PC and PA/DOPE/PC=10/50/40 liposomes were prepared. **7.1**-Liposomes (150 μL) were combined with 50 μL PA or PS liposomes in an Eppendorf tube. H_2O_2 (0.5 μL of a 9.8 M solution, final concentration = 20 mM) or TBS buffer was next added. After two hours of incubation, a 5 μL aliquot of the solution was diluted into 50 μL with TBS buffer, and Z-averages

were measured.

ZP analysis of liposome surface charge before and after treatment of H_2O_2

Zeta potential values were also measured on the same instrument. A 1 mM solution of PC-based liposomes containing 0%, 10%, or 20% **7.1** without any fluorescently-labeled lipids was prepared in 1 mM HEPES (pH=7.4, containing 30 mM NaCl). For endpoint measurements, the liposomes after H_2O_2 treatment were prepared by adding 0.5 μL of a 9.8 M H_2O_2 solution into 200 μL of 1 mM liposomes (final concentrations = 24.5 mM). After one hour incubation, a 200 μL aliquot of liposomes was diluted with 800 μL of buffer. The solutions were next transferred into a DTS1070 folded capillary cell ready for measurement. For time-dependent measurements, H_2O_2 was added to 1.2 mL liposomes to achieve the desired concentrations. After a certain amount of time incubation, 150 μL of liposomes were diluted with 850 μL buffer and subjected to ZP analysis. All measurements were taken at 20 ºC. Data were generated with at least three replicates.

Cellular delivery experiments

MDA-MB-231 Cell Culture.

Human epithelial breast cancer cells (MDA-MB-231) were obtained from ATCC (Manassas, VA). Cells were grown in 100 mm plates and then plated at 1×10^4 cells per well in a 96-well plate with clear flat bottom for cell delivery experiments. Cells were grown for 48 h to reach 80% confluency in Dulbecco's modified eagle medium (Gibco) supplemented with 10% (v:v) fetal bovine serum (Gibco), 50 U/mL penicillin/streptomycin (Gibco). Incubation was performed at 37 °C under 5% CO_2 with 95% humidity.

Fluorescence Microscopy

Solutions of liposomes (2 mM) with 0%, 10% or 20% **7.1** doped into PC containing 0.08% rhodamine L-α-phosphatidylethanolamine (Rd-PE) in 1×TBS buffer (pH=7.4, containing 25

mM Tris/Tris HCl, 0.13 M NaCl, 0.0027 M KCl) were prepared using the previously described thin-film hydration procedures. The 2 mM liposome solutions were incubated with 1 mM H_2O_2 for six hours at room temperature before being diluted with PBS^{++} buffer or media to 1 mM (final H_2O_2 concentration = 0.5 mM).

At 80% confluence, cells were treated with 100 µL per well of the corresponding 1 mM liposome solutions and incubated for 1 h at 37 °C. Cells were washed two times with 250 µL PBS^{++} pH 7.4, then fixed for 30 min at 37 °C by addition of 100 µL per well of 4% paraformaldehyde. Then, cells were washed two times with 250 µL PBS^{++} pH 7.4 and stained with NucBlue™ Fixed Cell ReadyProbes™ Reagent (DAPI, Fisher Scientific). Fluorometric analysis was performed using Gen5 software and Cytation 1 cell imaging multimode microplate reader (BioTek Instruments, Winooski, VT) with an RFP filter (Ex 531 / Em 593 nm) and DAPI filter (Ex 377 / Em 447 nm). Fluorescence microscopy images were acquired on the Cytation 1 Reader using 20X and 4X magnification. Averaged RFP fluorescence units for each sample were determined from images taken at 4X magnification. Replicates were performed using at least 3 batches of liposomes.

Chapter 8. Fluorescent probes based on cardiolipin and PE for high throughput assays of phospholipase inhibition

8.1. Background and project overview

Phospholipase enzymes are defined as lipolytic enzymes that can hydrolyze specific ester or phosphoester bonds of a phospholipid substrate, resulting in fatty acids and/or other lipophilic molecules.[327] Depending on different reactions they can catalyze, they are classified into four major categories, including phospholipase A, B, C, and D. While phospholipase A1 and A2 (PLA) cleave the *sn*-1 and *sn*-2 acyl chains, respectively, phospholipase B can cleave both *sn*-1 and *sn*-2 positions. For phospholipase C and D (PLC and PLD), they are both membrane-bound enzymes that can cleave before and after the phosphate group of the phospholipid substrate. Because phospholipases play important roles in biological systems, such as signal transduction[328,329] and production of lipid mediators,[330,331] dysregulation of certain phospholipases enzymes can result in severe diseases.[332-334] For example, PLD and several PLA2 isozymes have been implicated in the production of lysophosphatidic acid, which is overproduced in certain cancers and stimulates tumor invasiveness and reduces the sensitivity of cancer cells to chemotherapy.[335,336]

Systematic understanding of the phospholipase enzyme families is critical and has been a vibrant area of research, which can provide a better understanding of disease pathologies and a solid base to fundamental research.[337,338] Multiple analytical methods have been developed to identify active enzymes, including HPLC or TLC separation of radiolabeled lipids.[339] However, these traditional assays can only focus on endpoint products, which don't meet the demand of monitoring phospholipase activation in live cells. They also cannot be readily applied to high-throughput screening for kinetic analysis or inhibitor discovery. To overcome these obstacles, fluorogenic assays thus became a powerful tool for such purposes.[340] An early example utilizing bis-BODIPY functionalized PC analogue **8.1** (Figure 8.1A), which was reported by Simons and co-workers.[341] PLA2 enzymes cleave the *sn*-2 position of this lipid,

leading to disruption of internally pi-stacked bis-BODIPY fluorophores. This fluorescent probe could be applied to continuous monitoring of PLA2 enzyme activities towards neutrophils. Additional dequenching assays exploring FRET mechanisms have been intensively studied by the Prestwich group. Fluorogenic PC analog **8.2**, shown in Figure 8.1B, was used for real-time measurement of PLA2 chemical and cellular activities.[256] PLA2 enzymes cleaved the *sn*-2 position, where the fluorophore Dabcyl is located, and deactivated FRET to turn-on its fluorescence. Similarly, two fluorogenic substrate analogues **8.3** and **8.4** for lysoPLD enzymes were reported, as shown in Figure 8.1C.[342]

Outside of liposome projects, in this Chapter, we attempted to advance this field by developing alternative high-throughput assays for phospholipase inhibition. While a number of structural alterations have been made to common membrane lipids including PC and PE, minimal attention has been paid to lipids bearing more complex structures, possibly due to the synthetic challenges to obtain them via chemical approaches. Cardiolipin (CL), a negatively charged diphosphatidylglycerol lipid, is a unique compound that is predominant in mitochondrial membranes.[343] It contains two phosphatidic acid moieties connected with a glycerol backbone in the center to form a dimeric structure, and it has four alkyl groups and potentially carries two negative charges.[344] CL is exclusively synthesized in mitochondria and accounts for 15-20% of mitochondrial membranes. As a result, it can interact with a variety of mitochondrial proteins[345,346] and its biosynthesis is crucial to maintain mitochondrial activities.[347,348] Dysregulation of CL can lead to misfunction of cellular activities, including mitochondrial protein import, cell aging and apoptosis.[349-351] Thus, CL provides an exciting scaffold for fluorogenic phospholipase substrate development.

While commonly explored fluorescence mechanisms involve FRET, here, we sought to take advantages of the fluorescence properties pyrene, which is well-known for its excimer properties. Monomeric pyrene exhibits fluorescence emission peaks around 375-405 nm;

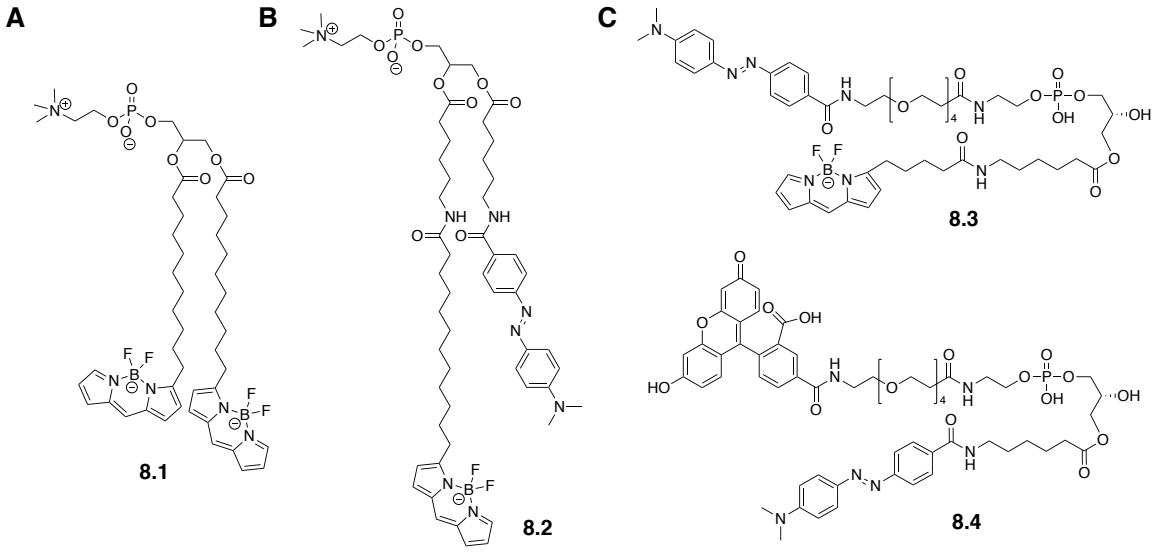


Figure 8.1. Structures of previous reports of fluorogenic analogues for measurement of phospholipase enzyme activities. A. PC-analogue **8.1** based on bis-BODIPY moieties for PLA2 enzymes. **B.** FRET-based PLA2 enzyme substrate **8.2** reported by the Prestwich group. **C.** Structures of fluorogenic lysoPLD enzyme substrates **8.3** and **8.4**.

however, when two pyrene molecules are in spatial proximity, they exhibit an additional emission band around 460 nm.[352,353] Due to these unique properties, pyrene excimer fluorescence has been exploited to study intra- and intermolecular interactions and spatial relationships in biomolecules, including proteins and biomembranes.[354-356] Studies have also shown the extent of pyrene excimer fluorescence emission could be utilized to reveal the distance and flexibility in certain biomacromolecules with complicated structures.[357]

8.2. Design and synthesis of cardiolipin probes 8.5 and 8.6

8.2.1. Initial synthetic route for 8.5

Taking all these considerations together, we attempted to develop fluorescent probes **8.5** and **8.6** containing two pyrene moieties based on a cardiolipin scaffold for high-throughput assays of phospholipase inhibition. Taking advantage of the pyrene excimer properties, these lipids are expected to exhibit fluorescent changes upon the addition of a wide variety of phospholipases. As illustrated in Figure 8.2B, addition of PLA2 or PLD can cleave the *sn*-2 acyl chain and the phosphodiester, respectively. In both cases, two pyrene molecules will fall apart from each other, leading to an expected decrease in excimer fluorescence, which can be utilized for detection purposes. Rauk et al reported a pyrene-labeled PC analogue that could act as a fluorogenic substrate for PLA2.[358] This work proved that pyrene excimer properties could be employed to study phospholipase activities and screen for inhibitors as medicinal lead compounds.

The proposed synthetic route for initial probe **8.5** is outlined in Scheme 8.1. Typical synthesis for CL lipids entails two separate parts, including the DAG synthesis and the middle glycerol backbone synthesis.[359-362] PMB protected **8.7** was first prepared from (*S*)-isopropylideneglycerol, followed by acetal deprotection to **8.8**. Desired monoacylated product **8.9** could be obtained using DCC as coupling reagent. When using EDC as the coupling reagent, only di-acylated product **8.9'** could be obtained, which is most likely due to the

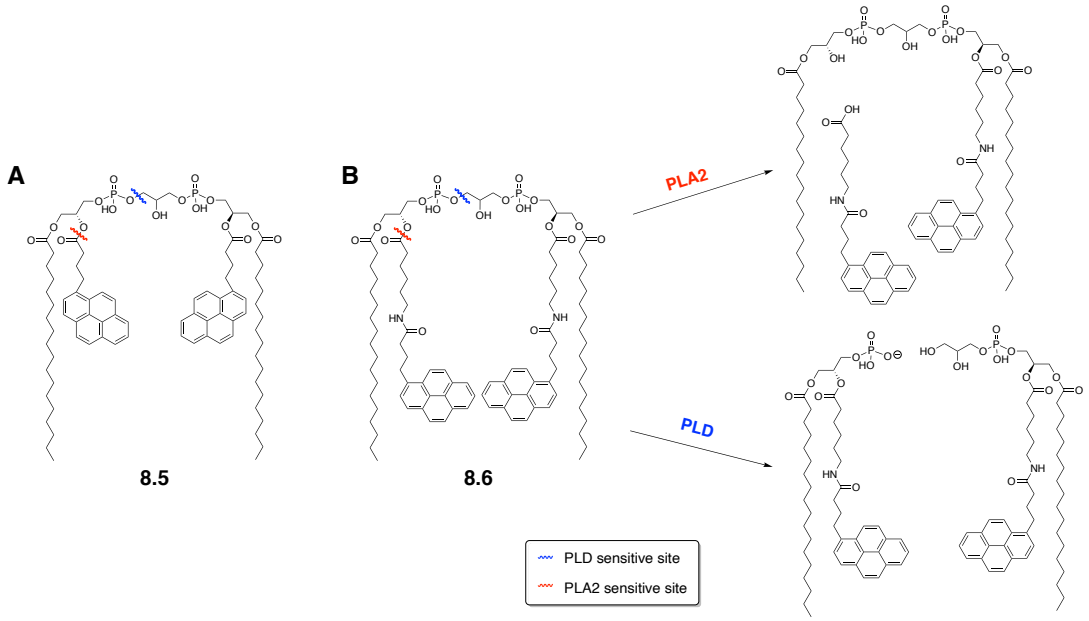
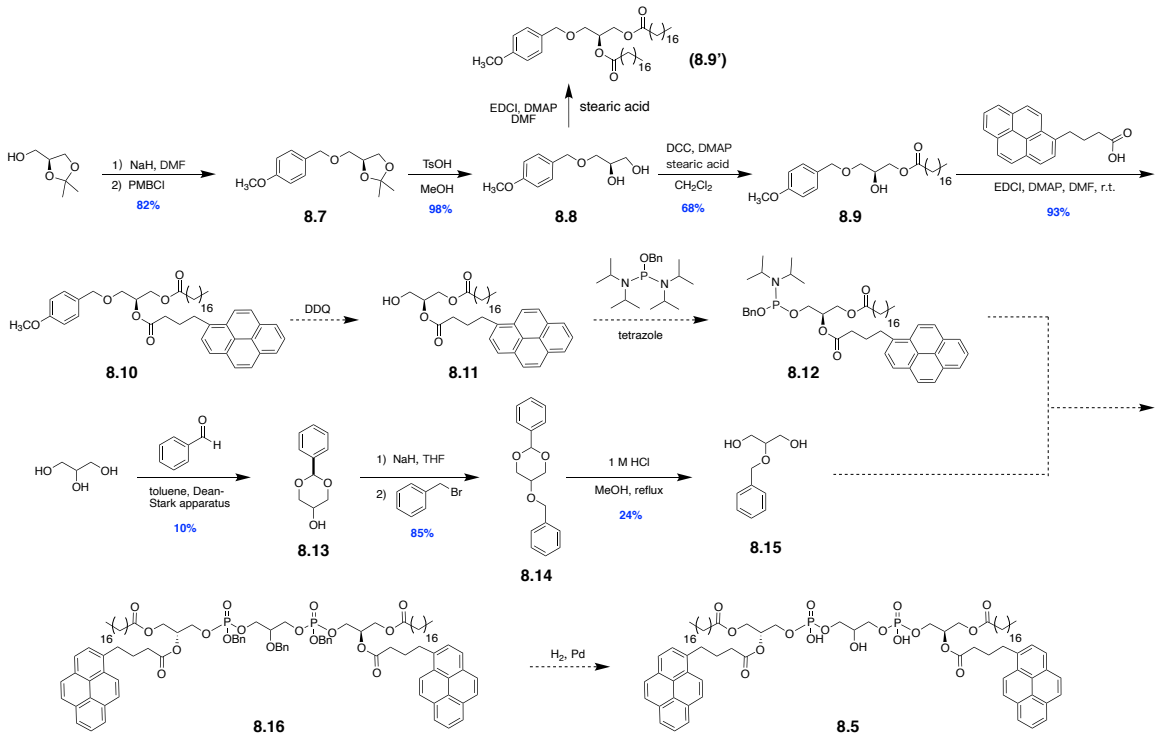


Figure 8.2. Structures of the cardiolipin probes we pursued containing two pyrene fluorophores. A. Initial design of probe **8.5**. **B.** Alternative design for probe **8.6** and expected hydrolysis reactions catalyzed by PLA2 and PLD enzyme enzymes.



Scheme 8.1. Proposed synthetic route for initially designed CL probe 8.5.

diminished steric interactions from less bulky EDC. A second esterification reaction using pyrene-1-butanoic acid was performed to produce **8.10**. PMB deprotection was expected to afford pyrene building block **8.11**. Benzyl protected glycerol backbone **8.15** was synthesized through three steps. Phosphoramidite chemistry was designed to convert **8.11** to **8.12** which could then be connected to **8.15** to build up the CL scaffold of **8.16**. Subsequent benzyl protection was expected to afford the final CL probe **8.5**.

8.2.2. Pyrene-DAG building block synthesis

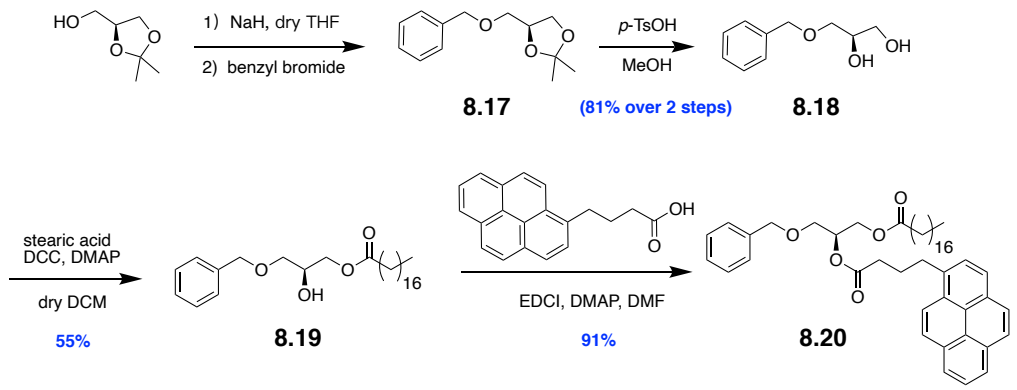
While the initial several steps worked well, we encountered synthetic problems when trying to deprotect the PMB group of **8.10** with the presence of pyrene in this molecule. Synthetic attempts are summarized in the Table 8.1. Oxidative cleavage with oxidants such as 2,3-dichloro-5,6-dicyano-1,4-benzoquinone (DDQ) and ceric ammonium nitrate ($(NH_4)_2Ce(NO_3)_6$, CAN) in Entry 1 led to pyrene oxidation, which was indicated by messy NMR peaks in the aromatic region. Acid-induced deprotection of **8.10** only resulted in migrated product, as is indicated from Entry 2, which could be determined by the chemical shift of the H on the glycerol *sn*-2 position. Reductive deprotection (Entry 3) did not work with hydrogen gas in the presence of Pd/C catalyst at normal pressure.

Observations in Entry 3 of Table 8.1 led us to pursue an alternative route where we switched the PMB into a Bn protecting group, considering no reduction was observed for pyrene at normal pressure. The route to synthesize Bn-protected pyrene-containing DAG is shown in Scheme 8.2. (*S*)-Isopropylideneglycerol was treated with benzyl chloride to afford **8.17** followed by acetal deprotection to **8.18**, esterification to **8.19**, and pyrene addition to **8.20**.

Unexpectedly, we met problems during Bn deprotection as well. Multiple reduction conditions were explored, including varying pressure of the hydrogen gas and Pd catalysts. The attempts are summarized in the following Table 8.2.

Table 8.1. Conditions explored to deprotect PMB groups of 8.10.

Entry	Condition	Outcome
1	DDQ/CAN	Pyrene oxidized
2	TFA/TfOH	100% migration
3	Pd/C	No reaction



Scheme 8.2. Synthetic route to benzyl-protected pyrene-containing DAG building block 8.20.

Table 8.2. Conditions explored to deprotect benzyl groups of 8.20.

Entry	Catalyst	Solvent	Outcome
1	10% Pd/C	EtOAc	Less than 50% conversion after 3 days
2	$Pd(OH)_2$	EtOAc/EtOH, 55 psi	Pyrene reduced; column free
3	$Pd(OH)_2$	EtOAc/EtOH	Pyrene partially reduced
4	10% Pd/C	EtOAc/EtOH	Trace amount of product

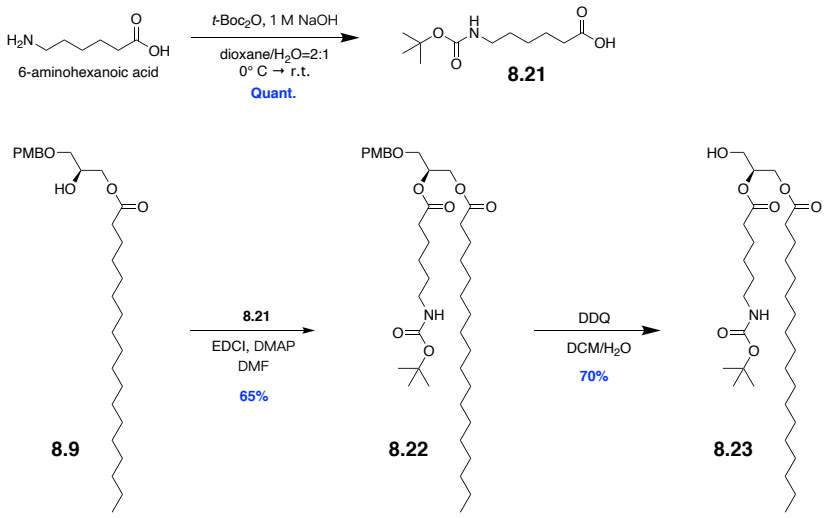
After realizing the presence of pyrene is problematic for deprotections, we came up with an alternative route (Scheme 8.3), where we introduced a linker between the lipid scaffold and pyrene moiety, so that pyrene could be potentially added in later stage of synthesis. Boc-protected amino-caproic acid **8.21** was synthesized and reacted with **8.9** to afford **8.22**, which could be deprotected with DDQ without any problem.

8.2.3. Protected glycerol backbone synthesis

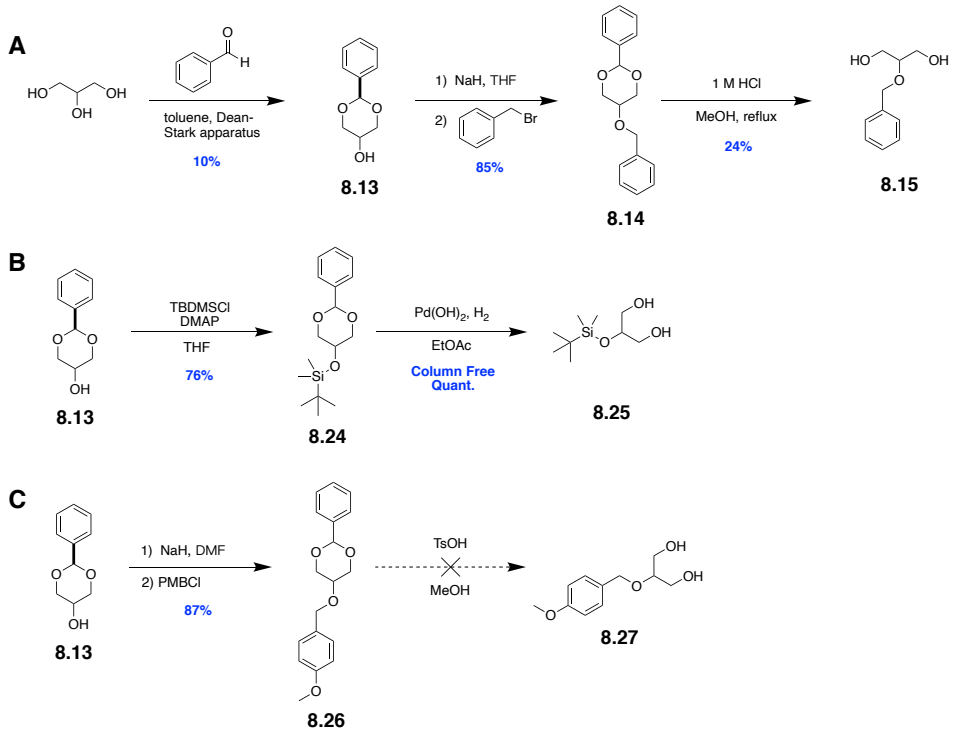
In addition, we synthesized a protected glycerol linker with different protecting groups including benzyl and silyl, as summarized in Scheme 8.4. To selectively protect the middle hydroxyl group, we had to protect both primary alcohols at the same time, which can be achieved by acetal formation by treating glycerol with benzyl aldehyde under reflux with a Dean-Stark trap to form **8.13**. However, formation of several by-products was observed in this reaction, including five-membered rings, six-membraned rings as well their stereoisomers. Although they could be distinguished by NMR based on the *sn*-2 proton chemical shift, it was challenging to separate them via column chromatography. Compound **8.13** was only successfully synthesized through a large-scale reaction utilizing 25 g glycerol as starting material. The desired product could be precipitated out when placed in a -20 °C freezer, though with a relatively low yield. Next, Bn or silyl were introduced into the middle hydroxyl group to form **8.14** and **8.24** followed by deprotection of the acetal with acid or hydrogen, respectively, to afford **8.15** and **8.25**. Attempts to synthesize the PMB-protected version of glycerol was also pursued by treating **8.13** with PMB-Cl. However, problems were met when we were trying to deprotect the acetal and leave PMB intact.

8.2.4. CL scaffold build-up

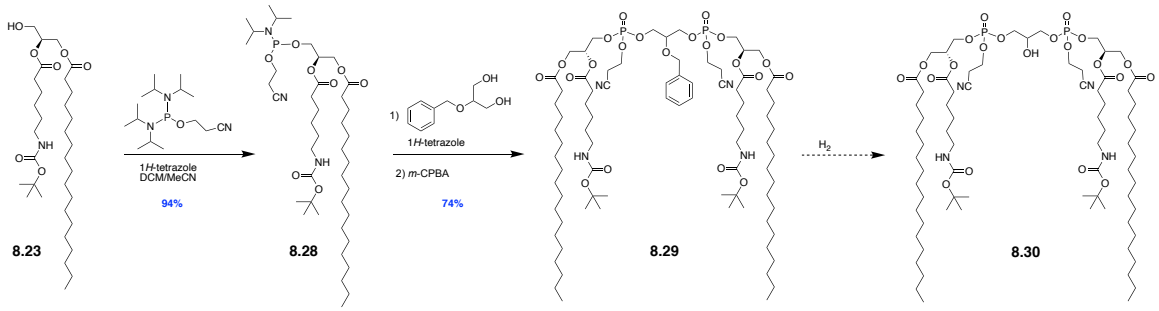
Our initial attempt to build up the CL scaffold focused on the Bn-protected glycerol backbone (Scheme 8.5). Phosphoramidite chemistry was first performed on **8.23** to obtain **8.28**, which was further treated with **8.15** followed by oxidization with *m*-CPBA to afford scaffold **8.29**.



Scheme 8.3. Synthetic route to the extended linker and the resulting alternative DAG scaffold 8.23.



Scheme 8.4. Synthetic routes to Bn- (A), silyl- (B) and PMB- (C) protected glycerol backbone.



Scheme 8.5. Proposed synthetic route to CL probe through Bn protected glycerol backbone.

Considering the problems we encountered when trying to deprotect Bn with pyrene present, we figured Bn needed to be removed before deprotection of Boc and addition of pyrene. However, problems were met again for benzyl protection, as is summarized in Table 8.3.

Next, we explored the possibility of synthesizing the silyl protected CL scaffold (Scheme 8.6). Similar phosphoramidite chemistry was performed twice, except the use of silyl protected glycerol backbone **8.25** to form scaffold **8.31**. Boc deprotection and amide coupling reaction were conducted to put the pyrenes onto the scaffold to form the silyl and cyanoethyl protected **8.32**.

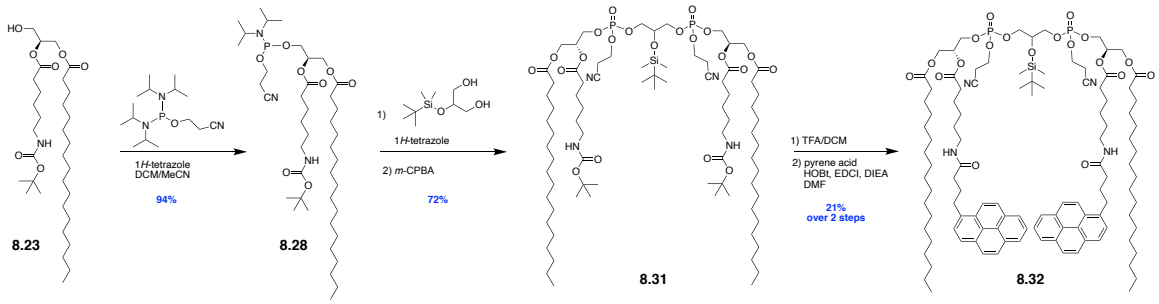
Moving forward, we started the exploration of different methods to deprotect cyanoethyl and silyl groups to obtain the final CL probe **8.6**. All the attempts are summarized in Table 8.4. The most promising trial was from entry 5. For the preparative TLC experiment (pTLC), plates were developed with chloroform/methanol/28% ammonia=65/25/5 and the strong fluorescent band with R_f = 0.5 was collected. This band looks extremely promising considering the desired probe has two negative charges. However, in its corresponding NMR spectra, all the peaks supposed to be on the CL scaffold went missing. The product looked more likely to be a long chain compound with pyrene attached. It is probably caused by the treatment with ammonium fluoride, which may be a too strong fluoride source.

8.3. Design and synthesis of the PE probe

Due to the challenges we encountered when synthesizing the CL probe, we alternatively explored a PE probe **8.33** containing pyrene moieties based on the same mechanism. Although a fluorogenic PE probe is not as an exciting target as CL probe, we could access the final product rapidly with the synthetic intermediates we have in hand. Additionally, considering the similarities in the probe design, **8.33** could be utilized to identify experimental conditions that could later be used for CL probe studies. The expected enzyme-catalyzed reactions are

Table 8.3. Conditions explored to deprotect the benzyl protecting group of 8.29.

Entry	Catalyst	Solvent or condition	Outcome
1	10% Pd/C	EtOAc	No rxn
2	$Pd(OH)_2$	EtOAc	TLC messy
3	$Pd(OH)_2$	EtOAc, 50 psi	No rxn
4	$PdCl_2$ (Activated by reducing w/ H_2)	EtOAc, 50 psi	No rxn



Scheme 8.6. Proposed synthetic route to CL probe through silyl protected glycerol backbone.

Table 8.4. Conditions explored to deprotect the silyl and cyanoethyl protected CL scaffold 8.32.

Entry	Condition	Outcome
1	1) 1.2 eq. TBAF, THF	TLC messy (phosphate migration detected)[359]
2	1) 28% NH_3 (aq), MeOH/DCM 2) 10 eq. TBAF, THF	Only removed cyanoethyl, trace amount of product from mass spec
3	1) 28% NH_3 (aq), MeOH/DCM 2) TBAF, DCM/MeOH	-- Giant TBAF peak on NMR
4	1) 28% NH_3 (aq), MeOH/DCM, w/o purification 2) 5.0 eq NH_4HF, MeOH, rt, overnight	Normal column followed by pTLC is needed to separate the promising product. Missing lots of peaks on NMRs.
5	10 eq. NH_4F, MeOH, 60 C	

shown in Figure 8.3. Treatment of PLA2 and PLD can cleave the *sn*-2 acyl chain and the phosphate, respectively, both of which are expected to result in the spatial separation of the two pyrene molecules leading to diminished excimer emission.

The synthetic route to **8.33** is shown in Scheme 8.7. **8.23** was first treated with Boc-protected ethanolamine **8.34** in the presence of tetrazole, followed by *m*-CPBA oxidation to afford **8.35**. Boc-deprotection and amide coupling reactions resulted in **8.36**, which was subjected to triethylamine mediated cyanoethyl deprotection to the final probe **8.33**.

8.4. Conclusions and future works

In this Chapter, we attempted to develop high-throughput assays for phospholipase inhibition. Initial designs focused on fluorogenic CL analogues, which contain two pyrene moieties. Taking advantage of the pyrene excimer properties, these lipids are expected to exhibit fluorescence changes upon the addition of a wide variety of phospholipases. While multiple synthetic attempts were made, we were not able to obtain the final probe. Alternatively, we synthesized a fluorogenic PE analogue **8.33** based on the same design strategy. Moving forward, we first propose to employ various assays to measure pyrene excimer fluorescence changes upon enzymatic cleavage of the specific bonds. Once we obtain preliminary results for different enzyme treatment and have modified experimental conditions in hand, we propose to involve **8.33** for *in vitro* high-throughput screening assays for phospholipase inhibition and activation. We also envision our probe can be applied to study important biological properties, including phospholipases in subcellular localization of enzyme activity, cellular signaling and *in vitro* drug discovery screening.

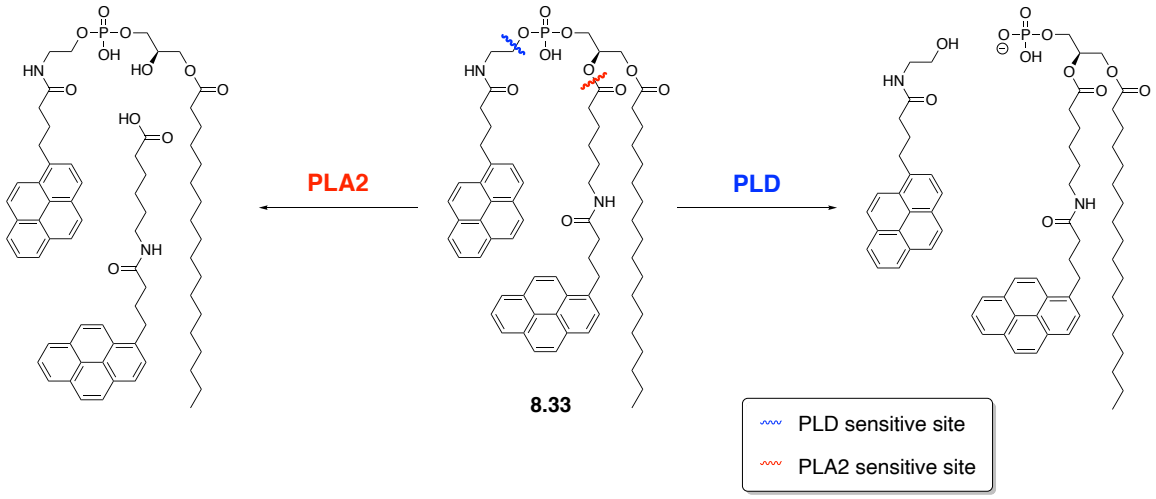
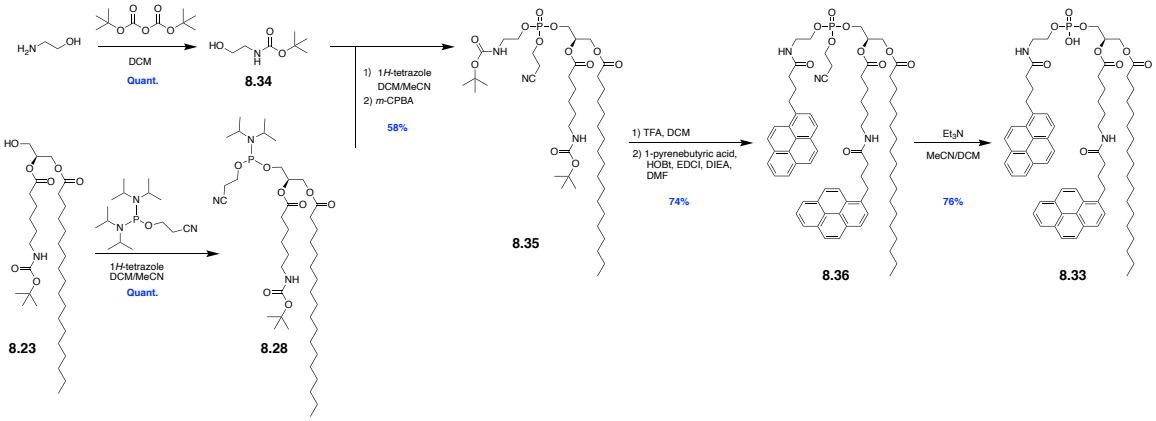
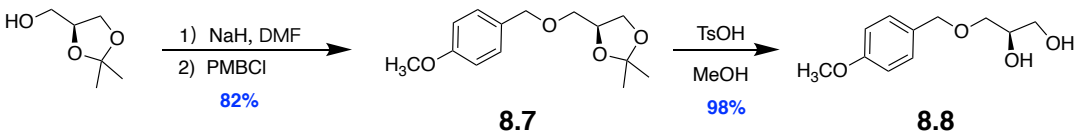


Figure 8.3. Structure and sensing mechanism of the alternative PE probe 8.33 containing two pyrene fluorophores. PLA2 and PLD enzyme treatment can cleave ester and phosdphodiester groups, resulting in the changes in pyrene excimer fluorescence.



Scheme 8.7. Synthetic route to pyrene probe 8.33 based on PE scaffold.

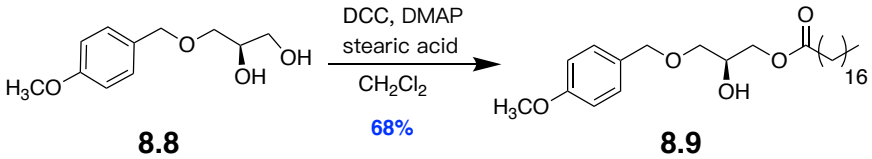
8.5. Synthesis



((*R*)-3-((4-Methoxybenzyl)oxy)propane-1,2-diol) (8.8)

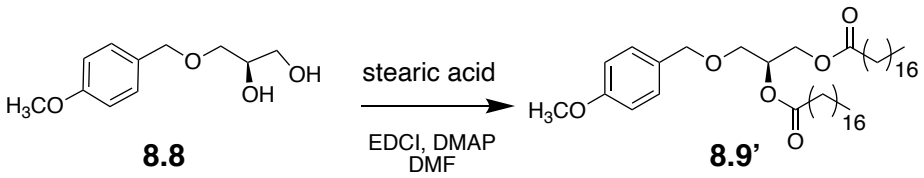
(*S*)-(2,2-Dimethyl-1,3-dioxolan-4-yl)methanol (1.05 g, 7.945 mmol) was dissolved in 5 mL dry DMF under nitrogen at 0 °C. NaH (0.35g, 8.74 mmol, 60% dispersion in mineral oil) was then added and the reaction mixture was further stirred for 15 minutes followed by addition of 4-methoxybenzyl chloride (1.125 mL, 8.74 mmol). After stirring at 0 °C for extra 10 min, the reaction mixture was removed from the ice bath and stirred at room temperature overnight. The reaction was carefully quenched by adding water and the mixture was extracted with 3 x 50 mL EtOAc. The combined organic layer was further washed with 5 x 100 water and once with 100 mL brine. After drying with Na_2SO_4, filtering and concentrating under reduced pressure, the residue was redissolved in MeOH. *p*-TsOH (0.15 g, 0.79 mmol) was then added. The reaction was stirred at room temperature overnight. After completion, the solvent was removed under reduced pressure and the residue was subjected to silica gel column chromatography. Gradient elution from 25% EtOAc-hexanes to 100% EtOAc afforded **8.8** as colorless oil (1.365 g, 6.43 mmol, 81% yield over 2 steps). R_f = 0.5 (100% EtOAc).

^{1}H NMR (500 MHz, Chloroform-*d*) δ 7.26 – 7.21 (m, 2H), 6.90 – 6.84 (m, 2H), 4.46 (s, 2H), 3.88 – 3.82 (m, 1H), 3.79 (s, 3H), 3.66 (dd, *J* = 11.3, 3.3 Hz, 1H), 3.58 (dd, *J* = 11.5, 5.5 Hz, 1H), 3.49 (qd, *J* = 9.7, 5.0 Hz, 2H), 2.81 (br, 2H). ^{13}C NMR (126 MHz, $CDCl_3$) δ 159.34, 129.76, 129.45, 129.44, 113.87, 113.86, 73.20, 71.43, 70.69, 64.04, 55.26. HRMS-DART: $[M+H]^+$ calcd for $C_{11}H_{17}O_4$, 213.1127; Found 213.0959.



((*S*)-2-Hydroxy-3-((4-methoxybenzyl)oxy)propyl stearate (8.9)

Compound **8.8** (0.6186 g, 2.914 mmol), stearic acid (0.7462 g, 2.623 mmol), *N*,*N*'-dicyclohexylcarbodiimide (DCC, 0.721 g, 3.5 mmol) and 4-dimethylaminopyridine (DMAP, 0.178 g, 1.457 mmol) were added into a 100 mL round bottom flask under nitrogen. The mixture was then dissolved with 20 mL dry DCM at 0 °C and further stirred at room temperature overnight. After completion, the DCU byproduct was filtered off with a Büchner funnel. The filtrate was collected and the solvent was evaporated under reduced pressure. Silica gel column chromatography using gradient elution from 100% hexanes to 25% EtOAc-hexanes afforded **8.9** as a white solid (0.86 g, 1.8 mmol, 68% yield). R_f = 0.26 (25% EtOAc-hexanes). ^{1}H NMR (500 MHz, Chloroform-*d*) δ 7.28 – 7.22 (m, 2H), 6.91 – 6.85 (m, 2H), 4.48 (s, 2H), 4.22 – 4.08 (m, 2H), 4.04 – 3.97 (m, 1H), 3.81 (s, 3H), 3.56 – 3.41 (m, 2H), 2.51 (br, 1H), 2.31 (t, *J* = 7.6 Hz, 2H), 1.66 – 1.55 (m, 28H), 1.25 (s, 27H), 0.88 (t, *J* = 6.9 Hz, 3H). ^{13}C NMR (126 MHz, $CDCl_3$) δ 174.09, 159.52, 129.89, 129.55, 129.46, 114.02, 114.00, 73.32, 70.71, 69.08, 65.51, 55.41, 34.31, 32.07, 29.84, 29.82, 29.80, 29.75, 29.61, 29.50, 29.42, 29.40, 29.28, 25.06, 22.83, 14.26.

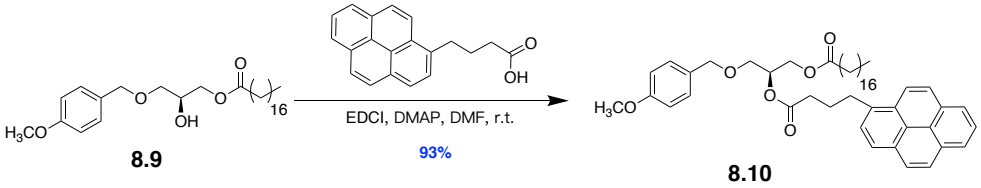


(*S*)-3-((4-Methoxybenzyl)oxy)propane-1,2-diyl distearate (8.9')

Stearic acid (113.8 mg, 0.4 mmol) and EDCI (68.31 mg, 0.44 mmol) were combined in a 50 mL RBF under Ar. 3 mL dry DMF was used to dissolve the starting materials and the reaction mixture was placed in a 0 °C with ice bath and stirred for 30 min. DMAP (9.7 mg, 0.08 mmol) as well as **8.8** (90 mg, 0.4 mmol) were added into the RBF. The reaction was stirred at room temperature overnight before being quenched by pouring into 100 mL 1N HCl. 25 × 3 mL DCM was used to extract the aqueous phase three time. The combined organic layer was then washed with water (25 mL) five times, once with 25 mL brine, dried over Na_2SO_4, filtered, and concentrated under reduced pressure. The crude was subjected to a column packed with silica

gel. Gradient elution with hexanes to 20% ethyl acetate-hexanes was needed to afford the product as a white solid. R_f = 0.5 (25% Ethyl acetate-hexanes)

^{1}H NMR (500 MHz, Chloroform-d) δ 7.26 – 7.23 (m, 2H), 6.90 – 6.86 (m, 2H), 4.48 (s, 2H), 4.22 – 4.08 (m, 2H), 4.04 – 3.98 (m, 1H), 3.80 (s, 3H), 3.55 – 3.42 (m, 2H), 2.44 (t, J = 7.4 Hz, 1H), 2.32 (dt, J = 10.4, 7.5 Hz, 3H), 1.62 (dtd, J = 14.5, 7.7, 4.7 Hz, 4H), 1.25 (d, J = 1.7 Hz, 55H), 0.88 (t, J = 6.9 Hz, 6H).



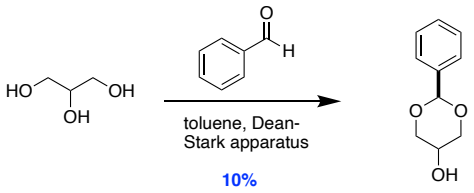
8.9 **8.10**

(*S*)-3-((4-Methoxybenzyl)oxy)-2-((4-(pyren-1-yl)butanoyl)oxy)propyl stearate (8.10)

Compound **8.9** (0.1918 g, 0.4 mmol), 1-pyrenebutyric acid (0.1384 g, 0.48 mmol), EDCI (0.06831 g, 0.44 mmol) as well as DMAP (9.77 mg, 0.08 mmol) were combined in a 50 mL RBF under Ar. After dissolving with 2 mL dry DMF, the reaction was stirred overnight at room temperature. The reaction was quenched by pouring into 100 mL water. The aqueous phase was extracted with 3 × 25mL chloroform until it was colorless. The combined organic layer was washed with 25 mL water five times and once with 25 mL brine. After being dried over Na_2SO_4, filtered, and concentrated under reduced pressure, the crude was purified with a silica gel column using gradient elution from hexanes to 20% ethyl acetate in hexanes. The product was obtained as a dark brown oil (0.2787g, 0.372 mmol, 93% yield). R_f = 0.56 (25% EtOAc-hexanes).

^{1}H NMR (500 MHz, Chloroform-*d*) δ 8.30 (d, *J* = 9.3 Hz, 1H), 8.20 – 8.15 (m, 2H), 8.13 – 8.08 (m, 2H), 8.03 (d, *J* = 0.7 Hz, 2H), 8.00 (t, *J* = 7.6 Hz, 1H), 7.86 (d, *J* = 7.8 Hz, 1H), 7.24 – 7.19 (m, 2H), 6.82 (d, *J* = 8.6 Hz, 2H), 5.36 – 5.24 (m, 1H), 4.51 – 4.42 (m, 2H), 4.38 (dd, *J* = 11.9, 3.7 Hz, 1H), 4.22 (dd, *J* = 11.9, 6.5 Hz, 1H), 3.62 – 3.53 (m, 2H), 3.44 – 3.33 (m, 2H), 2.52 – 2.42 (m, 2H), 2.31 – 2.14 (m, 4H), 1.62 – 1.49 (m, 2H), 1.32 – 1.16 (m, 30H), 0.92 – 0.87 (m, 3H). ^{13}C NMR (126 MHz, $CDCl_3$) δ 173.44, 172.74, 159.29, 135.64, 131.41, 130.89, 129.99,

129.67, 129.31, 128.73, 127.47, 127.42, 127.41, 127.34, 126.72, 125.83, 125.10, 124.99, 124.91, 124.81, 124.77, 123.28, 123.26, 113.80, 113.79, 113.78, 72.97, 70.32, 67.90, 62.71, 55.17, 34.11, 33.93, 32.69, 31.93, 29.70, 29.69, 29.67, 29.66, 29.64, 29.60, 29.58, 29.44, 29.36, 29.23, 29.08, 26.82, 24.85, 22.69, 14.12. HRMS-DART: $[M+H]^+$ calcd for $C_{49}H_{65}O_6$, 749.47814 Found: 749.46657

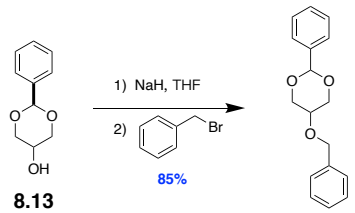


8.13

2-Phenyl-1,3-dioxan-5-ol (8.13)

Glycerol (24.31 g, 264 mmol), benzaldehyde (28.03 g, 264.1 mmol), and *p*-TsOH (115.1 mg, 0.61 mmol) were weighed into a 250 mL round bottom flask. 70 mL toluene was then added and the reaction was refluxed at 150 °C for 48 hours with a Dean-Stark trap. After being cooled back to room temperature, the mixture was washed with 100 mL saturated $NaHCO_3$, 100 mL brine, dried over Na_2SO_4 and filtered off. The filtrate was stored in a -20 °C freezer to precipitate the desired product, which was then quickly filtered at low temperature via vacuum filtration. **8.13** was obtained as a white solid (4.7 g, 26.4 mmol, 10% yield).

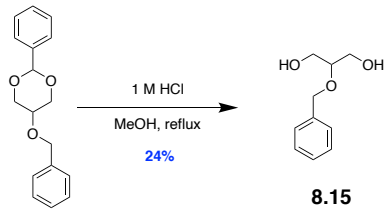
^{1}H NMR (500 MHz, Chloroform-*d*) δ 7.50 (dd, *J* = 7.1, 3.1 Hz, 2H), 7.38 (ddd, *J* = 7.0, 2.8, 1.7 Hz, 2H), 5.56 (d, *J* = 2.7 Hz, 1H), 4.23 – 4.11 (m, 4H), 3.63 (ddd, *J* = 11.2, 3.7, 1.9 Hz, 1H), 3.01 (dd, *J* = 11.3, 2.7 Hz, 1H). ^{13}C NMR (126 MHz, $CDCl_3$) δ 137.95, 129.25, 128.47, 126.01, 101.83, 72.45, 64.17. HRMS-DART: $[M+H]^+$ calcd for $C_{10}H_{13}NO_3$, 181.0865; Found 181.0928.



8.13 **8.14**

5-(Benzyloxy)-2-phenyl-1,3-dioxane (8.14)

Compound **8.13** (1 g, 5.54 mmol) was dissolved with 20 mL dry THF in a 100 mL RBF at 0 °C under Ar. NaH (60% dispersion in mineral oil, 0.3 g, 6.67 mmol) was added carefully portion wise. After stirring for 15 min, benzyl alcohol (0.8 mL, 6.67 mmol) was added dropwise. The reaction was allowed to warm up to room temperature and stirred overnight before being carefully quenched by addition of water. THF was removed under reduced pressure and the aqueous residue was extracted by 25 mL chloroform three times. The combined organic layer was washed by 50 mL water and 50 mL brine, respectively, before being dried over Na_2SO_4, filtered, and concentrated under reduced pressure. The crude was purified by silica gel column chromatography using gradient elution from hexanes to 20% EtOAc in hexanes to yield product as a white crystal (1.267 g, 4.71 mmol, 85% yield). R_f = 0.47 (25% EtOAc-hexanes). ^{1}H NMR (300 MHz, Chloroform-*d*) δ 7.63 – 7.57 (m, 2H), 7.47 – 7.32 (m, 8H), 5.58 (s, 1H), 4.73 (s, 2H), 4.38 (dd, *J* = 12.6, 1.6 Hz, 2H), 4.04 (dd, *J* = 12.6, 1.7 Hz, 2H), 3.34 (t, *J* = 1.8 Hz, 1H). ^{13}C NMR (75 MHz, $CDCl_3$) δ 138.18, 138.16, 128.83, 128.40, 128.13, 127.68, 127.64, 126.18, 101.28, 101.24, 70.28, 70.25, 70.22, 69.29, 69.27, 68.93. HRMS-DART: $[M+H]^+$ calcd for $C_{17}H_{19}O_3$, 271.1334; Found 271.1388.



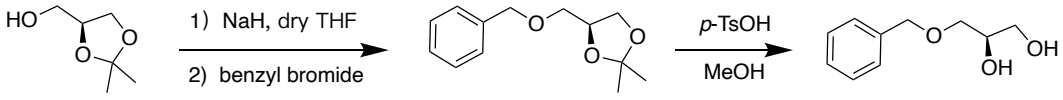
8.14 **8.15**

2-(Benzyloxy)propane-1,3-diol (8.15)

Compound **8.14** (0.432 g, 1.6 mmol) was dissolved with 30 mL methanol in a 100 mL RBF. 2 mL 1 N HCl was then added and the reaction was refluxed for 3 hours. After completion, the reaction was allowed to cool down to room temperature and water was added to dilute the mixture. Methanol was evaporated with a rotary evaporator and the aqueous residue was extracted with 25 mL chloroform three times. The combined organic layer was washed with 50

mL water and 50 mL brine before being dried with Na_2SO_4, filtered, and concentrated. Silica gel column chromatography was needed to purify the product as a white a solid (70 mg, 0.38 mmol, 24% yield). R_f = 0.5 (10% MeOH-chloroform).

^{1}H NMR (300 MHz, Chloroform-*d*) δ 7.45 – 7.27 (m, 5H), 4.66 (d, *J* = 0.8 Hz, 2H), 3.76 (qd, *J* = 11.7, 4.6 Hz, 4H), 3.64 – 3.57 (m, 1H), 1.98 (s, 2H). ^{13}C NMR (75 MHz, $CDCl_3$) δ 138.10, 128.72, 128.13, 127.97, 79.30, 72.08, 72.06, 62.38. HRMS-DART: $[M+H]^+$ calcd for $C_{10}H_{15}O_3$, 183.1021; Found 183.1087.



8.17 (81% over 2 steps) **8.18**

(*R*)-3-(Benzyloxy)propane-1,2-diol (8.18)

(*S*)-(2,2-Dimethyl-1,3-dioxolan-4-yl)methanol (1.07 g, 8.09 mmol) was weighed into a 50 mL RBF under nitrogen and dissolved with dry THF at 0 °C. NaH (60% dispersed in mineral oil, 0.38 g, 9.7 mmol) was carefully added into the RBF. After being further stirred for 30 min, benzyl bromide (1.15 mL, 9.7 mmol) was added. The reaction was allowed to warm up to room temperature and stirred overnight. Water was added dropwise to quench the reaction. THF was evaporated under reduced pressure and the aqueous residue was extracted twice with 25 mL chloroform. The combined organic layer was washed once with 25 mL H_2O, once with 25 mL brine, dried over Na_2SO_4, filtered, and concentrated using a rotary evaporator. The crude was redissolved in methanol and *p*-TsOH (0.2 g, 0.809 mmol) was added. The reaction was stirred at room temperature for six hours. Methanol was then removed under reduced pressure and the crude was subject to a column packed with silica gel. Gradient elution using hexanes to 100% EtOAc was needed to get the product as colorless oil (1.2 g, 6.58 mmol, 81% over two steps). R_f = 0.5 (100% EtOAc).

^{1}H NMR (500 MHz, Chloroform-*d*) δ 7.27 (d, *J* = 5.3 Hz, 4H), 7.22 (dq, *J* = 6.3, 4.0 Hz, 1H), 4.44 (s, 2H), 4.28 (s, 2H), 3.89 – 3.76 (m, 1H), 3.64 – 3.54 (m, 1H), 3.50 (dd, *J* = 11.7, 6.4 Hz, 1H), 3.41 (d, *J* = 5.4 Hz, 2H). ^{13}C NMR (126 MHz, $CDCl_3$) δ 137.69, 128.20, 127.59, 127.58,

127.54, 73.16, 71.33, 70.76, 63.67. HRMS-DART: $[M+H]^+$ calcd for $C_{10}H_{15}O_3$: 183.1021; Found: 183.0982.

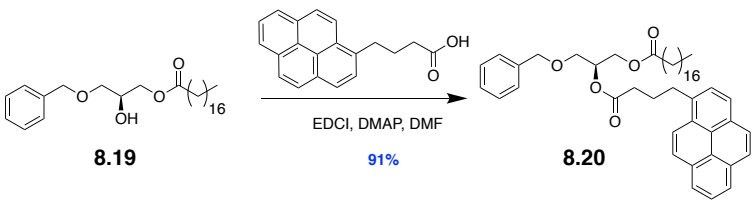


8.18 55% **8.19**

(*S*)-3-(Benzyloxy)-2-hydroxypropyl stearate (8.19)

Compound **8.18** (0.3611 g, 1.982 mmol), stearic acid (0.506 g, 1.78 mmol), DCC (0.49 g, 2.378 mmol), and DMAP (0.12 g, 0.99 mmol) were combined in a 100 mL RBF under nitrogen. 20 mL Dry DCM was added at 0 °C and the reaction mixture was stirred overnight. After completion, DCU by-product was filtered off and the filtrate was concentrated under reduced pressure. This process was repeated several times until no more DCU precipitated out from DCM. The crude was then purified with silica gel column chromatography using gradient elution from hexanes to 25% EtOAc-hexanes to yield product as a white solid (0.44 g, 0.98 mmol, 55% yield). R_f = 0.54 (25% EtOAc-hexanes).

^{1}H NMR (300 MHz, Chloroform-*d*) δ 7.44 – 7.26 (m, 5H), 4.56 (s, 2H), 4.24 – 4.09 (m, 2H), 4.08 – 3.98 (m, 1H), 3.60 – 3.44 (m, 2H), 2.54 (s, 1H), 2.32 (dd, *J* = 7.9, 7.2 Hz, 2H), 1.61 (t, *J* = 7.4 Hz, 2H), 1.26 (s, 31H), 0.93 – 0.83 (m, 3H). ^{13}C NMR (75 MHz, $CDCl_3$) δ 174.08, 137.80, 128.62, 128.02, 127.89, 73.66, 71.01, 69.09, 65.49, 34.30, 32.07, 29.84, 29.80, 29.75, 29.61, 29.51, 29.41, 29.28, 25.06, 22.84, 14.26. HRMS-DART: $[M+H]^+$ calcd for $C_{28}H_{49}O_4$: 449.3631; Found: 449.3559.



8.19 91% **8.20**

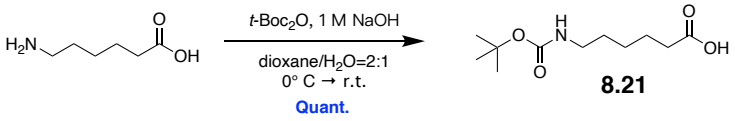
(*S*)-3-(Benzyloxy)-2-((4-(pyren-1-yl)butanoyl)oxy)propyl stearate (8.20)

Compound **8.19** (0.2032 g, 0.453 mmol), 1-pyrenebutyric acid (0.1567 g, 0.543 mmol), EDCI

(0.0773 g, 0.498 mmol), and DMAP (0.0111 g, 0.09 mmol) were weighed into a 50 mL RBF under nitrogen. 4 mL dry DMF was added at 0 °C. The reaction mixture was allowed to warm up to room temperature and further stirred overnight. After completion, the reaction was quenched by pouring into 100 mL water. 25 mL chloroform was used to extract the aqueous phase three times. The combined organic layer was further washed with 25 mL water five times, once with 25 mL brine, dried over Na_2SO_4, filtered, and concentrated under reduced pressure. The crude was then subjected to a column packed with silica gel using gradient elution from 100% hexanes to 10% EtOAc in hexanes. The product was obtained as a dark brown oil (0.296 g, 0.412 mmol, 91% yield). R_f = 0.67 (25% EtOAc-hexanes).

^{1}H NMR (500 MHz, Chloroform-*d*) δ 8.31 (d, *J* = 9.3 Hz, 1H), 8.17 (dq, *J* = 7.9, 1.2 Hz, 2H), 8.13 – 8.09 (m, 2H), 8.05 – 7.98 (m, 3H), 7.86 (d, *J* = 7.8 Hz, 1H), 7.34 – 7.26 (m, 4H), 5.33 (dtd, *J* = 6.5, 5.1, 3.7 Hz, 1H), 4.60 – 4.49 (m, 2H), 4.41 (dd, *J* = 11.9, 3.7 Hz, 1H), 4.25 (dd, *J* = 11.9, 6.4 Hz, 1H), 3.62 (dd, *J* = 5.1, 1.2 Hz, 2H), 3.44 – 3.36 (m, 2H), 2.55 – 2.44 (m, 2H), 2.31 – 2.17 (m, 4H), 1.57 (q, *J* = 7.4 Hz, 2H), 1.37 – 1.11 (m, 32H), 0.91 (t, *J* = 7.0 Hz, 3H).

^{13}C NMR (126 MHz, $CDCl_3$) δ 173.54, 172.85, 137.77, 135.74, 131.54, 131.02, 130.12, 128.86, 128.53, 127.90, 127.76, 127.59, 127.54, 127.47, 126.85, 125.96, 125.23, 125.05, 124.93, 124.90, 123.40, 73.44, 70.42, 68.39, 62.81, 34.24, 34.03, 32.81, 32.07, 29.84, 29.81, 29.78, 29.73, 29.58, 29.51, 29.37, 29.21, 26.93, 24.99, 22.84, 14.27. HRMS-DART: $[M+H]^+$ calcd for $C_{48}H_{63}O_5$: 719.4676; Found: 719.4732.



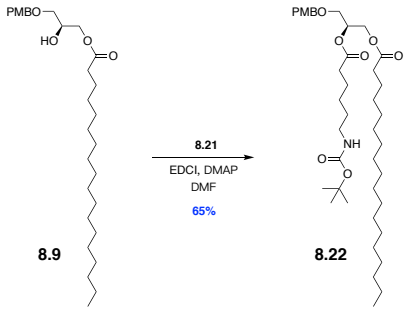
8.21

(6-((*tert*-Butoxycarbonyl)amino)hexanoic acid) (8.21)

6-Aminocaproic acid (2.62 g, 20 mmol) was dissolved in 30 mL dioxane/water (2/1, v/v). Then, the mixture was cooled to 0 °C with an ice bath. 1 M NaOH (20 mL) and *tert*-butyl dicarbonate (4.8 g, 22 mmol) were added into the flask respectively. The reaction was further stirred at room temperature for 3 hrs. Since carbon dioxide was released in this reaction, the flask was

left open to the atmosphere. After completion, the reaction mixture was concentrated and the basic residue was washed once with 100 mL EtOAc. The aqueous layer was acidified with 1 N HCl until pH reached 1 and was further extracted with 50 mL EtOAc twice. The combined organic layer was washed with water (100 mL), brine (100 mL), dried over Na_2SO_4, filtered, and concentrated under reduced pressure to afford **8.21** as a colorless oil which crystalized over time (Quantitative yield). R_f = 0.8 (100% EtOAc).

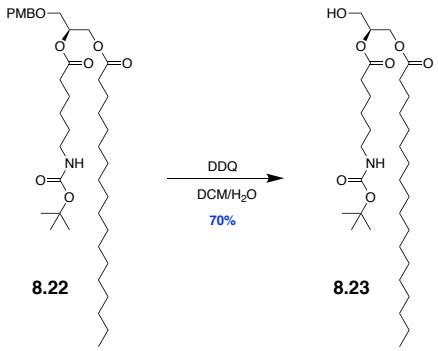
^{1}H NMR (300 MHz, Chloroform-*d*) δ 3.09 (q, *J* = 7.5, 7.0 Hz, 2H), 2.32 (t, *J* = 7.4 Hz, 2H), 1.73 – 1.55 (m, 2H), 1.54 – 1.28 (m, 13H). ^{13}C NMR (75 MHz, $CDCl_3$) δ 178.73, 156.18, 79.19, 40.38, 34.00, 29.69, 28.42, 26.24, 24.40.



((*S*)-2-((6-((*tert*-Butoxycarbonyl)amino)hexanoyl)oxy)-3-((4-methoxybenzyl)oxy)propyl stearate) (8.22)

Compound **8.9** (0.8687 g, 1.79 mmol), 1-Ethyl-3-(3-dimethylaminopropyl)carbodiimide (EDCI, 0.305 g, 1.97 mmol), and DMAP (0.0438 g, 0.359 mmol) were combined in a 50 mL round bottom flask under nitrogen. **8.21** (0.497g, 2.15 mmol) was dissolved in 5 mL dry DMF and added into the RBF dropwise at 0 °C. The reaction mixture was stirred overnight at room temperature and was then quenched by pouring into 150 mL water. The aqueous phase was extracted with 50 mL chloroform three times. The combined organic layer was further washed with 100 mL water five times and once with 100 mL brine. After being dried over Na_2SO_4, filtered, and concentrated to dryness, the crude was purified via silica gel column chromatography. Gradient elution from 100% hexanes to 20% EtOAc-hexanes yield **8.22** as a yellowish oil (0.806 g, 1.16 mmol, 65% yield). R_f = 0.65 (25% EtOAc-hexanes).

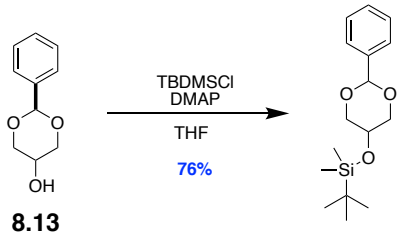
^{1}H NMR (500 MHz, Chloroform-*d*) δ 7.26 – 7.18 (m, 2H), 6.89 – 6.84 (m, 2H), 5.24 – 5.17 (m, 1H), 4.56 (s, 1H), 4.51 – 4.39 (m, 2H), 4.32 (dd, *J* = 11.9, 3.8 Hz, 1H), 4.21 – 3.94 (m, 2H), 3.79 (d, *J* = 1.3 Hz, 3H), 3.57 – 3.42 (m, 2H), 3.08 (q, *J* = 6.8 Hz, 2H), 2.37 – 2.17 (m, 4H), 1.60 (tt, *J* = 14.3, 7.3 Hz, 4H), 1.43 (s, 9H), 1.37 – 1.13 (m, 32H), 0.87 (t, *J* = 6.9 Hz, 3H). ^{13}C NMR (126 MHz, $CDCl_3$) δ 174.01, 173.48, 172.91, 159.43, 156.04, 129.85, 129.50, 129.41, 113.92, 79.12, 73.27, 73.05, 70.69, 70.24, 69.02, 67.98, 65.49, 62.72, 55.35, 40.46, 34.27, 34.24, 34.21, 32.04, 29.81, 29.80, 29.77, 29.74, 29.72, 29.60, 29.58, 29.47, 29.40, 29.37, 29.25, 29.23, 28.53, 26.31, 25.03, 24.99, 24.64, 22.80, 14.23. HRMS-DART: $[M+H]^+$ calcd for $C_{40}H_{70}NO_8$, 692.5101; Found 692.5327.



((*S*)-2-((6-((*tert*-Butoxycarbonyl)amino)hexanoyl)oxy)-3-hydroxypropyl stearate) (8.23)

Compound **8.22** (0.1285 g, 0.186 mmol) and 2,3-dichloro-5,6-dicyano-1,4-benzoquinone (DDQ, 0.084 g, 0.371 mmol) were weighed into a 50 mL flask. 5.5 mL DCM/water (10/1, v/v) was then added and the reaction was stirred vigorously at room temperature for 8 hours. The color of the reaction turned from dark green to bright orange. The reaction was finally quenched by addition of saturated $NaHCO_3$ solution. The mixture was extracted with 50 mL DCM three times. The combined organic layer was further washed with 100 mL water and 100 mL brine once, dried with Na_2SO_4, filtered, and concentrated under reduced pressure. The crude was separated through silica gel column chromatography using gradient elution from 10% EtOAc-hexanes to 50% EtOAc-hexanes. The product was obtained as a white solid (74 mg, 0.13 mmol, 70% yield). R_f = 0.5 (50% EtOAc-hexanes).

^{1}H NMR (500 MHz, Chloroform-*d*) δ 5.13 – 5.04 (m, 1H), 4.59 (t, *J* = 6.1 Hz, 1H), 4.37 – 4.18 (m, 2H), 3.73 (dd, *J* = 4.9, 3.7 Hz, 2H), 3.10 (q, *J* = 6.8 Hz, 2H), 2.33 (dt, *J* = 19.0, 7.6 Hz, 4H), 1.63 (dt, *J* = 23.1, 7.5 Hz, 4H), 1.43 (s, 13H), 1.25 (s, 28H), 0.87 (t, *J* = 6.9 Hz, 3H). ^{13}C NMR (126 MHz, $CDCl_3$) δ 173.68, 173.13, 156.12, 79.06, 72.21, 62.24, 61.16, 40.31, 34.08, 33.89, 31.91, 29.68, 29.64, 29.61, 29.47, 29.35, 29.27, 29.11, 28.40, 26.11, 24.87, 24.48, 22.67, 14.09.

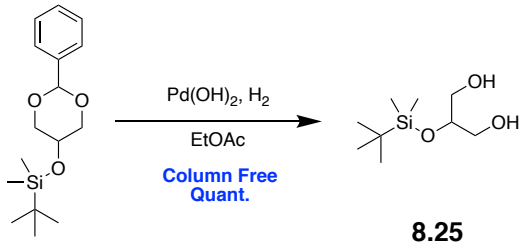


8.13 **8.24**

(*tert*-Butyldimethyl((2-phenyl-1,3-dioxan-5-yl)oxy)silane) (8.24)

Compound **8.13** (0.5 g, 2.77 mmol) and DMAP (0.541 g, 4.432 mmol) were added into a 100 mL round bottom flask under N_2. The solid was dissolved with 20 mL dry THF at 0 °C. After quickly adding *tert*-butyldimethylsilyl chloride (TBDMSCl, 0.501g, 3.33 mmol), the reaction was stirred at room temperature overnight. Water was then added to quench the reaction. After the removal of THF under reduced pressure, the aqueous residue was extracted with 50 mL DCM three times. The combined organic layer was washed with 100 mL water and 100 mL brine, dried over Na_2SO_4, filtered, and concentrated. Silica gel column chromatography using gradient elution from 100% hexanes to 10% EtOAc-hexanes afforded **8.24** as a colorless liquid (0.61g, 2.11 mmol, 76% yield). R_f = 0.51 (10% EtOAc-hexanes).

^{1}H NMR (300 MHz, Chloroform-*d*) δ 7.53 – 7.49 (m, 2H), 7.42 – 7.34 (m, 3H), 5.41 (s, 1H), 4.24 (ddt, *J* = 10.0, 5.1, 0.8 Hz, 2H), 4.08 – 3.94 (m, 1H), 3.60 (tdd, *J* = 10.0, 1.8, 0.9 Hz, 2H), 0.93 (s, 9H), 0.13 (s, 6H). ^{13}C NMR (75 MHz, $CDCl_3$) δ 138.45, 128.92, 128.37, 126.44, 101.02, 100.98, 71.86, 64.58, 64.54, 25.99, 18.35, -4.47. HRMS-DART: $[M+H]^+$ calcd for $C_{16}H_{27}SiO_3$, 295.1729; Found 295.1513.

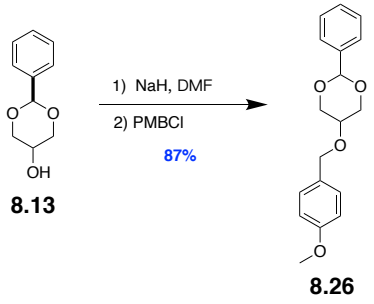


8.24 **8.25**

(2-((*tert*-Butyldimethylsilyl)oxy)propane-1,3-diol) (8.25)

Compound **8.24** (0.61 g, 2.11 mmol) was weighed into a 100 mL round bottom flask under nitrogen. $Pd(OH)_2$ on carbon (0.3 g, 50% wt of starting material) was quickly transferred into the flask followed by addition of 20 mL EtOAc. The nitrogen atmosphere was then carefully replaced by hydrogen gas. The reaction was stirred vigorously overnight. The palladium catalyst was carefully removed via vacuum filtration through a celite pad. Pure product was obtained after the removal of the solvent under reduced pressure at a quantitative yield.

^{1}H NMR (300 MHz, Chloroform-*d*) δ 3.82 (q, *J* = 4.8 Hz, 1H), 3.68 – 3.62 (m, 4H), 1.93 (br, 2H), 0.91 (s, 9H), 0.12 (s, 6H). ^{13}C NMR (75 MHz, $CDCl_3$) δ 72.72, 64.27, 25.93, 18.24, -4.53. HRMS-DART: $[M+H]^+$ calcd for $C_9H_{23}SiO_3$, 207.1416; Found 207.1205.



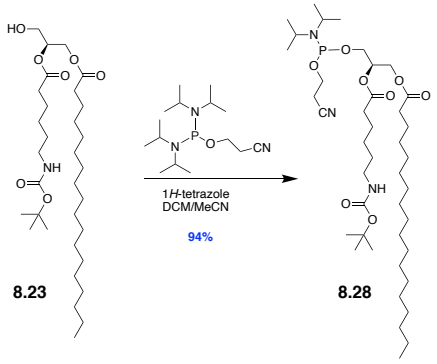
8.13 **8.26**

5-((4-Methoxybenzyl)oxy)-2-phenyl-1,3-dioxane (8.26)

Compound **8.13** (0.24 g, 1.33 mmol) was weighed into a 50 mL RBF under nitrogen. 2 mL dry DMF was used to dissolve the starting material at 0 °C. NaH (67 mg, 1.67 mmol, 60% dispersion in mineral oil) was then carefully added into the RBF, followed by addition of PMBCl (0.225 mL, 1.67 mmol). The reaction mixture was stirred overnight before being quenched by addition of water dropwise until no gas was released. The resulting mixture was next poured

into 100 mL water. 20 mL EtOAc was used to extract the aqueous phase three times. The combined organic layer was washed with 30 mL water five times, 30 mL brine, dried over Na_2SO_4, filtered, and concentrated under reduced pressure. The crude was purified using a column packed with silica gel. Gradient elution from 5% EtOAc in hexanes to 30% EtOAc-hexanes yield product as a yellow oil (0.3479 g, 1.16 mmol, 87 % yield). R_f = 0.4 (25% EtOAc-hexanes).

^{1}H NMR (300 MHz, Chloroform-*d*) δ 7.59 – 7.50 (m, 2H), 7.41 – 7.25 (m, 5H), 6.92 – 6.87 (m, 2H), 5.56 (s, 1H), 4.64 (s, 2H), 4.34 (dq, *J* = 12.7, 1.6 Hz, 2H), 4.06 – 3.99 (m, 2H), 3.80 (d, *J* = 0.5 Hz, 3H), 3.32 (p, *J* = 1.8 Hz, 1H). ^{13}C NMR (75 MHz, $CDCl_3$) δ 159.28, 138.21, 133.29, 130.20, 129.37, 128.91, 128.62, 128.21, 126.26, 113.93, 113.88, 101.40, 101.36, 70.00, 69.97, 69.94, 69.07, 68.93, 68.91, 64.92, 55.34, 55.29.

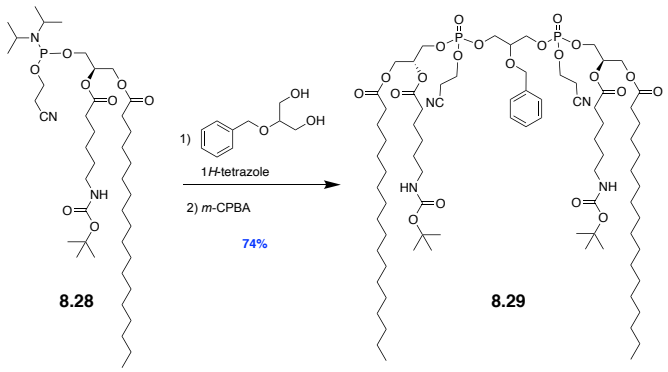


((2*R*)-2-((6-((*tert*-Butoxycarbonyl)amino)hexanoyl)oxy)-3-(((2-cyanoethoxy)(diisopropylamino)phosphaneyl)oxy)propyl stearate) (8.28)

Compound **8.23** (100 mg, 0.175 mmol) was weighed into a 50 mL round bottom flask under nitrogen and dissolved with dry DCM/MeCN (2mL/2.2mL). 1*H*-tetrazole (0.8 mL, 0.35 mmol, 0.45 M in MeCN) was added into the flask followed by 2-cyanoethyl *N*,*N*,*N*′,*N*′-tetraisopropylphosphorodiamidite (0.12 mL, 0.35 mmol). After being stirred at room temperature for 3 hours, the reaction was quenched by adding saturated $NaHCO_3$ solution. The mixture was extracted with 25 mL chloroform three times. The combined organic layer was washed with 50 mL water and 50 mL brine, dried over Na_2SO_4, filtered, and concentrated

under reduced pressure. The crude was purified with a column packed with silica gel and 10% EtOAc-hexanes containing 3% triethylamine. Gradient elution from 10% EtOAc-hexanes to 25% EtOAc-hexanes (all containing 3% triethylamine) afforded desired product as a yellow oil (125.7 mg, 0.16 mmol, 94% yield). R_f = 0.4 (25% EtOAc-hexanes).

^{1}H NMR (300 MHz, Chloroform-*d*) δ 5.17 (t, *J* = 5.2 Hz, 1H), 4.55 (br, 1H), 4.34 (td, *J* = 11.6, 3.8 Hz, 1H), 4.14 (ddd, *J* = 11.8, 8.5, 6.1 Hz, 1H), 3.88 – 3.50 (m, 6H), 3.15 – 3.00 (m, 2H), 2.62 (t, *J* = 6.4 Hz, 2H), 2.29 (dd, *J* = 9.9, 4.8 Hz, 4H), 1.75 – 1.46 (m, 6H), 1.43 (s, 9H), 1.24 (s, 30H), 1.16 (dd, *J* = 6.8, 3.7 Hz, 12H), 0.91 – 0.81 (m, 3H). ^{13}C NMR (75 MHz, $CDCl_3$) δ 173.50, 172.83, 156.07, 117.67, 79.18, 62.43, 61.79, 58.75, 58.50, 43.39, 43.21, 40.49, 34.24, 32.04, 29.88, 29.82, 29.78, 29.75, 29.61, 29.48, 29.42, 29.26, 28.54, 26.37, 25.02, 24.76, 24.67, 24.63, 22.81, 20.54, 20.45, 14.24. ^{31}P NMR (121 MHz, $CDCl_3$) δ 149.47, 149.34. HRMS-DART: $[M+NH_4]^+$ calcd for $C_{41}H_{82}O_8N_4P$, 789.5870; Found 789.3220.

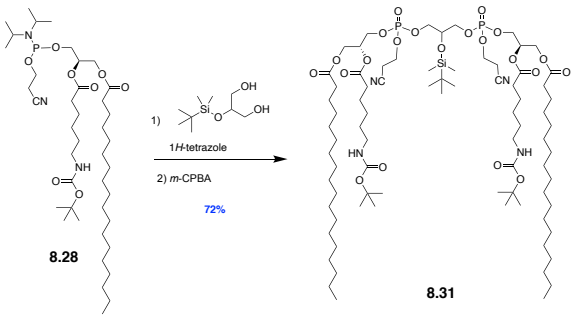


8.29

Compound **8.28** (116 mg, 0.15 mmol) and **8.15** (12.4 mg, 0.068 mmol) were combined in a 50 mL RBF under nitrogen. 2 mL dry DCM was used to dissolve the reaction mixture followed by addition of 1*H*-tetrazole (0.9 mL, 0.408 mmol, 0.45 M in MeCN). The reaction was stirred at room temperature. After three hours, it was brought to 0 °C with an ice bath. *m*-CPBA (122 mg, 0.408 mmol, 57% purity) was then added. After being stirred for extra 1.5 hours, the reaction was quenched by adding saturated $NaHCO_3$ solution. The reaction mixture was then extracted by 25 mL chloroform three times. The combined organic layer was washed once with 25 mL

water and once with 25 mL brine. After being dried over Na_2SO_4, filtered, and concentrated under reduced pressure, the crude was subjected to a column packed with silica gel. Gradient elution using chloroform to 5% MeOH in chloroform was needed to purify the product as a yellow oil (78.35 mg, 0.05 mmol, 74% yield). R_f = 0.48 (10% MeOH-chloroform); 0.32 (5% MeOH-chloroform).

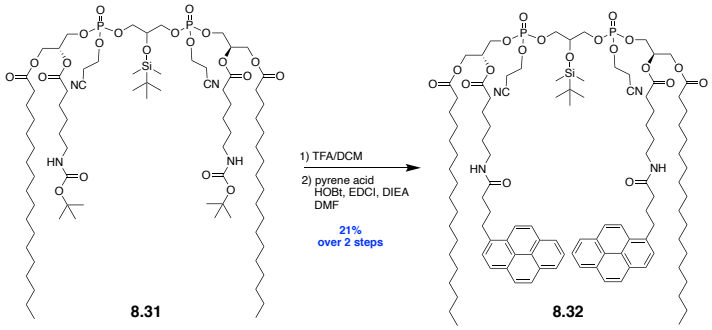
^{1}H NMR (500 MHz, Chloroform-*d*) δ 7.41 – 7.28 (m, 5H), 5.23 (dq, *J* = 3.9, 1.9 Hz, 2H), 4.74 – 4.54 (m, 4H), 4.36 – 4.06 (m, 16H), 3.87 (q, *J* = 5.1 Hz, 1H), 3.09 (q, *J* = 6.8 Hz, 4H), 2.83 – 2.66 (m, 4H), 2.37 – 2.26 (m, 8H), 1.69 – 1.54 (m, 11H), 1.43 (s, 23H), 1.38 – 1.20 (m, 64H), 0.88 (t, *J* = 6.9 Hz, 6H). ^{13}C NMR (126 MHz, $CDCl_3$) δ 173.39, 172.74, 156.14, 137.37, 128.93, 128.83, 128.72, 128.33, 128.22, 128.17, 128.15, 128.09, 127.92, 116.60, 79.18, 75.61, 72.50, 70.75, 69.84, 69.79, 69.56, 69.50, 66.17, 62.41, 62.39, 62.37, 61.76, 61.65, 44.67, 40.49, 34.26, 34.12, 34.10, 33.94, 32.07, 29.85, 29.83, 29.81, 29.79, 29.65, 29.51, 29.45, 29.29, 29.26, 28.58, 26.33, 24.97, 24.57, 23.80, 22.84, 19.77, 19.72, 19.66, 14.27. ^{31}P NMR (202 MHz, $CDCl_3$) δ -1.79, -1.81, -1.91, -1.96.



8.31

Compound **8.28** (75.3 mg, 0.0975 mmol) and **8.25** (9.15 mg, 0.0443 mmol) was added to a 50 mL RBF under nitrogen. Dry DCM (1.2 mL) was then used to dissolve the starting material followed by addition of 1*H*-tetrazole (0.6 mL, 0.266 mmol, 0.45 M in MeCN). After being stirred at room temperature for 3 hours, the reaction mixture was cooled to 0 °C with an ice bath. *m*-CPBA (80.53 mg, 0.266 mmol, 57% purity) was added carefully and the reaction was stirred for an extra 1.5 hours. Saturated $NaHCO_3$ solution was then used to quench the reaction. The

reaction mixture was extracted three times with 25 mL chloroform. The combined organic layer was washed with 100 mL water and 100 mL brine, dried over Na_2SO_4, filtered, and concentrated under reduced pressure. The crude was subjected to silica gel column chromatography and gradient elution from 100% chloroform to 5% methanol-chloroform yield **8.31** as a yellow oil (50.6 mg, 0.032 mmol, 72% yield). R_f = 0.48 (10% methanol-chloroform). ^{1}H NMR (500 MHz, Chloroform-*d*) δ 5.25 (q, *J* = 5.0 Hz, 2H), 4.64 (br, 2H), 4.38 – 4.01 (m, 17H), 3.10 (q, *J* = 6.8 Hz, 4H), 2.78 (t, *J* = 6.1 Hz, 4H), 2.32 (dt, *J* = 19.3, 7.5 Hz, 8H), 1.61 (dp, *J* = 21.4, 7.4 Hz, 10H), 1.43 (s, 22H), 1.25 (s, 58H), 0.88 (d, *J* = 9.0 Hz, 15H), 0.11 (d, *J* = 1.3 Hz, 6H). ^{13}C NMR (126 MHz, $CDCl_3$) δ 173.36, 172.69, 156.11, 116.55, 79.16, 70.14, 69.54, 69.40, 69.34, 69.14, 68.96, 68.14, 66.33, 66.17, 63.60, 62.69, 62.42, 61.85, 61.74, 61.42, 40.47, 34.11, 34.08, 32.06, 29.84, 29.81, 29.79, 29.78, 29.68, 29.64, 29.49, 29.43, 29.27, 28.73, 28.62, 28.51, 28.41, 26.33, 25.77, 24.96, 24.55, 22.82, 19.83, 19.77, 18.17, 14.26, -4.64, -4.75. ^{31}P NMR (121 MHz, $CDCl_3$) δ -1.66, -1.67, -1.74, -1.78. ESI-MS: $[M+H]^+$ calcd for $C_{79}H_{149}O_{21}N_4P_2Si$, 1579.9959; Found 1579.9930. ESI-MS: $[M+Na]^+$ calcd for $C_{79}H_{148}O_{21}N_4P_2SiNa$, 1601.9778; Found 1601.9748.

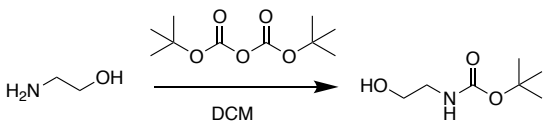


8.32

Compound **8.31** (48 mg, 0.03 mmol) was dissolved in 2 mL DCM in a large vial followed by addition of 2 mL trifluoracetic acid. The reaction was stirred at room temperature for 2 hours before being transferred into a 50 mL RBF. The solvent was removed under reduced pressure and the flask was placed under vacuum for 5 hours. After that, 1-pyrenebutyric acid (21.91 mg, 0.076 mmol) and hydroxybenzotriazole (HOBt, 11.64 mg, 0.076mmol) were added into the

flask under nitrogen. The mixture was dissolved by 2 mL dry DMF at 0 °C and stirred for 5 minutes. EDCI (14.57 mg, 0.076 mmol) was added into the reaction followed by *N*, *N*-diisopropylethylamine (DIEA, 25.12 µL, 0.152 mmol). The reaction was stirred overnight before being quenched by pouring into 100 mL 1 N HCl. The aqueous phase was extracted with 25 mL chloroform three times and the combined organic layer was washed with 50 mL water 5 times and once with 50 mL brine. After being dried over Na_2SO_4 and concentrated, the crude was purified through silica gel column chromatography using gradient elution from 100% chloroform to 10% methanol-chloroform. **8.32** was obtained as a yellow oil (12.25 mg, 6.4 µmol, 21% yield over 2 steps). R_f = 0.38 (5% methanol-chloroform).

^{1}H NMR (500 MHz, Chloroform-*d*) δ 8.29 (d, *J* = 9.2 Hz, 2H), 8.25 – 7.93 (m, 14H), 7.85 (d, *J* = 7.8 Hz, 2H), 5.83 – 5.70 (m, 2H), 5.22 (q, *J* = 5.0 Hz, 2H), 4.36 – 3.98 (m, 17H), 3.37 (t, *J* = 7.4 Hz, 4H), 3.21 (q, *J* = 6.7 Hz, 4H), 2.67 (dt, *J* = 12.9, 6.0 Hz, 4H), 2.25 (ddt, *J* = 31.9, 20.9, 7.0 Hz, 16H), 1.60 (ddt, *J* = 24.8, 17.2, 6.0 Hz, 12H), 1.47 (q, *J* = 7.3 Hz, 4H), 1.40 – 1.16 (m, 56H), 0.90 – 0.83 (m, 15H), 0.13 – 0.06 (m, 6H). ^{13}C NMR (126 MHz, $CDCl_3$) δ 173.37, 172.77, 172.69, 136.14, 131.53, 131.03, 130.03, 128.91, 127.61, 127.51, 127.48, 126.83, 126.00, 125.20, 125.10, 125.04, 124.91, 123.58, 116.55, 69.57, 69.51, 68.16, 68.11, 66.26, 66.22, 62.39, 61.57, 39.33, 36.14, 34.09, 34.02, 32.94, 32.07, 29.85, 29.83, 29.81, 29.78, 29.64, 29.51, 29.44, 29.33, 29.27, 27.61, 26.39, 25.76, 24.96, 24.50, 22.84, 19.75, 19.69, 18.16, 14.27, -4.70. ^{31}P NMR (121 MHz, $CDCl_3$) δ -1.75, -1.81, -1.85, -1.92. ESI-MS: $[M+H]^+$ calcd for $C_{109}H_{161}O_{19}N_4P_2Si$, 1920.09996; Found 1920.1007.



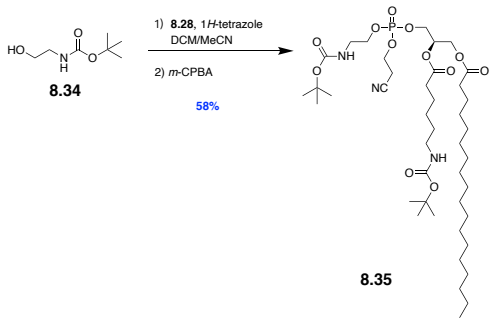
8.34

***tert*-Butyl (2-hydroxyethyl)carbamate (8.34)**

Di-tert-butyl dicarbonate (1.785 g, 8.18 mmol) was dissolved with 10 mL dry DCM in a 50 mL RBF at 0 °C under Ar. Ethanolamine (0.5 g, 8.18 mmol) was dissolved with 5 mL DCM in a vial and then added into the RBF dropwise. The reaction was warm up to rt and further stirred for

1 hr. Upon completion, the solvent was removed under reduced pressure and the crude was subjected to silica gel column chromatography. Gradient elution from 10% EtOAc in hexanes to 50% EtOAc in hexanes was needed to yield the product as a colorless oil (1.32 g, 8.18 mmol, quantitative yield). R_f = 0.3 (50% EtOAc-hexanes).

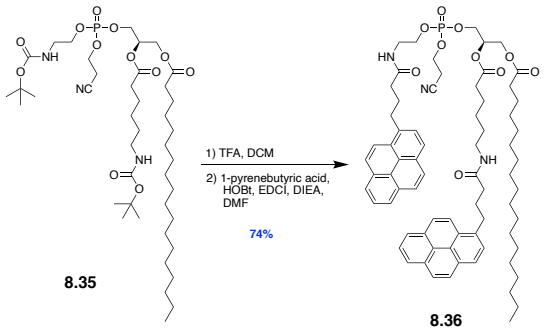
^{1}H NMR (300 MHz, Chloroform-*d*) δ 5.30 (s, 1H), 3.76 – 3.49 (m, 3H), 3.18 (d, *J* = 4.8 Hz, 2H), 1.36 (s, 9H). ^{13}C NMR (75 MHz, $CDCl_3$) δ 156.82, 79.50, 61.98, 43.04, 28.38.



(2*R*)-3-(((2-((*tert*-Butoxycarbonyl)amino)ethoxy)(2-cyanoethoxy)phosphoryl)oxy)-2-((6-((*tert*-butoxycarbonyl)amino)hexanoyl)oxy)propyl stearate (8.35)

Compound **8.28** (136.5 mg, 0.1768 mmol) was added to a 50 mL RBF under Ar. Compound **8.34** (34.2 mg, 0.212 mmol) was dissolved with 2.4 mL dry DCM in a 1 dr vial and was transferred in the RBF. 1*H*-tetrazole (1.2 mL, 0.5304 mmol, 0.45 M in MeCN) was next added. After being stirred at rt for 3 hours, the reaction mixture was cooled to 0 °C with ice bath. *m*-CPBA (0.16 g, 0.5304 mmol, 57% purity) was added carefully and the reaction was stirred for an extra 1.5 hours. Saturated $NaHCO_3$ solution was then used to quench the reaction. The reaction mixture was extracted three times with 50 mL chloroform. The combined organic layer was washed with 100 mL water and 100 mL brine, dried over Na_2SO_4, filtered, and concentrated under reduced pressure. The crude was subjected to silica gel column chromatography and gradient elution from 100% chloroform to 10% methanol-chloroform yield **8.35** as a yellow oil (83.6 mg, 0.0986 mmol, 58% yield). R_f = 0.48 (10% methanol-chloroform). ^{1}H NMR (300 MHz, $CDCl_3$) δ 5.29 – 5.08 (m, 2H), 4.65 (s, 1H), 4.35 – 4.03 (m, 9H), 3.44 – 3.32 (m, 2H), 3.07 (q, *J* = 6.2 Hz, 2H), 2.75 (t, *J* = 6.1 Hz, 2H), 2.31 (dt, *J* = 11.9, 7.5 Hz, 4H),

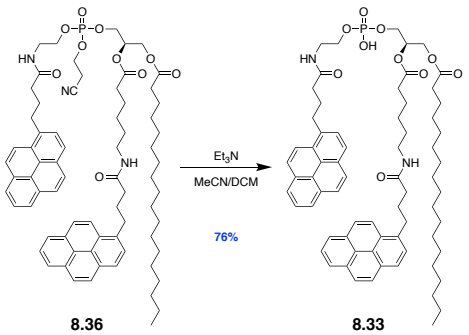
1.58 (dq, *J* = 13.4, 7.4 Hz, 5H), 1.41 (d, *J* = 2.8 Hz, 24H), 1.22 (s, 35H), 0.84 (t, *J* = 6.6 Hz, 3H). ^{13}C NMR (75 MHz, $CDCl_3$) δ 173.22, 172.59, 155.98, 155.80, 116.32, 79.62, 78.99, 69.40, 69.30, 67.68, 65.98, 62.20, 62.13, 61.41, 40.75, 40.29, 33.92, 31.87, 29.65, 29.61, 29.57, 29.43, 29.31, 29.23, 29.07, 28.39, 28.33, 26.12, 24.77, 24.38, 22.64, 19.67, 19.58, 14.08. ^{31}P NMR (121 MHz, $CDCl_3$) δ -1.55, -1.58.



(2*R*)-3-(((2-Cyanoethoxy)(2-(4-(pyren-1-yl)butanamido)ethoxy)phosphoryl)oxy)-2-((6-(4-(pyren-1-yl)butanamido)hexanoyl)oxy)propyl stearate (8.36)

Compound **8.35** (56.7 mg, 0.0668 mmol) was dissolved in 2 mL DCM in a large vial followed by addition of 2 mL trifluoracetic acid. The reaction was stirred at room temperature for 2.5 hours before being transferred into a 50 mL round bottom flask. The solvent was removed under reduced pressure and the flask was placed on high volume vacuum for 3 hours. After that, 1-pyrenebutyric acid (48.19 mg, 0.167 mmol) and hydroxybenzotriazole (HOBt, 25.6 mg, 0.167 mmol) were added into the flask under nitrogen. The solid mixture was dissolved by 2 mL dry DMF at 0 °C and stirred for 5 minutes. EDCI (21.6 mg, 0.334 mmol) was added into the reaction followed by *N*, *N*-Diisopropylethylamine (DIEA, 28 μL, 0.334 mmol). The reaction was stirred overnight before being quenched by pouring into 100 mL 1 N HCl. The aqueous phase was extracted with 25 mL chloroform three times and combined organic layer was washed with 100 mL water 5 times and once with 100 mL brine. After being dried over Na_2SO_4 and concentrated, the crude was purified through silica gel column chromatography using gradient elution from 100% chloroform to 10% methanol-chloroform. **8.36** was obtained as a yellow oil (59.2 mg, 0.05 mmol, 74% yield over 2 steps). R_f = 0.38 (5% methanol-chloroform).

^{1}H NMR (500 MHz, $CDCl_3$) δ 8.25 (dd, *J* = 9.1, 1.9 Hz, 2H), 8.18 – 8.03 (m, 8H), 7.97 (dd, *J* = 13.4, 6.1 Hz, 6H), 7.81 (dd, *J* = 7.7, 3.1 Hz, 2H), 6.40 (d, *J* = 6.3 Hz, 1H), 5.65 (d, *J* = 6.7 Hz, 1H), 5.24 – 5.13 (m, 1H), 4.28 – 4.02 (m, 8H), 3.57 – 3.48 (m, 2H), 3.43 – 3.29 (m, 4H), 3.12 (p, *J* = 6.4 Hz, 2H), 2.60 – 2.42 (m, 2H), 2.35 – 2.11 (m, 12H), 1.63 – 1.51 (m, 4H), 1.43 – 1.13 (m, 40H), 0.88 (t, *J* = 7.0 Hz, 3H). ^{13}C NMR (126 MHz, $CDCl_3$) δ 173.40, 173.39, 173.34, 172.86, 172.84, 172.76, 136.04, 135.96, 135.83, 131.49, 130.98, 130.06, 130.02, 130.00, 128.86, 128.83, 127.57, 127.52, 127.45, 127.43, 126.85, 126.81, 125.98, 125.93, 125.18, 125.16, 125.08, 125.05, 125.03, 125.00, 124.97, 124.90, 124.88, 123.50, 123.47, 123.41, 116.56, 69.52, 69.50, 69.47, 69.45, 67.62, 67.58, 66.31, 66.26, 66.23, 66.19, 62.31, 62.27, 61.50, 61.46, 39.75, 39.70, 39.25, 36.05, 35.89, 34.05, 34.02, 33.97, 33.96, 33.58, 32.83, 32.04, 29.82, 29.78, 29.73, 29.59, 29.47, 29.37, 29.19, 28.76, 27.54, 27.42, 26.81, 26.22, 26.21, 24.89, 24.42, 22.81, 21.63, 19.68, 19.63, 14.24. ESI-MS: $[M+H]^+$ calcd for $C_{72}H_{91}N_3O_{10}P$: 1188.6442; Found: 1188.6467. ESI-MS: $[M+Na]^+$ calcd for $C_{72}H_{90}N_3O_{10}PNa$: 1210.6262; Found: 1210.6294.



(2*R*)-3-((Hydroxy(2-(4-(pyren-1-yl)butanamido)ethoxy)phosphoryl)oxy)-2-((6-(4-(pyren-1-yl)butanamido)hexanoyl)oxy)propyl stearate (8.33)

Compound **8.36** (23.3 mg, 0.0196 mmol) was dissolved with 3 mL MeCN/DCM (2/1, v/v) in a 50 mL RBF under Ar. After adding 2 mL TEA, the reaction was further stirred at rt for 4 hr. Upon completion, the solvent was removed under reduced pressure and the crude was purified with silica gel column chromatography. Gradient elution from $CHCl_3$ to 65/25/4 $CHCl_3$/MeOH/H_2O was needed to yield the product as a yellow oil (17.176 mg, 0.015 mmol, 76%). R_f = 0.24 (10%

MeOH in $CHCl_3$). A UV lamp was used to monitor the column progress.

Note: 1. Although **8.33** was not that polar based on TLC, 20% MeOH in $CHCl_3$ could not pull it down from the column and this instead required a $CHCl_3$/MeOH/H_2O system, judging from the detection of the fluorescent bands with a handheld UV lamp. 2. These types of lipids are known to be hard to obtain decent NMRs, possibly due to solubility issues.

^{1}H NMR (500 MHz, 20% CD_3OD/Chloroform-*d*) δ 8.46 – 7.75 (m, 10H), 7.64 (dd, *J* = 12.3, 7.8 Hz, 1H), 5.02 (d, *J* = 25.3 Hz, 1H), 3.50 – 3.08 (m, 6H), 2.94 (q, *J* = 7.1 Hz, 2H), 2.28 – 1.84 (m, 8H), 1.59 – 0.96 (m, 34H), 0.92 – 0.52 (m, 3H). ^{13}C NMR (126 MHz, 20% CD_3OD/$CDCl_3$) δ 178.61, 175.77, 139.66, 135.25, 133.77, 131.27, 131.17, 130.54, 129.71, 128.77, 128.61, 127.08, 73.42, 64.99, 53.25, 53.08, 52.91, 52.74, 52.57, 52.40, 52.23, 50.04, 42.63, 39.78, 37.81, 36.60, 35.77, 33.54, 33.32, 33.20, 33.12, 32.92, 31.47, 29.91, 28.61, 28.25, 26.52, 17.84, 12.30. ^{31}P NMR (202 MHz, CD_3OD/$CDCl_3$) δ 1.02. ESI-MS: $[M-H]^-$ calcd for $C_{69}H_{86}N_2O_{10}P$: 1133.6020; Found: 1133.6031.

Chapter 9. Miscellaneous Synthesis

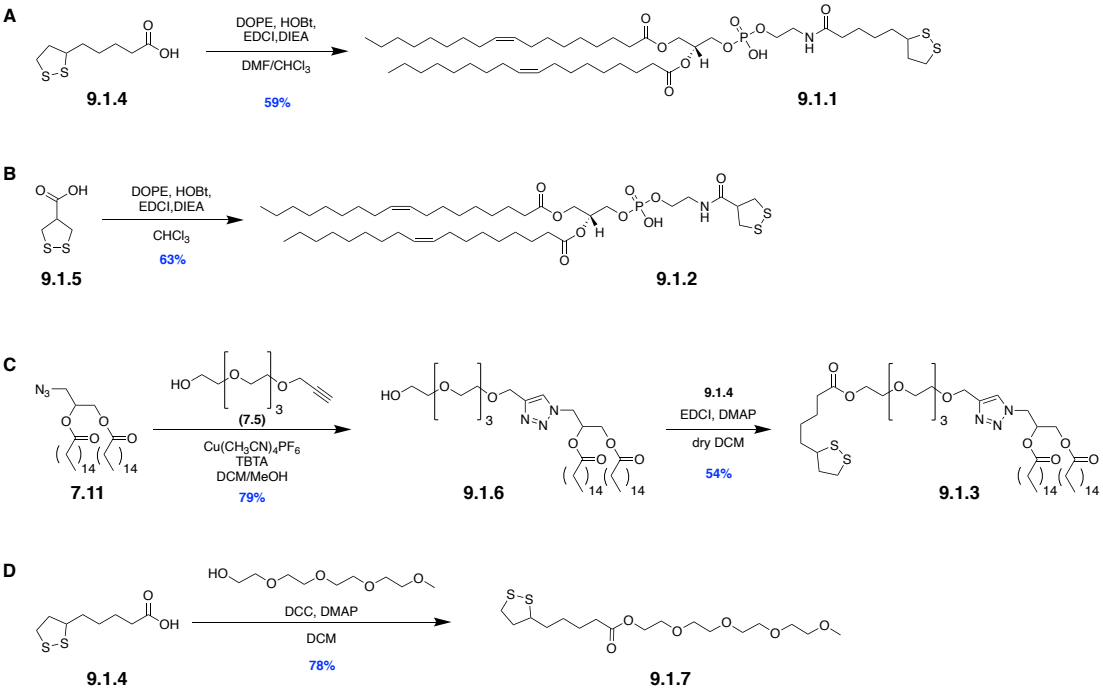
9.1. Design and synthesis of disulfide lipids for enhanced cellular delivery

(Part of the data used in this section was included in the manuscript by the authors: Qualls, Megan L.; Lou, Jinchao; McBee Dillon P.; Baccile, Joshua A.; Best, Michael D. Cyclic Disulfide Liposomes for Membrane Functionalization and Cellular Delivery, manuscript in submission)

9.1.1. Project overview

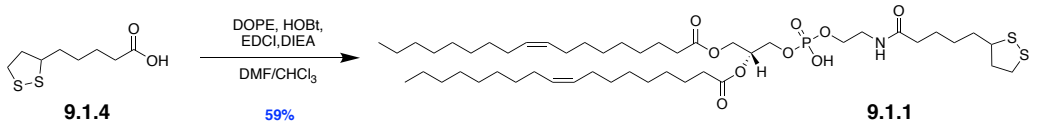
Disulfide exchange reactions involve the attack at the disulfide bond with a free thiol and the formation of a new mixed disulfide compound containing a portion of the original compound.[363] This type of reaction has been widely explored in dynamic covalent chemistry and protein aggregation/precipitation.[364,365] There are also reports showing that simple cyclic disulfides with high ring tension can mediate the uptake of giant substrates.[366] Taking advantage of these properties, we hypothesized that liposomes incorporating synthetic lipids modified with cyclic disulfides can exhibit enhanced cellular uptake. Since the disulfide bond can also be cleaved by addition of reductants such as glutathione (GSH) or tris(2-carboxyethyl)phosphine (TCEP),[367] we envision the resulting liposomal systems could also be redox-responsive. In collaboration with Megan Qualls in our group, I synthesized disulfide containing lipids **9.1.1**-**9.1.3**, as shown in Scheme 9.1.

DL-alpha-Lipoic acid **9.1.4** and asparagusic acid **9.1.5** were installed onto a DOPE scaffold through an amide coupling reaction to form lipids **9.1.1**-**9.1.2**, which contain a six-membered and five-membered cyclic disulfide ring, respectively. In a slightly different design, we synthesized lipid **9.1.3** by introducing a TEG linker in between the disulfide headgroup and the triazole lipid backbone. The presence of a hydrophilic TEG linker is expected to ensure that the disulfide ring is accessible on the liposome membrane surface for conjugation purposes. In addition, we synthesized a control hydrophilic compound **9.1.7** by directly coupling **9.1.4** with TEG mono methyl ether, although this compound turned out to be not water soluble.



Scheme 9.1. A-C. Synthetic routes to disulfide containing lipids 9.1.1-9.1.3. D. Synthetic route to a TEG-disulfide control compound 9.1.7.

9.1.2. Synthetic procedures

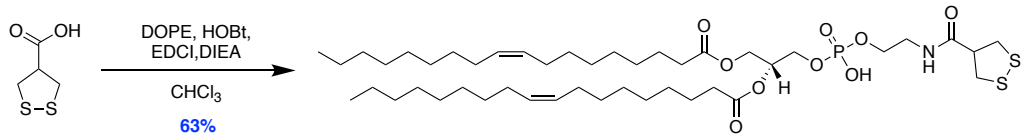


9.1.4 9.1.1

(2*R*)-3-(((2-(5-(1,2-Dithiolan-3-yl)pentanamido)ethoxy)(hydroxy)phosphoryl)oxy)propane-1,2-diyl dioleate (9.1.1)

DL-alpha-Lipoic acid (**9.1.4**, 33.28 mg, 0.1613 mmol), DOPE (100 mg, 0.1344 mmol) as well as HOBt (24.7 mg, 0.1613 mmol) were combined in a 50 mL RBF under Argon. 6 mL dry DMF/$CHCl_3$ was used to dissolve the starting materials at 0 °C. Next, EDCI (30.92 mg, 0.1613 mmol) was added into the reaction followed by DIEA (56 µL, 0.336 mmol). The reaction was allowed to warm up to room temperature and further stirred overnight before being quenched by pouring into 100 mL 1 N HCl. The aqueous layer was then extracted with 3×25 mL $CHCl_3$. The combined organic layer was next washed with 50 mL water five times and once with 50 mL brine. After being dried over Na_2SO_4, filtered, and concentrated under reduced pressure, the crude was subjected to silica gel column chromatography. Gradient elution from chloroform to 15% methanol in chloroform was needed to obtain **9.1.1** as a pale-yellow wax (74.2 mg, 0.0796 mmol, 59% yield). R_f = 0.47 (20% MeOH/$CHCl_3$).

^{1}H NMR (500 MHz, 20% CD_3OD-$CDCl_3$) δ 7.50 (t, *J* = 5.6 Hz, 1H), 5.23 – 5.14 (m, 4H), 5.06 (qd, *J* = 5.5, 3.1 Hz, 1H), 4.22 (dd, *J* = 12.1, 3.2 Hz, 1H), 3.83 – 3.69 (m, 4H), 3.42 (dq, *J* = 8.9, 6.3 Hz, 1H), 3.27 (q, *J* = 5.3 Hz, 2H), 3.07 – 2.91 (m, 2H), 2.32 (dq, *J* = 12.5, 6.5 Hz, 1H), 2.20 – 2.12 (m, 4H), 2.06 (t, *J* = 7.6 Hz, 2H), 1.86 (ddt, *J* = 9.3, 6.4, 2.5 Hz, 8H), 1.81 – 1.71 (m, 1H), 1.61 – 1.39 (m, 8H), 1.37 – 1.24 (m, 2H), 1.22 – 1.03 (m, 45H), 0.72 (t, *J* = 6.8 Hz, 6H). ^{13}C NMR (126 MHz, 20% CD_3OD-$CDCl_3$) δ 174.44, 173.76, 173.40, 129.88, 129.52, 129.50, 70.27, 70.21, 64.02, 63.45, 62.49, 56.29, 40.11, 39.91, 38.29, 35.89, 35.84, 34.48, 34.06, 33.91, 31.75, 29.60, 29.58, 29.51, 29.36, 29.16, 29.12, 29.09, 29.02, 29.00, 28.98, 28.95, 28.79, 27.05, 27.02, 25.29, 24.76, 24.70, 22.50, 13.82. ^{31}P NMR (202 MHz, CD_3OD-$CDCl_3$) δ -1.93.

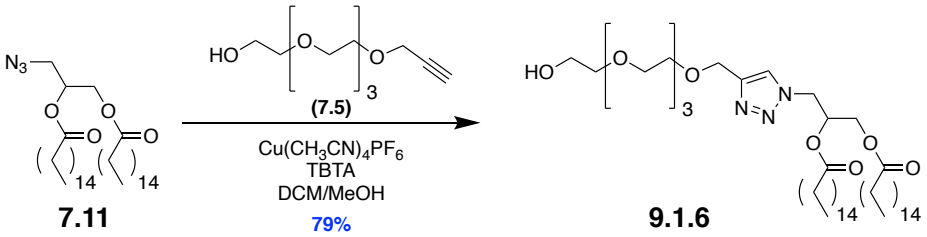


9.1.5 **9.1.2**

(2*R*)-3-(((2-(1,2-Dithiolane-4-carboxamido)ethoxy)(hydroxy)phosphoryl)oxy)propane-1,2-diyl dioleate (9.1.2)

Asparagusic acid (**9.1.5**, 24.23 mg, 0.1613 mmol), DOPE (100 mg, 0.1344 mmol) as well as HOBt (24.7 mg, 0.1613 mmol) were combined in a 50 mL RBF under Argon. 5 mL dry $CHCl_3$ was used to dissolve the starting materials at 0 °C. Next, EDCI (30.92 mg, 0.1613 mmol) was added into the reaction followed by DIEA (56 µL, 0.336 mmol). The reaction was allowed to warm up to room temperature and further stirred overnight before being quenched by pouring into 100 mL 1 N HCl. The aqueous layer was then extracted with 3×25 mL $CHCl_3$. The combined organic layer was next washed with 50 mL water and 50 mL brine. After being dried over Na_2SO_4, filtered, and concentrated under reduced pressure, the crude was subjected to silica gel column chromatography. Gradient elution from chloroform to 20% methanol in chloroform was needed to obtain **9.1.2** as a pale-yellow wax (74.7 mg, 0.085 mmol, 63% yield). R_f = 0.25 (20% MeOH/$CHCl_3$).

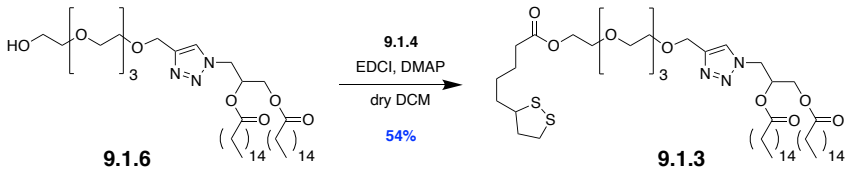
^{1}H NMR (500 MHz, 20% CD_3OD-$CDCl_3$) δ 5.22 – 5.12 (m, 4H), 5.05 (dt, *J* = 8.6, 4.3 Hz, 1H), 4.22 (dd, *J* = 12.0, 3.1 Hz, 1H), 3.99 (dd, *J* = 12.1, 7.0 Hz, 1H), 3.84 – 3.68 (m, 4H), 3.29 (t, *J* = 5.4 Hz, 2H), 3.19 (dddd, *J* = 30.7, 11.4, 7.4, 1.2 Hz, 4H), 3.06 (p, *J* = 7.4 Hz, 1H), 2.19 – 2.11 (m, 4H), 1.85 (dt, *J* = 9.1, 4.5 Hz, 8H), 1.43 (d, *J* = 6.5 Hz, 4H), 1.13 (d, *J* = 18.1 Hz, 44H), 0.72 (t, *J* = 7.0 Hz, 6H). ^{13}C NMR (126 MHz, 20% CD_3OD-$CDCl_3$) δ 173.81, 173.46, 172.74, 129.87, 129.86, 129.51, 129.49, 70.28, 70.22, 63.89, 63.48, 62.52, 51.97, 42.26, 40.24, 34.07, 33.91, 31.74, 29.59, 29.57, 29.35, 29.15, 29.11, 29.08, 29.01, 28.99, 28.97, 28.95, 27.04, 27.01, 24.76, 24.69, 22.49, 13.81. ^{31}P NMR (202 MHz, 20% CD_3OD-$CDCl_3$) δ -2.46



3-(4-(13-Hydroxy-2,5,8,11-tetraoxatridecyl)-1*H*-1,2,3-triazol-1-yl)propane-1,2-diyl dipalmitate (9.1.6)

Compound **7.5** (58.66 mg, 0.2526 mmol), **7.11** (150 mg, 0.2526 mmol), TBTA (13.27 mg, 0.025 mmol) and $Cu(CNCH_3)_4PF_6$ (9.32 mg, 0.025 mmol) were combined in a 50 mL RBF under Argon. After adding 5 mL MeOH/DCM (1:1, v/v), the reaction mixture was stirred overnight. Next, the solvent was removed under reduced pressure and the crude was purified via a silica gel column using gradient elution from DCM to 2% methanol in DCM. Compound **9.1.6** was obtained as a pale-yellow solid (165.4 mg, 0.2 mmol, 79%). R_f = 0.21 (5% MeOH-DCM).

^{1}H NMR (500 MHz, $CDCl_3$) δ 7.65 (s, 1H), 5.37 (p, *J* = 5.0 Hz, 1H), 4.67 (s, 2H), 4.62 – 4.53 (m, 2H), 4.30 (dd, *J* = 12.1, 4.3 Hz, 1H), 4.05 (dd, *J* = 12.1, 5.3 Hz, 1H), 3.71 – 3.60 (m, 14H), 3.59 – 3.56 (m, 2H), 2.34 – 2.21 (m, 4H), 1.57 (ddd, *J* = 29.6, 14.2, 7.1 Hz, 4H), 1.23 (s, 50H), 0.85 (t, *J* = 6.9 Hz, 6H). ^{13}C NMR (126 MHz, $CDCl_3$) δ 173.09, 172.55, 129.01, 123.56, 74.56, 72.49, 70.58, 70.50, 70.44, 70.42, 70.36, 70.30, 70.17, 69.64, 69.33, 69.07, 64.56, 62.01, 61.69, 61.57, 58.39, 50.04, 34.00, 33.96, 31.89, 29.66, 29.62, 29.59, 29.44, 29.32, 29.24, 29.22, 29.09, 29.00, 24.81, 24.71, 22.65, 14.08.

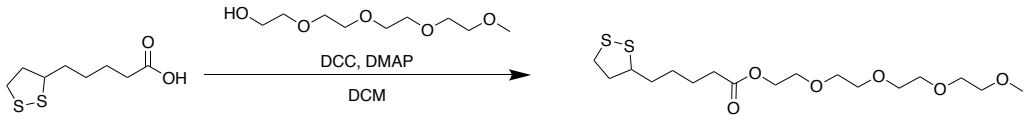


3-(4-(19-(1,2-Dithiolan-3-yl)-15-oxo-2,5,8,11,14-pentaoxanonadecyl)-1*H*-1,2,3-triazol-1-yl)propane-1,2-diyl dipalmitate (9.1.3)

Compound **9.1.6** (50 mg, 0.06 mmol), DL-alpha-lipoic acid **9.1.4** (13.7 mg, 0.067 mmol), DMAP (1.83 mg, 0.015 mmol) and EDCI (12.57 mg, 0.081 mmol) were dissolved with 5 mL dry DCM

in a 50 mL RBF under Ar. After overnight stirring, the solvent was removed under reduced pressure and the crude was directly subjected to silica gel column chromatography. Gradient elution from 100% hexanes to 70% EtOAc in hexanes was needed to obtain **9.1.3** as a pale-yellow solid. R_f = 0.35 (75% EtOAc-hexanes).

^{1}H NMR (500 MHz, $CDCl_3$) δ 7.61 (s, 1H), 5.38 (p, *J* = 5.0 Hz, 1H), 4.68 (s, 2H), 4.63 – 4.51 (m, 2H), 4.31 (dd, *J* = 12.1, 4.4 Hz, 1H), 4.25 – 4.18 (m, 2H), 4.07 (dd, *J* = 12.1, 5.2 Hz, 1H), 3.73 – 3.63 (m, 14H), 3.62 – 3.49 (m, 1H), 3.22 – 3.05 (m, 1H), 2.77 (s, 1H), 2.46 (dq, *J* = 12.2, 6.3 Hz, 1H), 2.39 – 2.23 (m, 6H), 1.91 (dt, *J* = 13.0, 6.9 Hz, 1H), 1.75 – 1.37 (m, 16H), 1.25 (s, 53H), 0.88 (t, *J* = 6.8 Hz, 6H). ^{13}C NMR (126 MHz, $CDCl_3$) δ 173.47, 173.11, 172.56, 145.55, 123.33, 70.58, 70.55, 70.54, 70.51, 70.50, 69.68, 69.33, 69.18, 64.57, 63.43, 62.04, 61.99, 56.32, 50.05, 40.21, 38.46, 34.58, 34.03, 33.98, 33.92, 31.91, 29.69, 29.65, 29.62, 29.47, 29.46, 29.35, 29.27, 29.24, 29.12, 29.03, 28.71, 24.83, 24.73, 24.60, 22.67, 14.10.



9.1.4 **9.1.7**

2,5,8,11-Tetraoxatridecan-13-yl 5-(1,2-dithiolan-3-yl)pentanoate (9.1.7)

DL-alpha-Lipoic acid **9.1.4** (0.2 g, 0.97 mmol), tetra ethylene glycol monomethyl ether (0.212 mL, 1.066 mmol), DCC (0.24 g, 1.16 mmol) and DMAP (59.25 mg, 0.485 mmol) were dissolved with 20 mL dry DCM in a 100 mL RBF at 0 °C. After overnight stirring, the DCU byproduct was filtered through gravity filtration and the filtrate was concentrated under reduced pressure. The crude was purified via a silica gel column using gradient elution from 25% EtOAc in hexanes to 75% EtOAc in hexanes. The product was obtained as a yellow oil (0.3 g, 0.756 mmol, 78% yield). R_f = 0.3 (75% EtOAc-hexanes).

^{1}H NMR (500 MHz, $CDCl_3$) δ 4.16 (dd, *J* = 5.5, 4.2 Hz, 2H), 3.65 – 3.62 (m, 2H), 3.61 – 3.51 (m, 10H), 3.51 – 3.48 (m, 2H), 3.32 (d, *J* = 1.3 Hz, 3H), 3.16 – 3.01 (m, 2H), 2.46 – 2.36 (m, 1H), 2.29 (t, *J* = 7.4 Hz, 2H), 1.92 – 1.79 (m, 1H), 1.70 – 1.55 (m, 4H), 1.49 – 1.34 (m, 2H). ^{13}C NMR (126 MHz, $CDCl_3$) δ 173.36, 71.90, 70.57, 70.55, 70.51, 70.49, 69.12, 63.43, 58.99,

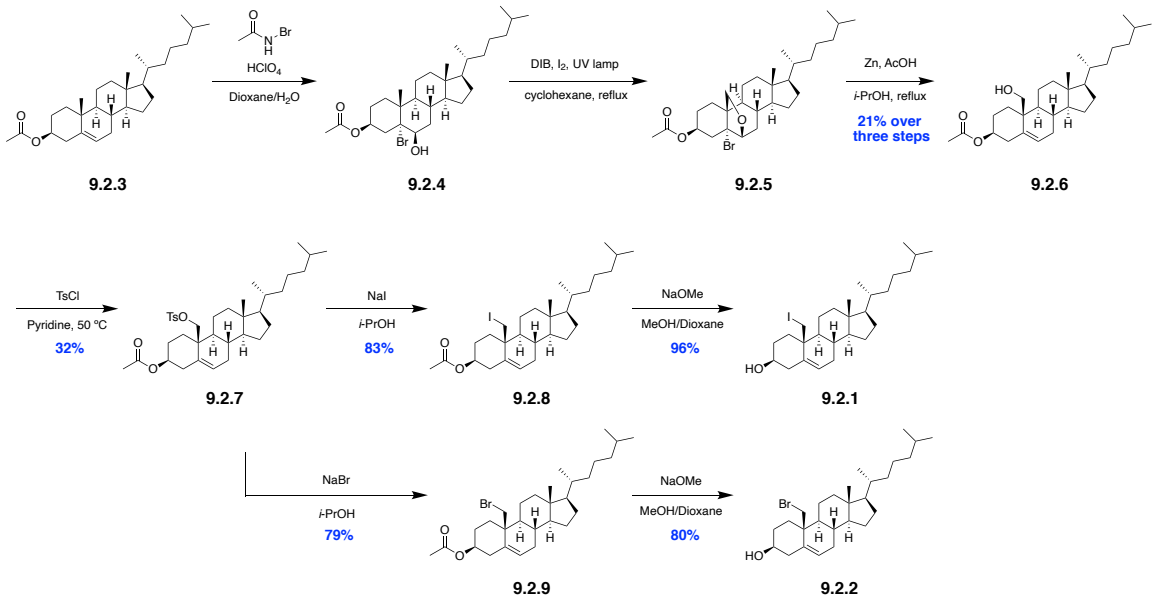
56.28, 40.18, 38.45, 34.55, 33.89, 28.68, 24.58. HRMS-DART: $[M+H]^+$ calcd for $C_{17}H_{33}S_2O_6$: 397.1718; Found: 397.1280.

9.2. Synthesis of 19-halogen substituted cholesterol analogues

9.2.1. Project overview

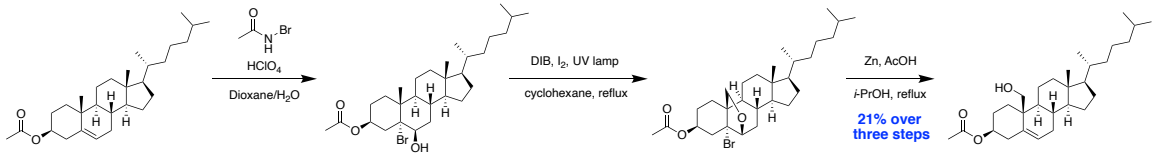
Cholesterol is a unique type of lipid that composes 20-40 mol% of eukaryotic plasma membranes.[368] It not only composes a significant amount of membranes but can also modulate membrane fluidity over a wide range of temperatures.[369] In addition, cholesterol can promote the formation of lipid rafts.[370] In collaboration with Dr. Fred Heberle in the UTK Chemistry department, we synthesized cholesterol analogues with halogen substituents on the C19 position, which can be potentially used in improving cryo-EM imaging of liposomes when these compounds are incorporated.

The synthetic routes for 19-iodo cholesterol **9.2.1** and 19-bromo cholesterol **9.2.2** are shown in Scheme 9.2. 19-Hydroxyl cholesterol **9.2.6** was synthesized from cholesteryl acetate **9.2.3** according to a previously reported protocol with slight modifications,[371] including the formation of bromohydrin intermediate **9.2.4**, radical reaction and the intramolecular ether formation of **9.2.5** and Zn-AcOH mediated reductive ring opening. Tosylation of the hydroxyl group of **9.2.6** resulted in **9.2.7**, which was reacted with NaI or NaBr in isopropanol to afford **9.2.8** and **9.2.9**, respectively. The final acetyl deprotection reaction with NaOMe resulted in the desired final targets. It is worth noting that when synthesizing **9.2.8**, we observed the formation of a rearranged by product, where the iodomethyl ended up at the C6 position and the double bonds switched to C5/C10. However, this type of rearrangement reaction was not observed for **9.2.9** synthesis.



Scheme 9.2. Synthetic routes to 19-iodo or 19-bromo cholesterol. Cholesteryl acetate **9.2.3** was treated with *N*-bromoacetamide and perchloric acid to form bromohydrin **9.2.4**, which was reacted with iodobenzene diacetate (DIB) and I_2 under UV irradiation to form **9.2.5**. Subsequent ring opening followed by tosylation resulted in **9.2.7**, which was treated with NaI or NaBr to introduce the halogens. Final deprotection afforded the 19-iodo cholesterol **9.2.1** and 19-bromo cholesterol **9.2.2**.

9.2.2. Synthetic procedures



9.2.3 9.2.4 9.2.5 9.2.6

(3*S*,5*R*,6*R*,8*S*,9*S*,10*R*,13*R*,14*S*,17*R*)-5-Bromo-6-hydroxy-10,13-dimethyl-17-((*R*)-6-methylheptan-2-yl)hexadecahydro-1*H*-cyclopenta[*a*]phenanthren-3-yl acetate (9.2.4)

Compound **9.2.3** (5 g, 11.67 mmol) was dissolved with 50 mL dioxane in a 250 mL RBF. 8 mL 0.5 N $HClO_4$ (prepared with 50 mL 70% $HClO_4$ and 100 mL H_2O) was added during stirring at rt. The reaction was performed at rt instead of in an ice bath, since the starting material precipitated out at 0 °C in dioxane. Next, *N*-bromoacetamide (2.4 g, 17.4 mmol) was added slowly and the reaction was stirred at rt for an extra one hour. After 15 min stirring, all the chemicals were dissolved, which resulted in an orange solution. Upon completion, the reaction was brought to °C with an ice bath, and 3 M thiosulfate was added dropwise to quench the reaction. The solvent was removed under reduced pressure and crude was redissolved with 100 mL H_2O and 100 mL ethyl ether. After collecting the organic layer, the aqueous layer was further extracted with 2 x 50 mL ether. The combined organic layer was further washed with 1 x 100 mL water and 1 x 100 mL brine, respectively, before being dried over Na_2SO_4, filtered, and concentrated under reduced pressure. ~4/5 of the crude was separated and purified through crystallization for analytical purposes. The rest of the crude was subjected to the next step without purification. For recrystallization, the crude was first dissolved in 20 mL hot hexanes. EtOAc was then added dropwise until all the solid dissolved. The solution was cooled down to room temperature and kept in a -20 °C freezer for further crystallization. Pure product was isolated through vacuum filtration as a white powder (1.0135 g, 1.928 mmol, 20 % yield). R_f = 0.55 (25% EtOAc-hexanes).

^{1}H NMR (500 MHz, $CDCl_3$) δ 5.48 (tt, *J* = 11.0, 5.7 Hz, 1H), 4.20 – 4.16 (m, 1H), 2.50 (dd, *J* = 13.5, 10.6 Hz, 1H), 2.29 – 2.16 (m, 2H), 2.05 (d, *J* = 1.4 Hz, 3H), 2.01 – 1.92 (m, 2H), 1.88 – 0.97 (m, 35H), 0.91 (d, *J* = 6.5 Hz, 3H), 0.86 (dd, *J* = 6.6, 2.3 Hz, 6H), 0.68 (s, 3H). ^{13}C NMR

(126 MHz, $CDCl_3$) δ 170.58, 86.83, 75.96, 72.26, 56.26, 55.87, 47.58, 42.85, 40.50, 39.82, 39.65, 38.59, 36.28, 35.92, 35.27, 34.75, 30.73, 28.35, 28.16, 26.51, 24.21, 23.96, 22.96, 22.71, 21.51, 21.45, 18.82, 18.18, 12.34.

(3*S*,5*R*,6*R*,8*S*,9*S*,10*R*,13*R*,14*S*,17*R*)-5-Bromo-13-methyl-17-((*R*)-6-methylheptan-2-yl)hexadecahydro-6,10-(epoxymethano)cyclopenta[*a*]phenanthren-3-yl acetate (9.2.5)

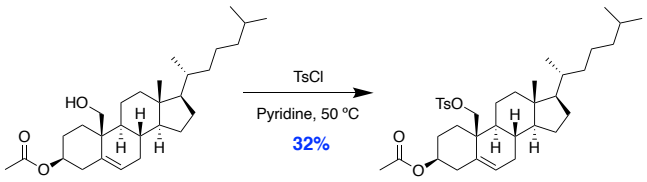
The crude from the first step was dissolved with 30 mL cyclohexane in a 100 mL RBF. Iodobenzene diacetate (DIB, 1.104 g, 3.43 mmol) and I_2 (0.35 g, 1.38 mmol) were next added. The reaction was heated under reflux with long UV irradiation (6 W handheld UV lamp, 354 nm) for three hours. Upon completion, the reaction was cooled down to room temperature and quenched with 3 M thiosulfate solution until the purple color turned into pale yellow. The mixture was extracted with 3 x 50 mL EtOAc. Next, the combined organic layer was further washed with 1 x 100 mL water and 1 x 100 mL brine, respectively, before being dried over Na_2SO_4, filtered, and concentrated under reduced pressure. A small portion of the crude was purified for analytical purposes. The rest of the crude was passed along to the next step without further purification. Pure product was isolated as a white solid. R_f = 0.7 (25% EtOAc-hexanes). ^{1}H NMR (500 MHz, $CDCl_3$) δ 5.24 – 5.14 (m, 1H), 4.05 (d, *J* = 4.7 Hz, 1H), 3.92 (d, *J* = 8.4 Hz, 1H), 3.74 (d, *J* = 8.3 Hz, 1H), 2.35 – 2.22 (m, 2H), 2.04 – 1.92 (m, 7H), 1.83 (dtd, *J* = 13.2, 9.5, 6.4 Hz, 1H), 1.73 – 1.66 (m, 2H), 1.64 (s, 1H), 1.63 – 1.57 (m, 1H), 1.57 – 1.44 (m, 6H), 1.44 – 1.33 (m, 3H), 1.32 (d, *J* = 4.4 Hz, 2H), 1.30 – 0.94 (m, 12H), 0.94 – 0.83 (m, 11H), 0.69 (s, 3H)

(3*S*,8*S*,9*S*,10*S*,13*R*,14*S*,17*R*)-10-(Hydroxymethyl)-13-methyl-17-((*R*)-6-methylheptan-2-yl)-2,3,4,7,8,9,10,11,12,13,14,15,16,17-tetradecahydro-1*H*-cyclopenta[*a*]phenanthren-3-yl acetate (9.2.6)

The crude from the last step as well as Zn (dust, 0.756 g, 11.63 mmol) were dissolved with *i*-PrOH in a 100 mL RBF. After addition of AcOH (1.88 mL, 32.87 mmol), the mixture was refluxed

for 1.5 hrs. Whether the reaction proceeded could be determined by the color change of the zinc dust from dark grey/black to light grey. Upon completion, the reaction was cooled down to rt, and the zinc dust was removed from filtration through a celite pad. The solvent was removed under reduced pressure and the crude was redissolved with 100 mL H_2O and 100 mL ethyl ether. After collecting the organic layer, the aqueous layer was further extracted with 2 x 50 mL ether. The combined organic layer was further washed with 1 x 100 mL water and 1 x 100 mL brine, respectively, before being dried over Na_2SO_4, filtered, and concentrated under rotary evaporator. The resulting crude was purified via silica gel column chromatography using gradient elution from hexanes to 15% EtOAc in hexanes as a white solid (0.2184 g, 0.49 mmol, 21% over two steps). R_f = 0.55 (25% EtOAc-hexanes).

^{1}H NMR (500 MHz, $CDCl_3$) δ 5.79 – 5.75 (m, 1H), 4.64 (tt, *J* = 11.5, 4.8 Hz, 1H), 3.83 (d, *J* = 11.3 Hz, 1H), 3.62 (dd, *J* = 11.1, 8.9 Hz, 1H), 2.42 (ddd, *J* = 13.0, 4.9, 2.2 Hz, 1H), 2.31 – 2.22 (m, 1H), 2.07 – 1.98 (m, 5H), 1.95 (dt, *J* = 13.8, 3.6 Hz, 1H), 1.91 – 1.73 (m, 3H), 1.67 – 0.93 (m, 24H), 0.93 – 0.88 (m, 4H), 0.86 (dd, *J* = 6.6, 2.3 Hz, 6H), 0.73 (s, 3H). ^{13}C NMR (126 MHz, $CDCl_3$) δ 170.65, 134.67, 128.47, 73.56, 62.87, 57.72, 56.25, 50.46, 42.67, 41.75, 40.15, 39.65, 38.37, 36.32, 35.92, 33.53, 33.24, 31.39, 28.38, 28.25, 28.16, 24.22, 23.97, 22.96, 22.71, 21.92, 21.53, 18.85, 12.36. HRMS-DART: $[M+H]^+$ calcd for $C_{29}H_{49}O_3$: 445.3682; Found 445.3737.



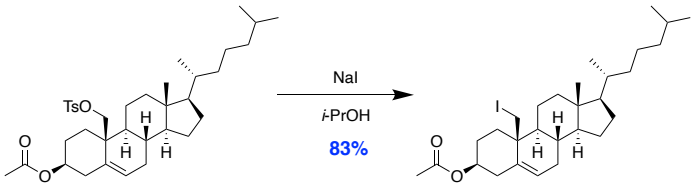
9.2.6 **9.2.7**

(3*S*,8*S*,9*S*,10*S*,13*R*,14*S*,17*R*)-13-Methyl-17-((*R*)-6-methylheptan-2-yl)-10-((tosyloxy)methyl)-2,3,4,7,8,9,10,11,12,13,14,15,16,17-tetradecahydro-1*H*-cyclopenta[*a*]phenanthren-3-yl acetate (9.2.7)

Compound **9.2.6** (0.1908 g, 0.429 mmol) was dissolved with 10 mL dry pyridine in a 100 mL

RBF under Ar. TsCl (98 mg, 0.514 mmol) was added and the reaction was heated at 50 °C overnight. After removing pyridine under reduced pressure, the crude was redissolved with 50 mL H_2O and 50 mL EtOAc. After collecting the organic layer, the aqueous layer was further extracted with 2 x 25 mL EtOAc. The combined organic layer was further washed with 1 x 100 mL water and 1 x 100 mL brine, respectively, before being dried over Na_2SO_4, filtered, and concentrated under reduced pressure. Silica gel column using gradient elution from hexanes to 10% EtOAc in hexanes was needed to afford the product as a white powder (83.6 mg, 0.139 mmol, 32 % yield). R_f = 0.24 (10% EtOAc-hexanes).

^{1}H NMR (500 MHz, $CDCl_3$) δ 7.78 (d, *J* = 8.2 Hz, 2H), 7.34 (d, *J* = 8.1 Hz, 2H), 5.58 (d, *J* = 4.7 Hz, 1H), 4.57 (tt, *J* = 11.3, 4.7 Hz, 1H), 4.10 (d, *J* = 10.2 Hz, 1H), 4.00 (d, *J* = 10.2 Hz, 1H), 2.45 (s, 3H), 2.37 – 2.30 (m, 1H), 2.16 – 2.02 (m, 2H), 2.01 (s, 3H), 1.98 – 1.89 (m, 2H), 1.80 (ddd, *J* = 19.2, 15.2, 9.5 Hz, 2H), 1.56 – 0.94 (m, 21H), 0.93 – 0.81 (m, 12H), 0.53 (s, 3H). ^{13}C NMR (126 MHz, $CDCl_3$) δ 170.58, 144.87, 133.39, 133.07, 129.94, 128.10, 128.07, 73.09, 69.84, 57.15, 56.15, 49.94, 42.41, 40.11, 39.91, 39.65, 38.09, 36.28, 35.88, 32.54, 32.52, 31.40, 28.26, 28.14, 27.79, 24.16, 23.95, 22.95, 22.69, 21.83, 21.78, 21.47, 18.81, 11.98. HRMS-DART: $[M+NH_4]^+$ calcd for $C_{36}H_{58}O_5SN$: 616.4036; Found: 616.4148.



9.2.7 **9.2.8**

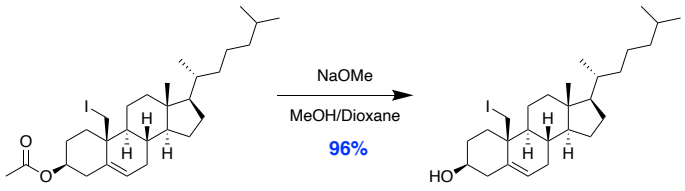
(3*S*,8*S*,9*S*,10*S*,13*R*,14*S*,17*R*)-10-(Iodomethyl)-13-methyl-17-((*R*)-6-methylheptan-2-yl)-2,3,4,7,8,9,10,11,12,13,14,15,16,17-tetradecahydro-1*H*-cyclopenta[*a*]phenanthren-3-yl acetate (9.2.8)

Compound **9.2.7** (42 mg, 0.07 mmol) and NaI (22.3 mg, 0.148 mmol) were dissolved with 5 mL isopropanol in a 50 mL RBF. The reaction was heated under reflux without N_2 protection for 24 hours. Upon completion, the solvent was removed under reduced pressure and the

crude was subjected to silica gel column. Gradient elution from hexanes to 10% EtOAc in hexanes was used to afford the product as a white solid (32 mg, 0.058 mmol, 83% yield). R_f = 0.55 (10% EtOAc-hexanes).

Note: Minor rearranged by product was separated from the column, which has an identical Rf as the product.

^{1}H NMR (500 MHz, $CDCl_3$) δ 5.67 – 5.62 (m, 1H), 4.60 (ddd, *J* = 16.4, 11.4, 4.9 Hz, 1H), 3.57 (d, *J* = 11.0 Hz, 1H), 3.31 (d, *J* = 10.9 Hz, 1H), 2.40 (ddd, *J* = 13.1, 5.0, 2.1 Hz, 1H), 2.15 (ddd, *J* = 14.0, 10.6, 2.5 Hz, 2H), 2.10 – 1.98 (m, 7H), 1.95 – 1.63 (m, 4H), 1.63 – 1.45 (m, 7H), 1.45 – 1.22 (m, 8H), 1.21 – 1.04 (m, 10H), 1.03 – 0.88 (m, 7H), 0.86 (dt, *J* = 6.5, 2.2 Hz, 8H), 0.77 (s, 3H). ^{13}C NMR (126 MHz, $CDCl_3$) δ 170.61, 135.46, 126.74, 73.21, 57.75, 56.20, 51.27, 42.75, 40.01, 39.67, 38.66, 38.18, 37.30, 36.32, 35.93, 31.96, 31.22, 28.36, 28.16, 28.01, 24.27, 23.97, 22.96, 22.71, 22.23, 21.51, 18.84, 12.44, 11.20.

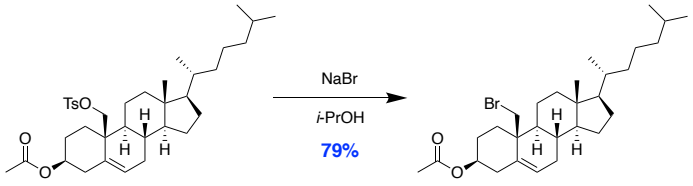


9.2.8 **9.2.1**

(3*S*,8*S*,9*S*,10*S*,13*R*,14*S*,17*R*)-10-(Iodomethyl)-13-methyl-17-((*R*)-6-methylheptan-2-yl)-2,3,4,7,8,9,10,11,12,13,14,15,16,17-tetradecahydro-1*H*-cyclopenta[*a*]phenanthren-3-ol (9.2.1)

Compound **9.2.8** (17.5 mg, 0.0316 mmol) was dissolved with 5 mL dioxane/MeOH (1:1, v/v) in a 50 mL RBF at rt. NaOMe solution (4.375 M in MeOH) was next added dropwise until the reaction mixture turned basic, as indicated by pH paper. The reaction progress was monitored through TLC techniques and completed within one hour. After being quenched by addition of 1 N HCl dropwise, the solvent was removed under reduced pressure and the crude was purified via a silica gel column using 25% EtOAc in hexanes. The product was obtained as a white solid (15.5 mg, 0.03 mmol, 96% yield). R_f = 0.44 (25% EtOAc-hexanes).

^{1}H NMR (500 MHz, $CDCl_3$) δ 5.65 – 5.58 (m, 1H), 3.61 – 3.48 (m, 2H), 3.30 (d, *J* = 10.9 Hz, 1H), 2.36 (ddd, *J* = 13.0, 4.9, 2.3 Hz, 1H), 2.08 (dddd, *J* = 21.7, 17.8, 9.0, 5.6 Hz, 5H), 1.90 – 1.65 (m, 4H), 1.59 – 0.97 (m, 24H), 0.95 – 0.82 (m, 12H), 0.77 (s, 3H). ^{13}C NMR (126 MHz, $CDCl_3$) δ 136.50, 125.75, 71.35, 57.84, 56.23, 51.33, 42.77, 42.34, 40.06, 39.67, 38.59, 37.55, 36.33, 35.93, 31.99, 31.85, 31.22, 28.37, 28.16, 24.28, 23.98, 22.96, 22.71, 22.27, 18.84, 12.45, 11.53. HRMS-DART: $[M+NH_4]^+$ calcd for $C_{27}H_{49}INO$: 530.2859; Found: 530.2890. $[M+H-H_2O]^+$ calcd for $C_{27}H_{44}I$: 495.2488; Found: 495.2498.

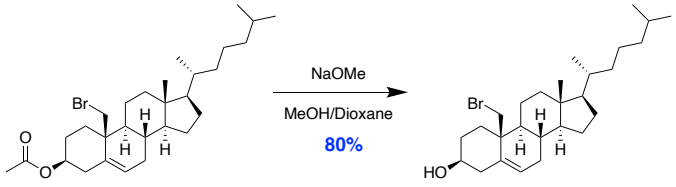


9.2.7 **9.2.9**

(3*S*,8*S*,9*S*,10*S*,13*R*,14*S*,17*R*)-10-(Bromomethyl)-13-methyl-17-((*R*)-6-methylheptan-2-yl)-2,3,4,7,8,9,10,11,12,13,14,15,16,17-tetradecahydro-1*H*-cyclopenta[*a*]phenanthren-3-yl acetate (9.2.9)

Compound **9.2.7** (20 mg, 0.0334 mmol) and NaBr (6.87 mg, 0.0668 mmol) were dissolved with 5 mL isopropanol in a 50 mL RBF. The reaction was heated under reflux without N_2 protection for 24 hours. Upon completion, the solvent was removed under reduced pressure and the crude was subjected to silica gel column. Gradient elution from hexanes to 10% EtOAc in hexanes was used to afford the product as a white solid (13.4 mg, 0.0264 mmol, 79% yield). R_f = 0.55 (10% EtOAc-hexanes). Note: No rearranged by product was observed in this case. ^{1}H NMR (500 MHz, $CDCl_3$) δ 5.67 (dd, *J* = 4.9, 2.5 Hz, 1H), 4.63 (ddd, *J* = 11.5, 6.6, 4.8 Hz, 1H), 3.74 (d, *J* = 11.2 Hz, 1H), 3.51 (d, *J* = 11.2 Hz, 1H), 2.46 – 2.38 (m, 1H), 2.26 – 2.13 (m, 3H), 2.10 – 1.99 (m, 6H), 1.96 – 1.76 (m, 4H), 1.72 (dd, *J* = 13.1, 4.0 Hz, 1H), 1.55 (dddd, *J* = 24.9, 16.9, 8.3, 3.3 Hz, 6H), 1.41 – 1.30 (m, 4H), 1.30 – 1.21 (m, 4H), 1.21 – 0.96 (m, 11H), 0.96 – 0.87 (m, 8H), 0.87 – 0.84 (m, 5H), 0.75 (s, 3H). ^{13}C NMR (126 MHz, $CDCl_3$) δ 170.62, 134.75, 127.30, 73.27, 57.62, 56.22, 51.01, 42.68, 40.09, 40.04, 39.67, 38.15, 36.32, 36.15,

36.00, 35.93, 32.45, 31.35, 28.36, 28.16, 28.00, 24.27, 23.98, 22.96, 22.71, 22.15, 21.51, 18.84, 12.34. HRMS-DART: $[M\text{-}CH_3CO_2]^{\cdot}$ calcd for $C_{27}H_{44}Br$: 447.2626; Found: 447.2796.



9.2.9 **9.2.2**

(3*S*,8*S*,9*S*,10*S*,13*R*,14*S*,17*R*)-10-(Bromomethyl)-13-methyl-17-((*R*)-6-methylheptan-2-yl)-2,3,4,7,8,9,10,11,12,13,14,15,16,17-tetradecahydro-1*H*-cyclopenta[*a*]phenanthren-3-ol (9.2.2)

Compound **9.2.9** (13.4 mg, 0.0264 mmol) was dissolved with 4 mL dioxane/MeOH (1:1, v/v) in a 50 mL RBF at rt. NaOMe solution (4.375 M in MeOH) was next added dropwise until the reaction mixture turned basic, as indicated by pH paper. The reaction progress was monitored through TLC techniques and completed within one hour. After being quenched by addition of 1 N HCl dropwise, the solvent was removed under reduced pressure and the crude was purified via a silica gel column using gradient elution from hexanes to 25% EtOAc in hexanes. The product was obtained as a white solid (9.8 mg, 0.021 mmol, 80% yield). R_f = 0.4 (25% EtOAc-hexanes).

^{1}H NMR (500 MHz, $CDCl_3$) δ 5.66 – 5.62 (m, 1H), 3.74 (d, *J* = 11.2 Hz, 1H), 3.56 (ddd, *J* = 16.0, 11.2, 4.9 Hz, 1H), 3.50 (d, *J* = 11.1 Hz, 1H), 2.39 (ddd, *J* = 13.1, 4.9, 2.3 Hz, 1H), 2.14 (tt, *J* = 10.2, 2.7 Hz, 2H), 2.09 – 1.99 (m, 2H), 1.99 – 1.67 (m, 3H), 1.61 – 1.43 (m, 6H), 1.43 – 0.92 (m, 16H), 0.92 – 0.84 (m, 10H), 0.75 (s, 3H). ^{13}C NMR (126 MHz, $CDCl_3$) δ 135.76, 126.33, 71.41, 57.73, 56.24, 51.09, 42.70, 42.31, 40.10, 40.02, 39.67, 36.38, 36.33, 36.28, 35.93, 32.51, 31.84, 31.35, 28.37, 28.17, 24.28, 23.98, 22.97, 22.71, 22.19, 18.84, 12.35. HRMS-DRAT: [M+H-H_2O] calcd for $C_{27}H_{44}Br$: 447.2626; Found: 447.2774. [M+H-HBr] calcd for $C_{27}H_{45}O$: 385.3470; Found: 385.3652.

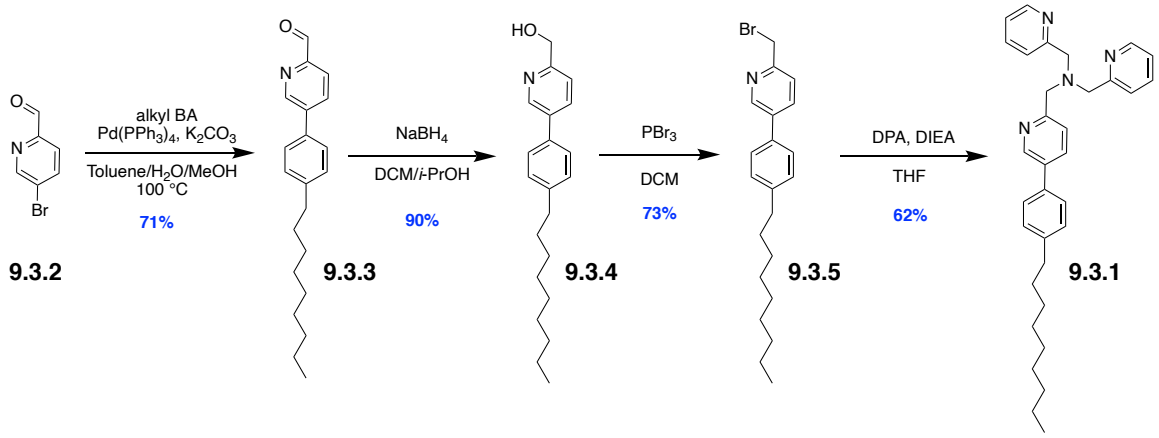
9.3. Synthesis of a zinc-responsive lipid based on a DPA scaffold

(The data used in this section has been published by the authors: Sagar, Ruhani; Lou, Jinchao; Watson, Alexa J. and Best, Michael D., Zinc triggered release of encapsulated cargo from liposomes via a synthetic lipid switch. *Bioconjugate Chem.* **2021**, 32, 2485-2496.)

9.3.1. Project overview

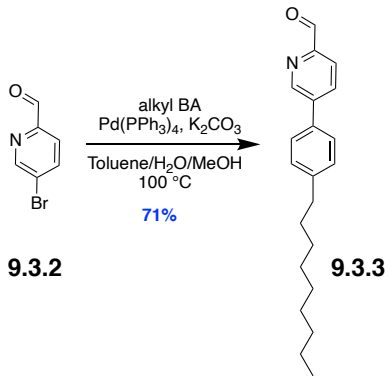
Zinc is an important ion in biological system. It is known to be associated with diseases[372-374] and is involved in regulating crucial processes, including immune response,[375] cell growth and proliferation,[376] and neurotransmission.[377] Taking a similar strategy as we presented in Chapters 2-4, our lab developed multiple zinc-responsive lipids that can undergo programmed conformational changes upon zinc-chelation. When these lipids are incorporated within the membrane bilayer, such conformational changes can disrupt the membrane integrity and induce the encapsulated cargo release. In a collaboration with Ruhani Sagar in our lab, I synthesized one of the target lipids **9.3.1** based on a DPA unit.

The synthetic route is shown in Scheme 9.3. A Suzuki coupling reaction between 5-bromopicolinaldehyde **9.3.2** and 4-(*n*-nonyl) benzeneboronic acid resulted in **9.3.3**, which was subjected to aldehyde reduction to **9.3.4**, bromination with PBr_3 to **9.3.5**, and DPA addition to **9.3.1**.



Scheme 9.3. Synthetic route to zinc-responsive lipid 9.3.1. 4-(*n*-Nonyl) benzene tail was installed onto **9.3.2** to **9.3.3**, followed by aldehyde reduction to **9.3.4**, bromination to **9.3.5** and DPA addition to **9.3.1**.

9.3.2. Synthetic procedures

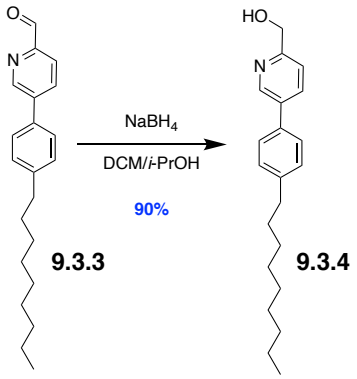


9.3.2 **9.3.3**

5-(4-Nonylphenyl)picolinaldehyde (9.3.3)

5-Bromopicolinaldehyde (**9.3.2**, 0.25 g, 1.344 mmol), 4-(*n*-nonyl) benzeneboronic acid (0.5 g, 2.016 mmol), tetrakis(triphenylphosphine)palladium(0) (15.53 mg, 0.01344 mmol) as well as K_2CO_3 (0.2786 g, 2.016 mmol) were combined in a 100 mL RBF under argon. After being dissolved with 25 mL toluene/H_2O/MeOH (2/2/1, v/v), the reaction mixture was heated at 100 ºC overnight. After completion, the reaction was cooled down to room temperature and the solvent was removed using a rotary evaporator. The residue was re-dissolved in 25 mL DCM and washed with 50 mL water. The aqueous layer was extracted twice more with 25 mL DCM. The combined organic layer was further washed with 50 mL water and 50 mL brine, respectively before being dried over Na_2SO_4, filtered, and concentrated under reduced pressure. The crude was next loaded onto silica gel and subjected to a column. Gradient elution from hexanes to 10% ethyl acetate in hexanes was needed to yield the product as a white solid (0.296 g, 0.956 mmol, 71% yield). R_f = 0.45 (10% EtOAc-hexanes).

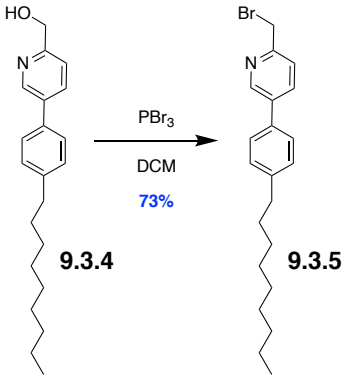
^{1}H NMR (500 MHz, $CDCl_3$) δ 10.11 (s, 1H), 9.02 – 8.98 (m, 1H), 8.06 – 7.99 (m, 2H), 7.56 (d, *J* = 8.2 Hz, 2H), 7.33 (d, *J* = 8.1 Hz, 2H), 2.70 – 2.64 (m, 2H), 1.69 – 1.60 (m, 2H), 1.39 – 1.21 (m, 13H), 0.90 – 0.83 (m, 3H). ^{13}C NMR (126 MHz, $CDCl_3$) δ 193.13, 151.38, 148.61, 144.53, 140.79, 134.94, 133.89, 129.54, 129.50, 127.36, 121.94, 115.26, 35.79, 31.99, 31.48, 29.65, 29.61, 29.43, 29.41, 22.78, 14.22. HRMS-DART: $[M+H]^+$ calcd for $C_{21}H_{28}NO$: 310.2171; Found: 310.1950.



(5-(4-Nonylphenyl)pyridin-2-yl)methanol (9.3.4)

Compound **9.3.3** (0.1896 g, 0.6123 mmol) was dissolved with 12 mL DCM/*i*-PrOH (3/1, v/v) under argon in a 100 mL RBF at 0 ºC. $NaBH_4$ (69.54 mg, 1.84 mmol) was then added. Next, the reaction mixture was warmed up to room temperature and further stirred for six hours. After completion, the reaction mixture was brought back to 0 ºC with an ice bath. 10% citric acid was added dropwise carefully until no hydrogen gas was released, and the reaction was further stirred for 20 min. The organic layer was collected and the aqueous layer was further extracted with 25 mL DCM twice. The combined organic layer was washed with 50 mL water and 50 mL brine. After being dried over Na_2SO_4, filtered, and concentrated under reduced pressure, the crude was purified using a column using gradient elution from hexanes to 50% EtOAc in hexanes. The product was obtained as a white solid (0.1706 g, 0.548 mmol, 90% yield). R_f = 0.2 (50% EtOAc-hexanes).

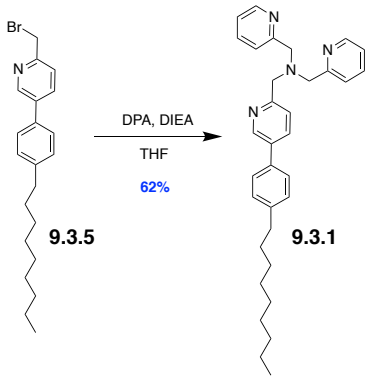
^{1}H NMR (500 MHz, Chloroform-*d*) δ 8.78 (s, 1H), 7.88 (dd, *J* = 8.1, 1.9 Hz, 1H), 7.52 – 7.47 (m, 2H), 7.32 (d, *J* = 8.1 Hz, 1H), 7.29 (d, *J* = 8.3 Hz, 2H), 4.82 (s, 2H), 2.70 – 2.61 (m, 2H), 1.64 (q, *J* = 7.3 Hz, 2H), 1.42 – 1.20 (m, 13H), 0.92 – 0.83 (m, 3H). ^{13}C NMR (126 MHz, $CDCl_3$) δ 157.48, 146.77, 143.35, 135.74, 135.34, 134.87, 129.35, 127.07, 120.61, 64.16, 35.78, 32.04, 31.61, 29.69, 29.66, 29.47, 22.82, 14.26. HRMS-DART: $[M+H]^+$ calcd for $C_{21}H_{30}NO$: 312.2327; Found: 312.2170.



2-(Bromomethyl)-5-(4-nonylphenyl)pyridine (9.3.5)

Compound **9.3.4** (0.1618 g, 0.52 mmol) was weighed into a 50 mL RBF under argon and dissolved with 20 mL dry DCM at 0 ºC. PBr_3 (0.74 mL, 7.79 mmol) was next added into the RBF dropwise carefully. The reaction was warmed up to room temperature and further stirred for six hours. After being cooled back to 0 ºC again, MeOH was added dropwise to quench the unreacted PBr_3. The mixture was poured into 100 mL H_2O in a separatory funnel and the DCM layer was collected. The aqueous layer was further extracted with 20 mL DCM twice. The combined organic layer was washed with 50 mL H_2O and 50 mL brine before being dried over Na_2SO_4, filtered, and concentrated under reduced pressure. The crude was purified with a short column packed with silica gel using elution of 10% EtOAc in hexanes. Compound **9.3.5** was obtained as a pale-yellow solid (0.1422 g, 0.38 mmol, 73% yield). R_f = 0.45 (10% EtOAc-Hexanes). Note: This compound can easily decompose at room temperature. It is desired to move onto next step as soon as possible.

^{1}H NMR (500 MHz, $CDCl_3$) δ 8.80 (s, 1H), 7.87 (dd, *J* = 8.1, 2.3 Hz, 1H), 7.49 (dd, *J* = 8.3, 2.1 Hz, 3H), 7.29 (d, *J* = 8.3 Hz, 2H), 4.61 (s, 2H), 2.69 – 2.62 (m, 2H), 1.69 – 1.60 (m, 2H), 1.39 – 1.20 (m, 13H), 0.92 – 0.85 (m, 3H). ^{13}C NMR (126 MHz, $CDCl_3$) δ 155.25, 148.10, 143.57, 136.16, 135.35, 134.60, 129.37, 127.12, 123.51, 35.78, 33.85, 32.03, 31.57, 29.69, 29.65, 29.47, 22.82, 14.25. HRMS-DART: $[M+H]^+$ calcd for $C_{21}H_{29}BrN$: 374.1483; Found: 374.1237.



1-(5-(4-Nonylphenyl)pyridin-2-yl)-*N*,*N*-bis(pyridin-2-ylmethyl)methanamine (9.3.1)

Compound **9.3.5** (43.6 mg, 0.1165 mmol) was dissolved with 10 mL dry THF in a 50 mL RBF under Ar. *N,N*-Diisopropylethylamine (DIEA, 23.34 µL, 0.134 mmol) and dipicolylamine (DPA, 24.12 µL, 0.134 mmol) were next added, respectively. The reaction was refluxed at 70 ºC overnight, accompanied by a color change from pale yellow to brown. After evaporating the solvent under reduced pressure, the crude was subjected to a column packed with neutral alumina. Gravity elution using 100% chloroform is enough to yield the purified product as a brown oil (35.4 mg, 0.072 mmol, 62% yield). R_f = 0.29 (5% Methanol in chloroform).

^{1}H NMR (500 MHz, $CDCl_3$) δ 8.75 (d, *J* = 1.9 Hz, 1H), 8.58 – 8.47 (m, 2H), 7.83 (dd, *J* = 8.1, 2.3 Hz, 1H), 7.70 – 7.57 (m, 5H), 7.47 (d, *J* = 8.2 Hz, 2H), 7.27 (d, *J* = 8.9 Hz, 2H), 7.14 (ddd, *J* = 7.2, 4.9, 1.2 Hz, 2H), 3.94 (d, *J* = 3.1 Hz, 6H), 2.66 – 2.62 (m, 2H), 1.63 (q, *J* = 7.3 Hz, 2H), 1.39 – 1.17 (m, 15H), 0.87 (t, *J* = 7.0 Hz, 3H). ^{13}C NMR (126 MHz, $CDCl_3$) δ 159.42, 157.82, 149.25, 147.53, 143.06, 136.57, 135.21, 135.11, 134.82, 129.25, 127.01, 123.17, 123.02, 122.15, 60.32, 60.00, 35.76, 32.02, 31.59, 29.84, 29.68, 29.64, 29.47, 29.45, 22.80, 14.24. HRMS-DART: $[M+H]^+$ calcd for $C_{33}H_{41}N_4$: 493.3331; Found: 493.2992.

9.4. Synthesis of azide-containing probes for metabolic labeling purposes

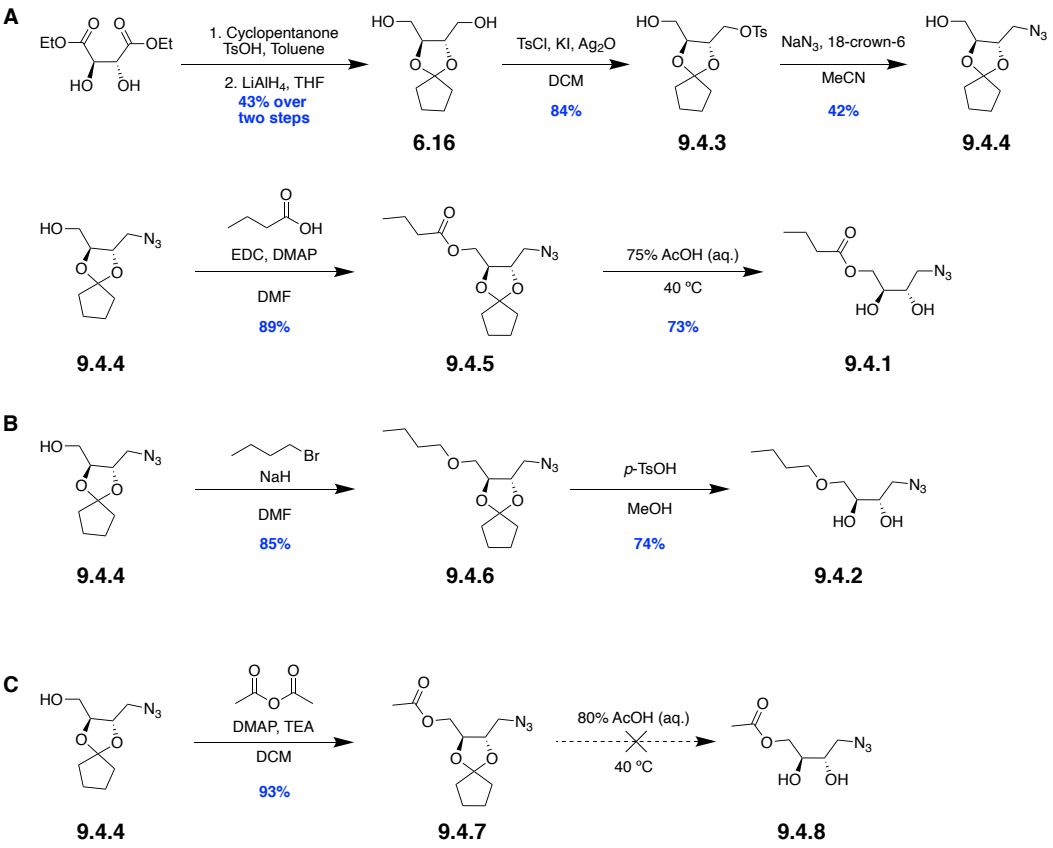
9.4.1. Project overview

Bioorthogonal chemistry has proven to be a powerful tool for chemical biology research since it was developed.[378-380] Previous reports have demonstrated that metabolic labeling utilizing small molecule precursors bearing clickable tags enables the imaging or detection of essential

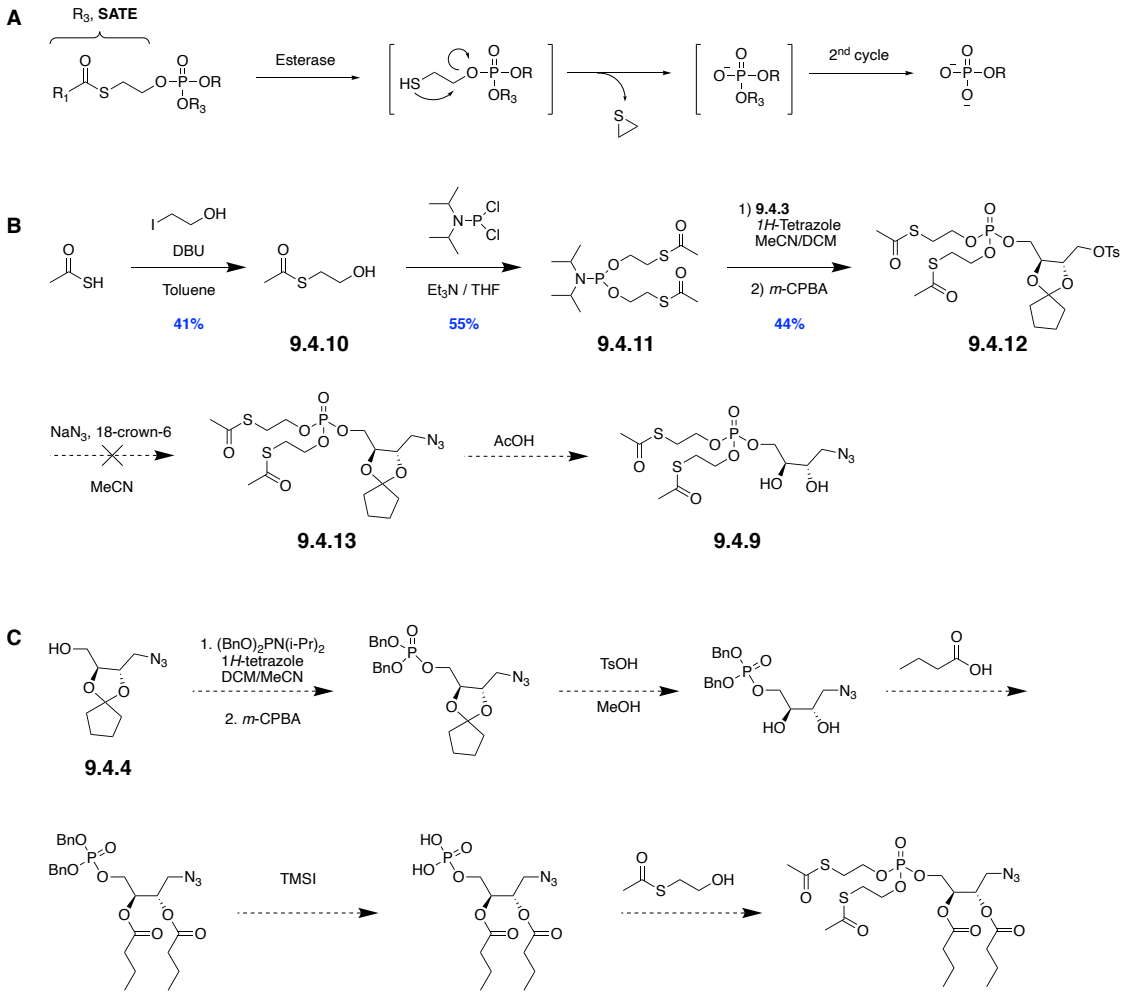
biomolecules.[381-384] After hijacking biosynthetic pathways, the probes can be converted into analogues of their target, allowing post-functionalization with fluorophores or affinity tags, which can reveal key information for signaling pathways, localization, development of new therapeutics, etc. In a collaboration with Christelle Ancajas in our lab, I synthesized glycerol-based probes **9.4.1** and **9.4.2** bearing an azide tag for metabolic infiltration of the yeast lipidome.

The structure and synthetic route for probe **9.4.1** is shown in Scheme 9.4A. It has a four-carbon short tail attached to the *sn*-3' position of glycerol through an ester bond. We hypothesized that the short fatty acid tail can increase the hydrophobicity of the probe, improving the yeast uptake. In addition, this ester bond can be hydrolyzed by cellular esterases and unveil the hydroxyl group of the *sn*-3' position. The resulting probe is thus expected to be able to label various of downstream lipids, including DAG, triacylglycerol (TAG), and all possible glycerol phospholipids. Monotosylation of **6.16** afforded **9.4.3**, which was treated with NaN_3 to install the azido tag.[288] Esterification with butyric acid, followed by deprotection of the acetal resulted in probe **9.4.1**. We additionally synthesized an ether version **9.4.2**, as a control probe. Since the ether bond cannot be cleaved when infiltrating the membrane and blocked the phosphate addition at the *sn*-3' position, we hypothesize that this probe is only able to label a limited amount of downstream lipids. Williamson ether synthesis was performed on intermediate **9.4.4** to afford **9.4.6**, followed by deprotection of the acetal to achieve **9.4.2**. Additional effort was made to synthesize the acetyl version of **9.4.8**; However, the synthesis was not successful.

Besides the above-mentioned glycerol-based probes, we also designed a PA-based probe **9.4.9** (Scheme 9.5B) for similar metabolic labeling applications. Due to the presence of polar phosphate PA headgroup that can affect probe uptake, we employed a *S*-acyl-2-thioethyl (SATE) protecting group to mask the highly negatively charged phosphates, which can undergo immolative processes upon intracellular esterase cleavage (Scheme 9.5A).[385,386]



Scheme 9.4. Synthetic routes to azido-glycerol-based probes for metabolic labeling purposes. A. Synthesis of **9.4.1** bearing a C4 ester tail at the *sn*-3' position. **B.** Synthesis of **9.4.2** bearing a C4 ether tail at the *sn*-3' position. **C.** Synthetic attempts to acetyl version **9.4.8**.

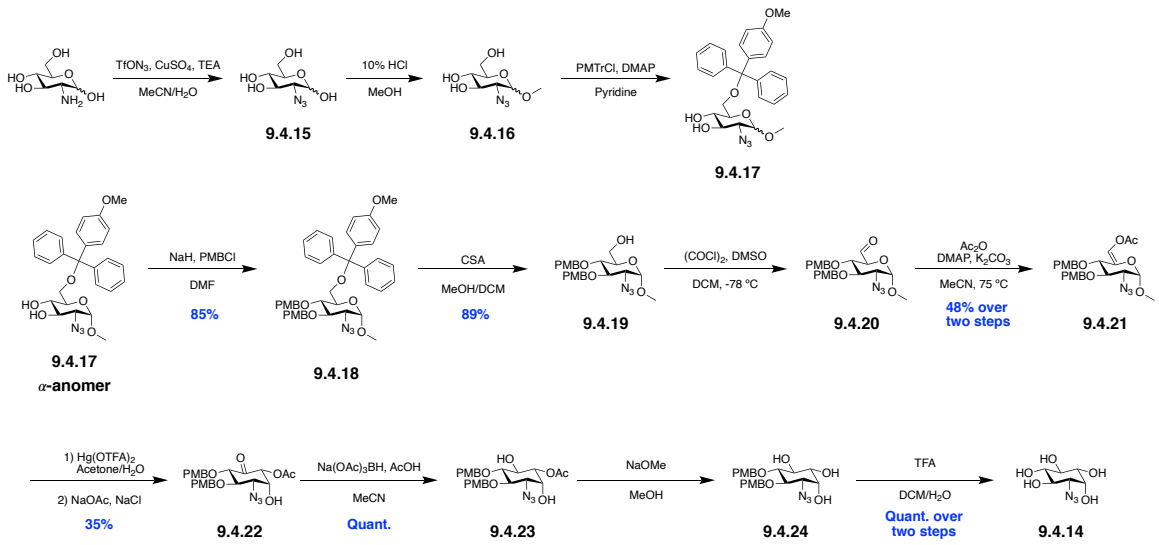


Scheme 9.5. Design and synthetic route to azido-PA probe. A. Release mechanism for SATE protected phosphate headgroup upon esterase enzyme mediated cleavage. **B.** Initial synthetic route for probe **9.4.9**. **C.** Proposed alternative route for synthesizing azido-PA probe.

Phosphoramidite reagent **9.4.11** was first synthesized in two steps (Scheme 9.5B)[387] and was next reacted with **9.4.3** to afford **9.4.12**. However, subsequent azide substitution turned out to be unsuccessful. Since the NaN_3 may react with the SATE protected phosphate headgroup, we provide an alternative route in Scheme 9.5C for potential future works, where the SATE cages are installed at the late stage of the synthesis.

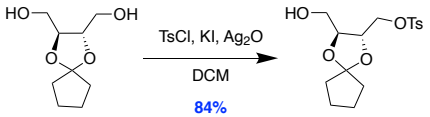
For a collaboration with the labs of Richard Anderson and Michael Sussman at the University of Wisconsin-Madison, we additionally synthesized inositol-based probe **9.4.14** containing an azido tag at the 3-position for metabolic labeling of PI lipids. The synthesis of the enantiopure version of this compound was previously reported by the Swartz group utilizing a Ferrier carbocyclization reaction as the key step.[388]

The synthetic route is shown in Scheme 9.6. D-Glucosamine hydrochloride was first reacted with freshly prepared triflic azide to form azido compound **9.4.15** through a diazo transfer reaction.[389] Methylation of the anomeric hydroxyl group of **9.4.15** resulted in **9.4.16**,[390] which was treated with *para*-methoxytrityl chloride to protect the primary alcohol group, leading to **9.4.17**, which existed a mixture of α and β anomers. The α anomer of **9.4.17** was separated via silica gel chromatography and was passed along to the next steps. After PMB protection and the deprotection of trityl groups using camphorsulfonic acid (CSA), the resulting primary alcohol **9.4.19** was subjected to a Swern oxidation to convert the alcohol group into an aldehyde group. Product **9.4.20** was treated with acetic anhydride to form the enol acetate of compound **9.4.21**, which was the precursor for a Ferrier carbocyclization reaction to build up the inositol ring scaffold of **9.4.22**. Reduction of the ketone with sodium triacetoxyborohydride ($Na(OAc)_3BH$) to **9.4.23**, deacetylation with NaOMe to **9.4.24**, and PMB deprotection with TFA resulted in the final probe **9.4.14**.



Scheme 9.6. Synthetic route to 3-azido inositol probe 9.4.14.

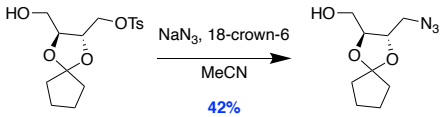
9.4.2. Synthetic procedures



6.16 **9.4.3**

((2*S*,3*S*)-3-(Hydroxymethyl)-1,4-dioxaspiro[4.4]nonan-2-yl)methyl 4-methylbenzenesulfonate (9.4.3)

This compound was synthesized according to the previous report from our group with slight modifications.[288] Multiple attempts were made and more than 0.1 eq of KI was essential to make this reaction work. Compound **6.16** (0.6 g, 3.19 mmol) was dissolved with 30 mL dry DCM in a 100 mL RBF under Ar. Next, Ag_2O (1.11 g, 4.78 mmol), TsCl (0.668 g, 3.5 mmol) and KI (0.159 g, 0.957 mmol) were added into the RBF. After stirring at 40 ºC for five hours, TLC indicated almost no starting material left. Ag_2O was removed via filtration through a short SiO_2 column. The filtrate was concentrated under reduced pressure and subjected to silica gel column chromatography. Gradient elution from hexanes to 40% EtOAc in hexanes was needed to yield the product as a clear oil (0.9234 g, 2.697 mmol, 84%). R_f = 0.41 (EtOAc-hexanes). ^{1}H NMR (500 MHz, $CDCl_3$) δ 7.77 (d, *J* = 8.3 Hz, 2H), 7.34 (d, *J* = 8.1 Hz, 2H), 4.11 (d, *J* = 4.9 Hz, 2H), 4.02 (dt, *J* = 7.3, 4.8 Hz, 1H), 3.89 (dt, *J* = 7.5, 4.3 Hz, 1H), 3.74 (d, *J* = 11.8 Hz, 1H), 3.65 – 3.58 (m, 1H), 2.43 (s, 3H), 2.15 (s, 1H), 1.92 – 1.70 (m, 4H), 1.63 (m, *J* = 15.0, 9.5, 5.1, 4.3 Hz, 4H). ^{13}C NMR (126 MHz, $CDCl_3$) δ 145.22, 132.64, 130.00, 128.07, 120.08, 78.13, 74.49, 69.16, 62.05, 37.30, 37.19, 23.62, 23.31, 21.72.



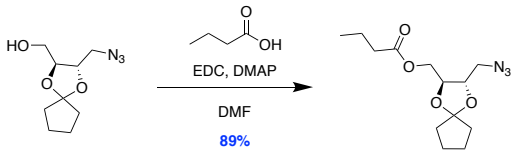
9.4.3 **9.4.4**

((2*S*,3*S*)-3-(Azidomethyl)-1,4-dioxaspiro[4.4]nonan-2-yl)methanol (9.4.4)

Compound **9.4.3** (0.22 g, 0.64 mmol), NaN_3 (0.125 g, 1.93 mmol) and 18-crown-6 (17 mg, 0.064 mmol) were weighed into a 100 mL RBF under argon and then dissolved with 15 mL MeCN. The reaction was stirred for 24 hours under reflux before being allowed to cool down

to room temperature. The solid left in the round bottom flask was filtered off through a celite pad and the filtrate was concentrated under vacuum. The resulting crude was subjected to silica gel column chromatography and gradient elution from hexanes to 50% EtOAc-hexane was used to yield **9.4.4** as a clear oil (57 mg, 0.267 mmol, 42% yield). R_f = 0.56 (50% EtOAc-hexanes).

^{1}H NMR (500 MHz, $CDCl_3$) δ 4.06 – 3.99 (m, 1H), 3.95 – 3.89 (m, 1H), 3.78 (dd, *J* = 11.9, 3.6 Hz, 1H), 3.70 – 3.61 (m, 1H), 3.50 (dd, *J* = 13.0, 4.3 Hz, 1H), 3.36 (dd, *J* = 13.0, 5.3 Hz, 1H), 2.12 (s, 1H), 1.91 – 1.56 (m, 8H). ^{13}C NMR (126 MHz, $CDCl_3$) δ 119.95, 78.65, 76.07, 62.13, 52.14, 37.43, 37.34, 23.59, 23.40. HRMS-DART: $[M+H-N_2]^+$ calcd for $C_9H_{16}NO_3$: 186.11302 ; Found: 186.0839.



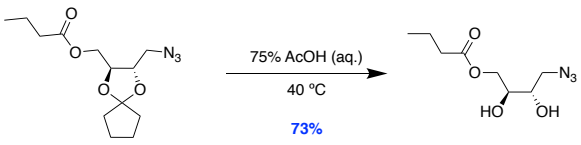
9.4.4 **9.4.5**

((2*S*,3*S*)-3-(Azidomethyl)-1,4-dioxaspiro[4.4]nonan-2-yl)methyl butyrate (9.4.5)

Compound **9.4.4** (52 mg, 0.244 mmol), butyric acid (24.6 µL, 0.268 mmol), DMAP (7.45 mg, 0.061 mmol), and EDCI (51.14 mg, 0.33 mmol) were dissolved with 3 mL dry DMF in a 50 mL RBF under Argon. After stirring at room temperature overnight, the reaction mixture was poured into a separatory funnel containing 100 mL H_2O. The aqueous layer was extracted with 3 × 25 mL EtOAc, and the combined organic layer was further washed with 5 × 50 mL H_2O and 1 × 50 mL brine. After being dried over Na_2SO_4, filtered, and concentrated under reduced pressure, the crude was purified with a column packed with silica gel and flushed with 10% EtOAc in hexanes. **9.4.5** was obtained as a clear oil (61.4 mg, 0.217 mmol, 89% yield). R_f = 0.43 (10% EtOAc-Hexanes).

^{1}H NMR (500 MHz, $CDCl_3$) δ 4.22 – 4.13 (m, 2H), 4.03 (dt, *J* = 7.3, 5.1 Hz, 1H), 3.94 (ddd, *J* = 7.3, 5.3, 4.1 Hz, 1H), 3.50 (dd, *J* = 13.1, 4.1 Hz, 1H), 3.35 (dd, *J* = 13.1, 5.3 Hz, 1H), 2.32 (t, *J* = 7.4 Hz, 2H), 1.92 – 1.76 (m, 4H), 1.74 – 1.60 (m, 6H), 0.94 (t, *J* = 7.4 Hz, 3H). ^{13}C NMR

(126 MHz, $CDCl_3$) δ 173.38, 120.34, 77.02, 76.06, 63.72, 52.03, 37.43, 37.28, 36.03, 23.59, 23.52, 18.45, 13.75.

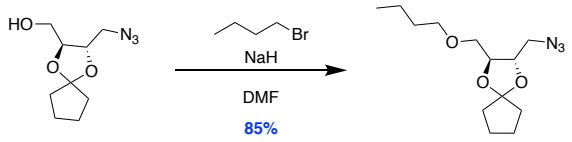


9.4.5 **9.4.1**

(2*S*,3*S*)-4-Azido-2,3-dihydroxybutyl butyrate (9.4.1)

Compound **9.4.5** (61.4 mg, 0.217 mmol) was dissolved with 6 mL 75% AcOH (4.5 mL AcOH and 1.5 mL H_2O) under Ar in a 50 mL RBF. After stirring the reaction overnight at 40 ºC, the solvent was removed under reduced pressure. The crude yellow oil was subjected to a silica gel column and purified with gradient elution from hexanes to 50% EtOAc in hexanes. The produce was obtained as a clear oil (34.4 mg, 0.158 mmol, 73% yield). R_f = 0.4 (50% EtOAc-hexanes).

^{1}H NMR (500 MHz, $CDCl_3$) δ 4.24 (dd, *J* = 11.7, 5.0 Hz, 1H), 4.17 (dd, *J* = 11.7, 6.5 Hz, 1H), 3.83 (p, *J* = 6.0 Hz, 1H), 3.78 – 3.72 (m, 1H), 3.51 – 3.41 (m, 2H), 2.64 (dd, *J* = 14.2, 5.9 Hz, 2H), 2.34 (t, *J* = 7.4 Hz, 2H), 1.66 (dt, *J* = 14.8, 7.4 Hz, 2H), 0.96 (t, *J* = 7.4 Hz, 3H). ^{13}C NMR (126 MHz, $CDCl_3$) δ 174.29, 70.35, 70.14, 65.46, 53.77, 36.13, 18.51, 13.77.



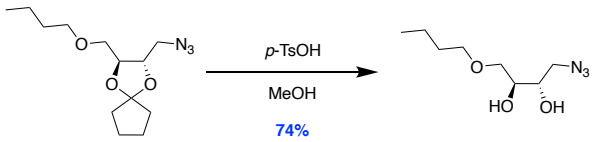
9.4.4 **9.4.6**

(2*S*,3*S*)-2-(Azidomethyl)-3-(butoxymethyl)-1,4-dioxaspiro[4.4]nonane (9.4.6)

Compound **9.4.4** (0.1 g, 0.469 mmol) was dissolved with 5 mL dry DMF at 0 ºC in a 50 mL RBF under Ar. NaH (56.28 mg, 1.407 mmol, 60% dispersant in mineral oil) was added carefully. After stirring for 5 min, 1-bromobutane (76.04 µL, 0.7 mmol) was added. The reaction mixture was stirred overnight at room temperature before carefully being quenched by adding water dropwise. After removal of the solvent under reduced pressure, the crude was redissolved with

25 mL EtOAc and 25 mL water. The organic layer was collected and the aqueous layer was further extracted with 2 × 25 mL EtOAc. Next, the combined organic layer was further washed with 5 × 50 mL H_2O and 1 × 50 mL brine. After being dried over Na_2SO_4, filtered, and concentrated under reduced pressure, the crude was purified with a column packed with silica gel. Gradient elution from hexanes to 10% EtOAc in hexanes yielded the product as a clear oil (107.1 mg, 0.398 mmol, 85% yield). R_f = 0.47 (10% EtOAc-Hexanes).

^{1}H NMR (500 MHz, $CDCl_3$) δ 4.02 – 3.91 (m, 2H), 3.63 – 3.57 (m, 1H), 3.55 – 3.42 (m, 4H), 3.37 – 3.29 (m, 1H), 1.91 – 1.76 (m, 4H), 1.68 (dtd, *J* = 11.2, 6.4, 5.7, 2.5 Hz, 4H), 1.55 (dq, *J* = 8.5, 6.5 Hz, 2H), 1.40 – 1.31 (m, 2H), 0.91 (t, *J* = 7.4 Hz, 3H). ^{13}C NMR (126 MHz, $CDCl_3$) δ 120.00, 78.19, 76.74, 71.81, 71.27, 52.53, 37.48, 37.32, 31.77, 23.63, 23.60, 19.41, 14.03. HRMS-DART: $[M+H-N_2]^+$ calcd for $C_{13}H_{24}NO_3$: 242.1752; Found: 242.1829.



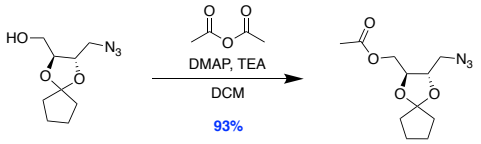
9.4.6 **9.4.2**

(2*S*,3*S*)-1-Azido-4-butoxybutane-2,3-diol (9.4.2)

Compound **9.4.6** (0.107 g, 0.398 mmol) was dissolved with 10 mL MeOH in a 50 mL RBF. After adding *p*-TsOH (6.8 mg, 0.0398 mmol), the reaction was stirred overnight at rt. Upon completion, 10 mg solid $NaHCO_3$ was added into the reaction to neutralize *p*-TsOH. The solvent was removed under reduced pressure and the crude was purified with a silica gel column using gradient elution from 10% EtOAc in hexanes to 50% EtOAc in hexanes. The product was obtained as a clear oil (60 mg, 0.295 mmol, 74% yield). R_f = 0.53 (50% EtOAc-hexanes).

^{1}H NMR (500 MHz, $CDCl_3$) δ 3.83 (ddd, *J* = 7.0, 5.1, 2.9 Hz, 1H), 3.75 – 3.69 (m, 1H), 3.61 – 3.54 (m, 2H), 3.51 – 3.42 (m, 3H), 3.38 (dd, *J* = 12.6, 5.0 Hz, 1H), 1.62 – 1.48 (m, 2H), 1.43 – 1.28 (m, 2H), 0.91 (t, *J* = 7.4 Hz, 3H). ^{13}C NMR (126 MHz, $CDCl_3$) δ 73.13, 71.80, 70.01, 53.70, 31.68, 19.37, 13.96. HRMS-DART: $[M+H]^+$ calcd for $C_8H_{18}N_3O_3$: 204.1348; Found: 204.1420.

$[M+H-N_2]^+$ calcd for $C_8H_{18}NO_3$: 176.1287; Found: 176.1338. $[M+NH_4]^+$ calcd for $C_8H_{21}N_4O_3$: 221.1614; Found: 211.1675

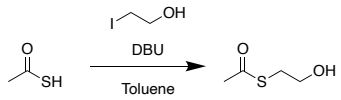


9.4.4 **9.4.7**

((2*S*,3*S*)-3-(Azidomethyl)-1,4-dioxaspiro[4.4]nonan-2-yl)methyl acetate (9.4.7)

Compound **9.4.4** (100 mg, 0.469 mmol) and DMAP (2.8 mg, 0.023 mmol) were dissolved with 10 mL dry DCM in a 50 mL RBF under Argon. After adding acetic anhydride (50 µL, 0.516 mmol) and triethylamine (0.13 mL, 0.938 mmol), the reaction was stirred at room temperature overnight. Next, the reaction mixture was poured into a separatory funnel containing 100 mL saturated $NaHCO_3$. The DCM layer was collected, and the aqueous layer was extracted with 2 × 25 mL DCM. The combined organic layer was further washed with 1 × 50 mL H_2O and 1 × 50 mL brine. After being dried over Na_2SO_4, filtered, and concentrated under reduced pressure, the crude was purified with a column packed with silica gel using gradient elution from 5%-15% EtOAc in hexanes. **9.4.7** was obtained as a clear oil (111.7 mg, 0.437 mmol, 93% yield). R_f = 0.18 (10% EtOAc-Hexanes).

^{1}H NMR (500 MHz, $CDCl_3$) δ 4.21 (dd, *J* = 11.8, 4.5 Hz, 1H), 4.15 (dd, *J* = 11.8, 5.6 Hz, 1H), 4.05 (ddd, *J* = 7.3, 5.6, 4.5 Hz, 1H), 3.94 (ddd, *J* = 7.3, 5.3, 4.2 Hz, 1H), 3.51 (dd, *J* = 13.1, 4.2 Hz, 1H), 3.36 (dd, *J* = 13.1, 5.3 Hz, 1H), 2.09 (s, 3H), 1.95 – 1.76 (m, 4H), 1.75 – 1.61 (m, 4H). ^{13}C NMR (126 MHz, $CDCl_3$) δ 170.78, 120.43, 76.96, 76.08, 64.08, 52.05, 37.45, 37.29, 23.63, 23.55, 20.91. HRMS-DART: $[M+H-N_2]^+$ calcd for $C_{11}H_{18}NO_4$: 228.1236; Found: 228.1273.

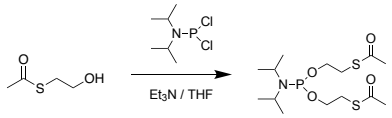


9.4.10

***S*-(2-Hydroxyethyl) ethanethioate (9.4.10)[387]**

Thioacetic acid (0.875 g, 1.15 mmol) was dissolved with 5 mL toluene at 0 ºC in a 50 mL RBF under Ar. After adding DBU (1.58 mL, 1.15 mmol) and 2-iodoethanol (0.78 mL, 10 mmol), the reaction was allowed to warm up to rt and further stirred overnight. There was a color change from colorless to orange and then yellow when adding the reagents. Upon completion, the reaction was diluted with 20 mL DCM and poured into a separatory funnel containing 100 mL H_2O. The DCM layer was collected, and the aqueous layer was extracted with 2 × 25 mL DCM. The combined organic layer was further washed with 1 × 50 mL H_2O and 1 × 50 mL brine. After being dried over Na_2SO_4, filtered, and concentrated under reduced pressure, the crude was purified with a column packed with silica gel using gradient elution from 10%-30% EtOAc in hexanes. **9.4.10** was obtained as a pale-yellow oil (0.4926 g, 4.1 mmol, 41% yield). R_f = 0.2 (25% EtOAc-Hexanes).

^{1}H NMR (300 MHz, $CDCl_3$) δ 3.56 (d, *J* = 5.4 Hz, 3H), 2.91 (t, *J* = 5.2 Hz, 2H), 2.21 (s, 3H). ^{13}C NMR (75 MHz, $CDCl_3$) δ 196.22, 60.99, 31.52, 30.34.



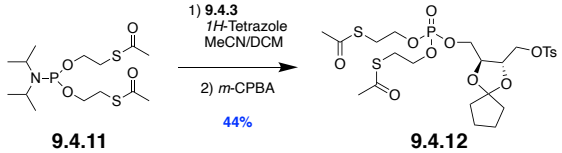
9.4.10 **9.4.11**

***S*,*S*'-((((Diisopropylamino)phosphanediyl)bis(oxy))bis(ethane-2,1-diyl)) diethanethioate (9.4.11)[387]**

Diisopropylphosphoramidous dichloride (0.414 g, 2.05 mmol) was dissolved in 15 mL dry THF at -78 ºC in a 100 mL RBF under Ar. **9.4.10** (0.4926 g, 4.1 mmol) and triethylamine (1.26 mL, 4.4 mmol) were dissolved with 3 mL THF in a separate vial and then added into the RBF dropwise. The reaction was warmed up to rt and further stirred for 4 hrs. Upon completion, the precipitate was removed via gravity filtration, and the filtrated was concentrated. The crude was purified with column packed with SiO_2 with elution of 10% EtOAc in hexanes to yield the product as a colorless oil (0.4135 g, 1.12 mmol, 55% yield). R_f = 0.74 (25% EtOAc-hexanes).

^{1}H NMR (500 MHz, $CDCl_3$) δ 3.76 (ddt, *J* = 10.6, 7.8, 6.5 Hz, 2H), 3.72 – 3.64 (m, 2H), 3.58 (ddd, *J* = 13.6, 6.8, 3.2 Hz, 2H), 3.12 (td, *J* = 6.5, 1.4 Hz, 4H), 2.33 (s, 6H), 1.17 (d, *J* = 6.8 Hz,

12H). ^{13}C NMR (126 MHz, $CDCl_3$) δ 195.59, 62.29, 62.15, 43.17, 43.07, 30.77, 30.72, 30.71, 24.78, 24.72. ^{31}P NMR (202 MHz, $CDCl_3$) δ 147.28. HRMS-DART: $[M+H]^+$ calcd for $C_{14}H_{29}NO_4PS_2$: 370.1276; Found: 370.1153.

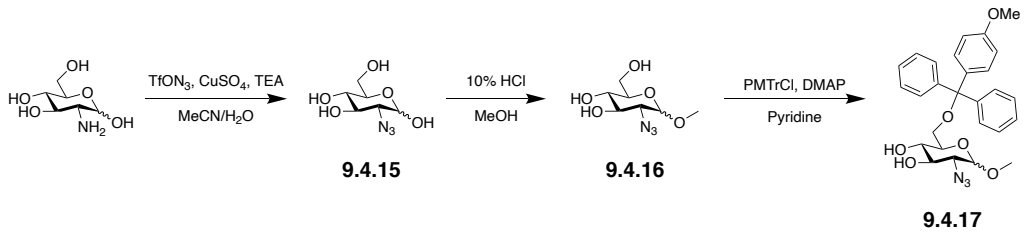


9.4.11 **9.4.12**

9.4.12

Compounds **9.4.3** (0.2474 g, 0.7225 mmol) and **9.4.11** (0.293 g, 0.795 mmol) were dissolved with 10 mL dry DCM in a 50 mL RBF under Ar. 1*H*-tetrazole (4.82 mL, 2.1675 mmol, 0.45 M in MeCN) was next added. After being stirred at rt for 6 hours, the reaction mixture was cooled to 0 °C with ice bath. *m*-CPBA (0.656 g, 2.1675 mmol, 57% purity) was added carefully and the reaction was stirred for an extra 3 hours. Saturated $NaHCO_3$ solution was then used to quench the reaction. The reaction mixture was extracted three times with 50 mL DCM. The combined organic layer was washed with 100 mL water and 100 mL brine, dried over Na_2SO_4, filtered, and concentrated under reduced pressure. The crude was subjected to silica gel column chromatography and gradient elution from 10% to 50% EtOAc in hexanes yielded **9.4.12** as a colorless oil (0.2 g, 0.32 mmol, 44% yield). R_f = 0.25 (50% EtOAc-hexanes).

^{1}H NMR (500 MHz, $CDCl_3$) δ 7.84 – 7.77 (m, 2H), 7.40 – 7.32 (m, 2H), 4.18 – 4.10 (m, 8H), 4.09 – 3.98 (m, 2H), 3.18 (t, *J* = 6.5 Hz, 4H), 2.45 (s, 3H), 2.37 – 2.34 (m, 6H), 1.76 (m, 3H), 1.69 – 1.58 (m, 5H). ^{13}C NMR (126 MHz, $CDCl_3$) δ 194.84, 145.30, 132.73, 130.09, 128.18, 120.77, 76.13, 76.07, 75.05, 68.94, 66.95, 66.91, 66.39, 66.34, 37.41, 37.39, 30.71, 30.70, 29.33, 29.27, 23.61, 23.56, 23.55, 21.82. ^{31}P NMR (202 MHz, $CDCl_3$) δ -1.97. HRMS-DART: $[M+H]^+$ calcd for $C_{24}H_{36}O_{11}PS_3$: 627.1157; Found: 627.1042.



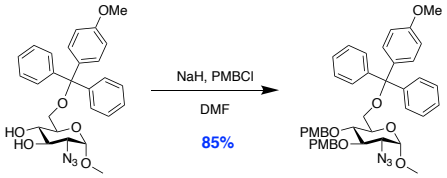
9.4.15 **9.4.16** **9.4.17**

(2*R*,3*S*,4*R*,5*R*,6*S*)-5-Azido-6-methoxy-2-(((4-methoxyphenyl)diphenylmethoxy)methyl)tetrahydro-2*H*-pyran-3,4-diol (9.4.17)

NaN_3 (0.436 g, 6.7 mmol) was dissolved in 8 mL dry MeCN at 0 ºC in a 50 mL RBF under Ar. Tf_2O (0.94 mL, 5.56 mmol) was then added dropwise carefully. The reaction was stirred at 0 ºC for two hours. A significant amount of salt precipitation could be observed during the reaction progress, which was filtered off through a fluted filter paper. The filtrate containing fresh $TfON_3$ was collected and ready to be used for the next step. In a separate 100 mL RBF, D-glucosamine hydrochloride (1 g, 4.64 mmol), $CuSO_4$ (7.4 mg, 0.0464 mmol), and triethylamine (1.3 mL, 9.276 mmol) were dissolved with 5 mL MilliQ purified water under Ar. The reaction was cooled to 0 ºC with an ice bath, and the previously prepared $TfON_3$ was added dropwise carefully. All the starting materials were dissolved at this moment and resulted in a clear blue/purple solution. After overnight stirring, the reaction turned green, and the solvent was removed under reduced pressure. The residual was re-dissolved with 10% HCl/MeOH (2.5 mL/22.5 mL concentrated HCl/MeOH) and stirred at 90 ºC for 24 hours. Upon completion, the reaction was allowed to cool down to rt. White precipitation could be observed at the bottom of the RBF. The solvent was removed, and the crude was re-dissolved with MeOH. Solid $NaHCO_3$ was added into the mix while stirring until the pH became neutral. Any solid present in the RBF was removed with a fluted filter paper. More solid precipitated out from the filtrate after the filtration, but that could be ignored as it did not affect the following steps. After removal of MeOH, the crude was re-dissolved with 15 mL dry pyridine under Ar and cooled to 0 ºC. Following the addition of PMTrtCl (2.1 g, 6.957 mmol), DMAP (60 mg, 0.464 mmol), and DIEA (1.6 mL, 9.276 mmol), the reaction was stirred overnight. Upon completion, the reaction was quenched by adding MeOH, and the majority of the pyridine

solvent was removed under reduced pressure. The residual ~5 mL reaction mixture was poured into a separatory funnel containing 150 mL H_2O. The aqueous layer was extracted with 3 × 25 mL DCM, and the combined organic layer was further washed with 5 × 50 mL H_2O and 1 × 50 mL brine. After being dried over Na_2SO_4, filtered, and concentrated under reduced pressure, the crude was purified with two columns packed with silica gel. Flash chromatography followed by a gravity column using gradient elution from 100% toluene to 30% EtOAc in toluene was needed to separate the pure α anomer of **9.4.17** as a fluffy sugar-like solid. The reaction yield could not be determined as this α anomer could never be completely separated from the β anomer. R_f = 0.34 (25% EtOAc-Toluene).

^{1}H NMR (300 MHz, $CDCl_3$) δ 7.46 (d, *J* = 7.2 Hz, 4H), 7.38 – 7.10 (m, 10H), 6.86 (d, *J* = 8.9 Hz, 2H), 4.78 (d, *J* = 3.5 Hz, 1H), 3.95 (dd, *J* = 10.1, 8.7 Hz, 1H), 3.80 (s, 3H), 3.67 (dt, *J* = 9.5, 4.7 Hz, 1H), 3.59 – 3.49 (m, 1H), 3.41 (d, *J* = 4.2 Hz, 5H), 3.26 (dd, *J* = 10.3, 3.5 Hz, 1H), 2.81 (s, 2H).



9.4.17
α-anomer

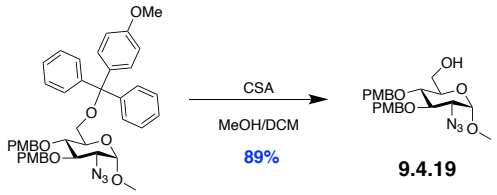
9.4.18

(2*S*,3*R*,4*R*,5*S*,6*R*)-3-Azido-2-methoxy-4,5-bis((4-methoxybenzyl)oxy)-6-(((4-methoxyphenyl)diphenylmethoxy)methyl)tetrahydro-2*H*-pyran (9.4.18)

Compound **9.4.17** (0.42 g, 0.854 mmol) was dissolved in 10 mL dry DMF under nitrogen at 0 °C. NaH (0.22 g, 5.49 mmol, 60% dispersion in mineral oil) was then added, and the reaction mixture was further stirred for 15 minutes, followed by the addition of 4-methoxybenzyl chloride (0.33 mL, 2.562 mmol). After stirring at 0 °C for an extra 10 min, the reaction mixture was removed from the ice bath and stirred at room temperature overnight. The reaction was carefully quenched by adding water, and the mixture was extracted with 3 x 50 mL EtOAc. The combined organic layer was further washed with 5 x 100 mL water and once with 100 mL brine. After drying with Na_2SO_4, filtering, and concentrating under reduced pressure, the crude was

purified through silica gel column chromatography using gradient hexanes to 15% EtOAc in hexanes to afford **9.4.18** as a fluffy sugar-like solid (0.531 g, 0.726 mmol, 85% yield). R_f = 0.18 (10% EtOAc-Hexanes).

^{1}H NMR (300 MHz, $CDCl_3$) δ 7.55 (dd, *J* = 6.7, 4.5 Hz, 4H), 7.46 – 7.20 (m, 10H), 6.98 – 6.75 (m, 8H), 4.94 (d, *J* = 3.4 Hz, 1H), 4.86 (s, 2H), 4.67 (d, *J* = 10.1 Hz, 1H), 4.30 (d, *J* = 10.1 Hz, 1H), 4.06 – 3.92 (m, 1H), 3.91 – 3.73 (m, 11H), 3.64 – 3.53 (m, 2H), 3.51 (s, 3H), 3.28 (dd, *J* = 10.0, 4.2 Hz, 1H).



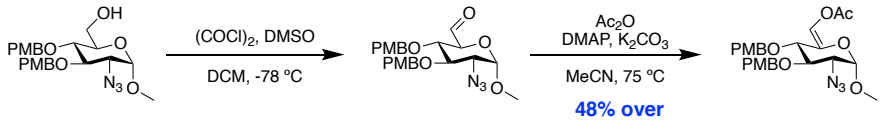
9.4.18 **9.4.19**

((2*R*,3*S*,4*R*,5*R*,6*S*)-5-Azido-6-methoxy-3,4-bis((4-methoxybenzyl)oxy)tetrahydro-2*H*-pyran-2-yl)methanol (9.4.19)

Compound **9.4.18** (0.1963 g, 0.268 mmol) was dissolved with 15 mL MeOH/DCM (2/1, v/v) in a 100 mL RBF. After adding camphorsulfonic acid (CSA, 10 mg, 0.04 mmol), the reaction was stirred for 1.5 hr at rt (determined via TLC, prolonged reaction time led to significantly lowered yield). Upon completion, 10 mg solid $NaHCO_3$ was added into the reaction to neutralize CSA. The solvent was removed under reduced pressure, and the crude was purified through silica gel column chromatography using gradient elution from 10% EtOAc in hexanes to 70% EtOAc in hexanes. The product was obtained as a clear oil (0.11 g, 0.24 mmol, 89% yield). R_f = 0.4 (50% EtOAc-hexanes).

^{1}H NMR (500 MHz, $CDCl_3$) δ 7.34 – 7.30 (m, 2H), 7.26 – 7.22 (m, 2H), 6.91 – 6.86 (m, 4H), 4.84 – 4.79 (m, 3H), 4.77 (d, *J* = 3.5 Hz, 1H), 4.60 (d, *J* = 10.8 Hz, 1H), 3.96 (dd, *J* = 10.1, 8.9 Hz, 1H), 3.80 (d, *J* = 2.7 Hz, 7H), 3.77 (d, *J* = 2.1 Hz, 1H), 3.73 – 3.63 (m, 2H), 3.59 – 3.53 (m, 1H), 3.40 (s, 3H), 3.37 (dd, *J* = 10.2, 3.5 Hz, 1H). ^{13}C NMR (126 MHz, $CDCl_3$) δ 159.58, 159.55, 130.17, 130.15, 129.95, 129.72, 114.10, 114.05, 98.81, 80.27, 77.76, 75.33, 74.83, 71.36,

63.88, 61.78, 55.43, 55.41, 55.35.



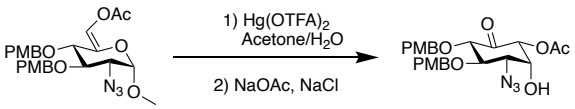
9.4.19 **9.4.20** **9.4.21**

(*Z*)-((3*S*,4*R*,5*R*,6*S*)-5-Azido-6-methoxy-3,4-bis((4-methoxybenzyl)oxy)tetrahydro-2*H*-pyran-2-ylidene)methyl acetate (9.4.21)

Oxalyl chloride (0.103 mL, 1.2 mmol) was dissolved with 5 mL dry DCM in a 100 mL RBF under Ar. The reaction was placed into a -78 °C N_2(Liq.)/EtOAc bath and stirred for 15 min. Next, DMSO (0.17 mL, 2.4 mmol) was added dropwise. After another 15 min stir, **9.4.19** (0.11 g, 0.239 mmol, dissolved in 3 mL dry DCM) was added dropwise, and the reaction was further stirred for 30 min. The temperature of the cooling bath was closely monitored during the whole reaction progress. Then, triethylamine (0.502 mL, 3.6 mmol) was added. After stirring for 15 min at -78 °C, the reaction was allowed to warm to rt. Solid precipitation could be observed in the RBF. The reaction mixture was poured into a separatory funnel containing 100 mL water. The DCM layer was collected and the aqueous layer was extracted with 2 × 25 mL DCM. The combined organic layer was further washed with 1 × 50 mL H_2O and 1 × 50 mL brine. After being dried over Na_2SO_4, filtered, and concentrated under reduced pressure, the crude was subjected to the next step without further purification (TLC indicated streaking, which made the separation challenging). The crude, DMAP (3.8 mg, 0.0312 mmol), K_2CO_3 (0.265 g, 1.92 mmol) were combined in a 50 mL RBF under Ar. Anhydrous MeCN (8 mL) and acetic anhydride (70 µL, 0.744 mmol) were next added. After being heated at 75 °C overnight, the solvent was removed under reduced pressure. The residual was redissolved with 25 mL water and 25 mL EtOAc. After collecting the organic layer, the aqueous layer was further extracted with 2 x 25 mL EtOAc. Next, the combined organic layer was washed with 1 x 100 water and once with 100 mL brine. After drying with Na_2SO_4, filtering, and concentrating under reduced pressure, the crude was purified with silica gel column chromatography using gradient elution from 0%-25% EtOAc in hexanes. **9.4.21** was obtained as a yellow oil (58.1 mg, 0.1163 mmol, 48% yield

over two steps). R_f = 0.34 (25% EtOAc-Hexanes). Note: Swern oxidation reaction can result in dimethyl sulfide as a byproduct, which has a notoriously unpleasant odor. Attention should be paid when working-up this reaction.

^{1}H NMR (500 MHz, $CDCl_3$) δ 7.27 (dd, *J* = 15.3, 8.6 Hz, 4H), 7.18 (d, *J* = 1.6 Hz, 1H), 6.92 – 6.81 (m, 4H), 4.89 (d, *J* = 3.3 Hz, 1H), 4.79 (d, *J* = 10.4 Hz, 1H), 4.72 – 4.65 (m, 3H), 3.98 (dd, *J* = 8.6, 1.7 Hz, 1H), 3.93 – 3.86 (m, 1H), 3.78 (d, *J* = 3.2 Hz, 6H), 3.49 (s, 3H), 3.45 (dd, *J* = 9.8, 3.3 Hz, 1H), 2.16 (s, 3H). ^{13}C NMR (126 MHz, $CDCl_3$) δ 167.36, 159.65, 159.56, 134.71, 130.00, 129.97, 129.92, 129.84, 129.66, 129.53, 123.56, 114.11, 114.01, 100.13, 79.25, 78.23, 75.24, 74.28, 63.01, 56.42, 55.40, 20.73. HRMS-DART: $[M+H-N_2]^+$ calcd for $C_{25}H_{30}NO_8$: 472.1971; Found:472.1972.

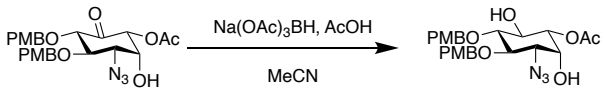


9.4.21 **9.4.22**

(1*R*,2*R*,3*S*,4*R*,5*S*)-3-Azido-2-hydroxy-4,5-bis((4-methoxybenzyl)oxy)-6-oxocyclohexyl acetate (9.4.22)

Compound **9.4.21** (58.1 mg, 0.116 mmol) was dissolved with 2 mL/0.5 mL acetone/H_2O in a 50 mL RBF at °C under Ar. $Hg(OTFA)_2$ (64.5 mg, 0.15 mmol) was added, which resulted in an orange suspension. After being stirred for 10 min, the reaction mixture was diluted with 5.5 mL acetone. Next, 3 N NaOAc solution (49 µL) and brine (81 µL) were added. The color of the reaction became lighter and orange droplets could be observed on the side of the RBF, which turned into dark green after 20 min stir. The reaction was stirred at rt for 24 hrs before being diluted with 10 mL H_2O. Acetone was removed under reduced pressure, and the resulting aqueous solution was extracted with 3 x 25 mL DCM. Next, the combined organic layer was washed with 1 x 100 mL water and once with 100 mL brine. After drying with Na_2SO_4, filtering, and concentrating under reduced pressure, the crude was purified with silica gel column chromatography using gradient elution from 10%-50% EtOAc in hexanes. Compound **9.4.22** was obtained as a yellow oil (20 mg, 0.0412 mmol, 35% yield). R_f = 0.4 (50% EtOAc-Hexanes).

^{1}H NMR (500 MHz, $CDCl_3$) δ 7.36 – 7.30 (m, 2H), 7.29 – 7.22 (m, 2H), 6.87 (dd, *J* = 8.6, 1.0 Hz, 4H), 5.20 (d, *J* = 1.9 Hz, 1H), 4.91 – 4.83 (m, 2H), 4.70 (d, *J* = 10.1 Hz, 1H), 4.47 (d, *J* = 10.9 Hz, 1H), 4.32 (d, *J* = 2.3 Hz, 1H), 4.20 (dd, *J* = 9.2, 1.0 Hz, 1H), 4.07 (t, *J* = 9.5 Hz, 1H), 3.81 (d, *J* = 1.3 Hz, 7H), 2.25 (s, 3H). ^{13}C NMR (126 MHz, $CDCl_3$) δ 197.32, 169.49, 159.58, 159.50, 130.15, 130.06, 129.53, 129.13, 113.93, 113.84, 84.24, 80.13, 75.57, 75.35, 73.32, 70.51, 62.92, 55.27, 20.47. HRMS-DART: $[M+H-N_2]^+$ calcd for $C_{24}H_{28}NO_8$: 458.1815; Found: 458.1846.



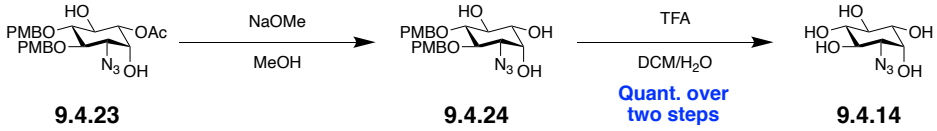
9.4.22 Quant. **9.4.23**

(1*R*,2*R*,3*S*,4*R*,5*R*,6*R*)-3-Azido-2,6-dihydroxy-4,5-bis((4-methoxybenzyl)oxy)cyclohexyl acetate (9.4.23)

Compound **9.4.22** (20 mg, 0.041 mmol) was dissolved with 2 mL anhydrous MeCN in a 6 dr vial at °C under Ar. After adding $Na(OAc)_3BH$ (78.58 mg, 0.37 mmol) and AcOH (0.14 mL, 2.46 mmol), the reaction mixture was stirred at rt. TLC indicated no starting material left after 1.5 hr. The reaction was next quenched by adding water dropwise before being poured into a separatory funnel containing 100 mL H_2O. The aqueous solution was extracted with 3 x 25 mL DCM. The combined organic layer was next washed with 1 x 100 mL water and once with 100 mL brine. After drying with Na_2SO_4, filtering, and concentrating under reduced pressure, the crude was purified via silica gel column chromatography using gradient elution from 25%-50% EtOAc in hexanes. **9.4.23** was obtained as a clear oil (20 mg, 0.041 mmol, quantitative yield). R_f = 0.2 (50% EtOAc-Hexanes).

^{1}H NMR (500 MHz, $CDCl_3$) δ 7.34 – 7.25 (m, 4H), 6.88 (d, *J* = 8.5 Hz, 4H), 4.87 (dd, *J* = 19.4, 10.6 Hz, 2H), 4.78 (d, *J* = 10.2 Hz, 1H), 4.71 (dd, *J* = 10.5, 3.2 Hz, 2H), 4.19 (t, *J* = 2.6 Hz, 1H), 4.03 (t, *J* = 9.8 Hz, 1H), 3.90 (t, *J* = 9.7 Hz, 1H), 3.80 (s, 7H), 3.48 (dd, *J* = 10.1, 2.5 Hz, 1H), 3.40 (t, *J* = 9.3 Hz, 1H), 2.15 (s, 3H). ^{13}C NMR (126 MHz, $CDCl_3$) δ 170.43, 159.48, 159.46, 130.25, 129.96, 129.77, 129.69, 129.55, 114.11, 113.92, 83.54, 79.64, 75.46, 75.33, 73.31,

70.49, 69.41, 63.85, 55.27, 29.69, 20.99. HRMS-DART: $[M+H-N_2]^+$ calcd for $C_{24}H_{30}NO_8$: 460.1971; Found: 460.2052.



9.4.23 **9.4.24** **Quant. over two steps** **9.4.14**

(1*R*,2*R*,3*R*,4*S*,5*R*,6*R*)-6-Azidocyclohexane-1,2,3,4,5-pentaol (9.4.14)

Compound **9.4.23** (20 mg, 0.0412 mmol) was dissolved with 3 mL/1 mL MeOH/DCM in a 6 dr vial. NaOMe solution (4.375 M in MeOH) was next added dropwise until the reaction mixture turned basic, as indicated by pH paper. The reaction progress was monitored through TLC techniques and was complete within one hour. After being quenched by the addition of 1 N HCl dropwise, the solvent was removed under reduced pressure. The crude was redissolved in 3 mL DCM in the same vial. TFA (0.5 mL), as well as H_2O (0.5 mL), were added to the reaction mixture. After stirring for 30 min, the solvent was removed under reduced pressure, and the crude was purified via silica gel column chromatography using gradient elution from DCM to 25% MeOH in DCM. The product was obtained as a white solid in a quantitative yield. R_f = 0.52 (25% MeOH-DCM).

^{1}H NMR (500 MHz, D_2O) δ 4.18 (t, *J* = 2.8 Hz, 1H), 3.76 (dd, *J* = 10.5, 9.4 Hz, 1H), 3.65 – 3.59 (m, 1H), 3.55 (dd, *J* = 10.0, 2.9 Hz, 1H), 3.45 (dd, *J* = 10.6, 2.7 Hz, 1H), 3.38 – 3.33 (m, 2H). ^{13}C NMR (126 MHz, D_2O) δ 65.60, 62.93, 62.21, 62.16, 61.72, 54.12. HRMS-DART: $[M+H-N_2]^+$ calcd for $C_6H_{12}NO_5$: 178.0715; Found: 178.0803. $[M+H-N_2-H_2O]^+$ calcd for $C_6H_{10}NO_4$: 160.0610; Found: 160.0684.

List of References

1. Jacobson, K.; Sheets, E. D.; Simson, R., Revisiting the fluid mosaic model of membranes. *Science* **1995,** *268* (5216), 1441-1443.
2. Wilfling, F.; Haas, J. T.; Walther, T. C.; Farese Jr, R. V., Lipid droplet biogenesis. *Curr. Opin. Cell Biol.* **2014,** *29*, 39-45.
3. Bangham, A. D.; Standish, M. M.; Watkins, J. C., Diffusion of univalent ions across the lamellae of swollen phospholipids. *J. Mol. Biol.* **1965,** *13* (1), 238-IN227.
4. Storck, E. M.; Özbalci, C.; Eggert, U. S., Lipid cell biology: a focus on lipids in cell division. *Annu. Rev. Biochem.* **2018,** *87*, 839-869.
5. Prescott, D. M., Regulation of cell reproduction. *Cancer Res.* **1968,** *28* (9), 1815-1820.
6. Huijbregts, R. P.; Topalof, L.; Bankaitis, V. A., Lipid metabolism and regulation of membrane trafficking. *Traffic* **2000,** *1* (3), 195-202.
7. Lee, A., Lipid–protein interactions in biological membranes: a structural perspective. *Biochim. Biophys. Acta, Biomembr.* **2003,** *1612* (1), 1-40.
8. Wang, X., Lipid signaling. *Curr. Opin. Plant Biol.* **2004,** *7* (3), 329-336.
9. Testerink, C.; Munnik, T., Phosphatidic acid: a multifunctional stress signaling lipid in plants. *Trends Plant Sci.* **2005,** *10* (8), 368-375.
10. Hammond, G. R.; Burke, J. E., Novel roles of phosphoinositides in signaling, lipid transport, and disease. *Curr. Opin. Cell Biol.* **2020,** *63*, 57-67.
11. Harayama, T.; Riezman, H., Understanding the diversity of membrane lipid composition. *Nat. Rev. Mol. Cell Biol.* **2018,** *19* (5), 281-296.
12. Fleischer, S.; Rouser, G.; Fleischer, B.; Casu, A.; Kritchevsky, G., Lipid composition of mitochondria from bovine heart, liver, and kidney. *J. Lipid Res.* **1967,** *8* (3), 170-180.
13. Casares, D.; Escribá, P. V.; Rosselló, C. A., Membrane lipid composition: Effect on membrane and organelle structure, function and compartmentalization and therapeutic avenues. *Int. J. Mol. Sci* **2019,** *20* (9), 2167.
14. Spector, A. A.; Yorek, M. A., Membrane lipid composition and cellular function. *J. Lipid Res.* **1985,** *26* (9), 1015-1035.
15. Gunstone, F. D., *Fatty acid and lipid chemistry*. Springer: 2012.
16. Yamashita, A.; Hayashi, Y.; Nemoto-Sasaki, Y.; Ito, M.; Oka, S.; Tanikawa, T.; Waku, K.; Sugiura, T., Acyltransferases and transacylases that determine the fatty acid composition of glycerolipids and the metabolism of bioactive lipid mediators in mammalian cells and model organisms. *Prog. Lipid Res.* **2014,** *53*, 18-81.
17. Kooijman, E. E.; Chupin, V.; Fuller, N. L.; Kozlov, M. M.; de Kruijff, B.; Burger, K. N.; Rand, P. R., Spontaneous curvature of phosphatidic acid and lysophosphatidic acid. *Biochemistry* **2005,** *44* (6), 2097-2102.
18. Li, Z.; Agellon, L. B.; Allen, T. M.; Umeda, M.; Jewell, L.; Mason, A.; Vance, D. E., The ratio of phosphatidylcholine to phosphatidylethanolamine influences membrane integrity and steatohepatitis. *Cell metab.* **2006,** *3* (5), 321-331.
19. McIntosh, T., Differences in hydrocarbon chain tilt between hydrated phosphatidylethanolamine and phosphatidylcholine bilayers. A molecular packing model.

Biophys. J. **1980,** *29* (2), 237-245.
20. Epand, R.; Fuller, N.; Rand, R., Role of the position of unsaturation on the phase behavior and intrinsic curvature of phosphatidylethanolamines. *Biophys. J.* **1996,** *71* (4), 1806-1810.
21. Vance, J. E.; Steenbergen, R., Metabolism and functions of phosphatidylserine. *Prog. Lipid Res.* **2005,** *44* (4), 207-234.
22. Fadok, V. A.; Bratton, D. L.; Frasch, S. C.; Warner, M. L.; Henson, P. M., The role of phosphatidylserine in recognition of apoptotic cells by phagocytes. *Cell Death Differ.* **1998,** *5* (7), 551-562.
23. Bevers, E. M.; Williamson, P. L., Getting to the outer leaflet: physiology of phosphatidylserine exposure at the plasma membrane. *Physiol. Rev.* **2016,** *96* (2), 605-645.
24. Janmey, P. A., Protein regulation by phosphatidylinositol lipids. *Cell Chem. Biol.* **1995,** *2* (2), 61-65.
25. Israelachvili, J. N.; Mitchell, D. J.; Ninham, B. W., Theory of self-assembly of lipid bilayers and vesicles. *Biochim. Biophys. Acta, Biomembr.* **1977,** *470* (2), 185-201.
26. Fong, W.-K.; Hanley, T. L.; Thierry, B.; Tilley, A.; Kirby, N.; Waddington, L. J.; Boyd, B. J., Understanding the photothermal heating effect in non-lamellar liquid crystalline systems, and the design of new mixed lipid systems for photothermal on-demand drug delivery. *Phys. Chem. Chem. Phys.* **2014,** *16* (45), 24936-24953.
27. Lou, J.; Best, M. D., Strategies for altering lipid self-assembly to trigger liposome cargo release. *Chem. Phys. Lipids* **2020,** *232*, 104966.
28. Tanford, C., Theory of micelle formation in aqueous solutions. *J. Phys. Chem.* **1974,** *78* (24), 2469-2479.
29. Fuller, N.; Rand, R., The influence of lysolipids on the spontaneous curvature and bending elasticity of phospholipid membranes. *Biophys. J.* **2001,** *81* (1), 243-254.
30. Jørgensen, I. L.; Kemmer, G. C.; Pomorski, T. G., Membrane protein reconstitution into giant unilamellar vesicles: a review on current techniques. *Eur. Biophys. J.* **2017,** *46* (2), 103-119.
31. Dua, J. S., Rana, A. C., Bhandari, A. K., Liposome: methods of preparation and applications. *Int. J. Pharm. Stud. Res.* **2012,** *3* (2), 14-20.
32. van Swaay, D.; deMello, A., Microfluidic methods for forming liposomes. *Lab Chip* **2013,** *13* (5), 752-767.
33. Marsh, D., *Handbook of lipid bilayers*. CRC press: 2019.
34. De Gier, J.; Mandersloot, J.; Van Deenen, L., Lipid composition and permeability of liposomes. *Biochim. Biophys. Acta, Biomembr.* **1968,** *150* (4), 666-675.
35. Blok, M.; Van der Neut-Kok, E.; Van Deenen, L.; De Gier, J., The effect of chain length and lipid phase transitions on the selective permeability properties of liposomes. *Biochim. Biophys. Acta, Biomembr.* **1975,** *406* (2), 187-196.
36. Kranenburg, M.; Smit, B., Phase behavior of model lipid bilayers. *J. Phys. Chem. B* **2005,** *109* (14), 6553-6563.
37. Israelachvili, J. N., Van der Waals forces in biological systems. *Q. Rev. Biophys.* **1973,** *6* (4), 341-387.
38. https://avantilipids.com/tech-support/liposome-preparation/lipids-for-liposome-formation.

39. Marsh, D., Thermodynamics of phospholipid self-assembly. *Biophys. J.* **2012,** *102* (5), 1079-1087.
40. Bangham, A.; De Gier, J.; Greville, G., Osmotic properties and water permeability of phospholipid liquid crystals. *Chem. Phys. Lipids* **1967,** *1* (3), 225-246.
41. Zhang, H., Thin-film hydration followed by extrusion method for liposome preparation. In *Liposomes*, Springer: 2017, pp 17-22.
42. Szoka, F.; Papahadjopoulos, D., Procedure for preparation of liposomes with large internal aqueous space and high capture by reverse-phase evaporation. *Proc. Natl. Acad. Sci.* **1978,** *75* (9), 4194-4198.
43. Zook, J. M.; Vreeland, W. N., Effects of temperature, acyl chain length, and flow-rate ratio on liposome formation and size in a microfluidic hydrodynamic focusing device. *Soft matter* **2010,** *6* (6), 1352-1360.
44. Huang, Z.; Li, X.; Zhang, T.; Song, Y.; She, Z.; Li, J.; Deng, Y., Progress involving new techniques for liposome preparation. *Asian J. Pharm. Sci.* **2014,** *9* (4), 176-182.
45. Laouini, A.; Jaafar-Maalej, C.; Limayem-Blouza, I.; Sfar, S.; Charcosset, C.; Fessi, H., Preparation, characterization and applications of liposomes: state of the art. *J. Colloid Sci. Biotechnol.* **2012,** *1* (2), 147-168.
46. Woodle, M. C.; Papahadjopoulos, D., [9] Liposome preparation and size characterization. *Methods Enzymol.* **1989,** *171*, 193-217.
47. Egelhaaf, S.; Wehrli, E.; Müller, M.; Adrian, M.; Schurtenberger, P., Determination of the size distribution of lecithin liposomes: a comparative study using freeze fracture, cryoelectron microscopy and dynamic light scattering. *J. Microsc.* **1996,** *184* (3), 214-228.
48. Ramos, A. P., Dynamic light scattering applied to nanoparticle characterization. In *Nanocharacterization Techniques*, Elsevier: 2017, pp 99-110.
49. Smith, M. C.; Crist, R. M.; Clogston, J. D.; McNeil, S. E., Zeta potential: a case study of cationic, anionic, and neutral liposomes. *Anal. Bioanal. Chem.* **2017,** *409* (24), 5779-5787.
50. Fröhlich, M.; Brecht, V.; Peschka-Süss, R., Parameters influencing the determination of liposome lamellarity by 31P-NMR. *Chem. Phys. Lipids* **2001,** *109* (1), 103-112.
51. Edwards, K. A.; Baeumner, A. J., Analysis of liposomes. *Talanta* **2006,** *68* (5), 1432-1441.
52. Eloy, J. O.; Claro de Souza, M.; Petrilli, R.; Barcellos, J. P.; Lee, R. J.; Marchetti, J. M., Liposomes as carriers of hydrophilic small molecule drugs: strategies to enhance encapsulation and delivery. *Colloids Surf. B* **2014,** *123*, 345-363.
53. Mitchell, M. J.; Billingsley, M. M.; Haley, R. M.; Wechsler, M. E.; Peppas, N. A.; Langer, R., Engineering precision nanoparticles for drug delivery. *Nat. Rev. Drug Discov.* **2021,** *20* (2), 101-124.
54. Schoenmaker, L.; Witzigmann, D.; Kulkarni, J. A.; Verbeke, R.; Kersten, G.; Jiskoot, W.; Crommelin, D. J., mRNA-lipid nanoparticle COVID-19 vaccines: structure and stability. *Int. J. Pharm.* **2021,** *601*, 120586.
55. Tenchov, R.; Bird, R.; Curtze, A. E.; Zhou, Q., Lipid nanoparticles-From liposomes to mRNA vaccine delivery, a landscape of research diversity and advancement. *ACS Nano* **2021**, 10.1021/acsnano.1c04996.

56. Gregoriadis, G.; Ryman, B. E., Liposomes as carriers of enzymes or drugs: a new approach to the treatment of storage diseases. *Biochem. J.* **1971,** *124* (5), 58P.
57. Gregoriadis, G., Drug entrapment in liposomes. *FEBS Lett.* **1973,** *36* (3), 292-296.
58. Allen, T. M.; Cullis, P. R., Liposomal drug delivery systems: from concept to clinical applications. *Adv. Drug Deliv. Rev.* **2013,** *65* (1), 36-48.
59. Muggia, F.; Hainsworth, J.; Jeffers, S.; Groshen, S.; Tan, M.; Greco, F. In *Liposomal doxorubicin (Doxil) is active against refractory ovarian cancer*, Proc. Am. Soc. Clin. Oncol., 1996; p 287.
60. Davidson, R. N.; Martino, L. D.; Gradoni, L.; Giacchino, R.; Russo, R.; Gaeta, G. B.; Pempinello, R.; Scott, S.; Raimondi, F.; Cascio, A., et al., Liposomal amphotericin B (AmBisome) in Mediterranean visceral leishmaniasis: a multi-centre trial. *QJM* **1994,** *87* (2), 75-81.
61. Chang, C.-C.; Liu, D.-Z.; Lin, S.-Y.; Liang, H.-J.; Hou, W.-C.; Huang, W.-J.; Chang, C.-H.; Ho, F.-M.; Liang, Y.-C., Liposome encapsulation reduces cantharidin toxicity. *Food Chem. Toxicol.* **2008,** *46* (9), 3116-3121.
62. Chang, H.-I.; Yeh, M.-K., Clinical development of liposome-based drugs: formulation, characterization, and therapeutic efficacy. *Int. J. Nanomed.* **2012,** *7*, 49-60.
63. Allen, T. M.; Hansen, C. B.; de Menezes, D. E. L., Pharmacokinetics of long-circulating liposomes. *Adv. Drug Deliv. Rev.* **1995,** *16* (2), 267-284.
64. Gabizon, A. A., Selective tumor localization and improved therapeutic index of anthracyclines encapsulated in long-circulating liposomes. *Cancer Res.* **1992,** *52* (4), 891-896.
65. Maruyama, K., Intracellular targeting delivery of liposomal drugs to solid tumors based on EPR effects. *Adv. Drug Deliv. Rev.* **2011,** *63* (3), 161-169.
66. Lentz, B. R.; Carpenter, T. J.; Alford, D. R., Spontaneous fusion of phosphatidylcholine small unilamellar vesicles in the fluid phase. *Biochemistry* **1987,** *26* (17), 5389-5397.
67. Gaber, B. P.; Sheridan, J. P., Kinetic and thermodynamic studies of the fusion of small unilamellar phospholipid vesicles. *Biochim. Biophys. Acta, Biomembr.* **1982,** *685* (1), 87-93.
68. Liu, D.; Mori, A.; Huang, L., Role of liposome size and RES blockade in controlling biodistribution and tumor uptake of GM1-containing liposomes. *Biochim. Biophys. Acta, Biomembr.* **1992,** *1104* (1), 95-101.
69. Gabizon, A.; Papahadjopoulos, D., Liposome formulations with prolonged circulation time in blood and enhanced uptake by tumors. *Proc. Natl. Acad. Sci.* **1988,** *85* (18), 6949-6953.
70. Barenholz, Y. C., Doxil®—the first FDA-approved nano-drug: lessons learned. *J. Control. Release* **2012,** *160* (2), 117-134.
71. Sercombe, L.; Veerati, T.; Moheimani, F.; Wu, S. Y.; Sood, A. K.; Hua, S., Advances and challenges of liposome assisted drug delivery. *Front. Pharmacol.* **2015,** *6*, 286.
72. Nakamura, Y.; Mochida, A.; Choyke, P. L.; Kobayashi, H., Nanodrug delivery: is the enhanced permeability and retention effect sufficient for curing cancer? *Bioconjugate Chem.* **2016,** *27* (10), 2225-2238.
73. Immordino, M. L.; Dosio, F.; Cattel, L., Stealth liposomes: review of the basic science, rationale, and clinical applications, existing and potential. *Int. J. Nanomed.* **2006,** *1* (3), 297.

74. Veronese, F. M., *PEGylated protein drugs: basic science and clinical applications*. Springer: 2009.
75. Ceh, B.; Winterhalter, M.; Frederik, P. M.; Vallner, J. J.; Lasic, D. D., Stealth® liposomes: from theory to product. *Adv. Drug Deliv. Rev.* **1997,** *24* (2-3), 165-177.
76. Paszko, E.; Senge, M. O., Immunoliposomes. *Curr Med Chem* **2012,** *19* (31), 5239-5277.
77. Weissmann, G.; Bloomgarden, D.; Kaplan, R.; Cohen, C.; Hoffstein, S.; Collins, T.; Gotlieb, A.; Nagle, D., A general method for the introduction of enzymes, by means of immunoglobulin-coated liposomes, into lysosomes of deficient cells. *Proc. Natl. Acad. Sci.* **1975,** *72* (1), 88-92.
78. Scharner, J.; Qi, S.; Rigo, F.; Bennett, C. F.; Krainer, A. R., Delivery of GalNAc-Conjugated Splice-Switching ASOs to Non-hepatic Cells through Ectopic Expression of Asialoglycoprotein Receptor. *Mol. Ther. Nucleic Acids* **2019,** *16*, 313-325.
79. D'souza, A. A.; Devarajan, P. V., Asialoglycoprotein receptor mediated hepatocyte targeting—Strategies and applications. *J. Control. Release* **2015,** *203*, 126-139.
80. Kelemen, L. E., The role of folate receptor α in cancer development, progression and treatment: cause, consequence or innocent bystander? *Int. J. Cancer* **2006,** *119* (2), 243-250.
81. Zwicke, G. L.; Ali Mansoori, G.; Jeffery, C. J., Utilizing the folate receptor for active targeting of cancer nanotherapeutics. *Nano Rev.* **2012,** *3* (1), 18496.
82. Snyder, E. L.; Dowdy, S. F., Cell penetrating peptides in drug delivery. *Pharm. Res.* **2004,** *21* (3), 389-393.
83. de Jong, H.; Bonger, K. M.; Löwik, D. W., Activatable cell-penetrating peptides: 15 years of research. *RSC Chem. Biol.* **2020,** *1* (4), 192-203.
84. Alam, S.; Mattern-Schain, S. I.; Best, M. D., Targeting and triggered release using lipid-based supramolecular assemblies as medicinal nanocarriers. In *Comprehensive Supramolecular Chemistry II*, Atwood, J. L., Ed. Elsevier: Oxford, 2017, https://doi.org/10.1016/B978-0-12-409547-2.12540-5pp 329-364.
85. Paliwal, S. R.; Paliwal, R.; Vyas, S. P., A review of mechanistic insight and application of pH-sensitive liposomes in drug delivery. *Drug Deliv.* **2015,** *22* (3), 231-242.
86. McCarley, R. L., Redox-responsive delivery systems. *Annu. Rev. Anal. Chem.* **2012,** *5*, 391-411.
87. Fouladi, F.; Steffen, K. J.; Mallik, S., Enzyme-responsive liposomes for the delivery of anticancer drugs. *Bioconjugate Chem.* **2017,** *28* (4), 857-868.
88. Lou, J.; Carr, A. J.; Watson, A. J.; Mattern-Schain, S. I.; Best, M. D., Calcium-responsive liposomes via a synthetic lipid switch. *Chem. Eur. J.* **2018,** *24* (14), 3599-3607.
89. Zhang, X.; Alves, D. S.; Lou, J.; Hill, S. D.; Barrera, F. N.; Best, M. D., Boronic acid liposomes for cellular delivery and content release driven by carbohydrate binding. *Chem. Commun.* **2018,** *54* (48), 6169-6172.
90. Lou, J.; Zhang, X.; Best, M. D., Lipid switches: Stimuli-responsive liposomes through conformational isomerism driven by molecular recognition. *Chem. Eur. J.* **2019,** *25* (1), 20-25.
91. Shum, P.; Kim, J.-M.; Thompson, D. H., Phototriggering of liposomal drug delivery systems. *Adv. Drug Deliv. Rev.* **2001,** *53* (3), 273-284.
92. Leung, S. J.; Romanowski, M., Light-activated content release from liposomes. *Theranostics*

2012, *2* (10), 1020.
93. Puri, A., Phototriggerable liposomes: current research and future perspectives. *Pharmaceutics* **2014,** *6* (1), 1-25.
94. Kneidl, B.; Peller, M.; Winter, G.; Lindner, L. H.; Hossann, M., Thermosensitive liposomal drug delivery systems: state of the art review. *Int. J. Nanomed.* **2014,** *9*, 4387.
95. Dicheva, B. M.; Koning, G. A., Targeted thermosensitive liposomes: an attractive novel approach for increased drug delivery to solid tumors. *Expert Opin. Drug Deliv.* **2014,** *11* (1), 83-100.
96. Sirsi, S. R.; Borden, M. A., State-of-the-art materials for ultrasound-triggered drug delivery. *Adv. Drug Deliv. Rev.* **2014,** *72*, 3-14.
97. Boissenot, T.; Bordat, A.; Fattal, E.; Tsapis, N., Ultrasound-triggered drug delivery for cancer treatment using drug delivery systems: from theoretical considerations to practical applications. *J. Control. Release* **2016,** *241*, 144-163.
98. Cullis, P. t.; Kruijff, B. d., Lipid polymorphism and the functional roles of lipids in biological membranes. *Biochim. Biophys. Acta, Biomembr.* **1979,** *559* (4), 399-420.
99. Pedersen, P. J.; Adolph, S. K.; Subramanian, A. K.; Arouri, A.; Andresen, T. L.; Mouritsen, O. G.; Madsen, R.; Madsen, M. W.; Peters, G. H.; Clausen, M. H., Liposomal formulation of retinoids designed for enzyme triggered release. *J. Med. Chem.* **2010,** *53* (9), 3782-3792.
100. Arouri, A.; Mouritsen, O. G., Anticancer double lipid prodrugs: liposomal preparation and characterization. *J. Liposome Res.* **2011,** *21* (4), 296-305.
101. Arouri, A.; Mouritsen, O. G., Phospholipase A(2)-susceptible liposomes of anticancer double lipid-prodrugs. *Eur. J. Pharm. Sci.* **2012,** *45* (4), 408-420.
102. Pedersen, P. J.; Christensen, M. S.; Ruysschaert, T.; Linderoth, L.; Andresen, T. L.; Melander, F.; Mouritsen, O. G.; Madsen, R.; Clausen, M. H., Synthesis and biophysical characterization of chlorambucil anticancer ether lipid prodrugs. *J. Med. Chem.* **2009,** *52* (10), 3408-3415.
103. Pedersen, P. J.; Viart, H. M.; Melander, F.; Andresen, T. L.; Madsen, R.; Clausen, M. H., Synthesis of tocopheryl succinate phospholipid conjugates and monitoring of phospholipase A(2) activity. *Bioorg. Med. Chem.* **2012,** *20* (13), 3972-3978.
104. Bayer, A. M.; Alam, S.; Mattern-Schain, S. I.; Best, M. D., Triggered liposomal release through a synthetic phosphatidylcholine analogue bearing a photocleavable moiety embedded within the sn-2 acyl chain. *Chem. Eur. J.* **2014,** *20* (12), 3350-3357.
105. Sun, Y.; Ji, Y.; Yu, H.; Wang, D.; Cao, M.; Wang, J., Near-infrared light-sensitive liposomes for controlled release. *RSC Adv.* **2016,** *6* (84), 81245-81249.
106. Mbarek, A.; Moussa, G.; Leblond Chain, J., Pharmaceutical applications of molecular tweezers, clefts and clips. *Molecules* **2019,** *24* (9), 1803.
107. Noble, G. T.; Stefanick, J. F.; Ashley, J. D.; Kiziltepe, T.; Bilgicer, B., Ligand-targeted liposome design: challenges and fundamental considerations. *Trends Biotechnol.* **2014,** *32* (1), 32-45.
108. Deshpande, P. P.; Biswas, S.; Torchilin, V. P., Current trends in the use of liposomes for tumor targeting. *Nanomedicine* **2013,** *8* (9), 1509-1528.
109. Pattni, B. S.; Chupin, V. V.; Torchilin, V. P., New developments in liposomal drug delivery. *Chem. Rev.* **2015,** *115* (19), 10938-10966.

110. Gillies, R. J.; Liu, Z.; Bhujwalla, Z., P-31-MRS measurements of extracellular pH of tumors using 3-aminophosphonate. *Am. J. Physiol.* **1994,** *267* (1), C195-C203.
111. van Sluis, R.; Bhujwalla, Z. M.; Raghunand, N.; Ballesteros, P.; Alvarez, J.; Cerdan, S.; Galons, J. P.; Gillies, R. J., In vivo imaging of extracellular pH using 1H MRSI. *Magn. Res. Med.* **1999,** *41* (4), 743-750.
112. Orrenius, S.; Gogvadze, V.; Zhivotovsky, B., Calcium and mitochondria in the regulation of cell death. *Biochem. Biophys. Res. Commun.* **2015,** *460* (1), 72-81.
113. Tu, M. K.; Levin, J. B.; Hamilton, A. M.; Borodinsky, L. N., Calcium signaling in skeletal muscle development, maintenance and regeneration. *Cell Calcium* **2016,** *59* (2-3), 91-97.
114. Ghosh, A.; Greenberg, M. E., Calcium signaling in neurons - Molecular mechanisms and cellular consequences. *Science* **1995,** *268* (5208), 239-247.
115. Grienberger, C.; Konnerth, A., Imaging calcium in neurons. *Neuron* **2012,** *73* (5), 862-885.
116. Gallo, E. M.; Cante-Barrett, K.; Crabtree, G. R., Lymphocyte calcium signaling from membrane to nucleus. *Nat. Immunol.* **2006,** *7* (1), 25-32.
117. Peacock, M., Calcium metabolism in health and disease. *Clin. J. Am. Soc. Nephrol.* **2010,** *5 Suppl 1*, S23-30.
118. Robertson, W. G.; Marshall, R. W.; Walser, M., Calcium measurements in serum and plasma—Total and ionized. *CRC Critical Reviews in Clinical Laboratory Sciences* **1979,** *11* (3), 271-304.
119. Prevarskaya, N.; Skryma, R.; Shuba, Y., Calcium in tumour metastasis: new roles for known actors. *Nat. Rev. Cancer* **2011,** *11* (8), 609-618.
120. Clapham, D. E., Calcium signaling. *Cell* **2007,** *131* (6), 1047-1058.
121. Stutzmann, G. E.; Mattson, M. P., Endoplasmic reticulum Ca2+ handling in excitable cells in health and disease. *Pharmacol. Rev.* **2011,** *63* (3), 700-727.
122. Verkhratsky, A., Physiology and pathophysiology of the calcium store in the endoplasmic reticulum of neurons. *Physiol. Rev.* **2005,** *85* (1), 201-279.
123. Bezprozvanny, I.; Mattson, M. P., Neuronal calcium mishandling and the pathogenesis of Alzheimer's disease. *Trends Neurosci.* **2008,** *31* (9), 454-463.
124. Kruman, II; Pedersen, W. A.; Springer, J. E.; Mattson, M. P., ALS-linked Cu/Zn-SOD mutation increases vulnerability of motor neurons to excitotoxicity by a mechanism involving increased oxidative stress and perturbed calcium homeostasis. *Exp. Neurol.* **1999,** *160* (1), 28-39.
125. Leal, S. S.; Gomes, C. M., Calcium dysregulation links ALS defective proteins and motor neuron selective vulnerability. *Front. Cell. Neurosci.* **2015,** *9*.
126. Ong, D. S. T.; Mu, T.-W.; Palmer, A. E.; Kelly, J. W., Endoplasmic reticulum Ca2+ increases enhance mutant glucocerebrosidase proteostasis. *Nat. Chem. Biol.* **2010,** *6* (6), 424-432.
127. Vitner, E. B.; Platt, F. M.; Futerman, A. H., Common and uncommon pathogenic cascades in lysosomal storage diseases. *J. Biol. Chem.* **2010,** *285* (27), 20423-20427.
128. MacDonald, J. F.; Xiong, Z. G.; Jackson, M. F., Paradox of Ca2+ signaling, cell death and stroke. *Trends Neurosci.* **2006,** *29* (2), 75-81.
129. Brochet, M.; Billker, O., Calcium signalling in malaria parasites. *Mol. Microbiol.* **2016,** *100* (3), 397-408.

130. Ward, P.; Equinet, L.; Packer, J.; Doerig, C., Protein kinases of the human malaria parasite Plasmodium falciparum: the kinome of a divergent eukaryote. *BMC Genomics* **2004,** *5*.
131. Glushakova, S.; Lizunov, V.; Blank, P. S.; Melikov, K.; Humphrey, G.; Zimmerberg, J., Cytoplasmic free Ca2+ is essential for multiple steps in malaria parasite egress from infected erythrocytes. *Malaria J.* **2013,** *12*, 12:41.
132. Tanabe, K.; Mikkelsen, R. B.; Wallach, D. F. H., Calcium-transport of plasmodium-chabaudi-infected erythrocytes. *J. Cell Biol.* **1982,** *93* (3), 680-684.
133. Krungkrai, J.; Yuthavong, Y., Enhanced Ca2+ uptake by mouse erythrocytes in malarial (plasmodium-berghei) infection. *Molec. Biochem. Parasitol.* **1983,** *7* (3), 227-235.
134. Wasserman, M.; Chaparro, J., Intraerythrocytic calcium chelators inhibit the invasion of Plasmodium falciparum. *Parasitol. Res.* **1996,** *82* (2), 102-107.
135. Garg, S.; Agarwal, S.; Kumar, S.; Yazdani, S. S.; Chitnis, C. E.; Singh, S., Calcium-dependent permeabilization of erythrocytes by a perforin-like protein during egress of malaria parasites. *Nat. Commun.* **2013,** *4*.
136. Sundaramoorthy, P.; Sim, J. J.; Jang, Y.-S.; Mishra, S. K.; Jeong, K.-Y.; Mander, P.; Chul, O. B.; Shim, W.-S.; Oh, S. H.; Nam, K.-Y., et al., Modulation of intracellular calcium levels by calcium lactate affects colon cancer cell motility through calcium-dependent calpain. *PLoS ONE* **2015,** *10* (1), e0116984.
137. Prevarskaya, N.; Skryma, R.; Shuba, Y., Targeting Ca2+ transport in cancer: close reality or long perspective? *Expert Opin. Ther. Targets* **2013,** *17* (3), 225-241.
138. Chan, K. T.; Bennin, D. A.; Huttenlocher, A., Regulation of adhesion dynamics by calpain-mediated proteolysis of focal adhesion kinase (FAK). *J. Biol. Chem.* **2010,** *285* (15), 11418-11426.
139. Viricel, W.; Mbarek, A.; Leblond, J., Switchable lipids: Conformational change for fast pH-triggered cytoplasmic delivery. *Angew. Chem. Int. Ed. Engl.* **2015,** *54* (43), 12743-12747.
140. Viricel, W.; Poirier, S.; Mbarek, A.; Derbali, R.; Mayer, G.; Leblond, J., Cationic switchable lipids: pH-triggered molecular switch for siRNA delivery. *Nanoscale* **2017,** *9* (1), 31-36.
141. Yaroslavov, A. A.; Sybachin, A. V.; Zaborova, O. V.; Migulin, V. A.; Samoshin, V. V.; Ballauff, M.; Kesselman, E.; Schmidt, J.; Talmon, Y.; Menger, F. M., Capacious and programmable multi-liposomal carriers. *Nanoscale* **2015,** *7* (5), 1635-1641.
142. Plaunt, A. J.; Harmatys, K. M.; Hendrie, K. A.; Musso, A. J.; Smith, B. D., Chemically triggered release of 5-aminolevulinic acid from liposomes. *RSC Adv.* **2014,** *4* (101), 57983-57990.
143. Grynkiewicz, G.; Poenie, M.; Tsien, R. Y., A new generation of Ca2+ indicators with greatly improved fluorescence properties. *J. Biol. Chem.* **1985,** *260* (6), 3440-3450.
144. Bannwarth, M.; Corrêa, I. R.; Sztretye, M.; Pouvreau, S.; Fellay, C.; Aebischer, A.; Royer, L.; Ríos, E.; Johnsson, K., Indo-1 derivatives for local calcium sensing. *ACS Chem. Biol.* **2009,** *4* (3), 179-190.
145. McCalmont, W. F.; Heady, T. N.; Patterson, J. R.; Lindenmuth, M. A.; Haverstick, D. M.; Gray, L. S.; Macdonald, T. L., Design, synthesis, and biological evaluation of novel T-Type calcium channel antagonists. *Bioorg. Med. Chem. Lett.* **2004,** *14* (14), 3691-3695.
146. Tsien, R. Y., Fluorescent probes of cell signaling. *Annu. Rev. Neurosci.* **1989,** *12* (1), 227-253.

147. Liu, Q.; Du, H.; Ren, X.; Bian, W.; Fan, L.; Shuang, S.; Dong, C.; Hu, Q.; Choi, M. M., Design of ratiometric emission probe with visible light excitation for determination of Ca2+ in living cells. *Anal. Chem.* **2014,** *86* (16), 8025-8030.
148. Greenspan, P.; Mayer, E. P.; Fowler, S. D., Nile red: a selective fluorescent stain for intracellular lipid droplets. *J. Cell. Biol.* **1985,** *100* (3), 965-973.
149. Liang, X.; Yue, X.; Dai, Z.; Kikuchi, J.-i., Photoresponsive liposomal nanohybrid cerasomes. *Chem. Commun.* **2011,** *47* (16), 4751-4753.
150. Vichai, V.; Kirtikara, K., Sulforhodamine B colorimetric assay for cytotoxicity screening. *Nat. Protoc.* **2006,** *1*, 1112.
151. Humphrey, S. J.; James, D. E.; Mann, M., Protein phosphorylation: a major switch mechanism for metabolic regulation. *Trends Endocrinol. Metab.* **2015,** *26* (12), 676-687.
152. Wilson, D. F., Oxidative phosphorylation: regulation and role in cellular and tissue metabolism. *J. Physiol.* **2017,** *595* (23), 7023-7038.
153. Zimmermann, H., Signalling via ATP in the nervous system. *Trends Neurosci.* **1994,** *17* (10), 420-426.
154. El-Moatassim, C.; Dornand, J.; Mani, J.-C., Extracellular ATP and cell signalling. *Biochim. Biophys. Acta, Mol. Cell Res.* **1992,** *1134* (1), 31-45.
155. Elston, T.; Wang, H.; Oster, G., Energy transduction in ATP synthase. *Nature* **1998,** *391* (6666), 510-513.
156. Martin, W. F.; Thauer, R. K., Energy in ancient metabolism. *Cell* **2017,** *168* (6), 953-955.
157. Nichols, C. G., K ATP channels as molecular sensors of cellular metabolism. *Nature* **2006,** *440* (7083), 470-476.
158. Ashcroft, S. J.; Ashcroft, F. M., Properties and functions of ATP-sensitive K-channels. *Cell. Signal.* **1990,** *2* (3), 197-214.
159. Bell, S. P.; Stillman, B., ATP-dependent recognition of eukaryotic origins of DNA replication by a multiprotein complex. *Nature* **1992,** *357* (6374), 128-134.
160. Vincent, J. A.; Kwong, T. J.; Tsukiyama, T., ATP-dependent chromatin remodeling shapes the DNA replication landscape. *Nat. Struct. Mol. Biol.* **2008,** *15* (5), 477-484.
161. Gilbert, S. M.; Oliphant, C. J.; Hassan, S.; Peille, A. L.; Bronsert, P.; Falzoni, S.; Di Virgilio, F.; McNulty, S.; Lara, R., ATP in the tumour microenvironment drives expression of nfP2X7, a key mediator of cancer cell survival. *Oncogene* **2019,** *38* (2), 194-208.
162. Zheng, L. M.; Zychlinsky, A.; Liu, C. C.; Ojcius, D. M.; Young, J. D., Extracellular ATP as a trigger for apoptosis or programmed cell death. *J. Cell Biol.* **1991,** *112* (2), 279-288.
163. Di Virgilio, F.; Dal Ben, D.; Sarti, A. C.; Giuliani, A. L.; Falzoni, S., The P2X7 receptor in infection and inflammation. *Immunity* **2017,** *47* (1), 15-31.
164. Di Virgilio, F.; Sarti, A. C.; Falzoni, S.; De Marchi, E.; Adinolfi, E., Extracellular ATP and P2 purinergic signalling in the tumour microenvironment. *Nat. Rev. Cancer* **2018,** *18* (10), 601-618.
165. Sun, W.; Gu, Z., ATP-responsive drug delivery systems. *Expert Opin. Drug. Deliv.* **2016,** *13* (3), 311-314.
166. He, Q.; Chen, J.; Yan, J.; Cai, S.; Xiong, H.; Liu, Y.; Peng, D.; Mo, M.; Liu, Z., Tumor

microenvironment responsive drug delivery systems. *Asian J. Pharm. Sci.* **2020,** *15* (4), 416-448.

167. Sameiyan, E.; Bagheri, E.; Dehghani, S.; Ramezani, M.; Alibolandi, M.; Abnous, K.; Taghdisi, S. M., Aptamer-based ATP-responsive delivery systems for cancer diagnosis and treatment. *Acta biomater.* **2021,** *123*, 110-122.
168. Chen, W.-H.; Yu, X.; Liao, W.-C.; Sohn, Y. S.; Cecconello, A.; Kozell, A.; Nechushtai, R.; Willner, I., ATP-responsive aptamer-based metal–organic framework nanoparticles (NMOFs) for the controlled release of loads and drugs. *Adv. Funct. Mater.* **2017,** *27* (37), 1702102.
169. Liao, W.-C.; Sohn, Y. S.; Riutin, M.; Cecconello, A.; Parak, W. J.; Nechushtai, R.; Willner, I., The application of stimuli-responsive VEGF- and ATP-aptamer-based microcapsules for the controlled release of an anticancer drug, and the selective targeted cytotoxicity toward cancer cells. *Adv. Funct. Mater.* **2016,** *26* (24), 4262-4273.
170. Mo, R.; Jiang, T.; Gu, Z., Enhanced anticancer efficacy by ATP-mediated liposomal drug delivery. *Angew. Chem. Int. Ed.* **2014,** *53* (23), 5815-5820.
171. Rice, D. R.; Clear, K. J.; Smith, B. D., Imaging and therapeutic applications of zinc(ii)-dipicolylamine molecular probes for anionic biomembranes. *Chem. Commun.* **2016,** *52* (57), 8787-8801.
172. Ngo, H. T.; Liu, X.; Jolliffe, K. A., Anion recognition and sensing with Zn (II)–dipicolylamine complexes. *Chem. Soc. Rev.* **2012,** *41* (14), 4928-4965.
173. Smith, B. D.; Anslyn, E.; Gokel, G.; Kubik, S.; Wang, B.; Hong, J.-I.; Hargrove, A.; Schmuck, C.; Rotello, D.; Gale, P., *Synthetic receptors for biomolecules: Design principles and applications*. Royal Society of Chemistry: 2015.
174. Williams, F. J.; Fiedler, D., A fluorescent sensor and gel stain for detection of pyrophosphorylated proteins. *ACS Chem. Biol.* **2015,** *10* (9), 1958-1963.
175. van den Brink-van der Laan, E. V.; Killian, J. A.; de Kruijff, B., Nonbilayer lipids affect peripheral and integral membrane proteins via changes in the lateral pressure profile. *Biochim. Biophys. Acta* **2004,** *1666* (1-2), 275-288.
176. Allen, T. M., Liposomal drug formulations. *Drugs* **1998,** *56* (5), 747-756.
177. Chen, Z.-P.; Levy, A.; Lightman, S. L., Nucleotides as extracellular signalling molecules. *J. Neuroendocrinol.* **1995,** *7* (2), 83-96.
178. Traut, T. W., Physiological concentrations of purines and pyrimidines. *Mol. Cell. Biochem.* **1994,** *140* (1), 1-22.
179. Zima, A. V.; Blatter, L. A., Inositol-1, 4, 5-trisphosphate-dependent Ca2+ signalling in cat atrial excitation–contraction coupling and arrhythmias. *J. Physiol.* **2004,** *555* (3), 607-615.
180. Jayaraman, T.; Ondriasova, E.; Ondrias, K.; Harnick, D. J.; Marks, A. R., The inositol 1, 4, 5-trisphosphate receptor is essential for T-cell receptor signaling. *Proc. Natl. Acad. Sci.* **1995,** *92* (13), 6007-6011.
181. Hughes, A.; Takemura, H.; Putney, J., Kinetics of inositol 1, 4, 5-trisphosphate and inositol cyclic 1: 2, 4, 5-trisphosphate metabolism in intact rat parotid acinar cells. Relationship to calcium signalling. *J. Biol. Chem.* **1988,** *263* (21), 10314-10319.
182. Jose, D. A.; Mishra, S.; Ghosh, A.; Shrivastav, A.; Mishra, S. K.; Das, A., Colorimetric sensor

for ATP in aqueous solution. *Org. Lett.* **2007,** *9* (10), 1979-1982.
183. Vance, J. A.; Devaraj, N. K., Membrane mimetic chemistry in artificial cells. *J. Am. Chem. Soc.* **2021,** *143* (22), 8223-8231.
184. Lasic, D. D.; Templeton, N., Liposomes in gene therapy. *Adv. Drug Deliv. Rev.* **1996,** *20* (2-3), 221-266.
185. Miller, A. D., Cationic liposomes for gene therapy. *Angew. Chem. Int. Ed.* **1998,** *37* (13-14), 1768-1785.
186. Allen, T., *Calcein as a tool in liposome methodology*. CRC Press, Boca Raton, Florida: 1984.
187. Ojida, A.; Park, S.-k.; Mito-Oka, Y.; Hamachi, I., Efficient fluorescent ATP-sensing based on coordination chemistry under aqueous neutral conditions. *Tetrahedron Lett.* **2002,** *43* (35), 6193-6195.
188. Fatouros, D. G.; Antimisiaris, S. G., Effect of amphiphilic drugs on the stability and zeta-potential of their liposome formulations: A study with prednisolone, diazepam, and griseofulvin. *J. Colloid Interface Sci.* **2002,** *251* (2), 271-277.
189. Farshbaf, S.; Anzenbacher, P., Fluorimetric sensing of ATP in water by an imidazolium hydrazone based sensor. *Chem. Commun.* **2019,** *55* (12), 1770-1773.
190. Holmsen, H.; Setkowsky, C. A.; Day, H. J., Effects of antimycin and 2-deoxyglucose on adenine nucleotides in human platelets. Role of metabolic adenosine triphosphate in primary aggregation, secondary aggregation and shape change of platelets. *Biochem. J.* **1974,** *144* (2), 385-396.
191. Ke, R.; Xu, Q.; Li, C.; Luo, L.; Huang, D., Mechanisms of AMPK in the maintenance of ATP balance during energy metabolism. *Cell Biol. Int.* **2018,** *42* (4), 384-392.
192. Vultaggio-Poma, V.; Sarti, A. C.; Di Virgilio, F., Extracellular ATP: A feasible target for cancer therapy. *Cells* **2020,** *9* (11).
193. Dosch, M.; Gerber, J.; Jebbawi, F.; Beldi, G., Mechanisms of ATP release by inflammatory cells. *Int. J. Mol. Sci.* **2018,** *19* (4).
194. van der Woude, I.; Visser, H. W.; ter Beest, M. B.; Wagenaar, A.; Ruiters, M. H.; Engberts, J. B.; Hoekstra, D., Parameters influencing the introduction of plasmid DNA into cells by the use of synthetic amphiphiles as a carrier system. *Biochim. Biophys. Acta, Biomembr.* **1995,** *1240* (1), 34-40.
195. Ong, W.; Yang, Y.; Cruciano, A. C.; McCarley, R. L., Redox-triggered contents release from liposomes. *J. Am. Chem. Soc.* **2008,** *130* (44), 14739-14744.
196. Wells, A.; Grandis, J. R., Phospholipase C-γ1 in tumor progression. *Clin. Exp. Metastasis* **2003,** *20* (4), 285-290.
197. Magno, L.; Lessard, C. B.; Martins, M.; Lang, V.; Cruz, P.; Asi, Y.; Katan, M.; Bilsland, J.; Lashley, T.; Chakrabarty, P., Alzheimer's disease phospholipase C-gamma-2 (PLCG2) protective variant is a functional hypermorph. *Alzheimer's Res. Ther.* **2019,** *11* (1), 1-11.
198. Yang, Y. R.; Kang, D.-S.; Lee, C.; Seok, H.; Follo, M. Y.; Cocco, L.; Suh, P.-G., Primary phospholipase C and brain disorders. *Adv. Biol. Regul.* **2016,** *61*, 80-85.
199. Veras, F. P.; Peres, R. S.; Saraiva, A. L.; Pinto, L. G.; Louzada-Junior, P.; Cunha, T. M.; Paschoal, J. A.; Cunha, F. Q.; Alves-Filho, J. C., Fructose 1, 6-bisphosphate, a high-energy

intermediate of glycolysis, attenuates experimental arthritis by activating anti-inflammatory adenosinergic pathway. *Sci. Rep.* **2015,** *5* (1), 1-11.

200. Niikura, K.; Metzger, A.; Anslyn, E. V., Chemosensor ensemble with selectivity for inositol-trisphosphate. *J. Am. Chem. Soc.* **1998,** *120* (33), 8533-8534.
201. Oh, D. J.; Ahn, K. H., Fluorescent sensing of IP3 with a trifurcate Zn (II)-containing chemosensing ensemble system. *Org. Lett.* **2008,** *10* (16), 3539-3542.
202. Do-Thanh, C.-L.; Rowland, M. M.; Best, M. D., Fluorescent bis-cyclen tweezer receptors for inositol (1, 4, 5)-trisphosphate. *Tetrahedron* **2011,** *67* (21), 3803-3808.
203. Ozpolat, B.; Sood, A. K.; Lopez-Berestein, G., Liposomal siRNA nanocarriers for cancer therapy. *Adv. Drug Deliv. Rev.* **2014,** *66*, 110-116.
204. Chen, R. F.; Knutson, J. R., Mechanism of fluorescence concentration quenching of carboxyfluorescein in liposomes: energy transfer to nonfluorescent dimers. *Anal. Biochem.* **1988,** *172* (1), 61-77.
205. Meers, P., Enzyme-activated targeting of liposomes. *Adv. Drug Deliv. Rev.* **2001,** *53* (3), 265-272.
206. Huang, Z.; Szoka Jr, F. C., Bioresponsive liposomes and their use for macromolecular delivery. In *Liposome technology*, CRC Press: 2018, pp 187-218.
207. Andresen, T. L.; Thompson, D. H.; Kaasgaard, T., Enzyme-triggered nanomedicine: Drug release strategies in cancer therapy (Invited Review). *Mol. Membr. Biol.* **2010,** *27* (7), 353-363.
208. Zhu, L.; Kate, P.; Torchilin, V. P., Matrix metalloprotease 2-responsive multifunctional liposomal nanocarrier for enhanced tumor targeting. *ACS Nano* **2012,** *6* (4), 3491-3498.
209. Elegbede, A. I.; Banerjee, J.; Hanson, A. J.; Tobwala, S.; Ganguli, B.; Wang, R.; Lu, X.; Srivastava, D. K.; Mallik, S., Mechanistic studies of the triggered release of liposomal contents by matrix metalloproteinase-9. *J. Am. Chem. Soc.* **2008,** *130* (32), 10633-10642.
210. Menger, F.; Johnston Jr, D., Specific enzyme-induced decapsulation. *J. Am. Chem. Soc.* **1991,** *113* (14), 5467-5468.
211. Linderoth, L.; Peters, G. H.; Madsen, R.; Andresen, T. L., Drug delivery by an enzyme-mediated cyclization of a lipid prodrug with unique bilayer-formation properties. *Angew. Chem. Int. Ed.* **2009,** *48* (10), 1823-1826.
212. Foged, C.; Nielsen, H. M.; Frokjaer, S., Liposomes for phospholipase A2 triggered siRNA release: Preparation and in vitro test. *Int. J. Pharm.* **2007,** *331* (2), 160-166.
213. Thamphiwatana, S.; Gao, W.; Pornpattananangkul, D.; Zhang, Q.; Fu, V.; Li, J.; Li, J.; Obonyo, M.; Zhang, L., Phospholipase A2-responsive antibiotic delivery via nanoparticle-stabilized liposomes for the treatment of bacterial infection. *J. Mater. Chem. B* **2014,** *2* (46), 8201-8207.
214. Davis, S.; Szoka, F., Cholesterol phosphate derivatives: synthesis and incorporation into a phosphatase and calcium-sensitive triggered release liposome. *Bioconjugate Chem.* **1998,** *9* (6), 783-792.
215. Cohen, R. B.; Nachlas, M. M.; Seligman, A. M., Histochemical demonstration of esterase in malignant tumors. *Cancer Res.* **1951,** *11* (9), 709.
216. Dong, H.; Pang, L.; Cong, H.; Shen, Y.; Yu, B., Application and design of esterase-responsive

nanoparticles for cancer therapy. *Drug Deliv.* **2019,** *26* (1), 416-432.
217. Yano, H.; Kayukawa, S.; Iida, S.; Nakagawa, C.; Oguri, T.; Sanda, T.; Ding, J.; Mori, F.; Ito, A.; Ri, M., et al., Overexpression of carboxylesterase-2 results in enhanced efficacy of topoisomerase I inhibitor, irinotecan (CPT-11), for multiple myeloma. *Cancer Sci.* **2008,** *99* (11), 2309-2314.
218. Rainier, S.; Bui, M.; Mark, E.; Thornas, D.; Tokarz, D.; Ming, L.; Delaney, C.; Richardson, R. J.; Albers, J. W.; Matsunami, N., et al., Neuropathy target esterase gene mutations cause motor neuron disease. *Am. J. Hum. Gen.* **2008,** *82* (3), 780-785.
219. Kunkel, H. G.; Ward, S. M., Plasma esterase activity in patients with liver disease and the nephrotic syndrome. *J. Exp. Med.* **1947,** *86* (4), 325-337.
220. Kaduszkiewicz, H.; Zimmermann, T.; Beck-Bornholdt, H. P.; van den Bussche, H., Cholinesterase inhibitors for patients with Alzheimer's disease: systematic review of randomised clinical trials. *Brit. Med. J.* **2005,** *331* (7512), 321-323.
221. Ostman, A.; Hellberg, C.; Bohmer, F. D., Protein-tyrosine phosphatases and cancer. *Nat. Rev. Cancer* **2006,** *6* (4), 307-320.
222. Zhao, S.; Sedwick, D.; Wang, Z., Genetic alterations of protein tyrosine phosphatases in human cancers. *Oncogene* **2015,** *34* (30), 3885-3894.
223. Kim, M.; Baek, M.; Kim, D. J., Protein tyrosine signaling and its potential therapeutic implications in carcinogenesis. *Curr. Pharm. Des.* **2017,** *23* (29), 4226-4246.
224. Kendall, M. J.; Cockel, R.; Becker, J.; Hawkins, C. F., Raised serum alkaline phosphatase in rheumartoid disease - An index of liver dysfunction. *Ann. Rheum. Dis.* **1970,** *29* (5), 537-&.
225. Ooi, K.; Shiraki, K.; Morishita, Y.; Nobori, T., High-molecular intestinal alkaline phosphatase in chronic liver diseases. *J. Clin. Lab. Anal.* **2007,** *21* (3), 133-139.
226. Li, J. W.; Xu, C.; Fan, Y.; Wang, Y.; Xiao, Y. B., Can serum levels of alkaline phosphatase and phosphate predict cardiovascular diseases and total mortality in individuals with preserved renal function? A systemic review and meta-analysis. *Plos One* **2014,** *9* (7).
227. Haarhaus, M.; Brandenburg, V.; Kalantar-Zadeh, K.; Stenvinkel, P.; Magnusson, P., Alkaline phosphatase: a novel treatment target for cardiovascular disease in CKD. *Nat. Rev. Nephrol.* **2017,** *13* (7), 429-442.
228. Asanuma, D.; Sakabe, M.; Kamiya, M.; Yamamoto, K.; Hiratake, J.; Ogawa, M.; Kosaka, N.; Choyke, P. L.; Nagano, T.; Kobayashi, H., et al., Sensitive beta-galactosidase-targeting fluorescence probe for visualizing small peritoneal metastatic tumours in vivo. *Nat. Commun.* **2015,** *6*, 7.
229. Bosmann, H. B.; Hall, T. C., Enzyme-activity in invasive tumors of human breast and colon. *Proc. Natl. Acad. Sci. U.S.A.* **1974,** *71* (5), 1833-1837.
230. Chatterjee, S. K.; Bhattacharya, M.; Barlow, J. J., Glycosyltransferase and glycosidase activities in ovarian-cancer patients. *Cancer Res.* **1979,** *39* (6), 1943-1951.
231. Zhang, J. J.; Cheng, P. H.; Pu, K. Y., Recent advances of molecular optical probes in imaging of beta-galactosidase. *Bioconjugate Chem.* **2019,** *30* (8), 2089-2101.
232. Kajimoto, T.; Node, M., Inhibitors against glycosidases as medicines. *Curr. Top. Med. Chem.* **2009,** *9* (1), 13-33.

233. Pinnaduwage, P.; Huang, L., β-Galactosidase-induced destabilization of liposome composed of phosphatidylethanolamine and ganglioside GM1. *Biochim. Biophys. Acta, Biomembr.* **1988,** *939* (2), 375-382.
234. Litzinger, D. C.; Huang, L., Phosphatodylethanolamine liposomes: drug delivery, gene transfer and immunodiagnostic applications. *Biochim. Biophys. Acta, Biomembr.* **1992,** *1113* (2), 201-227.
235. Domingo, J. C.; Mora, M.; De Madariaga, M. A., Role of headgroup structure in the phase behaviour of N-acylethanolamine phospholipids: hydrogen-bonding ability and headgroup size. *Chem. Phys. Lipids* **1994,** *69* (3), 229-240.
236. Newman, J.; Stiers, D.; Anderson, W.; Schmid, H., Phase behavior of synthetic N-acylethanolamine phospholipids. *Chem. Phys. Lipids* **1986,** *42* (4), 249-260.
237. Pak, C. C.; Ali, S.; Janoff, A. S.; Meers, P., Triggerable liposomal fusion by enzyme cleavage of a novel peptide–lipid conjugate. *Biochim. Biophys. Acta, Biomembr.* **1998,** *1372* (1), 13-27.
238. Pak, C. C.; Erukulla, R. K.; Ahl, P. L.; Janoff, A. S.; Meers, P., Elastase activated liposomal delivery to nucleated cells. *Biochim. Biophys. Acta, Biomembr.* **1999,** *1419* (2), 111-126.
239. Zhang, Z.-Y.; Smith, B. D., Synthesis and characterization of NVOC-DOPE, a caged photoactivatable derivative of dioleoylphosphatidylethanolamine. *Bioconjugate Chem.* **1999,** *10* (6), 1150-1152.
240. Loew, M.; Forsythe, J. C.; McCarley, R. L., Lipid nature and their influence on opening of redox-active liposomes. *Langmuir* **2013,** *29* (22), 6615-6623.
241. Wang, B.; Gangwar, S.; Pauletti, G. M.; Siahaan, T. J.; Borchardt, R. T., Synthesis of a novel esterase-sensitive cyclic prodrug system for peptides that utilizes a “trimethyl lock”-facilitated lactonization reaction. *J. Org. Chem.* **1997,** *62* (5), 1363-1367.
242. Chandran, S. S.; Dickson, K. A.; Raines, R. T., Latent fluorophore based on the trimethyl lock. *J. Am. Chem. Soc.* **2005,** *127* (6), 1652-1653.
243. Gonzaga, R. V.; do Nascimento, L. A.; Santos, S. S.; Machado Sanches, B. A.; Giarolla, J.; Ferreira, E. I., Perspectives about self-immolative drug delivery systems. *J. Pharm. Sci.* **2020,** *109* (11), 3262-3281.
244. Gisbert-Garzarán, M.; Manzano, M.; Vallet-Regí, M., Self-immolative chemistry in nanomedicine. *Chem. Eng. J.* **2018,** *340*, 24-31.
245. Yan, J.; Lee, S.; Zhang, A.; Yoon, J., Self-immolative colorimetric, fluorescent and chemiluminescent chemosensors. *Chem. Soc. Rev.* **2018,** *47* (18), 6900-6916.
246. Alouane, A.; Labruère, R.; Le Saux, T.; Schmidt, F.; Jullien, L., Self-immolative spacers: kinetic aspects, structure–property relationships, and applications. *Angew. Chem. Int. Ed.* **2015,** *54* (26), 7492-7509.
247. Lavis, L. D.; Chao, T.-Y.; Raines, R. T., Latent Blue and Red Fluorophores Based on the Trimethyl Lock. *ChemBioChem* **2006,** *7* (8), 1151-1154.
248. Levine, M. N.; Raines, R. T., Trimethyl lock: a trigger for molecular release in chemistry, biology, and pharmacology. *Chem. Sci.* **2012,** *3* (8), 2412-2420.
249. Greenwald, R. B.; Choe, Y. H.; Conover, C. D.; Shum, K.; Wu, D.; Royzen, M., Drug delivery systems based on trimethyl lock lactonization: Poly(ethylene glycol) prodrugs of amino-

containing compounds. *J. Med. Chem.* **2000,** *43* (3), 475-487.
250. Carl, P. L.; Chakravarty, P. K.; Katzenellenbogen, J. A., A novel connector linkage applicable in prodrug design. *J. Med. Chem.* **1981,** *24* (5), 479-480.
251. Gnaim, S.; Shabat, D., Quinone-methide species, a Gateway to functional molecular systems: From self-immolative dendrimers to long-wavelength fluorescent dyes. *Acc. Chem. Res.* **2014,** *47* (10), 2970-2984.
252. Zhou, W.; Andrews, C.; Liu, J.; Shultz, J. W.; Valley, M. P.; Cali, J. J.; Hawkins, E. M.; Klaubert, D. H.; Bulleit, R. F.; Wood, K. V., Self-cleavable bioluminogenic luciferin phosphates as alkaline phosphatase reporters. *ChemBioChem* **2008,** *9* (5), 714-718.
253. Amsberry, K. L.; Borchardt, R. T., The lactonization of 2'-hydroxyhydrocinnamic acid amides: a potential prodrug for amines. *J. Org. Chem.* **1990,** *55* (23), 5867-5877.
254. Chauvin, T.; Durand, P.; Bernier, M.; Meudal, H.; Doan, B. T.; Noury, F.; Badet, B.; Beloeil, J. C.; Toth, E., Detection of enzymatic activity by PARACEST MRI: a general approach to target a large variety of enzymes. *Angew. Chem. Int. Ed.* **2008,** *47* (23), 4370-4372.
255. Losey, E. A.; Smith, M. D.; Meng, M.; Best, M. D., Microplate-based analysis of protein-membrane binding interactions via immobilization of whole liposomes containing a biotinylated anchor. *Bioconjugate Chem.* **2009,** *20* (2), 376-383.
256. Feng, L.; Manabe, K.; Shope, J. C.; Widmer, S.; DeWald, D. B.; Prestwich, G. D., A real-time fluorogenic phospholipase A2 assay for biochemical and cellular activity measurements. *Cell Chem. Biol.* **2002,** *9* (7), 795-803.
257. Simberg, D.; Weisman, S.; Talmon, Y.; Barenholz, Y., DOTAP (and other cationic lipids): Chemistry, biophysics, and transfection. *Crit. Rev. Ther. Drug* **2004,** *21* (4), 62.
258. Whitehead, S. A.; McNitt, C. D.; Mattern-Schain, S. I.; Carr, A. J.; Alam, S.; Popik, V. V.; Best, M. D., Artificial membrane fusion triggered by strain-promoted alkyne-azide cycloaddition. *Bioconjugate Chem.* **2017,** *28* (4), 923-932.
259. Tanguy, E.; Wang, Q.; Moine, H.; Vitale, N., Phosphatidic acid: From pleiotropic functions to neuronal pathology. *Front. Cell. Neurosci.* **2019,** *13* (2).
260. Wang, H.-W.; Jiang, P.-L.; Lin, S.-F.; Lin, H.-J.; Ou, K.-L.; Deng, W.-P.; Lee, L.-W.; Huang, Y.-Y.; Liang, P.-H.; Liu, D.-Z., Application of galactose-modified liposomes as a potent antigen presenting cell targeted carrier for intranasal immunization. *Acta biomater.* **2013,** *9* (3), 5681-5688.
261. Blencowe, C. A.; Russell, A. T.; Greco, F.; Hayes, W.; Thornthwaite, D. W., Self-immolative linkers in polymeric delivery systems. *Polym. Chem.* **2011,** *2* (4), 773-790.
262. Allen, T. M.; Moase, E. H., Therapeutic opportunities for targeted liposomal drug delivery. *Adv. Drug Del. Rev.* **1996,** *21* (2), 117-133.
263. Gabizon, A. A., Liposome circulation time and tumor targeting - Implications for cancer chemotherapy. *Adv. Drug Del. Rev.* **1995,** *16* (2-3), 285-294.
264. Lasic, D. D.; Needham, D., The "Stealth" liposome: A prototypical biomaterial. *Chem. Rev.* **1995,** *95* (8), 2601-2628.
265. Czechura, P.; Tam, R. Y.; Dimitrijevic, E.; Murphy, A. V.; Ben, R. N., The importance of hydration for inhibiting ice recrystallization with C-linked antifreeze glycoproteins. *J. Am. Chem.*

Soc. **2008,** *130* (10), 2928-2929.
266. Wang, R.; Zhu, G.; Mei, L.; Xie, Y.; Ma, H.; Ye, M.; Qing, F.-L.; Tan, W., Automated modular synthesis of aptamer–drug conjugates for targeted drug delivery. *J. Am. Chem. Soc.* **2014,** *136* (7), 2731-2734.
267. Nathan, C.; Ding, A., SnapShot: reactive oxygen intermediates (ROI). *Cell* **2010,** *140* (6), 951-951. e952.
268. Fransen, M.; Nordgren, M.; Wang, B.; Apanasets, O., Role of peroxisomes in ROS/RNS-metabolism: implications for human disease. *Biochim. Biophys. Acta, Mol. Basis Dis.* **2012,** *1822* (9), 1363-1373.
269. Apel, K.; Hirt, H., Reactive oxygen species: metabolism, oxidative stress, and signal transduction. *Annu. Rev. Plant Biol.* **2004,** *55*, 373-399.
270. Radak, Z.; Zhao, Z.; Koltai, E.; Ohno, H.; Atalay, M., Oxygen consumption and usage during physical exercise: the balance between oxidative stress and ROS-dependent adaptive signaling. *Antioxid. Redox Signal.* **2013,** *18* (10), 1208-1246.
271. Sosa, V.; Moliné, T.; Somoza, R.; Paciucci, R.; Kondoh, H.; LLeonart, M. E., Oxidative stress and cancer: an overview. *Ageing Res. Rev.* **2013,** *12* (1), 376-390.
272. Fubini, B.; Hubbard, A., Reactive oxygen species (ROS) and reactive nitrogen species (RNS) generation by silica in inflammation and fibrosis. *Free Radical Biol. Med.* **2003,** *34* (12), 1507-1516.
273. Davalli, P.; Mitic, T.; Caporali, A.; Lauriola, A.; D'Arca, D., ROS, cell senescence, and novel molecular mechanisms in aging and age-related diseases. *Oxid. Med. Cell. Longev.* **2016,** *2016*, 3565127-3565127.
274. Szatrowski, T. P.; Nathan, C. F., Production of large amounts of hydrogen peroxide by human tumor cells. *Cancer Res.* **1991,** *51* (3), 794-798.
275. Ye, H.; Zhou, Y.; Liu, X.; Chen, Y.; Duan, S.; Zhu, R.; Liu, Y.; Yin, L., Recent advances on reactive oxygen species-responsive delivery and diagnosis system. *Biomacromolecules* **2019,** *20* (7), 2441-2463.
276. Tao, W.; He, Z., ROS-responsive drug delivery systems for biomedical applications. *Asian J. Pharm. Sci.* **2018,** *13* (2), 101-112.
277. Du, Y.; He, W.; Xia, Q.; Zhou, W.; Yao, C.; Li, X., Thioether phosphatidylcholine liposomes: A novel ROS-responsive platform for drug delivery. *ACS Appl. Mater. Interfaces* **2019,** *11* (41), 37411-37420.
278. Lippert, A. R.; Van de Bittner, G. C.; Chang, C. J., Boronate oxidation as a bioorthogonal reaction approach for studying the chemistry of hydrogen peroxide in living systems. *Acc. Chem. Res.* **2011,** *44* (9), 793-804.
279. Hoang, T. T.; Smith, T. P.; Raines, R. T., A boronic acid conjugate of angiogenin that shows ROS-responsive neuroprotective activity. *Angew. Chem. Int. Ed. Engl.* **2017,** *56* (10), 2619-2622.
280. Lou, J.; Best, M. D., A general approach to enzyme-responsive liposomes. *Chem. Eur. J.* **2020,** *26* (39), 8597-8607.
281. Jourden, J. L. M.; Daniel, K. B.; Cohen, S. M., Investigation of self-immolative linkers in the

design of hydrogen peroxide activated metalloprotein inhibitors. *Chem. Commun.* **2011,** *47* (28), 7968-7970.

282. Ellens, H.; Bentz, J.; Szoka, F. C., pH-induced destabilization of phosphatidylethanolamine-containing liposomes: role of bilayer contact. *Biochemistry* **1984,** *23* (7), 1532-1538.
283. Miyazawa, T.; Kamiyoshihara, R.; Shimizu, N.; Harigae, T.; Otoki, Y.; Ito, J.; Kato, S.; Miyazawa, T.; Nakagawa, K., Amadori-glycated phosphatidylethanolamine enhances the physical stability and selective targeting ability of liposomes. *R. Soc. Open Sci.* **2018,** *5* (2), 171249.
284. Sugihara, K.; Stucki, J.; Isa, L.; Voros, J.; Zambelli, T., Electrically induced lipid migration in non-lamellar phase. *J. Colloid Interface Sci.* **2012,** *386* (1), 421-427.
285. Smith, M. D.; Gong, D.; Sudhahar, C. G.; Reno, J. C.; Stahelin, R. V.; Best, M. D., Synthesis and convenient functionalization of azide-labeled diacylglycerol analogues for modular access to biologically active lipid probes. *Bioconjugate Chem.* **2008,** *19* (9), 1855-1863.
286. Kodali, D. R.; Tercyak, A.; Fahey, D. A.; Small, D. M., Acyl migration in 1,2-dipalmitoyl-sn-glycerol. *Chem. Phys. Lipids* **1990,** *52* (3), 163-170.
287. Barelli, H.; Antonny, B., Lipid unsaturation and organelle dynamics. *Curr. Opin. Cell Biol.* **2016,** *41*, 25-32.
288. Smith, M. D.; Sudhahar, C. G.; Gong, D.; Stahelin, R. V.; Best, M. D., Modular synthesis of biologically active phosphatidic acid probes using click chemistry. *Mol. Biosyst.* **2009,** *5* (9), 962-972.
289. Oude Blenke, E.; Mastrobattista, E.; Schiffelers, R. M., Strategies for triggered drug release from tumor targeted liposomes. *Expert Opin. Drug Deliv.* **2013,** *10* (10), 1399-1410.
290. Bibi, S.; Lattmann, E.; Mohammed, A. R.; Perrie, Y., Trigger release liposome systems: local and remote controlled delivery? *J. Microencapsul.* **2012,** *29* (3), 262-276.
291. Lee, Y.; Thompson, D. H., Stimuli-responsive liposomes for drug delivery. *WIREs Nanomed. Nanobi.* **2017,** *9* (5), e1450.
292. Madani, F.; Lindberg, S.; Langel, Ü.; Futaki, S.; Gräslund, A., Mechanisms of cellular uptake of cell-penetrating peptides. *J. Biophys.* **2011,** *2011*.
293. Zorko, M.; Langel, Ü., Cell-penetrating peptides: mechanism and kinetics of cargo delivery. *Adv. Drug Deliv. Rev.* **2005,** *57* (4), 529-545.
294. Foged, C.; Nielsen, H. M., Cell-penetrating peptides for drug delivery across membrane barriers. *Expert Opin. Drug Deliv.* **2008,** *5* (1), 105-117.
295. Koren, E.; Torchilin, V. P., Cell-penetrating peptides: breaking through to the other side. *Trends Mol. Med.* **2012,** *18* (7), 385-393.
296. Saar, K.; Lindgren, M.; Hansen, M.; Eiríksdóttir, E.; Jiang, Y.; Rosenthal-Aizman, K.; Sassian, M.; Langel, Ü., Cell-penetrating peptides: a comparative membrane toxicity study. *Anal. Biochem.* **2005,** *345* (1), 55-65.
297. Kilk, K.; Mahlapuu, R.; Soomets, U.; Langel, Ü., Analysis of in vitro toxicity of five cell-penetrating peptides by metabolic profiling. *Toxicology* **2009,** *265* (3), 87-95.
298. He, Y.; Li, F.; Huang, Y., Chapter six - Smart cell-penetrating peptide-based techniques for intracellular delivery of therapeutic macromolecules. In *Advances in Protein Chemistry and*

Structural Biology, Donev, R., Ed. Academic Press: 2018; Vol. 112, pp 183-220.

299. Huang, Y.; Jiang, Y.; Wang, H.; Wang, J.; Shin, M. C.; Byun, Y.; He, H.; Liang, Y.; Yang, V. C., Curb challenges of the “Trojan Horse” approach: Smart strategies in achieving effective yet safe cell-penetrating peptide-based drug delivery. *Adv. Drug Deliv. Rev.* **2013,** *65* (10), 1299-1315.
300. Lin, Y.; Mazo, M. M.; Skaalure, S. C.; Thomas, M. R.; Schultz, S. R.; Stevens, M. M., Activatable cell-biomaterial interfacing with photo-caged peptides. *Chem. Sci.* **2019,** *10* (4), 1158-1167.
301. Hansen, M. B.; van Gaal, E.; Minten, I.; Storm, G.; van Hest, J. C. M.; Löwik, D. W. P. M., Constrained and UV-activatable cell-penetrating peptides for intracellular delivery of liposomes. *J. Control. Release* **2012,** *164* (1), 87-94.
302. Shamay, Y.; Adar, L.; Ashkenasy, G.; David, A., Light induced drug delivery into cancer cells. *Biomaterials* **2011,** *32* (5), 1377-1386.
303. Jin, E.; Zhang, B.; Sun, X.; Zhou, Z.; Ma, X.; Sun, Q.; Tang, J.; Shen, Y.; Van Kirk, E.; Murdoch, W. J., Acid-active cell-penetrating peptides for in vivo tumor-targeted drug delivery. *J. Am. Chem. Soc.* **2013,** *135* (2), 933-940.
304. Lee, E. S.; Gao, Z.; Bae, Y. H., Recent progress in tumor pH targeting nanotechnology. *J. Control. Release* **2008,** *132* (3), 164-170.
305. Lee, E. S.; Gao, Z.; Kim, D.; Park, K.; Kwon, I. C.; Bae, Y. H., Super pH-sensitive multifunctional polymeric micelle for tumor pHe specific TAT exposure and multidrug resistance. *J. Control. Release* **2008,** *129* (3), 228-236.
306. He, H.; Sun, L.; Ye, J.; Liu, E.; Chen, S.; Liang, Q.; Shin, M. C.; Yang, V. C., Enzyme-triggered, cell penetrating peptide-mediated delivery of anti-tumor agents. *J. Control. Release* **2016,** *240*, 67-76.
307. Harris, T. J.; von Maltzahn, G.; Lord, M. E.; Park, J. H.; Agrawal, A.; Min, D. H.; Sailor, M. J.; Bhatia, S. N., Protease-triggered unveiling of bioactive nanoparticles. *Small* **2008,** *4* (9), 1307-1312.
308. Webb, B. A.; Chimenti, M.; Jacobson, M. P.; Barber, D. L., Dysregulated pH: a perfect storm for cancer progression. *Nat. Rev. Cancer* **2011,** *11* (9), 671-677.
309. Matsumura, Y.; Ananthaswamy, H. N., Toxic effects of ultraviolet radiation on the skin. *Toxicol. Appl. Pharmacol.* **2004,** *195* (3), 298-308.
310. Yang, J.; Yang, J.; Liang, S. H.; Xu, Y.; Moore, A.; Ran, C., Imaging hydrogen peroxide in Alzheimer’s disease via cascade signal amplification. *Sci. Rep.* **2016,** *6* (1), 35613.
311. Nicholls, D. G., Oxidative stress and energy crises in neuronal dysfunction. *Ann. N.Y. Acad. Sci.* **2008,** *1147* (1), 53-60.
312. Harrison, D.; Griendling, K. K.; Landmesser, U.; Hornig, B.; Drexler, H., Role of oxidative stress in atherosclerosis. *Am. J. Cardiol.* **2003,** *91* (3), 7-11.
313. Harrison, D. G.; Gongora, M. C.; Guzik, T. J.; Widder, J., Oxidative stress and hypertension. *J. Am. Soc. Hypertens.* **2007,** *1* (1), 30-44.
314. Li, J.-M.; Shah, A. M., ROS generation by nonphagocytic NADPH oxidase: potential relevance in diabetic nephropathy. *J. Am. Soc. Nephrol.* **2003,** *14*, S221-S226.

315. Weinstain, R.; Savariar, E. N.; Felsen, C. N.; Tsien, R. Y., In vivo targeting of hydrogen peroxide by activatable cell-penetrating peptides. *J. Am. Chem. Soc.* **2014,** *136* (3), 874-877.
316. Saczewski, F.; Balewski, Ł., Biological activities of guanidine compounds. *Expert Opin. Ther. Pat.* **2009,** *19* (10), 1417-1448.
317. Li, L.; Vorobyov, I.; Allen, T. W., The different interactions of lysine and arginine side chains with lipid membranes. *J. Phys. Chem. B* **2013,** *117* (40), 11906-11920.
318. Carlson, P. M.; Schellinger, J. G.; Pahang, J. A.; Johnson, R. N.; Pun, S. H., Comparative study of guanidine-based and lysine-based brush copolymers for plasmid delivery. *Biomater. Sci.* **2013,** *1* (7), 736-744.
319. Arisaka, A.; Mogaki, R.; Okuro, K.; Aida, T., Caged molecular glues as photoactivatable tags for nuclear translocation of guests in living cells. *J. Am. Chem. Soc.* **2018,** *140* (7), 2687-2692.
320. O'Neil, E. J.; DiVittorio, K. M.; Smith, B. D., Phosphatidylcholine-derived bolaamphiphiles via click chemistry. *Org. Lett.* **2007,** *9* (2), 199-202.
321. Hwang, D.; Nilchan, N.; Nanna, A. R.; Li, X.; Cameron, M. D.; Roush, W. R.; Park, H.; Rader, C., Site-selective antibody functionalization via orthogonally reactive arginine and lysine residues. *Cell Chem. Biol.* **2019,** *26* (9), 1229-1239.e1229.
322. Lou, J.; Best, M. D., Reactive oxygen species-responsive liposomes via boronate-caged phosphatidylethanolamine. *Bioconjugate Chem.* **2020,** *31* (9), 2220-2230.
323. Gong, D.; Smith, M. D.; Manna, D.; Bostic, H. E.; Cho, W.; Best, M. D., Microplate-based characterization of protein-phosphoinositide binding interactions using a synthetic biotinylated headgroup analogue. *Bioconjugate Chem.* **2009,** *20*, 310-316.
324. Rowland, M. M.; Bostic, H. E.; Gong, D.; Lucas, N.; Cho, W.; Best, M. D., Microarray analysis of Akt PH domain binding employing synthetic biotinylated analogs of all seven phosphoinositide headgroup isomers. *Chem. Phys. Lipids* **2012,** *165*, 207-215.
325. Utsugi, T.; Schroit, A. J.; Connor, J.; Bucana, C. D.; Fidler, I. J., Elevated expression of phosphatidylserine in the outer membrane leaflet of human tumor cells and recognition by activated human blood monocytes. *Cancer Res.* **1991,** *51* (11), 3062-3066.
326. Chan, T. R.; Hilgraf, R.; Sharpless, K. B.; Fokin, V. V., Polytriazoles as copper(I)-stabilizing ligands in catalysis. *Org. Lett.* **2004,** *6* (17), 2853-2855.
327. Aloulou, A.; Ali, Y. B.; Bezzine, S.; Gargouri, Y.; Gelb, M. H., Phospholipases: an overview. *Methods Mol. Biol.* **2012,** *861*, 63-85.
328. Dennis, E. A.; Rhee, S. G.; Billah, M. M.; Hannun, Y. A., Role of phospholipases in generating lipid second messengers in signal transduction 1. *FASEB J.* **1991,** *5* (7), 2068-2077.
329. Bonventre, J. V., Phospholipase A2 and signal transduction. *J. Am. Soc. Nephrol.* **1992,** *3* (2), 128-150.
330. Kramer, R. M.; Stephenson, D. T.; Roberts, E. F.; Clemens, J. A., Cytosolic phospholipase A2 (cPLA2) and lipid mediator release in the brain. *J. Lipid Mediators Cell Signalling* **1996,** *14* (1-3), 3-7.
331. Fourcade, O.; Simon, M.-F.; Viodé, C.; Rugani, N.; Leballe, F.; Ragab, A.; Fournié, B.; Sarda, L.; Chap, H., Secretory phospholipase A2 generates the novel lipid mediator lysophosphatidic acid in membrane microvesicles shed from activated cells. *Cell* **1995,** *80* (6),

919-927.
332. Oliveira, T. G.; Di Paolo, G., Phospholipase D in brain function and Alzheimer's disease. *Biochim. Biophys. Acta Mol. Cell Biol. Lipids* **2010,** *1801* (8), 799-805.
333. Record, M.; Poirot, M.; Silvente-Poirot, S., Emerging concepts on the role of exosomes in lipid metabolic diseases. *Biochimie* **2014,** *96*, 67-74.
334. Ramanadham, S.; Ali, T.; Ashley, J. W.; Bone, R. N.; Hancock, W. D.; Lei, X., Calcium-independent phospholipases A2 and their roles in biological processes and diseases. *J. Lipid Res.* **2015,** *56* (9), 1643-1668.
335. Awwad, H. M.; Geisel, J.; Obeid, R., The role of choline in prostate cancer. *Clin. Biochem.* **2012,** *45* (18), 1548-1553.
336. Mills, G. B.; Moolenaar, W. H., The emerging role of lysophosphatidic acid in cancer. *Nat. Rev. Cancer* **2003,** *3* (8), 582-591.
337. R Drake, C.; C Miller, D.; F Jones, E., Activatable optical probes for the detection of enzymes. *Curr. Org. Synth.* **2011,** *8* (4), 498-520.
338. Beisson, F.; Tiss, A.; Rivière, C.; Verger, R., Methods for lipase detection and assay: a critical review. *Eur. J. Lipid Sci. Technol.* **2000,** *102* (2), 133-153.
339. Van den Bosch, H.; Aarsman, A., A review on methods of phospholipase A determination. *Agents Actions* **1979,** *9* (4), 382-389.
340. Cho, W., Seeing is believing: Real-time cellular activity assay for phospholipase A2. *ACS Chem. Biol.* **2006,** *1* (2), 65-66.
341. Meshulam, T.; Herscovitz, H.; Casavant, D.; Bernardo, J.; Roman, R.; Haugland, R. P.; Strohmeier, G. S.; Diamond, R. D.; Simons, E. R., Flow cytometric kinetic measurements of neutrophil phospholipase A activation. *J. Biol. Chem.* **1992,** *267* (30), 21465-21470.
342. Ferguson, C. G.; Bigman, C. S.; Richardson, R. D.; van Meeteren, L. A.; Moolenaar, W. H.; Prestwich, G. D., Fluorogenic phospholipid substrate to detect lysophospholipase D/autotaxin activity. *Org. Lett.* **2006,** *8* (10), 2023-2026.
343. Houtkooper, R.; Vaz, F., Cardiolipin, the heart of mitochondrial metabolism. *Cell. Mol. Life Sci.* **2008,** *65* (16), 2493-2506.
344. Macfarlane, M. G., Structure of cardiolipin. *Nature* **1958,** *182* (4640), 946-946.
345. Robinson, N. C., Functional binding of cardiolipin to cytochrome c oxidase. *J. Bioenerg. Biomembr.* **1993,** *25* (2), 153-163.
346. Planas-Iglesias, J.; Dwarakanath, H.; Mohammadyani, D.; Yanamala, N.; Kagan, V. E.; Klein-Seetharaman, J., Cardiolipin interactions with proteins. *Biophys. J.* **2015,** *109* (6), 1282-1294.
347. Ren, M.; Phoon, C. K.; Schlame, M., Metabolism and function of mitochondrial cardiolipin. *Prog. Lipid Res.* **2014,** *55*, 1-16.
348. Dudek, J., Role of cardiolipin in mitochondrial signaling pathways. *Front. Cell Dev. Biol.* **2017,** *5*, 90.
349. McMillin, J. B.; Dowhan, W., Cardiolipin and apoptosis. *Biochim. Biophys. Acta Mol. Cell Biol. Lipids* **2002,** *1585* (2-3), 97-107.
350. Chicco, A. J.; Sparagna, G. C., Role of cardiolipin alterations in mitochondrial dysfunction and

disease. *Am. J. Physiol. Cell Physiol.* **2007,** *292* (1), C33-C44.
351. Schug, Z. T.; Gottlieb, E., Cardiolipin acts as a mitochondrial signalling platform to launch apoptosis. *Biochim. Biophys. Acta, Biomembr.* **2009,** *1788* (10), 2022-2031.
352. Birks, J.; Dyson, D.; Munro, I., 'Excimer'fluorescence II. Lifetime studies of pyrene solutions. *Proceedings of the Royal Society of London. Series A. Mathematical and Physical Sciences* **1963,** *275* (1363), 575-588.
353. Birks, J.; Christophorou, L., Excimer fluorescence spectra of pyrene derivatives. *Spectrochim. Acta* **1963,** *19* (2), 401-410.
354. Huang, J.; Wu, Y.; Chen, Y.; Zhu, Z.; Yang, X.; Yang, C. J.; Wang, K.; Tan, W., Pyrene-excimer probes based on the hybridization chain reaction for the detection of nucleic acids in complex biological fluids. *Angew. Chem. Int. Ed.* **2011,** *50* (2), 401-404.
355. Yang, C. J.; Jockusch, S.; Vicens, M.; Turro, N. J.; Tan, W., Light-switching excimer probes for rapid protein monitoring in complex biological fluids. *Proc. Natl. Acad. Sci.* **2005,** *102* (48), 17278-17283.
356. Sahoo, D.; Narayanaswami, V.; Kay, C. M.; Ryan, R. O., Pyrene excimer fluorescence: a spatially sensitive probe to monitor lipid-induced helical rearrangement of apolipophorin III. *Biochemistry* **2000,** *39* (22), 6594-6601.
357. Bains, G. K.; Kim, S. H.; Sorin, E. J.; Narayanaswami, V., The extent of pyrene excimer fluorescence emission is a reflector of distance and flexibility: analysis of the segment linking the LDL receptor-binding and tetramerization domains of apolipoprotein E3. *Biochemistry* **2012,** *51* (31), 6207-6219.
358. Hendrickson, H. S.; Rauk, P. N., Continuous fluorometric assay of phospholipase A2 with pyrene-labeled lecithin as a substrate. *Anal. Biochem.* **1981,** *116* (2), 553-558.
359. Abe, M.; Kitsuda, S.; Ohyama, S.; Koubori, S.; Murai, M.; Miyoshi, H., Concise procedure for the synthesis of cardiolipins having different fatty acid combinations. *Tetrahedron Lett.* **2010,** *51* (15), 2071-2073.
360. Abe, M.; Nakano, M.; Kosaka, A.; Miyoshi, H., Syntheses of photoreactive cardiolipins for a photoaffinity labeling study. *Tetrahedron Lett.* **2015,** *56* (17), 2258-2261.
361. Ali, S. M.; Ahmad, M. U.; Koslosky, P.; Kasireddy, K.; Murali Krishna, U.; Ahmad, I., Synthesis of short and long chain cardiolipins. *Tetrahedron* **2006,** *62* (29), 6990-6997.
362. Inuki, S.; Ohta, I.; Ishibashi, S.; Takamatsu, M.; Fukase, K.; Fujimoto, Y., Total synthesis of cardiolipins containing chiral cyclopropane fatty acids. *J. Org. Chem.* **2017,** *82* (15), 7832-7838.
363. Fava, A.; Iliceto, A.; Camera, E., Kinetics of the thiol-disulfide exchange. *J. Am. Chem. Soc.* **1957,** *79* (4), 833-838.
364. Black, S. P.; Sanders, J. K.; Stefankiewicz, A. R., Disulfide exchange: exposing supramolecular reactivity through dynamic covalent chemistry. *Chem. Soc. Rev.* **2014,** *43* (6), 1861-1872.
365. Gilbert, H. F.; McLean, V., Molecular and cellular aspects of thiol-disulfide exchange. *Adv. Enzymol. Relat. Areas Mol. Biol.* **1993,** *63*, 69-69.
366. Chuard, N.; Gasparini, G.; Moreau, D.; Lorcher, S.; Palivan, C.; Meier, W.; Sakai, N.; Matile,

S., Strain-promoted thiol-mediated cellular uptake of giant substrates: Liposomes and polymersomes. *Angew. Chem. Int. Ed. Engl.* **2017,** *56* (11), 2947-2950.
367. Burns, J. A.; Butler, J. C.; Moran, J.; Whitesides, G. M., Selective reduction of disulfides by tris(2-carboxyethyl) phosphine. *J. Org. Chem.* **1991,** *56* (8), 2648-2650.
368. Mouritsen, O. G.; Zuckermann, M. J., What's so special about cholesterol? *Lipids* **2004,** *39* (11), 1101-1113.
369. Presti, F. T., *The role of cholesterol in regulating membrane fluidity*. 1985; Vol. 4, p 97-145.
370. Silvius, J. R., Role of cholesterol in lipid raft formation: lessons from lipid model systems. *Biochim. Biophys. Acta, Biomembr.* **2003,** *1610* (2), 174-183.
371. Taspinar, Ö.; Wilczek, T.; Erver, J.; Breugst, M.; Neudörfl, J. M.; Schmalz, H. G., Synthesis of the 8, 19-epoxysteroid eurysterol A. *Chem. Eur. J.* **2020,** *26* (19), 4256-4260.
372. Koh, J.-Y., Zinc and disease of the brain. *Molecular neurobiology* **2001,** *24* (1), 99-106.
373. Maret, W., Zinc and human disease. *Met. Ions Life Sci.* **2013,** *13*, 389-414.
374. Walker, C. F.; Black, R. E., Zinc and the risk for infectious disease. *Annu. Rev. Nutr.* **2004,** *24*, 255-275.
375. Fraker, P. J.; Haas, S. M.; Luecke, R. W., Effect of zinc deficiency on the immune response of the young adult A/J mouse. *J. Nutr.* **1977,** *107* (10), 1889-1895.
376. MacDonald, R. S., The role of zinc in growth and cell proliferation. *J. Nutr.* **2000,** *130* (5), 1500S-1508S.
377. Toth, K., Zinc in neurotransmission. *Annu. Rev. Nutr.* **2011,** *31*, 139-153.
378. Bertozzi, C. R., A decade of bioorthogonal chemistry. *Acc. Chem. Res.* **2011,** *44* (9), 651-653.
379. Devaraj, N. K., The future of bioorthogonal chemistry. *ACS Cent. Sci.* **2018,** *4* (8), 952-959.
380. Scinto, S. L.; Bilodeau, D. A.; Hincapie, R.; Lee, W.; Nguyen, S. S.; Xu, M.; am Ende, C. W.; Finn, M.; Lang, K.; Lin, Q., Bioorthogonal chemistry. *Nat. Rev. Methods Primers* **2021,** *1* (1), 1-23.
381. Biegas, K. J.; Swarts, B. M., Chemical probes for tagging mycobacterial lipids. *Curr. Opin. Chem. Biol.* **2021,** *65*, 57-65.
382. Best, M. D., Click chemistry and bioorthogonal reactions: Unprecedented selectivity in the labeling of biological molecules. *Biochemistry* **2009,** *48* (28), 6571-6584.
383. Hang, H. C.; Wilson, J. P.; Charron, G., Bioorthogonal chemical reporters for analyzing protein lipidation and lipid trafficking. *Acc. Chem. Res.* **2011,** *44* (9), 699-708.
384. Ricks, T. J.; Cassilly, C. D.; Carr, A. J.; Alves, D. S.; Alam, S.; Tscherch, K.; Yokley, T. W.; Workman, C. E.; Morrell-Falvey, J. L.; Barrera, F. N., et al., Labeling of phosphatidylinositol lipid products in cells through metabolic engineering by using a clickable myo-inositol probe. *ChemBioChem* **2019,** *20* (2), 172-180.
385. Périgaud, C.; Gosselin, G.; Lefebvre, I.; Girardet, J.-L.; Benzaria, S.; Barber, I.; Imbach, J.-L., Rational design for cytosolic delivery of nucleoside monphosphates:“SATE” and “DTE” as enzyme-labile transient phosphate protecting groups. *Bioorg. Med. Chem. Lett.* **1993,** *3* (12), 2521-2526.
386. Schultz, C., Prodrugs of biologically active phosphate esters. *Bioorg. Med. Chem.* **2003,** *11* (6), 885-898.

387. Lefebvre, I.; Perigaud, C.; Pompon, A.; Aubertin, A.-M.; Girardet, J.-L.; Kirn, A.; Gosselin, G.; Imbach, J.-L., Mononucleoside phosphotriester derivatives with S-acyl-2-thioethyl bioreversible phosphate-protecting groups: intracellular delivery of 3'-azido-2', 3'-dideoxythymidine 5'-monophosphate. *J. Med. Chem.* **1995,** *38* (20), 3941-3950.
388. Ausmus, A. P.; Hogue, M.; Snyder, J. L.; Rundell, S. R.; Bednarz, K. M.; Banahene, N.; Swarts, B. M., Ferrier carbocyclization-mediated synthesis of enantiopure azido inositol analogues. *J. Org. Chem.* **2020,** *85* (5), 3182-3191.
389. Yan, R.-B.; Yang, F.; Wu, Y.; Zhang, L.-H.; Ye, X.-S., An efficient and improved procedure for preparation of triflyl azide and application in catalytic diazotransfer reaction. *Tetrahedron Lett.* **2005,** *46* (52), 8993-8995.
390. Li, Y.; Zhou, Y.; Ma, Y.; Li, X., Design and synthesis of novel cell wall inhibitors of Mycobacterium tuberculosis GlmM and GlmU. *Carbohydr. Res.* **2011,** *346* (13), 1714-1720.

Appendix

All NMR characterization spectra are included in a separate pdf file as an attachment.

Vita

Jinchao Lou (娄锦超) was born and raised in Wuxi, Jiangsu Province, China. Her interest in chemistry arose in high school, and she has been determined to study chemistry since. Beginning in 2012, she attended Northwest Normal University in Lanzhou, China, and obtained her bachelor's degree of Science in Chemistry in 2016. From her freshman year, she participated in undergraduate research in a supramolecular chemistry lab under the supervision of Dr. Qi Lin, where she learned the basics of research. In Spring 2016, she conducted research in Dr. Leyong Wang's lab at Nanjing University as a visiting undergraduate research assistant, where she obtained intensive experience in organic synthesis. After that, she was accepted to the chemistry Ph.D. program at the University of Tennessee at Knoxville in August 2016. Jinchao joined Dr. Michael Best's research group in January 2017. Her graduate research mainly focused on developing various stimuli-responsive liposomes for triggered release purposes.